JULY 1980 134 9-24-80 JRC

MASTER

DI 1222

LBL-10686
UC-13

EARTH SCIENCES DIVISION

ANNUAL REPORT 1979

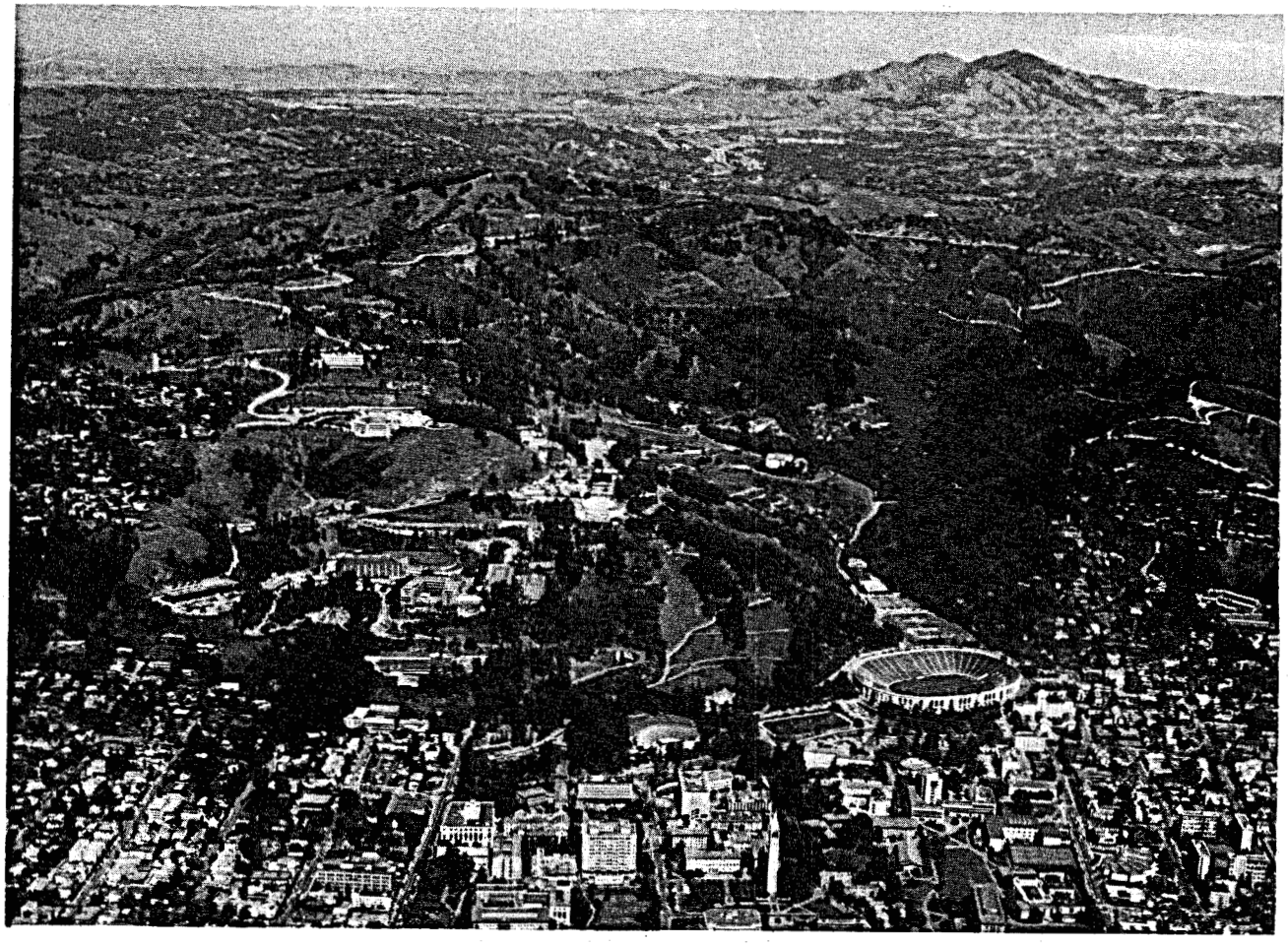

LAWRENCE BERKELEY LABORATORY
UNIVERSITY OF CALIFORNIA
BERKELEY, CALIFORNIA 94720

Prepared for the U.S. Department of Energy under Contract W-7405-ENG-48

DISTRIBUTION OF THIS DOCUMENT IS UNLIMITED

DISCLAIMER

This report was prepared as an account of work sponsored by an agency of the United States Government. Neither the United States Government nor any agency Thereof, nor any of their employees, makes any warranty, express or implied, or assumes any legal liability or responsibility for the accuracy, completeness, or usefulness of any information, apparatus, product, or process disclosed, or represents that its use would not infringe privately owned rights. Reference herein to any specific commercial product, process, or service by trade name, trademark, manufacturer, or otherwise does not necessarily constitute or imply its endorsement, recommendation, or favoring by the United States Government or any agency thereof. The views and opinions of authors expressed herein do not necessarily state or reflect those of the United States Government or any agency thereof.

DISCLAIMER

Portions of this document may be illegible in electronic image products. Images are produced from the best available original document.

LEGAL NOTICE

This book was prepared as an account of work sponsored by an agency of the United States Government. Neither the United States Government nor any agency thereof, nor any of their employees, makes any warranty, express or implied, or assumes any legal liability or responsibility for the accuracy, completeness, or usefulness of any information, apparatus, product, or process disclosed, or represents that its use would not infringe privately owned rights. Reference herein to any specific commercial product, process, or service by trade name, trademark, manufacturer, or otherwise, does not necessarily constitute or imply its endorsement, recommendation, or favoring by the United States Government or any agency thereof. The views and opinions of authors expressed herein do not necessarily state or reflect those of the United States Government or any agency thereof.

Printed in the United States of America
Available from
National Technical Information Service
U.S. Department of Commerce
5285 Port Royal Road
Springfield, VA 22161
Price Code: A10

LBL-10686

EARTH SCIENCES DIVISION ANNUAL REPORT 1979

LAWRENCE BERKELEY LABORATORY
UNIVERSITY OF CALIFORNIA
BERKELEY, CALIFORNIA 94720

DISCLAIMER

This book was prepared as an account of work sponsored by an agency of the United States Government. Neither the United States Government nor any agency thereof, nor any of their employees, makes any warranty, express or implied, or assumes any legal liability or responsibility for the accuracy, completeness, or usefulness of any information, apparatus, product, or process disclosed, or represents that its use would not infringe privately owned rights. Reference herein to any specific commercial product, process, or service by trade name, trademark, manufacturer, or otherwise, does not necessarily constitute or imply its endorsement, recommendation, or favoring by the United States Government or any agency thereof. The views and opinions of authors expressed herein do not necessarily state or reflect those of the United States Government or any agency thereof.

Prepared for the U.S. Department of Energy under Contract W-7405-ENG-48

DISTRIBUTION OF THIS DOCUMENT IS UNLIMITED

CONTENTS

Introduction 1

GEOTHERMAL ENERGY DEVELOPMENT

Geothermal Exploration Technology 4

INTERPRETATION OF ELECTRICAL AND ELECTROMAGNETIC SURVEY DATA 4
H. F. Morrison, K. H. Lee, E. Mozley, and M. Hoversten

FIELD PROCESSING OF MAGNETOTELLURIC DATA 5
J. Clarke, T. D. Gamble, W. M. Goubau, R. Koch, and R. Miracky

AUTOMATED SEISMIC PROCESSOR 7
T. V. McEvilly, E. L. Majer, J. Bartschi, J. Heinsen, and R. O'Connell

CONTROLLED-SOURCE ELECTROMAGNETIC MEASUREMENTS AT GEOTHERMAL SITES IN NEVADA 11
M. J. Wilt, N. E. Goldstein, R. Haught, and M. Stark

GEOPHYSICAL AND GEOCHEMICAL INVESTIGATIONS AT MT. HOOD, OREGON 15
N. E. Goldstein, H. A. Wollenberg, E. Mozley, and M. J. Wilt

KLAMATH BASIN GEOTHERMAL RESOURCE AND EXPLORATION TECHNIQUE EVALUATION 19
M. A. Stark, N. E. Goldstein, and H. A. Wollenberg

MAGNETOTELLURIC STUDIES IN THE HIGH CASCADE, OREGON 24
N. E. Goldstein, R. Miracky, W. M. Goubau, and T. D. Gamble

Geothermal Energy Conversion Technology 26

BINARY FLUID EXPERIMENT 26
B. W. Tleimat

ACTIVITIES IN DIRECT-CONTACT HEAT EXCHANGE 27
P. M. Rapier

Reservoir Engineering 31

MEXICAN-AMERICAN COOPERATIVE PROGRAM AT THE CERRO PRIETO GEOTHERMAL FIELD, BAJA CALIFORNIA, MEXICO 31
M. J. Lippmann, P. A. Witherspoon, and N. E. Goldstein

REGIONAL GEOLOGIC SETTING OF THE CERRO PRIETO GEOTHERMAL FIELD 36
S. P. Vonder Haar and J. H. Howard

SUBSURFACE GEOLOGY OF THE CERRO PRIETO GEOTHERMAL FIELD 39
S. P. Vonder Haar, J. Noble, M. T. O'Brien, and J. H. Howard

NUMERICAL MODELING STUDIES OF THE CERRO PRIETO RESERVOIR 44
M. J. Lippmann and K. P. Goyal

SIMULATION OF REINJECTION AT CERRO PRIETO USING AN IDEALIZED TWO-RESERVOIR GEOLOGICAL MODEL 52
C. F. Tsang, D. C. Mangold, and M. J. Lippmann

RESISTIVITY STUDIES AT CERRO PRIETO 57
M. J. Wilt and N. E. Goldstein

MAGNETOTELLURIC STUDIES AT CERRO PRIETO 61
T. D. Gamble, W. M. Goubau, R. Miracky, J. Clarke, and N. E. Goldstein

PRECISION GRAVITY STUDIES AT THE CERRO PRIETO GEOTHERMAL FIELD 66
R. B. Grannell, D. W. Tarman, R. C. Clover, R. M. Leggewie, P. S. Aronstam, R. C. Kroll, and J. Eppink

GEOTHERMAL RESERVOIR ENGINEERING MANAGEMENT PROGRAM: DEVELOPMENTS IN FISCAL 1979 66
J. H. Howard and W. J. Schwarz

EVALUATION OF CITY WELL 1, KLAMATH FALLS, OREGON 69
S. M. Benson, C. B. Goranson, and R. C. Schroeder

EVALUATION OF THE SUSANVILLE, CALIFORNIA, GEOTHERMAL RESOURCE, 1979 76
S. M. Benson, C. B. Goranson, J. P. Haney, and R. C. Schroeder

RECENT MODIFICATIONS OF THE NUMERICAL CODE CCC 87
G. S. Bodvarsson, M. J. Lippmann, and T. N. Narasimhan

DEVELOPMENT OF THE TWO-PHASE RESERVOIR SIMULATION PROGRAM, SHAFT79 91
K. Pruess, R. C. Schroeder, and P. A. Witherspoon

PROPERTIES OF H_2O-CO_2 MIXTURES FOR GEOTHERMAL RESERVOIR AND WELLBORE SIMULATORS 95
E. R. Iglesias and R. C. Schroeder

PRELIMINARY STUDIES OF THE RESERVOIR CAPACITY AND LONGEVITY OF THE BACA GEOTHERMAL FIELD, NEW MEXICO 98
G. S. Bodvarsson, S. P. Vonder Haar, M J. Wilt, and C. F. Tsang

MODELING TRANSIENT TWO-PHASE FLOW IN A WELLBORE 103
C. W. Miller

CORRECTION OF DOWNHOLE PRESSURE TRANSIENTS MEASURED WITH A FLUID-FILLED CAPILLARY TUBE 105
C. W. Miller and J. M. Zerzan

WELLBORE STORAGE EFFECTS IN GEOTHERMAL WELLS 107
C. W. Miller

HYDRAULICS OF A WELL INTERCEPTING A SINGLE HORIZONTAL FRACTURE
G. S. Bodvarsson, T. N. Narasimhan, and C. F. Tsang 109

PRELIMINARY STUDY OF SUBSIDENCE AT WAIRAKEI, NEW ZEALAND, USING A NUMERICAL MODEL 112
T. N. Narasimhan and K. P. Goyal

USE OF PRESSURE TRANSIENT ANALYSIS IN MODELING THE HYDRAULIC FRACTURING PROCESS 115
W. A. Palen and T. N. Narasimhan

Geothermal Environmental Research 118

GEOTHERMAL SUBSIDENCE RESEARCH PROGRAM 118
J. E. Noble

INDUCED SEISMICITY STUDIES AT THE CERRO PRIETO, MEXICO, AND EAST MESA, CALIFORNIA, GEOTHERMAL FIELDS 123
E. L. Majer and T. V. McEvilly

REMOVAL OF SILICA FROM CERRO PRIETO BRINES 125
O. Weres and L. Tsao

THEORETICAL STUDIES OF CERRO PRIETO BRINES CHEMICAL EQUILIBRIA 127
E. R. Iglesias and O. Weres

GEOSCIENCES

Basic Sciences Studies 132

BUOYANCY FLOW AND THERMAL STRATIFICATION IN AQUIFER HOT-WATER STORAGE 132
G. Hellstrom, C. F. Tsang, and J. Claesson

DAILY SENSIBLE HEAT STORAGE IN AQUIFERS FOR SOLAR ENERGY SYSTEMS
C. F. Tsang, P. Fong, C. W. Miller, and M. J. Lippmann 133

ONE-DIMENSIONAL CHEMICAL TRANSPORT IN AN ADVECTION-DOMINATED SYSTEM 136
T. N. Narasimhan

RESPONSE OF AQUIFERS TO EARTH TIDES 137
T. N. Narasimhan and B. Y. Kanehiro

PROBABILISTIC SIMULATION OF TRANSIENT SUBSURFACE FLOW USING A NUMERICAL SCHEME 141
T. N. Narasimhan and T. Buscheck

A NOTE ON VOLUME AVERAGING 143
T. N. Narasimhan

GROUNDWATER MODELING IN SUBSURFACE NUCLEAR WASTE DISPOSAL—AN OVERVIEW 144
T. N. Narasimhan

ROLE OF PORE PRESSURE ON DEFORMATION IN GEOLOGIC PROCESSES 145
T. N. Narasimhan

AN ANALYTIC STUDY OF GEOTHERMAL RESERVOIR PRESSURE RESPONSE TO COLD-WATER INJECTION 148
Y. W. Tsang and C. F. Tsang

THERMAL EFFECTS IN WELL TEST ANALYSIS 150
D. C. Mangold, C. F. Tsang, M. J. Lippmann, and P. A. Witherspoon

THERMODYNAMICS OF HIGH-TEMPERATURE BRINES 154
K. S. Pitzer, D. J. Bradley, P. Z. Rogers, and J. C. Peiper

BEHAVIOR OF ROCK-FLUID SYSTEMS AT ELEVATED PRESSURES AND TEMPERATURES 156
W. H. Somerton

SOLUBILITY OF LOW ALBITE IN NaCl SOLUTIONS AT 250°C 159
J. M. Neil and J. A. Apps

THERMODYNAMIC PROPERTIES OF SILICATE MATERIALS 165
I. S. E. Carmichael, M. S. Ghiorso, L. Moret, S. A. Nelson, M. Rivers, and J. Stebbins

CHEMICAL TRANSPORT IN NATURAL SYSTEMS 166
C. L. Carnahan

THERMAL CONDUCTIVITY OF AQUEOUS NaCl SOLUTIONS FROM 20°C TO 330°C 167
H. Ozbek and S. L. Phillips

AQUEOUS SOLUTIONS DATA BASE TO HIGH TEMPERATURES AND PRESSURES, SODIUM CHLORIDE SOLUTIONS 170
S. L. Phillips, R. J. Otto, H. Ozbek, and M. Tavana

Applied Research Studies 174

ENHANCED RECOVERY WITH MOBILITY AND REACTIVE TENSION AGENTS 174
C. J. Radke and W. H. Somerton

HIGH-PRECISION MASS SPECTROMETRY 177
M. C. Michel and W. R. Keyes

STATE-OF-THE-ART TRACER TECHNIQUES 178
S. M. Klainer and J. A. Apps

CRYSTALLOGRAPHIC PROPERTIES USING THE NQR TECHNIQUE 180
S. M. Klainer and J. A. Apps

TRACE ANALYSIS OF GROUNDWATERS 184
S. M. Klainer and J. A. Apps

SURVEY OF AQUIFER THERMAL ENERGY STORAGE PROJECTS 186
C. F. Tsang, D. L. Hopkins, and G. Hellstrom

MULTIPLE-WELL VARIABLE-RATE WELL TEST ANALYSIS OF THE AUBURN UNIVERSITY AQUIFER THERMAL ENERGY STORAGE FIELD DATA 188
C. A. Doughty, D. G. McEdwards, and C. F. Tsang

NUMERICAL SIMULATION OF AUBURN UNIVERSITY FIELD EXPERIMENTS 190
C. F. Tsang, T. Buscheck, and C. A. Doughty

NUCLEAR WASTE ISOLATION

Swedish-American Cooperative Program 196

THERMOMECHANICAL EXPERIMENTS AT STRIPA 196
M. Hood, T. Chan, and P. Nelson

FRACTURE HYDROLOGY STUDIES AT STRIPA 201
J. E. Gale, C. R. Wilson, and P. A. Witherspoon

MACROPERMEABILITY STUDIES AT STRIPA 205
C. R. Wilson, J. C. S. Long, R. M. Galbraith, A. O. DuBois, M. J. McPherson, and P. A. Witherspoon

A PROGRAM OF GEOLOGIC STUDIES AT STRIPA 207
H. A. Wollenberg, L. Andersson, and S. Flexser

Research and Development Investigations 209

REVIEW OF THE STATE-OF-THE-ART OF NUMERICAL MODELING OF THERMO-HYDROLOGIC FLOW IN FRACTURED ROCK MASSES 209
J. S. Y. Wang, R. A. Sterbentz, and C. F. Tsang

MIGRATION OF RADIONUCLIDES IN GEOLOGIC MEDIA 211
T. H. Pigford

ULTRA-LARGE ROCK CORE EXPERIMENTS 212
D. J. Watkins, R. Thorpe, W. E. Ralph, R. Hsu, and S. Flexser

$^{234}U/^{238}U$ DISEQUILIBRIUM STUDIES 215
M. C. Michel and W. R. Keyes

SEARCH FOR UNDERGROUND OPENINGS FOR IN-SITU TEST FACILITIES IN CRYSTALLINE ROCK 217
H. A. Wollenberg, B. Strisower, D. J. Corrigan, A. N. Graf, and M. T. O'Brien

THERMOCHEMICAL MODELING OF MASS TRANSPORT PROCESSES IN THE NEAR-CANISTER REGION OF A BASALTIC NUCLEAR WASTE REPOSITORY 220
L. V. Benson and P. C. Lichtner

THEORETICAL AND EXPERIMENTAL EVALUATION OF WASTE TRANSPORT IN SELECTED ROCKS 221
R. J. Silva, L. V. Benson, A. W. Yee, and G. A. Parks

MARINE SCIENCES

Ocean Thermal Energy Conversion 226

ENVIRONMENTAL AND RESOURCE ASSESSMENT PROGRAM FOR OCEAN THERMAL ENERGY CONVERSION 226
P. Wilde

COMPILATION OF MARINE GEOLOGIC AND OCEANOGRAPHIC DATA OFF THE WEST COAST OF THE UNITED STATES 230
P. Wilde

APPENDIXES

APPENDIX A: PUBLICATIONS 233

APPENDIX B: EARTH SCIENCES DIVISION STAFF 238

INTRODUCTION

The programs of the Earth Science Division constitute a broad and varied spectrum of research on topics important to the nation's energy future. Programmatically our fundamental and applied research activities include assessment, recovery, and use of underground resources; developing the knowledge and techniques to safely isolate nuclear waste in geologic repositories; mitigating the environmental impact of energy exploitation developments; and studying geologic storage of thermal energy. The individual projects span the possibilities from basic scientific investigations of underlying geologic phenomena to mission-directed resolution of underground engineering problems. Linking all of these earth sciences studies is a common focus on the earth's deep crustal regime and the development of increased knowledge about the regime's dynamic behavior. By its complex multifaceted nature, the crustal environment cannot be fully scrutinized by the experimental researcher in a laboratory nor by the geologist on a field survey. A complete scientific understanding of the dynamic physical and chemical behavior of geologic systems requires an earth sciences team approach with the support of sophisticated laboratory and field facilities. The Earth Sciences Division is such a scientific team composed of about 20 University faculty members, 140 professional researchers, and 35 graduate students. Their research activities can be either generic in nature, focusing on specific geology, geochemistry, geophysics, hydrology, rock mechanics, reservoir engineering and mining engineering questions, or of a broader scope requiring all the talents and energies of a multidisciplinary professional team. Most enjoy the opportunity to do both by dividing their time between scientific problems topical to their discipline and comprehensive projects of broader national importance. All researchers make full use of LBL's excellent analytical facilities, research laboratories, computational capabilities, and field experiment equipment.

The articles herein are indicative of our researchers' level of sophistication, breadth of interests, and variety of applications.

GEOTHERMAL ENERGY DEVELOPMENT

The Earth Sciences Division program in Geothermal Energy Development began in 1973 in response to the national goal of developing alternate energy sources for electric and non-electric applications. The program initially consisted of: an exploration assessment of sites in northern Nevada for a proposed demonstration plant; development of a binary-fluid conversion process for high-temperature, low-salinity brines; and various geochemical studies related to brine chemistry, scaling, and corrosion. An additional support project, the National Geothermal Information Resource (GRID) was begun to compile a data bank on topics related to geothermal energy.

Many of these general programs continue in modified or expanded form and others have begun in recent years. Most have been funded by the U.S. Department of Energy, Division of Geothermal Energy; the U.S. Bureau of Reclamation has contracted with LBL for site specific studies. Within this section of the Annual Report we present our current geothermal research activities subdivided into four principal areas: (1) Geothermal Exploration Technology, (2) Geothermal Energy Conversion Technology, (3) Reservoir Engineering, and (4) Geothermal Environmental Research.

Exploration Technology projects deal with generic research to improve our ability to locate and define a geothermal reservoir using surface, mainly geophysical, techniques. Historically, our emphasis has been on electrical, electromagnetic, and seismic techniques because of the expertise available to us at the University of California, Berkeley, and because of the recognized need to evaluate and develop these techniques to the point where they can be better used by industry. Tests and demonstrations of research results are done by LBL at various geothermal sites as part of site-specific resource assessments (e.g., Mt. Hood and Klamath Falls, Oregon, and northern Nevada sites) or as site-specific reservoir definition studies (e.g., Cerro Prieto). Technology transfer to industry in this and other program areas is an ever-present concern; one that is accomplished through workshops, conferences, and consultations with geothermal developers and field demonstrations.

Geothermal Energy Conversion Technology projects develop basic data and analytical tools in heat exchange and thermodynamics needed for the development of moderate-temperature geothermal resources. LBL has been studying the thermodynamic properties of isobutane/isopentane mixtures to learn how to optimize binary Rankine cycle heat conversion to electric power for various resource temperatures. We are also managing the design, fabrication and testing of a 500-kW pilot plant using a direct-contact heat exchanger. This energy conversion process may have potential importance to the economics of second-generation geothermal power plants.

Reservoir Engineering studies can be subdivided into two main areas: fundamental research and reservoir case studies. Under the first, LBL manages a Geothermal Reservoir Engineering Management Program (GREMP) for the U.S. Department of Energy Division of Geothermal Energy, for which LBL prepares and implements a research program involving various academic, industry, and other research groups. Tied into the overall plan are the separate in-house research efforts consisting of (a) the development and testing of new and improved geothermal well test equipment, field techniques, and interpretative methods; (b) the development of reservoir simulation codes capable of dealing with two-phase conditions in the reservoir well-bores and mixtures of H_2O-CO_2 gases; and (c) modeling the hydraulic stimulation of reservoirs. In the area of reservoir case studies, LBL directs for DOE a U.S./Mexican cooperative study of the Cerro Prieto, Baja California, geothermal field. The elements of this study are geology-hydrology, geochemistry, geophysics, and reservoir testing and modeling. We have also provided advice on reinjection. LBL also assists DOE in evaluating reservoir data for the Valles Caldera, New Mexico, the site of a 50-MW demonstration plant.

Geothermal Environmental Research consists of subsidence, induced seismicity, and brine chemistry. LBL manages for DOE a Geothermal Subsidence Research Program (GSRMP) for which we prepare and implement research efforts into the causes, prediction, monitoring, and mitigation of subsidence. Research contracts are given to academic, industry, and other laboratory groups. In addition, LBL also maintains an in-house research component which has been chiefly concerned with and has succeeded in developing a numerical code that provides new insight into the possible physical mechanisms of the complex subsidence at Wairakei, New Zealand.

Induced seismicity work, which ties in closely with subsidence and the general topic of reservoir dynamics under production conditions, involves monitoring at East Mesa and Cerro Prieto.

Geothermal Exploration Technology

INTERPRETATION OF ELECTRICAL AND ELECTROMAGNETIC SURVEY DATA

H. F. Morrison, K. H. Lee, E. Mozley, and M. Hoversten

INTRODUCTION

As part of a continuing research and development program directed towards interpreting electrical and electromagnetic survey data, a number of computer programs have been written to calculate the response of one-, two-, and three-dimensional subsurface structures to electromagnetic sources. Sources of interest are plane electromagnetic waves (for magnetotelluric studies) and current loop magnetic dipoles (for controlled-source EM studies.)

In addition, an integrated interpretation procedure has been developed and used on magnetotelluric field data from Mt. Hood, Oregon.

PROGRESS IN FISCAL YEAR 1979

In this section we summarize the features of various computer programs that have been developed or improved upon during fiscal year 1979.

Program DECAY

DECAY calculates the electric and magnetic fields on or above a layered earth in both the frequency and time domains. The EM source is a current loop of arbitrary radius on or above the surface. The earth response is calculated in the frequency domain via equations given by Morrison et al. (1969). To obtain the time-domain response for a given current waveform, we multiply the waveform harmonics by the earth response and these products are added in a Fourier series to give the transient response.

Program GRADMAG

GRADMAG calculates the induced electric fields within a layered earth for a current loop source. The E fields are calculated as a function of frequency and transformed to the time domain. This program is being used to understand the relationships between the induced E field in the ground and the observed electric and magnetic fields on the surface.

Program TDINVER

TDINVER is a weighted-least-squares algorithm for finding layered models that fit time-domain electromagnetic sounding data. This program is now under development and will be refined in the coming year.

Program HYBRID

Program HYBRID calculates the electric and magnetic fields scattered by a three-dimensional inhomogeneity of finite extent buried in a one- or two-layer half space. The algorithm is based on two independent sets of equations: (1) a system of finite-element equations derived from a variational integral and (2) a set of equations obtained from the integral relations between the field at the boundary and the field inside the boundary. The maximum size of the inhomogeneity that we can model with the program is limited up to 10 x 10 x 10 array. The program uses 47K decimal words in small core memories (SCM) along with four disk files. Both magnetic dipole (vertical or horizontal) and plane wave sources can be used.

Program MSE2D

Program MSE2D has been written exclusively for a magnetic dipole source on or above a two-dimensional half space, where the extent of the inhomogeneity can be arbitrary. The method used is a finite element technique with a mesh limited to 55 x 18 nodes in x and z directions, respectively. The memory requirement is 46K in SCM, 295K in LCM, and one disk file.

Program ESE2D

The algorithm for this program is exactly the same as the one used for MSE2D. The only difference is that program ESE2D calculates the fields for a grounded electric dipole source. This program is used in the evaluation of the controlled-source AMT technique.

Program TEMINTG

Program TEMINTG has been written to study scattering by a simple two-dimensional inhomogeneity where the primary field is a normally incident plane wave with arbitrary orientation with respect to the inhomogeneity. The technique used is the integral equation point-matching method. The TE-mode plane wave solution was given by Hohmann (1971). The integral equation solution for the TM-mode incident has been developed recently by Lee (1980). If the inhomogeneity contains less than 100 cells we find that this program is less expensive to run than the finite element solution developed by Ryu (1971). This program uses 38K words of SCM and 123K words of LCM.

Interpretation of MT Data from Mt. Hood, Oregon

For processing and displaying of multi-site magnetotelluric data we have developed programs capable of treating and displaying large amounts of data, e.g., regional strike and impedance estimates as a function of frequency as well as angle of rotation and position.

Three different one-dimensional inversion techniques have been used on selected MT field data from Mt. Hood, Oregon, and the results were compared. The first method used, and the one most relied upon, was the discrete iterative inversion

method developed by Jupp and Vozoff (1977). Second, the iterative-continuous method by Oldenberg (1979) was used in a limited manner. This technique iteratively constructs a model minimizing the residual error and evaluates the model via Backus-Gilbert techniques. The third approach was a continuous inversion based on non-uniform transmission line solutions via rational approximations developed by Becher and Sharpe (1969). Stability problems were encountered which limited the use of this approach.

For the second stage of interpretation we concentrated on local areas where a two-dimensional conductivity structure dominates the frequency response of the earth. Two approaches were used. First, we used forward modeling using programs by Lee (1978) and Lee and Pridmore (1979) to first approximate the observed responses. Then, where possible, an automatic inversion scheme by Jupp and Vozoff (1977) was used. This method is similar to their one-dimensional inversion, with the forward problem being calculated by the network methods developed by Madden (1972).

A study of effect of topography on MT data was begun. The initial studies were done using an integral equation method developed by Oppliger (1980). This provided the dc current distributions in the region for plane wave sources.

PLANS FOR WORK IN FISCAL YEAR 1980

One of the top priorities will be to document the computer programs developed in 1979, and to provide user's instructions.

Independent of the forward-modeling technique development, we will also give a high priority to the generalized direct inverse problem associated with EM waves. Initial studies have uncovered a new technique which may allow us to reconstruct the shape and location of a scatterer directly from the reflected tangential electric and magnetic fields measured on an arbitrary surface. This approach to EM interpretation will be evaluated for simple scattering bodies, such as circular cylinder.

REFERENCES CITED

Becher, C. N., and Sharpe, C. B., 1969. A synthesis approach to magnetotelluric exploration. Radio Science, v. 4, no. 11, p. 1089.

Hohmann, G. W., 1971. Electromagnetic scattering by two-dimensional inhomogeneities in the earth. (Ph.D. dissertation) Berkeley, University of California.

Jupp, D. L. B., and Vozoff, K., 1975. Stable iterative methods for the inversion of geophysical data. Geophysical Journal R. Astr. Soc., v. 42, p. 957.

____, 1977. Two-dimensional magnetotelluric inversion. Geophys. Journal R. Astr. Soc., v. 50, p. 333.

Lee, K. H., 1978. Program TEM-two dimensional plane wave scattering solution by the finite element method for a two-dimensional conductivity distribution. Berkeley, University of California.

____, 1980. A solution for TM-mode plane waves incident on a two-dimensional inhomogeneity. To be submitted to Geophysics.

Madden, J. R., 1972. Transmission systems and network analogies to geophysical forward and inverse problems. Cambridge, Mass., Massachusetts Institute of Technology Technical Report N000-14-67-A 0204-0045.

Morrison, H. F., Phillips, R. J., and O'Brien, D. P., 1969. Quantitative interpretation of transient electromagnetic fields over a layered half space. Geophysical Prospecting, v. 17, no. 1, p. 82.

Oldenburg, D. W., 1979. One-dimensional inversion of natural source magnetotelluric observations. Geophysics, v. 44, no. 7, p. 1218.

Oppliger, G. L., 1980. Program MTOPO: Electric potential solution in the vicinity of a three-dimensional topographic feature (Ph.D. dissertation). Berkeley, University of California.

Ryu, J., 1971. Low frequency electromagnetic scattering (Ph.D. dissertation). Berkeley, University of California.

FIELD PROCESSING OF MAGNETOTELLURIC DATA

J. Clarke, T. D. Gamble, W. M. Goubau, R. Koch, and R. Miracky

INTRODUCTION

Recent advances in semiconductor technology have reached the point that battery-operated microcomputers can now analyze magnetotelluric data in the field. In 1979 we completed the construction of a system based on a Digital Equipment Corporation LSI-11 microcomputer for in-field magnetotelluric analysis and used it for the execution of several surveys.

PROGRESS IN 1979

The LSI-11 has proven to be a very fieldworthy instrument, performing in real time a data analysis essentially identical to that formerly done on the CDC-7600 computer at LBL. The system operates on approximately 200 W provided by 12-V golf-cart batteries. The limited capacity of the battery power supply, however, restricts the peripheral equipment that can be used in the field and this limits the quality and modes of results presentation. Therefore, our present analyses are limited to those selected by the operator to evaluate the quality and sufficiency of the data. Final data selection and graphic display are performed in the laboratory.

Figure 1 is a block diagram of the complete magnetotelluric data collection system. Our mag-

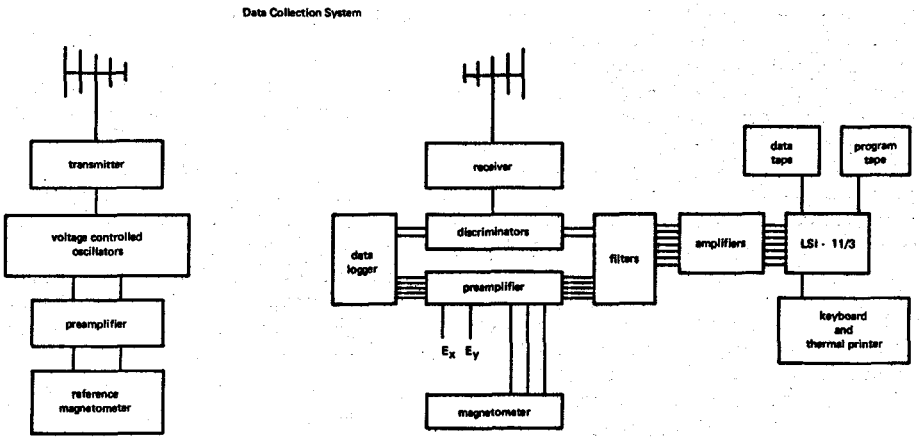

Figure 1. Block diagram of the magnetotelluric data collection system. (XBL 7910-13064)

netotelluric measurements are always made with the remote reference technique (Gamble, 1978; Gamble et al., 1979a,b). The equipment at the remote site, shown at the left of the figure, consists of a dc SQUID magnetometer, preamplifier, and FM analog telemetry equipment. Horizontal components of the magnetic field changes at the remote site are telemetered to the base station. At the base station the horizontal components of the electric field and three components of the magnetic field are preamplified, the remote signals are received, and then two simultaneous operations, described below, are performed on all seven channels.

All seven channels are digitized at a sampling rate of 1 Hz by the data logger so that the long-period digital data can be stored for later analysis. Simultaneously, the signals are bandpass filtered, digitized at a selectable rate by the LSI-11 microcomputer, and analyzed in real time to determine the average autopower and crosspowers between all channels. These average powers are written on magnetic tape to be the permanent record of the high frequency measurements. A second tape deck is used to load the programs into the computer.

The operation of the programs is outlined in Figure 2. The analysis is split into two main programs, GGUT and RESULTS, to maximize the capacity of the hardware. GGUT is written entirely in MACRO assembly language to maximize the speed of the real-time calculations and to minimize the size of the program. GGUT controls the digitization of the data, performs the Fourier analysis and compu-

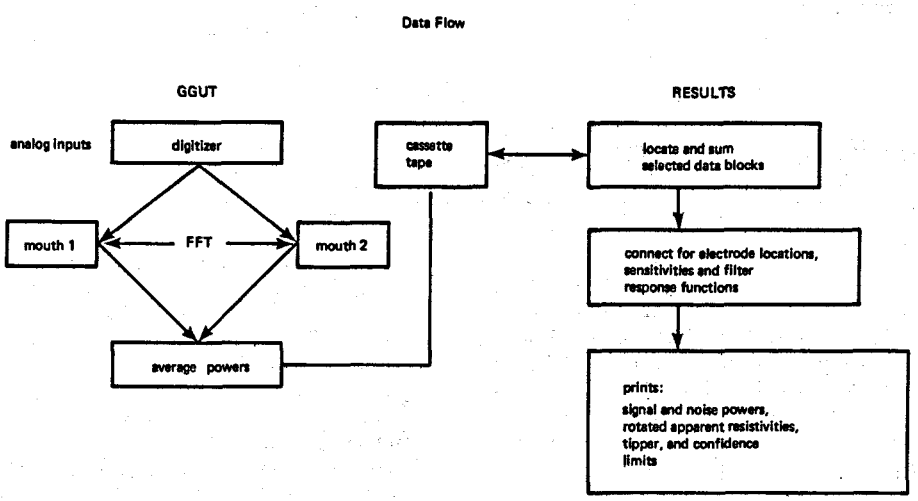

Figure 2. In-field processing of magnetotelluric data. (XBL 7910-13065)

tation of average powers, and writes them on the data tape. RESULTS is written in FORTRAN for ease of modification and to provide more sophisticated input-output formats. It reads the average powers of selected blocks of data from the data tape and prints out the results desired by the operator on a thermal printer.

The analysis proceeds as follows. The digitizer samples the channels under the control of a programmable clock. This digitization rate is limited to about 6 kHz by the software and could be easily increased to the hardware limit of about 40 kHz. When a 1024-point data segment has been completed, the digitization continues to fill a second input buffer while the Fourier analysis is performed on the first data segment. The average powers are computed within frequency windows equally spaced on a logarithmic scale and are added to the average powers from previous data segments. This analysis requires 16 seconds for several channels of data. If the analysis is not completed by the time the second input buffer fills, then the sampling is simply discontinued until the analysis is complete and the first buffer is free again. When the operator feels that sufficient data have been collected he halts the collection and directs the LSI-11 to write the average powers on the data tape. The RESULTS program then reads and averages selected blocks of average powers from the data tape, corrects these for electrode lengths, dipole orientations, filter response functions, and magnetometer sensitivities. The results are printed, as specified by the operator. These may include the signal-to-noise ratios of any measurement, the rotated apparent resistivities with their phases, rotation angles, skewnesses and tipper magnitudes, and phases, all with their probable errors. Examples of data collected and analyzed with this system are included in another article in this volume, "Magnetotelluric Studies at Cerro Prieto."

PLANS FOR FISCAL YEAR 1980

The LSI-11 microcomputer has proven to be a fieldworthy instrument powerful enough for all the calculations involved in real-time magnetotelluric data analysis. More importantly, as a research tool, the system can be reprogrammed to perform almost any analysis of electromagnetic measurements involving up to 16 channels of data. Thus it is an integral tool for further studies involving simultaneous measurements at several sites. Such studies may include investigating the coherence length of the incident electromagnetic fluctuations, determining the noise spectra, and performing relative calibrations of various types of magnetometers in the field.

REFERENCES CITED

Gamble, T. D., 1978. Remote reference magnetotellurics with SQUID (Ph.D. dissertation). Berkeley, University of California, and Lawrence Berkeley Laboratory, LBL-8062.

Gamble, T. D., Goubau, W. M., and Clarke, J. 1979a. Magnetotellurics with a remote magnetic reference. Geophysics, v. 44, no. 1, p. 43-68.

____, 1979b. Error analysis for remote reference magnetotellurics. Geophysics, v. 44, no. 1, p. 959-968.

AUTOMATED SEISMIC PROCESSOR

T. V. McEvilly, E. L. Majer, J. Bartschi, J. Heinsen, and R. O'Connell

SYSTEM DESCRIPTION

As first conceived, the Automated Seismic Processor (ASP) is a low-power (1 W/per channel), fast 16-bit, in-field seismic data processing computer (McEvilly et al., 1979). The ASP is designed around the RCA 1802 COSMAC CMOS microprocessor. Its principle use is for microearthquake detection and analysis. In 1979 a 16-channel ASP was built. It has essentially met all specified requirements. ASP is a parallel processing device with 15 microcomputers (WORKERS) responsible for feeding preprocessed data to a central microcomputer (the BOSS) for final processing (Figure 1). Each WORKER as well as the BOSS is capable of addressing 32 K of memory, either PROM or RAM. Presently the WORKERS each contain 4 K of RAM and 12 K of PROM. The BOSS contains 8 K of RAM and 24 K of PROM memory. The WORKER and BOSS programs are configured as shown in Figure 2. The routines SYSTEM, MISC, and SINTP are service programs that handle the intialization of the CPU, the basic interrupts and the calls and returns between the BOSS and WORKER computers. These routines also handle the BOSS messages, printing of output, input processing and the manipulation of data. 'Worker' in the WORKER, and 'boss' in the BOSS are the main computer programs from which all calls to the different subroutines are made.

ICALC in the WORKER handles the ADC interrupt routines that sample the data, remove the dc component, form the long-term-average (LTA), the short-term-average (STA), check for trigger, and time the arrival of the P-phase, if there is a trigger, all in real time between samples. At present, the maximum sample rate is 100 samples/sec with the CPU clock rate at 2 MHz. By increasing the clock rate to 3 MHz and cleaning up the program it is anticipated that a sample rate of 200 samples/sec can be achieved. Except for the FFT routines, all arithmetic in the WORKER is done in fixed point format. Also, every effort is made to use multiplication and division by twos. FIX is the RCA fixed point arithmetic package. Figure 3 is an example of the worker operations. If $x(t_i)$ is the original time series (the mean is first removed by subtracting a 4096 point long-term average), then a new time series $x'(t_i)$ is formed as:

$$x'(t_i) = \frac{\sum_{n-16}^{n} |x(t_i)|}{n}$$

i.e., rectifying the time series and smoothing with an n-point boxcar. For microearthquake data

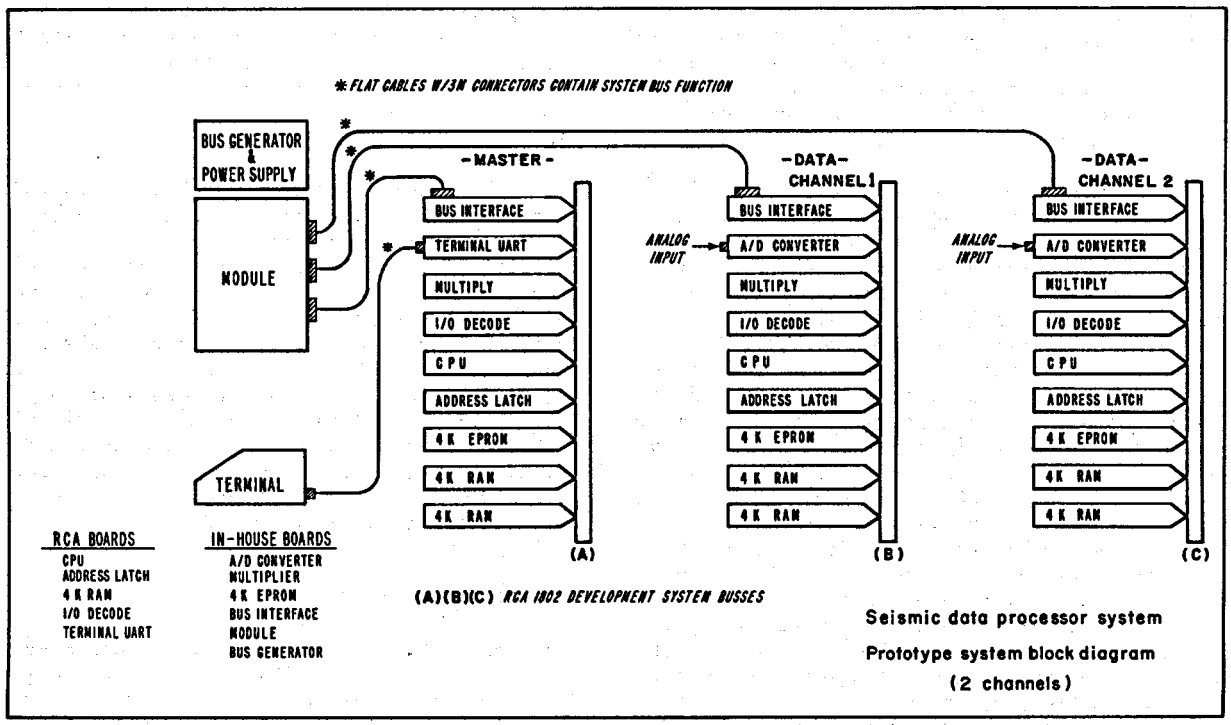

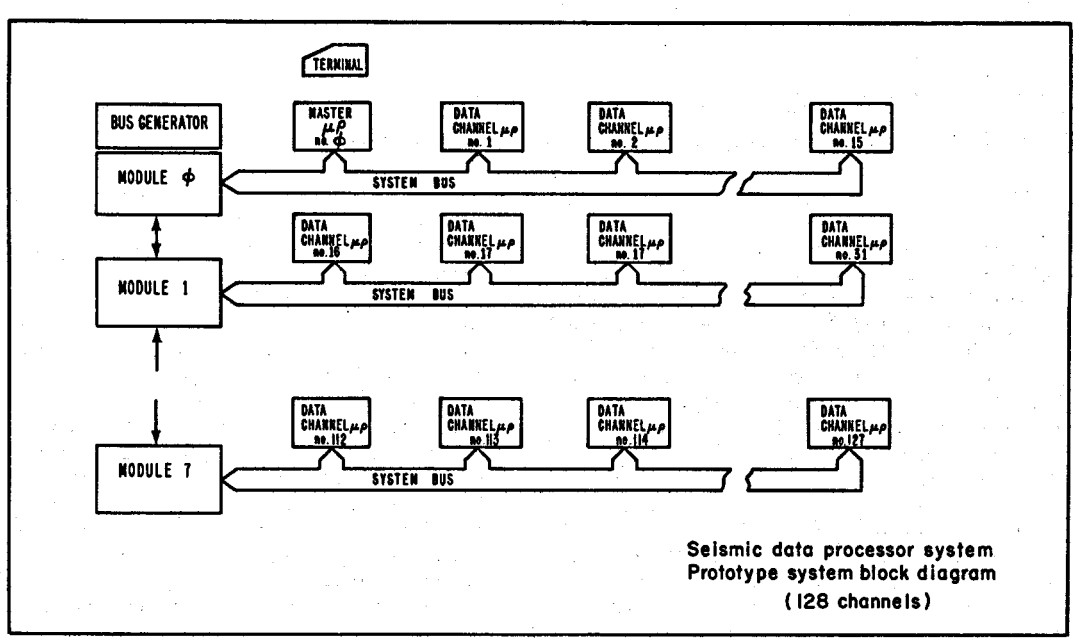

Figure 1. Top: Block diagram, two-channel prototype seismic data aquisition/processing system, showing card structures for BOSS (master) and WORKER (channel) modules. Bottom: Generalized block diagram of 128-channel seismic field system, illustrating 16-channel modular architecture. (XBL 7812-14137; XBL 7812-14138)

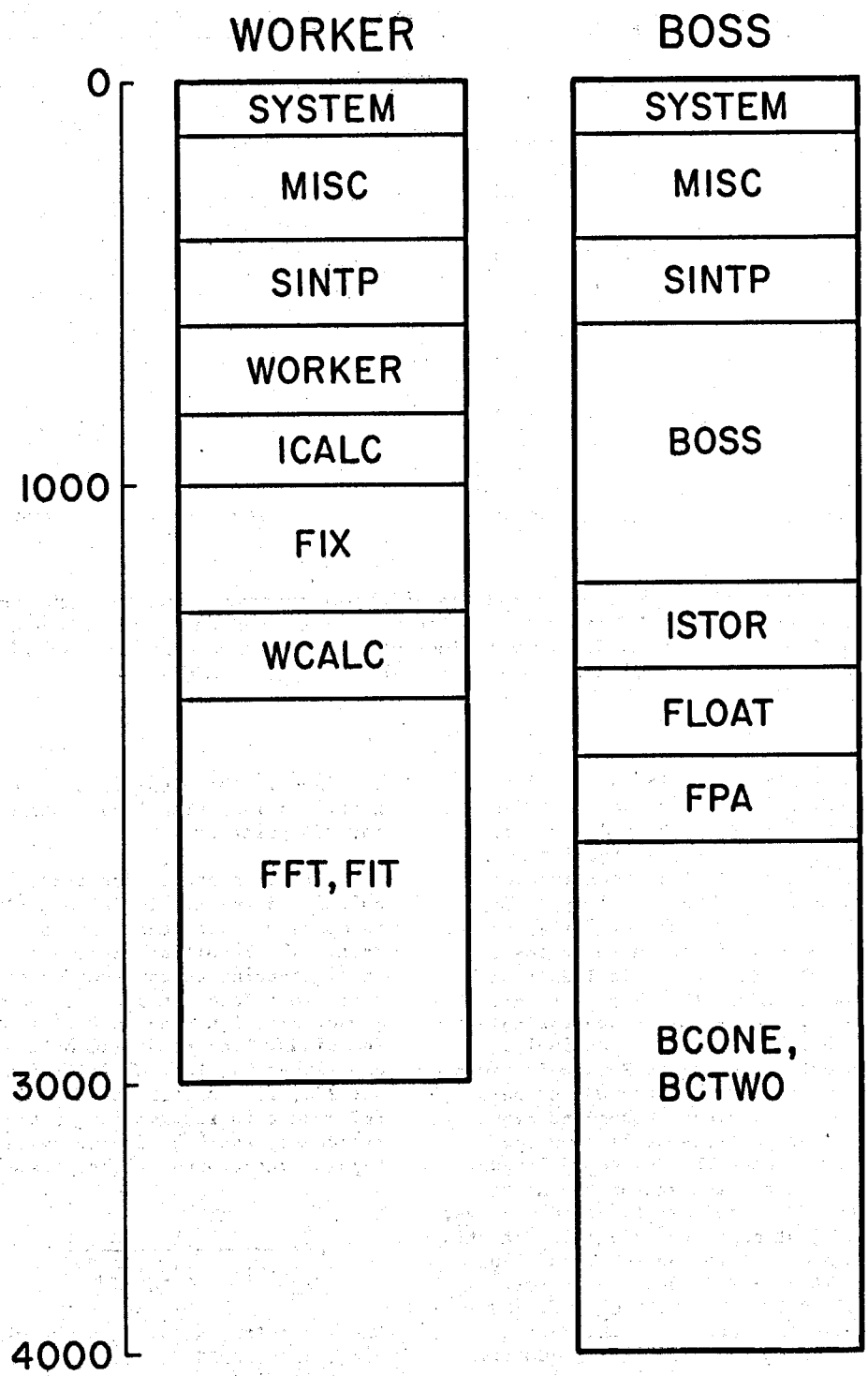

Figure 2. System program maps for WORKER and BOSS showing program location and lengths. Numbers are in hexadecimal. (XBL 807-7257)

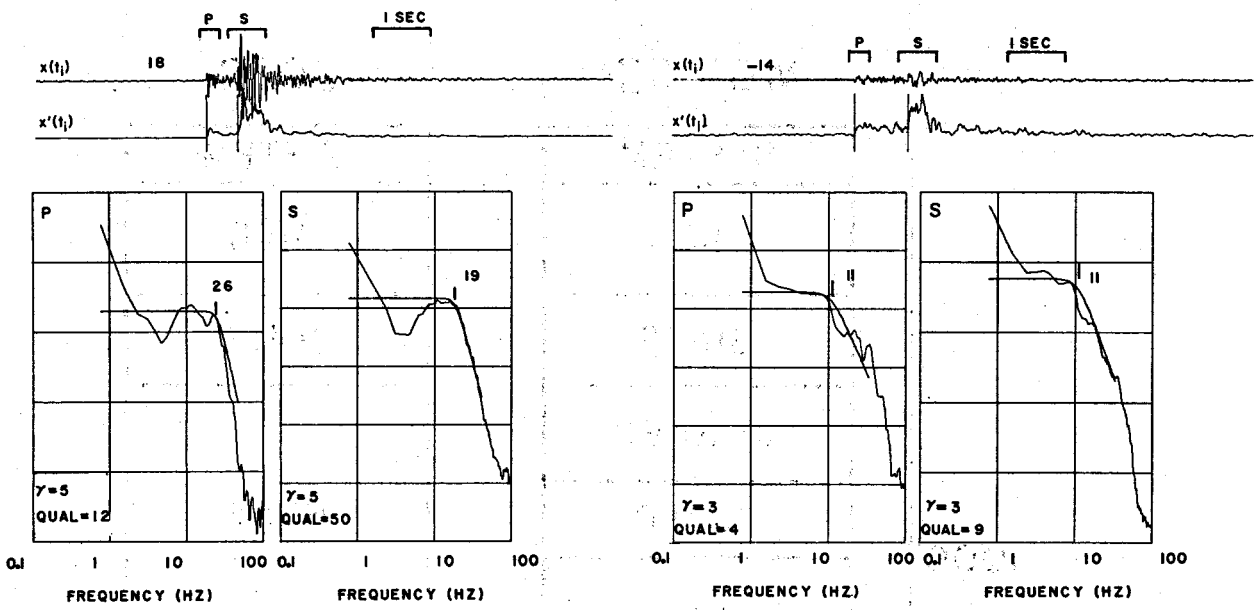

Figure 3. Examples of ASP processing and two different events. Shown on each event are the P and S windows selected for FFT processing polarity of the events (18 and -14) quality of P waves and S waves (P = 12,4, S = 50,9), arrival times of P and S waves [bars on $x'(t_i)$] corner frequences (26,19,11,11) and high frequency slope values (γ = 5,5,3,3).

(XBL 802-8307)

sampled at 200 samples/sec, n = 16 was found to be the optimum window. $x'(t_i)$ is then analyzed for detection and timing of the P- and S-waves, as shown in Figure 3. To do so, a 16-point short-term average (STA) and a 4096 long-term average (LTA) are taken on $x'(t_i)$. When STA = C_1 * LTA, a trigger point is found. However, the time when STA = C_2 * LTA, ($C_2 < C_1$), is taken to be the P-wave arrival time, PT. Because C_2 is less than C_1, PT will always be before the trigger point. Typical values for C_1 and C_2 (C_1,C_2 are variable input parameters) are 3 and 1.25 respectively. After an event is detected and the P-wave is timed, further processing requires that the worker be put in a "hold" mode to prevent subsequent event detection. The LTA and STA are still computed but detection is disabled. The P-wave amplitude, PA, is found by taking the average of the next 64 points after the PT. The quality of the P-wave, PQ, is PA/(the LTA just prior to trigger). At this point, PT, PA, PQ are sent to the BOSS. An S-wave is detected when STA = C_3 * PA and its arrival time, ST, is at STA = C_4 * PA, with C_3 = 2, and C_4 = 1.5. SA, S-wave amplitude, is the average of the next 128 points after ST. S-wave quality, SQ = SA/(LTA just prior to P-wave trigger). With ST and PT, the S-P time, DT, is calculated and variable window lengths around the P- and S-waves for the FFTs are selected. ST, SA, SQ, and DT are then sent to BOSS. The polarity of the P-wave, PP, is then calculated and sent to BOSS, PP is formed by summing the four points after PT, then dividing this difference by the LTA prior to the P-wave trigger. The sign of this result, + = up, - = down, is the direction of the first motion, and its magnitude is the quality of the polarity determination, i.e., the degree of sharpness of the onset. The event is over when the STA of $x'(t_i)$ is less than 1.25 * (LTA prior to trigger) for 256 points.

After an end is detected, the FFTs are then calculated and fit in FFT and FIT. Before an FFT is done, a cosine taper is applied to the demeaned data. The resulting spectra are then smoothed with an eight-point boxcar and corrected for instrument response before the long period level, corner frequency and high frequency roll-off are calculated. The window lengths depend on the DT (S-P time), and are either 64, 128, or 256 points for the P-wave, and 128, 256, or 512 points for the S-wave. Each FFT result is fit for long period level, corner frequency, and high frequency slope, γ, with a γ-pole Butterworth filter, i.e.,

$$A = \frac{1}{[1 + (f/f_o)^2\gamma]^{1/2}}$$

These results, along with the window lengths used, are sent to BOSS for further processing. After completion of the FFT, WORKER is ready to start looking for another event. However, until BOSS sends a release to each WORKER the hold mode is still in effect. This is to insure that BOSS has completed its duties before another set of data is taken in.

The order of messages on the line between BOSS and the WORKERS is determined by a system priority, with BOSS having number one priority. This allows BOSS to perform abortions on the WORKERS if certan specified parameters or quality

criteria are not met, and to return the WORKERS to looking for another event if BOSS determines that the event presently being processed is marginal. Upon power-on, the user is interrogated by BOSS to determine triggering levels, minimum detection, and quality criteria, desired BOSS processing, station coordinates, number of stations, and other input parameters. All communication to the WORKERS is through the BOSS via keyboard input. All output is also performed by BOSS on a small printer.

'Boss' in the BOSS computer is the main routine which controls the rest of the BOSS programs. ISTOR picks up the BOSS messages (i.e., PT, PA, PQ, ST, SA, SQ, DT, PP, FFT results) and stores them in tables corresponding to the WORKER Number. FLOAT and EPA handle the fixed point to floating point conversion and the floating point arithmetic which is done in BOSS. Presently the arithmetic is done with an RCA software package. However, to increase the speed of calculation an Arithmetic Logic Unit is planned to handle all the floating point arithmetic in BOSS. Because the ALU requires a relatively large amount of power, it will only be used in BOSS. The WORKERS handle the floating point multiplication through an in-house designed hardware multiply board.

BCONE and BCTWO are the routines which contain the different modes of operation within BOSS. The different modes are:

1. Event count, total number of events that meet specified requirements.
2. b-values, both cumulative and interval, using PA and SA (maximum likelihood).
3. Event location.
4. Poisson's ratio using Wadati's method.
5. Source characteristics (moment, stress drop, displacement, fault area) from the spectral characteristics.

Also planned but not yet incorporated in the BOSS is the fault plane solution. Presently the first motions are printed out for each station. Another mode is the debug mode which prints out all the data from the BOSS tables. These tables contain the information sent from each worker for a particular event. Any combination in any order of the above modes may be chosen.

FUTURE ACTIVITIES

ASP will be housed in a field van presently being modified. Its first field test will be in Spring 1980 at a geothermal site with known seismic activity. Another ASP presently under construction will be used for monitoring acoustic emissions at the climax stock nuclear waste repository at the Nevada test site. Besides geothermal exploration ASP will also be used for monitoring geothermal reservoir dynamics associated with fluid withdrawal and reinjection.

CONTROLLED-SOURCE ELECTROMAGNETIC MEASUREMENTS AT GEOTHERMAL SITES IN NEVADA

M. J. Wilt, N. E. Goldstein, R. Haught, and M. Stark

INTRODUCTION

In 1976 LBL, in conjunction with U.C. Berkeley, made preliminary measurements with a prototype large-moment, horizontal-loop EM prospecting system (Jain, 1978) in a geothermal area in Nevada. Encouraging results from this work led to the development of the EM-60 horizontal-loop system (Morrison, et al., 1978), which has now been operated for over 500 hours at various geothermal sites in Nevada and Oregon.

The objectives of the controlled-source EM project are to develop new hardware and software tools for geothermal exploration. The LBL program is designed to fill the gap in existing technology with EM and to demonstrate the technical feasibility and cost-effectiveness of the technique to industry.

The EM method may be a significant improvement over existing techniques [dc resistivity and magnetotellurics (MT)] in geothermal exploration for three reasons. (1) The depth of exploration with EM is approximately equal to the distance between the transmitter and receiver; this is almost five times the source receiver separation for dc resistivity. (2) The EM method is faster and less expensive than dc resistivity or MT. (3) Distant lateral inhomogeneities, which often affect MT data, have relatively minor significance for EM because the strength of the fields strongly decreases with increasing distance from the transmitter.

SYSTEM DESCRIPTION

With the EM-60 system the earth is energized by means of alternating magnetic field created by a square-wave current applied to a horizontal loop (Figure 1). Power is provided by a Hercules gasoline engine linked to an aircraft 60-kW 400-Hz, three-phase alternator. The output is full-wave rectified and capable of providing 150 V at up to 400 A to the loop. The current waveform is created with a transistorized switch, controlled remotely by the operator who sets the fundamental frequency over the ranges of 10^{-3} to 10^{3} Hz (Morrison et al., 1978). In practice, four turns of #6 welding wire in a circular loop, 50 m in radius, yields a dipole moment of about 3×10^{6} mks, corresponding to a current of 65 A. This configuration has been found satisfactory for most normal exploration activities where the maximum depth of exploration is 1 to 3 km.

The fields are detected at a point 1 to 4 km distant from the transmitter with a three-component SQUID magnetometer oriented to measure the vertical, radial, and tangential components with respect to the loop. Signals are amplified, anti-alias fil-

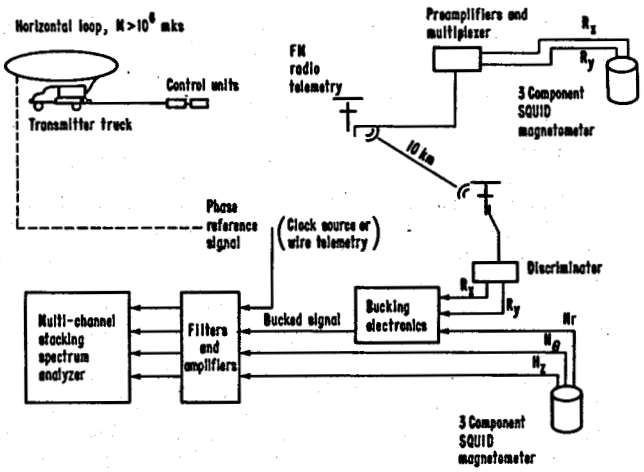

Figure 1. Schematic diagram of the EM-60 horizontal loop electromagnetic prospecting system as used in Nevada in 1979. (XBL 797-11400)

tered and input to a six-channel, programmable, multi-frequency phase-sensitive receiver. Through the receiver key-pad the operator sets parameters controlling signal processing: (a) fundamental period of the waveform to be processed; (b) maximum number of harmonics to be analyzed, up to 15; (c) number of cycles in increments of 2^N to be stacked prior to Fourier decomposition; and (d) number of input channels of data to be processed. Processing results in a raw amplitude estimate for each component and a phase estimate relative to the phase of the current in the loop. Phase referencing is maintained with a hard-wire link between a shunt on the loop and the receiver and this reference voltage is applied directly to channel 1 of the receiver for phase comparison. Raw amplitude estimates must be later corrected for dipole moment and distance between loop and magnetometer.

In practice the hard-wire link was found to be a source of noise, particularly above 50 Hz. This has required the elimination of the absolute phase reference at high frequencies in favor of relative phase measurements between vertical and radial components. With relative phase measurements interpretation is based on the ellipticity and tilt angle of magnetic field rather than amplitude-phase of the vertical and radial fields.

Basic interpretation is accomplished by comparing field curves with calculated curves. Usually, amplitude-phase or ellipticity spectra are fit to one-dimensional layer model curves by trial and error or direct inversion. Two-dimensioal modeling, although possible, is currently cumbersome and prohibitively expensive (Lee, 1979).

ACTIVITIES IN 1979

The most significant change to field procedures in 1979 was the addition of a reference magnetometer to the system for geomagnetic "noise" cancellation. At low frequencies (≤0.1 hz) natural geomagnetic signal amplitude increases roughly as 1/f while the signal sought decreases as 1/f. The net result is an effective signal-to-noise ratio that decreases as $1/f^2$, making noise cancellation imperative for recovery of low-frequency information. In practice, the reference magnetometer is placed at least 10 to 12 km from the transmitter loop, so that the observed fields will consist only of the geomagnetic fluctuations (Figure 1). Once installed, the reference magnetometer can often remain fixed over the course of a survey. The remote signals are transmitted to the mobile receiver station from the transmitter via FM radio telemetry. Before the loop is energized, the remote signals are inverted, adjusted in amplitude, and then added to the base station geomagnetic signal to produce essentially a null signal. A good example of this simple noise cancellation scheme is shown in Figure 2. The resulting signal-to-noise improvement of roughly 20 dB has allowed us to obtain reliable data to 0.05 Hz, a gain of three or four important data points on the sounding curve. These points are invaluable for resolution of deeper horizons.

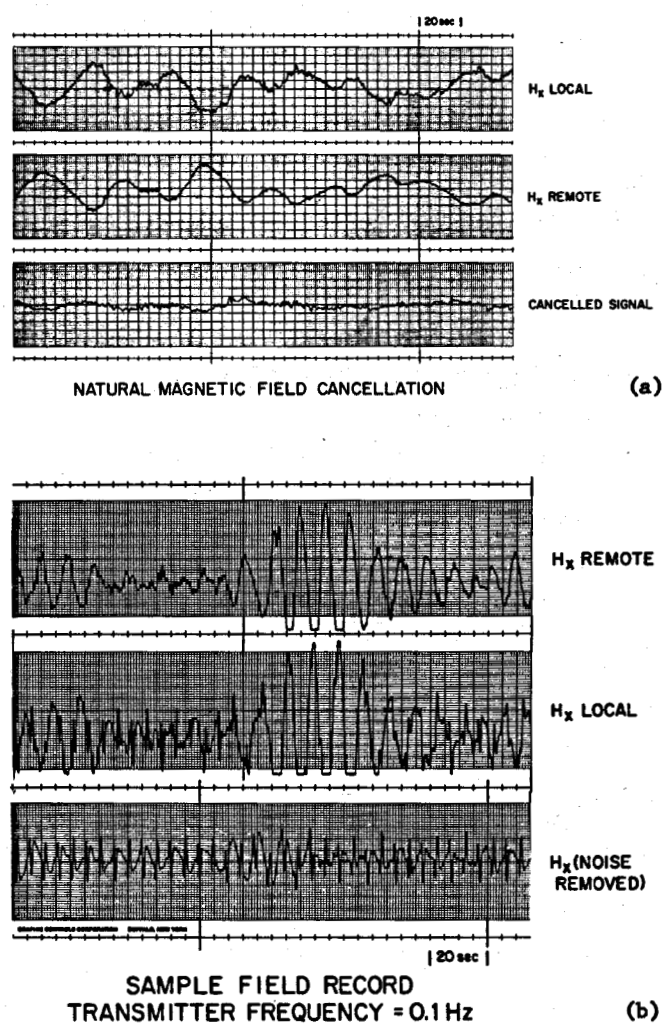

Figure 2. Example of data improvement using the telluric noise cancellation scheme. (a) Natural geomagnetic signal and initial cancelling at the receiver site with transmitter off; (b) the same system but with transmitter on.
(a) XBL 7911-13079; (b) XBL 7911-13078

As part of the DOE Industry Case Studies Program for the northern Basin and Range province, LBL conducted EM-60 surveys at three geothermal target areas in northern Nevada: Panther Canyon in Grass Valley, Soda Lake near Fallon, and McCoy west of Austin (Figure 3). Using the noise cancellation scheme, we obtained two soundings per day during favorable weather conditions. A total of more than 40 soundings were made at the three sites, some under conditions of high wind, low temperatures and snow. Because most of the data were collected between August and November, a complete analysis and interpretation is not yet ready. A summary of findings, however, for each prospect area is reported below:

Panther Canyon

At this site eight receiver stations relative to one transmitter loop were occupied along two orthogonal survey lines originally used by LBL for dipole-dipole resistivity profiling (Beyer, 1977). Good quality data were obtained from 0.1 to 500 Hz. The data were collected to investigate the geometry and extent of a long, narrow conductive body originally detected with the dc resistivity measurements. The body may be related to a heat flow high centered over the same region so its determination may have some geothermal significance.

In Figure 4 the two-dimensional dipole-dipole resistivity model calculated by Beyer (1977) is shown over the section corresponding to the long dimension of the conductive body; also shown is the EM-60 sounding profile over the same line. Although the two models give similar information, the differences in the techniques are: (a) the acquisition cost of the dipole-dipole data is approximately three times that of EM-60 data; (b) the EM profile is based on one-dimensional inversions so that the depths to the various horizons are weighted average values for the region between the transmitter and receiver; the EM soundings therefore give a smooth version of the resistivity cross-section.

Samples of EM-60 amplitude-phase spectra soundings are given in Figures 5 and 6; the error bars signify one standard deviation. The fit to a three-layer model is fairly good, but note that data were interpreted only to 50 Hz because high noise due to the use of the reference wire prohibited obtaining higher frequency amplitude-phase data. Ellipticity data, however, could usually be interpreted to 500 Hz.

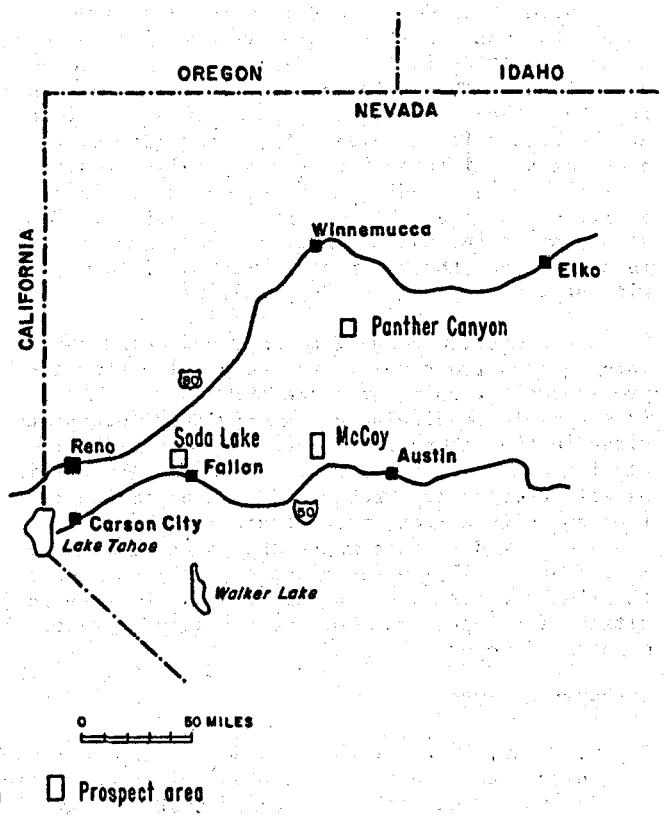

Figure 3. Prospect location map for the 3 EM-60 surveys conducted in 1979 by LBL. (XBL 802-6771)

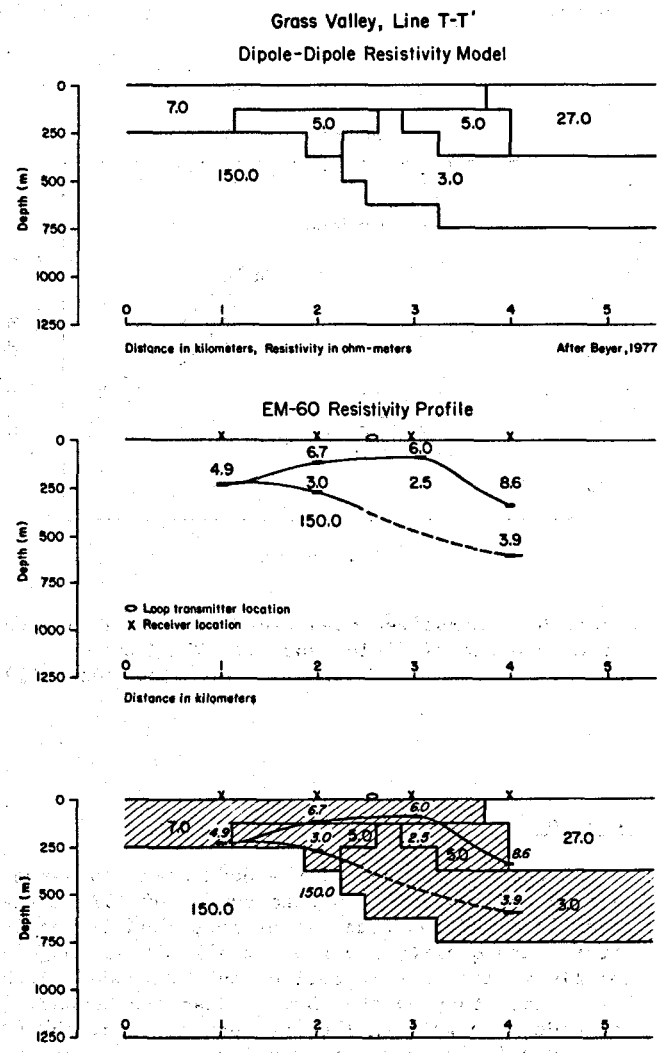

Figure 4. Resistivity cross section over a conductive body in Panther Canyon: (a) two-dimensional dipole-dipole resistivity model (after Beyer, 1977); (b) profile of one-dimensional EM-60 electromagnetic soundings; (c) a comparison of parts a and b. (XBL 802-6775)

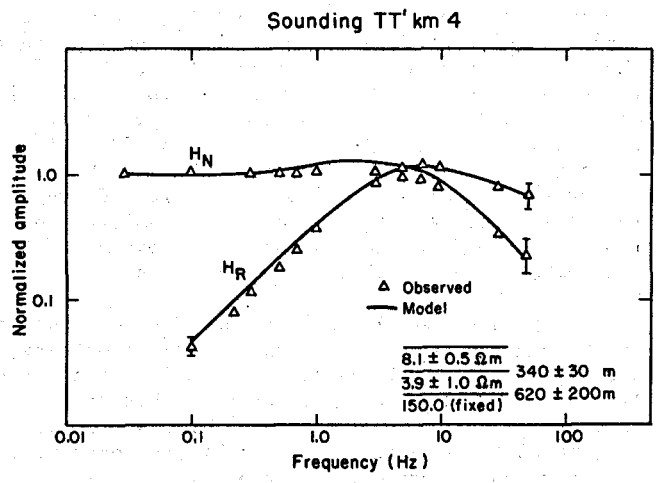

Figure 5. Normalized magnetic field amplitude spectra normal and radial fields sounding TTS Panther Canyon. (XBL 802-6816)

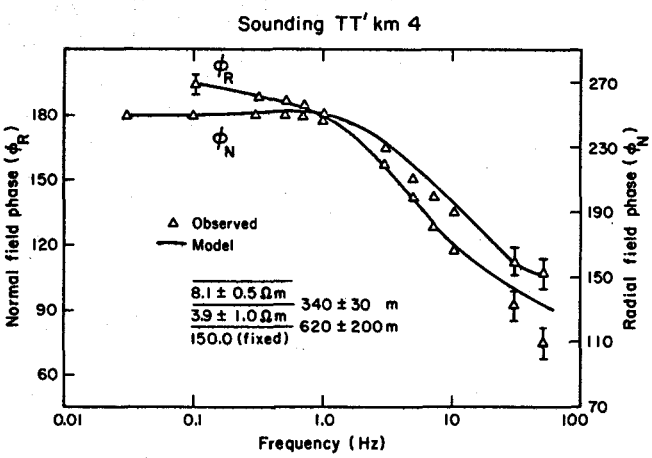

Figure 6. Normalized magnetic field phase spectra normal and radial fields sounding TTS Panther Canyon. (XBL 802-6815)

Soda Lake

A one week survey of the Soda Lake geothermal anomaly was conducted in late summer of 1979. The study involved two transmitter loops and 13 receiver sites; data quality was good at all sites. Magnetotelluric and seismic reflection data made available to the study by the Chevron Resource Company has aided somewhat in the interpretation of the EM data by allowing us to better fix certain parameters (Hill et al., 1979).

From the EM data we hoped to determine the depth to and thickness of an extensive gently dipping conductive zone which may serve as the reservoir for hydrothermal fluids. A resistive volcanic horizon detected first from magnetotelluric data lies some 1 to 2 km below the surface and may form a confining layer for the hot water zone. The definition of this layer is also important.

Preliminary analysis indicates that the conductive zone is well determined at all sites, but interpretation of the deeper horizons is somewhat more difficult.

McCoy

The McCoy prospect located in a remote mountainous area some 40 miles west of Austin was the most difficult survey attempted because of the mountainous terrain and the two- and three-dimensional geology (Olsen et al., 1979). Although 19 stations were occupied, about 50 percent of the data cannot yet be interpreted with existing software. Modifications to the existing layered model inversion codes should help in interpreting data distortions due to loop misorientation and topography, but two-dimensional modeling may be necessary to interpret other data.

ACTIVITIES PLANNED FOR 1980

All data obtained in 1979 will be interpreted to the fullest extent possible. Results will be compiled and issued in short technical reports. Results will also be turned over to the Earth Science Laboratory, University of Utah Research Institute (ESL/UURI), who have the responsibility of preparing complete case histories for each of the study areas.

During the course of the field surveys we found that the phase reference wire was introducing noise, resulting in lower accuracy at frequencies above 50 Hz. This problem was remedied by eliminating the reference wire and determining ellipticity at the higher frequencies. As a consequence, the one-dimensional inversion program will be modified to interpret a sounding curve composed of mixed amplitude-phase and ellipticity data points. We also plan to include a highly accurate quartz clock in our system, thereby giving us phase information without the need for a hard-wire link.

System software will be improved. There remains a need for simplifying and accelerating the procedures for going from the printed tapes taken in the field to displaying the finished interpretations in the laboratory. This may be done by including a tape recorder in the system. In addition, we will address the problem of interpreting data from an inlined loop; more precisely, the common case in rugged terrain where the point of measurement does not lie in the plane of the loop. Here the fields observed can be treated as the superposition of effects from both vertical and horizontal magnetic dipoles.

REFERENCES CITED

Beyer, J. H., 1977. Telluric and resistivity techniques applied to the geophysical investigation of Basin and Range geothermal systems, Part III: The analysis of data from Grass Valley, Nevada (Ph.D. dissertation). Berkeley, University of California, Department of Engineering Geosciences, LBL-6325, 313 p.

Hill, P. G., Layman, E. B., Swift, C. M., and Yungul, S. H., 1979. Soda Lake, Nevada thermal anomaly, in Expanding the geothermal frontier. Transactions, Geothermal Resources Council Annual Meeting, v. 3.

Jain, B., 1978. A low frequency electromagnetic prospecting system (Ph.D. dissertation). Berkeley, University of California, Department of Engineering Geosciences, LBL-7042.

Lee, Ki Ha, 1978. Electromagnetic scattering by a two-dimensional inhomogeneity due to an oscillating magnetic dipole (Ph.D. dissertation). Berkeley, University of California, Department of Engineering Geosciences, LBL-8275.

Morrison, H.F., Goldstein, N. E., Hoversten, N., Oppliger, G., and Riveros, C., 1978. Description, field test and data analysis of a controlled-source EM system EM-60. Berkeley, Lawrence Berkeley Laboratory, LBL-7088.

Olsen, H. J., Dellachaic, F., Pilkington, D., and Large, A. L., 1979. The McCoy geothermal prospect status report of a possible new discovery in Churchill and Lander counties, Nevada, in Expanding the geothermal frontier. Transactions, Geothermal Resources Council Annual Meeting, v. 3.

GEOPHYSICAL AND GEOCHEMICAL INVESTIGATIONS AT MT. HOOD, OREGON

N. E. Goldstein, H. A. Wollenberg, E. Mozley, and M. J. Wilt

INTRODUCTION

Mt. Hood is a Holocene volcano located 80 km east of Portland, Oregon. It is one of many stratocones in the High Cascade Range extending from northern California to southern British Columbia (Figure 1). In 1977, the U.S. Department of Energy, U.S. Geological Survey, U.S. Forest Service and Oregon Department of Geology and Mineral Industries (DOGAMI) began a program to evaluate the geothermal resource potential of this volcano. It was selected because of its proximity to a major city, the abundance of federally controlled land on which to work, evidence for a heat source, and growing interest of private developers in a source of hot water for the local area.

As part of the program, LBL was assigned the responsibility of conducting and coordinating surveys dealing with rock, gas, and water geochemistry, and electrical resistivity.

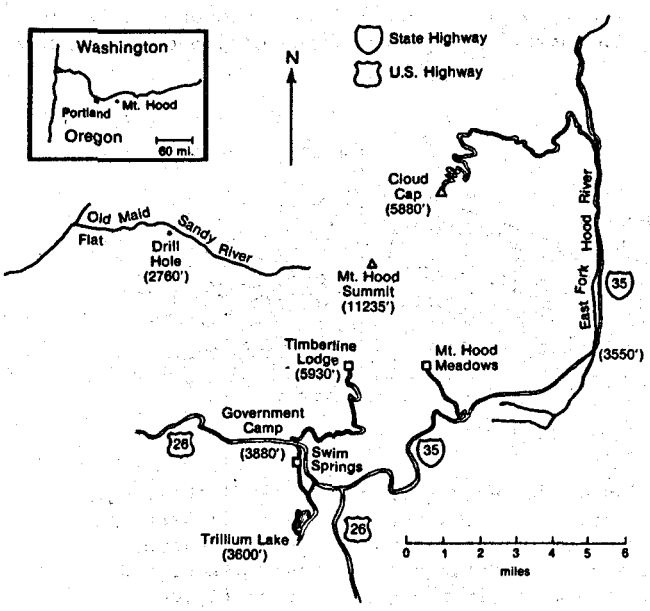

Figure 1. Location map of Mt. Hood area. (XBL 784-644)

ACTIVITIES IN FISCAL YEAR 1979

Geochemical Studies

Samples of warm- and cold-spring water, water from a geothermal test well in Old Maid Flat, fumarolic gases, and rocks were collected and analyzed for major chemical constituents and trace elements. This project culminated in fiscal year 1979 with a report by Wollenberg et al. (1979), presenting and summarizing the analytical data and proposing an interpretation of the hydro-geochemical system of Mt. Hood.

The only warm-spring area on Mt. Hood is Swim Springs, located on the south flank. Orifices at Swim Springs were sampled repeatedly with little overall change noted in water chemistry between summer and winter. Oxygen and hydrogen isotope data and mixing calculations based on analyses of Swim Springs and numerous cold springs indicate that a large component of the warm water at Swim Springs is from near-surface runoff. Chemical geothermometry suggests that temperatures at depth in the Swim Springs system are within the range 104 to 170°C; the temperature of unmixed hot water may exceed 200°C. Higher-than-background chloride contents and specific conductances of cold springs on the south flank of the mountain (Figure 2) suggest that there is a small component of thermal water in these sources.

A geothermal model of Mt. Hood is proposed wherein snow- and glacier-melt water near the summit comes in close proximity to the hot central "neck" of the mountain, manifested by the summit-crater fumaroles (Figure 3). The hot water migrates downslope, mixing with cold water along its path; a small portion of the mixed warm water surfaces at Swim Springs.

Another possible explanation for the presence of warm water at Swim Springs is deep circulation along a fault zone. An east-west oriented fault zone in the vicinity of Swim Springs has been suggested from analyses of earthquake epicentral data (R. Couch, 1977, personal communication). However, to date, other geological and geophysical investigations have not confirmed the fault zone. If a fault zone were present and it contained permeable

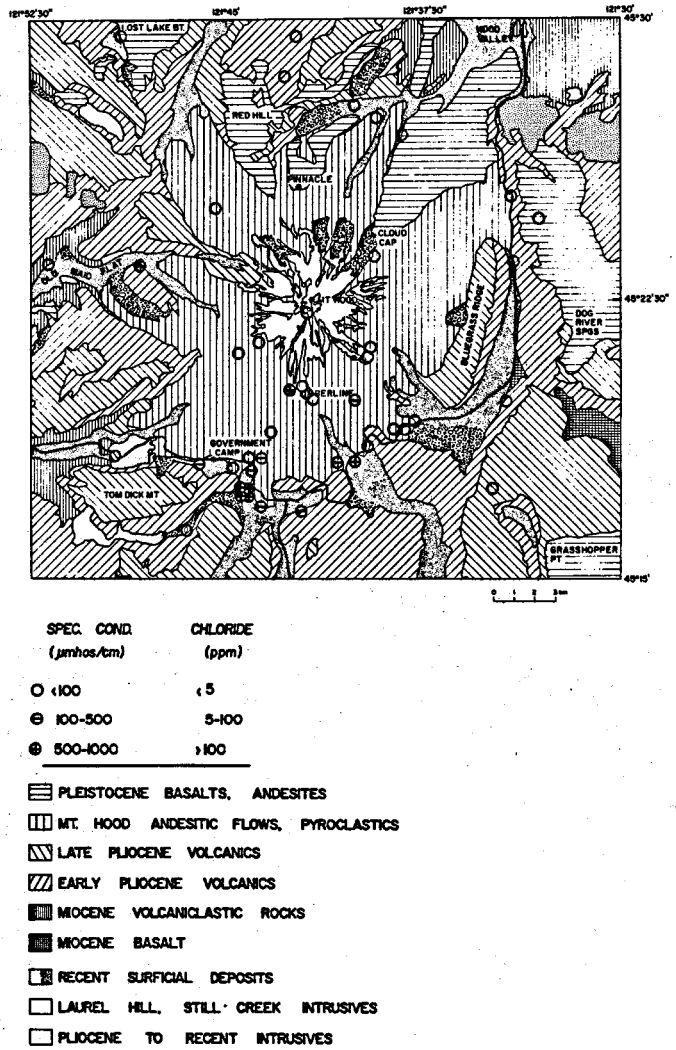

Figure 2. Specific conductance and chloride content of waters, plotted on the geologic map of Mt. Hood (after Wise, 1968). (XBL 802-8179)

zones, these could serve as conduits for deep circulation of meteoric water. It is more likely that if a fault zone is present, it would serve as an impermeable barrier to warm water moving downslope, causing some impoundment and the emanation at Swim Springs. Neither the fault-zone nor the downslope moving warm water mechanisms for Swim Springs are mutually exclusive; both could be operating.

We were surprised to detect the platinum-group element, iridium, in warm- and cold-spring waters and in a sample of altered andesite. Iridium is generally considered to be associated with basic to ultrabasic igneous rocks; its association with an andesite volcano is believed to be without precedent.

Geophysical Studies

Field surveys consisting of telluric-magnetotelluric (MT) observations and controlled-source electromagnetic (EM) soundings were made in 1977 and 1978, respectively. Field work done in 1979 consisted of occupying several widely spaced MT stations in connection with the High Cascade project. The major effort during fiscal year 1979 was to analyze and to interpret the large amount of data previously obtained at the stations shown in Figure 4.

Of the nine controlled-source EM soundings performed with the newly developed EM-60 system (Figure 5) four were successfully analyzed in terms of layered-earth models. Two were not interpretable because intervening terrain between transmitter and receiver gave results that badly distorted the sounding curves. Three soundings from the loop in Summit Meadow, at the southern base of the mountain, await interpretation based on two-dimensional models.

Interpretations are based on either (a) a combined inversion using the four components of amplitude and phase of the normal (i.e., normal to plane of loop) and radial magnetic fields, or (b) ellipticity of the magnetic field vector traced out by the normal and radial field components. Figures 6

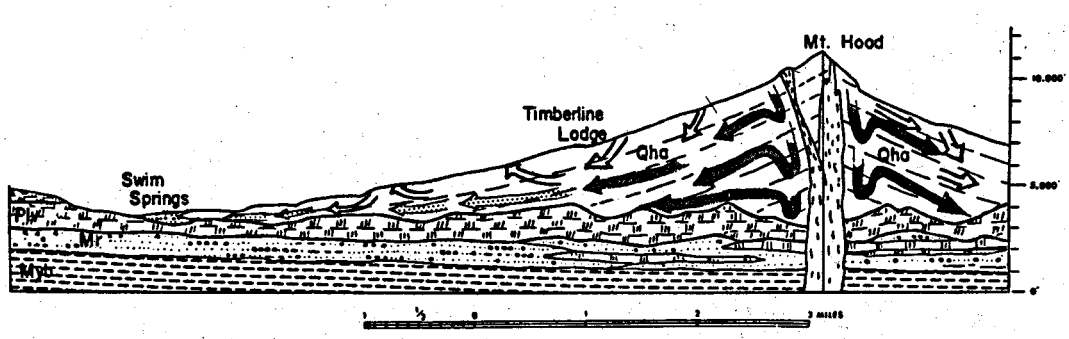

Figure 3. North-south geologic cross section of Mt. Hood (after Wise 1968) showing, schematically, the hypothesized circulation paths of hot water (dark arrows) heated near the volcano's central neck, mixed warm water (lighter arrows), and cold water (unshaded arrows). The warm water emanating at Swim Springs is strongly mixed, and cold water in springs on the south flank of the mountain may contain a small component of the deeper-flowing hot water. Myb = Yakima Basalt; Mr = Rhododendron Formation; Plv = Lower Pliocene basalt and andesite; Qha = Mt. Hood andesite flows. (XBL 792-8469)

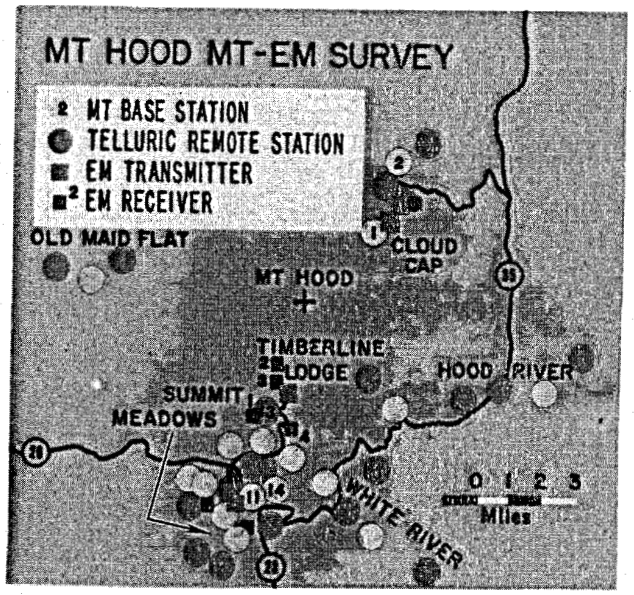

Figure 4. Magnetotelluric and controlled-source electromagnetic stations around Mt. Hood. (BBC 7911-15939)

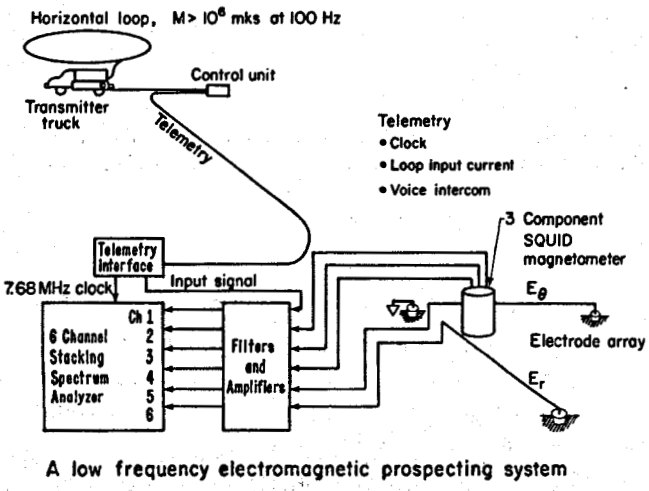

Figure 5. Schematic of the EM-60 system. (XBL 786-2575)

and 7 illustrate the amplitude-phase inversion at Cloud Cap Station and Figure 8 shows the corresponding ellipticity inversion (Wilt et al., 1979). Both analyses show a good conductor beneath a resistive surface layer 650 to 690 m thick. The thickness of the conductor could not be resolved, but its presence had previously been noted from the magnetotelluric work (Goldstein and Mozley, 1978).

The telluric-magnetotelluric data obtained by the contractor (Geonomics, Inc.) were totally reprocessed using both remote electric and magnetic field references in an attempt to obtain more reliable MT sounding curves to interpret (Goubau, et al., 1978; Gamble et al., 1979a,b). It was found that electric and magnetic references gave improved

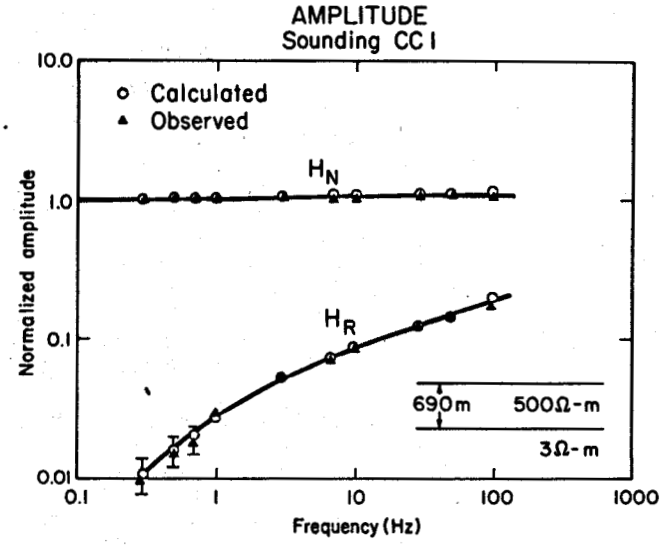

Figure 6. Magnetic field amplitude spectra for Cloud Cap sounding CC1. (XBL 796-7522)

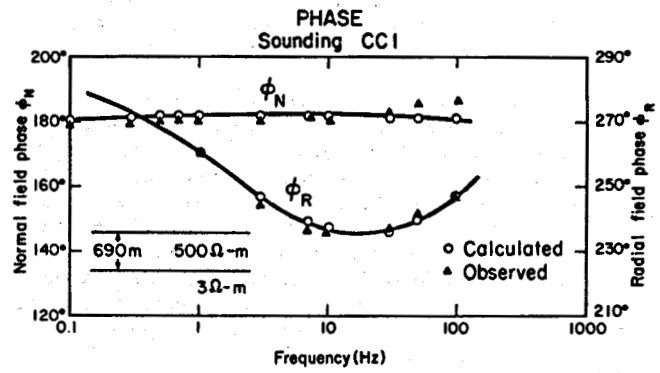

Figure 7. Magnetic field phase spectra for Cloud Cap sounding CC1. (XBL 796-7525)

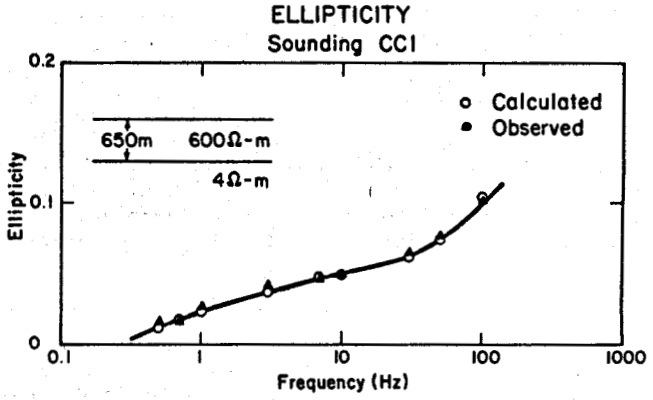

Figure 8. Magnetic field ellipticity spectrum for Cloud Cap sounding CC1. (XBL 796-7524)

results (i.e., smaller error bars) but the magnetic reference seemed to be better for noise cancellation.

Because the Cloud Cap MT data gave results that appeared reasonable to interpret by means of one-dimensional inversions and because of the conductor found at 600 m depth, considerable effort went into a suitable interpretation of the stations in this cluster (Figure 9). These stations are on a fairly young basalt-andesite flow, one of several that are associated with eruptive centers (satellitic vents) on the north side of the volcano and dated at approximately 12,000 years B.P. Figure 10 shows a resistivity cross section along line B-B' derived from the one-dimensional inversions. This profile is normal to the electrical strike determined from the MT measurements, and we show only the results for the electric field parallel to strike. Here again we see clear evidence for a conductive zone, diminishing somewhat with distance from the summit. This zone may be due to hot water, heated either near the summit or near the Cloud Cap eruptive center, and cooling as it mixes with cold meteoric water downslope. This interpretation is consistent with the geochemical interpretation discussed above. At a depth of 2+ km we also see a discontinuity near station 2 that seems to be the cause of the east-west strike. This has been interpreted as a possible cauldron-feature: resistive basement relatively high northward and a chaotic zone of rocks closer to the summit.

The conductive second layer is also noted near Timberline Lodge on the south flank. There the MT data suggest a shallower and thinner zone, but the two-dimensional effects appear to have distorted the sounding curves. The EM-60 results show that the conductive zone lies at a depth of 500 m and has a resistivity of >10 ohm-m compared with 2 to 3 ohm-m at Cloud Cap. The warm water emanations at Swim Springs confirm that the conductive second layer may indeed signify a zone of heated water moving down the mountain.

ACTIVITIES PLANNED FOR FISCAL YEAR 1980

Geochemical Studies

The data on the chemistry of waters from cold and warm springs and wells was presented in a report to the American Geophysical Union's Fall 1979 meeting.

Geophysical Studies

During fiscal year 1980 the remaining MT data will be analyzed to the fullest extent possible, and a final report will be issued giving, in detail, the results of all EM and MT work. There are no plans to conduct additional EM or MT measurements in 1980.

REFERENCES CITED

Gamble, T. D., Goubau, W. M., and Clarke, J., 1979a. Magnetotelluric with a remote magnetic reference. Geophysics, v. 44, p. 43-68.

____, 1979b. Error analysis for remote reference magnetotellurics. Geophysics, v. 44, p. 959-968.

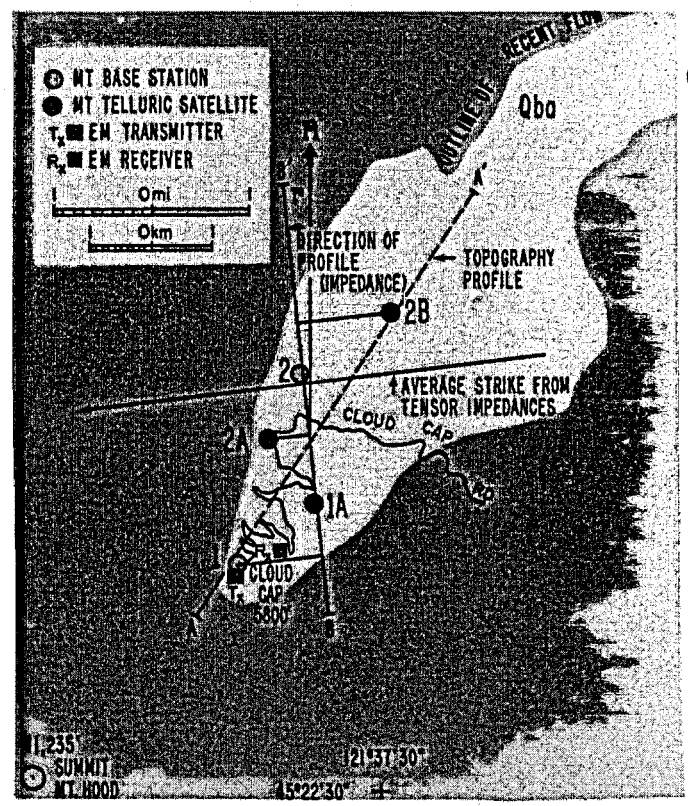

Figure 9. Magnetotelluric and controlled-source EM stations at Cloud Cap. (BBC 7911-15943)

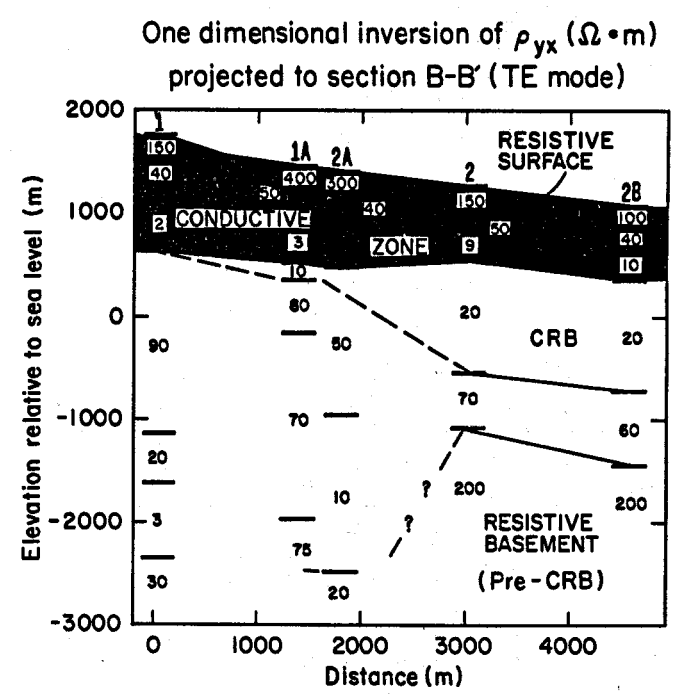

Figure 10. Interpreted resistivity cross section at Cloud Cap. (BBC 7911-15937)

Goldstein, N. E., and Mozley, E., 1978. A telluric-magnetotelluric survey at Mt. Hood, Oregon--a preliminary study. Berkeley, Lawrence Berkeley Laboratory, LBL-7050.

Goubau, W. M., Gamble, T. D., and Clarke, J., 1978. Magnetotelluric data analysis: removal of bias. Geophysics, v. 43, p. 1157-1166.

Wilt, M., Goldstein, N. E., Hoversten, M., and Morrison, H. F., 1979. Controlled-source EM experiments at Mt. Hood, Oregon. Geothermal Resources Council, Transactions, v. 3, p. 789-792.

Wise, W. S., 1968. Geology of Mt. Hood, Oregon. Oregon Dept. Geol. Min. Ind., v. 62, p. 81-98.

____, 1969. Geology and petrology of the Mt. Hood area: A study of the High Cascade volcanism. Geol. Soc. Am. Bull., v. 80, p. 969-1006.

Wollenberg, H. A., Bowen, R. G., Bowman, H. R., and Strisower, B., 1979. Geochemical studies of rocks, water, and gases at Mt. Hood, Oregon. Berkeley, Lawrence Berkeley Laboratory, LBL-7092.

KLAMATH BASIN GEOTHERMAL RESOURCE AND EXPLORATION TECHNIQUE EVALUATION

M. A. Stark, N. E. Goldstein, and H. A. Wollenberg

INTRODUCTION

The Klamath Basin, located in south-central Oregon and northern California, has been a locus of geothermal exploration for several years. Three Known Geothermal Resource Areas (KGRAs) have been identified in the area; they are delineated in Figure 1. Hundreds of warm springs and wells, mostly in Klamath Falls KGRA, are used in space heating and other direct applications. The waters range in temperature up to 145°C, and several companies and government agencies have searched for hotter water or steam suitable for electric power generation. Outside the main geothermal area in the city two exploratory deep holes have been drilled thus far in the basin but without finding hot water or steam. Interest in the region has consequently waned over the last two or three years.

In an attempt to restimulate exploration activity, LBL, working with the State of Oregon's Department of Geology and Mineral Industries (DOGAMI) and the U.S. Geological Survey (USGS) has attempted to collect, integrate, and reinterpret all available exploration data from both public and private sources. Our primary goals were to develop a conceptual model for the hydrothermal system, to suggest targets for further exploration, and to evaluate the exploration techniques on a site-specific basis.

The Klamath graben can be traced from 80 km from the Medicine Lake volcanic field in northern California to Crater Lake, Oregon, attaining a width of 15 km. The local geologic structure is characterized by numerous northwest-trending normal faults with occasional northeast-trending cross-faults. Important rock units are late Tertiary and Quaternary extrusive rocks and a late Tertiary lacustrine and volcanic unit known as the Yonna Formation.

The results from our fiscal year 1978 study are discussed in Stark et al. (1979). In that report we examined geophysical data concentrated in the Swan Lake Valley and Klamath Hills areas (Figure 1). These included data from magnetotelluric (MT), audio-magnetotelluric (AMT), roving dipole resistivity, aeromagnetic, and gravity surveys. Two-dimensional computer modeling was used to develop subsurface resistivity and density models to satisfy the data. Both areas showed evidence for electrically conductive bodies associated with normal faulting and cross-faulting. In the Klamath Hills area, the conductive zone coincides with a shallow hot well area along the southwestern margin of the hills. In the Swan Lake Valley area, there are indications of a dike-shaped conductive zone in Meadow Lake Valley, but only minor evidence of surface hydrothermal activity. We also found geophysical evidence for a concealed cross fault between the Klamath Hills and Olene Gap.

ACCOMPLISHMENTS FOR 1979

In fiscal year 1979 we concentrated our efforts on data from the west and east shores of Upper Klamath Lake. Figure 1 shows the survey areas covered. Since this was the last year of the project, we also emphasized geological and geochemical considerations in an effort to understand the system as a whole. The work is reported in Stark et al. (1980).

Figure 2 shows the locations of dipole-dipole, roving dipole, and Schlumberger resistivity surveys carried out on the west shore of the lake. By means of two-dimensional computer modeling we were able to find earth resistivity models to satisfy these data. Our model for Line DDG, near Spence Mountain, is shown in Figure 3. This area was of interest because it was the site of a 2000-ft hole, which was designed, in part, to investigate a local resistivity-low inferred from the electrical surveys. Our model (Figure 3), which satisfies both the dipole-dipole (DDG, Figure 2) and the Schlumberger (KF3, Figure 2) data, indicates that low resistivities should not be expected less than 4000 ft beneath the drill site.

Similar conductive anomalies were detected on other resistivity lines on the west shore of Upper Klamath Lake. Our models indicate conductive horizons at depths from 1200 to 10,000 ft; the horizons are usually shallower beneath the valleys. Because these extensive conductive units effectively short-circuit the current, there is no evidence for a resistive basement in the soundings.

It is not known whether the conductive units represent anomalously high temperatures at shallow depth. We have suggested possible drill tests near

Known geothermal resources area boundary

Dipole-dipole and Schlumberger survey area (Harding-Lawson, 1974)

Schlumberger sounding and roving dipole survey area (Geoterrex, 1975)

Schlumberger, time domain electromagnetic, and roving dipole survey area (Argonaut, 1975)

Gravity and magnetics (VanDeusen, 1978) covers whole area

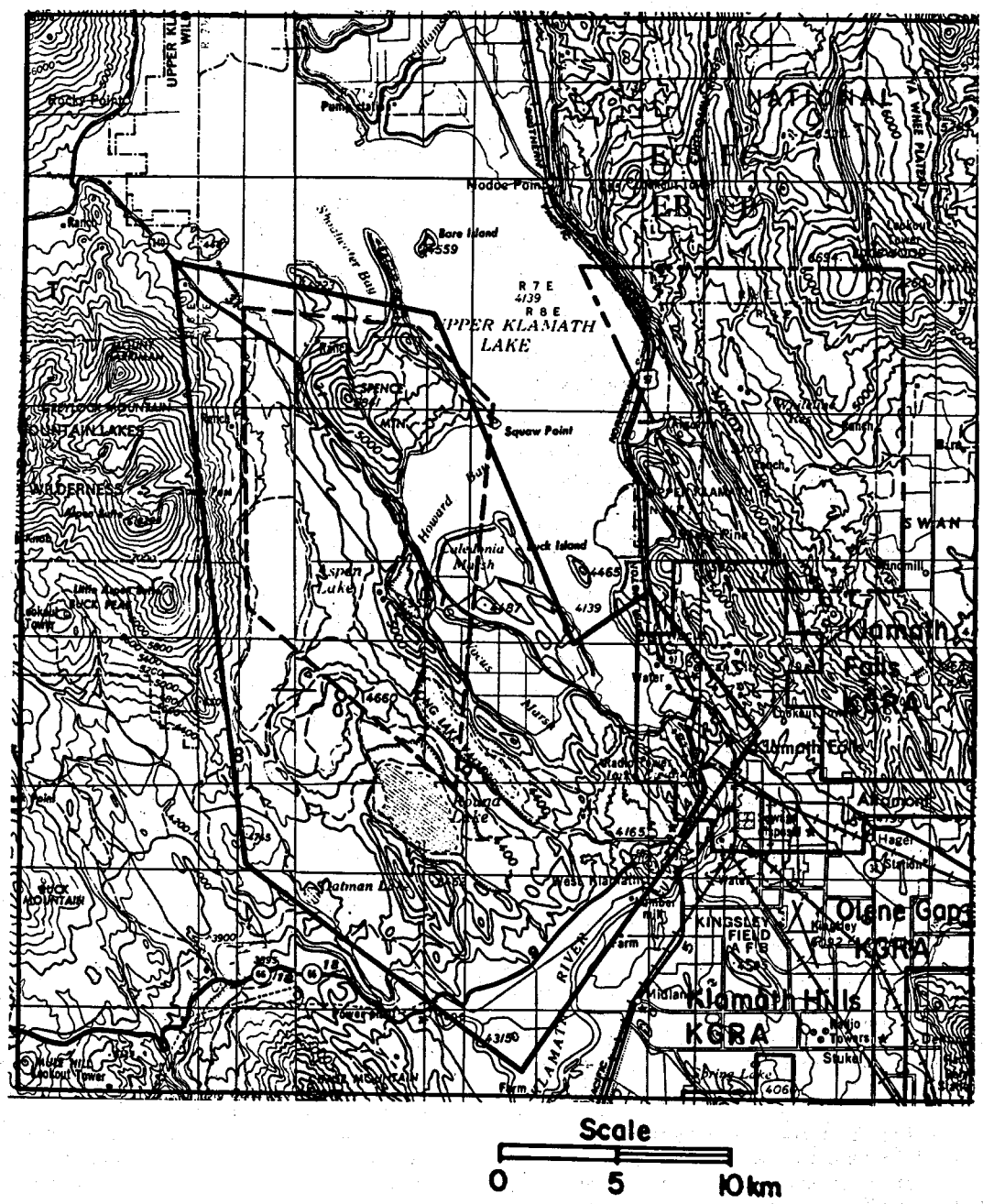

Figure 1. Index map of geophysical survey areas.
(XBL 798-11451)

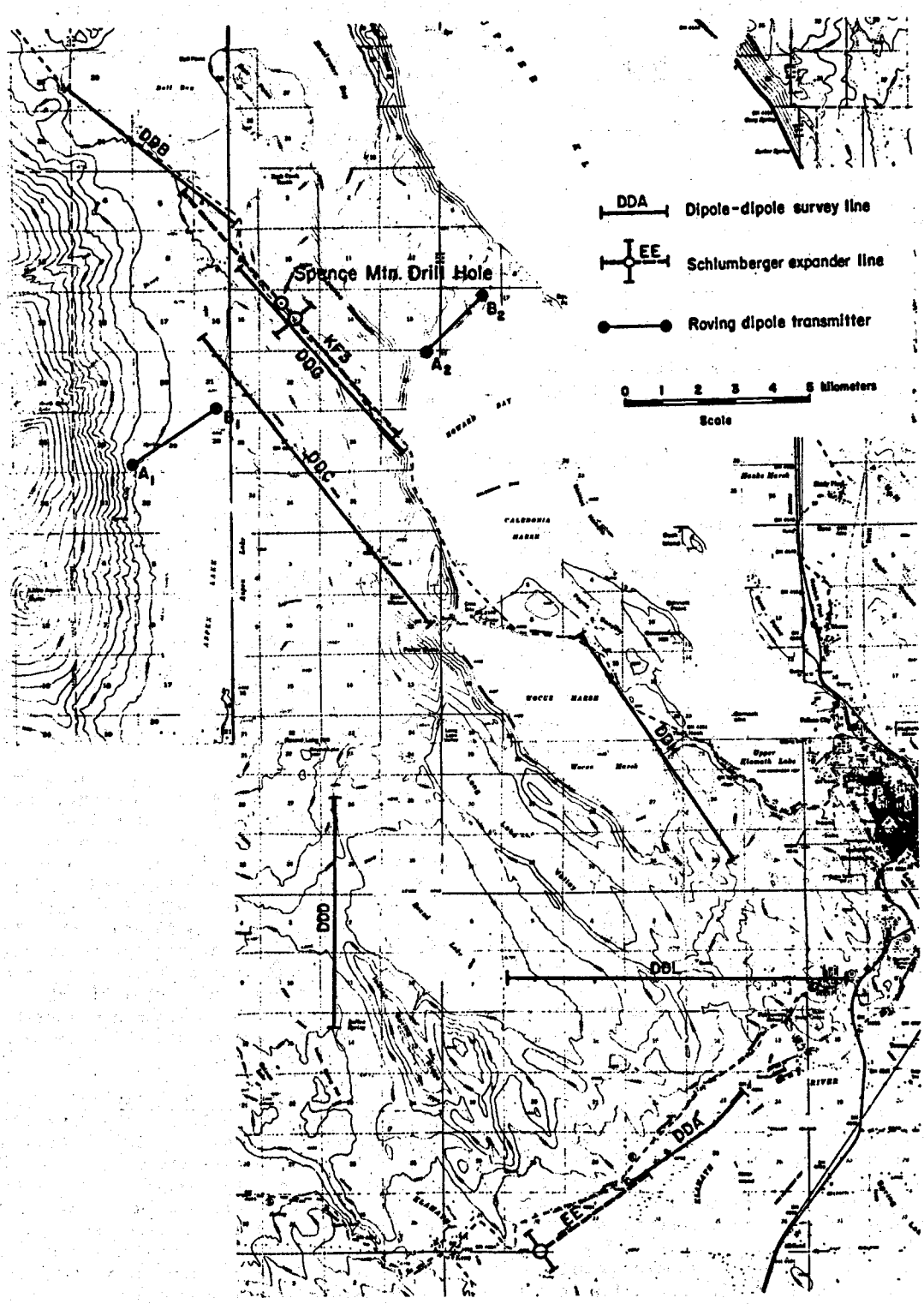

Figure 2. Location map of electrical resistivity surveys, west shore of Klamath Lake. (XBL 798-11149)

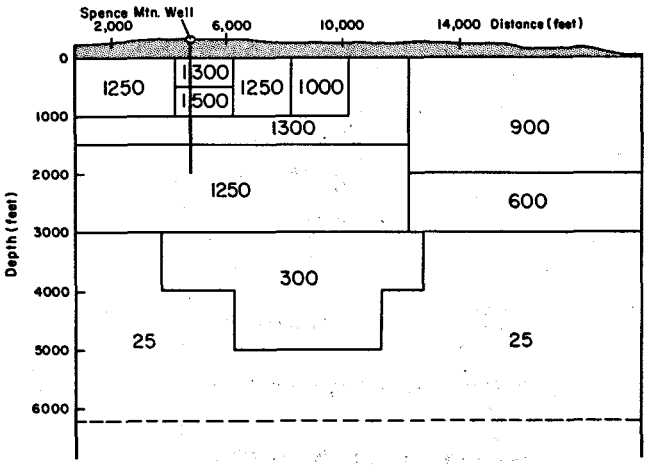

Figure 3. Two-dimensional resistivity model for line DDG: values in ohm-m. (XBL 798-11452)

lines DDL and DDA where the conductive horizons come closest to the surface.

On the east shore of the lake (Figure 1) we examined roving dipole, Schlumberger, and electromagnetic survey data. We made no effort at quantitative reinterpretation of these data. Qualitatively, the data show decreasing resistivity with depth, especially in Plum Valley (east of Naylox Mountain in Figure 1), and south of Whiteline Reservoir. The latter anomaly is adjacent to Meadow Lake Valley, site of a strong MT apparent resistivity low discussed in Stark et al. (1979). Soundings should be undertaken to investigate the specific anomalies.

We also analyzed regional geochemical and geological information. Reservoir temperature estimates for the Klamath Basin hot water aquifer were made independently by Sammel (1976) and by Koenig and Gardner (1972) based on silica and Na:K geothermometers. Both workers estimated equilibration temperatures in the 120 to 130°C range, and they both invoked the possibility of a deeper steam reservoir to explain the high sulfate content of the waters. Since publication of these studies, higher temperatures have been measured in a new well in Klamath Falls city. The new well is 1200-ft deep with a reported bottom-hole temperature of 145°C.

Sammel (1976) also measured specific electrical conductivities of well and spring waters. We analyzed the relationship between conductivity and temperature in these waters. In the Klamath Falls/Olene Gap area, the expected trend prevails, i.e., the hotter waters are more conductive. South and west of Olene Gap, however, the opposite trend emerges, with the warmer waters associated with lower conductivity. This trend, though less clear-cut, is partly due to saline groundwater in the marsh environment. This hypothesis does not explain all the data; we have recommended additional geochemical work to investigate the history of these waters.

We also examined geologic maps and aerial infrared imagery, tying these into the geophysical data in a basin-wide tectonic analysis. Figure 4 shows an idealized conception of an offset in the graben axis. The northeast-trending fault between the Klamath Hills and Olene Gap was inferred in Stark et al. (1979) based on audio-magnetotelluric, gravity, and aeromagnetic data. The other northeast-trending fault, located northwest of the Klamath River, was inferred in Stark et al., (1980) based on remote sensing, gravity, and aeromagnetic data. We believe that the graben has been offset along these faults in the right-lateral strike-slip sense.

These cross-faults seem to be regional features; the one northwest of the river may extend through Klamath Falls and Swan Lake Valley. Intersections of these cross-faults with the northwest-trending normal faults seem to be favorable locations for near-surface geothermal activity.

In this work we have had a chance to evaluate the exploration techniques on a site-specific basis. Our impressions follow:

1. Remote Sensing. Aerial infrared photographs proved most useful in substantiating the presence of cross-faulting inferred from other methods.

2. Geochemistry. Available wells and springs should always be inventoried at an early stage of exploration. The new 145°C well in Klamath Falls has shown that the reservoir temperature estimates by Sammel (1976) and Koenig and Gardner (1972) should be regarded as minimum values. We found the specific conductivity measurements useful in interpretating resistivity anomalies.

3. Gravity and Magnetics. These methods are hampered by the fundamental non-uniqueness problem of potential field data, particularly in the volcanic terrain of the Klamath Basin where rock magnetizations and densities can be so variable. In conjunction with other information, however, the data can be extremely useful for tracing faults and for estimating depth to basement. In this area, direct associations of gravity and/or magnetic anomalies with geothermal targets are not recommended. Structural and lithologic changes can account for more variation than geothermal processes such as hydrothermal metamorphism and elevated Curie point isotherms.

4. Roving Dipole Resistivity. This is a useful reconnaissance tool, but the data are difficult to interpret quantitatively unless supplemented by data from other resistivity methods. Schlumberger and EM soundings were conducted at the Whiteline Reservoir for control, but in retrospect these soundings might have been more usefully employed at a later time to define targets outlined by the roving dipole survey. Similarly, the west shore roving dipole survey should have been completed and analyzed before the dipole-dipole and Schlumberger work began there. Computer modeling can help pinpoint the sources of the often-deceptive roving dipole anomalies.

5. Schlumberger and Dipole-Dipole Resistivity. Schlumberger and dipole-dipole sounding can offer detailed, quantitative earth resistivity information

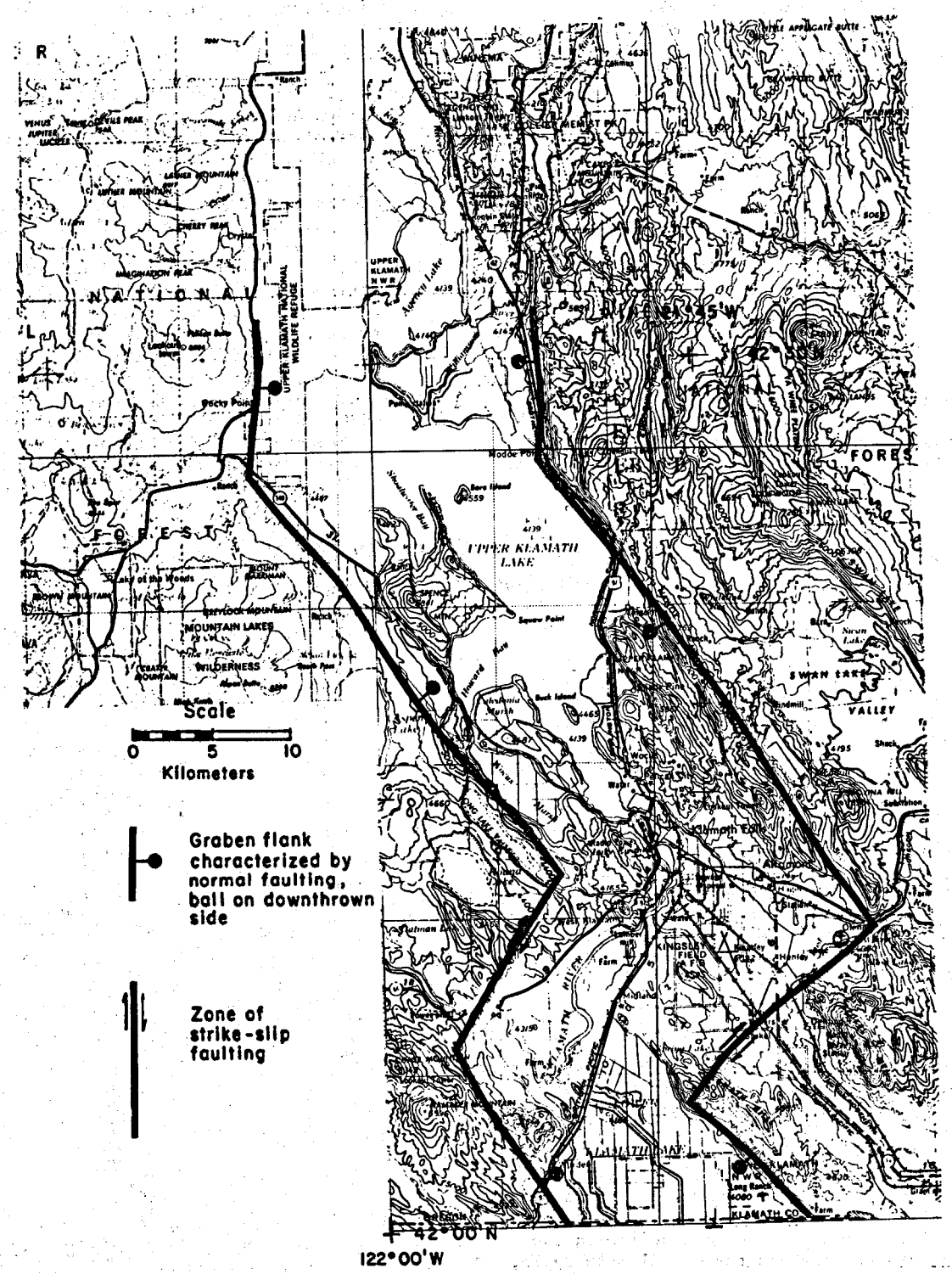

Figure 4. Idealized tectonic map of Klamath graben.
(XBL 7910-13077)

if the surveys are properly implemented. If possible, lines should be laid out perpendicular to geologic strike, so that two-dimensional modeling can be used effectively to separate lateral resistivity changes from changes with depth. We found that collinear, overlapping Schlumberger and dipole-dipole soundings were necessary to allow a well-constrained interpretation. Finally, joint computer modeling of the data sets should be undertaken. When these conditions are satisfied, a quantitative subsurface resistivity picture emerges that can be valuable in selecting a drill target.

6. Time Domain EM. The data we received are rather difficult to interpret. We certainly applaud efforts to develop and deploy field equipment to make these measurements, but at this time most interpreters are limited to very simple models. If more powerful methods of analysis can be developed, the technique could become quite useful.

7. Temperature Gradient Surveys. These seemed to be only marginally useful in the exploration efforts to which they pertained. In the Klamath Basin, there appear to be difficulties related to the complicated groundwater flow which reduce the effectiveness of these methods.

PLANS FOR FISCAL YEAR 1980

The second of the two technical reports (Stark et al., 1980) will be completed, reviewed by an industry committee, and issued at midyear.

REFERENCES CITED

Koenig, J., and Gardner, M., 1972. Geochemical interpretation of spring and well waters south-central Oregon and adjacent California. Berkeley, Geothermix.

Sammel, E. A., 1976. Hydrologic reconnaissance of the geothermal area near Klamath Falls, Oregon. U.S. Geological Survey Open File Report WRI 76-127.

Stark, M., Goldstein, N.E., Wollenberg, H., Strisower, B., Hege, M., and Wilt, M., 1979. Geothermal exploration assessment and interpretation, Klamath Basin, Oregon: Swan Lake and Klamath Hills areas. Berkeley, Lawrence Berkeley Laboratory, LBL-8186.

Stark, M., Goldstein, N. E., and Wollenberg, H. A., 1980. Geothermal exploration assessment and interpretation, Upper Klamath Lake area, Klamath Basin, Oregon. Berkeley, Lawrence Berkeley Laboratory, LBL-10140 (draft).

MAGNETOTELLURIC STUDIES IN THE HIGH CASCADE, OREGON

N. E. Goldstein, R. Miracky, W. M. Goubau, and T. D. Gamble

INTRODUCTION

In 1979, the U.S. Geological Survey, as part of its Geothermal Research Program, began a number of long-term geologic, geophysical, geochemical, and hydrologic studies of the Cascade Range on both regional and local scales. Upon completion, this work will provide basic information for an assessment of the geothermal potential of the Cascades, one of the major active volcanic belts in the world. To help support these studies, the U.S. Department of Energy, Division of Geothermal Energy, has contributed financially to the geoelectric studies. In connection with this involvement, LBL has undertaken magnetotelluric soundings in concert with similar work by the U.S. Geological Survey and a commercial contractor.

PROGRESS IN FISCAL YEAR 1979

During August and September 1979, LBL performed a reference magnetic-magnetotelluric (MT) survey at widely spaced stations along two east-west lines (Figure 1). The northern line, lat 45°30', extends from the Willamette Valley, southwest of Portland, across the Cascades at Mt. Hood, and terminates between the Deschutes and John Day Rivers in the Deschutes-Umatilla plateau province. The southern line, 42°15', extends from Cave Junction in the Siskyou Mountains eastward through Klamath Falls, terminating in the Basin and Range provinces, at about long 121°W. These lines, referred to as the Mt. Hood and Klamath lines, respectively, are two of six MT lines straddling the High Cascade Range. The others were surveyed by a contractor to the U.S. Geological Survey (Geotronics, Inc.), but these are conventional MT stations without the magnetic reference. LBL station separations vary between

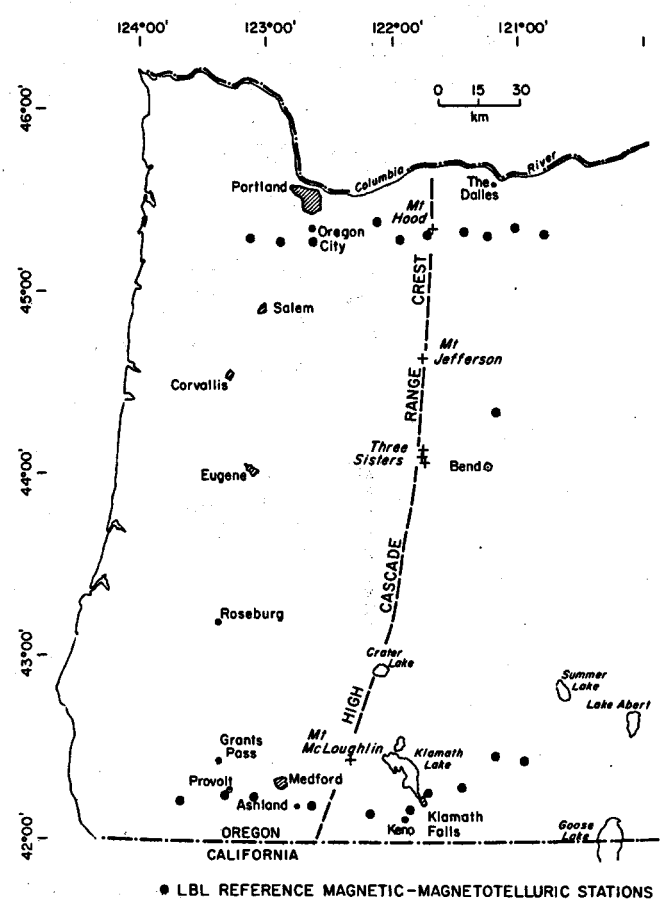

Figure 1. Location of LBL magnetotelluric stations for the High Cascade Program. (XBL 803-6821)

10 and 30 miles, resulting in a station density too coarse to permit anything more than a very general look at deep features across the Cascades. As we learned in our previous MT work around Mt. Hood, the impedance tensor can change rapidly over short distances (e.g., 2 to 3 km).

Readings were made at ten stations along each line; and two other stations were occupied in west-central Oregon, near Bend. The latter were occupied to obtain comparative results for the three MT data aquisition and processing systems being used for the geoelectric studies.

In general, results from Mt. Hood line are disappointing in terms of usable data obtained. Changes made to the DEC LSI-11 computer's software prior to the field work caused a system error that went undetected in laboratory runs. This resulted in the total loss of usable data at frequencies above 0.1 Hz. Low-frequency data were collected, but severe man-made noise between Portland and Mt. Hood caused the SQUID magnetometers to lose lock often, degrading the quality of the low-frequency data. Results from the Klamath line are much better; man-made noise was not a problem there, and data with low error bars were obtained over the 10- to 1000-sec range. The regional MT results clearly define the 50-km-wide Klamath Graben and suggest a relatively shallow heat source within the graben.

PLANS FOR FISCAL YEAR 1980

The magnetotelluric data will be processed to the fullest extent possible. Results will be plotted both as individual station soundings and as pseudosections of apparent resistivities, tipper, and tipper phase. The results will be turned over to the U.S. Geological Survey for open-filing and an LBL report will be prepared.

Geothermal Energy Conversion Technology

BINARY FLUID EXPERIMENT

B. W. Tleimat

The objective of the Binary Fluid Experiment (BFE) is to obtain data on heat-transfer film coefficient for the heating and condensing of working fluids proposed for use in binary-cycle geothermal power plants.

The experiment simulates the binary cycle using steam as the heat source for the working fluid instead of geothermal brine, and using a throttling valve instead of a turbine. Depending on the temperature range of the geothermal brine, the working fluid may be water, ammonia, isobutane and other light hydrocarbons, other fluids, or appropriate mixtures thereof. Although isobutane has received the most attention for use in geothermal power plants using the binary cycle, mixtures of isobutane and isopentane are being considered.

In specifying heat-transfer equipment for a process, the designer is usually armed with well-tested information on the performance of similar equipment under similar or identical conditions. In an unusual application, such as specifying heat-transfer equipment in a geothermal binary cycle plant using isobutane as the working fluid, designers usually refer to the heat-transfer coefficient prediction method embodied in the empirical correlation equations, such as those of Dittus and Boelter, Colburn, Sieder and Tate, and of others found in standard works. These general correlations are based on fluid transport properties and give the mean, or most probable value of a large amount of reliable experimental data. Unfortunately, because of the large influence sometimes exerted on heat transfer by minor and frequently unrecognized variations in conditions, a designer can only be reasonably sure that the performance of an individual heat exchanger will be within ±35% of the mean. Consequently, to assure fulfillment of a performance guarantee on a design embodying a minor innovation, the designer would select a heat-transfer coefficient value at the lower limit, that is, 35% less than the mean.

The correlation equations for the prediction of the heat-transfer coefficients need accurate and reliable data on the transport properties of the fluid at the operating conditions. Lack of data at these conditions makes the designer's task difficult at best. This lack of data is especially true for designs where the working fluid is in the supercritical region. This is important because computer studies (LBL's GEOTHM, for example) indicate that heating the secondary fluid in the supercritical region will result in high cycle efficiency. Consequently, the most effective and reliable method for specifying equipment design parameters is to determine the heat-transfer coefficient experimentally at the proposed operating conditions.

The BFE (Tleimat) has the capability of providing definitive baseline heat-transfer coefficient data for the heating and condensing of hydrocarbon mixtures of interest over the ranges of temperatures and pressures relevant to geothermal power plants.

The BFE is located at the University of California's Richmond Field Station. Figure 1 is a photograph of part of the apparatus and Figure 2 is a schematic flow diagram of the apparatus showing the major components. A detailed description of the apparatus is given elsewhere (Tleimat and Laird, 1979; Tleimat et al., 1979a,b).

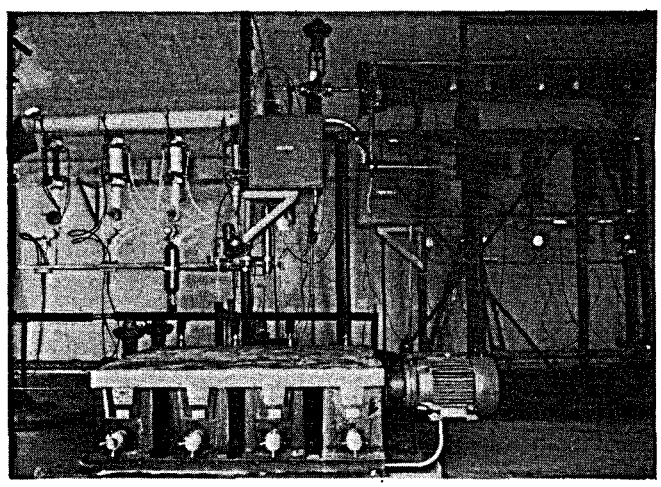

Figure 1. Binary Fluid Experiment showing high-pressure pump in the foreground; isobutane heater and its special condensate flowmeters in the upper left; isobutane throttling valve in the middle; and surface desuperheater, isobutane condenser and its special condensate flowmeters in the upper right. (CBB 780-15079)

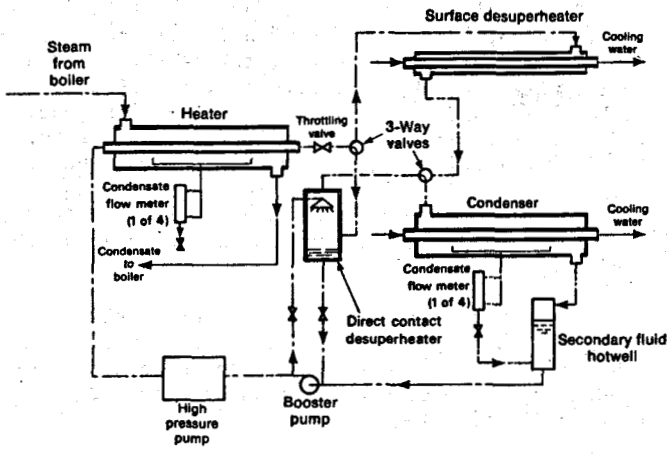

Figure 2. Schematic flow diagram of the Binary Fluid Experiment. (XBL 783-7893)

ACCOMPLISHMENTS DURING 1979

Data on the heating of isobutane at supercritical pressure (600 psia) and at various flow rates and temperatures were obtained. Simultaneously data on the condensation of isobutane at various temperatures and condensation rates were obtained. These data were analyzed. The results of the analysis were published in two reports (Tleimat et al., 1979a,b).

The system was charged with a mixture of 80/20 by mole of isobutane-isopentane in April. Trial runs were made and preliminary data were obtained. These data were examined to determine the need for additional instruments to obtain heat-transfer data on mixtures.

The system was shut down in June to install thermocouples in the vapor space in the condenser. These thermocouples will be used to determine the temperature profile in the vapor space along the length of the tube. Sampling valves were also installed at the condensate outlet from each of the condensate meters. These samples will be analyzed to determine the composition of the condensate along the length of the tube and the effect of composition on condensation film coefficient.

FUTURE PLANS

Data will be obtained on heat-transfer film coefficients for heating and condensing mixtures of different compositions in the loop. These data will be analyzed to determine the effects of varying compositions on the performance of the heater and condenser and the need for further tests.

REFERENCES CITED

Tleimat, B. W., Laird, A. D. K., Rie, H., and Hsu, I. C., 1978. Heat transfer coefficients for isobutane, in Earth Sciences Division Annual Report 1978. Berkeley, Lawrence Berkeley Laboratory, LBL-8648, p. 47-51.

Tleimat, B. W., and Laird, A. D. K., 1979. Investigation of heat transfer coefficients of binary cycle working fluids, in Earth Sciences Division Annual Report 1977. Berkeley, Lawrence Berkeley Laboratory, LBL-7028, p. 109-112.

Tleimat, B. W., Laird, A. D. K., Rie, H., Hsu, I. C., and Seban, R. A., 1979a. Hydrocarbon heat transfer coefficients; preliminary isobutane results. Berkeley, Lawrence Berkeley Laboratory, LBL-8645, 45 p.

Tleimat, B. W., Laird, A. D. K., Hsu, I. C., and Rie, H., 1979b. Baseline data on film coefficient for heating isobutane inside a tube at 4.14 MPa (600 psia). ASME publication 79-HT-14.

ACTIVITIES IN DIRECT-CONTACT HEAT EXCHANGE

P. M. Rapier

INTRODUCTION

The U.S. Department of Energy's Division of Geothermal Energy has undertaken a program to delineate and demonstrate the economic advantage of the Direct Contact Heat Exchange (DCHX) process in generating power from liquid-dominated geothermal resources. Following a proof-of-concept phase and pilot plant construction, the program elements will measure and demonstrate both subsystem and overall system performance. Development of technically and economically viable process designs will be followed by estimates of the cost of electric energy produced by such optimized plants.

1979 ACTIVITIES

During fiscal year 1979, LBL was engaged in both overall system and subsystem program elements related directly to the DCHX. These activities included the following.

Data and operational notes were assembled for proof-of-concept and reduction to practice of an equilibrium-flash boiler section, which was to be used directly on top of the 500-kW pilot plant DCHX preheater section of the tower (Rapier, 1978). The notes show a volumetric heat transfer coefficient for this section of up to five times that theoretically obtainable with alternative liquid/liquid volumetric boilers (Urbanek, 1978).

Mathematical models were developed for:

1. Determining the setting depth in a geothermal well for a downhole pump (Rapier, 1979a).

2. Performing a multistage flash evaporator of n stages for degassing geothermal brine feeds to a DCHX power plant (Rapier, 1979b).

3. Modifying the GEOTHM binary fluid code for passive simulaion of the direct-contact process.

A general code for the direct-contact mixtures and process, including economics, remains to be done.

4. DCHX preheater, boiler, and in-shell condenser model with brine chemistry (Perona, 1979). In-tube condenser, equilibrium-flash boiler, heat-and-mass balance for entire 500-kW pilot plant remain to be done.

At DOE's request, we reviewed unsolicited proposals submitted to DOE on various aspects of the DCHX.

Pilot Plant

Figure 1 is a simplified flowchart for the 500-kW plant. Incoming brine is first pressurized to 175 psia by a downhole pump to insure single-phase flow, and enters the plant at 320 to 340°F and 220 gpm, at the flash tank. Here, about 85% of the well gases are flashed off along with a small amount of steam, to prevent them from entering the turbine cycle. The heat from the off-gases is used to vaporized about 2.6% of the isobutane working fluid, which powers the turbine. The degassed brine from the flash tank next enters the brine booster pump, which pressurizes it to 458 psia and sprays it into a special equilibrium-flash boiler section at the top of the 35-ft-high, 40-in.-diameter DCHX tower. Here the preheated isobutane is flash-evaporated by live steam and brine from the spray and enters the boiler dome along with 1.4% residual steam.

In the boiler dome, the vapors are demisted. Then they are admitted at a rate of 99,400 lb/hr and a temperature of about 253°F into a radial inflow turbine. From the turbine exit the vapors flow into an evaporative condenser, where they are liquified, and then into the hotwell, where about 1400 lb/hr of water is separated from the isobutane. The isobutane reaches the isobutane return pump at about 94°F and 70 psia and is pressurized to 485 psia for injection into the base of the DCHX column through a large droplet distributor.

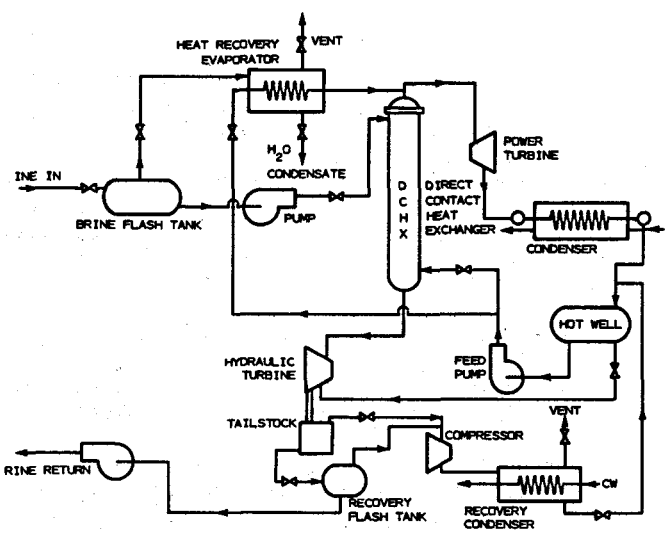

Figure 1. Flowchart for 500-kW DCHX pilot plant. (XBL 801-6739)

Spent brine leaves the tower base at 150°F and 450 psia, passes through a hydraulic turbine for recovery of the flow-work, thence through two stages of isobutane vapor recovery, and finally to the brine discharge pump and reinjection pond. Flow-work recovery at the hydraulic turbine reduces the external power requirement of the brine booster pump by about 50%. Isobutane recovery from the spent brine is estimated to be about 95%, so that less than 10 ppm will remain in the brine going to the reinjection pond.

The energy yield of the pilot plant per unit of well flow is expected to range between 5.2 and 3.6 Whr/lb of brine depending upon the build-up of condenser back pressure as shown by Figure 2 (Barber-Nichols, 1979).

Supporting Studies on Effects of Noncondensables

Noncondensables entering the pilot plant in the brine supply affect all subsystems adversely, starting with the geothermal well itself. Their presence in the brine, particularly when reinjecting will help provide compatibility in the geothermal strata; yet, they must be absent in the DCHX working fluid, where they disrupt operations of the DCHX unit, the turbine, the condenser, and the hydrocarbon recovery system.

In the wellbore and in the brine supply lines to the plant, noncondensables create two-phase flow problems, such as burping, scaling, and plugging. LBL's solution to this has been to set a newly developed electrically driven REDA pump at a 600-ft depth in the East Mesa 8-1 well. This setting depth is 50% greater than the theoretical minimum depth

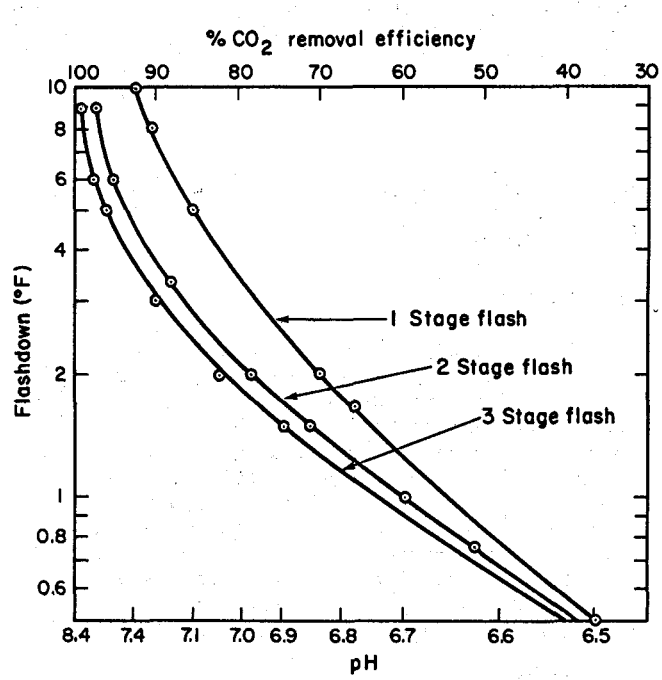

Figure 2. Carbon dioxide removal efficiency and pH of brine after a given flashdown taken over one, two, and three stages. Calculated for 8-1 well data, based on initial 6.27 pH and 422 ppm alkalinity, as bicarbonate ion. (XBL 803-6819)

of 402 ft after four years flow at 220 gpm as determined by LBL's calculator code (Rapier, 1979a). This 50% increase includes the manufacturer's recommended NPSH plus a reasonable safety factor. No evidence of two-phase flow has been observed since startup, and so this first-of-its-kind downhole pump installation is now regarded as an adequate solution to this problem.

The single-stage flash tank of the pilot plant is expected to provide experimental data for the design of a fully commerical multistage flash (MSF) degasser, capable of removing 96% of the gas, thus allowing a close approach to the ideal gas-free operation. Figure 3 shows the gas removal efficiency and pH of the flashed brine for a given flash-down taken over one, two, and three stages (Rapier, 1979b). The heat-recovery efficiency of the MSF degasser is expected to be close to unity, inasmuch as it possesses several features not found on the experimental flash tank:

1. The steam condensate from each stage drips directly into the brine, so that the total brine supplied enters the DCHX unit. This returns all of the enthalpy to the process.

2. The steam condenses within the stage at about the brine temperature instead of in a separate heat recovery vessel at a much lower temperature and pressure. This provides a maximum temperature for boiling the isobutane in the condenser tubes of the stage.

3. The noncondensables are subcooled before being discharged, so that steam losses from the vent are inconsequential.

4. The back-pressure condensing principle employed from stage to stage insures an equilibrium flash in each stage and provides fly-wheel stability to the operation by coupling the heat and mass flows of the process and eliminating nonessential controls.

Noncondensables, remaining in the brine entering the DCHX, will build up an equilibrium concentration in the recirculating isobutane working

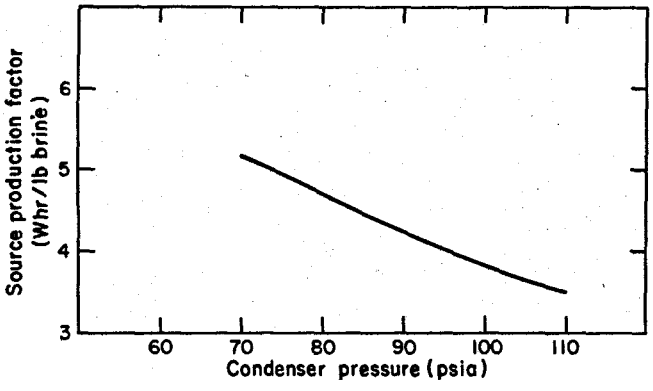

Figure 3. Influence of condenser pressure on system performance: brine flow = 26.5 lb/s; turbine efficiency = 0.8. (XBL 803-6818)

fluid that depends upon their entering rate. They recirculate through the turbine to form as much as 1% of the total mass flow, but do not contribute a corresponding enthalpy drop, thereby reducing the turbine efficiency. They also add their partial pressure to the working-fluid condensing pressure, reducing the available pressure ratio across the turbine. In an unvented condenser, the pressure builds up to an equilibrium point such that noncondensables can be transferred from the working fluid to the spent brine stream at the same rate as they are entering the DCHX unit. The recycled noncondensables form a blanket through which the isobutane must diffuse to reach the heat exchange surface, and thereby lower the heat transfer coefficient by as much as 50% (Urbanek, 1979, p. 7-1). Consequently, for a given cooling system to perform its duty the condensing temperature and pressure of the isobutane will have to rise. Additionally, because of the recycled noncondensable load, vapors from the turbine exit will reach the condenser more highly superheated than for a pure isobutane vapor. Consequently, desuperheating will be more of a problem.

In the isobutane vapor recovery section following the hydraulic turbine, noncondensables can aid in stripping the 200 ppm soluble isobutane from the brine; however, the resulting gas mixture is more difficult and costly to condense and separate than pure isobutane. The most cost-effective procedure is to remove the noncondensables ahead of the DCHX unit.

Recommended for future investigation are the following problems: in the upper part of the DCHX preheater section, dissolution of the recycling concentrated noncondensable gases from the isobutane droplets, prior to any active boiling, may stifle the expected liquid/liquid heat transfer, blanket the droplets, buoy them to the surface prematurely, form metastable cellular gas structures, and otherwise disrupt the orderly counter-current heat exchange of the device. Preflashing the brine ahead of the DCHX unit and use of sieve trays beneath the equilibrium-flash boiler section are feasible solutions to these gas difficulties.

At the condenser, higher-than-expected back-pressures may occur because of bypassing of superheated vapors and subcooling of the condensate. Desuperheating at the turbine exit, together with the use of a vent compressor/condenser may reduce these irreversibilities.

REFERENCES CITED

Barber-Nichols Engineering Company, 1978. 500 kW pilot plant design review, July 20, 1978. Barber-Nichols Engineering Company.

____, 1979. Final report, direct contact heat exchanger 10 kW power loop test series no. 2. Berkeley, Lawrence Berkeley Laboratory, LBL-7036, v. 2, p. 5.

Fulton, R. L., 1979. Developments in direct-contact heat exchange, in Earth Science Division annual report 1978. Berkeley, Lawrence Berkeley Laboratory, LBL-8648, p. 55-57.

Perona, J., 1979. Periodic Reports for DGE on Analysis of Mass Transfer Processes in Geothermal Power Cycles Utilizing Direct Contact

Heat Exchanger. Knoxville, University of Tennessee.

Rapier, P. M., 1978. Proposed design for direct contact isobutane boiler. Berkeley, Lawrence Berkeley Laboratory, LBL Engineering Note, UCID-8029, GT1808, Serial M5194, May 23, 1978.

____, 1979a. Calculations for the proposed downhole pumping of East Mesa 8-1 well at 220 gpm. Berkeley, Lawrence Berkeley Laboratory, LBL Engineering Note, LBID-008, GT1808, Serial M5314, March 16, 1979.

____, 1979b. SR-59 program for vapor pressure of geothermal brine at constant alkalinity vs pH, flashdown °C versus number of MSF stages, carbonate composition and percent CO_2 removal for each stage. Berkeley, Lawrence Berkeley Laboratory, LBL Engineering Note, LBID-096, GT1702, Serial M5391, May 16, 1979.

Urbanek, M. W., 1978. Development of direct-contact heat exchangers for geothermal brines, DDS Engineers, Final report, October 1977-June 1978. Berkeley, Lawrence Berkeley Laboratory, LBL-8558.

____, 1979. Experimental testing of a direct-contact heat exchanger for geothermal brine, Final report, December 1979. ORNL/SUB-79/13564/1 and ORNL/SUB-79/45736/1 DSS-079.

Reservoir Engineering

MEXICAN-AMERICAN COOPERATIVE PROGRAM AT THE CERRO PRIETO GEOTHERMAL FIELD, BAJA CALIFORNIA, MEXICO

M. J. Lippmann, P. A. Witherspoon, and N. E. Goldstein

INTRODUCTION

The Cerro Prieto field is located in the Salton Trough just south of the California/ Baja California border (Figure 1). The field is the site of a cooperative effort between Mexico and the United States to understand the behavior of a geothermal system under full-scale fluid exploitation.

The Comisión Federal de Electricidad of Mexico (CFE), which manages and operates the field, began generating electric power at Cerro Prieto in 1973. Last April, the original 75-MWe power output was doubled to 150 MWe as the third and fourth 37.5MW higher-pressure single-flash units were placed in operation.

At the present time, about 480 MWt contained in hot separated waters are being wasted. To recover some of the energy of these 169°C waters, now being disposed of into an evaporation pond at a rate of about 3000 tonnes/day; a 30-MWe lower-pressure double-flash unit is scheduled for commercial operation in 1982 (Hernandez, 1979).

The total generating capacity at the field is expected to reach 400 MWe by 1985. The probable total capacity of the Cerro Prieto field is estimated to be about 1000 MWe and that of the entire Mexicali Valley is believed to be much larger (Mañon and Guiza, 1979). Based on CFE's resource estimates, the available geothermal power will exceed the local demand for electricity, and CFE has tentatively agreed to sell large blocks of electrical power to San Diego Gas and Electric Company, of southern California.

The intensive drilling program initiated in 1976 continues. At the present time about 65 deep wells have been completed (Figures 2 and 3). The new wells in the eastern and southeastern parts of the field confirmed the existence of a very hot (>320°C) reservoir below 2000 m depth (Alonso et al., 1979).

Geothermal studies are now being performed as part of a cooperative project, which was established

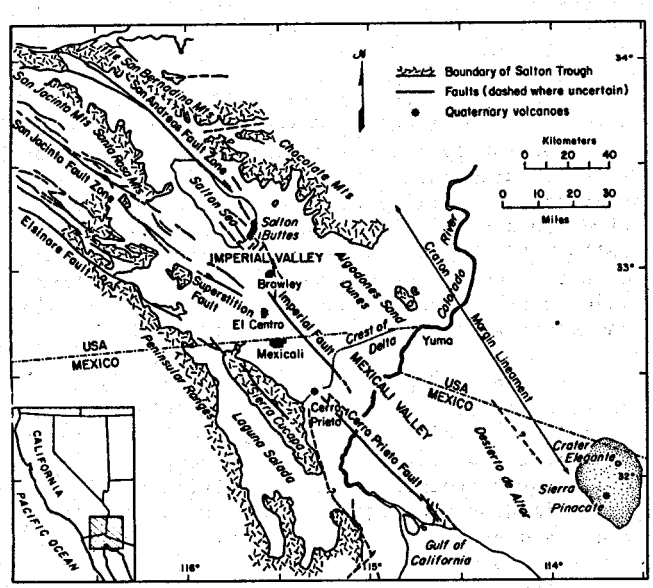

Figure 1. Salton Trough (or Salton Sea/Sea of Cortez Trough) showing the location of the Imperial and Mexicali Valley and the Cerro Prieto field. (XBL 801-6718)

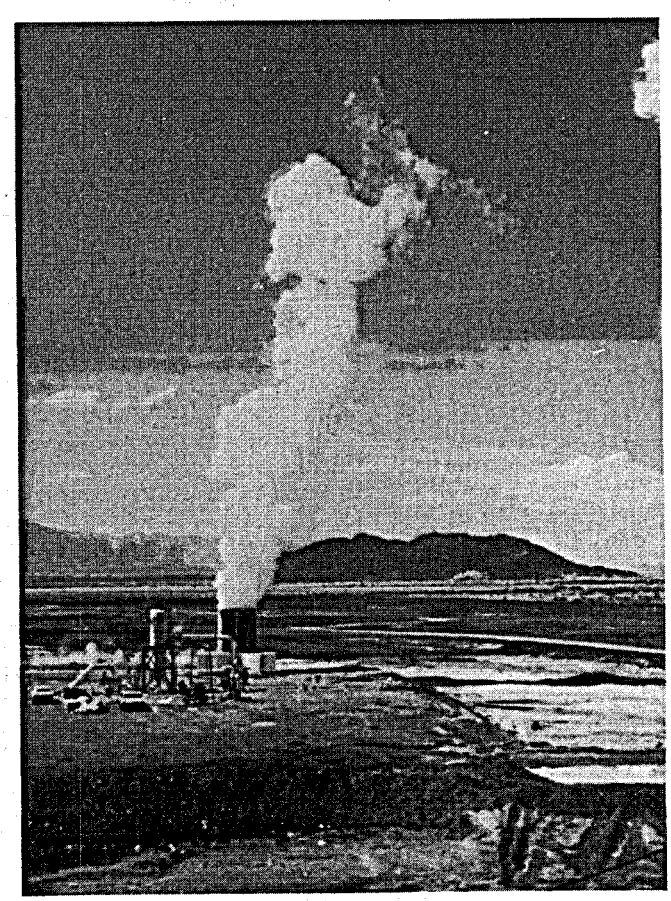

Figure 2. One of the wellhead installations. Cerro Prieto Volcano and Sierra Cucapa in the background. (CBB 802-1912)

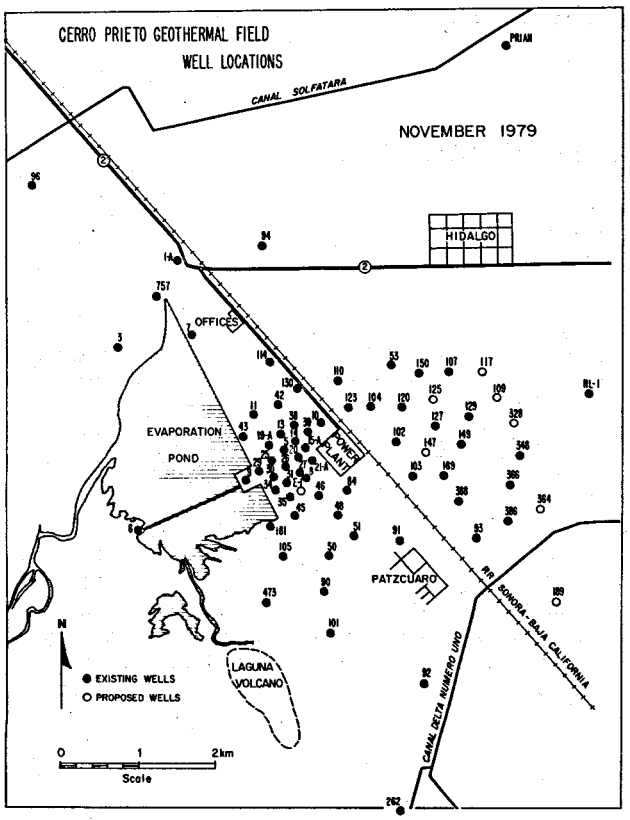

Figure 3. Cerro Prieto geothermal field--well locations. (XBL 7911-13432)

and operated through an agreement signed on July 21, 1977, between CFE and the U.S. Department of Energy (DOE). Lawrence Berkeley Laboratory (LBL) coordinates U.S. technical activities carried out under this project. The Coordinadora Ejecutiva de Cerro Prieto of CFE is organizing all Mexican participation (Witherspoon et al., 1978).

The Cerro Prieto project incorporates studies of the geologic, hydrogeologic, geochemical, and geophysical settings of the geothermal field, as well as investigations of its structural, reservoir engineering, and subsidence characteristics. The primary objective of the program is to develop an understanding of the geologic setting and hydrothermal circulation of this geothermal system.

Cerro Prieto is considered an ideal system for studying the long-term response of a liquid-dominated geothermal field in continuous production. Much of the information obtained here will be applicable to the development of geothermal resources in similar geologic settings such as the Mexicali Valley, Mexico, and the Imperial Valley, California. This information will be useful for geothermal development in other parts of the world.

FISCAL YEAR 1979 ACTIVITIES

Most of the results obtained since the beginning of this international project in 1977 have been published in the Proceedings of the First Symposium on the Cerro Prieto Field, San Diego, California, September 20-22, 1978 (Lawrence Berkeley Laboratory, 1978) or will be included in those of the Second Symposium, Mexicali, Baja California, October 17-19, 1979, expected to be issued by CFE in the latter part of 1980.

Further details of the activities and results described below are discussed elsewhere in this volume.

Geology

Data from surface geophysical surveys, well sample descriptions and analysis, and geophysical well logs were used to obtain new insights into the stratigraphy, structure, hydrothermal alteration, reservoir properties, and geohydrology of the area.

Lyons and van de Kamp (1980) completed a comprehensive geologic study using geophysical well logs and surface geophysical results, in addition to borehole lithology and mineralogy. They developed a new regional depositional model which indicates the reservoir rocks occupy a transition zone from an upper delta plain environment to the east to a marine environment west of the field. They recognized three principal types of faults: (1) older faults offsetting only the deeper part of the geologic section, (2) reactived older faults with smaller offset or reversed sense of offset above some horizon, and (3) young faults offsetting the entire section. Some of the faults previously identified by other workers were not recognized by them. For example, the major fault previously assumed to run almost along the railroad track (Michoacan fault) seems not to contiune farther south than about well M-103.

The vertical transition from unconsolidated and semiconsolidated to consolidated sediments, the so-called A/B boundary, was found not to occur at one stratigraphic horizon, but cuts across the sedimentary strata suggesting localized post-depositional alteration.

Vonder Haar and Howard (1979) hypothesize that where the important northwest-southeast Michoacan fault obliquely intersects shorter northeast-southwest trending faults (e.g., near M-103) there is greater permeability and increased natural convective fluid flow. In addition, a shear zone near wells M-48, M-91, and M-101 seems to enhance the distribution of the geothermal fluids away from the major northwest-southeast faults, thus increasing the recharge capacity of the field.

By means of petrological and geochemical studies of well cuttings and cores, Elders et al. (1980) have confirmed the existence in the reservoir of a systematic sequence of temperature-dependent hydrothermal minerals (Figure 4). These are formed by progressive dehydration, decarbonation, and exchange reactions. Minor variations in mineral assemblages in different parts of the systems were observed. These are due to differences in permeability, pCO_2 and in some cases to localized episodic temperature fluctuations.

The thermal metamorphism of organic particles (phytoclasts) found in Cerro Prieto sedimentary

MINERAL ZONATION IN CERRO PRIETO SANDSTONES

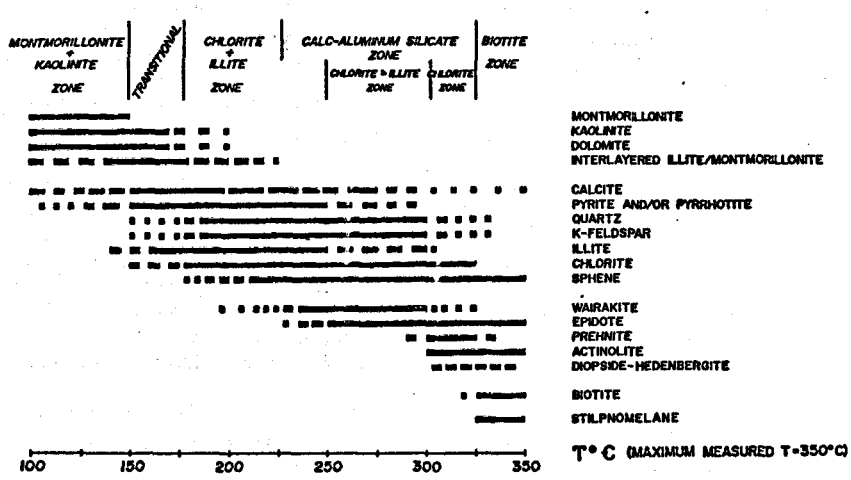

Figure 4. Mineral zonation in Cerro Prieto sandstones (from Elders et al., 1980). (XBL 804-9162)

rocks indicate that the measured temperatures in the deeper portions of the geothermal wells are equilibrium reservoir temperatures (Elders et al., 1980).

Paleomagnetic studies of rocks from the Cerro Prieto volcano suggested that it originated about 110,000 years B.P., and that volcanism continued intermittently until about 10,000 years ago (de Boer, 1979).

Geophysics

During 1979 CFE and LBL and their contractors continued surface geophysical surveys throughout the area. LBL concentrated its efforts on improving the structural model of the field and using resistivity, gravity, and seismicity to monitor changes due to fluid production. On the other hand, CFE extended exploration surveys to other potentially promising areas in the Mexicali Valley.

Based on independent dipole-dipole dc resistivity and magnetotelluric surveys performed and interpreted by LBL, the reservoir rocks currently exploited show up as more resistive (4 ohm-m) than the surrounding rock (~1.5 ohm-m). Although this is contrary to the widely held theory that hot reservoir rocks will appear as low resistivity zones, a correlation between surface resistivity data and borehole geologic data shows that the higher resistivities can be accounted for by hydrothermal metamorphism that has reduced the porosity of the mud and shale units (Wilt et al., 1979; Goubau et al., 1979). Surface measurements have also provided subsurface information that may help CFE in planning step-out drilling.

A repeat precision gravity survey at monuments over and around the field was made in 1979 (Grannell et al., 1979). Two-thirds of the station observations have an estimated error less than 9 gal, sufficient to permit detection of mass changes taking place within 2 km of the surface. To within the accuracy of the 1978 and 1979 sets of measurements, no mass changes are evident. This suggests that over the 2-year period the circulation system remained in approximate dynamic equilibrium.

Geochemistry

Based on chemical and isotopic studies of the Cerro Prieto brines, Truesdell et al. (1979) conclude that the fluids derive from a mixture of partially evaporated sea water and Colorado River waters, which were extensively altered compositionally by high-temperature reactions involving the reservoir rocks (Figure 5). Their results also have shown that exploitation of the field has greatly changed the pressure, temperature, state, and chemistry of the aquifer fluids.

A geochemical study of the different surface manifestations in the Cerro Prieto field (Elders et al., 1980) suggests: (1) there is a close relationship between the hot springs in the area and the deep geothermal reservoir, and (2) there has been a change in the spring's chemical characteristics since 1968 in response to the large-scale fluid extraction from the field.

Subsidence

Last year the first-order leveling and precise horizontal-control networks established in 1978 were surveyed for the second time. The comparison of the measurements from the first and second vertical surveys indicated localized vertical subsidence and uplifts in the area, ranging from -28.0 mm to +33.0 mm (García and Mendéz, 1979).

Trilateration surveys indicated that horizontal ground-surface movement was also occurring (Figure 6). The portion of the local net covering the geothermal production zone showed a northwest-southeast contraction that may be as great as 31 μ strain/yr. Movements in the area surrounding the production

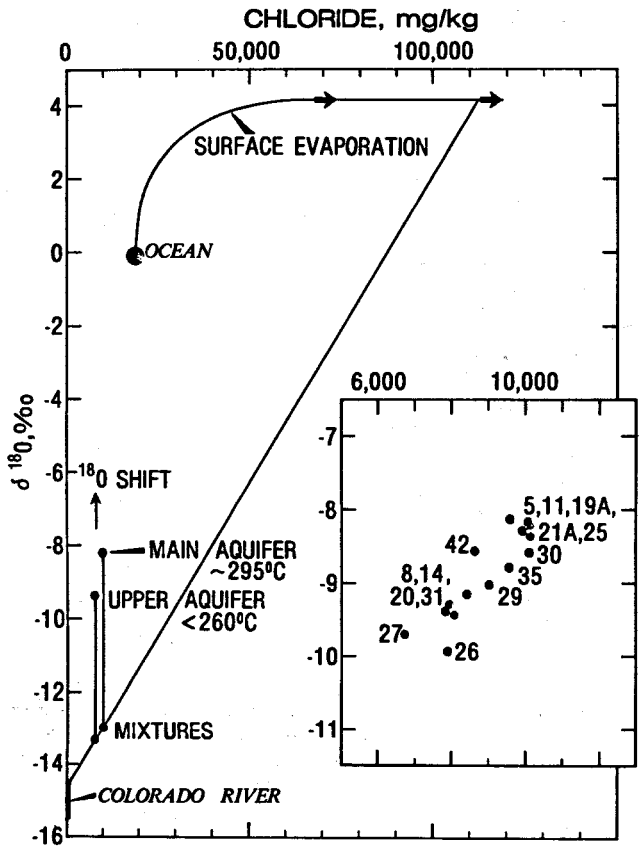

Figure 5. Isotopic composition and chloride content of Cerro Prieto reservoir, Colorado River and ocean waters, showing the effect of surface evaporation, mixture, and high temperature reactions (from Truesdell et al., 1979). (XBL 804-9163)

zone are small and show a northeast-southwest extension of about 0.7 μ strain/yr. The regional net resurvey showed a small expansion on all axes with a maximum of about 0.7 μ strain/yr in a northeast-southwest direction (Massey, 1979).

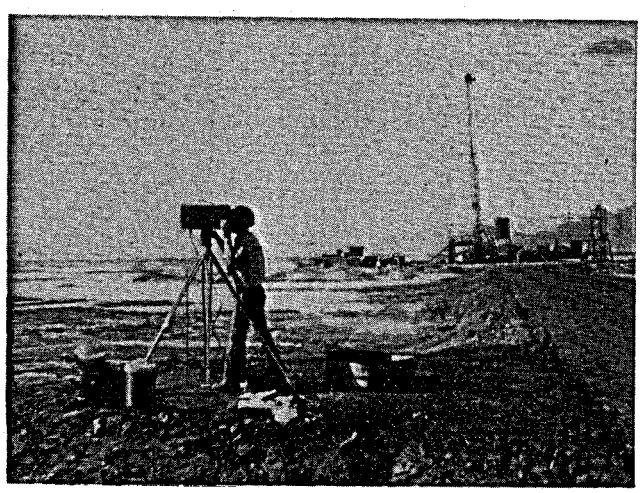

Figure 6. Electronic distance measurement equipment being used at a horizontal control station of the local network (USGS photograph). (BBC 784-4885)

Reservor Engineering

During fiscal year 1979 LBL advised CFE in their well testing program, performed a number of field tests, and assisted in interpreting the data obtained. The results from two-rate flow and interference tests confirmed that permeability of the reservoir is on the order of tens of millidarcies.

LBL carried out a two-rate flow test in one of the wells using a downhole tool modified by Sandia Laboratories (Figure 7). The test demonstrated that the modified high-temperature tools could operate at temperatures of up to 340°C for 12-hr periods. The maximum downhole time seems to be determined by the failure of the O-rings, and not of the clocks (Alonso et al., 1979).

Physical and mechanical properties of cores continued to be determined under high temperature and pressure conditions (Abou-Sayed and Schatz, 1979). Simplified models of the field were used to determine its boundary condition and recharge rates and to simulate its behavior during production and injection.

Reinjection

In August 1979 CFE began reinjection of untreated 165°C brines into well M-9. The test is being carefully monitored. Downhole measurements in M-9 are periodically carried out. Pressure and temperature of neighboring producing wells are being monitored to detect any changes resulting from the test.

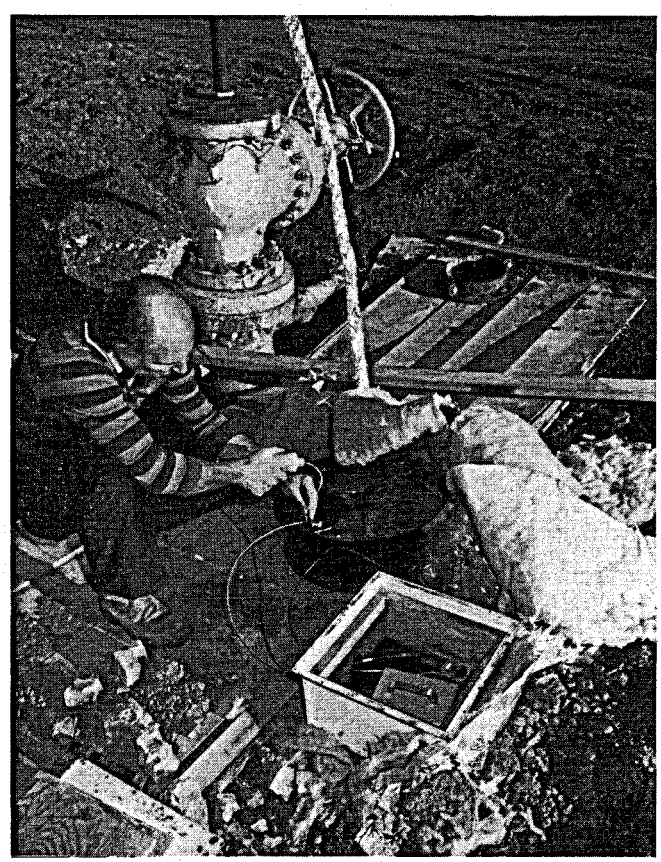

Figure 7. Technician checking instrumentation during a well test. (BBC 782-2269)

Because a 30 MW low-pressure turbine will be on line in 1982, large amounts of 100°C brines supersaturated with silica will then be available for reinjection. To avoid major problems in the pipes and reservoir, the excess silica will have to be eliminated before reinjection.

In support of these future reinjection operations under low temperature conditions, Weres et al. (1980) carried out laboratory experiments and theoretical calculations to evaluate different brine treatment processes. They found that part of the dissolved silica quickly polymerizes to form suspended colloidal silica. This colloidal silica will flocculate and settle rapidly by raising the pH and stirring the brine. The theoretical equilibrium calculations indicated that the increase of pH of the brine to remove silica might cause some precipitation of carbonates. If this occurs the problem could be eliminated at reasonable cost.

Mexico has begun pilot plant-scale tests to determine the isothermal (~100°C) rate of silica polymerization for different pH values. Also, sedimentation tests with and without flocculants are being conducted.

Conferences

During this fiscal year no symposium open to the general public was held. However, a number of internal planning and technical meetings between Mexican and U.S. scientists and engineers were organized to discuss the latest results and future directions of the coorperative program.

The proceedings of the first symposium, in Spanish and English, were issued as an LBL report (Lawrence Berkeley Laboratory, 1978) and will be published in a special issue of the journal Geothermics.

PLANNED ACTIVITIES FOR FISCAL YEAR 1980

LBL will continue to coordinate the U.S. activitites at Cerro Prieto under the CFE/DOE cooperative program. Discussions will be held between DOE/LBL and CFE to extend the present agreement to one of the geothermal areas of central Mexico, possibly Los Azufres field in the state of Michoacan.

The geological model of the Cerro Prieto field will be updated in light of new data from wells, field surveys, and laboratory work, which will be carried out during the next year. The interpretation of well logs, analysis of cores, and drill cuttings will continue.

The dipole-dipole and precision gravity networks will be resurveyed for the third time to maintain the monitoring activities within the production area. Additional magnetotelluric measurements will be carried out. The induced seismicity array will be refurbished by the installation of improved downhole geophones.

The geochemical model to explain the different processes occurring in the reservoir as well as to determine its evolution and recharge will be developed further based on the analysis of reservoir rocks and fluids.

The regional and local horizontal networks will be resurveyed to monitor crustal deformations related to tectonic and man-made activities.

Improved high-temperature downhole tools will be used in well tests to gather additional data on the characteristics of individual wells and of the different geothermal aquifers. The numerical simulation of field behavior will continue at an accelerated pace in view of the need to estimate the long-term capacity of the field and to predict the effects on the reservoir of large-scale reinjection of waste brines.

Internal technical meetings with DOE and CFE will be held periodically to review results and plan future activities. On October 17-19, 1979, the Second Symposium on the Cerro Prieto Geothermal Field was held in Mexicali. Preparations for the Third Symposium (San Francisco, March 1981) will begin during this fiscal year.

REFERENCES CITED

Abou-Sayed, A., and Schatz, J. F., 1979. Physical and mechanical properties of cores from the Cerro Prieto geothermal field, in Abstracts, Second Symposium on the Cerro Prieto Geothermal Field. Mexicali, Comisión Federal de Electricidad.

Alonso E., H., Domínguez A., B., Lippmann, M. J., Molinar C., R., Schroeder, R. E., and Witherspoon, P. A., 1979. Update of reservoir engineering activities at Cerro Prieto. Berkeley, Lawrence Berkeley Laboratory, LBL-10209.

de Boer, J., 1979. Paleomagnetic dating of the Cerro Prieto volcano, in Abstracts, Second Symposium on the Cerro Prieto Geothermal Field. Mexicali, Comisión Federal de Electricidad.

Elders, W. A., Hoagland, J. R., Vallette, J. N., Williams, A., Barker, C., and Collier, P., 1980. A comprehensive study of samples from geothermal reservoirs: petrology and geochemistry of subsurface and surface samples from the Cerro Prieto geothermal field, Baja California, Mexico. University of California at Riverside (report in press).

Hernández G., J. L., 1979. Algunas precisiones en torno a la Unidad 5. Boletín Instituto Investigaciones Eléctricas, v. 3, no. 10, p. 7-10.

Hurtado, R., Díaz, R., Mercado, S., Garibaldi, F., Cortéz, C., and Fausto, J. J., 1979. Brine treatment for reinjection and reinjection tests without treatment, in Abstracts, Second Symposium on the Cerro Prieto geothermal field. Mexicali, Comisión Federal de Electricidad.

García, J. R., and Mendéz, V. P., 1979. First-order leveling surveys at Cerro Prieto, in Abstracts, Second Symposium on the Cerro Prieto geothermal field. Mexicali, Comisión Federal de Electricidad.

Goubau, W. M., Stark, M., Gamble, T. D., Goldstein, N. E., and Miracky, R., 1979. Magnetotelluric studies at Cerro Prieto, in Abstracts, Second Symposium on the Cerro Prieto Geothermal Field. Mexicali, Comisión Federal de Electricidad.

Grannell, R. B., Tarman, D. W., Aronstam, P., Clover, R. C., Leggewie, R. M., Eppink, J., and Kroll, R., 1979. Precision gravity

measurements in the Cerro Prieto geothermal area, in Abstracts, Second Symposium on the Cerro Prieto Geothermal Field. Mexicali, Comisión Federal de Electricidad.

Lawrence Berkeley Laboratory, 1978. Proceedings, First Symposium on the Cerro Prieto Geothermal Field, Baja California, Mexico, September 20-22, 1978, San Diego, California. Berkeley, Lawrence Berkeley Laboratory, LBL-7098.

Lyons, D. J., and van de Kamp, P. C., 1980. Subsurface geological and geophysical study of the Cerro Prieto geothermal field. Berkeley, Lawrence Berkeley Laboratory, LBL-10540.

Mañon M., A. and Guiza L., J., 1979. El proyecto de optimización del aprovechamiento de fluidos geotérmicos en opinión de dos expertos. Boletín Instituto Investigaciones Eléctricas, v. 3, no. 4, p. 22.

Massey, B. L., 1979. Measured crustal strain, Cerro Prieto geothermal field, Baja California, Mexico, in Abstracts, Second Symposium on the Cerro Prieto Geothermal Field. Mexicali, Comisión Federal de Electricidad.

Truesdell, A. H., Nehring, N. L., Thompson, J. M., Coplen, T. B., DesMarais, D. J., Janik, C. J., and Mehl, D. C., 1979. Geochemical studies of the Cerro Prieto reservoir fluid, in Abstracts, Second Symposium on the Cerro Prieto Geothermal Field. Mexicali, Comisión Federal de Electricidad.

Vonder Haar, S. and Howard, J. H., 1979. Intersecting faults and sandstone stratigraphy at the Cerro Prieto geothermal field, in Abstracts, Second Symposium on the Cerro Prieto Geothermal Field. Mexicali, Comisión Federal de Electricidad.

Weres, O., Tsao, L., and Iglesias, E., 1980. Chemistry of silica in Cerro Prieto brines. Berkeley, Lawrence Berkeley Laboratory, LBL-10166.

Wilt, M. J. and Goldstein, N. E., 1979. Resistivity monitoring at Cerro Prieto, in Abstracts, Second Symposium on the Cerro Prieto Geothermal Field. Mexicali, Comisión Federal de Electricidad.

Witherspoon, P. A., Alonso E., H., Lippmann, M. J., Mañon M., A., and Wollenberg, H. A., 1978. Mexican-American Cooperative Program at the Cerro Prieto geothermal field. Berkeley, Lawrence Berkeley Laboratory, LBL-7095.

REGIONAL GEOLOGIC SETTING OF THE CERRO PRIETO GEOTHERMAL FIELD

S. P. Vonder Haar and J. H. Howard

INTRODUCTION

A synthesis of geological information on the Salton Trough from the Salton Sea region south to the Upper Gulf of California was completed during the past fiscal year.

Satellite photography and field research established important relationships between a probable deep heat source, fluid migration, and magnitude of the geothermal fields (Vonder Haar and Puente C., 1979a; Meidav and Howard, 1979). Our understanding of regional volcanism and subsurface stratigraphy was enhanced by paleomagnetic and micropaleontology studies. Merging of concepts on San Andreas type wrench faulting with oceanic transform fault theory (Vonder Haar and Puente C., 1979b) provided insight into the apparently significant role of northeast-southwest trending cross-faults in geothermal fields in the Salton Trough, including Cerro Prieto.

THE YEAR'S ACTIVITIES

The wedge-shaped region termed the Salton Trough extends from the Salton Sea to the uppermost Gulf of California (Figure 1) and is noted for recent volcanism, strike-slip faulting and geothermal fields. This region is bounded on the east by the poorly defined Craton Margin Lineament (see Figure 2) and the Sierra Pinacate volcanics. On the west, the San Felipe basin-bounding fault zone and the combined Elsinore/San Jacinto fault zones form a sharp boundary. Slicing through the trough are the Cerro Prieto fault, the Imperial fault and still other faults. Faults in the trough are best conceived of as hybrid types having features of both San Andreas style wrench faults and oceanic transform faults. Earlier ideas of passive pull-apart basins or transform faults that leak magma (Elders et al., 1972) have been refined.

Fault blocks between the Cerro Prieto and Imperial faults appear to be 1 to 4 km on a side. Oblique intersections of northeast-southwest trending fault shear zones with these two major faults

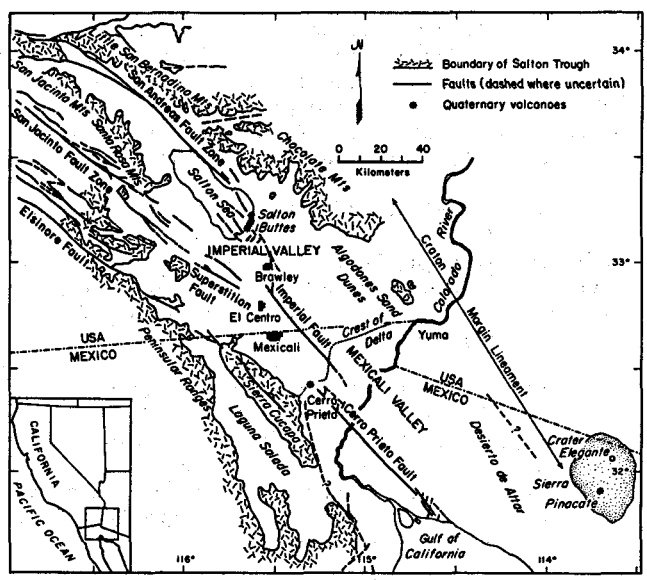

Figure 1. Regional geology of the Cerro Prieto geothermal field showing major faults and sites of paleomagnetic studies (see Vonder Haar, Noble, and Puente C., 1979). (XBL 801-6718)

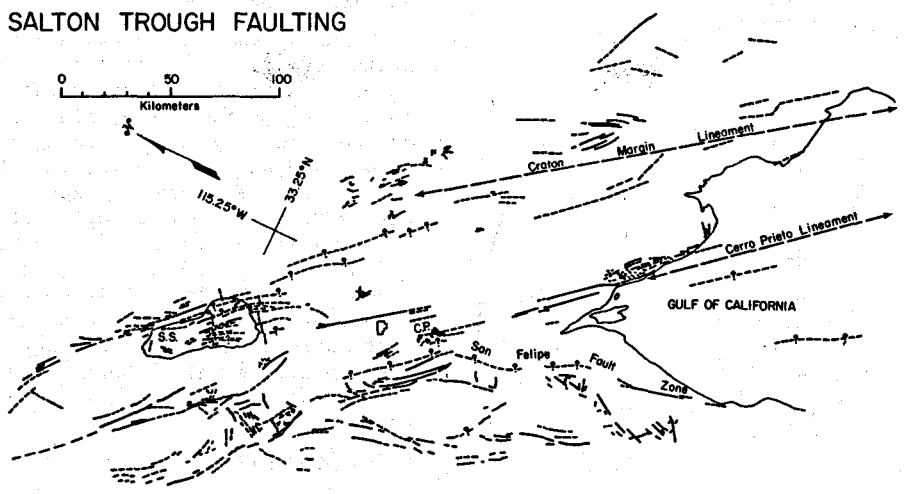

Figure 2. Compilation of faults in the Salton Tough showing the Cerro Prieto Lineament as a major hybrid transform fault zone. Note the prevalent and long northwest-southeast trending faults with much shorter intersecting faults of northeast-southwest trends. Faults indicated by lines, dashed where discontinuous or subsurface; ? indicates uncertain location. Critical data evaluation from published work; S.S. indicates Salton Sea; C.P. is the Cerro Prieto geothermal area (from Vonder Haar and Puente C., 1979a). (XBL 797-7515A)

indicate sites for the most productive wells. In addition, these cross-cutting northeast-southwest faults help move the convective fluid flow away from the deep penetrating hybrid transform faults. Thus the areal extent of the rapid recharge zone is increased.

Of major importance to the regional stratigraphy was the discovery of a mid-Tertiary (approximately 15 m.y. old) foraminifer Cassigerinella chipolensis (Figure 3). This planktonic marine microfossil was found in well cuttings from the Cerro Prieto geothermal field. These specimens are not laboratory contaminates and have not been found in the drilling mud (Cotton and Vonder Haar, 1980). If the presence of Cassigerinella chipolensis is confirmed, the current conceptualization of the opening of the Gulf of California after mid-Tertiary, only 11 million years ago, and the California Pacific coast mid-Tertiary history will need to be revised.

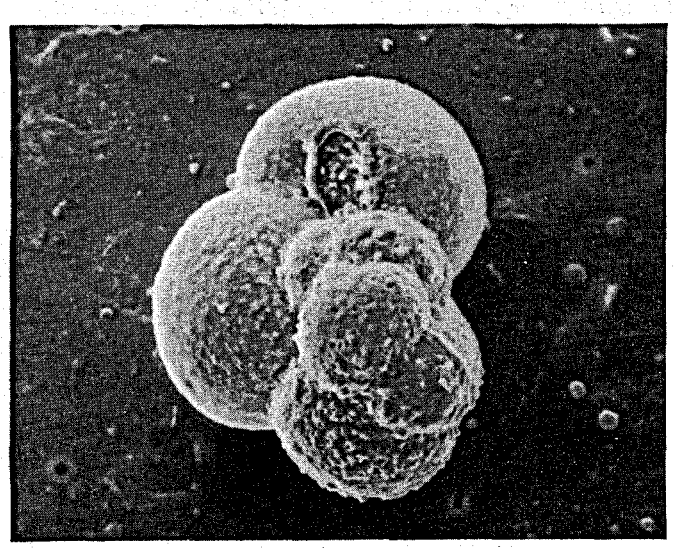

Figure 3. Cassigerinella chipolensis; a mid-Tertiary planktonic microfossil found in Cerro Prieto geothermal well cuttings (see Cotton and Vonder Haar, 1979). Scanning electron microphotograph provided by J. L. Lamb, Exxon Production Research; actual diameter of the microfossil is 0.7 mm. (XBB 790-13447)

Timing of geologic events in the region and the variation in volcanism were clarified by paleomagnetic studies. Figure 4 illustrates polar excursion paths and data for the Salton Buttes, Crater Elegante, and Cerro Prieto. Deviating thermomagnetic directions in volcanism representing the second and fifth or sixth pulse of volcanism suggest that Cerro Prieto originated approximately 110,000 years B.P. and continued to be active intermittently until about 10,000 years ago (de Boer and Vonder Haar, 1980). The Crater Elegante, Salton Buttes, and Cerro Prieto poles differ enough to support the conclusion that volcanic activity throughout the trough was not contemporaneous.

Analogs to the Cerro Prieto region were investigated in relation to both early rifting phases (see Vonder Haar and Howard, 1978) and to transform faulting. In addition to the Gulf of California basin studies (Lonsdale and Lawver, 1979), the in-situ structural observations along Transform fault "A" in the FAMOUS area of the Mid-Atlantic ridge provided clear insights into tectonism (see Figure 5). Geophysical studies and well drilling in the Cerro Prieto region furnished a model that compared favorably with these analogs if the increased deltaic sedimentation rate and thickening continental basement near Cerro Prieto are considered.

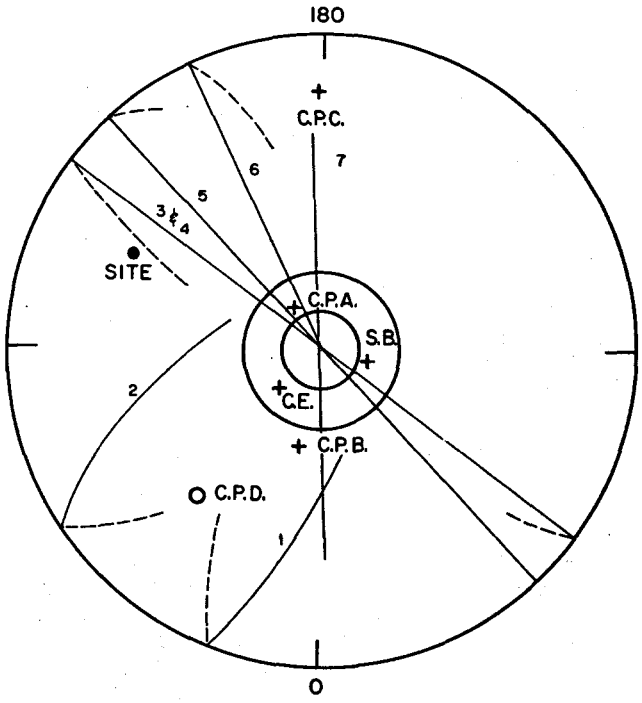

Figure 4. Polar paths for major magnetic excursions in the Brunhes period: (1) Gothenburg (~10,000 years B.P.), (2) Starno (~12.000 years B.P.), (3) Lake Mungo, (4) Laschamp, (5) Lake Bitwa, (6 and 7) Blake (119,000 to 108,000 years B.P.); with the virtual geomagnetic poles for Cerro Prieto (CPA, CPB, CPC, CPD), Salton Buttes (SB), and Crater Elegante (CE). CPD represents a pole in the southern hemisphere--a magnetic reversal. (XBL 7912-13474)

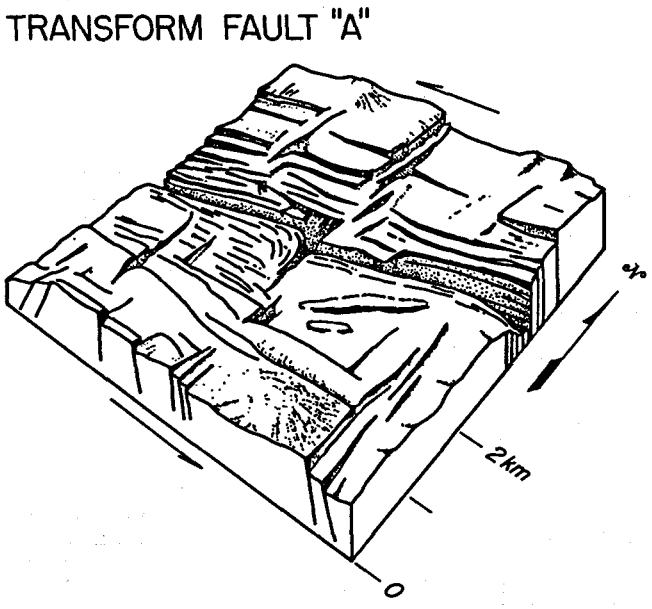

Figure 5. Interpretive block diagram of Transform fault "A" in the Mid-Atlantic Ridge showing structural domains. The ramps, cross-faults and 200-m-wide active zone of strike-slip movement within a 4-km-wide fault trough suggest the possible complexity of faulting along the Cerro Prieto and Imperial faults and within the producing geothermal fields (after Choukroune et al., 1978).(XBL 797-7583)

PLANNED ACTIVITIES

During the coming fiscal year, work on the neotectonism and regional stratigraphy is planned. In particular we will study the Sierra Cucapa, only 10 km west of the Cerro Prieto geothermal zone, for fracture density and fracture styles around the normal and strike-slip faults. This will aid in studies of the production zone at 2 to 3.5 km depth at the Cerro Prieto field. Heat flux and detailed faulting at the southern end of the Imperial fault are not nearly as well understood as at the northern terminus of the Cerro Prieto fault. Geophysical data that reach across the Salton Trough would be most useful. Micropaleontology of key outcrop and subsurface wells should prove as exciting and beneficial as the initial work on Cerro Prieto well samples.

REFERENCES CITED

Choukroune, P., Francheteau, J., and Le Pichon, X., 1978. In situ structural observations along Transform Fault A in the FAMOUS area, Mid-Atlantic Ridge. Geol. Soc. Amer. Bull., v. 89, p. 1013-1029.

Cotton, M. L., and Vonder Haar, S., 1980. Microfossils from Cerro Prieto geothermal wells, Baja, California, Mexico. Berkeley, Lawrence Berkeley Laboratory, LBL-10303.

de Boer, J., and Vonder Haar, S., 1980. Paleomagnetism of the Quaternary Cerro Prieto, Crater Elegante, and Salton Buttes volcanic cones in the northern Gulf of California rhombochasm. Berkeley, Lawrence Berkeley Laboratory, (in prep.).

Elders, W. A., Rex, R. W., Meidav, T., Robinson, P. T., and Biehler, S., 1972. Crustal spreading in southern California: Science, v. 178, no. 4056, p. 15-24.

Lonsdale, P., and Lawver, L. A., submitted 1979. Submersible study of immature plate boundary zones in the Gulf of California. Geol. Soc. Amer. Bull., 8 p.

Meidav, T. and Howard, J. H., 1979. An update of tectonics and geothermal resource magnitude of the Salton Sea geothermal resource. Transactions, v. 3, Geothermal Resources Council Annual Meeting, 24-27 September 1979, Reno, Nevada, p. 445-448.

Vonder Haar, S. and Howard, J. H., 1978. Geology and geothermal resources of the Salton Trough California in relation to rift zone tectonics; International Symposium on the Rio Grande Rift, Santa Fe, New Mexico. Program and Abstracts Vol., p. 97-99.

Vonder Haar, S. and Puente C., I., 1979a. Fault intersections and hybrid transform faults in the southern Salton Trough geothermal area, Baja California, Mexico. Geothermal Resources Council Annual Meeting, 24-27 September 1979, Reno, Nevada, Transactions, v. 3, p. 761-764.

_____, 1979b. Transform faulting related to geothermal energy in Baja California, Mexico. Geol. Soc. Amer. Annual Meeting, San Diego, Nov. 5-8, Abstracts and Programs, v. 11, no. 7, p. 533.

Vonder Haar, S., Noble, J. E., and Puente C., I., 1979. Vertical movement along the Cerro Prieto transform fault, Baja California, Mexico--A mechanism for geothermal energy renewal. Berkeley, Lawrence Berkeley Laboratory, LBL-8905.

SUBSURFACE GEOLOGY OF THE CERRO PRIETO GEOTHERMAL FIELD

S. P. Vonder Haar, J. Noble, M. T. O'Brien, and J. H. Howard

INTRODUCTION

A subsurface evaluation of the Cerro Prieto geothermal field was undertaken to furnish information for use in reservoir simulation models. Structure, stratigraphy, hydrothermal alteration and reservoir properties were studied. Data used included well logs, well cuttings and cores, and surface geophysical surveys. Detailed information from reports by Elders et al. (1979), and Lyons and van de Kamp (1980), were integrated into ongoing Cerro Prieto geothermal research at LBL. The approach taken in this summary and the concepts developed for Cerro Prieto are applicable to geothermal exploration and reservoir development in other regions.

THIS YEAR'S ACTIVITIES

Structural features at Cerro Prieto are dominated by a major northeast-southwest strike slip fault zone termed the Cerro Prieto Fault (Vonder Haar and Puente, C., 1980) and cross-cutting north-northeast to south-southwest faults. Figure 1 illustrates these faults based on revised interpretations of well log correlations, linear surface features, thermal spring locations, seismic reflection and refraction profiles, and gravity and magnetic maps. Faulting is complex in terms of the history of episodic fault movements. Only dip-slip displacement can be recognized, whereas there may also be a significant lateral component.

A variety of subsurface cross sections have been compiled. One useful style is based on lithofacies analysis (Figure 2) of mechanical well logs in conjunction with cutting and core (Figure 3) descriptions. Based on lithofacies analysis and geochemical data it was possible to delineate densification and hydrothermally altered zones and temperature-sensitive hydrothermal mineral horizons

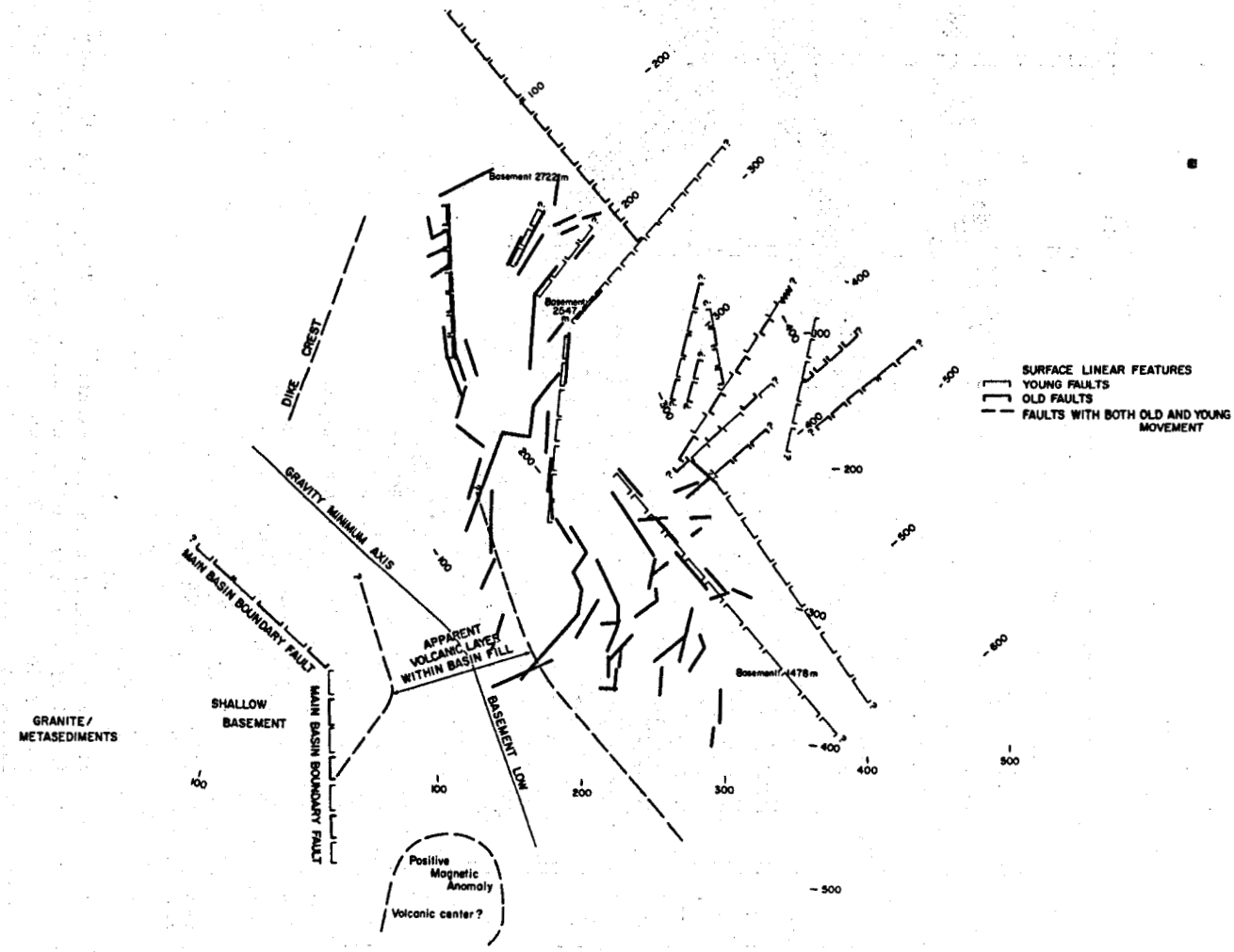

Figure 1. Index map for the Cerro Prieto geothermal field showing wells, faulting, seismic reflection lines and geologic cross sections. (XBL 801-6753)

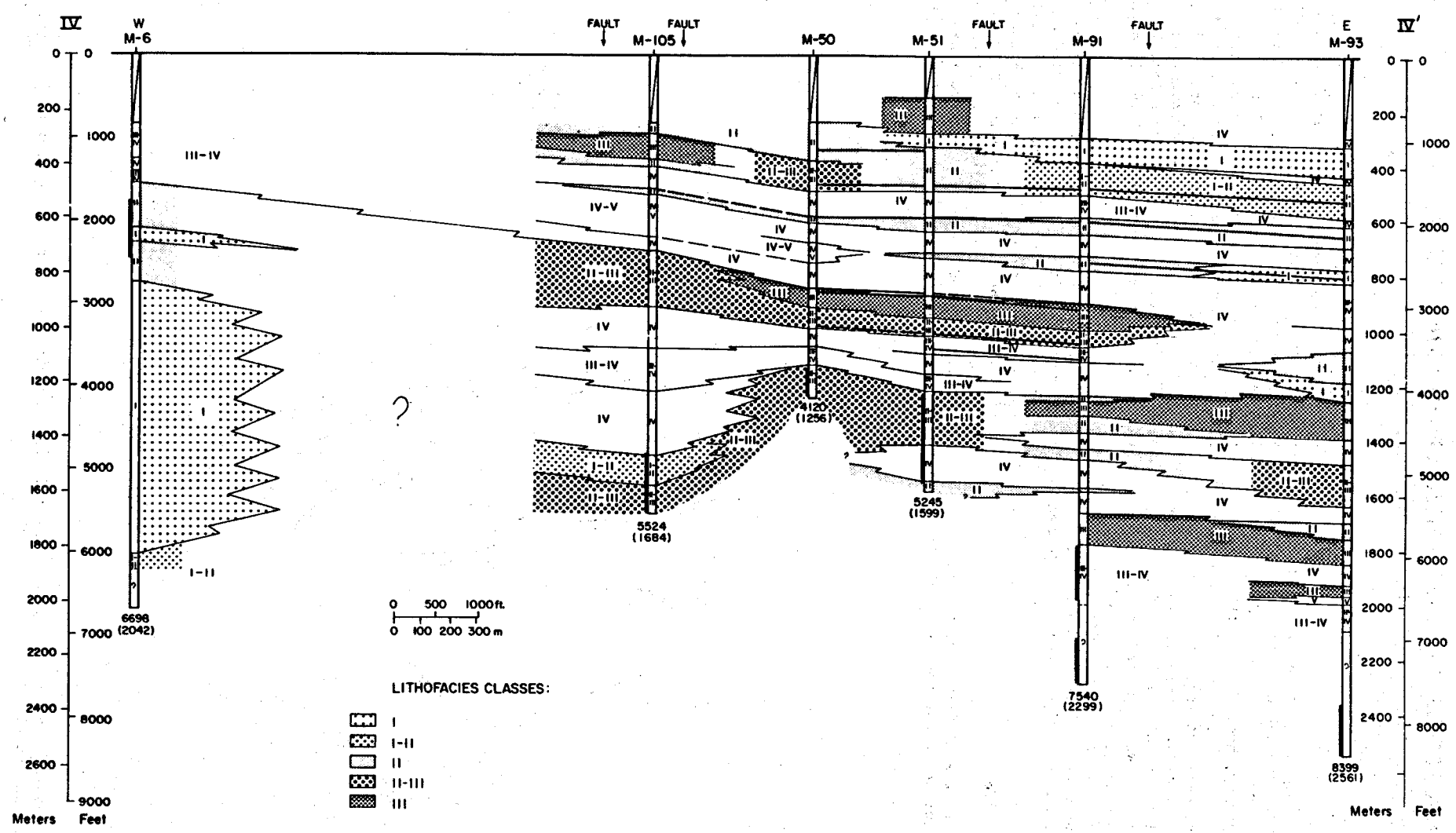

Figure 2. Lithofacies cross-section IV-IV' spanning the southern portion of the geothermal field. Correlation markers in thse deltaic units are sparse. Class I contains approximately 90% sandstone grading down to Class V, which is predominantly siltstones and shales (see Lyons and van de Kamp, 1979).
(XBL 801-6731A)

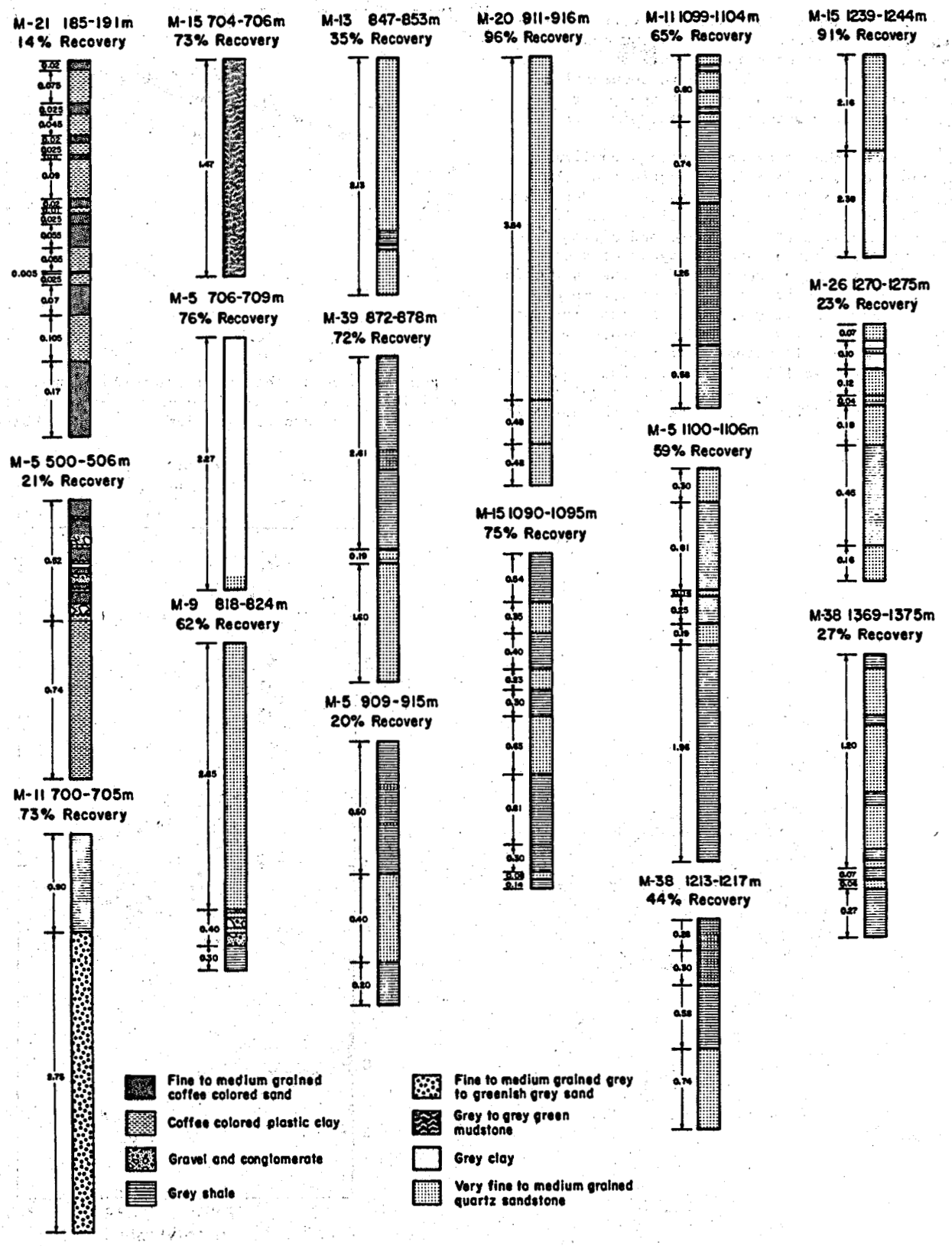

Figure 3. Summary of rock types recovered by coring from Cerro Prieto geothermal wells. Note the abundance of deltaic sandstone and the transition near 700 m depth from sediment to hydrothermally altered rock. Numbers next to the cores, such as 0.62, indicate the length in meters of core pieces recovered. (XBL 7910-13058)

(Figure 4) in order to estimate reservoir temperature and flow characteristics. Contour maps of reservoir properties such as resistivity (Figure 5) are available for use in documenting somewhat subtle shifts in sediment type, porosity and thus fluid flow within the reservoir area.

Studies of the cores and cuttings confirmed the presence of microfossils in portions of the field, as shown in Table 1 (Cotton and Vonder Haar, 1979). In addition to being useful paleoenvironmental indicators, these carbonate and silica fossils substantiate our alteration hypothesis of localized and selective removal of sediments within the densified reservoir units. Secondary porosity is commonplace. Porosity shifts are also apparent in density and porosity versus depth plots as shown in Figure 6. Dramatic visual confirmation of porosity and permeability clogging, using scanning electron microscopy, (Figure 7) has been related to both the x-ray diffraction work and the downhole mechanical properties.

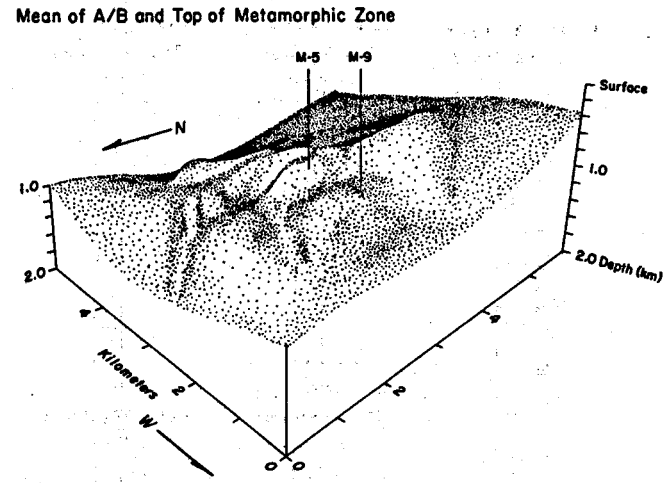

Figure 4. Map of the depth below which shale resistivities exceed 5 ohm-m (top of high-resistivity shales). Contours are in feet. (XBL 801-6723)

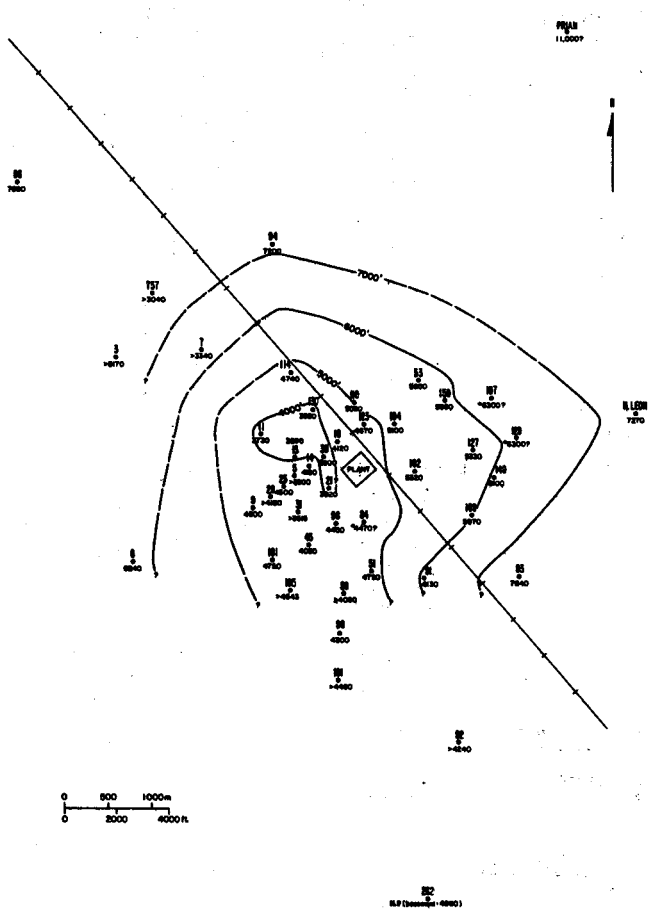

Figure 5. Three-dimensional computer presentation of a capping type domal surface in the Cerro Prieto geothermal field. This surface represents the mean depth of the unconsolidated sediment to rock contact (Puente C. and de la Peña L., 1980); and the top of the metamorphic zone based on hydrothermal mineral alterations (data from Elders et al., 1979). (XBL 803-6851)

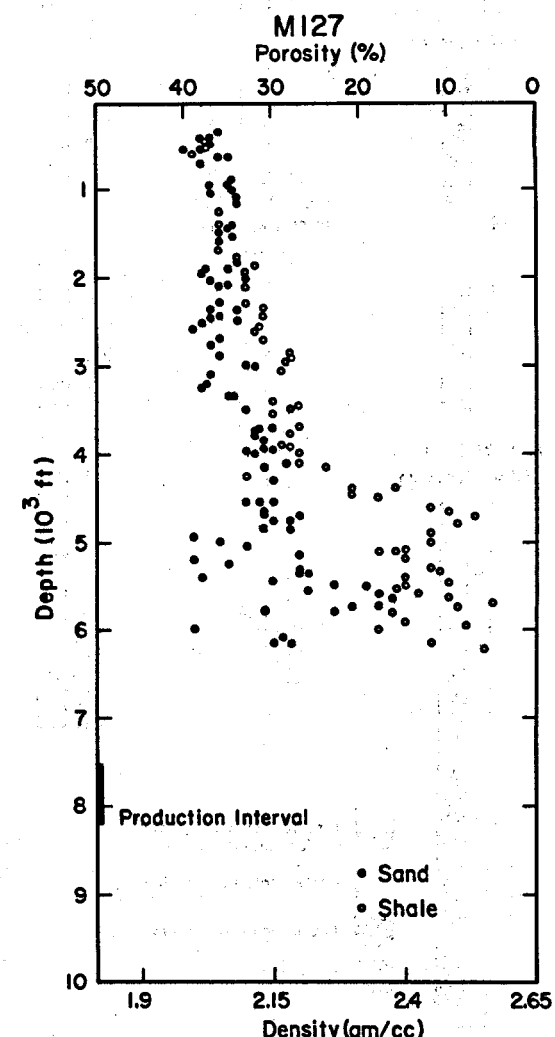

Figure 6. Plot of porosity and density versus depth for well M-127, determined from well logs. Some sandstone porosities in the altered zone at depth are even higher than those above the A/B boundary. These higher porosity sandstones interbedded with metamorphosed, low density shales imply secondary porosity that contributes to the reservoir zone. (XBL 802-6769)

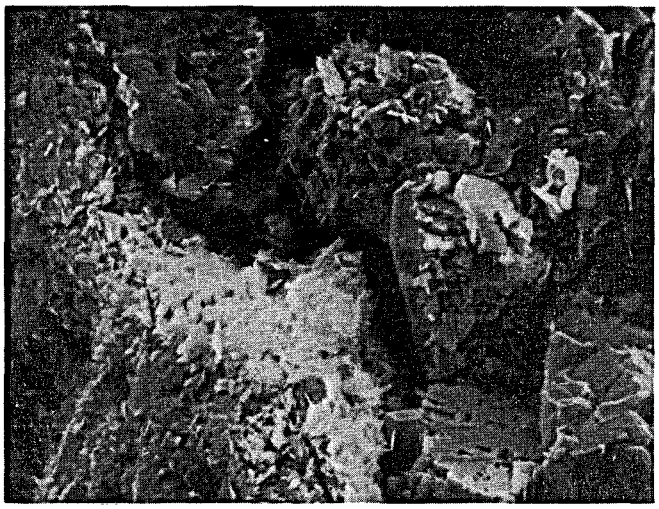

Figure 7. Scanning electron microphotograph of a core chip from well M-38 at 1372 m below the surface; field of view across the photograph is 100 μm (=0.1 mm). This sample lies within the zone of the first occurrence of prehnite (280°C) defined by Elders et al. (1979). Note the variety of clay-like minerals, leached crystal faces and new crystal faces. (XBB 797-9451)

PLANNED ACTIVITIES

In fiscal year 1980, we will clarify geological reservoir features of the Cerro Prieto geothermal field by comparing them with geophysical data and regional groundwater flow concepts. In particular we will relate the role of secondary porosity and deeper fracture flow in metamorphosed deltaic rocks to transmissivity and storativity. A geologic model will be confirmed and tested for prediction of reservoir behavior and production characteristics.

SECONDARY POROSITY STUDIES

Secondary sandstone porosity extends the depth range for effective sandstone porosity far below the depth limit for effective primary porosity. Generation and primary migration of geofluids occurs mainly below the range of effective primary porosity. The path of primary migration and the site of accumulation of geofluids are, therefore, commonly controlled by the distribution of secondary porosity.

The reservoir aspects of fields producing from secondary sandstone porosity more closely resemble carbonate reservoirs than fields with primary sandstone porosity. The distribution of secondary porosity in a sandstone formation may not show a direct relationship with depositional lithofacies or burial history and can be difficult to predict with conventional subsurface methods. However, detailed geologic and petrologic analysis of the factors that control the occurrence of secondary porosity often greatly enhance the understanding and prediction of its distribution. Sandstone reservoirs with secondary porosity have special problems but they also offer special opportunities for both the explorationist and the exploitationist. It is necessary, firstly, to recognize the secondary nature of the porosity of these reservoirs; secondly, to interpret controls and timing of the origin of their porosity; thirdly, to evaluate any factors that may have played a role in preserving this porosity; and fourthly, to survey the existing pore geometry in order to optimize the methods and economics of finding and recovering geofluids.

The detailed analyses of the petrological attributes of secondary porosity will require the use of advanced analytical techniques, such as cathode luminescence petrography, scanning electron microscopy, pore cast examination, microprobe analysis, and stable isotope analysis. In many sandstones, an amount of important information will be obtained simply by careful and methodical use of conventional petrographic microscopy.

The results of these detailed analyses will be integrated into the geologic model of the Cerro Prieto geothermal field.

REFERENCES

Cotton, M. L., and Vonder Haar, S., 1979. Microfossils from Cerro Prieto geothermal wells, Baja California, Mexico. Berkeley, Lawrence Berkeley Laboratory, LBL-10303.

Elders, W. A., Hoagland, J. R., Williams, A., Barker, C., Valette, J. N., and Collier, P., 1979. A study of Cerro Prieto geothermal well samples. University of California Riverside Publication (final report in preparation).

Lyons, D. J., and van de Kamp, P. C., 1980. Subsurface geological and geophysical study of the Cerro Prieto geothermal field. Berkeley, Lawrence Berkeley Laboratory, LBL-10540.

Vonder Haar, S. P., and Puente, C., I., 1980. Fault intersection and hybrid transform faults in the Southern Salton Trough geothermal area, Baja California, Mexico. Trans. Geothermal Resources Council, Annual Meeting, v. 3, 24-27 September, 1979, Reno, Nevada, p. 761-764.

Puente C., I. and de la Peña L., 1979. Geological model of the Cerro Prieto geothermal field, in Proceedings of the Second Symposium on the Cerro Prieto geothermal field. Mexicali, Comisión Federal de Electricidad.

NUMERICAL MODELING STUDIES OF THE CERRO PRIETO RESERVOIR

M. J. Lippmann and K. P. Goyal

INTRODUCTION

The Cerro Prieto geothermal field is presently producing 150 MW of electric power. In April 1979 the capacity of the power plant was doubled (from 75 to 150 MW) as two new units came into operation. Consequently, the fluid production rate has increased from about 2800 to 4200 tonnes per hour. Bermejo et al. (1979) estimate that about 1.2 x 10^8 tonnes of steam-brine mixture has been extracted from the field as of late 1978.

Improved estimates of the total capacity of the field will be essential in studying the feasibility of further developments of the area.

A realistic geohydrological model is of fundamental importance in estimating the capacity and longevity of the Cerro Prieto field. A number of papers presented at the Second Symposium of the Cerro Prieto Field (October 17-19, 1979, Mexicali, Baja California, Mexico) discussed the various efforts under way to establish the dimensions, structure and stratigraphy of the field, the properties and interconnection between the various aquifers, and the circulation of fluid and heat within the geothermal system and across its boundaries.

ACTIVITIES IN FISCAL YEAR 1979

During this year the aim of the modeling studies on the Cerro Prieto field were to determine its preproduction recharge and discharge conditions. As a first step, a simplified geological model of the system was developed on the basis of the available data. Then, the heat and mass flow through this model were calculated numerically using a computer program. The location, temperature and strength of the reservoir recharge and discharge areas, the thermal and hydraulic boundaries of the model, and the properties of the different materials were varied in an attempt to reproduce the preproduction temperatures given by Mercado (1976), and Elders et al. (1978). No efforts were made to match early reservoir pressures since pre-1973 pressure data are only available for few wells in the central part of the field.

The sources and sinks identified by this study could also be used for simulating the behavior of the field after 1973. However, their characteristics would change due to large-scale production. The mass inflow from the sources into the reservoir is expected to increase significantly in this open system and a decrease is anticipated at the sinks due to exploitation. In addition, areas surrounding the producing reservoir are also expected to drain (cold or hot) fluids in response to the changes in the pressure distribution in the field.

Relevant Work

Knowledge about the recharge and discharge characteristics of the field is essential to predict its future behavior. Based on data from recent and earlier studies, zones of recharge and directions of flow of the recharged fluid may be inferred. Unfortunately not all the data point to exactly the same zones and directions.

On the other hand, no precise locations at depth are available for the zones where some of the fluid and heat transported across the geothermal reservoir find their way to the surface. It is safe to say that heat is conducted through the caprock, and that fluids, and heat carried by convection, are discharged to the surface along the main fault zones in the area.

Using well temperatures, pressures, enthalpy, flow data and geothermochemical correlations of the fluids discharged by the wells, Mercado (1976) developed a hydrogeological model of the Cerro Prieto area. He postulated that: (1) hot fluids ascending in the eastern and central zones of the field flow toward the west, (2) the heat source is located in the eastern and deeper part of the field, (3) the reservoir is recharged mainly from the west (in the area of alluvial fans of the Sierra Cucapa) and also to some extent from the east by the underflow of the Colorado River water. Figures 1 and 2 show the preproduction temperature distributions in the field along two different cross-sections (Mercado, 1976).

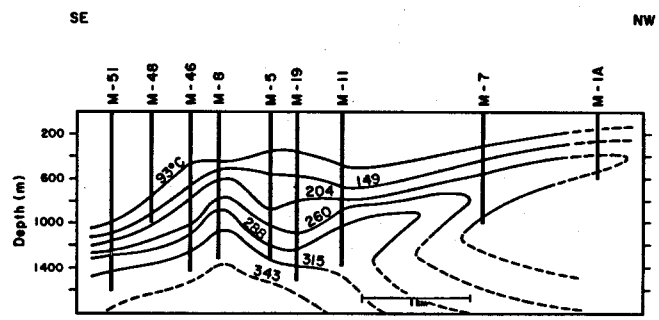

Figure 1. Preproduction temperature distribution in the reservoir along a southeast-northwest cross-section (adapted from Mercado, 1976).

(XBL 804-7028)

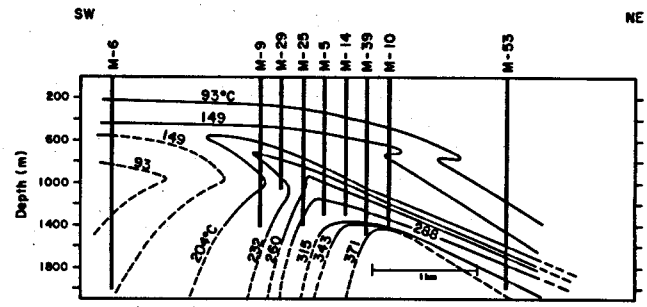

Figure 2. Preproduction temperature distribution in the reservoir along a southwest-northeast cross-section (adapted from Mercado, 1976).

(XBL 804-7027)

According to Truesdell et al. (1979) the comparison of measured deuterium contents of the Cerro Prieto geothermal waters and the interpolated composition of cold Mexicali Valley ground waters suggest that the recharge to the system could have occurred along a narrow zone running from Mexicali on the north, passing just west of the field and curving northeast to the Mesa Arenosa on the east. This recharge from the west agrees with part of Mercado's (1976) model.

Corwin et al. (1979) correlated the dipolar self-potential anomaly detected in the Cerro Prieto area with geothermal activity. They concluded that the surface anomaly could be the result of a vertical fault or fracture zone along which a vertical component of fluid or heat flow exists. Based on these data the hot water upflow zone is distributed along an approximately north-south area passing near well M-48.

Elders et al. (1978) recognized a number of regularly distributed mineral zones in the field by examining cores and drill cuttings. They developed maps indicating depths to the first occurrence of some temperature diagnostic minerals. The mineral distributions suggest that the hottest fluids rose along a north-south trending zone passing near well M-105. This zone is displaced toward the west with respect to the one inferred from the self-potential study (Corwin et al., 1979).

The isotopic and mineralogic data represent the preproduction condition of the system, that is before 1973 when large scale exploitation of the field began.

Numerical Computer Program and Methodology

The numerical computer code CCC developed at Lawrence Berkeley Laboratory was used in these studies. The program solves the heat and mass flow equations for liquid saturated media. Details on the Integrated Finite Difference Method, and on the explicit-implicit iterative procedure used in this program, are given elsewhere (Edwards, 1972; Narasimhan and Witherspoon, 1976; Lippmann et al., 1977).

In all cases the numerical computations were run until a steady-state pressure and temperature distribution was obtained in the simulated system. The computed temperatures were then compared with Mercado's (1976) temperature distributions (Figures 1 and 2).

Using these comparisons as a guide, the characteristics of the sources, sinks, and boundary conditions were modified to improve the match. The changes were not arbitrarily made but were based on available geological and reservoir engineering information.

A number of different models were used to reproduce Mercado's preproduction temperature distributions. Only the results of two of the cases studied will be discussed here. As will be shown, it was not possible to reach good agreements. We suspect that the simplified geological model and boundary conditions used in the simulations were responsible for some of the poor matches obtained.

Recent studies (Lyons and Van de Kamp, 1980) indicate that the lithology of the field is quite complex, with lithofacies changes controlling largely the fluid flow within the system.

Geological Model

Using the information available in mid-1979, a simplified geological model of Cerro Prieto was developed for use in simulations. The faults believed to be bounding and intersecting the area initially developed by CFE (Cerro Prieto I) are shown on Figure 3. Based on these data, the region modeled to reproduce the preproduction conditions of the field was restricted to the area indicated on Figure 4.

Basically, the lithologic column introduced by Abril and Noble (1979) was incorporated in the model (Figure 5). According to them in this area the column may be subdivided into three units. The upper one (Unit A) consists of unconsolidated sediments, the middle one (Unit B) of consolidated materials, and the lower one (Unit C) of granodioritic and metamorphic rocks. Unit A acts as the leaky caprock of the geothermal system, while Unit C constitutes its impermeable bedrock. Unit B, overlying the basement formed by alternating sandstone and shale layers, can be divided into five major subunits.

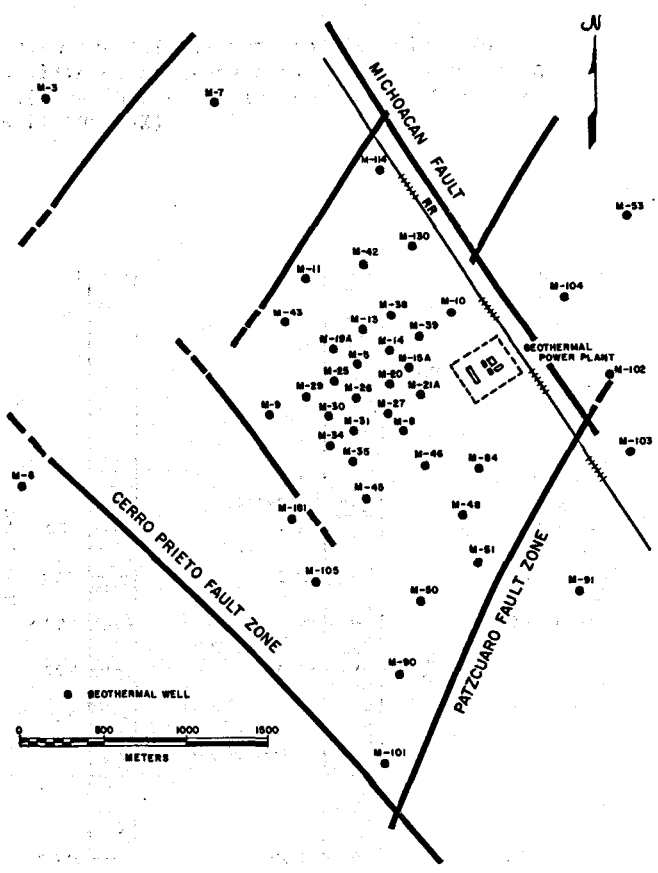

Figure 3. Fault map for the area initially developed at Cerro Prieto (from Vonder Haar and Howard, 1980). (XBL 804-7025)

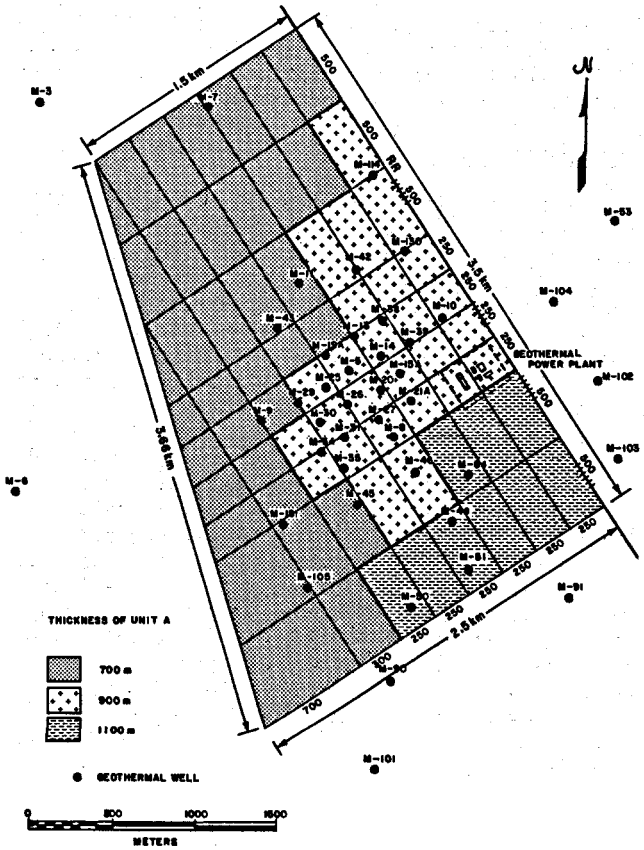

Figure 4. Plan view of the area modeled and mesh used. Contrasting hatchings correspond to different thicknesses of Unit A (unconsolidated sediments). (XBL 799-11561)

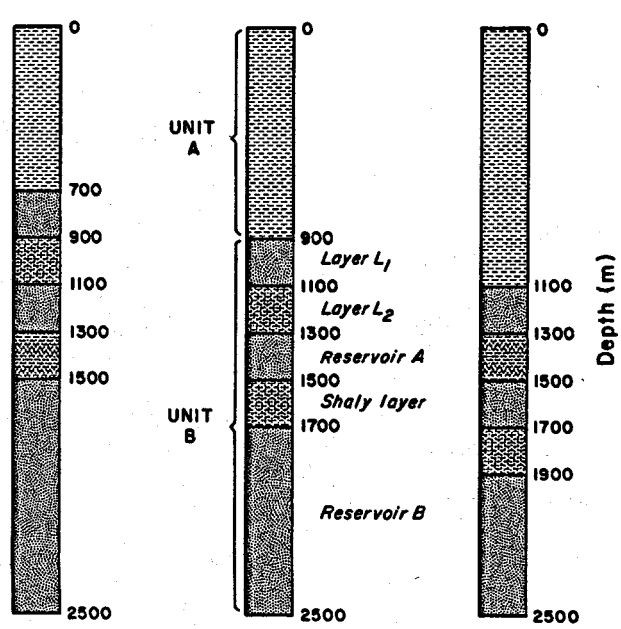

Figure 5. Basic lithologic columns used in the model for the areas with different Unit A thicknesses (see Figure 4). (XBL 7910-13037)

The top layer L_1 consists of sandstone lenses and shales. Below Layer L_1 is Layer L_2, which is characterized by rocks with high content of carbonate cement. The underlying sandy strata, separated by a shaly layer, are the main geothermal reservoirs A and B at Cerro Prieto.

The total thickness of the sedimentary column varies within the Cerro Prieto field. The depth to the block-faulted basement increases significantly towards the east (Fonseca and Razo, 1980). For simulation purposes the top of the bedrock was assumed to be at a constant depth of 2500 m throughout the modeled area.

An isopach map of Unit A, based on data provided by CFE, is given in Figure 6. For the simulations the variable thickness of this unit was modeled as shown in Figure 4. By assuming constant thicknesses for the different subunits of Unit B, three basic lithologic columns were used in the model (Figure 5). It is believed (A. Mañon, personal communication) that in the central part of the Cerro Prieto I area there is preferential fluid movement in a northeast-southwest direction due to presence of more permeable facies or highly fractured rocks. This feature was incorporated in the model as discussed below.

Mesh Used in the Simulations

The three-dimensional region studied was subdivided into 560 nodes (or elements). The vertical column, 2500 m thick, was subdivided into

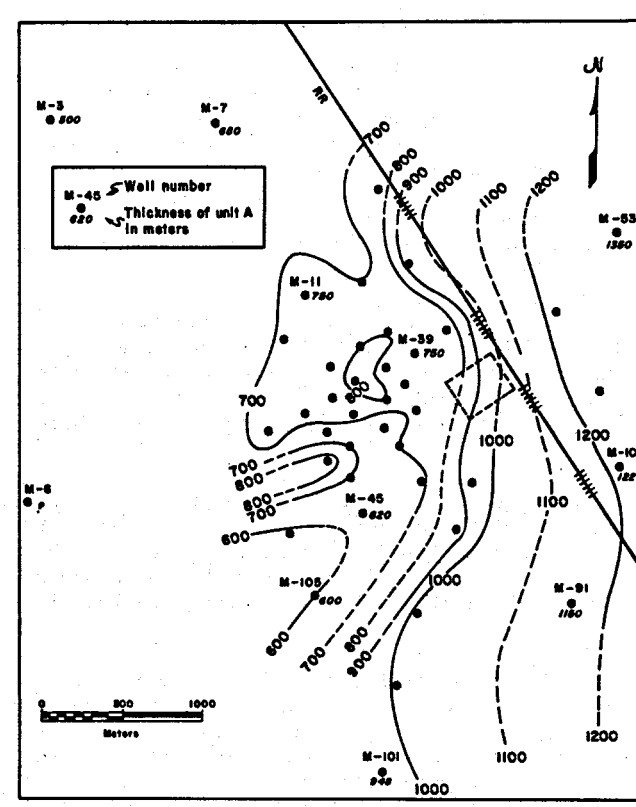

Figure 6. Unit A isopach map. (XBL 804-7026)

8 horizontal levels (each having 70 nodes). The lowest level (100 level) is 600 m thick, above it the 200 to 700 levels each 200 m thick, and the upper level (800 level) is 700 m thick. The different thicknesses were needed to account for the different lithologic columns used in the model (Figure 5).

Figure 7 depicts the numbering used for the nodes in the 400 level, a similar numbering scheme was used in the other levels. In this three-digit system, the first digit represents the level, while the number of the node is represented by the other two. Thus, node 818 lies in the 800-level layer and is vertically above nodes 118, 218, 318, 418, 518, 618, and 718. In the horizontal plane, its shape is exactly the same as that of node 418. Figure 7 shows the northeast-southwest trending high permeability area, representing a coarser facies or a fractured zone in the field. The higher permeable material was restricted to the 400 level only.

Boundary and Initial Conditions

Boundary conditions that have to be specified in the model are: (1) type of boundaries whether open or closed to heat and mass flow, (2) temperatures and pressures at the boundaries, (3) location and strength of sources and sinks, and (4) temperature of fluid entering the system.

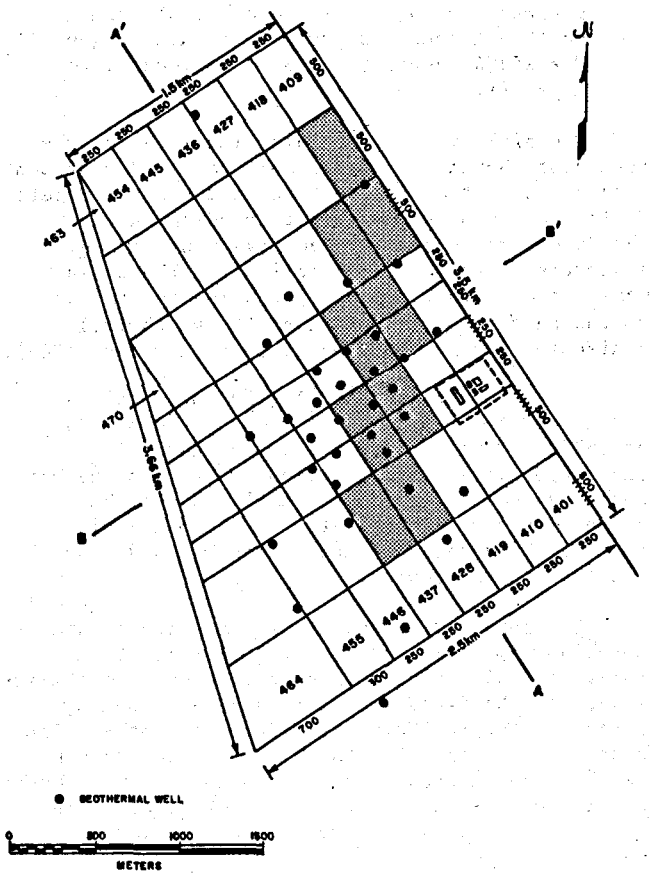

Figure 7. Plan view of the mesh used in the computations. Hatched area indicates an area of higher permeability in the 400 level (1400 m depth). Node numbering for the 400 level, and the location of the A-A' and B-B' cross-sections are also shown. (XBL 799-11558A)

In the various models developed for the Cerro Prieto I area most of these conditions were varied to study their effect on the preproduction temperature distributions. However, in both cases discussed here we made the following assumptions. (1) The inflow and outflow of fluids into and from the region were modeled by placing sources and sinks in some nodes located at the boundaries (i.e., near geologic faults). (2) All vertical boundaries were closed to heat flow. (3) The top and bottom boundaries were held at constant temperatures. The top surface was assumed to be at 25°C; the bottom at 150°C. (4) The total mass flow rate across the model (from the sources towards the sinks) was arbitrarily assumed to be 2.95×10^7 kg/day. This rate is about 2.15 times the preproduction discharge of the surface manifestations in the area as reported by Mercado (1968). We considered that before 1973 a significant fraction of the heat and mass inflow into the geothermal field rose to the surface mainly through the fault zones.

Hydrostatic pressure and linear temperature-depth distribution were used as initial conditions for the system.

Fluid and Rock Properties

We assumed that (1) the fluid in the system was liquid and had constant properties, and (2) the properties of the solid matrix are isotropic and constant.

For the fluid, we used pure water properties at 250°C. The solid matrix properties are given in Table 1 and are representative of the different lithologies included in the model.

No temperature or pressure dependency of the properties was used to reduce the cost of computations, because we felt that this simplification would not significantly affect the computed steady state temperature distributions. We planned to include temperature and pressure dependencies once an acceptable match between computed and Mercado (1976) temperatures was obtained.

Model 1

In model 1 and in the one discussed later, we considered that the recharge and discharge areas were closely associated with the bounding faults. We assumed the inflow of fluids into the system to be distributed as follows (Table 2):

1. 22% of the total mass recharge is at 350°C. The sources are located in the lower part of Reservoir B (100 level), near the intersection of the Michoacán and Pátzcuaro faults (Figure 3).

2. 61% of the recharge comes from colder water sources located in the upper part of Reservoir B (levels 200 and 300, at 208°C and 188°C, respectively), near the southwest region of the system, along the Cerro Prieto fault zone.

Table 1. Properties used for the solid matrix.

Material	Density (kg/m^3)	Heat capacity ($J/kg \cdot {}^oC$)	Thermal cond. ($J/m \cdot day \cdot {}^oC$)	Intrinsic permeability (md)	Porosity
Unit A	2500	935	1.92×10^5	10^{-3}	0.20
Layer L_1	2650	825	2.8×10^5	20	0.10
Layer L_2	2700	860	1.85×10^5	5	0.10
Reservoir A	2650	825	2.8×10^5	50	0.10
Shaly layer	2700	860	1.85×10^5	5	0.10
Reservoir B	2650	825	2.8×10^5	80	0.10
Highly permeable	2650	825	2.8×10^5	100	0.10

Table 2. Model 1, locations and characteristics of sources and sinks.

SOURCES

Node	Mass flow rate (kg/day)	Temperature (°C)
101	2.5×10^6	350
110	2.5×10^6	350
119	1.5×10^6	350
264	2.5×10^6	208
265	2.5×10^6	208
266	1.5×10^6	208
267	1.5×10^6	208
268	1.0×10^6	208
364	2.5×10^6	188
365	2.5×10^6	188
366	1.5×10^6	188
367	1.5×10^6	188
368	1.0×10^6	188
608	5.0×10^6	250

SINKS

Node	Mass flow rate (kg/day)	Node	Mass flow rate (kg/day)
527	1.00×10^6	727	1.00×10^6
536	1.00×10^6	736	1.00×10^6
545	1.00×10^6	745	1.00×10^6
554	1.00×10^6	754	1.00×10^6
562	2.00×10^6	762	2.00×10^6
563	0.50×10^6	763	0.50×10^6
564	3.50×10^6	764	3.50×10^6
565	2.75×10^6	765	2.75×10^6
566	2.00×10^6	766	2.00×10^6

3. 17% of inflow of fluid is concentrated at the intersection of the Michoacán fault and a northeast-southwest trending fault (Figure 3). The 250°C source (node 608) is located in Layer L_1.

The sinks where the fluids leave the system were distributed around its northwest and southwest corners, near the intersection of the Cerro Prieto fault and northeast-southwest trending faults. The discharge occurs through Layers L_1 and L_2, at levels 700 and 500 respectively. The sinks were arranged in a manner approximately similar to the surface distribution of the geothermal manifestations in the area given by Mercado (1968).

The bottom of the model (2500-m depth) was considered to be a constant temperature boundary at 150°C. This low value was used to duplicate the temperatures of the regions away from the hot recharge zones. Around the inflow zones the temperatures near the bottom of the model will be reflecting those of the recharge fluids and not that of the boundary.

The computed steady-state temperatures are described by various temperature distribution maps. The effect of sources and lower permeability layers on the fluid flow can be established by analyzing the isotherms at different depths. The hotter waters entering the system at the deeper levels move in response to the pressure distribution resulting from the sources and sinks located in the model; it tends to move around the less permeable layers.

The isotherms at 1000 m (600 level) and 1400 m (400 level) are given in Figures 8 and 9, respectively. In Figure 8 the 250°C isotherm in the northeast part reflects the effect of the source in node 608. The high temperatures in the south-central part of the system are caused by the hot

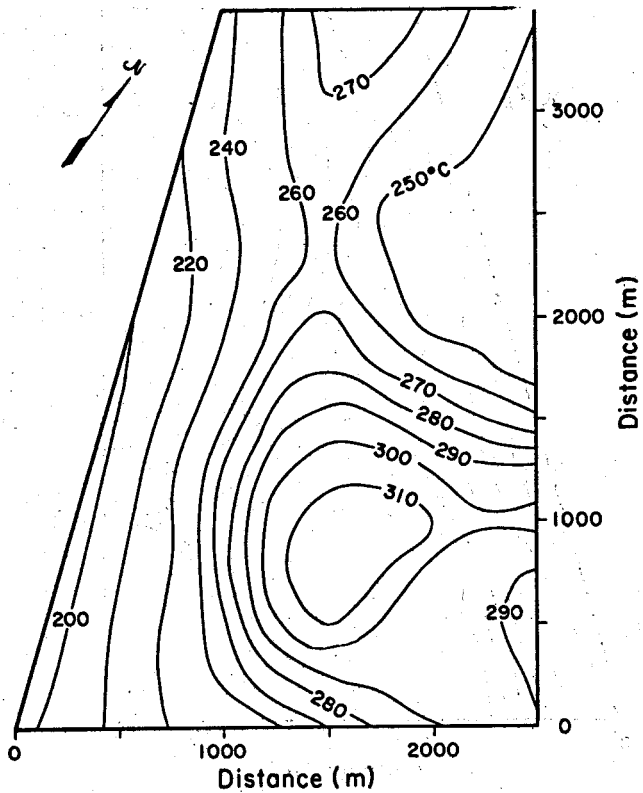

Figure 8. Model 1. Isotherms at the 600-level (1000-m depth). (XBL 804-7033)

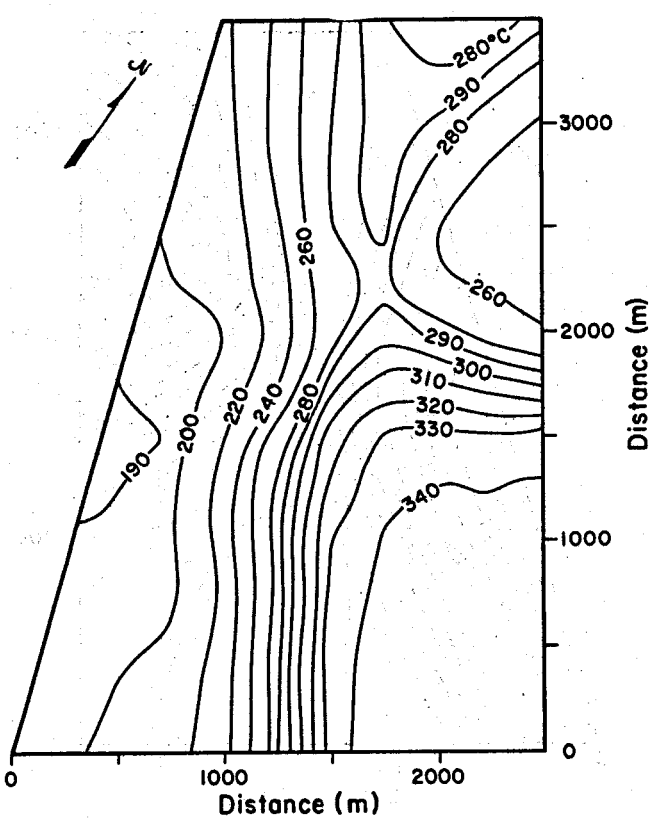

Figure 9. Model 1. Isotherms at the 400-level (1400-m depth). (XBL 804-7034)

water rising from beneath. In Figure 9, the isotherms in the southeast corner indicate the movement and cooling of the water as it flows away from the 350°C sources. The 190°C isotherm toward the west shows the influence of 188°C sources located in the 300 level; the 260°C isotherm towards the northeast shows that of 250°C sources in the 600 level.

The calculated temperatures along the sections A-A' and B-B' are shown in Figures 10 and 11. These plots, when compared with the temperatures given in Figures 1 and 2, indicate that in the southeast-northwest section, the computed temperatures are higher everywhere except in the area near the center of Figure 10. In this region the temperatures seem to be dominated by the strength and temperatures of the sources located at the southeast corner of the field. A comparison of Figures 2 and 11 indicates that the temperatures match favorably near well M-9 and in the central part of the field. Generally the calculated temperatures are higher than those of Mercado.

Model 2

To obtain a better match, the sources in the 100-level were displaced toward the southwest corner of the system, the 200-level sources were taken out, and their flow rates were added to those at the 100 level. The temperature of the sources at the 300 and 600 levels were changed to 200°C (Table 3). The sinks in this model were assumed to be equal to those in Model 1 (Table 2). The temperature of the lower boundary was again fixed at 150°C.

Isotherms at 1000- and 1400-m depths (600 and 400 levels) are given in Figures 12 and 13. Temperatures have changed with respect to those of Figures 8 and 9 in response to the change of source characteristics.

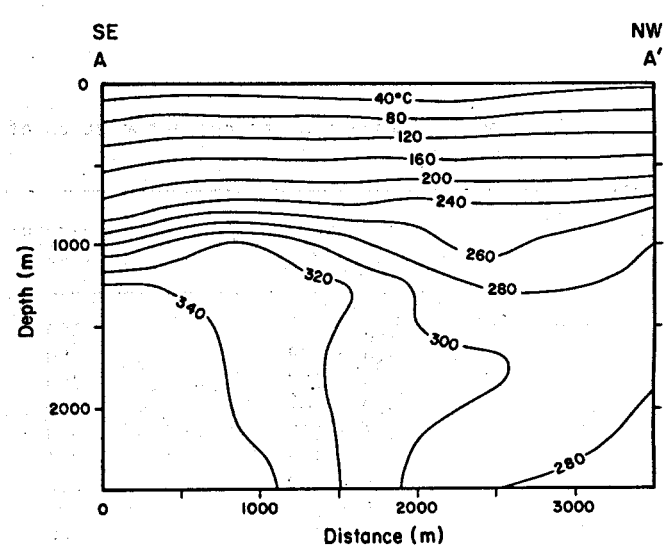

Figure 10. Model 1. Temperature distribution along the A-A' cross-section. (XBL 804-7037)

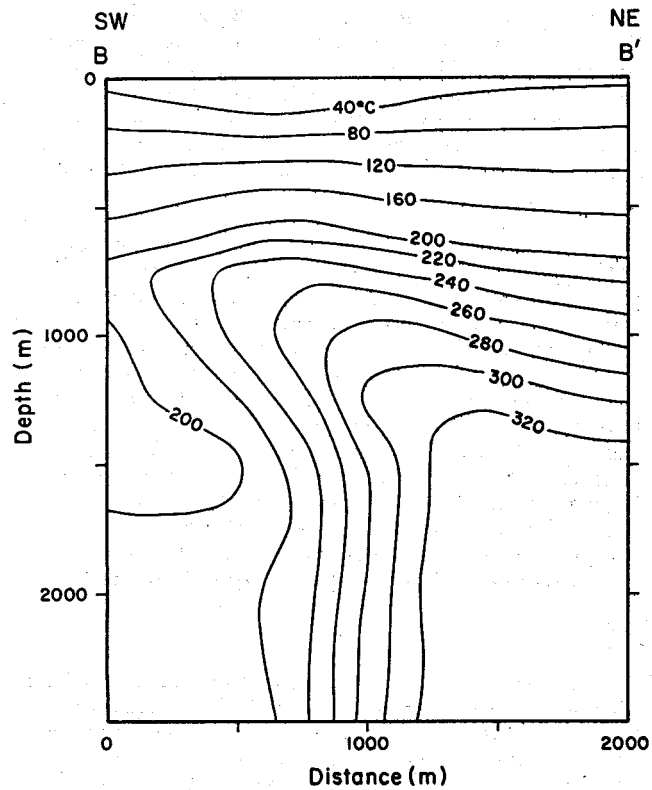

Figure 11. Model 1. Temperature distribution along the B-B' cross-section. (XBL 804-7032)

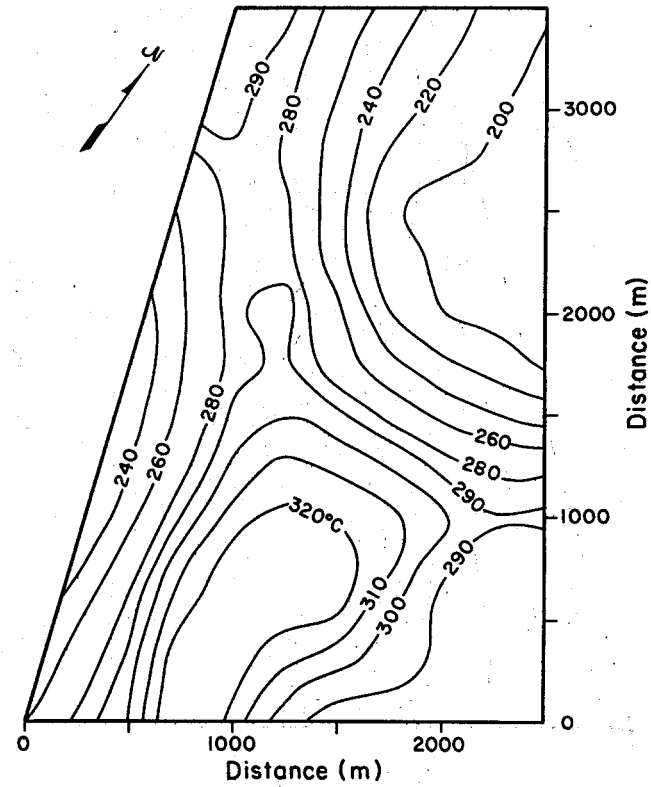

Figure 12. Model 2. Isotherms at the 600 level (1000-m depth). (XBL 804-7035)

Isotherms along section A-A' are shown in Figure 14. A comparison with Figure 1 indicates that the calculated temperatures at well M-8 are close to Mercado's. Temperatures in the central part of Figure 14 also match favorably those in Figure 1. The calculated temperatures are sligthly higher in the southeastern part of the field. Isotherms along section B-B' are shown in Figure 15.

Table 3. Model 2, location and characteristics of sources.

Node	Mass flow rate (kg/day)	Temperature (°C)
128	2.5×10^6	350
137	3.0×10^6	350
146	3.0×10^6	350
155	3.0×10^6	350
164	2.5×10^6	350
165	1.5×10^6	350
364	2.5×10^6	200
365	2.5×10^6	200
366	1.5×10^6	200
367	1.5×10^6	200
368	1.0×10^6	200
608	5.0×10^6	200

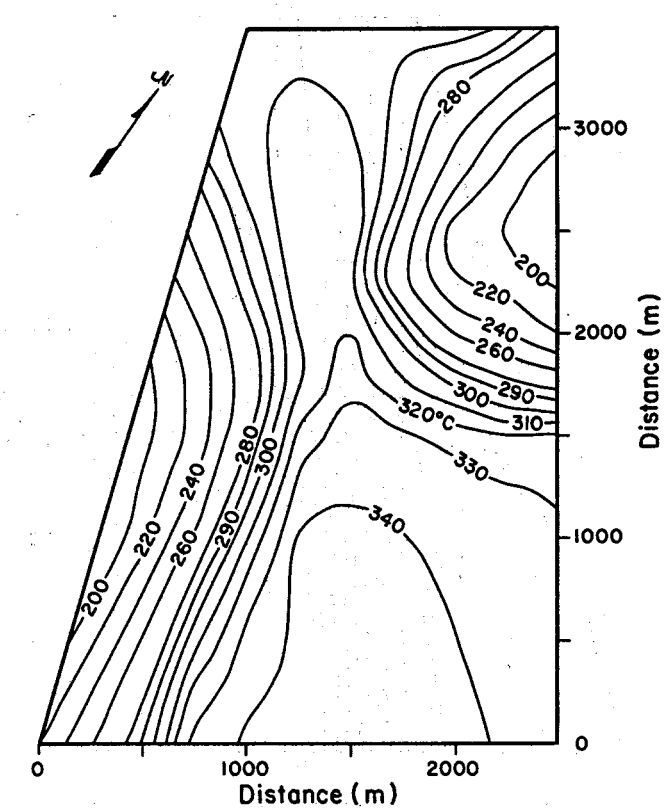

Figure 13. Model 2. Isotherms at the 400 level (1400-m depth). (XBL 804-7036)

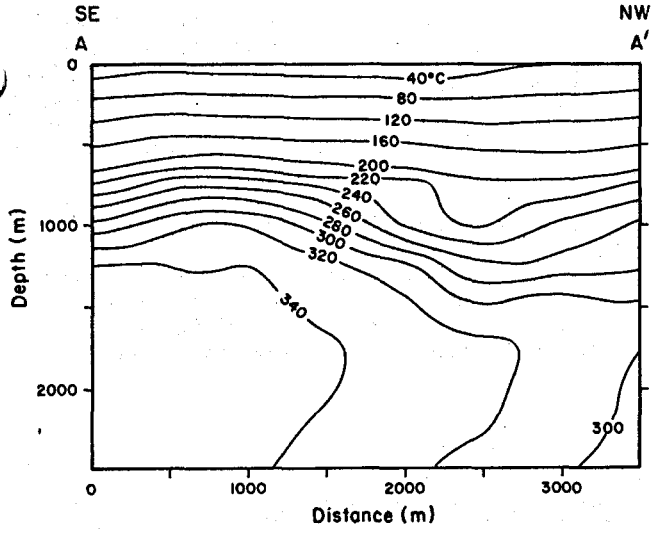

Figure 14. Model 2. Temperature distribution along the A-A' cross section. (XBL 804-7030)

A comparison of these temperatures with those in Figure 2 shows that the calculated temperatures are, in general, higher than the preproduction temperatures given by Mercado (1976).

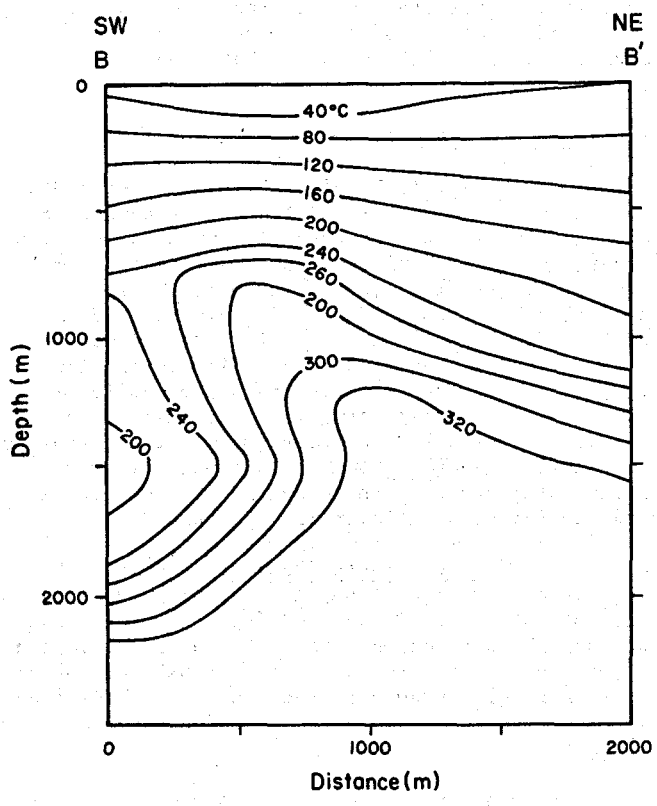

Figure 15. Model 2. Temperature distribution along the B-B' cross section. (XBL 804-7029)

PLANNED ACTIVITIES FOR FISCAL YEAR 1980

In order to establish the preproduction recharge and flow characteristics of the Cerro Prieto field, more temperature and early pressure data will be obtained. The geological model of the field to be used in the computations will be modified based on new information expected to become available during fiscal year 1980.

A three-stage program in reservoir modeling of the field response to large-scale fluid production (started in 1973) will be initiated. It will begin with the simulation of the initial production area, working up to a simulation of the entire known Cerro Prieto geothermal field.

REFERENCES CITED

Abril G., A., and Noble, J. E., 1979, Geophysical well-log correlations along various cross-sections of the Cerro Prieto geothermal field, in Proceedings, First Symposium on the Cerro Prieto geothermal field, Baja California, Mexico, September 1978. Berkeley, Lawrence Berkeley Laboratory, LBL-7098, p. 41-48.

Bermejo M., F., Cortéz A., C., and Aragón A., A., 1979. Physical and thermodynamic changes observed in the Cerro Prieto geothermal reservoir, in Proceedings, First Symposium on the Cerro Prieto geothermal field, Baja California, Mexico, September 1978. Berkeley, Lawrence Berkeley Laboratory, LBL-7098, p. 300-332.

Corwin, R. F., Morrison, H. F., Díaz, C. S., and Rodríguez B., J., 1979. Self-potential studies at the Cerro Prieto geothermal field, in Proceedings, First Symposium on the Cerro Prieto geothermal field, Baja California, Mexico, September 1978. Berkeley, Lawrence Berkeley Laboratory, LBL-7098, p. 204-210.

Edwards, A. L., 1972. TRUMP: A computer program for transient and steady state temperature distribution in multidimensional systems. Livermore, Lawrence Livermore Laboratory, UCRL-14754, Rev. 3.

Elders, W. A., Hoagland, J. R., Olson, E. R., McDowell, S. D. and Collier, P., 1978. A comprehensive study of samples from geothermal reservoirs: Petrology and light stable isotope geochemistry of twenty-three wells in the Cerro Prieto geothermal field, Baja California, Mexico. Riverside, University of California, UCR/IGPP-78/26.

Fonseca L., H., and Razo M., A., 1980. Gravimetric magnetometric and seismic reflection studies at the Cerro Prieto geothermal field, in Proceedings, Second Symposium on the Cerro Prieto Geothermal Field, Baja California, Mexico, October 1979. Mexicali, Comisión Federal de Electricidad (in preparation).

Lippmann, M. J., Tsang, C. F., and Witherspoon, P. A., 1977. Analysis of the response of geothermal reservoirs under injection and production procedures: Dallas, Society of Petroleum Engineers, SPE-6537.

Lyons, D. J., and van de Kamp, P. C., 1980. Subsurface geological and geophysical study of the Cerro Prieto geothermal field: Berkeley, Lawrence Berkeley Laboratory, LBL-10540.

Mercado G., S., 1968. Localización de zonas de máxima actividad hidrotermal por medio de

proporciones químicas, campo geotérmico de Cerro Prieto B. C.: Presented at the III Congreso Mexicano de química pura y aplicada March 21-23, 1968, Guadalajara, México.
____, 1976. Movement of geothermal fluids and temperature distribution in the Cerro Prieto geothermal field, Baja California, Mexico, in Proceedings, Second United Nations Symposium on the Development and Use of Geothermal Resources, May 1975: Washington, D.C., U.S. Government Printing Office, v. 1, p. 487-494.
Narasimhan, T. N., and Witherspoon, P. A., 1976. An integrated finite difference method for analyzing fluid flow in porous media: Water Resources Research, v. 12, no. 1, p. 57-64.
Truesdell, A. H., Rye, R. O., Pearson, F. J., Jr. Olson, E. R., Nehring, N. L., Huebner, M. A., and Coplen, T. B., 1979. Preliminary isotopic studies of fluids from the Cerro Prieto geothermal field, in Proceedings, First Symposium on the Cerro Prieto geothermal field, Baja California, Mexico, September 1978; Berkeley, Lawrence Berkeley Laboratory, LBL-7098, p. 95-99.
Vonder Haar, S., and Howard, J. H., 1980. Intersecting faults and sandstone stratigraphy at the Cerro Prieto geothermal field. Berkeley, Lawrence Berkeley Laboratory, LBL-9546.

SIMULATION OF REINJECTION AT CERRO PRIETO USING AN IDEALIZED TWO-RESERVOIR GEOLOGICAL MODEL

C. F. Tsang, D. C. Mangold, and M. J. Lippmann

INTRODUCTION

Most of the papers published on the hydrodynamic and thermal effects of reinjection in geothermal fields assume a single reservoir with uniform transmissivity and storativity. However, there is evidence that the Cerro Prieto geothermal field is a two-reservoir system and that each reservoir has different hydraulic properties (Abril and Noble, 1979). Since the case of two-reservoir fields has not been adequately studied, the present research attempts to analyze the thermohydrological response of this kind of geothermal system to various alternative schemes of reinjection. Parameters relevant to the Cerro Prieto system are used so that the results will be useful in the planning of future reinjection operations at this field.

ACTIVITIES IN FISCAL YEAR 1979

In the present analysis LBL computer program CCC (Lippmann et al., 1977) is used, which is capable of modeling the complex geological and boundary conditions of a geothermal system. CCC also simulates the major physical factors involved in the movement of the injected waters: (1) forced convective flow between the production and injection areas; (2) heat exchange among injected water, rock matrix, and native waters; (3) density-buoyancy effects, and (4) influence of temperature-dependent viscosity on fluid flow. But the problems associated with the chemistry of the fluids and the porous media, such as injectibility of the wells, injected/native groundwater compatibility, and water-rock interactions, will not be covered here. These matters are addressed in a number of other papers at the second Cerro Prieto symposium.

Reinjection Modeling

In any type of modeling study we may distinguish two broad categories: special studies and detailed simulations. In the case of reinjection, special studies investigate particular topics of interest, such as optimal injection well patterns and the effects of temperature-dependent properties (e.g. Tsang et al., 1979). On the other hand, detailed simulation studies are appropriate only after a realistic geologic model of the system (i.e. its geometry, physical properties, boundary and initial conditions) is developed. In this general framework, we address a special study of reinjection operations in a geothermal field. The study is concerned with the peculiarities of carrying out this type of operation in a system consisting of two separate reservoirs. One particular purpose for employing in this research a simpler idealized model is to begin to determine the best strategies for reinjection so that they can be tested later in more realistic simulations.

Two-Reservoir Systems

1. Single Well Model. The simplified radially symmetric two-reservoir model used for this case with its initial temperature distribution is shown in Figure 1. The reservoir hydraulic and thermal properties are displayed in Table 1. These data are all taken from an earlier simulation study of Cerro Prieto (Lippmann et al., 1979). Note from the table that the permeability in the lower aquifer is 80 md whereas in the upper aquifer it is 50 md. The intervening layer has a permeability of 0.5 md, which is two orders of magnitude smaller, but still not negligible. For simplicity, the aquifers are assumed to be uniformly 100 m thick and the intervening layer is 50 m thick.

a. Pressure effects (production only). In this series of simulations a constant production rate of 1000 m^3/hr is assumed (approximately 40% of the 1978 production rate at Cerro Prieto). The injection rate is at 500 m^3/hr, one-half of the production rate. Three different boundary conditions were employed to study pressure effects during production.

The open boundary case corresponds to an aquifer of large radial extent, with a constant potential boundary simulating "full" recharge conditions 2.3 km away from the well. The semi-open boundary case had a leaky flow barrier at the same distance

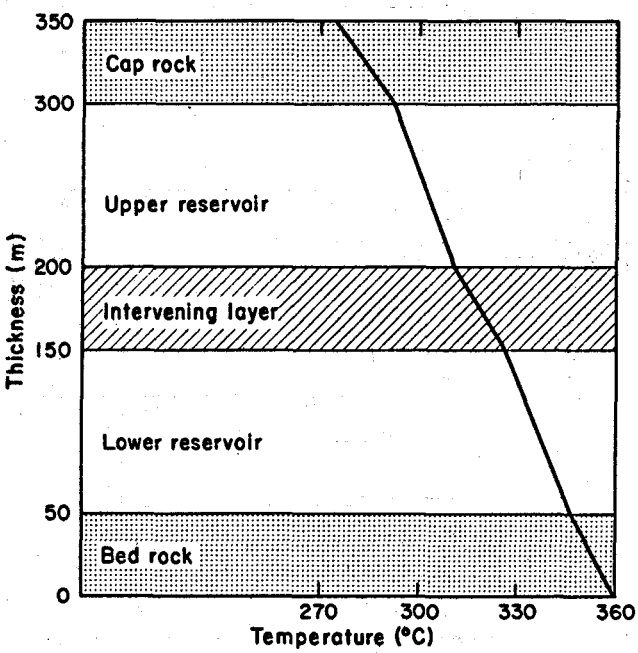

Figure 1. Cross section of the two-reservoir model used and its initial temperature profile. (XBL 803-6829)

to simulate "partial" recharge. The closed boundary case was used as a limiting case, with no recharge through the barrier. The letters A, B, and C on Table 2 are the locations where temperature and pressure were determined as the upper aquifer was produced: A is near the well in the upper aquifer, and B and C are 100 m away from the well in the upper and lower aquifers, respectively.

The results of the simulations for 5 and 10 years are displayed in Table 2. In comparing pressure reductions for the upper and lower aquifers at either 5 or 10 years, the results show maximum differences of only 13% after 5 years, and 10% after 10 years. This demonstrates considerable hydraulic communication through the intervening layer. The results also show the effect of boundary conditions.

b. Temperature effects (injection). In Figures 2 and 3 the temperature fronts are indicated for injection into the upper and lower aquifer after 10 years, respectively. The open boundary or "full" recharge condition was employed. In the upper aquifer case the thermal front has begun to penetrate through the intervening layer due to the downward flow of the higher-density-injected cold water. In the lower aquifer case there is some dispersion of the thermal front within the aquifer, but with little effect on the intervening layer. This is encouraging, because it shows that thermal fronts do not easily migrate through the intervening layer.

Table 1. Material properties used in the single-well and doublet simulations.

Property	Lower reservoir	Intervening layer	Upper reservoir	Bedrock/ Caprock
Intrinsic permeability (md)	80	0.5	50	0.005
Porosity	0.22	0.40	0.20	0.40
Specific storage (m^{-1})	10^{-4}	1.6×10^{-3}	10^{-4}	1.6×10^{-3}
Thermal conductivity (cal/sec·cm°C)	10×10^{-3}	7.5×10^{-3}	10×10^{-3}	6.0×10^{-3}
Heat capacity (cal/g°C)	0.250	0.230	0.250	0.230

Table 2. Pressure drawdowns for the single well production simulations.

Case	Pressure drawdowns (psi) 1 to 5 yrs	1 to 10 yrs
At Point A		
Open	36	40
Semi-open	38	61
Closed	39	64
At Point B		
Open	36	40
Semi-open	38	61
Closed	39	64
At Point C		
Open	32	36
Semi-open	33	58
Closed	35	61

The box below the thermal front diagrams in Figures 2 and 3 records pressure changes in the upper and lower aquifers, respectively, at radial distances of 500 m and 1000 m. These pressures agree with the results of the production tests mentioned above. Despite the much lower permeability of the intervening layer, pressures are readily transmitted through it from the injected reservoir to the other reservoir. This indicates that reinjection may be useful to maintain overall reservoir pressures even through an intervening layer which inhibits or slows down thermal fronts, thereby prolonging the useful life of a geothermal field.

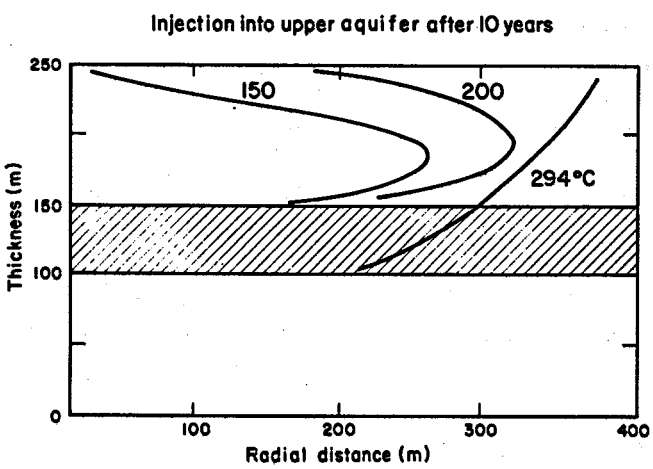

Pressure increase (psi) measured at

Aquifer	500m	1000m
Upper	54	19
Lower	33	22

Figure 2. Isotherms and pressure changes simulated for 10 years of single-well injection into the upper reservoir. (XBL 803-6833)

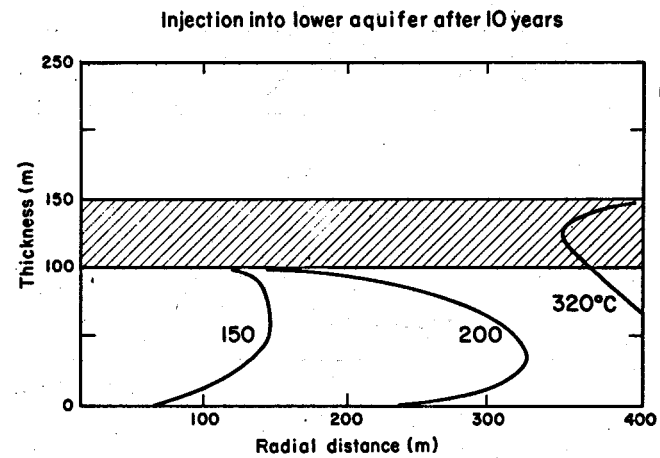

Pressure increase (psi) measured at

Aquifer	500m	1000m
Upper	16	9
Lower	54	28

Figure 3. Isotherms and pressure changes simulated for 10 years of single-well injection into the lower reservoir. (XBL 803-6835)

2. Doublet Model. As a further development in modeling reinjection, the slightly more realistic case of a simultaneous system of production and injection was simulated. Figure 4 illustrates the mesh for a two-layer doublet system which is produced from the upper reservoir at the rate of 2000 m^3/hr and is injected with 150°C water at the rate of 1000 m^3/hr into either the upper or lower reservoir. The three-dimensional mesh makes use of symmetry along the line connecting the production and injection wells, but otherwise it is similar to

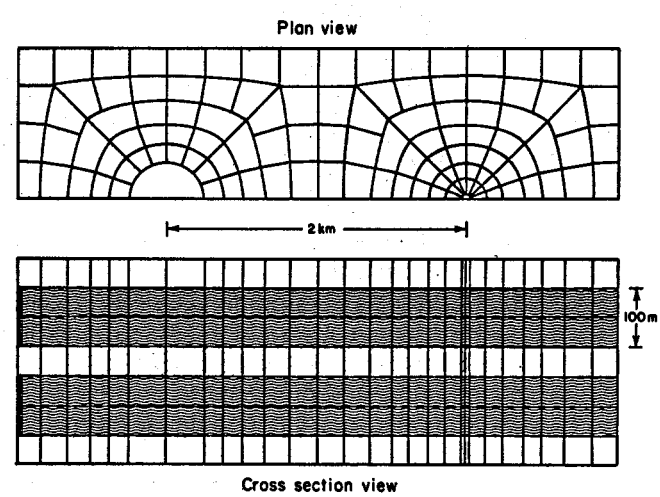

Figure 4. Plan and cross section views of the doublet mesh. (XBL 803-6844)

the single well model, with the same seven layers, thickness and reservoir properties. The simulated area is 4 km by 1 km, with a 2 km spacing between production and injection wells, surrounded by a closed boundary.

The outcomes of the simulations at 10 years are displayed in Figures 5 and 6 for injection into the upper and lower reservoirs, respectively. The upper panel shows the temperature fronts for the upper reservoir, the middle one is a cross section view with the intervening layer shaded, while the lower panel shows the temperature fronts for the lower reservoir. (In examining the contours recall that the upper and lower reservoirs are at different temperatures initially.) The results are similar to the single-well case.

The pressure response is given in Table 3. Pressures are shown as the differences between the pressure changes resulting from simultaneous production and injection, and those due to production only. The results indicate that the overall increase in presssure from injection is on the order of 100 psi at 1 km from the production well. Again, as in the single well model, there appears to be very good pressure communication through the intervening layer, because the reservoirs without injection have pressures which are within 10-15% of those of the reservoirs with injection. The lower pressure at the producing well for the upper injection case appears to be caused by the thermal effects described below.

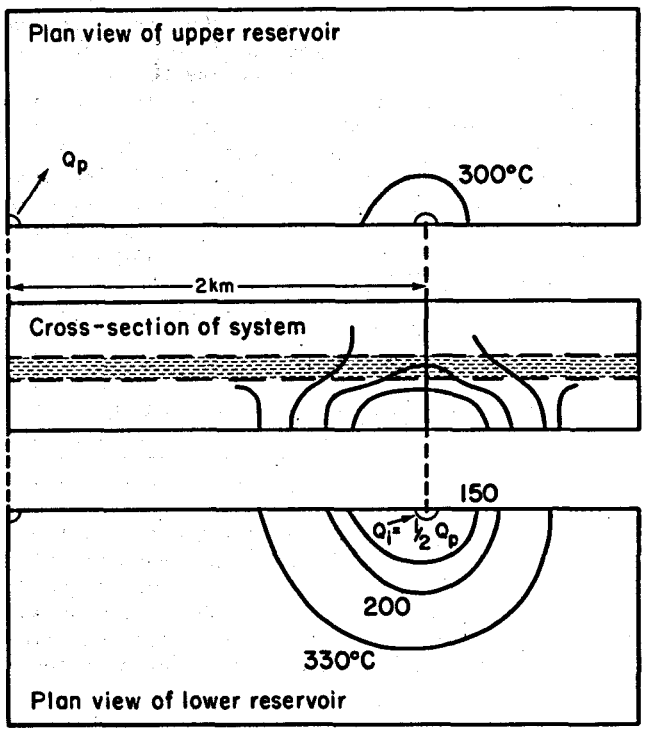

Figure 6. Isotherms simulated for 10 years of doublet injection into the upper reservoir. (XBL 803-6828)

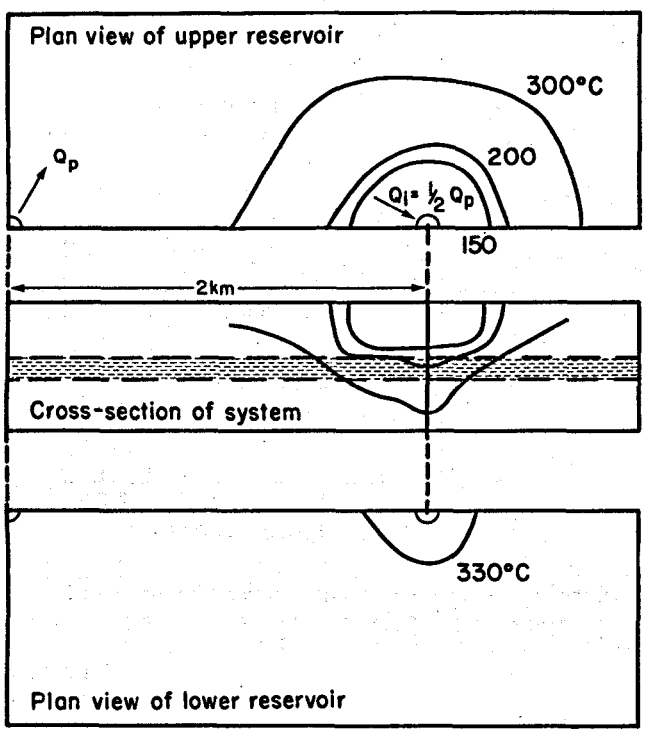

Figure 5. Isotherms simulated for 10 years of doublet injection into the lower reservoir. (XBL 803-6826)

Table 3. Pressure changes for doublet injection simulations after 10 years.*

Cases (psi)	At production well		1 km from prod well	
	Upper Reservoir	Lower Reservoir	Upper Reservoir	Lower Reservoir
Upper injection	78	80	132	120
Lower injection	81	88	120	138
Lower injection (intervening layer permeability = 5 md)	226	-3	148	116

* $P_{i,p} - P_p$ (psi) where $P_{i,p}$ = change in pressure in the case of simultaneous injection and production; and P_p = change in pressure in the case of production only.

The pressure response for the upper injection case over the 10-year period is shown in Figure 7. The pressure profile between the production area and the injection well displays a transition region between the injected 150°C water and the surrounding 302°C water. In this region, the viscosity changes significantly due to fluid temperature differences (a ratio of nearly 2:1), producing a moving thermal barrier which can be responsible for larger than usual pressure declines in well test analysis (Mangold et al., 1979). The accompanying graph in Figure 8 suggests the influence of this effect on pressure response in a comparison between the cases of upper and lower injection. After 10 years of injection into the upper reservoir, the production well area actually has a lower pressure than the lower injection case, probably due to the thermally produced viscosity barrier in the upper aquifer. For injection into the lower reservoir, the pressures in the upper aquifer are not as affected by such a barrier since it is restricted to the lower aquifer. Such results indicate that a combination of viscosity and buoyancy effects are needed in order to adequately describe the physical processes of reinjection, especially in a two-reservoir system. These matters will be the subject of a further investigation.

Thus the doublet model further confirms that in a more realistic model of a two-reservoir system, reinjection will be useful to maintain reservoir pressure while restricting the thermal front to the neighborhood of the injection area.

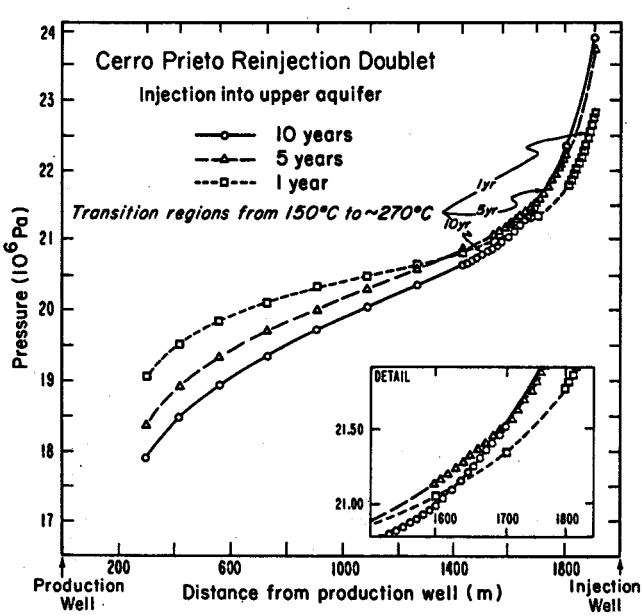

Figure 7. Radial pressure distribution simulated for 1, 5, and 10 years of doublet injection into the upper reservoir, showing the transition region between hot and cold waters. (XBL 803-6832)

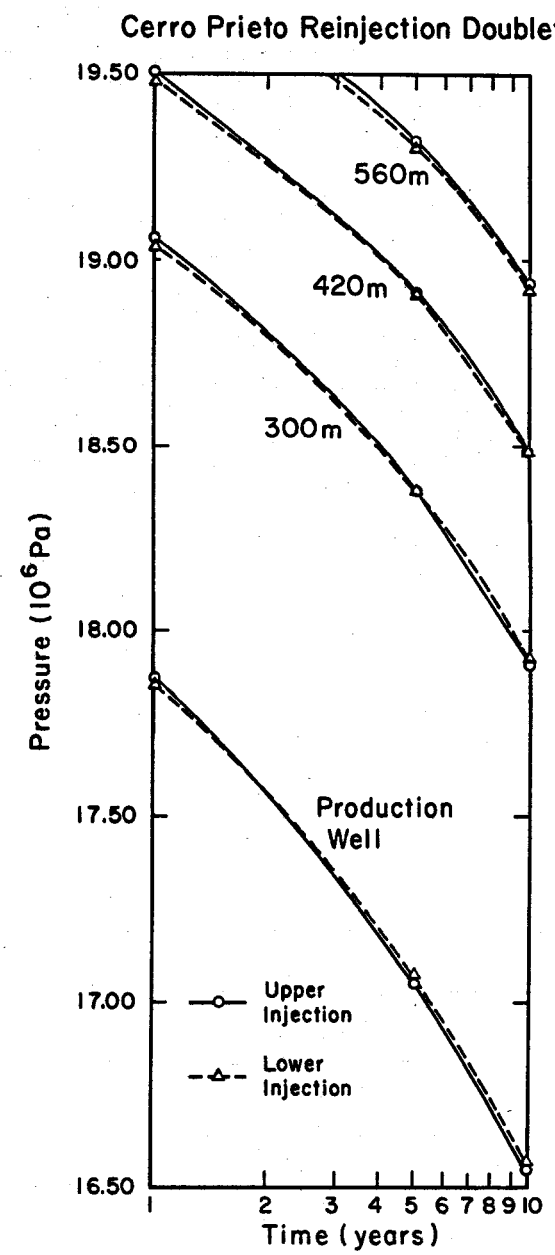

Figure 8. Pressure changes near the production area simulated for 1, 5, and 10 years of doublet injection into the upper and lower reservoirs. (XBL 803-6836)

CONCLUSION

In this paper we have introduced an idealized two-reservoir model to explore some of the effects of reinjection in a geothermal field. For both the single-well model and the doublet model the results indicate that reservoir pressures will be adequately maintained even when an intervening layer of low permeability is present. The same intervening layer may nevertheless be an effective barrier to the movement of cold fronts, due to the action of gravity and viscosity on the flow of denser colder waters. This shows promise for developing reinjection strategies which can be tested on more detailed simulation models for specific sites such as the Cerro Prieto field.

PLANS FOR FISCAL YEAR 1980

In further research we hope to conduct a sensitivity analysis on some of the main parameters used in this study, especially permeability. Clearly, there is also a need to study the flow of the colder water toward the production well for a longer period of time than 10 years. Such matters as simulation of permeability anisotropy and optimum well spacing for injection may have to wait until detailed geological models become available. Idealized models like the ones employed in this study, however, are useful for suggesting practical reinjection operation strategies for optimizing the development of geothermal energy resources.

REFERENCES CITED

Abril G., A. and Noble, J. E., 1979. Geophysical well-log correlations along various cross sections of the Cerro Prieto Geothermal Field, in Proceedings, First Symposium on the Cerro Prieto Geothermal Field, Baja California, Mexico, September, 1978. Berkeley, Lawrence Berkeley Laboratory, LBL-7098, p. 41-48.

Lippmann, M. J., Bodvarsson, G. S., Witherspoon, P. A., and Rivera R., J., 1979. Preliminary simulation studies related to the Cerro Prieto Field, in Proceedings, First Symposium on the Cerro Prieto Geothermal Field, Baja California, Mexico, September, 1978. Berkeley, Lawrence Berkeley Laboratory, LBL-7098, p. 375-387.

Lippmann, M. J., Tsang, C. F., and Witherspoon, P. A., 1977. Analysis of the response of geothermal reservoirs under injection and production procedures. SPE 6537, presented at the 47th Annual California Regional Meeting SPE-AIME, Bakersfield, California, April 1977.

Mangold, D. C., Tsang, C. F., Lippmann, M. J., and Witherspoon, P. A., 1979. A study of thermal effects in well test analysis. SPE-8232, presented at the 54th Annual Fall Technical Conference SPE-AIME, Las Vegas, Nevada, September 1979. Berkeley, Lawrence Berkeley Laboratory, LBL-9769.

Tsang, C. F., Bodvarsson, G. S., Lippmann, M. J., and Rivera R., J., 1979. Some aspects of the response of geothermal reservoirs to brine reinjection with application to the Cerro Prieto Field, in Proceedings, First Symposium on the Cerro Prieto Geothermal Field, Baja California, Mexico, September, 1978. Berkeley, Lawrence Berkeley Laboratory, LBL-7098, p. 396-403.

RESISTIVITY STUDIES AT CERRO PRIETO

M. J. Wilt and N. E. Goldstein

INTRODUCTION

In 1978 Lawrence Berkeley Laboratory, in cooperation with Comisión Federal de Electricidad, began a program of dipole-dipole resistivity studies at the Cerro Prieto geothermal field (Wilt et al., 1979). Dipole-dipole resistivity measurements were conducted in 1978 and 1979 along two long east-west survey lines; one (E-E') crossing the central part of the production area near the power plant, and the other (D-D') passing about 4 km north of the plant and immediately south of the Cerro Prieto volcano (Figure 1). The utmost care was taken to achieve the best accuracy obtainable with the available instrumentation.

The goals of this project are to determine how well the boundaries of the geothermal field can be defined with surface resistivity measurements, and to determine if changes in reservoir conditions due to production (e.g. formation of a vapor zone, changes in porosity at the periphery of the reservoir) may be monitored by means of accurate surface resistivity measurements.

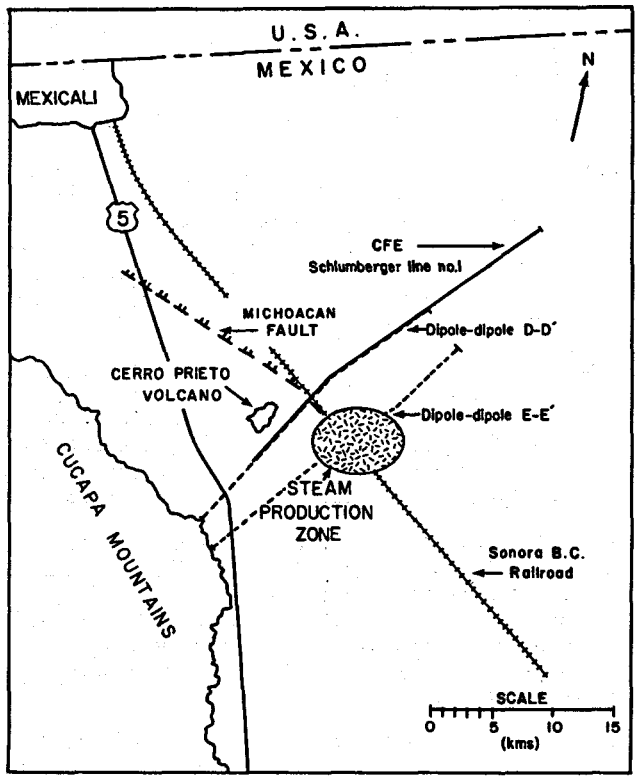

Figure 1. Project location map, LBL resistivity project. (XBL 788-1632)

PROGRESS IN FISCAL YEAR 1979

In fiscal year 1979, line E-E' was remeasured with 1-km dipoles but at significantly greater accuracy than in 1978 to provide better modeling constraints and to establish a reliable baseline for future observations of resistivity changes (Wilt et al., 1980). The LBL 25-kW motor generator was used as the power source both years, but greater accuracy was achieved in 1979 because of superior receiver instrumentation, mechanical improvements to the power source, and the experience gained from the previous year.

Measurements on line E-E' were extended 4 km farther eastward and the maximum transmitter receiver separations were increased from N = 6 to N = 8, thereby yielding a greater depth of exploration. In addition, telluric profile measurements were made along line E-E' to test the applicability of this relatively fast and inexpensive method for resolving subsurface structure.

The expanded and more accurate results were used to develop an improved two-dimensional resistivity cross-section for line E-E' (Figures 2 and 3). New model perturbation studies were performed to identify points of maximum likely interest; i.e., those measurement points where reservoir changes might be most easily recognized, and to examine the magnitude of resistivity change for several possible reservoir changes. An analysis of measurement errors was done with the 1978 and 1979 data and the two sets were compared to see (1) if new measurements (1979) fall within the predicted errors and (2) if data accuracy is sufficient to isolate any changes in reservoir conditions.

Telluric data taken in 1979 were analyzed, and errors were evaluated to determine if it is possible to use this method for resistivity monitoring.

Results of Dipole-Dipole Studies

The following is a summary of some of our findings:

1. The dipole-dipole data gathering technique was improved in 1979 to where estimated measurement errors are less than 3% for most points. This is sufficient accuracy to observe changes in resistivity that may occur over a short time interval due to reservoir dynamics associated with production.

2. Further resistivity modeling has better defined the resistivity structure of the eastern part of the field. The model suggests that the resistive body associated with the producing zone (Figure 3) dips eastward at 30 to 50 degrees to a depth of greater than 2.0 km. A narrow, steeply dipping conductive zone lies immediately east of the resistive body and may correspond to a zone of recharge or faulting (Lyons et al., 1980).

3. The resistivity modeling suggests a deep source of fluid beyond the eastern part of the field. This is shown as the 4.0 ohm-m layer at 2.5 to 3.0 km depth. There is also some evidence that this deep zone is in hydrologic communication with existing shallower production (Elders et al., 1979).

4. Model perturbation studies show that apparent resistivity changes due to model variations normally occur as banded or grouped points of anomalous apparent resistivities. The signature of such models (Figure 4) may allow detection and identification of changes in the presence of noise. The study also helped define an "area of interest" of 60 measurement points particularly associated with changes in the reservoir formation.

5. Interpretation of telluric profile measurements done over line E-E' yields a significant amount of reconnaissance information about the field. Because of inherent measurement uncertainty, however, the method seems unsuitable for monitoring purposes.

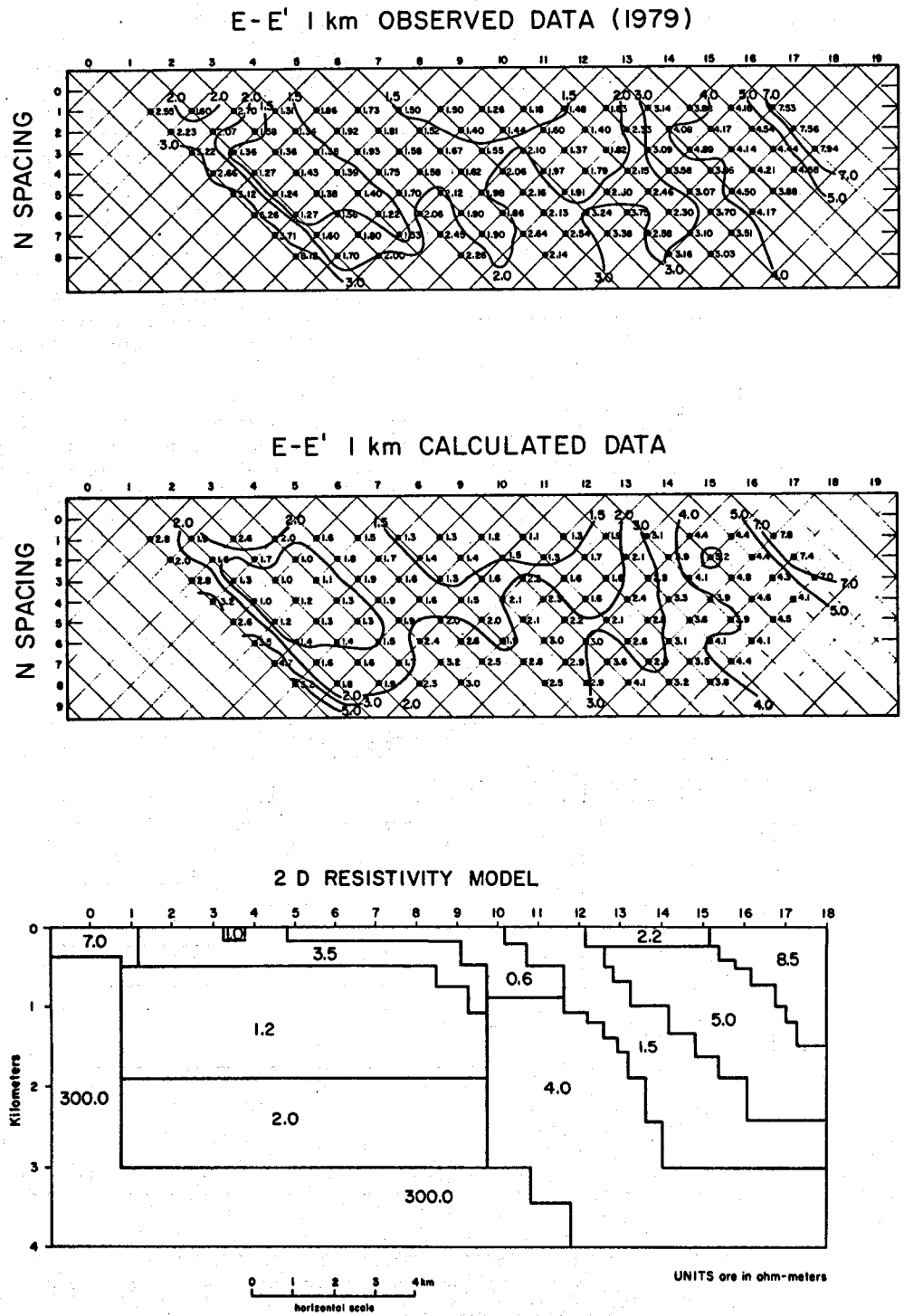

Figure 2. Dipole-dipole resistivity profile, line E-E', 1979: observed data, calculated data, and two-dimensional resistivity model. (XBL 7910-13040A)

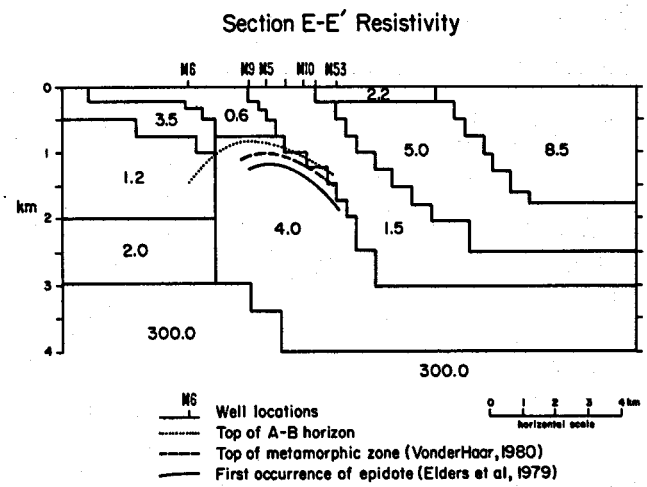

Figure 3. Expanded two-dimensional resistivity model showing well locations and plots of the consolidated-unconsolidated sediment interface, the top of the metamorphic zone, and the first occurrence of the metamorphic mineral epidote. (XBL 801-6761)

PLANS FOR FISCAL YEAR 1980

In fiscal year 1980 line E-E' will be remeasured to an accuracy of 3% or better for all points. In addition, a detailed analysis will be performed on observed changes in apparent resistivity with emphasis on those 60 points most closely associated with the reservoir. Further model perturbation studies will be performed and some three-dimensional computer models will be calculated that account for the rapid changes in resistivity near the edges of the field that were observed with magnetotelluric measurements (Gamble et al., 1979). These three-dimensional models will be of use in constructing more realistic perturbation models.

In the hope of futher improving the accuracy of our measurements two changes will be made to the recording system: (1) a telluric monitor will be added for direct telluric noise cancellation, and (2) a multichannel signal processor will be used for improved signal averaging and filtering. For larger transmitter-receiver separations telluric noise is often greater than the signal and this noise must be effectively cancelled to achieve the

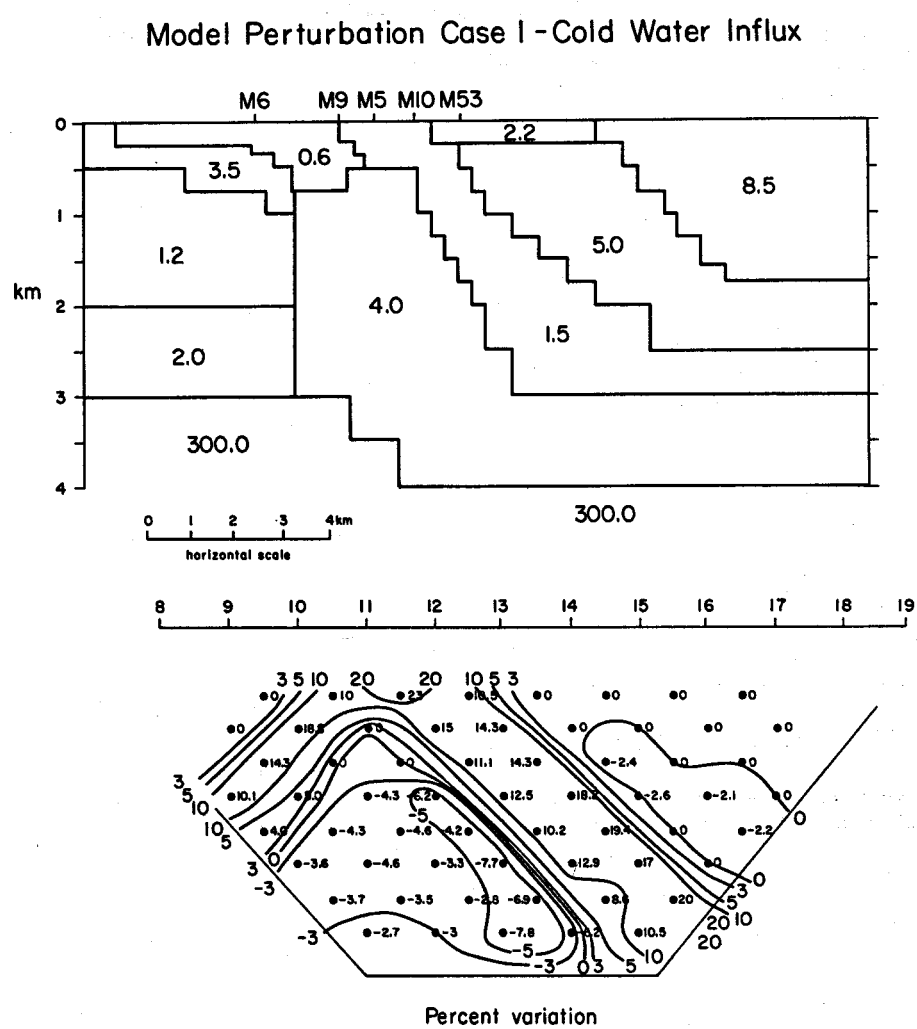

Figure 4. Model perturbation study to simulate the effect of cold water influx into the upper portion of the reservoir (compare model with Figure 3). Percent variations are differences between the calculated data from Figure 2 and the calculated data from the perturbed model. (XBL 801-6759)

required accuracy. This can be done either by subtracting it directly from recordings or by averaging many cycles of data, assuming that the telluric noise will average to zero; we intend to do both.

For noise removal a telluric monitor will be placed 10-15 miles away from the dipole-dipole line so that no transmitted signal is contained in remote signals. The monitor will consist of an electric dipole, amplifiers and filters, and a radio transmitter to telemeter data to the recording van. The remote signal is then adjusted in amplitude, inverted, and added to the local tellurics, to reach a null signal. The transmitter is then switched on and data is taken in a normal manner.

Automatic signal averaging for noise reduction will be done with the new multichannel, microprocessor-controlled wave analyzer originally designed for use with an electromagnetic system. Its flexible design permits its use as a general geophysical receiver (Morrison et al., 1978). The addition of this instrument will allow superior filtering of noise, adjustable cycle averaging to a maximum of over 2000 cycles, and harmonic analysis of transmitted square waves. Since this receiver has six channels it will allow us to increase survey speed by making several measurements simultaneously.

REFERENCES CITED

Elders, W. A., and Hoagland, J. R., 1979. Studies of water/rock interaction in the Cerro Prieto geothermal field, Baja California, Mexico, in Abstracts, Second Symposium on the Cerro Prieto Geothermal Field, Baja California, Mexico: Mexicali, Comisión Federal de Electricidad.

Gamble, T. D., Goubau, W. M., Goldstein, N. E., Miracky, R., Stark, M., and Clark, J., 1980. Magnetotelluric studies at Cerro Prieto, in Proceedings, Second Symposium on the Cerro Prieto Geothermal Field, Baja California, Mexico, October 1979. Mexicali, Comisión Federal de Electricidad.

Lyons, D. J., van de Kamp, P., Vonder Haar, S., Noble, J., and Howard, J. H., 1980. Subsurface stratigraphy at the Cerro Prieto geothermal field, in Proceedings, Second Symposium on the Cerro Prieto Geothermal Field, Baja California, Mexico, October 1979. Mexicali, Comisión Federal de Electricidad.

Morrison, H. F., Goldstein, N. E., Hoversten, M., Oppliger, G., and Riveros, C., 1979. Description field test and data analysis of a controlled source EM system (EM-60). Berkeley, Lawrence Berkeley Laboratory, LBL-7088.

Wilt, M., Goldstein, N. E., and Razo, M. A., 1979. LBL resistivity studies at Cerro Preito, in Proceedings, First Symposium on the Cerro Prieto Geothermal Field, Baja California, Mexico, September 1978. Berkeley, Lawrence Berkeley Laboratory, LBL-7098, p. 179-188.

Wilt, M., and Goldstein, N. E., 1980. Resistivity monitoring at Cerro Prieto, in Proceedings, Second Symposium on the Cerro Prieto Geothermal Field, Baja California, Mexico, October 1979. Mexicali, Comisión Federal de Electricidad.

MAGNETOTELLURIC STUDIES AT CERRO PRIETO

T. D. Gamble, W. M. Goubau, R. Miracky, J. Clarke, and N. E. Goldstein

INTRODUCTION

Seventeen magnetotelluric soundings have been performed near the current geothermal production zone at Cerro Prieto, Mexico. These measurements indicate, among other things, a zone of relatively high resistivity enclosing the region of current brine producion. This narrow zone plunges at a shallow angle to the south-southeast. The three-dimensional nature of this resistive body, combined with the long range influence of the high resistivity Cucapa Mountain Range and other regional features, makes a rigorous quantitative evaluation impractical. Nonetheless, the qualitative picture is clear; and a rough model drawn from crude quantitative considerations has been shown to be in good agreement with dipole-dipole resistivity measurements and well log data from the area. The relatively high resistivity is apparently due to hydrothermal metamorphism of the sediments by geothermal activity, with an attendant loss of porosity, in a zone of faulting parallel to the regional strike, about 15° west of north.

PROGRESS IN FISCAL YEAR 1979

Figure 1 is a map of the sites of the magnetotelluric soundings performed in 1978 and 1979. They form three lines: D to the north of the plant, E parallel to D through the present production

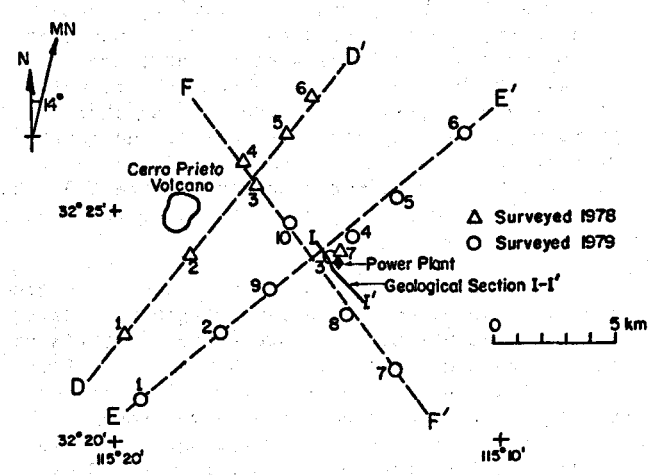

Figure 1. Location of magnetotelluric stations at Cerro Prieto, Baja California. (XBL 791-12866)

field, and F also through the present field but perpendicular to the others and parallel to the geologic strike. All the measurements were made using the remote reference technique (Gamble 1978; Gamble et al. 1979a,b,c,d; Gamble, 1980). The Sierra Cucapa range is about 10 km to the west of Cerro Prieto; and the southern extension of the Imperial Valley fault lies about 12 km to the east, both sub-parallel to line F.

Magnetotelluric measurements can determine two response functions of the earth. One is the tipper, $\underline{T}$, which relates the vertical to the horizontal components of the magnetic field by $H_z = \underline{T} \cdot \underline{H}$. The second is the impedance tensor $\underline{Z}$, which relates the horizontal components of the electric field to the horizontal components of the magnetic field by $\underline{E} = \underline{Z}\underline{H}$. Z is usually described by the apparent resistivity, which is the resistivity of a homogeneous earth that would give the same ratio of electric to magnetic field powers as is observed at a given frequency. This apparent resistivity is proportional to the squared magnitude of the off-diagonal components of $\underline{Z}$. For the real, inhomogeneous earth, resistivity is a function of frequency. Apparent resistivity and tipper information are often conveniently represented in pseudosection form, where the lateral axis specifies the position along a survey line and the vertical scale is the logarithm of the period. The depth of penetration of the electromagnetic waves is roughly proportional to the square root of the period, so the vertical axis corresponds very roughly to logarithmic depth.

We present a small sample of the pseudosections of the data from these soundings. Figure 2 is a pseudosection of the tipper magnitude for current going across the strike, for line F. There is a very large maximum at station 3, just north of the power plant, at periods of about 1 second. The tipper indicates lateral changes in resistivity, so this pseudosection indicates a large north-south gradient of resistivity just north of the plant. The phase of the tipper (not shown) indicates that the more resistive material is to the south. Figure 3 is a pseudosection of the apparent resistivity for the same line, F, and current direction, across the regional strike. Here we see more directly a region of higher resistivity to the south indicated by an area of high apparent resistivity, greater than 3 ohm-m, south of station 3. The contour of 3 ohm-m apparent resistivity closes at longer periods, but this does not mean that the actual resistivity decreases at the greatest depths. Rather, we are seeing the influence of the resistive barrier of the Cucapa granites to the west. This barrier blocks off the current at great depths, causing a lower apparent resistivity for the longer periods.

Because of lateral resistivity changes in geologically complex areas, we rarely encounter data that can be quantitatively interpreted in terms of a simple one-dimensional (i.e., horizontally layered) earth. The only station for which the measurements appear consistent with a one-dimensional model over most of the frequency range is station 6 on line E, the station farthest from the Cucapas. We used a program developed by Oldenburg (1979) to invert the data from this sounding. The results are shown in Figure 4. The crosses indicate the

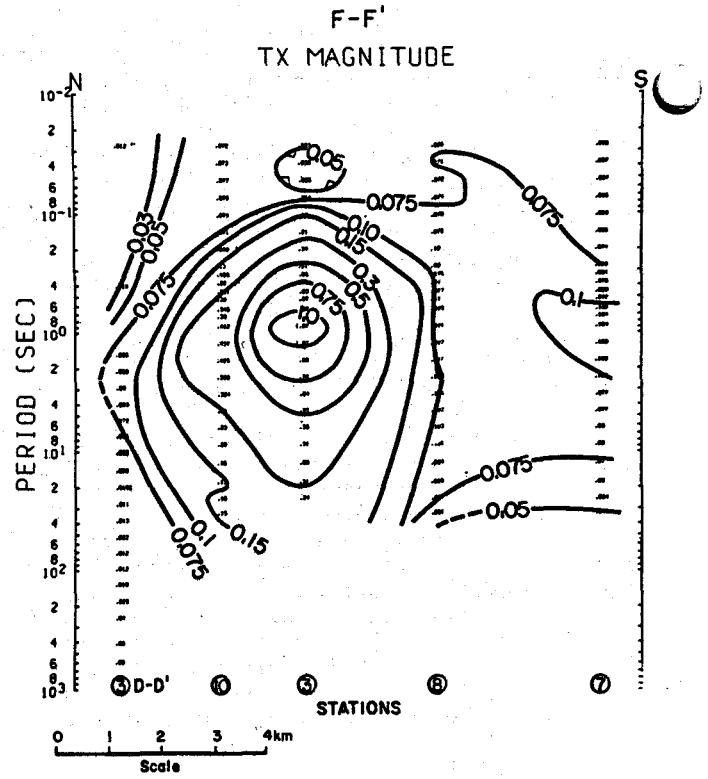

Figure 2. Observed tipper magnitude for line F-F', current perpendicular to regional geologic strike. (XBL 799-11504)

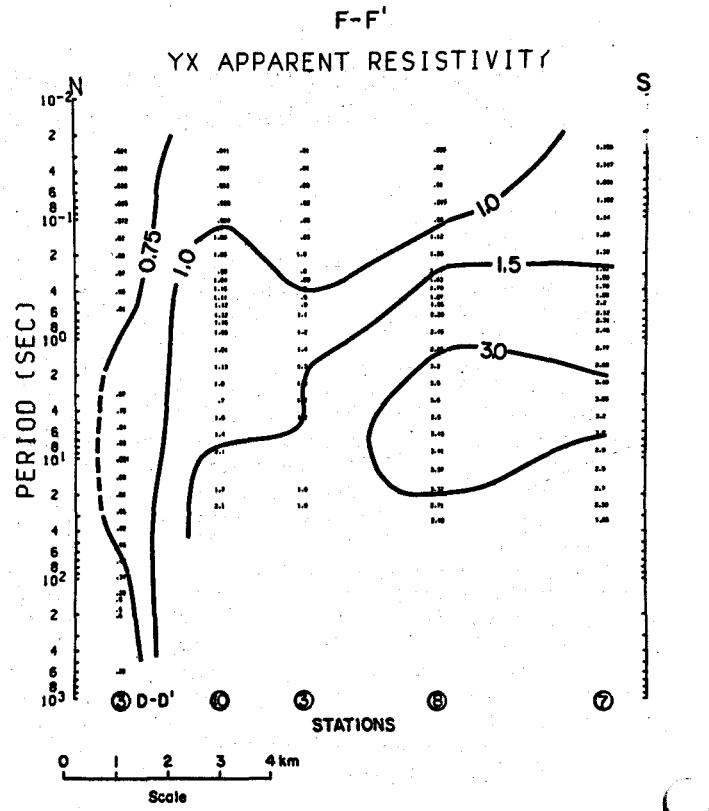

Figure 3. Apparent resistivity pseudosection along line F-F', current perpendicular to regional geologic strike. (XBL 799-11507)

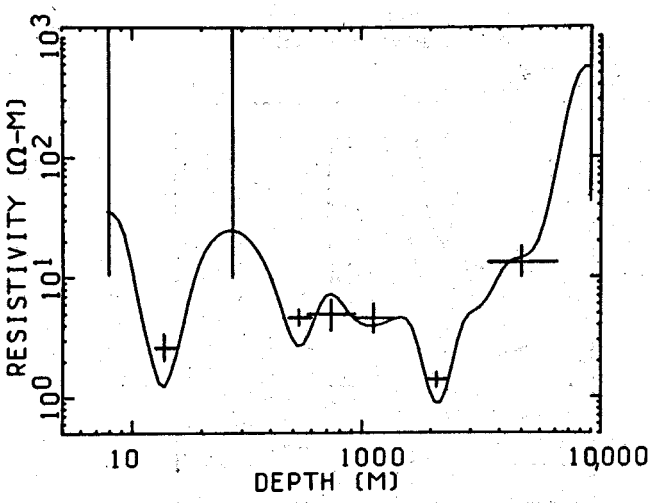

Figure 4. One-dimensional inversion results for station 5, line E-E'; electric field parallel to regional strike (crosses explained in text). (XBL 7910-12330A)

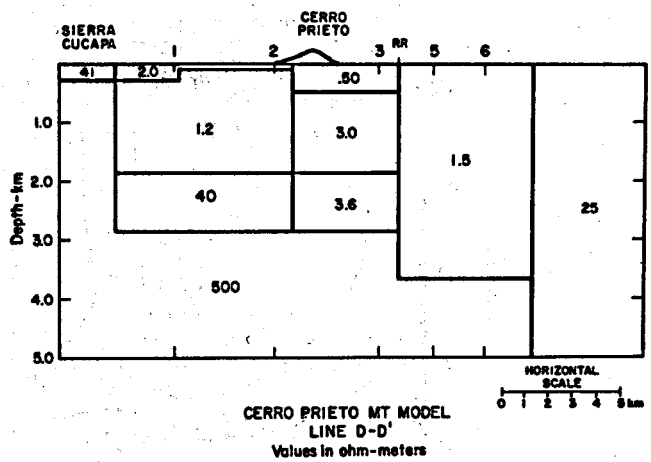

Figure 5. Two-dimensional interpretation of resistivity fitting the magnetotelluric results at stations along line D-D'. (XBL 796-7534A).

resolution of the sounding. The vertical bars indicate a range of depths over which the resistivity was average, whereas the horizontal bars indicate the standard deviation of this average resistivity due to the uncertainty of the measurements. Between depths of 200 and 2000 m, resistivities tend to decrease, a consequence of water salinity changing from nearly fresh at the surface (Colorado River water) to fossil sea water trapped in the deeper sediments. The low resistivity anomaly (1 ohm-m) between 1.9 and 2.5 km depth, could be caused by a combination of high temperature and high salinity. Results from well Neuvo Leone I in the general area confirm this condition.

The soundings along line D are relatively consistent with a two-dimensional earth; i.e., there is no indication of a large lateral change in resistivity in the strike direction. Therefore, we have attempted to match the observed pseudosections to those for a two-dimensional model. A preliminary model, which was included in the 1978 annual report, roughly matched the long period data from this line (Gamble et al., 1979b). This model has been refined to obtain a much better match to all the measurements. This subsurface resistivity along line D is presented in Figure 5. To illustrate how well the model satisfies the data, Figure 6 shows a comparison of calculated and observed apparent resistivity pseudosections. Although Figure 6 portrays only the case for current perpendicular to strike (the TE mode), the model also satisfies current perpendicular to strike (the TM mode). For this particular line, agreement between model and observed results is particularly good. The values of resistivity were found for the blocks shown in Figure 5.

The 41 ohm-m block at the western end of line D is included to account for the conduction paths within the Cucapa mountains above the level of the plain. Also, relatively resistive rocks were required east of station 6 to help fit the data. Thus we had to introduce a rather artificial 25 ohm-m block of undetermined depth extent beyond the eastern end of the line. The low resistivity surface zone in the middle of the line is well resolved, and is coincident with the geothermal surface manifestations near the Cerro Prieto volcano. The measurements are consistent with 1.7 or 1.8 ohm-m resistivity from 0.5 to 3.0 km depth below stations 3, 5, and 6, although a slightly better match is obtained with the values of 3.0 and 3.6 ohm-m below station 3, as shown. This more resistive zone, bounded approximately by the Cerro Prieto fault on the west and the Michoacán fault on the east, is better defined by means of dipole-dipole resistivity than by MT. The zone corresponds to a region of hydrothermal metamorphism and reduced porosity as determined from a study of well cuttings (Elders et al., 1979).

Because of the large lateral changes of resistivity in the regional strike direction over the field, indicated earlier by Figures 2 and 3, we have not attempted to match these soundings to a two-dimensional model. Instead, we have conceptualized a rough three-dimensional model based on a qualitative consideration of all relevant pseudosections. Sections of this model along lines E and F, plotted to a logarithmic depth scale, are shown in Figures 7 and 8, respectively. The resistive body in the vicinity of the power plant presents a large cross section along line F but only a relatively small one along line E. It is not connected to the resistive zone near the surface to the east on line E and does not extend any farther south than the southernmost station on line F. It comes within 500 m of the surface in the region of the power plant and plunges at a shallow angle to the south. We have no stations distributed across strike near the middle of this resistive zone, so we cannot determine its width, although it appears narrow. It could be a single vertical dike-like body of resistive material, a number of such narrow bodies, or a zone of anisotropic conductivity, more conductive along strike.

Dipole-dipole resistivity measurements have been performed along lines D and E. The models developed from these measurements are in close agreement along those lines with rough model from

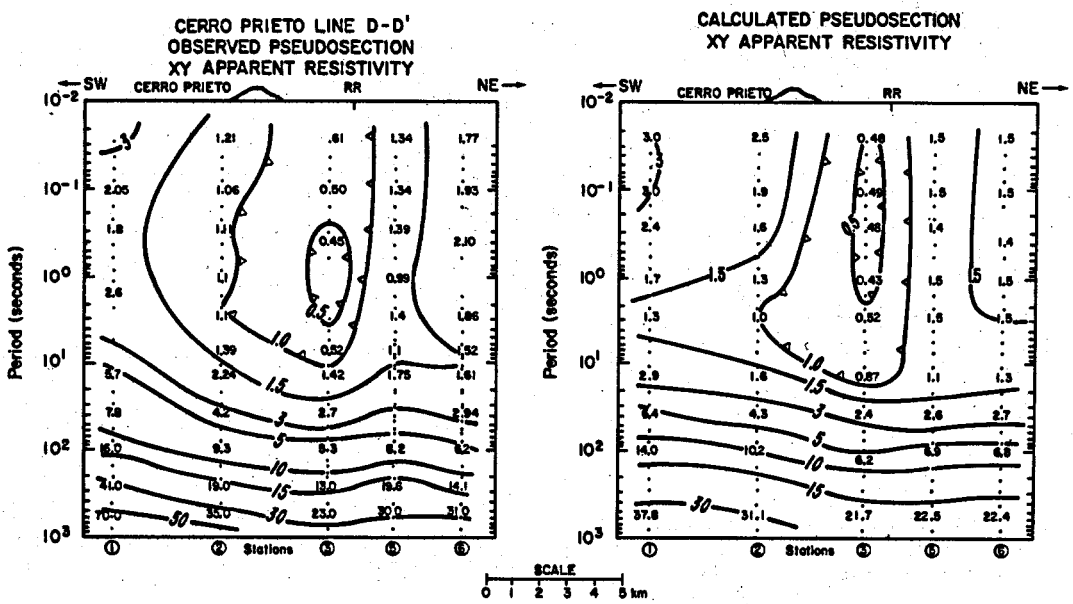

Figure 6. Observed and calculated apparent resistivity pseudosections, line D-D', current parallel to geologic strike. (XBL 796-7532)

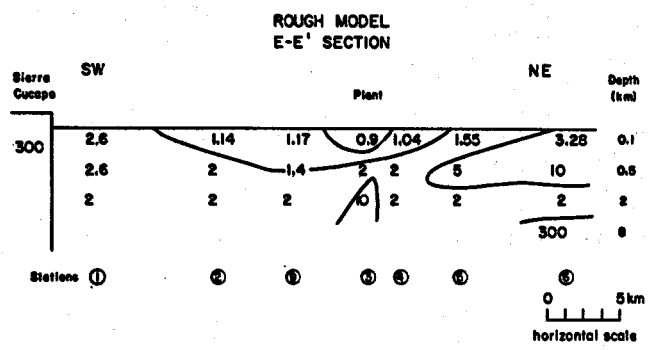

Figure 7. Semi-quantitative estimate of subsurface resistivity distribution along line E-E', vertical scale logarithmic. (XBL 799-1150A)

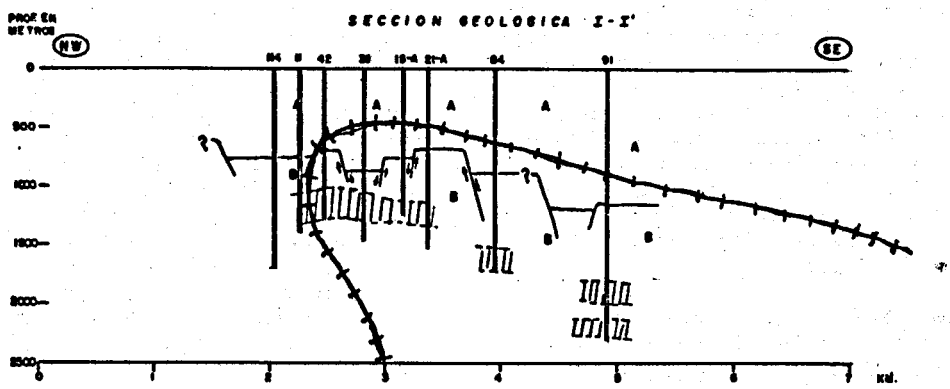

Figure 8. Approximate relationship between the dipping resistive zone and subsurface geology. (XBL 7910-12260)

the magnetotelluric measurements (Wilt and Goldstein, 1979). In fact the match between the measured and calculated responses for the dc resistivity mode has been signficantly improved by the inclusion of features from the "rough" magnetotelluric model into the dipole-dipole model.

Except where the resistive zone is shallowest, north of the power plant, the top of the zone corresponds well to the first occurrence of significant hydrothermal alteration as determined from well samples. Very little mineralogical data are available from wells to the north, but what is available does not show any sharp increase in the depth to the altered zone. We are reminded that the bulk resistivity properties as measured from the surface are determined by many factors, such as the grain of fracturing in fault zones. They all must be included to explain the resistivity structure; and we do not have any really satisfactory explanation of the lateral change of resistivity to the north.

It is likely that the history of geothermal activity at Cerro Prieto has included phases of induration of the sediments by hydrothermal solutions interrupted by faulting and fracturing that opened new paths for hydrothermal solutions and provided convective pathways for dissolution and resulting secondary porosity of the sandstones (Lyons, 1979, personal communication.). However, the gross features of the structure in the current production zone can be explained most simply in terms of hydrothermal alteration of the sediments by geothermal fluids emanating from a source at depth about 4 km to the south-southeast of the present plant and flowing along the general regional strike in a zone of faulting to the north-northwest. A well of great capacity has been recently completed about 3 km to the southeast of the plant, supporting this picture.

The conductive layer at 2 km depth to the east may indicate that the circulation system now extends to this region and that recharge to the production zone may also be coming from reservoir rocks underlying the central portion of the Mexicali Valley.

PLANNED ACTIVITIES FOR 1980

We plan to add another line of stations parallel to lines D and E, about 4 km south of the plant, over the apparent root of the resistive zone. We hope this line will yield significant information about the hydrothermal flow around the source of the heat.

A more fundamental objective is to improve interpretation of magnetotelluric measurements. At present there is no program that can calculate the responses that would be observed for our rough model. Magnetotelluric measurements can be performed to almost arbitrary accuracy with the use of a remote reference; but the promise of magnetotellurics will not be fulfilled until some quantitative means is developed for direct approximate inversion of the measurements to determine the conductivity structure of the ground in complex situtations.

REFERENCES CITED

Elders, W. A., Hoagland, J. R., McDowell, S. E., and Cobo, R. J., 1979. Hydrothermal mineral zones in the geothermal reservoir of Cerro Prieto, in Proceedings, First Symposium on the Cerro Prieto Geothermal Field, Baja California, Mexico, September 1978. Berkeley, Lawrence Berkeley Laboratory, LBL-7098, p. 68-75.

Gamble, T. D., 1978. Remote reference magnetotellurics with SQUID (Ph.D. dissertation). Berkeley, Lawrence Berkeley Laboratory, LBL-8062.

Gamble, T. D., Goubau, W. M. Goldstein, N. E., and Clarke, J., 1979a. Referenced magnetotellurics at Cerro Prieto, in Proceedings of the First Symposium on the Cerro Prieto Geothermal Field, Baja California, Mexico: Berkeley, Lawrence Berkeley Laboratory, LBL-7098.

____, 1979b. Magnetotelluric survey at Cerro Prieto, in Earth Sciences Division Annual Report 1978. Berkeley, Lawrence Berkeley Laboratory, LBL-8648, p. 41-42.

Gamble, T. D., Goubau, W. M., and Clarke, J., 1979c. Magnetotellurics with a remote magnetic reference. Geophysics, v. 44, no. 1, p. 53-68.

____, 1979d. Error analysis for remote reference magnetotellurics. Geophysics, v. 44, no. 5, p. 959-968.

Gamble, T. D. Goubau, W. M., Goldstein, N. E., Miracky, R., Stark, M. and Clarke, J., October 1980. Magnetotelluric studies at Cerro Prieto, in Proceedings, Second Symposium on the Cerro Prieto Geothermal Field, Baja California, Mexico, October 1979. Mexicali, Comisión Federal de Electricidad.

Oldenburg, D. W., 1979. One dimensional inversion of natural source magnetotelluric observations. Geophysics, v. 44, no. 7, p. 1218-1244.

Wilt, M., and Goldstein, N. E., 1979. Resistivity monitoring at Cerro Prieto, in Proceedings, Second Symposium on the Cerro Prieto Geothermal Field, Baja California, Mexico, October 1979. Mexicali, Comisión Federal de Electricidad.

PRECISION GRAVITY STUDIES AT THE CERRO PRIETO GEOTHERMAL FIELD

R. B. Grannell,* D. W. Tarman,† R. C. Clover,* R. M. Leggewie,* P. S. Aronstam,* R. C. Kroll,* and J. Eppink†

From January to March 1979, 60 permanent gravity stations in the Cerro Prieto geothermal field were reoccupied for the collection of data, a year after their initial occupation in early 1978 (Chase et al., 1978; Grannell et al., 1979). For the collection of both data sets, each station was occupied four times and was replicated four times at an individual occupation, for a total of 16 readings. Two LaCoste and Romberg G-model gravity meters were used. In a looping technique, individual stations were surveyed between two base station occupations, taken up to five hours apart. This procedure allowed identification of tares and partial removal of instrumental drift.

The data were reduced to observed gravity values using meter calibrations and the appropriate corrections for both earth tides and instrumental drift. The station values were then referred to a bedrock base, presumed stable and nonsubsiding over short time intervals, (several years). This base is located on granitic rocks in the Sierra Cucupa, west of the geothermal field.

A comparison of reduced data from the two periods shows no significant gravity changes in that interval. This result is consistent with the results of first- and second-order leveling carried out by CFE within and adjacent to the Cerro Prieto geothermal field. The possible reasons for lack of gravity changes are fourfold: (1) insufficient time at the current rate of production to produce measurable changes; (2) local recharge to offset mass losses; (3) drawdown in an area not covered by the gravity survey (possible to the west); and (4) changes too small to be detected at the current level of precision (10 to 17 μ gals).

*California State University, Long Beach
†California State Polytechnic University, San Luis Obispo

REFERENCES CITED

Chase, D. S., Clover, R. C., Grannel, R. B., Leggewie, R. M., Eppink, J., Tarman, D. W., and Goldstein, N. E., 1979. Precision gravity studies at Cerro Prieto, in Proceedings, First Symposium on the Cerro Prieto Geothermal Field, Baja California, Mexico, September 1978. Berkeley, Lawrence Berkeley Laboratory, LBL-7098, p. 249-256.

Grannell, R. B., Tarman, D. W., Aronstam, P., Clover, R. C., Leggewie, R. M., Eppink, J., and Kroll, R., 1979. Precision gravity measurements in the Cerro Prieto geothermal area, in Abstracts, Second Symposium on the Cerro Prieto Geothermal Field, Baja California, Mexico. Mexicali, Comision Federal de Electricidad, p. 37-39.

GEOTHERMAL RESERVOIR ENGINEERING MANAGEMENT PROGRAM: DEVELOPMENTS IN FISCAL 1979

J. H. Howard and W. J. Schwarz

INTRODUCTION

Fiscal year 1979 was the third year of LBL's responsibility for the Geothermal Reservoir Engineering Management Program (GREMP) on behalf of the U. S. Department of Energy, Division of Geothermal Energy. The concept behind this program is explained in Lawrence Berkeley Laboratory report LBL-7000. Its history since 1977 is summarized in Earth Science Division Annual Reports of 1977 and 1978.

Fiscal 1979 was marked by the conclusion of a number of contracts supported by the program and by relative decline in the number of new contracts when compared with 1978. Overall, the GREMP program has shown typical signs of growth and maturity: fiscal 1977 was devoted largely to planning and getting the program initiated; fiscal year 1978 was characterized by an appreciable amount of new contracting; and fiscal year 1979 was devoted to the conclusion of many contracts and a call for serious review and possible redirection and reorganization of the effort.

ACTIVITIES IN FISCAL YEAR 1979

Administrative Highlights

New contracts were let in fiscal year 1979 for work on tracers in geothermal reservoirs (with Vetter Research) and for work on declines of geothermal well production (with E. Zais and Associates). Contracts with Princeton University, University of California at Riverside, and Stanford University, which started under the NSF-RANN program, were continued.

From its start at LBL through this fiscal year, 23 distinguishable research projects have been addressed through the efforts of 14 institutions. This work is summarized in Figure 1, which shows the relationship of these various projects to the overall GREMP plan. Table 1 gives a brief statement of explanation of each of these projects.

SUMMARY OF PROJECTS RELATIVE TO ORIGINAL PLAN

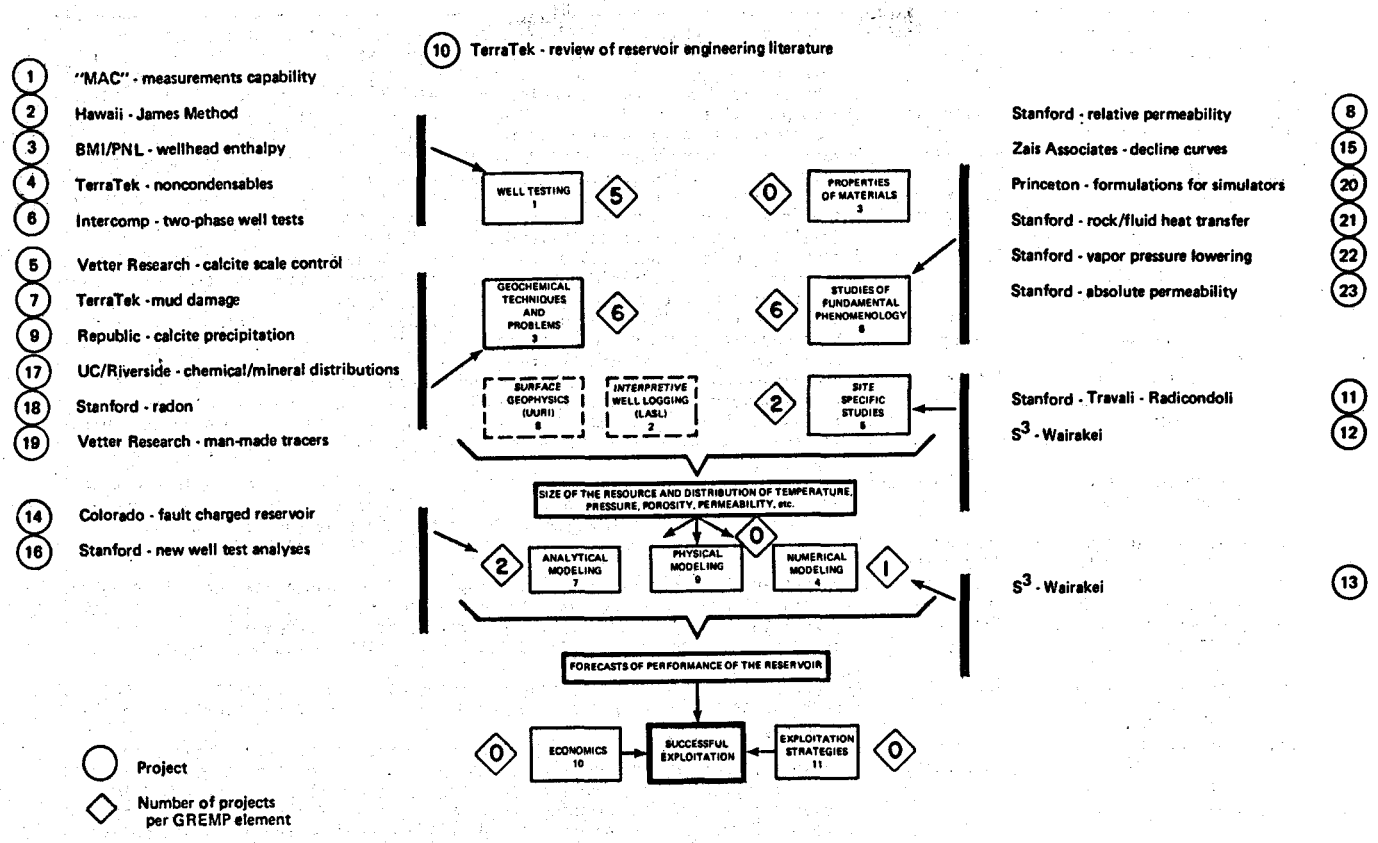

Figure 1. Summary of projects with respect to elements of original GREMP plan. (XBL 7911-13434)

The GREMP publication series, which was started in fiscal year 1978 was continued and now includes six publications with two more of the series in press (as of January 1980).

The newsletter "News from GREMP" was continued through fiscal year 1979 and now includes six issues. This series has set a good precedent for communication of technical results (with an active mailing list of 600), and has encouraged the issuing of similar series for other programs like GREMP.

Certain areas of work have yet to be addressed by the program. These include, economics and exploitation strategies. Generally, projects-not-done are a consequence of recommended low priority for support by the Review Task Force for GREMP and due to fund limitations.

Technical and Scientific Progress

Technical work addressed to date through GREMP is summarized in Figure 1 and Table 1. Attention is called to the projects completed (marked with an asterisk), and to publications about those works. Space does not permit even a short statement on the progress for each project during fiscal year 1979. However, noted below are three achievements of special interest.

1. TerraTek instrument development for measurement of noncondensables on a real-time basis. This instrument has been successfully field tested and is now at the stage of being perfected for practical use. Several companies have expressed interest in its purchase or lease when it is available commercially.

2. UC/Riverside work on petrology of Cerro Prieto geothermal field. The significance of minerals, as an index of temperature in the field, has been sufficiently well established that the minerals seen in cuttings have been used as a basis for decisions to abandon or to deepen a well. This achievement is particularly noteworthy inasmuch as the motive for investigation was an improvement in understanding of metamorphosis in geothermal reservoirs, a fundamental scientific question.

3. Vetter Research (and Republic Geothermal Incorporated) on use of a chemical additive to control calcite precipitation. Calcite fouling is a serious practical problem in the production of geothermal fluids and this research defined the circumstances under which an additive DEQUEST 2060 can virtually eliminate calcite precipitation.

Table 1. Summary of Geothermal Reservoir Engineering projects supported by USDOE/DGE through Lawrence Berkeley Laboratory.

ID#	Brief project name	Contractor	Brief summary of work
1.	Status of reservoir related measurements*	Measurement Analysis Corp.	A comprehensive appraisal of measurement needs and instrumentation for geothermal applications has been completed, indicating that commercially available technology and instrumentation exists in principle for all wellhead and process plant measurement requirements, except two-phase flow (Lamers, 1979).
2.	Theoretical basis for James method	University of Hawaii	The purpose of this project is to understand the theoretical basis of James' empirical method for estimating mass flow and enthalpy (Cheng, 1979).
3.	Measurement of enthalpy at wellhead*	Battelle Pacific Northwest Laboratory	Several calorimetry methods for measuring geothermal wellhead enthalpies were reviewed. A mixing tee condenser was recommended for use when cooling water is available. When not, a multiphase tank was recommended. Work on engineering drawings of a sampling system and a mixing tee condenser (Cliff et al., 1979a) have been prepared (Cliff et al., 1979b).
4.	Measurements of noncondensible gases at wellhead	TerraTek	Engineering design construction and testing of a device with the capability to monitor noncondensible gas concentrations continuously in geothermal discharges has been completed (Harrison et al., 1979).
5.	Control of calcite precipitation by additives*	Vetter Research	Scale inhibitor tests performed at Republic Geothermal Inc., East Mesa wells have shown that Dequest can economically eliminate calcite precipitation in the discharge flow stream (Vetter, 1979).
6.	Analysis of well tests of two-phase reservoir	Intercomp	Favorable comparison of Intercomp's proprietary geothermal wellbore and reservoir simulators with the experimental and numerical results from three other models has been completed. Data on two-phase well tests have been assembled for analysis (Aydelotte and Taylor, 1979) and the Hawaiian well HCP-4 has been studied.
7.	Formation damage of drilling mud	TerraTek	Laboratory simulation of drilling mud damage to geothermal reservoir rocks has been initiated. Parameters to be considered are pressure, temperature, reservoir fluid chemistry, mud composition, and time (Butters, 1979).
8.	Relative permeability of steam and water	Stanford University	Relative permeability data have been collected by Counsil (1978).
9.	Calcite formation by inappropriate production practices	Republic Geothermal, Inc.	Carbonate-rich geothermal brine is being passed through containers of granular materials in order to evaluate the mechanism and rate of calcite precipitation within the pore space. The ultimate practical purpose of the activity is to plan better remedial "acid jobs" on calcite-fouled geothermal wells (Michaels, 1979).
10.	Literature review of reservoir exploitation*	TerraTek	An annotated bibliography covering reservoir modeling, exploitation strategies, and interpretation of production trends has been prepared (Harrison and Randall, 1979).
11.	Study of the Travali Radicondoli geothermal areas in Italy	Stanford University	Geology and pressure-production history of Serrazzano reservoir have been reviewed. Bottomhole temperatures and pressures have been calculated from wellhead measurements. Areal distribution of pressure has been mapped for seven different times spanning the last 15 years. A conceptual model of Travali Radicondoli geothermal field was developed on the basis of the available field data (Miller et al., 1978).
12.	Data collection for the Wairekei field, New Zealand*	Systems, Science and Software	All geological, geochemical, geophysical, and wellbore data from January, 1953 to December, 1976 has been collected and synthesized (Pritchett et al., 1978).
13.	Simulation of past and future performance at Wairakei,	Systems, Science and Software	With the data collected and synthesized (#12 above), an attempt is under way to match the pressure, enthalpy and subsidence history during past production of the Wairakei, New Zealand, field (Pritchett et al., 1979).
14.	Prototype of a fault-charged geothermal reservoir*	University of Colorado	A physical, viable, mathematical model of an unexploited geothermal system has been constructed in terms of a fault zone controlled charging of a reservoir (Kassoy and Goyal, 1979).
15.	Review of decline curves appropriate to geothermal reservoirs	E. Zais and Associates	The purpose of this project is to review decline curve procedures used in the petroleum industry, determine which procedures are applicable to geothermal systems, and establish a theoretical basis for applicability.
16.	New analytical well test methods for geothermal reservoirs	Stanford University	The utility of parallelipiped models has been investigated (Ramey et al., 1978).
17.	Studies of mineral facies and stable isotopes and their relations to geothermal reservoirs	University of California, Riverside	Cuttings and core samples, obtained from the six wells drilled during the year 1977 were studied and interpreted to define the current temperatures in the field (Elders et al., 1978).
18.	Understanding the significance of radon in geothermal reservoirs.	Stanford University	The variation of radon associated with geothermal reservoir production has been analyzed and interpreted for several reservoirs throughout the world (Kruger et al., 1978).
19.	Studies of the use of tracers in geothermal reservoirs	Vetter Research	A program of literature review and laboratory evaluation of tracers suitable for use in geothermal reservoirs has been initiated.
20.	Study of basic formulation of simulation of geothermal reservoirs.	Princeton University	Multiphase flow equations have been derived for a deformable porous medium. Equations for heat and mass transfer in a fractured reservoir have also been formulated. A computer code BIFEPS (Block Interactive Finite Element Processed Scheme) has been developed to solve nonlinear transient problems with one or two governing equations in two or three dimensions.(Pinder et al., 1978).
21.	Studies of heat transfer from rock to fluid	Stanford University	Heat flow from rock to water has been studied as a function of a number of parameters including the size of rock fragments (Kruger et al., 1979).
22.	Vapor pressure lowering phenomena of geothermal fluids	Stanford University	The project demonstrated that vapor pressure may be lowered as a consequence of a number of chemical and petrophysical parameters (Miller et al., 1979). parameters (Miller et al., 1979).
23.	Absolute permeability of geothermal fluids	Stanford University	The effects of temperature and chemical composition of the rock types on relative permeability has been investigated (Miller et al., 1978).

* Project completed.

It should also be noted that the Fifth Annual Stanford Geothermal Reservoir Engineering Workshop was held. This workshop is of special significance to GREMP. To some extent, it measures the existence and viability of a geothermal reservoir engineering professional working community and also reveals the extent to which students (tomorrow's geothermal reservoir engineers) are entering the community. These concerns are a part of the GREMP program, and judging from the workshop, it would be fair to say that the community is alive and well, and that an adequate number of students are entering the community.

Activities Planned for Fiscal Year 1980

Several changes are planned for the GREMP program in fiscal year 1980. It is anticipated that primary responsibility for administering the program will begin a transfer to DOE/SAN. A major revision of the plans for GREMP is ecpected to take place. From a technical point of view the following activities are expected to receive emphasis, as budgets allow:

1. Evaluating the basic validity of computerized reservoir simulators and the effectiveness with which they can be applied to specific reservoirs (to be handled by DOE/SAN)

2. Evaluating techniques of measurement of two-phase mass flow

3. Relating well cuttings and core to porosity and permeability.

In addition, of course, projects under contract should continue in force to their successful conclusion.

REFERENCES CITED

Cliff, W. C., Apley, W. J., and Creer, J. M., 1979. Evaluation of potential geothermal wellhead flow sampling and calorimetry methods. Berkeley, Lawrence Berkeley Laboratory, LBL-9248, GREMP-7.

Elders, W. A., Hoagland, J. R., Olson, E. R., McDowell, S. D., and Collier, P., 1978. A comprehensive study of samples from geothermal reservoirs. Riverside, University of California, UCR/IGPP-78/26 (also LBL-9088, GREMP-4).

Harrison, Roger, and Randall, Georgia, 1979. Annotated research bibliography for geothermal reservoir engineering. Berkeley, Lawrence Berkeley Laboratory, LBL-8664, GREMP-1.

Kassoy, D. R., and Goyal, K. P., 1979. Modeling heat and mass transfer at the Mesa anomaly, Imperial Valley, California. Berkeley, Lawrence Berkeley Laboratory, LBL-8784, GREMP-3.

Lamers, Michael D., 1979. An appraisal of measurement methods for geothermal well system parameters. Berkeley, Lawrence Berkeley Laboratory, LBL-9090, GREMP-6.

Lawrence Berkeley Laboratory, Earth Sciences Division, 1977. Geothermal reservoir engineering management program plan (GREMP plan). Berkeley, Lawrence Berkeley Laboratory, LBL-7000, 135 p.

Lawrence Berkeley Laboratory, 1978. Earth Sciences Division annual report 1978. Berkeley, Lawrence Berkeley Laboratory, LBL-8648, 251 p.

Pritchett, J. W., Rice, L. F., and Garg, S. K., 1978. Summary of reservoir engineering data: Wairakei geothermal field. Berkeley, Lawrence Berkeley Laboratory, LBL-8669, GREMP-2.

Vetter, O. J., 1979. Scale inhibitor tests at East Mesa. Berkeley, Lawrence Berkeley Laboratory, LBL-9089, GREMP-5.

EVALUATION OF CITY WELL 1, KLAMATH FALLS, OREGON

S. M. Benson, C. B. Goranson, and R. C. Schroeder

ABSTRACT

A city-wide geothermal space heating project is currently under development at Klamath Falls, Oregon. The first phase of the project will require two production wells. Geothermally heated water will be used to heat 14 city, county, state, and federal buildings. At peak load the heating system will require approximately 750 gpm of 200°F (or greater) geothermal brine.

The first production well was spudded on August 29, 1979. During drilling a major lost circulation zone was encountered between 340 and 360 ft depth. At this time the well was cleaned, reamed, cased to 300 ft, and then pump tested. The well was pumped for a total of 15-1/2 hr. A maximum flow rate of 680 gpm, with 77 ft of drawdown, was held constant for 7-1/2 hr. Discharge temperature was approximately 218°F.

Three observation wells were monitored to determine the impact of producing large quantities of brine on the many private geothermal wells already in use for space heating. Preliminary indications are that the water level decline in the area will be small (2 to 3 ft). However, further testing is recommended to determine the effects of reservoir heterogeneity on the water level decline.

INTRODUCTION

A city-wide geothermal space heating project is currently under development at Klamath Falls, Oregon. Phase I of the project involves drilling two production wells, constructing a pipeline to transport the geothermal brine, designing a heat-exchanger system, and retrofitting 14 city, county, state, and federal buildings to use geothermally heated water. A flow rate of approximately 750 gpm of 200°F brine is required to meet the maximum heat load for Phase I of the project.

The first of two production wells was spudded on August 21, 1979. The selection of the drill site was based on several factors: proximity to the most active thermal region, availability of land, and distance from the existing private geothermal wells already in use. As part of the overall resource delineation study, lithologic logs from roughly 40 wells have been collected and examined. From these, two likely production zones have been identified. The first is at a depth of 200 ft, and the second is at a depth of 750 ft. While drilling the first well, a lost circulation zone was encountered between 340 and 360 ft. At this time, the well was reamed to 17-1/2 in. A 12-in. casing was then set at 300 ft. The well was pump tested for a total of 15-1/2 hr.

The purpose of the pump-test was twofold. First, the flow rate, well drawdown, and the wellhead production temperature was measured to determine the feasibility of using this aquifier as the production zone for Phase I of the district heating project. It was also necessary to measure the impact of producing large quantities of fluid from this zone on the many private geothermal wells in the area. If excessive drawdown of the surrounding wells took place, it would not be possible to use this aquifer as a producing zone for the project. A short term interference test (8 hr) was run in conjunction with a productivity test to determine inter-well communication and, if possible, to predict the effect of sustained production on the surrounding wells. The results of the tests will be discussed here.

WELL COMPLETION AND LITHOLOGY

A summary of the drilling rate, lost circulation zones, and lithology for City Well-1 is shown in Table 1. As is typical of the wells in this area, a sequence of roughly 250 ft of lacustrine and volcanic sediments overlie larger units of black, grey and "red" basalts. Several substantial lost circulation zones were encountered, one at about 195 ft and a second at 350 ft. The first occurred in a brown shale, and the second in an altered reddish basalt previously identified as a potential producing aquifer. When the second zone was encountered, the well was reamed to 17-1/2 in. and a 12-in. casing was cemented from ground level down to 300 ft. From 300 to 360 ft the well was left uncased.

WELL TEST DESIGN

The well test was designed with three primary objectives:

1. To determine if the shallow aquifier is suitable as a production zone for Phase I of the district heating program.

2. To obtain a more comprehensive model of the hydrogeology of the Klamath Falls KGRA (Known Geothermal Resource).

3. To assist in obtaining a data base to be used in establishing a resource management program.

To accomplish these objectives, a productivity test and a short term interference test were performed simultaneously. In this paper we will discuss the results of this test insofar as they pertain to the development of the district heating project.

Several factors must be taken into account in determining if the shallow aquifer is a suitable production zone for Phase I of the district heating program. First, flowing wellhead temperatures must be greater than 200°F to satisfy the heat-exchanger design specifications. A flow rate of 350 gpm with less than 250 ft of drawdown in the well must be obtained (one-half the required total flow rate based on peak load demands.) Finally, there must be a negligible impact (both thermal and hydrologic) on the many private geo-thermal wells in use for space heating, domestic hot water, and industrial processing.

PRODUCTION TEST RESULTS

For the production test, City Well-1 was pumped for a total of 15-1/2 hr. Table 2 summarizes the pumping time, flow rate, flowing wellhead temperature, and drawdown. During the test, a maximum pumping rate of approximately 680 gpm with 77 ft of drawdown was held constant for 7-1/2 hr. Discharge temperatures measured at this time varied between 217 and 219°F. The small drawdown at this rate far exceeded estimates for the shallow aquifer production capacity.

The water level in the pumped well was measured using an electric probe. The primary flow rate measuring device used was an orifice plate with a bourdon tube pressure gauge on the upstream side of the orifice. Because the brine flashed downstream of the orifice, the accuracy of the measured flow rate is poor. However, other methods were also used to estimate the flow rates, and those values were in close agreement with those obtained from the orifice measurement. The estimated flow rates are probably not accurate to better than 15% of the stated value. Higher flow rates could have been obtained with a deeper pump setting if the surface equipment (discharge pipe, pump platform, pump packing) had been more suitable (water well pumping equipment was used). Wellhead temperatures were measured continuously upstream from the orifice using an RTD probe. These values are believed to be accurate to ±0.2°F.

INTERFERENCE TESTING

Three observation wells were used to monitor the impact of pumping large volumes of fluid from City Well-1. Figure 1 shows the location of these wells. Two of the wells, the Head Well and the Adamcheck Well, are in an area where a large number of geothermal wells are currently in use. The monitor wells are completed in a similar manner and to similar depths as the many existing wells in this area. These monitor wells will most likely reflect the behavior in other existing wells.

In Figure 2 the well completion and well lithology are shown for each well. As shown in

TABLE 1 DRILLING AND COMPLETION HISTORY OF CITY WELL

KLAMATH FALLS CITY WELL 1

SPUD DATE AND TIME - AUGUST 21, 1979, 1640 HOURS

COMPLETION DATE - SEPTEMBER 17, 1979

CASING RECORD - 300 FT OF 12 IN BLANK CASING

DEPTH-FT	DRILLING RATE FT/HR	MUD TEMP °C	MUD LOSSES/ WARM ENTRY	LITHOLOGIC COLUMN	SAMPLE DESCRIPTION--PRELIMINARY
					0-2 FT - TOP SOIL
10	50	--	--		2-20 FT - DIATOMITE, WHITE, SILICA FILLED VEINS
20	50	--	--		20-47 FT - DIATOMITE, WHITE
30	60	16	--		47-66 FT - DIATOMITE, SOME GREY SHALE
40	60	16	--		
50	50	17	--		
60	18	20	--		66-93 FT - GREY SHALE AND CLAY
70	17	21	--		
80	17	23	--		
90	17	24	--		93-104 FT - BLACK SHALE
100	17	26	--		
110	30	29	--		104-116 FT - GREY SHALE
120	40	30	--		
130	40	32	--		116-147 FT - BROWN SHALE AND CLAY
140	40	34	--		
150	40	35	--		147-152 FT - GREY SHALE AND CLAY
160	40	36	- WARM WATER		152-160 FT - BROWN SHALE AND GREY TUFF
170	30	39	ENTRY 160-170FT		160-170 FT - GREY TUFF AND SHALE
180	25	37	- WARM WATER		
190	30	41	ENTRY 178-185 FT		170-198 FT - BROWN SHALE
195	20	40	- SUBSTANTIAL		
200	20	29	MUD LOSS-195 FT		198-243 FT - BLUE AND GREY SHALE
210	20	29			
220	20	29	- LOSING MUD		
230	20	30	195-245 FT		243-253 FT - STREAM DEPOSIT OVERLYING BLACK BASALT, CONSIDERABLE 'BLUE' QUARTZ VEINING
240	5	31			
250	3	31	- LOST CIRCULATION		253-276 FT - GREY BASALT-SOFT
260	3	31	AT 248 FT		
265	10	31			276-279 FT - GREY BASALT-HARD
270	10	32	- CONTINUOUS		
280	15	36	SLOW LOSS OF MUD		279-285 FT - REDDISH BROWN BASALT
285	5	35	- LOST CIRCULATION		
290	3	39	292-298 FT		285-341 FT - HARD GREY BASALT AND CLAY
300	2	37	- LOSING MUD		
310	3				
320	3				
330	3				
340	2	MUD TEMP INCREASING	- LOSING MUD 340 - 360 FT		341 FT - END OF HARD BASALT
350	20				341-360 FT - RED BASALT
360	20				

TABLE 2 SUMMARY OF PRODUCTION TEST (CITY WELL 1)

TIME	FLOWRATE	TEMPERATURE	PUMPING LEVEL	DRAWDOWN
5 HRS	260 GPM	212° F	111 FT	35 FT
2 HRS	480 GPM	215°F	115 FT	39 FT
1 HRS	550 GPM	217°F	125 FT	49 FT
7.5 HRS	680 GPM	217-219°F	153 FT	77 FT

STATIC WATER LEVEL	∿ 76 FT
WELL DEPTH	∿360 FT
CASING SIZE	12 IN
OPEN INTERVAL	300-350 FT
PUMP SETTING	200 FT (5 IN. COLUMN, 8 IN. BOWLS)

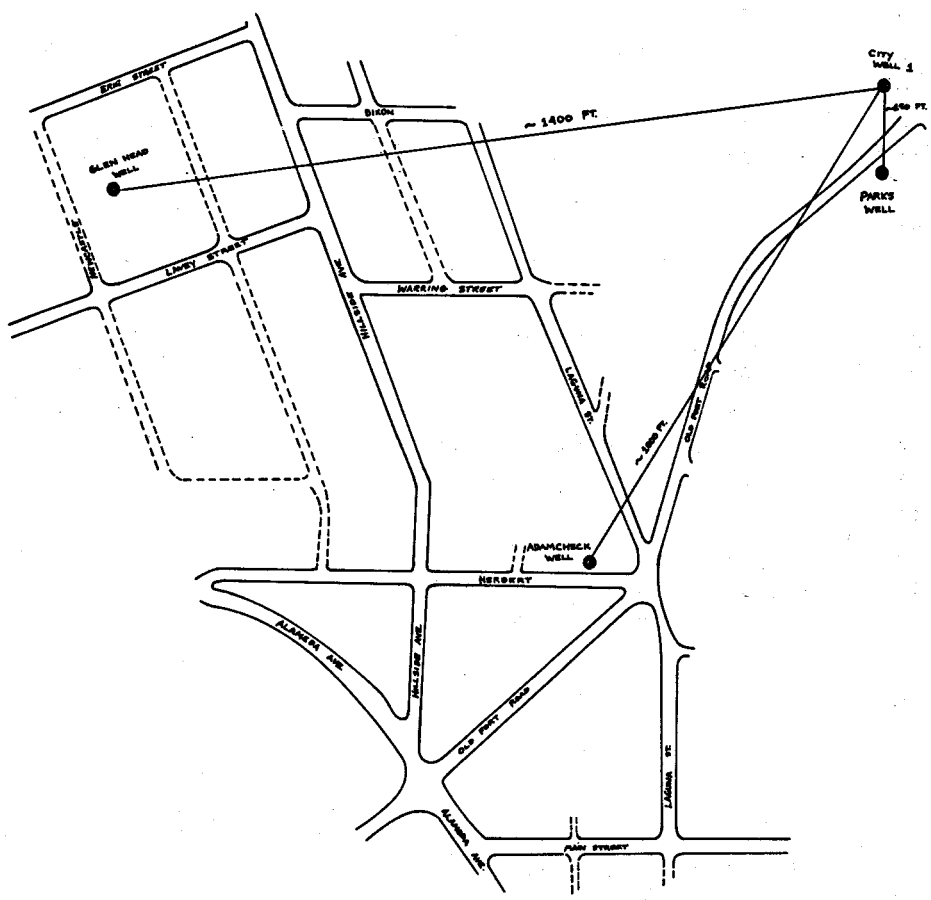

Figure 1. Locations of monitor wells and City Well-1. (XBL 802-8113)

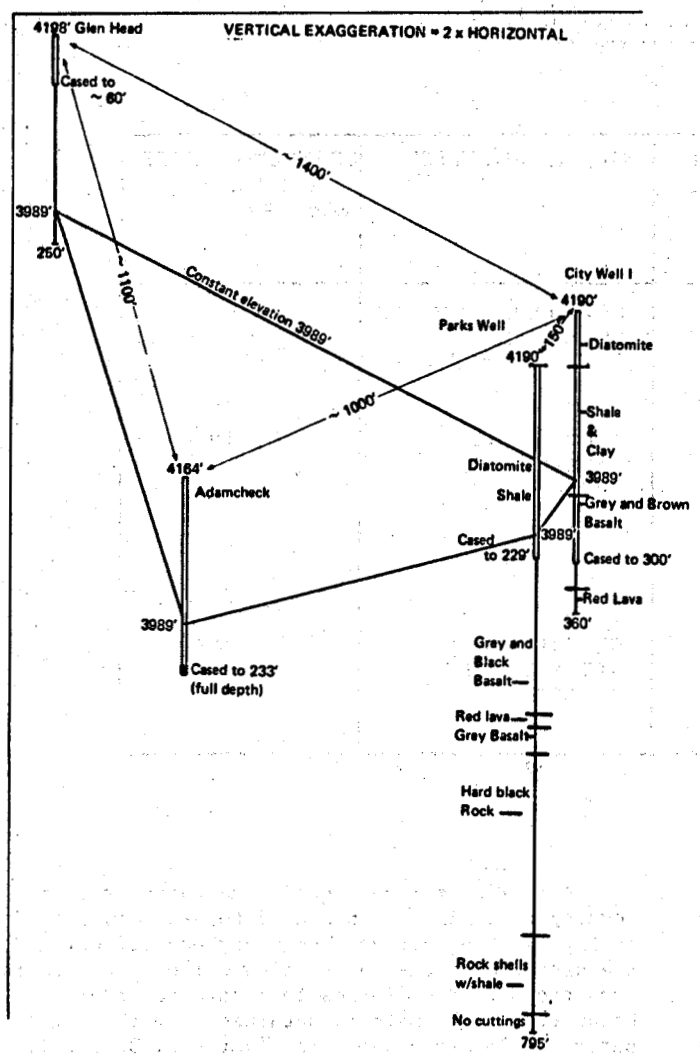

Figure 2. Fence diagram of monitor wells and City Well-1. (XBL 801-6744)

the figure, two of the wells, Head and Adamcheck, are shallower than the city well. The lithologic logs from these wells are not available at this time. Well logs from several surrounding wells indicate that these two wells penetrate approximately 200 ft of lacustrine sediments, which are underlain by a highly permeable volcanic tuff or pumice. It is doubtful that these wells penetrate the red basalt strata, which is the production zone for the city well. The difficulties encountered in correlating individual strata from one well to another indicate complex faulting in the area (or lake bed sediments deposited in a tectonically active area). The Parks Well is open to the same reservoir interval as the city well. However, correlation on individual strata between the two wells is not obvious.

INTERFERENCE MONITORING EQUIPMENT

Water levels in the Adamcheck Well and the Head Well were monitored using Leopold-Stevens continuous-recording water level devices. Changes in water level of 1/2 in. can be easily resolved. Background data were obtained from these wells for several months before the test. At the onset of the cold season in September, a decline of the water levels took place at a similar rate in all of the monitor wells. The water level was dropping at a rate of approximately 3 ft/mo. when the pump test began. Figure 3 shows the water level data obtained during the interference test.

Water level changes in the Parks Well were measured using a downhole Paro-Scientific pressure transducer. The transducer measures changes of water level by measuring the weight of the column of water above it. The instrument has a resolution of approximately 0.01 psi (better than 1/2 in.). Pressure data are recorded automatically at specified time intervals ranging from 1 sec to 2 hr. For this test, data points were recorded at 10-sec intervals each time the pump was turned on or off and at 2-min intervals when water level changes occurred less rapidly. Table 3 summarizes the instrumentation and the location of the wells used in the test. Figure 4 shows the data obtained from the Parks Well during the interference test.

INTERFERENCE TEST ANALYSIS

The rapid drop in water levels at the onset of production from City Well-1 indicates a high degree of hydrologic reservoir continuity. Response time at the Parks Well (150 ft) was less than 10 sec after the pump was turned on. At the other two observation wells, response time was short but difficult to measure because of the non-digital time display. Interference tests can be used to determine the reservoir parameters that control reservoir drawdown. Together with an accurate hydrogeologic model of the reservoir, these parameters can be combined to predict how the system will respond to pumping (and/or injection) with any arbitrary flow rate schedule and well configuration.

Interference test data are usually analyzed using a simplified reservoir model. The model assumed in this analysis was that on which the Theis solution is based. This model assumes the production well fully penetrates an isothermal, isotropic, homogeneous, porous medium of infinite

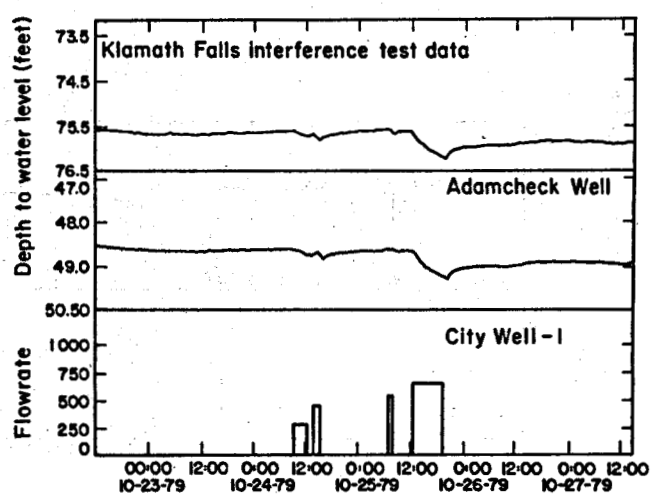

Figure 3. Interference test data from the Head Well and the Adamcheck Well. (XBL 801-131)

TABLE 3 SUMMARY OF INTERFERENCE TEST

WELL	LOCATION	DISTANCE TO CITY WELL 1	INSTRUMENTATION	DRAWDOWN AFTER 7 1/2 HRS @ 680 GPM
PARKS	OLD FORT RD.	180 FT	DOWNHOLE PRESSURE TRANSDUCER	1.2 FT
ADAM-CHECK	HERBERT & LAGUNA ST.	1000 FT	CONTINUOUS WATER LEVEL RECORDER	7 IN
HEAD	NEWCASTLE	1420 FT	CONTINUOUS WATER LEVEL RECORDER	7 IN

areal extent and constant thickness. The data from the Adamcheck Well and the Head Well are shown matched to the Theis curve in Figures 5 and 6 respectively. The match of the data is acceptable for these small measured drawdowns. The transmissivity values calculated range from 1.4×10^7 to 1.5×10^7 md-ft/cp and the storativity values range from 2.4×10^{-3} to 7.8×10^{-3} ft/psi. The data begin departing from the Theis curve toward the end of the test, indicating that some sort of hydrologic boundary or reservoir heterogeneity may be affecting the reservoir response. Another explanation for the departure from the Theis curve is that the reservoir water level trend recorded before the test is affecting the drawdown.

A nonlinear least-squares matching program developed at LBL was then used to determine if an impermeable reservoir boundary was affecting the drawdown at the observation wells. The program uses the method of images to locate reservoir boundaries. The matches obtained from the computer analysis are shown in Figures 7, 8, and 9. Two of the wells, the Adamcheck Well and the Parks Well, suggest that an impermeable boundary may be affecting the data. The location of this boundary, however, is nonunique. A longer test with a constant background pressure is necessary to determine both the existence and location of a boundary. Table 4 summarizes the results obtained from the computer analysis.

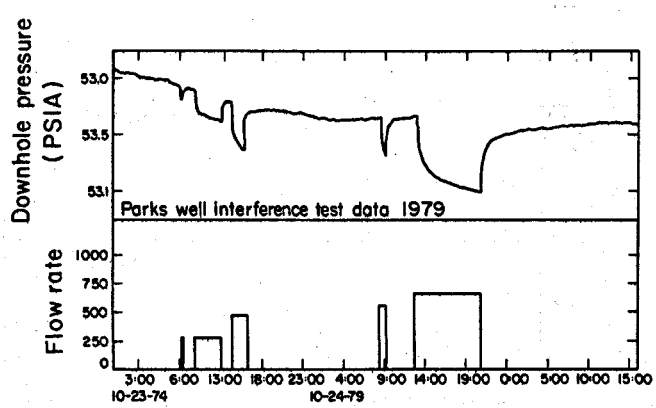

Figure 4. Interference data from Parks Well. (XBL 801-132)

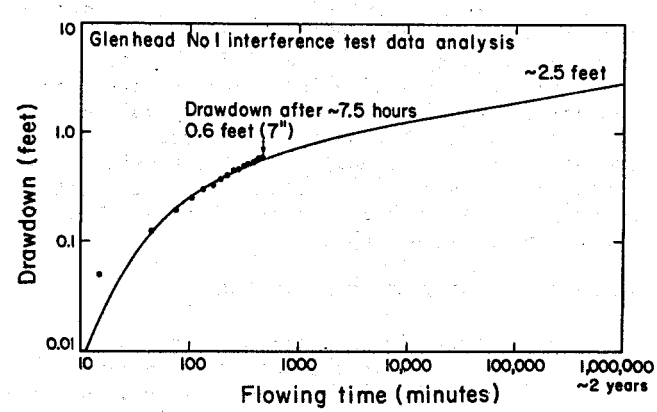

Figure 5. Theis curve match of interference test data from the Head Well. (XBL 801-134)

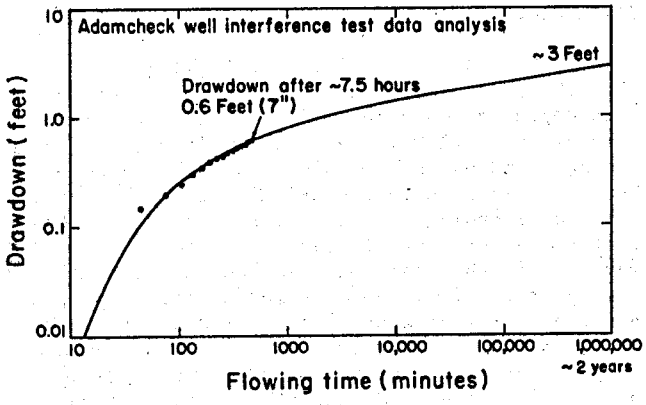

Figure 6. Theis curve match of the Adamcheck well interference data. (XBL 801-133)

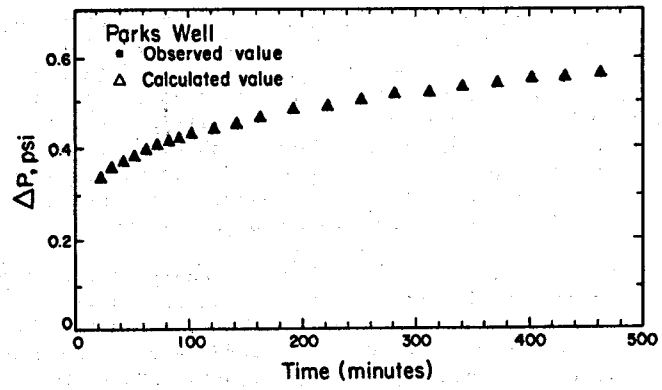

Figure 8. Computer match of the Parks Well interference test data. (XBL 801-137)

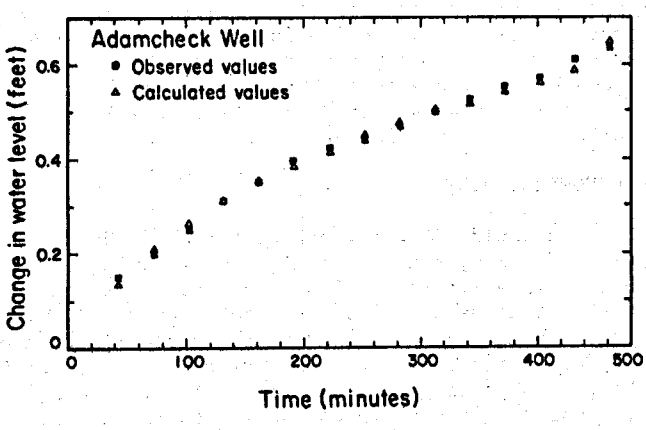

Figure 7. Computer match of the Adamcheck Well interference data. (XBL 801-135)

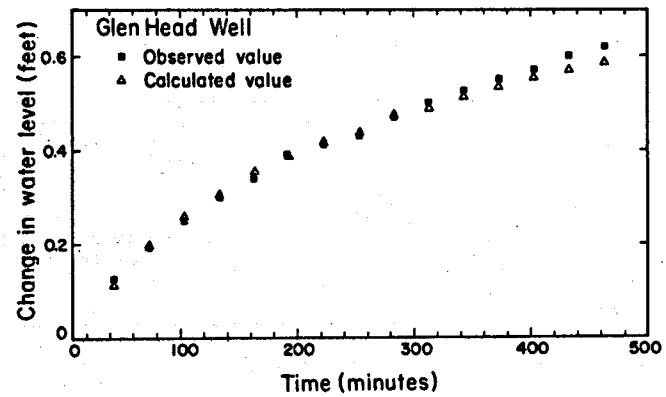

Figure 9. Computer match of the Head Well interference test data. (XBL 801-136)

TABLE 4 COMPUTER MATCH OF WELL DATA

WELL	DISTANCE TO CITY WELL-1	KH/μ (MD·FT/CP)	ϕCH (FT/PSI)	DISTANCE TO BOUNDARY
ADAMCHECK	1000 FT	$2.6 \cdot 10^{7}$	$1.1 \cdot 10^{-3}$	2280 FT
GLEN HEAD	1400 FT	$1.7 \cdot 10^{7}$	$1.4 \cdot 10^{-3}$	
PARKS	200 FT	$3.3 \cdot 10^{7}$	$9.1 \cdot 10^{-4}$	4300 FT

Figure 10 shows a log ΔS vs log t/r^2 plot for all of the observation wells. If the reservoir model discussed above was accurate, the data should plot as one curve. The discrepancy could be caused by any of several factors: reservoir heterogeneity, fractures, reservoir boundaries, partial penetration, dual porosity and so on. To accurately discern the cause of the discrepancy, an interference test of longer duration would be necessary.

The values obtained from the analysis indicate that the shallow reservoir permeability is very high. Assuming an aquifer thickness of 40 ft, and a viscosity value of 0.3 cp (220°F water), the calculated permeability value is approximately 100 darcies. The porosity value extracted from the storativity value (ϕcH) using a compressibility of 5×10^{-5} psi^{-1} is approximately 0.5. This is anomalously high, indicating that the values used for the compressibility and reservoir thickness are uncertain.

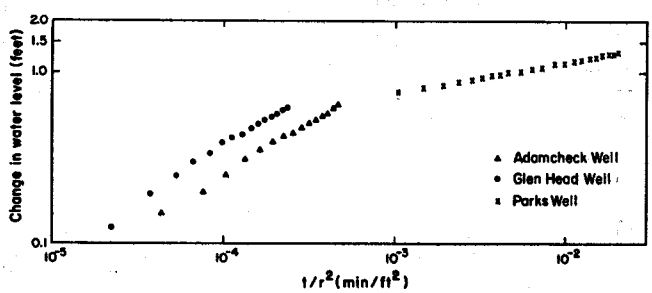

Figure 10. Log Δs vs log $(\Delta t/r^2)$ plot of the interference test data. (XBL 801-6747)

CONCLUSIONS

The tests of the Klamath City Well #1 show that the shallow test aquifer is capable of sustained production of at least 680 gpm at a temperature of about 218°F. Rapid water level changes in the surrounding wells indicate a high degree of hydrodynamic reservoir continuity through several distinct lighologic units. This would indicate that a fracture network may be controlling fluid movement in the reservoir. Calculated transmissivity values from the interference test indicate a permeability of approximately 100 darcies. When the pressure behavior over the 8-hr interference test are extrapolated to several years, drawdowns of 2 to 3 ft are predicted at a sustained production rate of 680 gpm. However, the data show a departure from the Theis curve match near the end of the test interval. This departure could imply greater drawdowns than predicted by these tests. At present no unique explanation can be given to account for this departure. To accurately predict the effects of sustained production over the lifetime of this project a longer test must be conducted to determine the effects of reservoir heterogeneity on the water level decline in sur-rounding wells. Present indications, from reservoir testing at the Klamath Falls, are that this system has a very promising potential for development of a large-scale district heating project.

ACKNOWLEDGEMENTS

We would like to thank G. Parks, G. Head, C. Adamscheck, and T. Fillmore for allowing us to use their wells in previous and subsequent reservoir tests at Klamath Falls. We also thank John Lund, Paul Lienau, and Gene Culver from Oregon Institute of Technology Geo-Heat Utilization Center for their help in obtaining information on the Klamath Falls resource. Finally, we would like to thank Harold Derrah, Assistant City Manager of Klamath Falls, for his patience and help.

EVALUATION OF THE SUSANVILLE, CALIFORNIA, GEOTHERMAL RESOURCE, 1979

S. M. Benson, C. B. Goranson, J. P. Haney, and R. C. Schroeder

INTRODUCTION

The Susanville geothermal anomaly is located in northeast California. The presence of several shallow hot-water wells and a natural hot spring initially identified in this area as a prospective candidate for the development of geothermal energy. Increased fossil fuel cost and the high price of transporting liquified natural gas to the area stimulated interest in developing the resource for a city-wide space-heating program. Since late 1978, the U.S. Bureau of Reclamation and Lawrence Berkeley Laboratory's Earth Sciences Division have collaborated on a geothermal resource evaluation project at Susanville, California. As part of this project, 12 exploratory temperature gradient holes were drilled, subsurface geologic and geophysical data were analyzed, and a well test was conducted.

The town of Susanville lies at the intersection of three major geologic regimes, the Sierra Nevada Range to the southwest, the Modoc Plateau to the northwest, and the Basin and Range Province which extends into Nevada (Rudser, 1978; U.S. Bureau of Reclamation, 1976a,b,c). Subsurface geology is characterized by interbedded basalt flow, agglomerates, and alluvial conglomerates. Subsurface and surface geologic structure indicate extensive block faulting, with the dominant trend in a northwesterly direction. Subsurface temperature contours indicate the occurrence of the geothermal anomaly is fault related.

WELLS IN THE CITY OF SUSANVILLE

Six geothermal wells had been drilled in Susanville before the 1970s. These wells had been used for heating a greenhouse, space heating, and heating a swimming pool. Because these wells (Naef well, LDS Church well, Roosevelt Swimming Pool, and Davis well) were drilled long ago little detailed information on well lithology, temperature, completion, and total depth is available.

The U.S. Bureau of Reclamation has drilled 12 exploratory wells and five shallow temperature gradient holes. The locations of the twelve exploratory wells are shown in Figure 1. Well sites were chosen in an attempt to define the areal extent of the geothermal anomaly. Depths of the well ranged from 135 to 640 m. Well diameters were 6 in. and were completed with a 2-in. sealed casing. Two of the wells, Suzy-4 and Suzy-6, were completed with 4-in. and 6-in. casings, respectively. The total depths, casing size, and completion schedule are shown in Figures 2 and 3.

Detailed interpretation of the formation lithology and geophysical bore logs have been completed. Several distinct units, probably offset by faults, have been identified. All of the wells, however, penetrated a sequence of basalt, mud-flow and ash-flow agglomerates. Several of the wells on the southern portion of the anomaly penetrate alluvial conglomerates. The contact zones between the basalt layers and the conglomerates have been identified as the major geothermal production zones. The agglomerate and the conglomerates may also contribute to the geothermal production.

TEMPERATURE DISTRIBUTION

Temperature profiles obtained from the wells are shown in Figures 4, 5, and 6. Several of the wells in the southwest portion of the anomaly dis-

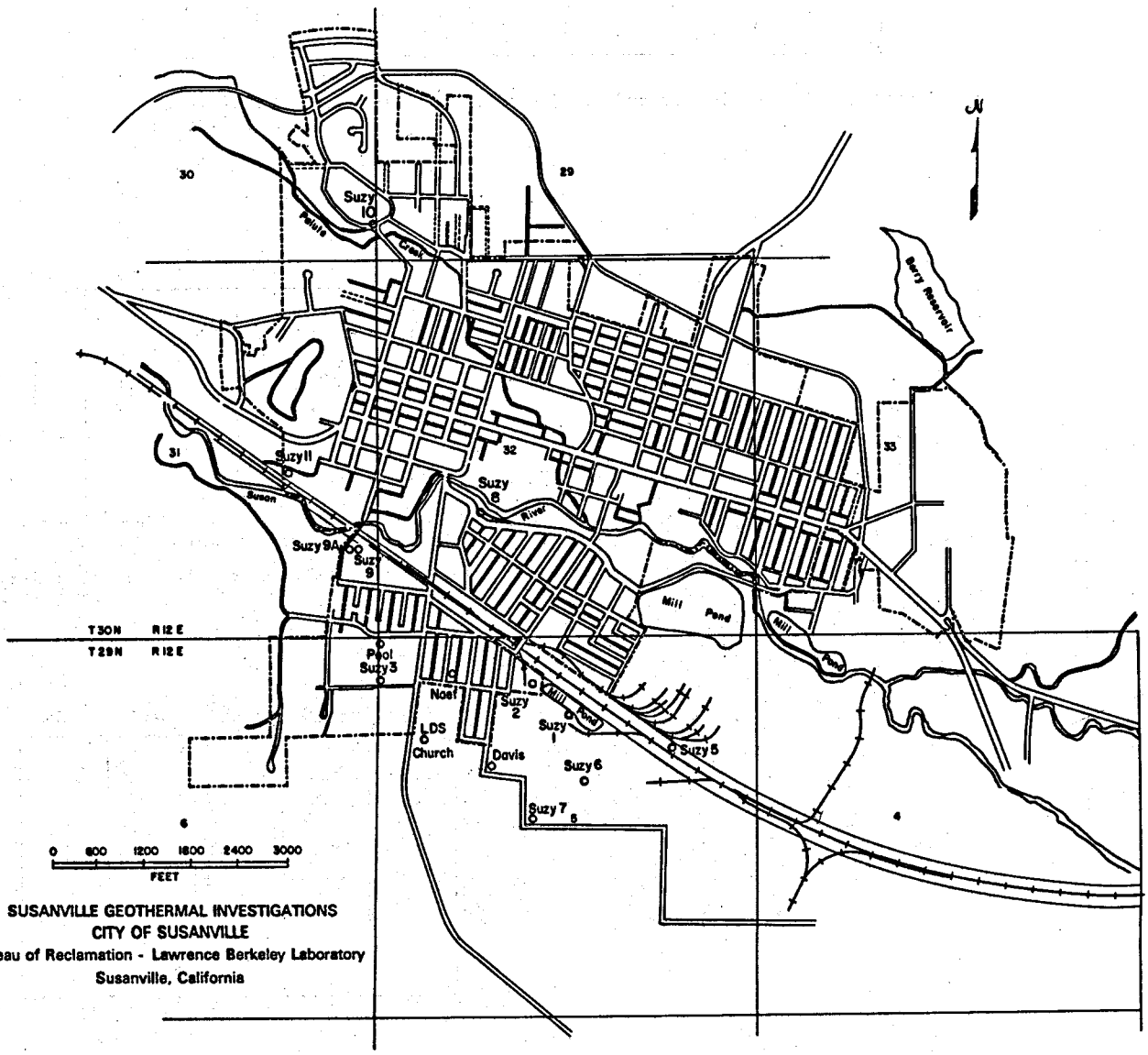

Figure 1. Geothermal well locations in Susanville, California. (XBL 801-6767)

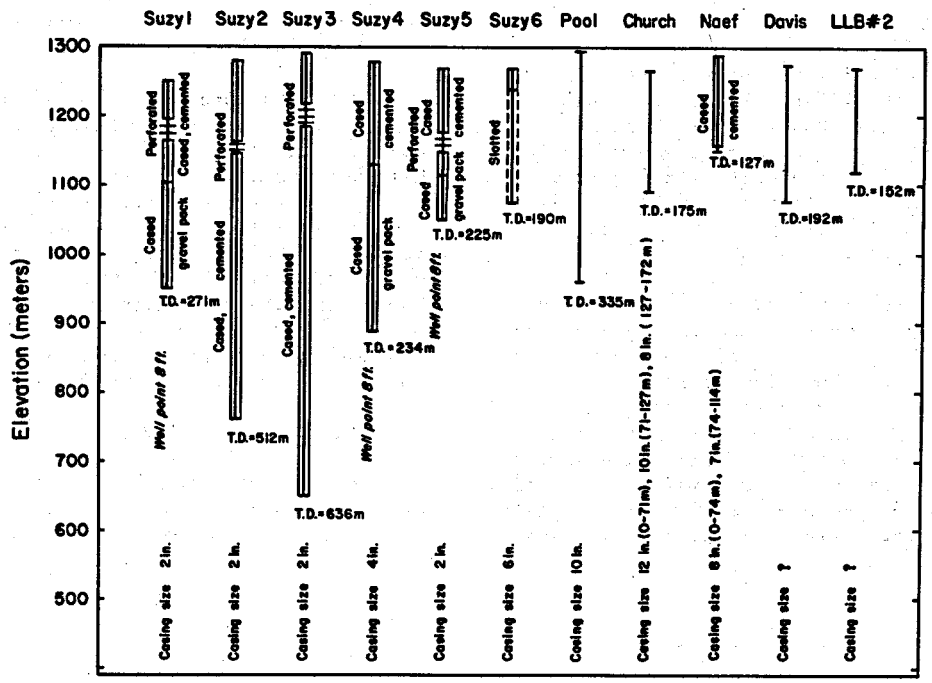

Figure 2. Completion record of the wells in Susanville, California. (XBL 795-7442)

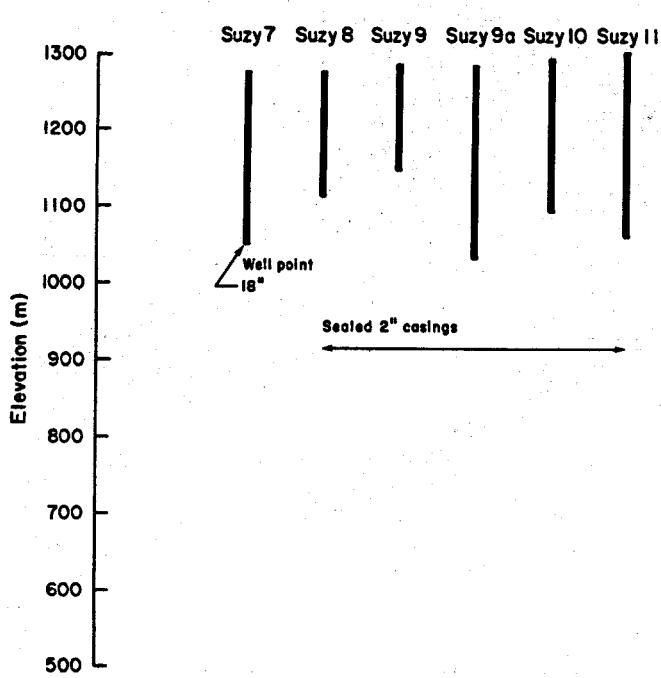

Figure 3. Well completions of Suzy-7 through Suzy-11, Susanville, California. (XBL 7912-13485)

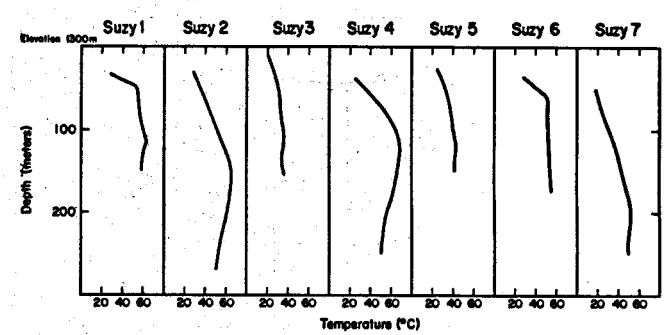

Figure 4. Temperature profiles in wells Suzy-1 to Suzy-7. (XBL 795-7495)

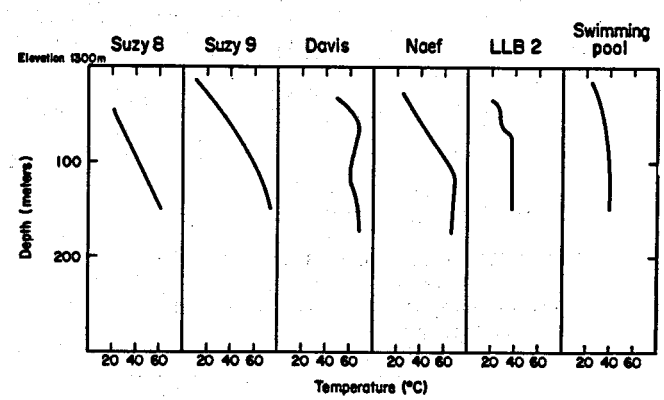

Figure 5. Temperature profiles for wells Suzy-8, Suzy-9 and several older wells in Susanville, California. (XBL 795-7496)

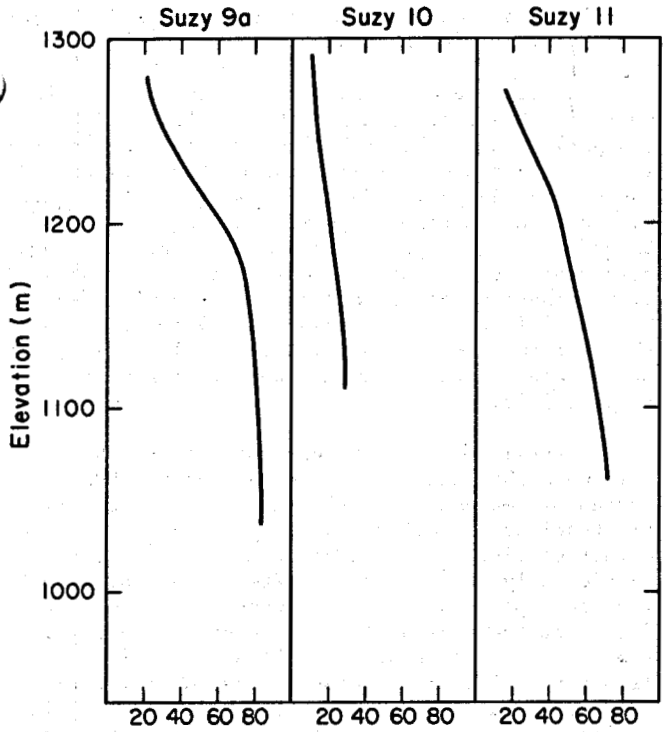

Figure 6. Temperature profiles for Suzy-9a through Suzy-11. (XBL 7912-13486)

play temperature reversals with depth. The temperature reversals take place at depths between 100 and 150 m. The reversals nearly coincide with the contact zones between the basalt and the conglomerate, which is further evidence that the producing aquifer(s) occur at the contact zones in those wells. Maximum temperatures range from 35°C to 70°C. The hottest wells are Suzy-9 and Suzy-9a. No temperature reversals take place, indicating the possibility of higher temperatures with depth. However, the productivity of this section of the reservoir is unknown. Further testing in this area will indicate the productivity of these higher-temperature zones.

Temperature contours at 50 m (1250-m elevation) and 100 m (1200-m elevation) are shown in Figures 7 and 8. The contours are asymmetrically shaped around a northwest-trending axis. The anomaly is sharply bounded to the west, indicating a hydrologic or geologic discontinuity (e.g., a fault or fracture zone). To the south, east, and north, the thermal anomaly gradually abates. Analysis of cores and geophysical data suggests cooler groundwater from saturated strata are mixing with geothermal fluids in these areas. The asymmetrically shaped thermal anomaly and the noticeable temperature reversals in the southern portion of the field suggest heated fluids are upwelling along a northwest-trending fault. They are then dispersed into the reservoir along the most permeable strata. In the southern portion of the anomaly, the basalt-conglomerate interface appears to be the most permeable.

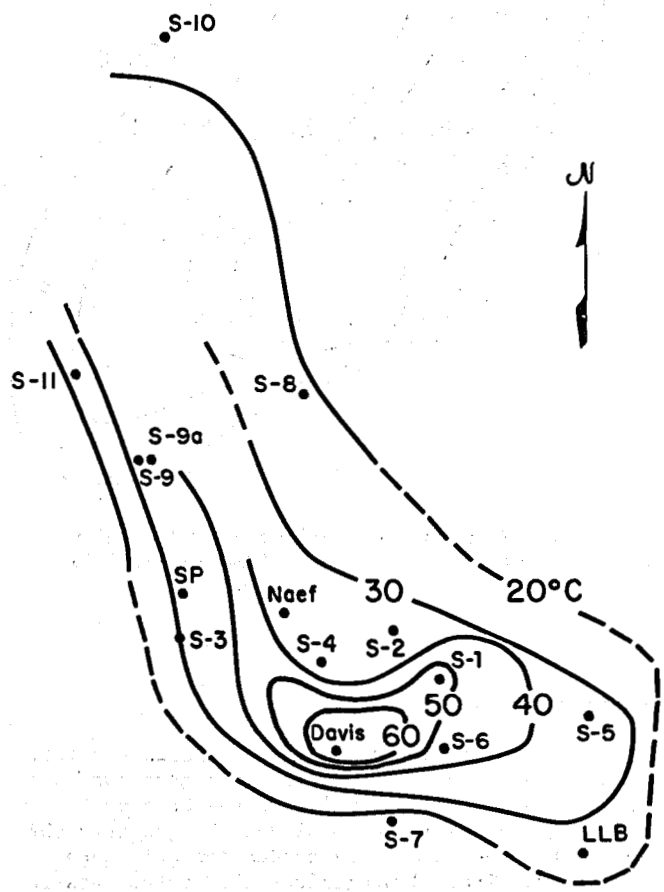

Figure 7. Temperature contours at 50 m below ground level. (XBL 806-7212)

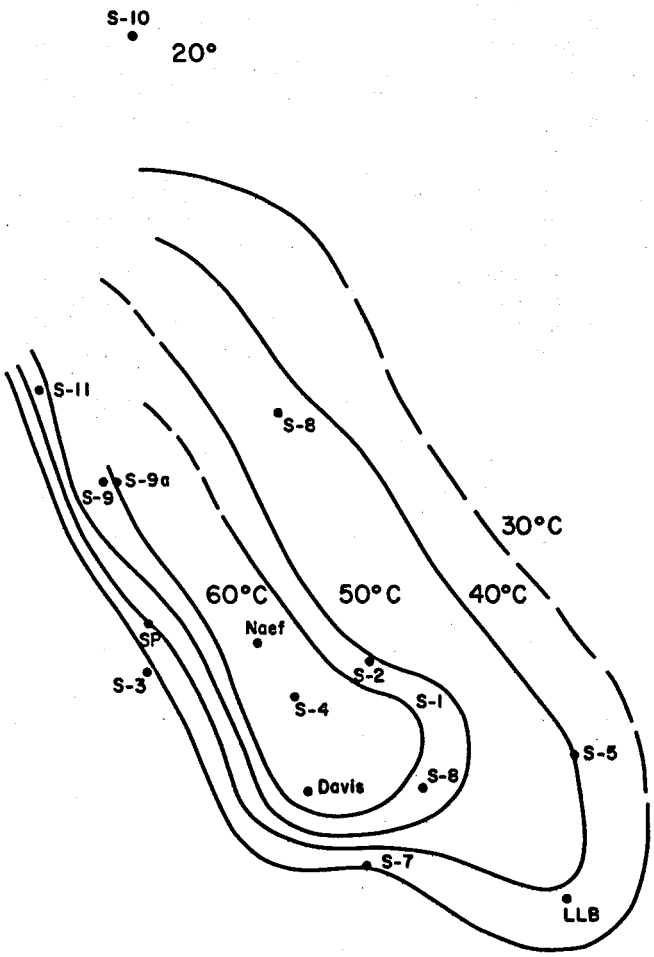

Figure 8. Temperature profiles at 100 m below ground level. (XBL 7912-13487)

RESERVOIR TESTING

A well test was conducted by LBL in December 1978 and January 1979. During this test two wells were pumped, the Davis well and the Roosevelt swimming pool well. Water level changes in eight observation wells and one production well were monitored. Table 1 summarizes the instrumentation and wells used. The test consisted of four segments. The first segment consisted of obtaining background data before pumping the Davis well. However, due to the extremely cold weather the LDS Church well was produced for space heating. To avoid or minimize any transients associated with the church well flow, the rate was held constant at approximately 90 gpm throughout the background data collection period and the subsequent pumping of the Davis well. The second segment of the test consisted of pumping the Davis well at a rate of 250 gpm for a period of 9 days. The well was then shut in and the build-up was observed. Several days after the Davis well was shut in, the LDS Church well was shut in for 12 hr, then pumped again for several days; shut in for 12 hr and then pumped continuously for the duration of the test. During the last segment of the test the Roosevelt swimming pool well was pumped at a rate of ~275 gpm for three days and then shut in.

The magnitude of drawdowns at the observation wells in this test were from 0.3 to 1.5 m (0.4 to 2.4 psi). The wells with 2-in. casing were instrumented with nitrogen-filled tubing (Suzy-1, Suzy-2, Suzy-3, and Suzy-5). Well Suzy-4 was instrumented with a downhole Paro-scientific pressure transducer, LLB-2 was instrumented with a Hewlett Packard downhole transducer. The Naef well was instrumented with a continuously recording water-level gauge. Water-level data (and pressure data) obtained during the test for the Naef well, Davis well, Suzy-3, Suzy-4 and Lassen Lumber and Box are shown in Figures 9-13.

Several months of background data at the Naef well were obtained before the test by the U.S. Bureau of Reclamation. Figure 14 shows the daily fluctuations of ±0.2 ft superimposed on larger magnitude fluctuations throughout the summer months. Particularly curious is the water level build-up that took place over several weeks in the early fall. At the present time the cause is unknown. However, several possible explanations exist. If rainfall were particularly heavy during this period, influx of this water from either overlying sediments or the river could cause this behavior. Or, the cessation of irrigation after the summer months could cause a pressure build-up in the reservoir. Both of these possibilities are highly speculative, but pressure data do indicate that the reservoir is effected by external sources.

The sharp peaks and valleys in the data starting at the beginning of September are caused by production at the LDS Church well. An expanded section of these data, shown in Figure 15, reveals three build-ups and drawdowns corresponding to the Church well being shut in for several hours and then pumped again. Analysis of these data returned a transmissivity value of 3.6×10^6 md-ft/cp and a storativity value of 2.3×10^{-4} ft/psi. The best match of the data obtained indicated the pressure response was influenced by an impermeable reservoir boundary. The location of this barrier cannot be established with one observation well. The best match obtained between calculated and observed pressures is shown in Figure 16.

Those wells instrumented with nitrogen-filled tubing (Suzy-1, Suzy-2, Suzy-3, and Suzy-5) were strongly affected by daily temperature and atmospheric pressure changes. This noise obscured both the initial pressure and the drawdown (if any) caused by the production well(s). These data are not considered to be suitable for analysis. The data obtained at Suzy-4 and at the Lassen Lumber and Box wells illustrate drawdowns of 2 psi and 0.5 psi, respectively. Both of these wells show two peculiar features as compared with other wells (see Figures 9, 12, and 13). First, they both show a gradual pressure decrease several days before the Davis well was shut in. Second, they both displayed a pressure build-up before shutting in the Davis well. For this reason, the data from these wells are not suitable for complete analysis.

Because both of these wells incurred a drawdown due to the Davis well production it can be

Table 1. Summary of instrumentation and wells used in Susanville, California well tests.

Well	Test Classification	Measurement Parameter	Instrumentation	Resolution	Comments
Naef	Observation	Water Level	Leupold-Stevens type A water level recorder, owned by USBR	0.1 ft	Clear evidence of communication between Davis well, church well and the swimming pool well. Accuracy of data uncertain between 12/16/78 to 12/20/79 due to sticking of water level recorder.
Davis	Production-observation	Pressure	40 ft of tubing in pipe-pump annulus, connected Paroscientific pressure transducer	0.01 psi	After 12/19/79 probable nitrogen leak in tubing which caused subsequent pressure change. Clear evidence of communication with the Church well.
		Wellhead temperature	Platinum RTD	0.1°F	
		Flow	Orifice and Pitot tube	20%	
LDS Church	Production	Flow	Flow measured using container and stopwatch	20%	
LLB 2	Observation	Pressure	Hewlett-Packard pressure probe and	0.01 psi	
		Temperature	Gearhart-Owen temperature tool set at 425 ft	0.1°F	
Suzy-1	Observation	Pressure	50 ft tubing connected to Paroscientific pressure transducer	0.01 psi	The perforation job was not successful. No pressure change due to flowing wells was recorded.
Suzy-3	Observation	Pressure	250 ft tubing and chamber connected to Paroscientific pressure transducer	0.01 psi	
Suzy-4	Observation	Pressure	Downhole Paroscientific transducer set 5000 ft	0.01 psi	
Suzy-5	Observation	Pressure	200 ft tubing and chamber connected to Paroscientific pressure transducer	0.01 psi	Did not respond to the reservoir pressure due to unsuccessful perforation job.
Roosevelt Swimming Pool	Production	Flow	Private communication	20%	

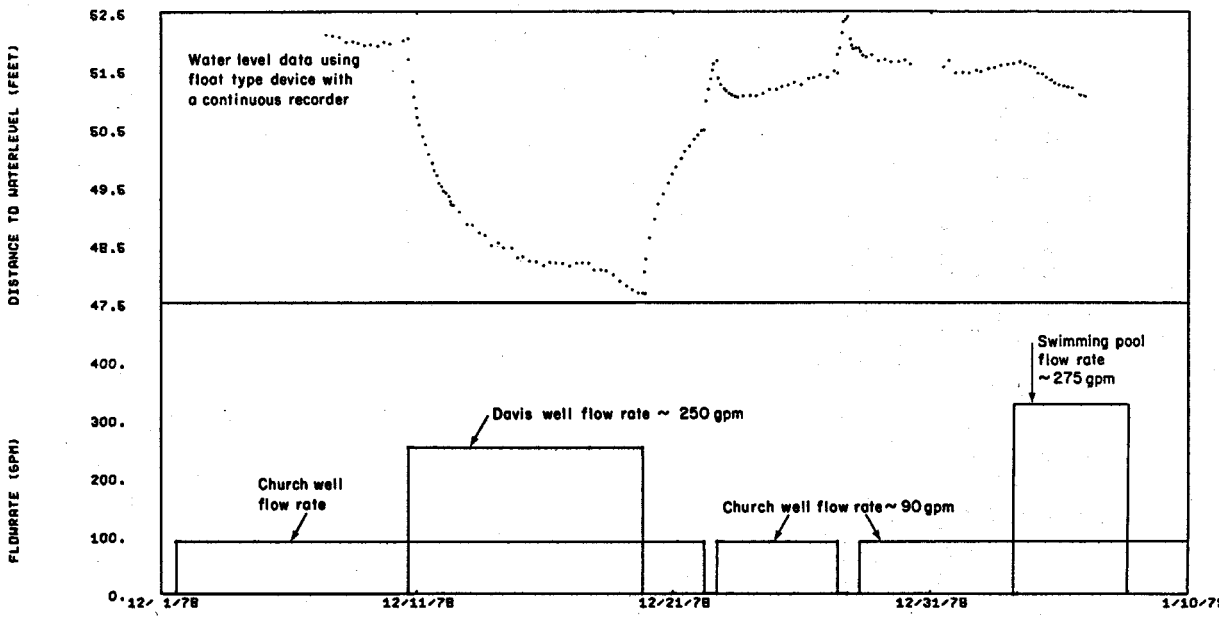

Figure 9. Naef well interference data. (XBL 795-7441)

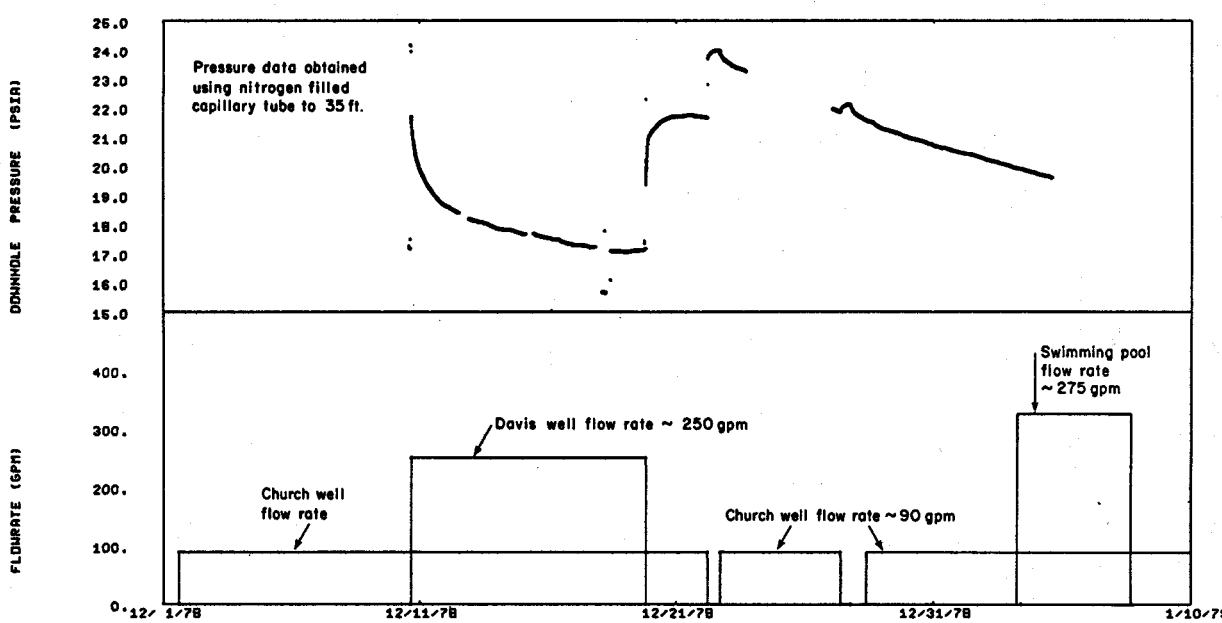

Figure 10. Davis well production data. (XBL 795-7439)

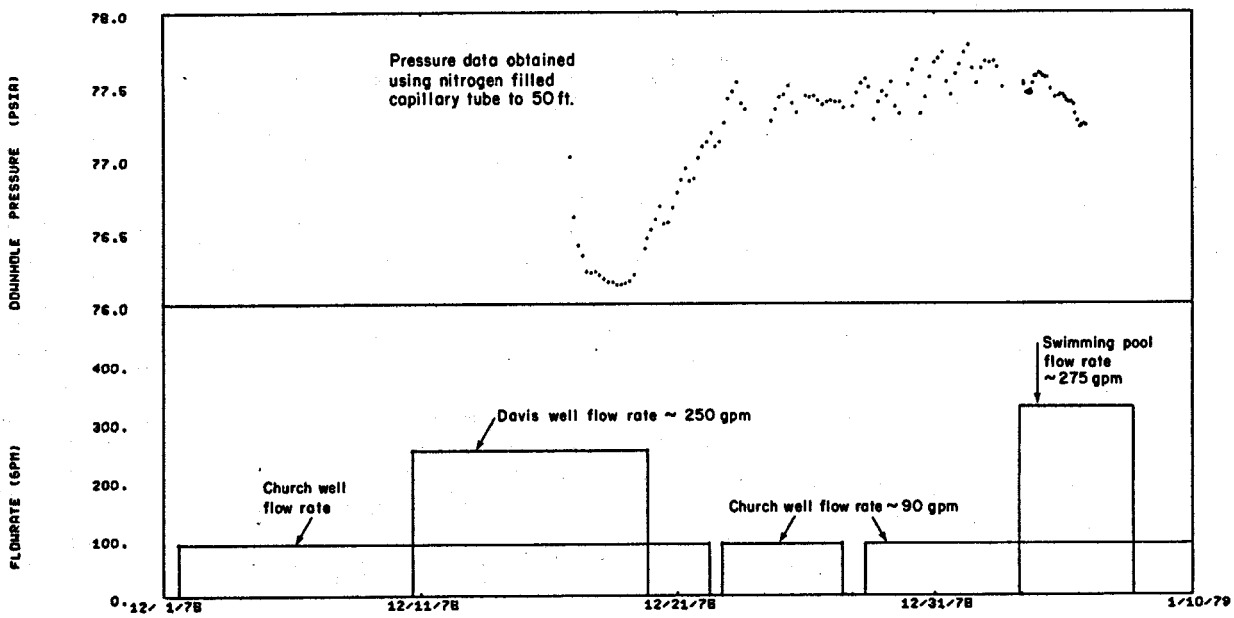

Figure 11. Suzy-3 interference data. (XBL 795-7438)

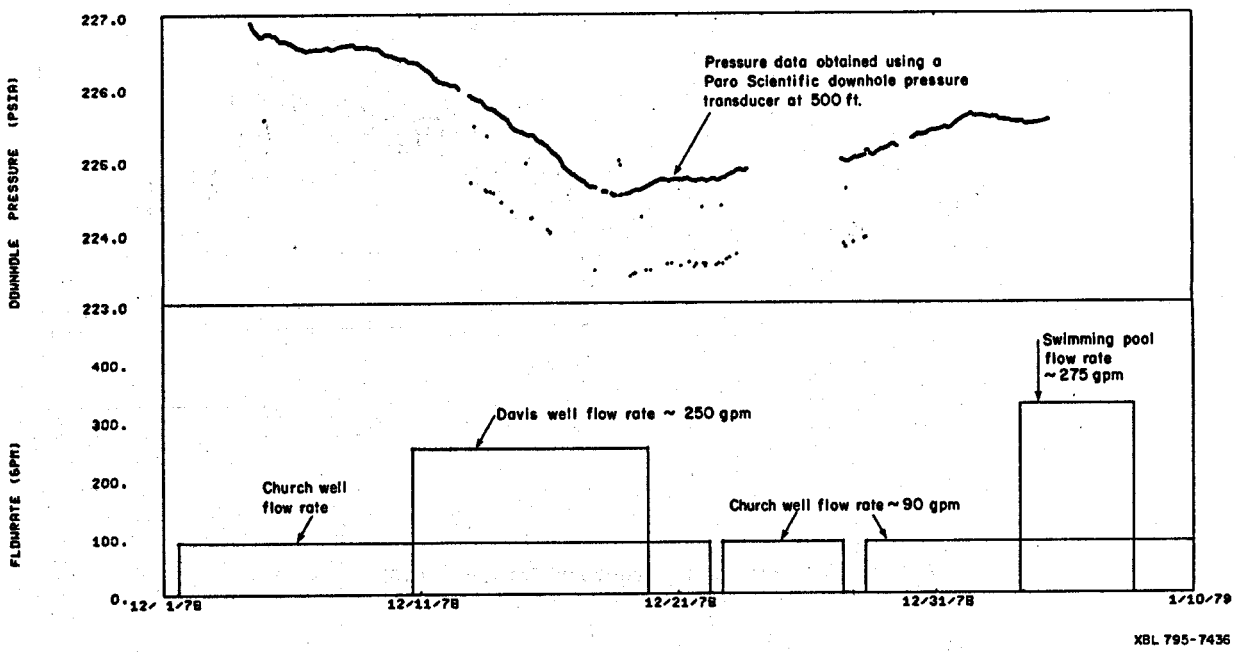

Figure 12. Suzy-4 interference data. (XBL 795-7436)

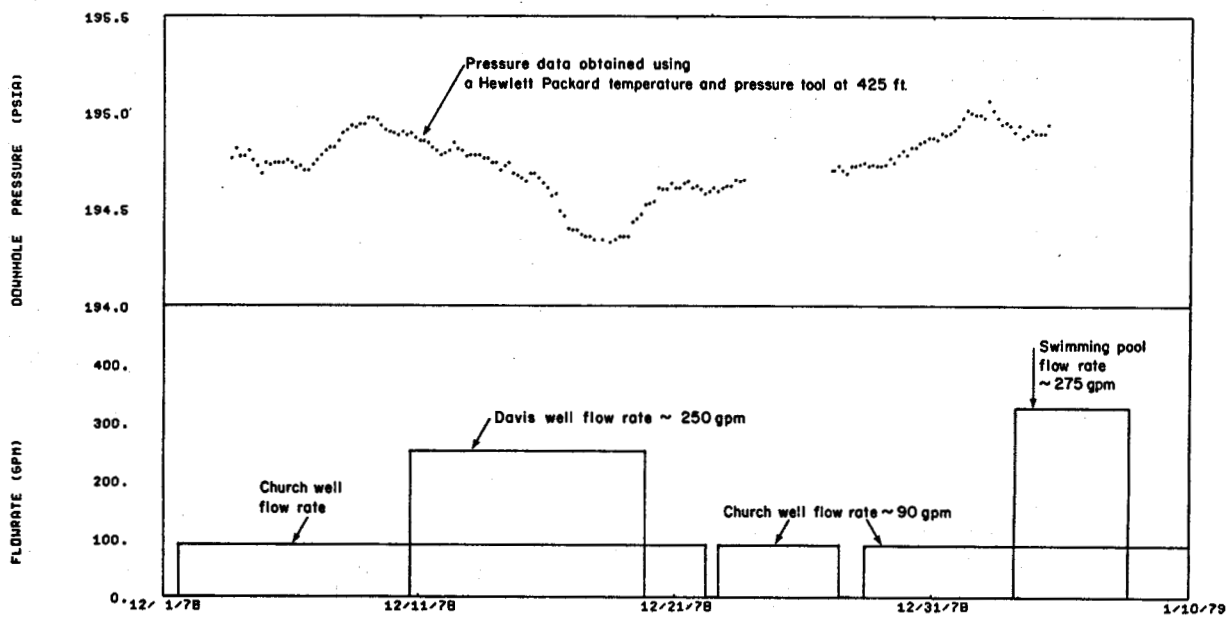

Figure 13. LLB-2 interference data. (XBL 795-7440)

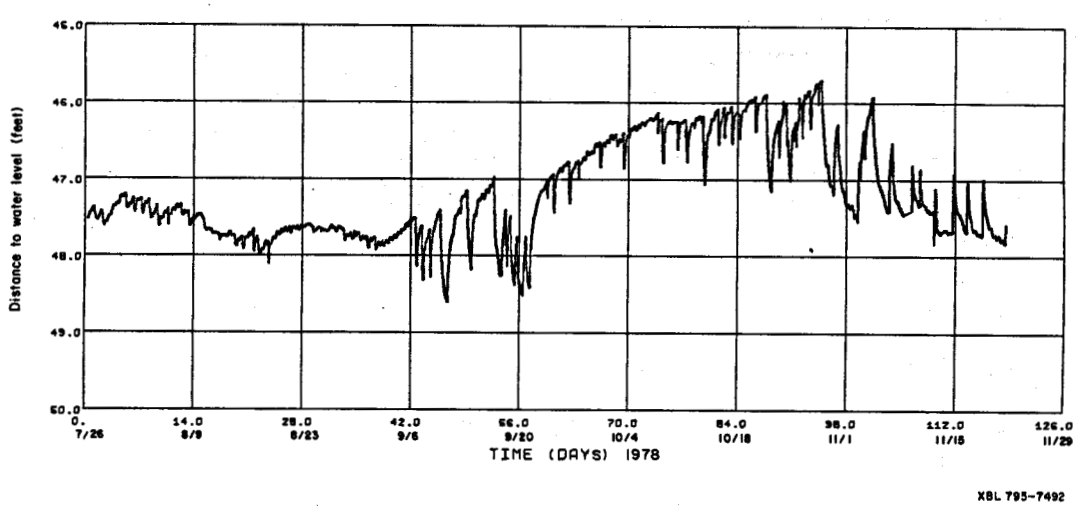

Figure 14. Naef well pre-test data. (XBL 795-7492)

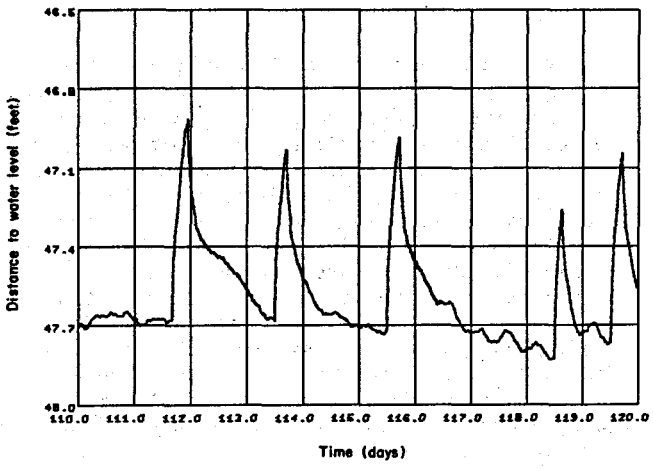

Figure 15. Expanded section of the Naef well pretest data showing five build-up and drawdowns caused by the church well production. (XBL 795-7493)

inferred that the pressure is affected by the Davis well production and by an external source: e.g., atmospheric pressure, ambient temperature, or an influx of fluids to the reservoir from some unknown source(s) such as local precipitation or melting snow.

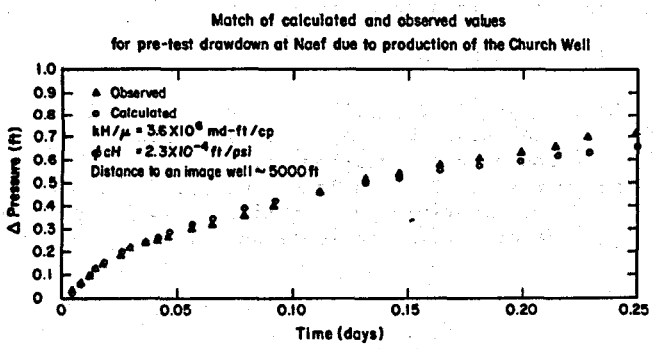

Figure 16. Match of calculated and observed drawdowns at the Naef well due to the church well production. (XBL 796-7508)

WELL TEST DATA ANALYSIS

Pressure data obtained from an observation well that is affected by the production of more than one well or by variable flow rates requires computer-assisted analysis methods. A nonlinear least-squares computer-matching program developed at LBL was used to analyze observation water level data from the Naef well (McEdwards and Tsang, 1977). The program employs the line source solution (Theis), which calculates pressure drawdowns assuming an isotropic, isothermal, homogeneous porous medium of constant thickness. The production well is modeled as a line source that fully penetrates the reservoir. The program can also be used to search for vertical reservoir boundaries (impermeable or constant potential). Vertical boundaries are modeled using the method of images.

The interference data from the Naef well were first analyzed using the production data from all three producing wells (Church, Davis, and Roosevelt swimming pool wells). This analysis revealed that an acceptable match of the pressure data could not be obtained with one set of reservoir parameters (kH/μ, ϕcH, geometry). For this reason, the data were analyzed in two parts. The drawdown at the Naef well caused by the Davis well was analyzed assuming that the production of the Church well had no pressure transients associated with it during the Davis well production. An instrument malfunction at the Naef well made only the first six days of data analyzable. Analysis yields a kh/μ values of 2.3×10^6 md-ft/cp and ϕcH of 7.2×10^{-4} ft/psi. Figure 17 shows the best match obtained between the observed and calculated response. The best match of observed and calculated values indicate the pressure response was influenced by an impermeable boundary.

Pressure and discharge temperature data at the Davis well were obtained for the duration of the test. However, due to instrumentation problems only data from the drawdown (12/10/78 to 12/19/78) is considered reliable. These data were analyzed by the Miller-Dyes-Hutchinson (semi-log) technique (Earlougher, 1977). The data are shown plotted on semi-log paper in Figure 18. After the first several hundred minutes the data fall on a single straight line indicating that no boundary is influencing the pressure response. The calculated transmissivity is 7.3×10^5 mid-ft/cp. The discharge temperature stabilized at 59°C.

Table 2 summarizes the reservoir parameters obtained from analysis of the well test data. The relatively high transmissivity values and low storativity values are indicative of a fracture dominated producing aquifer.

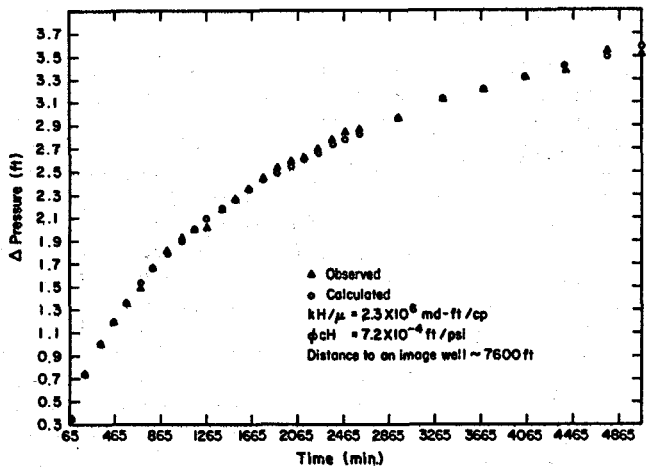

Figure 17. Match of calculated and observed values for the drawdown at the Naef well due to production of the Davis well. (XBL 796-7507)

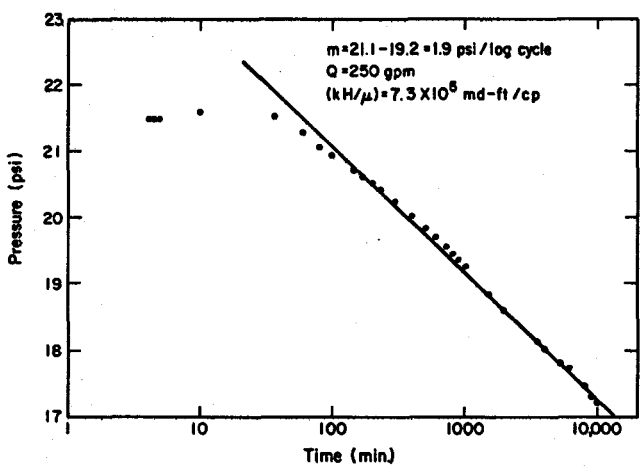

Figure 18. Semi-log plot of the drawdown data from the Davis well. (XBL 796-7505)

CONCLUSION

The occurrence of the Susanville geothermal resource appears to be fault related. Temperature contours and temperature profiles suggest that heated fluids are upwelling on a northwest-trending fault. The heated fluids are then dispersed into the reservoir along the highly permeable (fracture) agglomerate-basalt interface. The geothermal anomaly is larger in lateral extent than was first estimated. However, studies show that the portion of the resource that is above 40°C is partially confined both laterally and vertically. The areal confinement is on three sides of the northwest. The vertical confinement appears to be related to the presence of fractures at the agglomerate-(conglomerate-) basalt interface in the southwest portion of the anomaly.

Well tests show a high lateral permeability associated with the fractured basalt-agglomerate interface. Porosity values are low, supporting evidence of a fracture-dominated producing aquifer. Drilling in the northwestern portion of the anomaly has encountered fluids of higher temperatures than found in the southern portion of the geothermal anomaly. Further well testing will be required to determine the productivity of the higher temperature fluids in this area of the anomaly.

ACKNOWLEDGMENT

We would like to thank Wes Davis and D. Naef for use of their wells during testing in the Susanville area. We are also thankful to Lyle Tomlin and Dick Richardson from the U.S. Department of the Interior, Bureau of Reclamation, Mid-Pacific Region, for their help in obtaining reservoir information at Susanville. The information obtained from J. Jesky and C. Richardson of the City of Susanville is also acknowledged.

REFERENCES CITED

Earlougher, R. C., 1977. Advances in well test analysis. Dallas, Society of Petroleum Engineers, monograph, v. 5.

McEdwards, D. G., and Tsang, C. F., 1977. Variable rate multiple well testing analysis, in Proceedings, Invitational Well Testing Symposium.

Table 2. Reservoir parameters obtained from analysis of well test data.

Observation Well	Pumped Well	kh/μ (md-ft/cp)	φch (ft/psi)	Indication of reservoir boundaries
Naef	Church	3.6×10^6	2.3×10^{-4}	Barrier boundary
Naef	Davis	2.3×10^6	7.2×10^{-4}	Barrier boundary
Naef	Roosevelt Swimming Pool	3.4×10^6	3.9×10^{-2}	None
Davis	Davis	4.3×10^5	Not obtained	None

Berkeley, Lawrence Berkeley Laboratory, LBL-7027, p. 92-99.
Rudser, R. J., 1978. The geology and geothermal potential of Susanville, Lassen County, California (M.S. thesis). Davis, University of California.
U.S. Bureau of Reclamation, 1976a. Susanville geothermal investigations: special report 1976. Sacramento, U.S. Bureau of Reclamation, Mid-Pacific Region.
____, 1976b. Susanville geothermal investigations: Supplemental technical data: special report 1976. Sacramento, U.S. Bureau of Reclamation, Mid-Pacific Region.

RECENT MODIFICATIONS OF THE NUMERICAL CODE CCC

G. S. Bodvarsson, M. J. Lippmann, and T. N. Narasimhan

INTRODUCTION

The numerical code CCC (convection, conduction and consolidation) developed at LBL, solves the energy and mass balance equations and the one-dimensional consolidation for liquid water flow in porous media. The program can be used to simulate one-, two-, or three-dimensional heterogeneous, isotropic, nonisothermal saturated systems. The thermal and hydraulic properties of the water and rock matrix can be temperature or pressure dependent. The program, which was based on programs SCHAFF (Sorey, 1975) and TRUST (Narasimhan, 1975), employs an integrated finite-difference method to discretize the flow regime, and to define the numerical formulation (Edwards, 1972; Narasimhan and Witherspoon, 1976).

The earlier version of CCC (Lippmann et al., 1977) solved the mass and energy equation alternatively by interlacing them in time (leap-frogging method), as shown schematically in Figure 1. The flow equation solves for the pressure and the Darcy velocities, assuming that the temperature-dependent properties remain constant. The energy equation is then solved for the temperature changes, assuming that the Darcy velocity and the pressure-dependent properties remain constant. Because the pressure generally changes much faster than the temperature, much smaller time steps had to be taken in the flow cycles than in the energy cycles for accurate simulation of the pressure behavior.

There were two key factors behind the decision to modify CCC. In the approach employed by the older version, some very important coupling terms between the energy and the mass equations were neglected. In addition, the temperature- and pressure-dependent (nonlinear) parameters were not accurately evaluated during the course of the simulation.

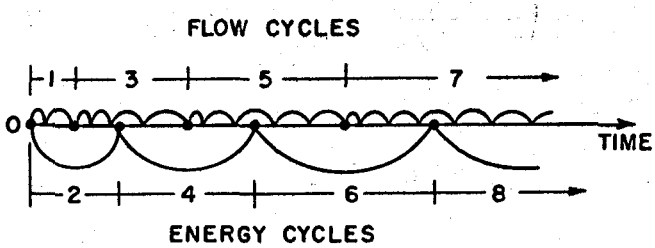

Figure 1. Interlacing of flow and energy calculation. (XBL 7611-7862)

In the modified version of CCC, developed during fiscal year 1979, the two basic balance equations are solved simultaneously using an efficient sparse solver (Duff, 1977). This approach allows all coupling terms to be taken into account and the temperature or pressure dependent coefficients to be accurately evaluated during each time step. Furthermore, the modified version allows much larger time steps to be taken, resulting in a drastic reduction in the simulation costs.

In this report we will give the formulation of the governing equation enabling direct solution by the sparse solver. The assumptions employed in the formulation will be discussed and the solution technique briefly described. Finally, some validation examples will be given, and the advantages of the new formulation listed.

ACTIVITIES IN FISCAL YEAR 1979

Governing Equations

The governing equations for nonisothermal flow of slightly compressible fluid through porous media are the mass and the energy balance equations. These can be written in integral form as follows:

$$\text{mass balance}: \quad \frac{\partial}{\partial t}\int_V \frac{S_s}{g} P dV = -\int_S \rho \vec{v}_d \cdot \vec{n}\, dS + \int_V G_f dV \tag{1}$$

$$\text{energy balance}: \quad \frac{\partial}{\partial t}\int_V (\rho c)_M T dV = \int_S K_M \vec{\nabla} T \cdot \vec{n}\, dS - \int_S \rho c_F \delta T\, \vec{v}_d \cdot \vec{n}\, dS + \int_V G_h dV \tag{2}$$

In the mass balance equation, the left-hand side (LHS) represents the rate of mass accumulation whereas the terms on the right-hand side (RHS) represent the fluxes into the volume element and the sources within the element. Similarly, the LHS of the energy equation consists of the accumulation term whereas the three terms on the RHS represent conductive and convective heat transfer and the source term, respectively.

Equations (1) and (2) must be supplemented by an equation of motion and a number of constitutive relations to fully describe the phenomena being considered. For the equation of motion, the validity of Darcy's law is assumed:

$$\vec{v}_d = -\frac{k}{\mu}(\vec{\nabla}P - \eta\rho g) \tag{3}$$

Constitutive relations must be specified for each of the temperature- or pressure-dependent properties of the fluid and the rock matrix. In the program, these relations have been incorporated either as equations or tabulated values.

Assumptions

The formulation of the model as described by equations (1) and (2) was based on several assumptions. The most significant ones are:

1. Fluid motion is governed by Darcy's law.
2. The fluid and the rock matrix are in local thermal equilibrium.
3. Work due to the effects of viscous dissipation, acceleration, and compressibility is neglected.

Formulation

In this section, the governing equations (equations 1 and 2) will be written in matrix form to be readily handled by the sparse solver. Re-writing equation (1) using numerical notation for a node n and adjacent nodes m, the equation becomes:

$$\frac{(S_sV)_n}{g}\frac{\Delta P}{\Delta t} = \sum_m \left[\left(\frac{k\rho A}{\mu}\right)_{n,m}\frac{(P_m - P_n)}{D_{n,m}+D_{m,n}} - \left(\frac{k\rho^2\eta A}{\mu}\right)_{n,m} g\right] + (G_fV)_n \tag{4}$$

Adopting an implicit formulation to relax constraints in the time steps results in the following equations:

$$P_n = P_n^o + \lambda\Delta P_n \tag{5}$$

$$P_m = P_m^o + \lambda\Delta P_m \tag{6}$$

Here λ is a weighting factor that is limited to the range 0.5 to 1.0 for unconditionally stable solutions. Substituting (5) and (6) into (4) yields,

$$\frac{(S_sV)_n}{g}\frac{\Delta P}{\Delta t} = \sum_m \left[\left(\frac{k\rho A}{\mu}\right)_{n,m}\frac{P_m^o + \lambda\Delta P_m - P_n^o - \lambda\Delta P_n}{D_{n,m}+D_{m,n}} + \left(\frac{k\rho^2\eta A}{\mu}\right)_{n,m} g\right] + (G_fV)_n \tag{7}$$

Equation (7) can be written in matrix form as follows:

$$\left[1 + \frac{\Delta tg}{(S_sV)_n}\sum_m \frac{\lambda}{D_{n,m}+D_{m,n}}\left(\frac{k\rho A}{\mu}\right)_{n,m}\right]\Delta P_n - \left[\frac{\Delta tg}{(S_sV)_n}\sum_m \frac{\lambda}{D_{n,m}+D_{m,n}}\left(\frac{k\rho A}{\mu}\right)_{n,m}\right]\Delta P_m = \frac{\Delta tg}{(S_sV)_n}\left\{(G_fV)_n + \sum_m\left[\left(\frac{k\rho A}{\mu}\right)_{n,m}\frac{(P_m^o - P_n^o)}{D_{n,m}+D_{m,n}} - \left(\frac{k\rho^2\eta A}{\mu}\right)_{n,m} g\right]\right\} \tag{8}$$

In terms of the matrix equation [A][x] = [b], the coefficients of the ΔP_n's represent the diagonal values of the A matrix, while the coefficients of the ΔP_m's are the off-diagonal values. The RHS of equation (8) gives the values of the known vector b.

Similarly, after incorporation of Darcy's law, the energy equation (2) can be written using numerical notation as follows:

$$[(\rho c)_M V]_n \frac{\Delta T_n}{\Delta t} = \sum_m \left[\frac{(K_MA)_{n,m}}{D_{n,m}+D_{m,n}}(T_m - T_n) + \left(\frac{\rho c_F A k}{\mu}\right)_{n,m}(T_{n,m} - T_n)\left(\frac{P_m - P_n}{D_{n,m}+D_{m,n}} - \eta\rho g\right)\right] + (G_hV)_n \tag{9}$$

In equation (9), $T_{n,m}$ represents the interface temperature between nodes n and m, and using upstream weighting, it can be expressed as:

$$T_{n,m} = aT_n + (1-a)T_m \tag{10}$$

In equation (10), a is the upstream weighting factor and it may be varied between 0.5 and 1. Substitution of (10) into (9) yields

$$[(\rho c)_M V]_n \frac{\Delta T_n}{\Delta t} = \sum_m \left[\frac{(K_MA)_{n,m}}{D_{n,m}+D_{m,n}}(T_m - T_n) + \left(\rho c_F A\frac{k}{\mu}\right)_{n,m}(1-a)(T_m - T_n) \times \left(\frac{P_m - P_n}{D_{n,m}+D_{m,n}} - \eta\rho g\right)\right] + (G_hV)_n \tag{11}$$

Again we introduce the implicit formulation:

$$T_n = T_n^o + \lambda\Delta T_n$$

$$T_m = T_m^o + \lambda\Delta T_m$$
$$P_n = P_n^o + \lambda\Delta P_n \qquad (12)$$
$$P_m = P_m^o + \lambda\Delta P_m$$

$$[(\rho c)_M V]_n \frac{\Delta T_n}{\Delta t} = \sum_m \left\{ \frac{(K_M A)_{n,m}}{D_{n,m}+D_{m,n}} \left[T_m^o + \lambda\Delta T_m - T_n^o - \lambda\Delta T_n\right] + \left(\rho c_F A \frac{k}{\mu}\right)_{n,m} (1-a)\left[T_m^o + \lambda\Delta T_m - T_n^o - \lambda\Delta T_n\right] \times \left[\frac{P_m^o + \lambda\Delta P_m - P_n^o - \lambda\Delta P_n}{D_{n,m}+D_{m,n}} - \eta\rho g\right]\right\} + (G_h V)_n \qquad (13)$$

If the generation term $(QV)_n$ represents more a sink (fluid produced), it vanishes, but in the case of a source (injection), it becomes

$$G_f \bar{c}_F \left[T_i - (T_n^o + \lambda\Delta T_n)\right] \qquad (14)$$

Here $\bar{c}_F$ represents the specific heat of the injected fluid. Substitution of (14) into (13) yields:

$$[(\rho c)_M V]_n \frac{\Delta T_n}{\Delta t} = \sum_m \left\{ \frac{(K_M A)_{n,m}}{D_{n,m}+D_{m,n}} \left(T_m^o + \lambda\Delta T_m - T_n^o - \lambda\Delta T_n\right) + \left(\rho c_F A \frac{k}{\mu}\right)_{n,m} (1-a)\left[T_m^o + \lambda\Delta T_m - T_n^o - \lambda\Delta T_n\right]\left[\frac{P_m^o + \lambda\Delta P_m - P_n^o - \lambda\Delta P_n}{D_{n,m}+D_{m,n}} - \eta\rho g\right]\right\} + G_f \bar{c}_F \left[T_i - (T_n^o + \lambda\Delta T_n)\right] \qquad (15)$$

We now proceed and expand neglecting terms involving the products of Δp and ΔT; the equation becomes

$$[(\rho c)_M V]_n \frac{\Delta T_n}{\Delta t} = \sum_m \left\{ \frac{(K_M A)_{n,m}}{D_{n,m}+D_{m,n}} (T_m^o + \lambda\Delta T_m - T_n^o - \lambda\Delta T_n) + \left(\rho c_F A \frac{k}{\mu}\right)_{n,m} (1-a)\left[-\eta\rho g\,(T_m^o + \lambda\Delta T_m - T_n^o - \lambda\Delta T_n) + (T_m^o - T_n^o)\frac{(P_m^o - P_n^o)}{D_{n,m}+D_{m,n}} + \frac{\lambda}{D_{n,m}+D_{m,n}}(\Delta T_m - \Delta T_n)(P_m^o - P_n^o) + \frac{\lambda}{D_{n,m}+D_{m,n}}(T_m^o - T_n^o)(\Delta P_m - \Delta P_n)\right]\right\} + G_f \bar{c}_F \left[T_i - (T_n^o + \lambda\Delta T_n)\right] \qquad (16)$$

$$\left\{1 + \frac{\Delta t\lambda}{[(\rho c)_M V]_n} G_f \bar{c}_F + \frac{\Delta t\lambda}{(\rho c V)_n} \sum_m \frac{(K_M A)_{n,m}}{D_{n,m}+D_{m,n}} - \frac{\Delta t\lambda(1-a)}{[(\rho c)_M V]_n} \sum_m \left(\frac{\eta\rho^2 g c_F A k}{\mu}\right)_{n,m} + \frac{\Delta t\lambda}{(\rho c V)_n} (1-a) \sum_m \left(\frac{\rho c_F A k}{\mu}\right)_{n,m} \frac{P_m^o - P_n^o}{D_{n,m}+D_{m,n}}\right\} \Delta T_n$$
$$- \left\{ \frac{\Delta t\lambda}{[(\rho c)_M V]_n} \sum_m \frac{(K_M A)_{n,m}}{D_{n,m}+D_{m,n}} - \frac{\Delta t\lambda}{[(\rho c)_m V]_n} \times (1-a) \sum_m \left(\frac{\eta\rho^2 g c_F A k}{\mu}\right)_{n,m} + \frac{\Delta t\lambda}{[(\rho c)_M V]_n} \times (1-a) \sum_m \left(\frac{\rho c_F A k}{\mu}\right)_{n,m} \frac{P_m^o - P_n^o}{D_{n,m}+D_{m,n}}\right\} \Delta T_m$$
$$+ \left[\frac{\Delta t\lambda}{[(\rho c)_M V]_n} (1-a) \sum_m \left(\frac{\rho c_F A k}{\mu}\right)_{n,m} \frac{(T_m^o - T_n^o)}{D_{n,m}+D_{m,n}}\right] \Delta P_n$$
$$- \left[\frac{\Delta t}{[(\rho c)_M V]_n} (1-a) \sum_m \left(\frac{\rho c_F A k}{\mu}\right)_{n,m} \frac{(T_m^o - T_n^o)}{D_{n,m}+D_{m,n}}\right] \Delta P_m$$
$$= \frac{\Delta t}{[(\rho c)_M V]_n} \left\{ G_f \bar{c}_F (T_i - T_n^o) + \sum_m \left[\frac{(K_M A)_{n,m}}{D_{n,m}+D_{m,n}} \times (T_m^o - T_n^o) - (1-a) \sum_m \left(\frac{\eta\rho^2 g c_F A k}{\mu}\right)_{n,m} (T_m^o - T_n^o) + (1-a) \sum_m \left(\frac{\rho c_F A k}{\mu}\right)_{n,m} \frac{(T_m^o - T_n^o)(P_m^o - P_n^o)}{D_{n,m}+D_{m,n}}\right]\right\} \qquad (17)$$

It can be noted that the unknowns in equation (17) are not only the temperature changes at the nodes but also the pressure changes. The latter were neglected during a time step in the older version of CCC.

For a complete coupling of the mass and the energy equations, equations (6) and (13) can be written in simplified forms as follows:

$$C_{n,n}\Delta P_n - C_{n,m}\Delta P_m = b_n \tag{18}$$

$$K_{i,i}\Delta T_n - K_{i,j}\Delta T_m + K_{i,n}\Delta P_n - K_{i,m}\Delta P_m = B_i \tag{19}$$

The coefficients in equations (18) and (19) are all nonlinear, i.e., a function of pressure and temperature. These equations are handled by an iterative procedure to be discussed later. Figure 2 shows the combined equations (8) and (17) expressed in matrix form.

The Solution Technique

The sets of linear equations (19) and (20) are solved by an efficient direct solver (Duff, 1977). Basically the solver uses LU decomposition and a Gaussian elimination procedure. The matrix of coefficients (the A matrix) is preordered using permutation matrices P^1 and Q^1 such that the resultant matrix is in block lower triangular form. Gaussian elimination is then performed within each diagonal block in order to obtain factorization into the lower triangular (L_K) and the upper triangular (U_K). Finally, the factorization is used to solve the matrix equations.

The flow chart of the modified code is shown in Figure 3. After the input mode has been completed, the program determines the time step to be taken and estimates the values of the nonlinear coefficients based upon anticipated changes in temperature and pressure. Then the values in the A matrix and the B vector are calculated, and the set of linear equations solved by the sparse solver. If the nonlinear coefficients used in the calculations are not accurate enough, the program starts an iterative loop, which terminates when sufficient accuracy has been obtained. Then the program provides output or ends the problem if instructed to do so; otherwise it advances to the next time step.

Validation

The present code has been validated against a number of analytical solutions. For each case, the new version of CCC gives results identical to or better than the old version. For the transient-heat/transient-flow case, the new version should give considerably more accurate results than the older one. However, an appropriate analytical solution for comparison is not yet available.

$$\begin{bmatrix} C_{11} & & & & & & & \\ & C_{22} & & C_{n,m} & & & & \\ & & \ddots & & & & & \\ & C_{n,m} & & C_{nn} & & & & \\ & & & & K_{11} & & & \\ K_{i,n} & & & & & K_{22} & & K_{i,j} \\ & & & & & & \ddots & \\ K_{i,m} & & & & K_{i,j} & & & K_{ii} \end{bmatrix} \begin{bmatrix} \Delta P_1 \\ \Delta P_2 \\ \vdots \\ \Delta P_n \\ \Delta T_1 \\ \Delta T_2 \\ \vdots \\ \Delta T_n \end{bmatrix} = \begin{bmatrix} b_1 \\ b_2 \\ \vdots \\ b_n \\ B_1 \\ B_2 \\ \vdots \\ B_n \end{bmatrix}$$

Figure 2. The formulated equations expressed in matrix form. (XBL 806-7214)

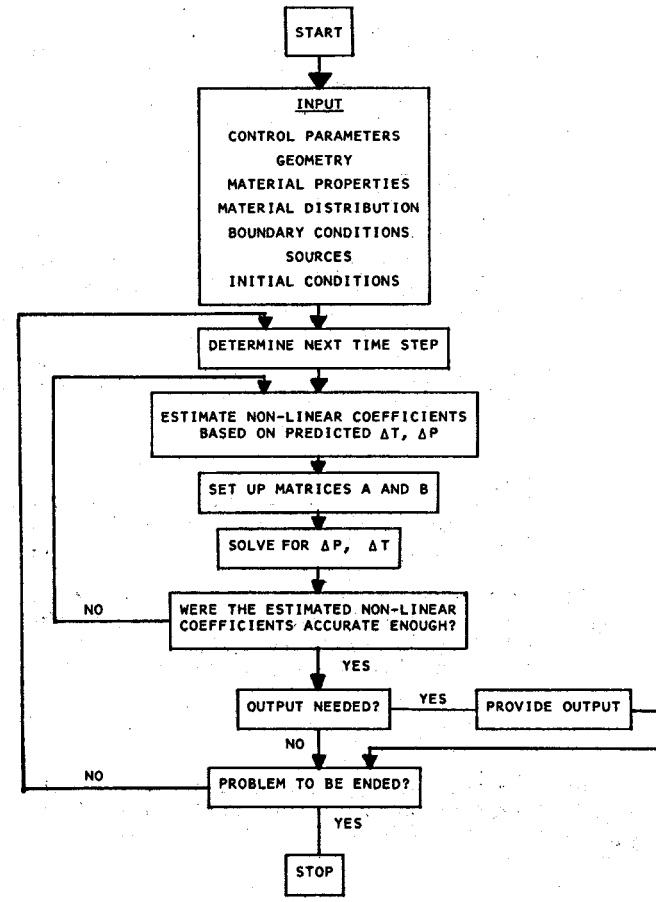

Figure 3. Flow chart for the new version of the computer code CCC (XBL 806-10532)

Advantages of the New Formulation

Some of the main advantages of the new formulation are listed below.

1. The governing equations are solved simultaneously and therefore all of the coupling terms are included.
2. An iterative scheme has been implemented to ensure accurate determination of the nonlinear coefficients.
3. The new code gives as good or better accuracy than the older version for the same time steps. No analytical solution has been found for the transient-flow/transient-heat case, but the new code should give considerably better results than the older one.
4. The direct solution technique allows much larger time steps to be taken and consequently less computational effort is needed. Preliminary comparison between the two versions indicates that the new code is 10 to 100 times more cost efficient than the older one.

PLANNED ACTIVITIES DURING FISCAL YEAR 1980

During the next fiscal year, the new version will be further improved. We intend to:

1. Establish a better criterion for determining the next time step, and streamline computations when the flow field is under quasi-steady conditions.
2. Incorporate the Newton-Raphson iterative scheme for accurate determination of the nonlinear coefficients.
3. Incorporate in the formulation the thermal expansion of the solid matrix.

REFERENCES CITED

Duff, I.S., 1977. MA28--a set of FORTRAN subroutines for sparse unsymmetric linear equations. Harwell/Oxfordshire, Great Britain, Report AERE-R8730.

Edwards, A.L., 1972. TRUMP: A computer program for transient and steady state temperature distribution in multidimensional systems. Lawrence Livermore Laboratory, UCRL-14754, Rev. 3, 259 p.

Lippmann, M.J., Tsang, C.F., and Witherspoon, P.A., 1977. Analysis of the response of geothermal reservoirs under injection and production procedures. Dallas, Society of Petroleum Engineers, SPE-6537, 15 p.

Narasimhan, T.N., 1975. A unified numerical model for saturated-unsaturated groundwater flow (Ph.D. dissertation, Berkeley, University of California), 244 p.

Narasimhan, T.N., and Witherspoon, P.A., 1976. An integrated finite-difference method for analyzing fluid flow in porous media. Water Resources Research, v. 12, no. 1, p.57-64.

Sorey, M.L., 1975. Numerical modeling of liquid geothermal systems (Ph.D. dissertation, Berkeley, University of California), 65 p.

DEVELOPMENT OF THE TWO-PHASE RESERVOIR SIMULATION PROGRAM, SHAFT79

K. Pruess, R. C. Schroeder, and P. A. Witherspoon

INTRODUCTION

Over the last year, work on two-phase geothermal reservoir simulation was focused on two areas. First, we made a major effort to increase the efficiency and accuracy of the simulator SHAFT78 through the use of more powerful mathematical and numerical methods. This work has resulted in the completion of a new simulator, called SHAFT79. Second, we applied SHAFT79 to diverse geothermal reservoir problems.

MATHEMATICAL AND NUMERICAL METHODS

Applications of SHAFT78 had shown that, although it was possible to obtain accurate solutions to difficult problems, including phase transitions, the maximum permissible time steps were severely restricted. For example, in a simulation of the Serrazzano geothermal reservoir (see below) typical time steps were a few hours, and the simulaton required typically 15 sec CPU-time on the CDC-7600 per day of physical time. Computations were so costly and cumbersome that SHAFT78 could only be applied to very simple idealized model problems. SHAFT79 solves the same equations as SHAFT78, but in a much more efficient way. Typical time steps in the Serrazzano simulation with SHAFT79 are 10 to 50 days, with computation times of typically 0.3 sec CPU-time on the CDC-7600 per day of physical time.

In this section, we shall briefly review the methods used in SHAFT79 as they were developed through step-by-step revisions of SHAFT78. More specific details can be found in the papers by Pruess et al. (1979a,b).

The main shortcoming of SHAFT78 is the once-through sequential method used for solving the strongly coupled mass- and energy-transport equations. Our attempt to improve this with an iterative sequential method was unsuccessful. Numerical tests as well as a subsequent analytical derivation showed that the strength of the coupling is such that convergence could only be obtained for small time steps.

The next step was implementation of a completely simultaneous, iterative solution. This in itself did not yet allow longer time steps, because the iterative matrix method used in SHAFT78 for solving the linearized equations requires a diagonally dominant matrix. The off-diagonal matrix elements turn out to be proportional to the time step size Δt, which restricts the permissible time steps to virtually the same maximum as in the sequential iterative method, above.

Subsequently, the iterative matrix method was replaced with an efficient direct solver as developed by Duff (1977). Duff's program package uses clever storage and pre-ordering procedures combined with LU-decomposition and Gaussian elimination. It is ideally suited for solving non-symmetric matrix equations with random sparcity structure, such as arise in the integrated finite-difference description of fluid and heat flow in porous rock.

The resulting simultaneous iterative solution method with fully implicit time differencing and direct solver permits large time steps. A convenient measure of time-step size is in terms of "throughput," which is defined as ratio of the fluid mass flowing through the surface of an element in one time step to the fluid mass initially in place in that element. Throughputs with SHAFT78 were typically on the order of 10^{-2} or smaller, whereas with SHAFT79 throughputs of 10-500 can often be obtained.

There remains one flaw in the methodology outlined so far. Namely, the nonlinear equations are replaced in an iterative way with a sequence of linear equations. Convergence occurs when, for a given time step, a set of equivalent linear equations is obtained. This procedure works as long as the nonlinearities are not too severe, but it fails completely for phase transitions. The final step in developing the algorithm of SHAFT79, then, was to implement a Newton/Raphson method for actually solving the nonlinear equations rather than replacing them iteratively with linear ones. With this methodology, SHAFT79 can accurately perform large time steps whether or not phase transitions occur during the time step.

Data inputting and printing of output were also rewritten to accommodate the new computational structure, and to improve usability of the program.

Accuracy of SHAFT79 was verified by comparison with SHAFT78 and with calculations published in the literature.

APPLICATIONS

Table 1 gives an overview of the types of systems and processes that have been modeled with SHAFT79. Below are presented results of selected SHAFT79 simulations, which illustrate the range of applications. (Parameters for the individual cases are given in the figure captions.) Relative permeabilities were obtained from Corey's equations, with residual immobile steam saturation S_{sc} equal to zero, and residual immobile water saturation S_{wc} varying between 0.40 and 0.70.

DEPLETION OF A RESERVOIR WITH SHARP STEAM/WATER INTERFACE

When steam is produced from above a liquid water table, boiling commences near the top of the water zone. This gives rise to a drop in temperature and pressure, whereby a two-phase layer between water and steam zones is established. Water moves upward into the two-phase zone, releasing pressure below the boiling front and advancing it downward (Pruess, 1979b). In the examples studied (see Figure 1), the top of the two-phase zone does not dry up until after the boiling front has reached the bottom of the reservoir. This occurs after 6.4 years for the "high permeability" case (A in Figure 1), and after 9.6 years for the "low permeability" case (B in Figure 1). Vapor saturation at the top of the water table then reaches 46.7% for case A and 78.9% for case B. Pressure at the steam/two-phase interface, at a depth of 500 m, declines very slowly during the advancing of the boiling front in case A. The reason for this is that the most rapid boiling occurs at the bottom of the two-phase zone. This provides a supply of hotter steam, which flows up from depth and tends to maintain temperature and hence pressure at the top of the two-phase zone. In case B this mechanism for pressure maintenance is much less effective because of the power permeability.

INJECTION OF COLD WATER

Cold-water injection into a steam reservoir gives rise to a hydrodynamic front and, trailing behind it, a temperature front. In the finite-difference simulation of this process subsequent

Table 1. Simulation studies with SHAFT79.

Geometry	Type of problem	Simulated processes
1-D, rectangular	Depletion of two-phase geothermal reservoirs[3]	Various production and injection schemes for reservoirs with uniform initial conditions or with sharp steam/water interfaces
1-D, cylindrical	Two-phase flow near wells	Production from two-phase zones; cold water injection into two-phase and superheated steam zones, respectively
2-D, rectangular	Krafla geothermal reservoir (Iceland)[4]	Different space and time patterns of production and injection
2-D, cylindrical	High-level nuclear waste repository[5]	Long-term evolution of temperatures and pressures near a powerful heat source (in progress)
3-D, regular	Two-phase interference test in Cerro Prieto (Mexico)	(in progress)
3-D, irregular	Serrazzano geothermal reservoir (Italy)[3]	Detailed field production from 1960 to 1966

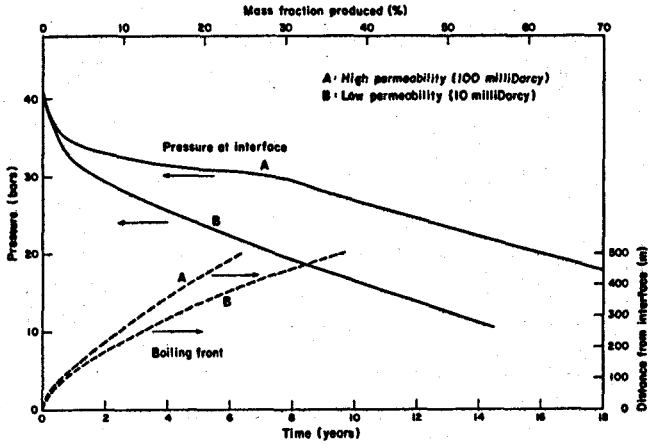

Figure 1. Depletion of a reservoir with sharp steam/water interface. The reservoir is a vertical column of 1 km depth with a volume of 1 km^3 and "no flow" boundaries. For purposes of numerical simulation it is subdivided into 44 horizontal elements. Initially, the bottom half is filled with liquid water, the top half with superheated steam, with temperature T = 252°C and pressures carefully equilibrated under gravity. (Rock parameters: density = 2000 kg/m^3; specific heat = 1232 J/kg °C; porosity = 10%; residual immobile water saturation = 70%.) Depletion occurs uniformly at the top with a constant rate of 50 kg/sec. The curves are for a permeability of 10^{-13} m^2 (A) and 10^{-14} m^2 (B), respectively. Typical time steps in the simulation are 2 - 5 x 10^6 sec, corresponding to throughputs of up to 250. (XBL 7911-13094)

elements undergo phase transitions from superheated steam to two-phase conditions to subcooled water. Figure 2 shows the fronts at two different times. It is apparent that the fronts are propagated according to the parameter t/R^2. The volume swept by the temperature front is close to 1/4 of the volume swept by the hydrodynamic front. This reflects the fact that, at a porosity of 20%, the volumetric heat capacity of water is about 1/4 of the volumetric heat capacity of the rock/water mixture.

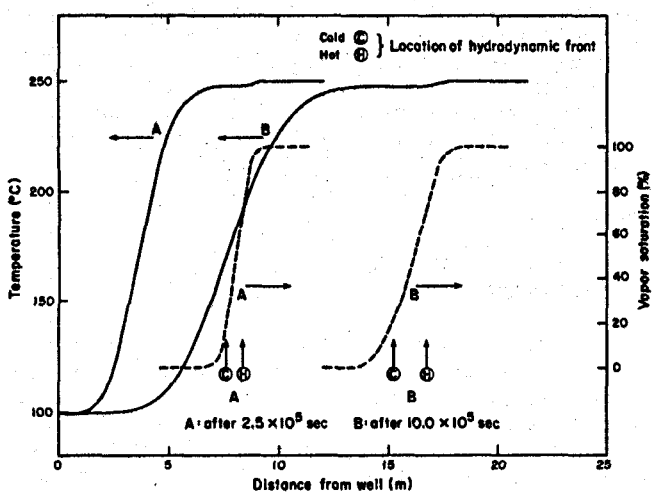

Figure 2. Injection of cold water into a steam zone. The reservoir is a cylinder with large radius, initially filled with superheated steam at T = 250°C, pressure = 38 bars. Water with T = 99.3°C is injected along the center line at a constant rate of 0.14 kg/s m. The numerical simulation employs an axisymmetric grid as used by Garg (1978). (Rock parameters: density = 2650 kg/m^3; specific heat = 1000 J/kg °C; porosity = 20%; heat conductivity = 5.25 W/m °C; permeability = 10^{-13} m^2; residual immobile water saturation = 40%.) The simulation uses time steps from 2500 to 10,000 sec, with throughputs of up to 6. The arrows labeled C and H show the locations of the hydrodynamic front if all injected water were to remain at injection temperature (C) or were heated up to initial reservoir temperature (H). (XBL 7911-13092)

SIMULATION OF KRAFLA FIELD

Figure 3 shows a vertical two-dimensional grid as used by Jonsson for simulating production and injection at Krafla, Iceland (Jonsson, 1980). The reservoir is initially entirely filled with liquid water close to saturated conditions. Various production and injection schemes were explored in an attempt to optimize injection, i.e., to combine pressure and temperature maintenance during production with minimal sacrifices in terms of decreasing vapor saturation, S. Figure 4 shows typical results. Jonsson finds that deep injection is preferable to shallow injection. Complete problem specifications and discussions of results are given by Jonsson (1980).

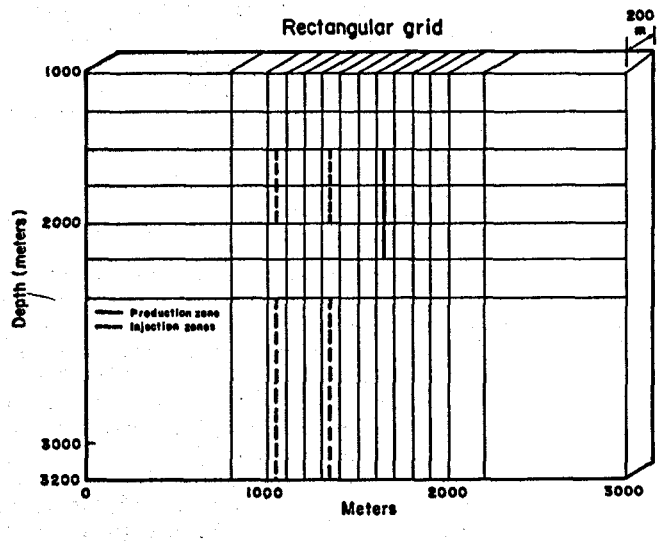

Figure 3. Two-dimensional grid for simulation of Krafla, Iceland (Jonsson, 1980). (XBL 7910-13062)

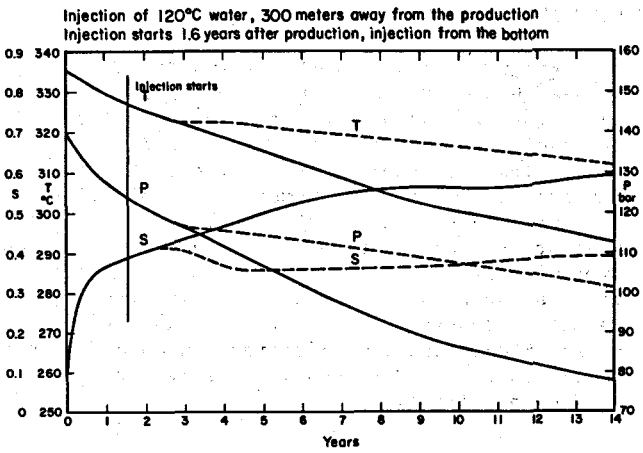

Figure 4. Simulated performance of Krafla reservoir. Temperature, pressure, and vapor saturation at the well block are given as function of time with injection (dashed lines) and without injection (solid lines). Production rate is 45 kg/sec and injection rate is 22.5 kg/sec. Typical time steps in the simulation are 1.25 x 10^6 sec, with throughputs of about 0.1 (Jonsson, 1980). (XBL 798-11415K)

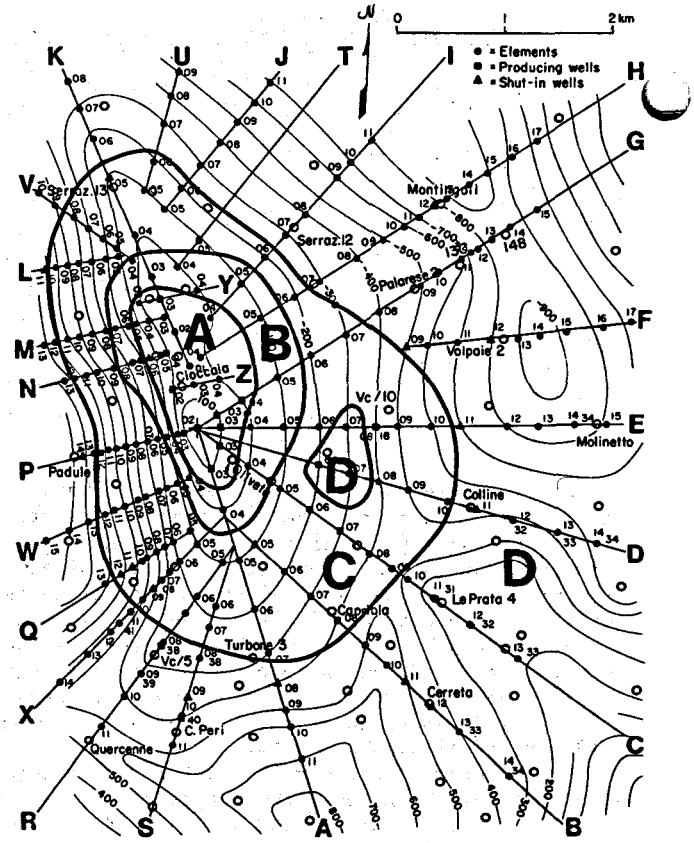

Figure 5. Aerial map of Serrazzano geothermal reservoir. The thin contour lines show elevations of the cap rock as determined from drill logs. The straight lines labeled A to Z indicate the locations of geological cross sections used in constructing a three-dimensional finite difference grid (Weres, 1977). Locations of elements (nodes) are also shown. A - D are regions of different permeability as determined in the simulation: A = 0.75 x 10^{-12} m^2; B = 0.25 x 10^{-12} m^2; C = 0.75 x 10^{-13} m^2; D = 0.15 x 10^{-13} m^2. (XBL 7910-12576)

SIMULATION OF SERRAZZANO FIELD

The most complex simulation effort undertaken with SHAFT79 to date is a case study (history match) of the Serrazzano reservoir. Serrazzano is one of the distinct zones of the extensive geothermal area near Larderello in central Tuscany, Italy. Detailed production data gathered since 1939 and an extensive body of geologic and hydrologic work make Serrazzano an attractive example for developing geothermal reservoir simulation methodology (see Pruess, 1979b). Figure 5 gives a map of the reservoir, and Figure 6 shows the geologically accurate mesh as developed by Weres (1977). Conceptual model of the reservoir and parametrization of the problem are discussed in Pruess (1979b) and Weres (1977).

Many parameters are only partially known, and are determined in trial-and-error fashion by comparing simulated reservoir performance with field observations. A valuable criterion for determining absolute permeabilities is that well blocks must remain very close to steady flow conditions. Our most complete simulation so far covers the period from 1960 to 1966. With the permeability distribution as indicated in Figure 5, we achieve steady flow for all wells producing since 1961 or earlier to within 2% for the entire 6-yr period modeled (i.e., the difference between inflow and production for any well block never exceeds 2%).

From mass balance considerations it can be shown that most of the fluid reserves in Serrazzano are in place in liquid form. Little is known, however, about the distribution of pore water in the reservoir. Making the tentative assumption that liquid water is distributed throughout most of the reservoir, we compute a pressure decline (see Figure 7) which is slower than observed in the field by a factor of approximately 3.5. In the simulation, pressure declines slowly because boiling is spread out over a large volume. We conclude that in most of the reservoir volume no liquid water is present, and we shall modify our initial conditions accordingly in subsequent simulations. We also need to correct some imbalances in initial conditions, which are apparent from the initial nonmonotonic behavior of pressure in Figure 7.

CONCLUSION

The simulator SHAFT79 uses efficient methods for computing mass- and energy-transport in geothermal reservoirs, and allows for a flexible description of irregular geometric features. A broad range of applications, including idealized systems as well as large field problems, demonstrates its

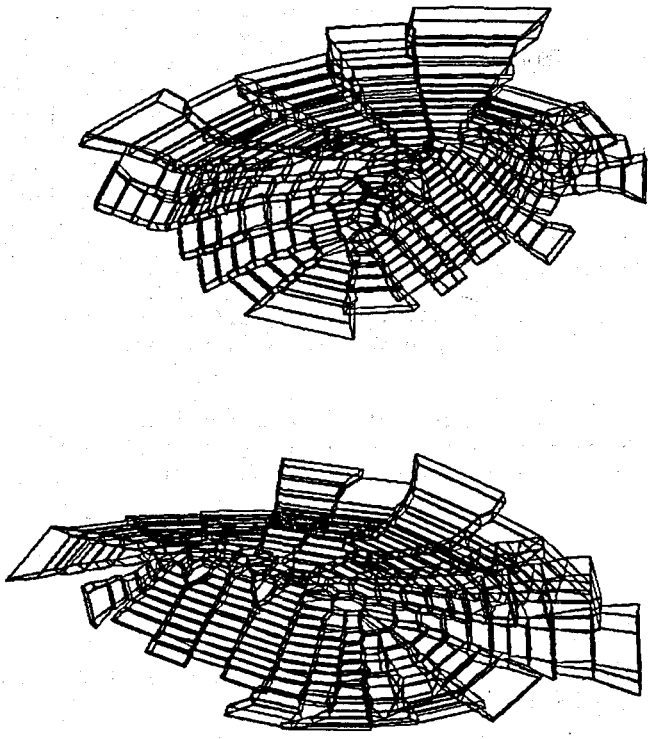

Figure 6. Serrazzano grid. The computer-generated geologically accurate grid of the Serrazzano reservoir as developed by Weres (1977) is shown in two rotated perspective views. This three-dimensional grid represents a reservoir that is a curved thin sheet approximately 1 km from top to bottom, with an aerial extension of about 25 km^2. It has 234 polyhedral elements, with 679 polygonal interfaces between them. There are up to 10 interfaces per element. (XBL 787-9570)

usefulness for geothermal reservoir studies. Further development work is presently under way to improve on some of the restrictive approximations made in the formulation of the physical model.

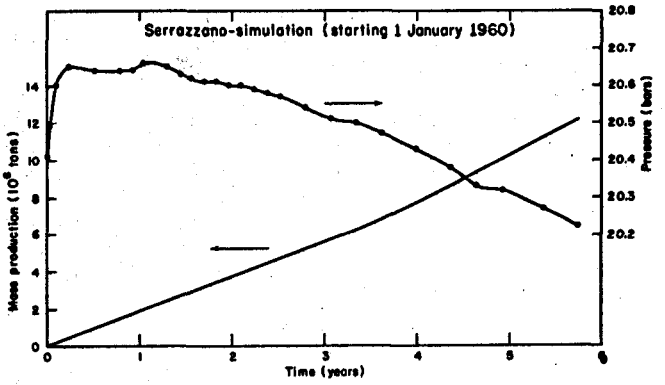

Figure 7. Average reservoir steam pressure and cumulative fluid production as calculated in Serrazzano simulation. Typical time steps in the simulation are 10 to 50 days, with throughputs of up to 65. (XBL 7911-13093)

REFERENCES CITED

Duff, I. S., 1977. A set of FORTRAN subroutines for sparse unsymmetric linear equations. Harwell/Oxfordshire, Great Britian, Report AERE-R 8730.

Garg, S. K., 1978. Pressure transient analysis for two-phase liquid water/steam geothermal reservoirs. Dallas, Society of Petroleum Engineers, paper SPE-7479.

Jonsson, V., 1980. Two-dimensional model of injection into a liquid-dominated two-phase production reservoir. Berkeley, Lawrence Berkeley Laboratory, LBL-10003 (in prep.).

Pruess, K., Zerzan, J. M., Schroeder, R. C., and Witherspoon, P. A., 1979a. Description of the three-dimensional two-phase simulator SHAFT78 for use in geothermal reservoir studies. Dallas, Society of Petroleum Engineers, paper SPE-7699.

Pruess, K., Bodvarsson, G., Schroeder, R. C., Witherspoon, P. A., Marconcini, R., Neri, G., and Ruffilli, C., 1979b. Simulation of the depletion of two-phase geothermal reservoirs. Dallas, Society of Petroleum Engineers, paper SPE-8266.

PROPERTIES OF H_2O-CO_2 MIXTURES FOR GEOTHERMAL RESERVOIR AND WELLBORE SIMULATORS

E. R. Iglesias and R. C. Schroeder

INTRODUCTION

Discharges from hydrothermal reservoirs often contain considerable amounts of noncondensible gases (White et al., 1971; Burgassi et al., 1975; Weres et al., 1977). By far the dominant species is the weakly polar, slightly soluble carbon dioxide molecule (Ellis and Mahon, 1977; Wahl, 1977). The total pre-exploitation CO_2 content of these reservoirs ranges probably as high as several percent by mass (e.g., Sutton and McNabb, 1977; Gislason et al., 1978). These high gas contents result in hydrothermal fluid thermodynamic properties significantly different from those of pure water. Properties

affected include pressure, density, enthalpy, compressibility, vapor saturation, etc. (Strauss and Schubert, 1979a,b; Grant, 1977).

The current LBL geothermal reservoir and wellbore simulators assume pure water as the only fluid component in the system. We therefore felt that a wider and more realistic prediction capability required inclusion of CO_2 as a second component to these codes. Two-component simulators would find immediate application in modeling CO_2-rich hydrothermal fields (e.g., the Serrazzano, Italy, and Krafla, Iceland, reservoirs).

Implementation of the envisioned multiphase, multicomponent simulators requires formulation of the physical properties of the H_2O-CO_2 mixtures and development of appropriate computational techniques. We feel that the computational tools developed for pure water simulators can be adapted to handle this problem. In this report, we focus on the description of a simplified thermodynamic model of water-carbon dioxide mixtures that has been formulated. Unlike previous studies (e.g., Zyvoloski and O'Sullivan, 1980; Strauss and Schubert, 1979a,b; Grant, 1977; Sutton, 1976), which consider only two-phase situations, this model applies to compressed solutions, two-phase mixtures, and superheated gas mixtures.

A SIMPLE MODEL

The basic assumption is that of thermodynamic equilibrium. Within the typical ranges spanned by the relevant thermodynamic variables in hydrothermal reservoirs, a water-carbon dioxide mixture may be in three different states: a compressed liquid solution, a liquid in equilibrium with a vapor phase, and a "superheated" gas.

In a two-phase situation, the liquid phase contains dissolved gas, and the gas phase is a mixture of steam and CO_2. We assume that CO_2 partitions between the two phases according to Henry's Law. The total pressure is computed as the sum of the saturation pressure of pure water P_1^* and the partial pressure of CO_2, P_2. The gas phase density is taken to be equal to the saturated steam density ρ_{1G}^* divided by the steam mass fraction in the gas phase y_1. Furthermore, the liquid density is estimated as the saturated water density ρ_{1L}^* divided by the water mass fraction in the solution x_1. The gaseous CO_2 specific enthalpy h_{2G} is computed from an analytical fit to experimental data due to Sweigert et al. (1946); by addition of h_{2G} with the heat of solution we obtain the specific enthalpy of the dissolved CO_2, h_{2G}. The enthalpies for the liquid and gaseous phases are computed from:

$$h_L = x_1 \, h_{1L}^* + x_2 \, h_{2L} \qquad (1)$$

$$h_G = y_1 \, h_{1G}^* + y_2 \, h_{2G} \quad , \qquad (2)$$

where the asterisks refer to saturated water properties. Other thermodynamic variables of interest, such as total density, vapor and liquid saturation, and internal energy are derived from the formulation just described.

In the compressed liquid region the CO_2 partial pressure is computed from Henry's Law, and the water partial pressure P_1 by the difference $(P-P_2)$. The water density ρ_{1L} (P,T) is taken from steam tables, and the liquid density is estimated as $\rho_L = \rho_{1L}/x_1$. The liquid specific enthalpy is computed from expression (1), replacing h_{1L}^* by h_{1L} which accounts for the effects of pressure in the water enthalpy.

The partial pressures of steam and CO_2 in the superheated gas region are estimated as $P_1 = y_1 \, P$, $P_2 = y_2 \, P$ (Sutton, 1976). The gas density is taken as $\rho_G = \rho_{1G}(P_1,T)/y_1$. The specific gas enthalpy is computed from expression (2), replacing h_{1G}^* by h_{1G}.

Approximate analytical expressions for the boundaries of the two-phase region, boiling and dew curves, have been derived as follows:

$$P_B(\lambda,T) = P_1^*(T) + 18 \, K(T)/[(44/\lambda) - 26]$$

$$P_D(\lambda,T) = P_1^*(T)/(1-\lambda) \quad , \qquad (3)$$

where K (T) is Henry's Law constant and λ the total CO_2 mass fraction.

Illustrative results are presented in Figures 1 through 4. Clearly, two-phase situations develop

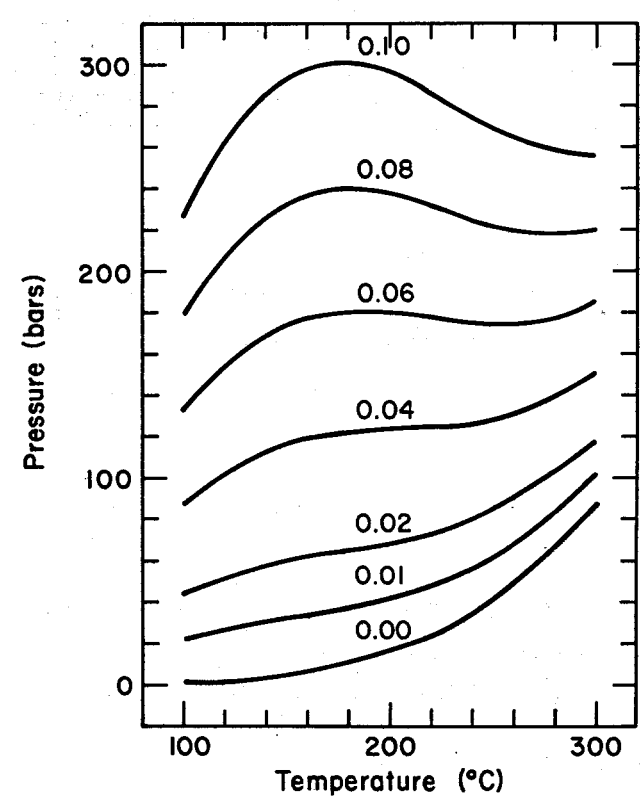

Figure 1. Boiling curves for H_2O-CO_2 mixtures. Total CO_2 mass fractions are indicated on the curves. (XBL 795-853)

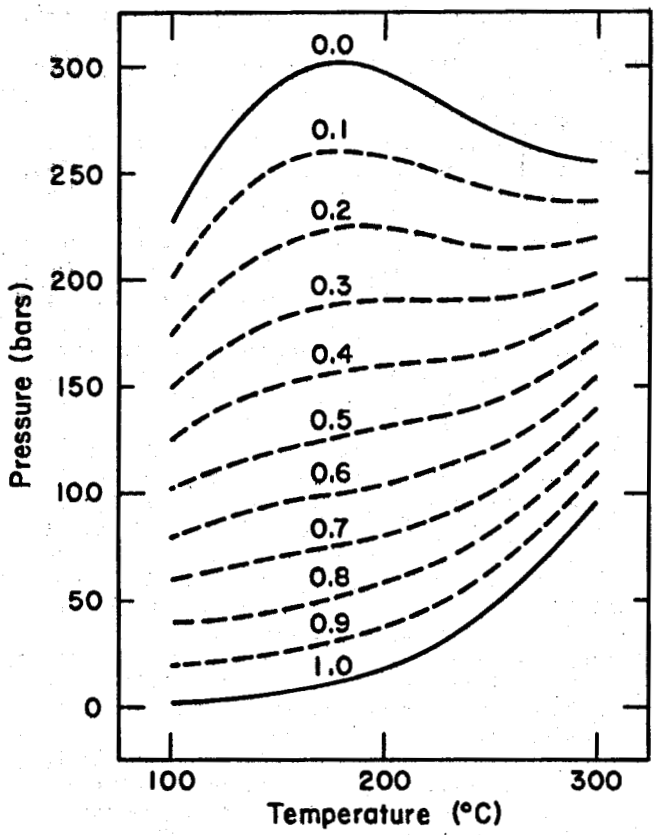

Figure 2. Vapor saturation curves (values of S_v indicated on the curves) for an H_2O-CO_2 mixture. The total CO_2 mass fraction is $\lambda = 0.1$. (XBL 801-6762)

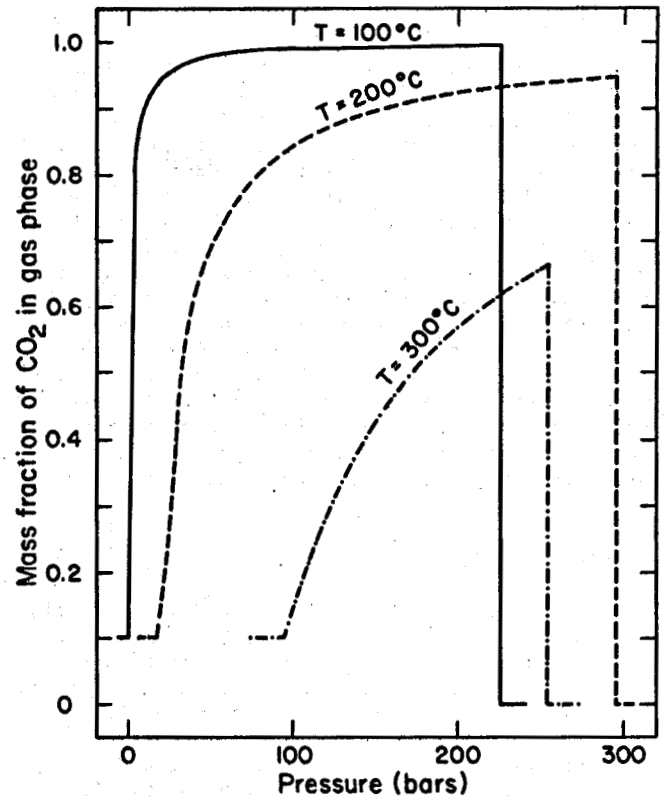

Figure 3. CO_2 mass fraction in the vapor phase as a function of pressure and temperature. The total CO_2 mass fraction is 0.1. (XBL 801-6763)

for pressures and temperatures at which pure water exists as a compressed liquid, even for relatively small CO_2 total mass fractions. This may have significant implications in fluid reserve assessment and well test interpretation. Figure 1 indicates the interesting possibility of inverse isobaric condensation and evaporation taking place at high (≥5%) carbon dioxide contents; this may introduce peculiar effects in hydrothermal fluid flow patterns. Our results also indicate that CO_2 may significantly contribute to the fluid enthalpy, particularly in reservoir gas caps where the carbon dioxide mass fraction is high.

This simple model is also currently being implemented in a steady-state wellbore code (Miller, 1979, personal communication).

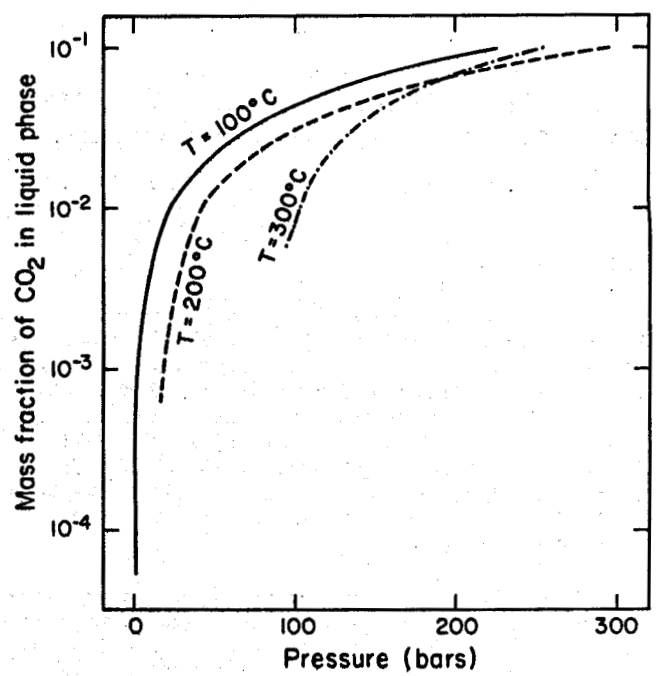

Figure 4. CO_2 mass fraction in the liquid phase as a function of pressure and temperature. The total CO_2 mass fraction is 0.1. (XBL 801-6764)

SUMMARY

The main advantage of the model just described is its simplicity. Only the thermodynamic properties of the pure components plus Henry's Law are used to estimate the properties of the mixture. In this economical way a qualitative understanding of compressed CO_2-H_2O solutions, two-phase and superheated gas mixtures is achieved. The accuracy of the model, however, is only fair, degrading rapidly with increasing temperatures, pressures and concentrations. This is of course because the simple assumptions adopted become inadequate outside a fairly restricted range of values of P, T, and λ. To overcome these difficulties a new, more accurate model is currently under development. The new model treats the mixture nonidealities on a rigorous thermodynamic basis, including corrections for pressure, temperature, and composition effects.

REFERENCES CITED

Burgassi, P., Stefani, G. C., Cataldi, R., Rossi, A., Squarci, P., and Taffi, L., 1976. Recent developments of geothermal exploration in the Travale-Radicondoli area, in Proceedings, Second United Nations Symposium on the Development and Use of Geothermal Resources, San Francisco, May 1975. Washington, D.C., U.S. Government Printing Office, v. 3, p. 1571-

Ellis, A. J., and Mahon, N. A. J., 1977. Chemistry and geothermal systems. New York, Academic Press.

Gislason, G., Armannsson, A., and Hauksson, T., 1978. Thermal behavior and dissolved gases in the Krafla geothermal system, Iceland. Icelandic National Energy Authority, report, OSJHD-7846.

Grant, M. A., 1977. Broadlands: a gas dominated geothermal field. Geothermics, v. 6, no. 9, p. 9-29.

Strauss, J. M., and Schubert, T., 1979a. Effect of CO_2 on the buoyancy of geothermal fluids. Geophysics Research Letters, v. 6. no. 1, p. 5-8.

____, 1979b. Thermodynamic properties for the convection of steam-water-CO_2 mixtures. Reprint submitted to the American Journal of Science, March 1979.

Sutton, F. M., 1976. Pressure-temperature curves for a two-phase mixture of water and carbon dioxide. New Zealand Journal of Science, v. 20, p. 297.

Sutton, F. M., and McNabb, A., 1977. Boiling curves at Broadlands geothermal field, New Zealand. New Zealand Journal of Science, v. 20, p. 333.

Sweigert, R. L., Weber, P., and Allen, R. L., 1946. Thermodynamic properties of gases: carbon dioxide. Ind. Engin. Chem., v. 30, . 185.

Wahl, E. F., 1977. Geothermal energy utilization. New York, Wiley-Interscience.

Weres, O., Tsao, K., and Wood, B., 1977. Resource, technology, and environment at The Geysers. Berkeley, Lawrence Berkeley Laboratory, LBL-5231.

White, D. E., Muffler, L. J. P., and Truesdell, A. H., 1971. Vapor-dominated hydrothermal systems compared with hot-water systems. Economic Geology, v. 66, p. 75-97.

Zyvoloski, G. A., and O'Sullivan, M. J., 1980. Simulation of a gas dominated, two-phase geothermal reservior. SPE Journal, v. 20, p. 52-58.

PRELIMINARY STUDIES OF THE RESERVOIR CAPACITY AND LONGEVITY OF THE BACA GEOTHERMAL FIELD, NEW MEXICO

G. S. Bodvarsson, S. P. Vonder Haar, M J. Wilt, and C. F. Tsang

INTRODUCTION

The Baca geothermal field is located in the Valles Caldera, New Mexico, about 55 miles north of Albuquerque. The field is being developed by the Union Oil Company of California and the Public Service Company of New Mexico (PNM). To date, 18 geothermal wells have been drilled in the Valles Caldera, varying in depth from 2000 to 9000 ft (Union and PNM, 1978). Six of the wells have been drilled in the Sulfur Creek area, the remainder along Redondo Creek (Figure 1).

The wells in the Sulfur Creek area have penetrated a high-temperature but low-productivity formation. In the Redondo Creek area, the wells have encountered a high-temperature ($\geq 550^{o}F$) liquid-dominated reservoir.

It is extremely important to make reliable estimates of the mass of hot water in place (reservoir capacity) and the length of time the reservoir can supply steam for a 50-MW power plant (reservoir longevity). Reservoir longevity depends both on the reservoir capacity and on the overall development plan for the field (flow rates, injection, etc.). Our paper (Bodvarsson et al., 1979) represents the first in a series of studies of the reservoir capacity and longevity of the Baca field.

THE YEAR'S ACTIVITIES

In this first study, the reservoir capacity was estimated by volumetric means using existing geological, well, and geophysical data. An initial study of reservoir longevity was also made using the two-phase numerical simulator SHAFT79 (Preuss et al., 1979) developed at LBL. Because of the lack of available data, we made a number of assumptions during the course of the study. Therefore, the results presented are preliminary estimates only.

Figure 1 is a base map of the Valles Caldera showing temperature contours, resistivity survey lines, and major faults. Geologic cross sections of the Valles Caldera region are shown in Figure 2 (see also Dondanville, 1971; Slodowski, 1977; Bailey

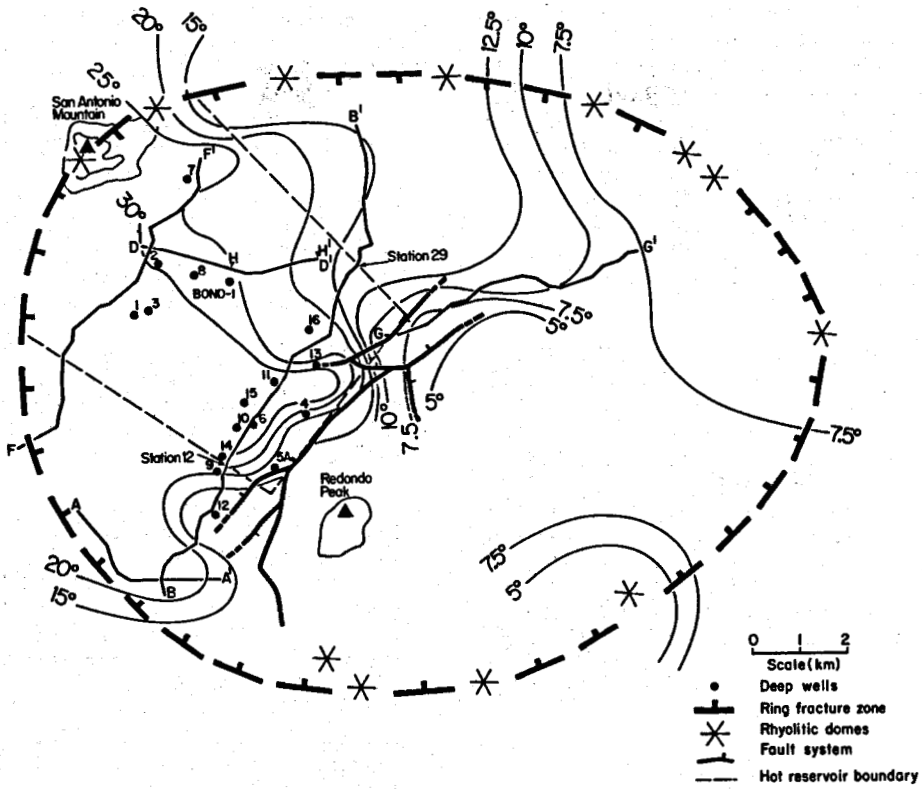

Figure 1. Base map of the Valles Caldera showing shallow temperature gradients (°F), geophysical survey lines (e.g., A-A'), specific faults, and the estimated hot reservoir boundary. (XBL 7912-13349)

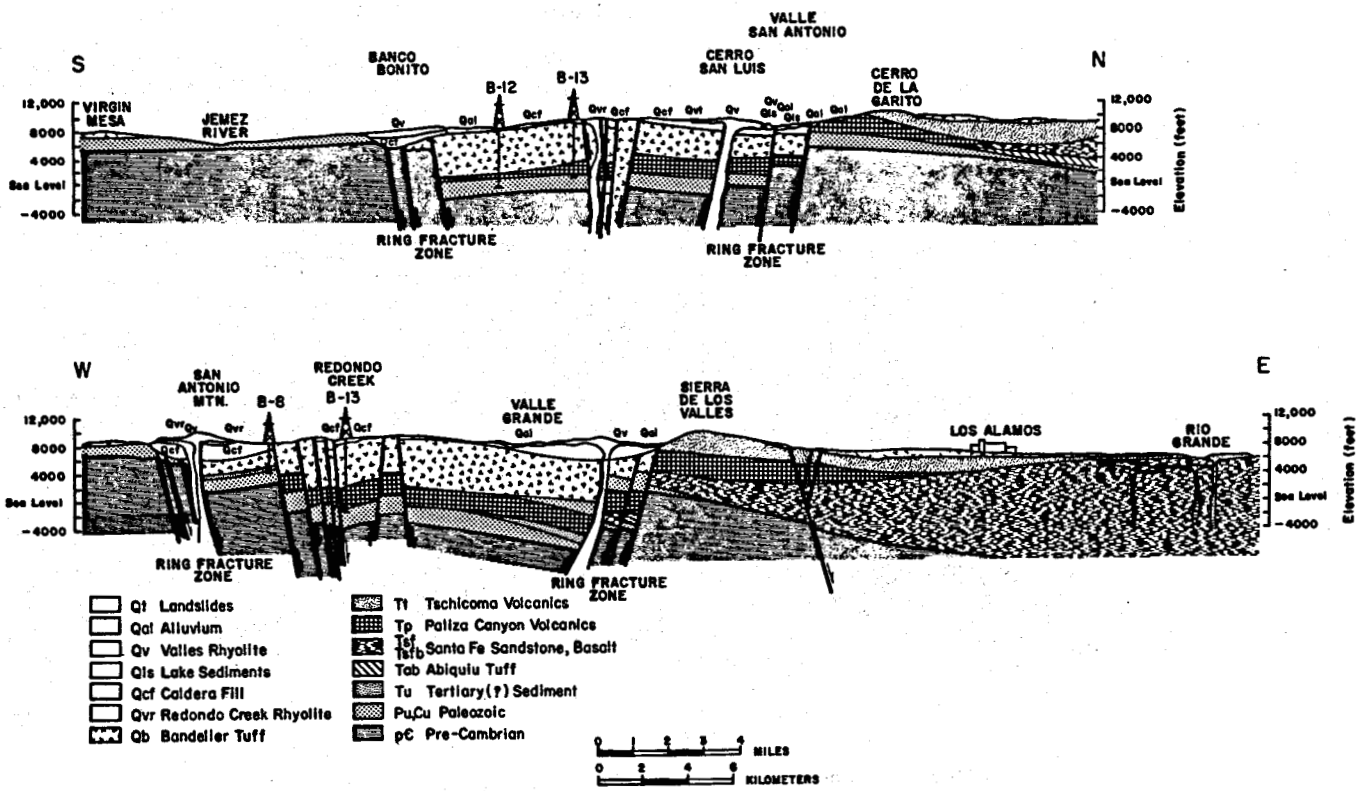

Figure 2. Geologic cross sections of the Valles Caldera Region. (XBL 799-11548A)

and Smith, 1978). The Bandelier tuff, the producing formation at Baca, is composed of several members of closely welded to nonwelded rhyolitic tuff and tuff breccia. Up to 6300 ft of this rock has been penetrated by the wells in Redondo Creek, but the bulk of the produced fluid comes from the deeper, more permeable layers. From temperature logs of the wells in the Redondo Creek area, an average reservoir thickness of 2000 ft was estimated. An average reservoir porosity of 5% was estimated from well resistivity logs and core data (Core Laboratories, 1975).

Geophysical data (Union Oil Co., 1972; Geonomics, 1976) shallow temperature contours and deep temperature data (Union Oil Co. and PNM, 1978) were used in estimating the areal extent of the reservoir. The reservoir temperature contours (Figure 3) are not very reliable due to the limited amount of data, but they do indicate a sharp temperature gradient southeast of the main temperature anomaly. This boundary coincides with a major northeast-southwest fault (Figure 1) that may act as an impermeable barrier. Figure 4 shows the shallow temperature gradients and the telluric profiles along line B-B', which is directed along the length of Redondo Canyon. An estimation of the hot reservoir boundaries in the north-south direction is made from these data. The results are indicated by the dotted line in Figure 4.

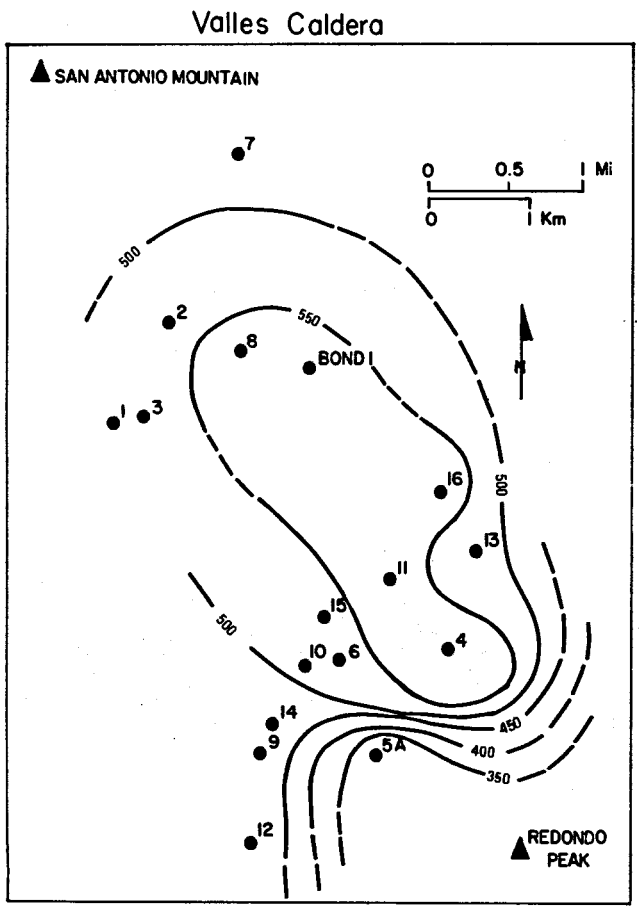

Figure 3. Deep reservoir temperature contours (3000 ft above sea level), in degrees. (XBL 794-7414B)

The data presently available are too limited to allow the western boundary of the hot reservoir to be established. To allow an optimistic estimation, the hot reservoir in this direction was assumed to extend to the ring fracture zone. Some geophysical data, and the fact that the Sulfur Creek wells are dry, seem to indicate a more reasonable boundary close to the Bond-1 well.

Using the above criteria, the areal extent of the hot reservoir was estimated to be 40 km^2 and the porosity-thickness product to be 100 ft. These values correspond to a reservoir capacity of 2.2 x 10^{12} lb of hot fluid in place.

The longevity of the Baca field has been studied using the numerical simulator SHAFT79 (Preuss et al., 1979). The reservoir was simulated using one basic rectangular mesh, with dimensions corresponding to those estimated in the previous section. In a few case studies, elements were added to obtain the required boundary conditions. Due to symmetry, only half of the system was modeled (Figure 5). Wells were not simulated individually, but rather the fluid was produced uniformly over one node representing half of the well field (assumed to be 1 km^2).

The parameters used in the simulation are given in Table 1. Most of these were taken directly from data reports released to the public by Union Oil Company. The relative permeability curves used were the Corey curves (Faust and Mercer, 1979), with residual liquid and steam saturations of 0.30 and 0.05 respectively.

Five cases were studied using a constant mass flow rate. The value used was based upon the amount of steam theoretically required for a 50-MW power

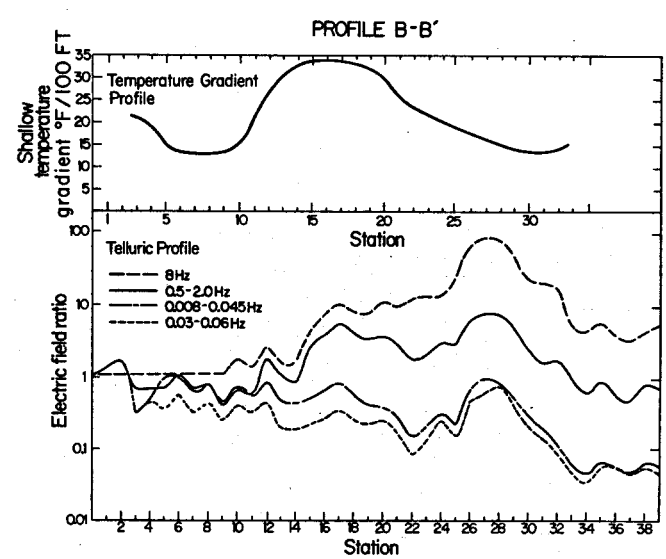

Figure 4. Shallow temperature gradients and telluric profiles along line B-B'. (XBL 7912-13350)

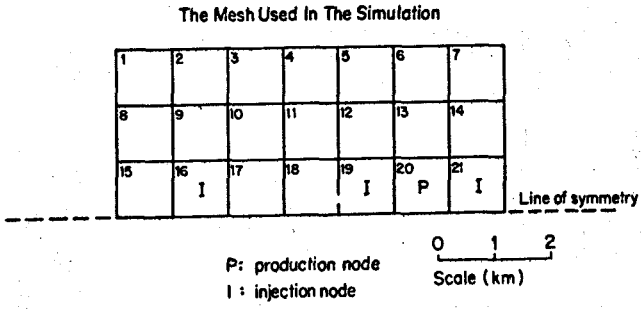

Figure 5. The mesh used in the longevity study for "closed" reservoir cases. (XBL 7912-13354)

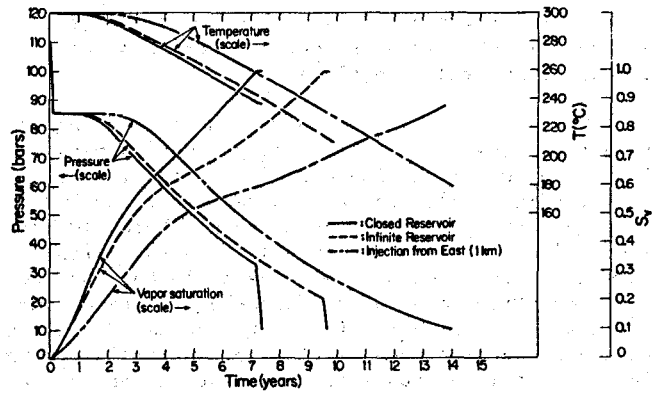

Figure 6. The temperature, pressure, and vapor saturation behavior in the production node for three of the constant flow rate cases. (XBL 7912-13352)

plant and a constant value of the mass fraction of steam in the separators (Union Oil Co. and PNM, 1978). The five cases studied were a bounded reservoir, an infinite reservoir, and three injection cases. Each case was run until the pressure in the production node dropped below the designated wellhead pressure of 10 bars (Union Oil Co. and PNM, 1978). The longevity of the field in each case was defined as the time it took to reach this point. In Figure 6, the pressure, temperature, and vapor saturation at the production node are plotted versus time for three of these cases.

The simulation of the closed reservoir was terminated after 7.4 years due to the low pressure in the production node. As Figure 6 shows, the pressure falls very rapidly at first until the production node goes two-phase. Under two-phase conditions, the pressure is related not to the density but to the temperature. The pressure first stabilizes after the node becomes two-phase because of the large heat capacity of the node and the low initial boiling rates. Later, the pressure declines gradually with the temperature. When saturation reaches 1.0, the pressure again becomes dependent on density, and the low inflow of fluid from adjacent nodes (due to the low absolute permeability and the effect of the relative permeability curves) causes the pressure to drop very rapidly.

For the infinite case, the pressure in the production region dropped below 10 bars after about 10 years, again due to the limited flow of the fluids into the production node (low-permeability effects). It therefore appears that the controlling

Table 1. Parameters used in simulation.

Constant flow rate	Q_T = 330 kg/s
Rock heat capacity	C_v = 950 J/kg°C
Permeability thickness	kh = 6,000 md ft
Thermal conductivity	λ = 2.0 J/s·m·°C
Porosity thickness	ϕH = 100
Initial pressure	P_i = 110 bars
Initial temperature	T_i = 300°C
Enthalpy of saturated steam in flash tank	H_{sv} = 2,772,000 J/kg
Enthalpy of saturated liquid in flash tank	H_{sl} = 734,380 J/kg
Steam requirement for a 50-MW plant	Q_{sv} = 892,000 lbs/hr
Enthalpy of the fluid entering the well	H_{wv}
Steam quality in flash tank	S_{qv}
Total flow rate	Q_t

factor limiting the reservoir longevity is the low permeability-thickness product rather than the amount of hot water in place.

Three injection cases were simulated using an injection flow rate of half the production mass flow rate; water was injected into nodes 16, 19, and 21 (Figure 5). For all three cases, the pressure into the production node dropped below 10 bars after 13 or 14 years. Figure 6 shows that with injection, the pressure falls below 10 bars before the production node reaches superheated steam conditions. This behavior is due to increased boiling in the production node because more water is coming in. The boiling causes the temperature, and consequently the pressure, to drop steadily.

A few cases were run using a time dependent flow rate based upon the steam quality in the separators and the theoretical steam requirement for a 50-MW power plant. Four cases were run using this approach: a closed reservoir, a semi-closed reservoir, an infinite reservoir, and a closed reservoir with recharge from deeper layers. In the semi-closed case, the northeast and the southwest boundaries were expanded from 3 to 10 km, leaving the other two boundaries unchanged. No injection runs were made, because very little separated water was obtained after about three years of simulation, and the injection of such a small amount of water would not alter the results significantly. Figure 7 shows the calculated flow rate as a function of time for the bounded reservoir case.

The closed reservoir case and the semi-closed reservoir case give very similar results; the pressure in the production node drops below 10 bars after 25 and 26 years, respectively. For the "infinite reservoir" case, the required amount of steam was supplied for 35 years before the pressure fell below 10 bars.

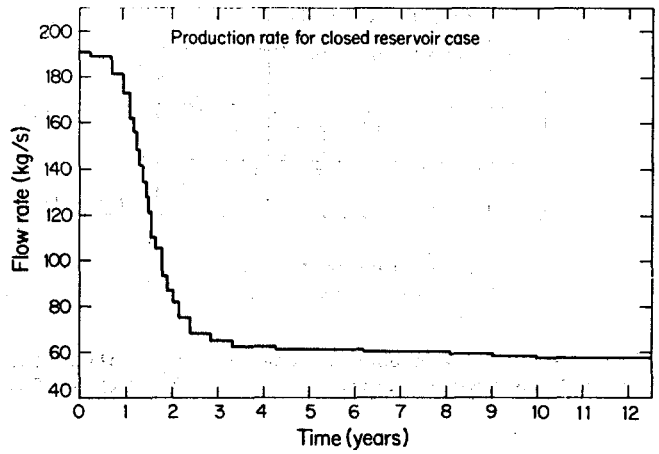

Figure 7. Production rate versus time for the closed boundary case. (XBL 7912-13353)

Finally, a run was made assuming that the reservoir was recharged from deeper layers through a 20 m wide fault zone extending along Redondo Creek (recharging nodes 5, 13, and 20). The fault zone was modeled as a constant pressure boundary 600 m below the assumed reservoir, having a permeability-thickness product of 60,000 md.ft. The results obtained indicate a reservoir longevity of 49 years under these conditions. Table 2 summarizes the primary results from all of the cases studied.

In conclusion, the study indicates a reservoir capacity on the order of 2.2×10^{12} lbs of hot fluid and a longevity of 7 to 50 years for the Baca geothermal field. The primary factor limiting the longevity of the field is the low permeability-thickness factor (kh), which causes very localized boiling around the production region.

Table 2. Summary of cases and primary results.

				Conditions at the end of the run			
Case	Flow rate	Boundary conditions	Injection	Time (yrs)	Pressure (bars)	Temp. (°C)	Vapor saturation
1	Constant	Closed	None	7.4	10	237	1.0
2	Constant	"Infinite"	None	9.6	10	214	1.0
3	Constant	Closed	4 km to NW	12.9	10	180	0.99
4	Constant	Closed	1 km to NW	13.7	10	180	0.91
5	Constant	Closed	1 km to NE	14.0	10	180	0.87
6	Variable	Closed	None	25	10	214	1.0
7	Variable	"Semi-infinite"	None	26	10	213	
8	Variable	"Infinite"	None	35	10	185	1.0
9	Variable	Bounded with a fault	None	50	10	180	0.48

PLANNED ACTIVITIES FOR 1980

During the next fiscal year, additional studies of the longevity of the Baca field will be carried out. The effects of relative permeabilities and the size of the production area will be studied, and construction of a geological model of the field will be initiated.

REFERENCES CITED

Bailey, R. A., and Smith, R. L., 1978. Volcanic geology of the Hemez Mountains, New Mexico, in, J. W. Hawley, ed., Circular 163. New Mexico Min. Mines, p. 184-196.

Bodvarsson, G. S., Vonder Haar, S., Wilt, M. J., and Tsang, C. F., 1979. Preliminary studies of the reservoir capacity and the longevity of the Baca geothermal field, New Mexico. Berkeley, Lawrence Berkeley Laboratory, LBL-10227, 18 p.

Core Laboratories, Inc., 1975. Special core analysis study of Baca no. 13 well. Union Oil Company.

Dondanville, R. F., 1971. Hydrological geology of the Valles Caldera, New Mexico. Union Baca Project Report, 36 p.

Faust, C. R., and Mercer, J. W., 1979. Geothermal reservoir simulation; numerical solution techniques for liquid and vapor dominated hydrothermal systems. Water Resources Research, v. 15, no. 1, p. 31-46.

Geonomics, Inc., 1976. Magnetotelluric-telluric profile survey of the Valles Caldera prospect. Union Oil Company.

Grant, M., 1979. Interpretation of downhole measurements at Baca. Proc. 4th Workshop on Geothermal Reservoir Engineering, Stanford University.

Pruess, K., Zerzan, J. H., Schroeder, R. C., and Witherspoon, P. A., 1979. Description of the three-dimensional two-phase simulator SHAFT78 for use in geothermal reservoir studies. Paper presented at Petr. Eng. Meeting in Denver, Colorado, February 1-2, 1979.

Slodowski, T. R., 1977. Geological resume of the Valles Caldera. Union Baca Project Report, 11 p.

Union Oil Company of California, 1972. Additional electrical geophysical surveys of the Valles Caldera area. Union Oil Company.

Union Oil Company of California and Public Service Company of New Mexico, 1978. Geothermal Demonstration Plant--Technical and Management Proposal to DOE, 120 p.

MODELING TRANSIENT TWO-PHASE FLOW IN A WELLBORE

C. W. Miller

INTRODUCTION

For a complete analysis of a geothermal system, it is necessary to model flow in the wellbore and in the reservoir. Several numerical codes to simulate the two-phase flow in the wellbore have been reported in the geothermal literature including those of Gould (1974), Juprasert and Sanyal (1977), and Sigiurs and Farouq (1979). However, they all assume steady state flow. Such types of models can be used to approximate downhole conditions from wellhead measurements or vice versa but only after the well has been flowing at a constant rate for a while. They are not useful in describing the wellbore flow during a well test. At early times, after a flow rate change has been made at wellhead, the mass flow rate into the well ($\dot{m}_{in}$) does not equal the mass flow rate out of the well ($\dot{m}_{out}$), because wellbore storage is important. Under such circumstances, a steady-state model, which naturally assumes $\dot{m}_{in} = \dot{m}_{out}$, is not appropriate. Wellhead data taken during this early time cannot be related accurately to downhole pressures using a steady-state model, and a transient model is needed. Besides relating wellhead and downhole pressures during a well test, one can use such a code to understand the initial pressure changes with time in the well after a flow rate change. Because of heat transfer in the wellbore and the relatively large value of permeability-thickness found in a geothermal field, the drawdown or buildup curve does not necessarily coincide with what is predicted by well test analysis developed by the petroleum industry (Miller, 1979a).

ACTIVITIES IN 1979

A transient two-phase numerical code that solves one-dimensional flow including heat and mass transfer has been developed. The wellbore model has been coupled to a reservoir model of simple, one-phase radial flow in a porous medium. The program WELBORE solves the equations of mass, momentum, and energy and uses an equation of state to relate the density to pressure and energy. The Navier Stokes equation is used for the momentum equation in contrast to assuming Darcy flow as for flow in a porous medium. Thermodynamic equilibrium is assumed so the equation of state is given by an analytical representation of the the steam tables. For the initial development of the model, the velocities of the two-phases were assumed equal. The four unknowns that must be determined are pressure, energy, density, and velocity.

The basic approach is to solve the four equations using a finite-difference approximation with a partially implicit method. Terms that would impose very restrictive time steps because of the fluid compressibility were solved implicitly while the other terms were evaluated explicitly for ease and computational efficiency. The solution procedure is: (1) to write the change in density, $d\rho$, in terms of the change in pressure, dP, and the change in enegy, de; (2) to solve the energy equation for the quantity de; and (3) to combine the continuity and momentum equation to give an expression for the new pressure in terms of known values. Combining the equations results in an

expression

$$AP = B$$

where A is a tri-diagonal matrix, which can easily be inverted, and B is a matrix that is a function of the old values of density, pressure, velocity, and energy.

To use this method, the equation of state is written in the form

$$d\rho = (\partial\rho/\partial P)_e \, dP + (1/\rho)\,(\partial\rho/\partial e)\;\; \rho de$$

instead of $\rho = fn(P,e)$. At the end of the calculation, the computed density is compared to the density calculated from $\rho = fn(P,e)$. If there is any significant difference, the pressure is calculated a second time using an average of the derivatives $\partial\rho/\partial P$ and $(1/\rho)\,(\partial\rho/\partial e)$. More details are given in Miller (1979b).

The transient wellbore code was used to investigate the propagation of a pressure pulse down the wellbore after a flow rate change was made at wellhead. Figures 1 and 2 illustrate the pulse as a function of time for flow in a liquid filled well and for flow in the well, where the fluid flashes part of the way up the bore. In the first figure (liquid filled well), one sees that initially there is no change downhole until the pulse has time to propagate through the bore. Once the pulse reaches the well/reservoir boundary, it interacts with that boundary. In some cases the pulse is partially reflected, propagating back up the bore. The change in wellhead and downhole pressures will be different until this transient motion dies out.

In Figure 2, one sees the pulse propagation in a fluid that is flashing in the bore. In this case, the pulse reflects off the flash point and oscillations in pressure occur in the two-phase region. Again, changes in wellhead pressure are quite different from downhole transients and are not representative of the reservoir itself. Nevertheless, given appropriate boundary conditions, one can use the transient code to solve for the flow in the bore and to essentially eliminate the well as an unkonwn. Even without the correct boundary conditions, one could first estimate the properties of the reservoir and then use the wellbore code with a reservoir model to determine if these properties gave the measured values of pressure and flow rate.

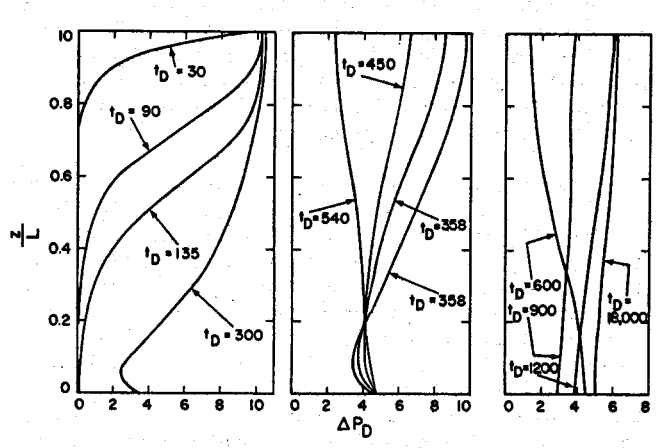

Figure 1. Propagation of pressure pulse down a well as a function of time for a liquid-filled well. (XBL 794-7404)

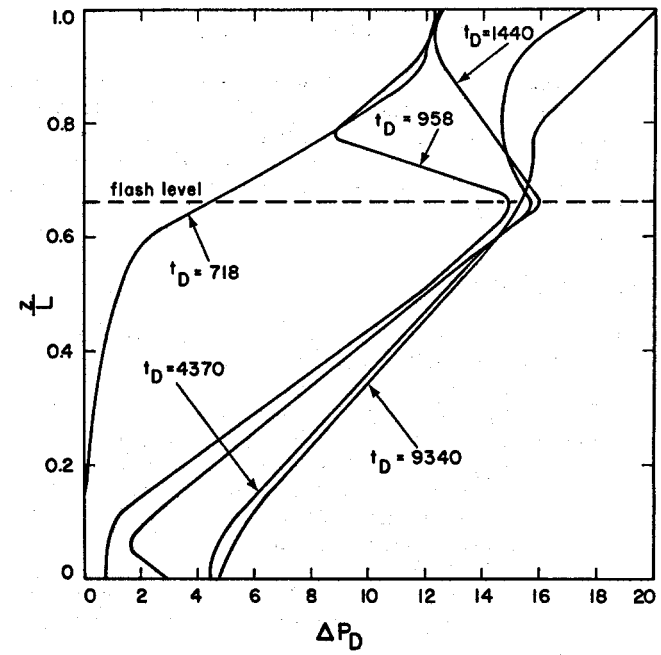

Figure 2. Propagation of a pressure pulse down a wellbore in a two-phase well as a function of time. (XBL 794-7403)

FURTHER INVESTIGATIONS

Several different combinations of boundary conditions are possible with the program WELBORE. They include: (1) downhole pressure and wellhead flow rate; or (2) wellhead and downhole pressures. It is also of interest to be able to specify wellhead pressure and wellhead flow rate and to determine the downhole pressure and flow rate. Work is being initiated on including this option. Also to improve the model, slip is being added, i.e., the velocities of the two phases will not be assumed to be equal. The slip will be given by empirical correlations. With the slip in the model, an attempt will also be made to relate wellhead data to what actually happens downhole. To further improve the model, a second component, say CO_2, will be added. Then one can look at the flow of two components as well as two phases.

REFERENCES CITED

Gould, T. L., 1974. Vertical two phase steam water flow in geothermal wells. Journal of Petroleum Technology, v. 26, p. 883-892.

Jupraset, S., and Sanyal, S. K., 1977. A numerical simulator for flow in geothermal wellbores. Geothermal Resources Council Transactions, v. 1, p. 159-161.

Miller, C. W., 1979a. Wellbore storage in geothermal wells. Dallas, Society of Petroleum

Engineers, SPE-8203.
____, 1979b. Numerical model of transient two phase flow in a wellbore. Berkeley, Lawrence Berkeley Laboratory, LBL-9056.

Sugiurs, T., and Farouq, S. M., 1979. A comprehensive wellbore steam-water flow model for steam injection and geothermal applications. Dallas, Society of Petroleum Engineers, SPE-7966.

CORRECTION OF DOWNHOLE PRESSURE TRANSIENTS MEASURED WITH A FLUID-FILLED CAPILLARY TUBE

C. W. Miller and J. M. Zerzan

INTRODUCTION

One of the limiting factors in the well testing of a geothermal reservoir is the ability to measure downhole pressure transients. Many existing pressure tools, developed for the petroleum industry, cannot withstand the high temperature and high salinity of the geothermal brine. The main problem is the pressure transducer itself. One method that has been used to alleviate the problem is to keep the pressure transducer at wellhead and to transmit downhole pressure changes to wellhead through a fluid-filled capillary tube. The fluid used in the tube should not flash or condense at the temperatures and pressures of interest. Also, the diameter of the tubing must be small enough so that the tubing can be handled at wellhead and lowered into the well. Such a system is marketed for use by the petroleum and geothermal field by the Sperry Sun Company and has been used at Lawrence Berkeley Laboratory for a number of well tests. However, an analysis was done on the system in the previous year (Miller and Haney, 1978), and it was shown that the fluid transmission line delayed and distorted the pressure signal significantly. The time delay of the system was on the same order of magnitude or longer than the response time of the reservoir in many cases. The effect of tubing diameter, fluid type, temperature changes, and temperature and pressure levels were investigated. Nevertheless, because of the desirability of being able to continuously monitor the downhole pressure during a test, and the unavailability of alternate methods at the moment, the system is still being used or being considered for many well tests. The main effort then in 1979 was to investigate whether one could determine an accurate method of correcting for the effect of the measuring instrument, the fluid transmission line in this case.

ACTIVITIES IN 1979

In the previous work, the fluid transmission system was modeled for the fluid being either a gas or a liquid. Given the pressure disturbance generated downhole, one could calculate, then, what would arrive at the wellhead. For the liquid-filled tube, the propagation of the pressure disturbance was controlled by a diffusion-like equation because of the large friction effects. For a gas-filled tube, the pressure disturbance had to be modeled by a wavelike equation that had a damping term to account for the frictional losses. However, to correct for the effects of the fluid transmission line on the signal, one must be able to solve the inverse problem. That is, given the measured pressure signal, it is necessary to determine the downhole pressure that caused the signal. The problem is not straightforward because the specification of the cause of the disturbance (the measured pressure) does not result in a well-posed problem. A unique solution may not exist, meaning that different disturbances could result in the same signal arriving at the pressure transducer. At present, it has been possible to obtain reasonable solutions to this inversion problem for the case of the liquid-filled tube, because the equation governing the signal propagation was linear in most cases, and when it was nonlinear, the coefficients were a function of the position only and not a function of position and time. For the gas-filled tubing, the equation governing the signal propagation is highly nonlinear, and it is not clear that a unique solution exists for the measured data. An inversion technique was applied to the liquid case and excellent results were obtained.

As stated above, the liquid-filled tubing was modeled by a diffusion-like equation. This same type of equation is important in heat conduction problems, and the solution to this inverse problem has been considered previously. Exact solutions are available for the linear case (Burggraf, 1964). However, the exact solution requires a continuous pressure measurement in time, because the inverse solution is a convergent series dependent on derivatives of pressure with time. The more distorted the signal, the more higher-order derivatives are needed. Accurate measurements of these derivatives may not be realistic.

Another method of inverting data is the nonlinear estimation technique used by Beck (1970). The method is to minimize the difference between the calculated response of the system for a guessed value of pressure or the derivative of the pressure at the bottom of the well and the measured response over some time interval. Because there is a delay in time before the changes downhole can be measured at the wellhead, the minimization is done over a number of "future times," with the number of future times depending on just how long the delay is. If a signal takes 10 sec to produce a "measurable" value at wellhead, then the minimization is done over the time t^{ℓ} to t^{ℓ} + 10 sec. For a longer delay, the minimization is done over a longer time A measurable value depends on the accuracy of the pressure transducer used. More details of the method are given by Miller and Zerzan (1979).

The method was used to invert the measured data. Results of the inversion are given in Figures 1 through 3. For the first two cases, the measured data were obtained by using a simulation drawdown curve and then finding out what would be measured at wellhead for that curve. Then these

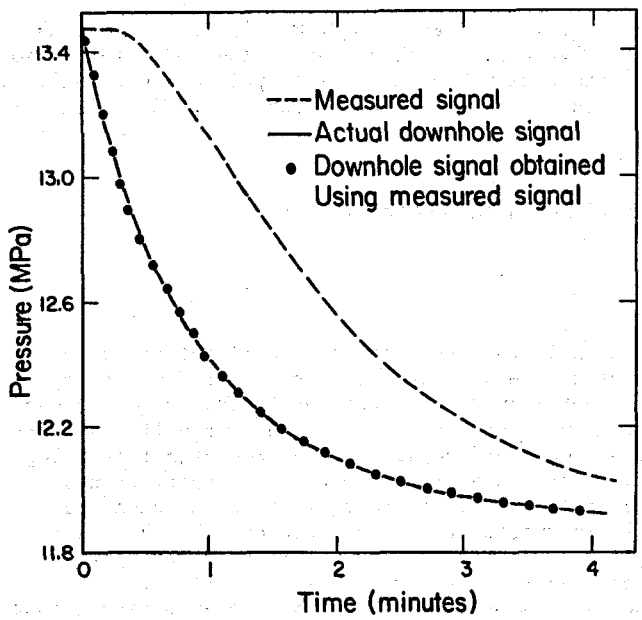

Figure 1. Comparison of a simulated downhole pressure signal and the signal obtained using the "measured" signal; diffusivity of oil is 40,000 m^2/sec and tube length is 2400 m. (XBL 797-2060)

"measured data" were inverted using the minimization technique to try to obtain the original drawdown curve. For Figure 1, the simulation was done for a high-temperature oil with a diffusion coefficient of 40,000 m^2/sec. For Figure 2, the simulation was for a low-temperature oil, resulting in a diffusion coefficient of only 6,000 m^2/sec. In both cases, the tubing was 2400 m in length with an inner diameter of 0.14 cm. For the first case, the minimization had to be over 8 sec, whereas in

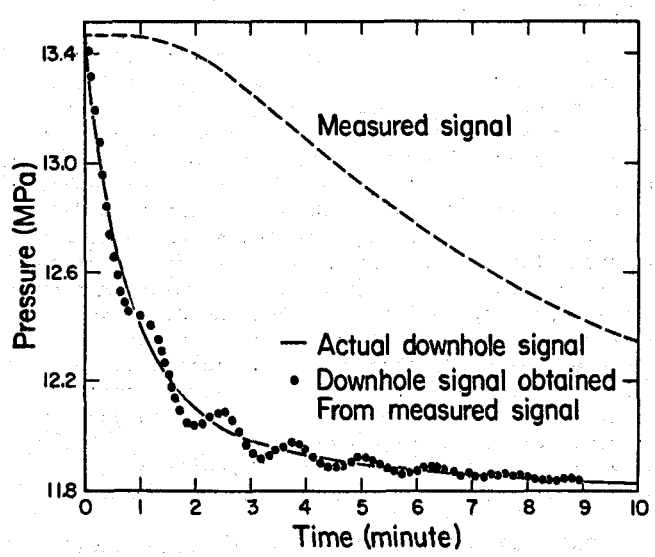

Figure 2. Comparison of a simulated downhole pressure signal and the signal obtained using the "measured" pressure response at wellhead; diffusivity is 6000 m^2/sec and tubing length is 2400 m. (XBL 797-2059)

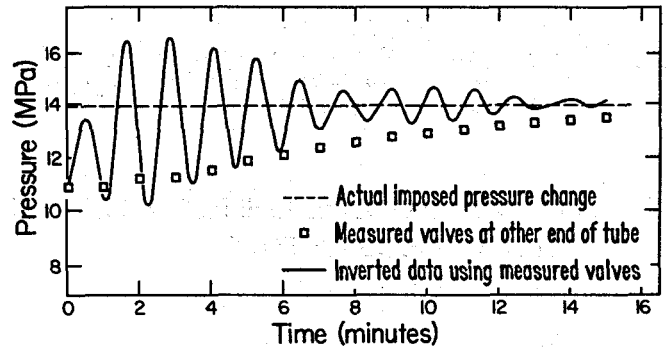

Figure 3. Comparison of an actual step change in pressure and the signal obtained using the measured pressure response; diffusivity is 6000 m^2/sec and tubing length is 2400 m. (XBL 797-2081)

the second case it was necessary to use a delay of 40 sec. For the same drawdown curve, a more distorted curve will be measured as the signal delay time increases. Also, as the drawdown curve increases in steepness, the measured signal increases in distortion. As the curve distorts more, oscillations appear when solving the inverse case. Nevertheless, the oscillations are symmetic about the actual solution. Realizing this result, one could obtain the solution by first inverting the signal, and then, knowing that the actual solution is not oscillatory, one obtains the actual solution by assuming that the oscillations are symmetric about it. Using this assumed solution, one can recalculate the expected values and compare with the measured one.

To check the inverse technique, the numerical solution was compared to an experiment. However, the only experimental data available were for the case where a step change from 10.9 to 14.0 MPa was imposed at one end of a capillary tube and then the pressure signal was measured at the second end. This situation is one of the "worst cases," i.e., a very steep change with a long delay time (40 sec). The measurements were obtained for a tube 2400 m long with an inner diameter of 0.14 cm and for 10 centistoke silicone oil at 20 C. Figure 3 shows the imposed change, the measured pressure at the second end of the tube, and the values calculated when trying to invert the data. The oscillations are larger than the original step change, so the inversion in this case should not be taken too seriously, but it must be noted that even in this case, the oscillations are damped and symmetric about the actual signal. If one followed the above method of calculating the inverse solution and then taking the average of the oscillations, the solution obtained even in this case would be fairly reasonable.

A method of correcting for the measuring instrument has been determined for the liquid-filled capillary tubing. It must be noted, though, that the fluid is affected by any temperature changes in the well during a test. The temperature changes show up as a source of the pressure in the modeling of the fluid transmission line. To invert the measured data at wellhead, one must have some idea

of the changes in temperature with time, which is a large limitation on the use of the instrument.

PLANNED ACTIVITIES

It is still of interest to consider the highly nonlinear problem of the inverse case for a gas-filled tube. One reason is that the gas is significantly less affected by temperature changes then the liquid-filled tube. Secondly, given a method of modeling the two-phase transient flow in the wellbore itself (Miller, 1979), another possible way of obtaining the downhole pressure transients is to use the wellhead data itself without having to resort to a fluid transmission line. Such a technique will be considered in the future.

REFERENCES CITED

Burggraf, O. R., 1964. An exact solution of the inverse problem in heat conduction theory and applications. Journal of Heat Transfer, v. 86C, p. 373.

Beck, J. V., 1970. Nonlinear estimation applied to the nonlinear inverse heat conduction problem. International Journal of Heat and Mass Transfer, v. 13, p. 703-716.

Miller, C. W., 1979. A numerical model of transient two phase flow in a wellbore. Berkeley, Lawrence Berkeley Laboratory, LBL-9056.

Miller, C. W., and Haney, J., 1979. Response of pressure changes in a fluid filled capillary tube, in Proceedings, Second Invitational Well Testing Symposium. Berkeley, Lawrence Berkeley Laboratory, LBL-8883.

Miller, C. W., and Zerzan, J. M., 1979. Downhole pessure changes measured with a fluid filled capillary tube. Dallas, Society of Petroleum Engineers, SPE-8233.

WELLBORE STORAGE EFFECTS IN GEOTHERMAL WELLS

C. W. Miller

The established techniques of well testing in the petroleum industry, which are used to assess the characteristics of oil and gas reservoirs, have been extended to the geothermal field. However, there are several important differences between a geothermal field and an oil or gas reservoir, and it is necessary to understand how these differences will influence the analysis of well test data. There are two important differences. (1) The value of kh/μ (permeability-thickness/viscosity) is usually much larger in a geothermal field than an oil or gas reservoir because of the large value of h and relatively small value of μ. (2) Heat loss in the wellbore during a well test of a geothermal field can be important while it is ignored for a test of an oil or gas field. The increased value of kh/μ means that for the same storage capacity of the reservoir, the time for the reservoir to be able to supply the desired flow rate for a given pressure drop will decrease. The significance of this effect is that as the time for the reservoir to respond decreases, the nonuniform transients in the well itself can become important. The drawdown in a well test has been derived previously assuming that the fluid in the wellbore is well-mixed and responds uniformly in time to pressure changes, i.e. an infinite speed of propagation. As the reservoir responds faster the latter assumption is not valid and vastly different wellbore storage curves are obtained. The second problem of heat loss always exists in the testing of a geothermal field and is important even when the semilog straight-line region is expected.

ACTIVITIES IN 1979

Work was one on understanding and characterizing the expected drawdown pressure response during a well test of a geothermal field. The effort was directed at understanding the early time changes affected by the relatively large value of kh/μ and also the longer time effect of heat transfer.

Wellbore storage is the capacity for the well itself to absorb or supply any part of the mass flow rate out of the well/reservoir system. When the mass flow rate at the surface is increased (or decreased), the change in pressure is felt initially only in the well. After a certain amount of time, depending on the properties of the reservoir and the conditions in the well, the reservoir will start to supply part of the flow. As transient changes in the well die out, the sandface flow rate increases and approaches the surface flow rate, and one can think of the time for this to occur as the time constant of the reservoir.

If the pressure changes with time in the well are not a function of position, then a graph of pressure versus time on a log-log plot will have unit slope, implying that the well supplies the flow rate changes in a uniform manner. All wellbore storage curves generated in the petroleum industry have this unit slope. However, there is a finite time for changes made at the surface to arrive downhole, and it is not possible for the well to respond initially in a uniform manner. During that time, the wave generated when a change is made in flow rate at the surface is important and the measurement of pressure changes with time (dP/dt) at any one point in the well cannot characterize the average of dP/dt. Before a well-mixed condition is valid, the wave nature of the original disturbance must be damped out. There are cases when the reservoir can supply fluid before dP/dt in the well is uniform. For these cases, a unit slope of log P vs log t is not measured and another nondimensional time has been derived to characterize the resultant curves.

For a given value of C_D (ratio of the storage capacity of the well to that of the reservoir), it has been possible to derive a quantity t_{RW}, which is the ratio of the time for the reservoir to respond to that of the well. The quantity was

determined to be

$$\frac{\mu}{kh} \quad \frac{r_w^2}{2} \quad \frac{1}{\rho_{s.f.}} \left(\frac{\partial\rho}{\partial P}\right)_s^{1/2}$$

where r_w is the radius of the well, $\rho_{s.f.}$ is the density of the fluid at the sandface, and $(\partial\rho/\partial P)_s^{1/2}$ is the average isentropic compressibility of the fluid in the well. Using a transient numerical model of the flow in the wellbore (Miller, 1979a), it has been possible to determine the expected drawdown response for a homogeneous single-phase reservoir with either single-phase or two-phase flow in the wellbore for the adiabatic case.

Figure 1 illustrates the results of these calculations for a $C_D = 25$, giving the nondimensional pressure P_D, versus the nondimensional time, t_D. Plotted in the figure are: (1) the $C_D = 0$ case for a finite well radius; (2) the drawdown curve generated assuming the fluid in the wellbore responds uniformly; and (3) the actual drawdown curves that result as the value of the t_{RW} decreases. After a flow change has been made at wellhead, nothing is measured downhole until the disturbance arrives. However, once the wave reaches the well/reservoir interface, the pressure change increases abruptly and approaches the wellbore storage curve based on the uniform theory. If the reservoir cannot supply the surface flow rate for the pressure pulse that arrives downhole, then the well must continue to supply the desired flow rate and P_D vs t_D curve approaches the unit slope. Most oil and gas fields are in this category. But as kh/μ increases for the same value of C_D, the reservoir is capable of supplying a much larger quantity of fluid in a shorter time and the measured P_D vs t_D curve approaches the uniform theory curve at times later than the expected unit slope. Curves of this steep nature have been observed in geothermal field tests (Narasimhan and Witherspoon, 1977) and were not previously explained. As t_{RW} decreases, the reservoir

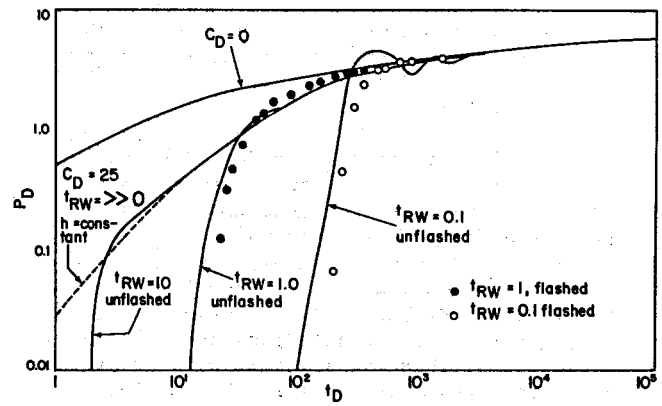

Figure 1. Nondimensional pressure vs nondimensional time for different values of t_{RW} with $C_D = 25$. Calculations are done for fluid that is both flashed and unflashed. (XBL 794-7402)

may be able to supply more fluid than the well could for the same pressure drop and oscillations would be measured. The quantity t_{RW} was shown to describe this early time behavior in many cases and details are given in Miller (1979b).

The effect of heat transfer on the well tests was also considered. Heat transfer is especially important when a new well is tested because the rock surrounding the bore is still relatively cool. However, heat transfer will always be important in a two-phase well because of the large temperature changes that occur when the flash level rises or falls. Even after the early-time wellbore storage changes are over, heat transfer can alter the slope of the semilog plot of P vs log t from $q\mu/4\pi kh$ (q is the volume flow rate) requiring a different analysis of the data than has been developed in the petroleum industry.

Figure 2 is a plot of P vs t for a buildup and a subsequent drawdown test. To simulate the heat

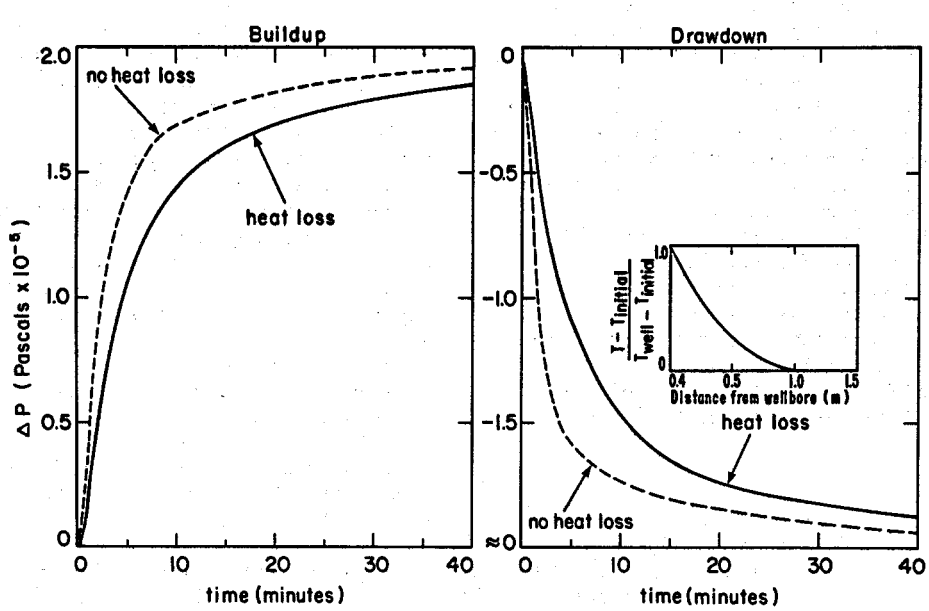

Figure 2. Effect of heat transfer on the buildup and drawdown curve. (XBL 794-7412)

loss from the well, a typical geothermal temperature gradient was assumed far from the well and a small temperature buildup was used near the bore. A nondimensional representative temperature profile is given by the insert in the figure. This is a typical temperature buildup. The effects shown in the figure will increase for colder wells. In Figure 2, the graph on the left is a plot of the pressure buildup and then drawdown when the heat loss is ignored. The graph on the right is a plot of those properties when heat transfer is allowed to take place. The figure shows that the heat transfer causes the pressure to initially change at a slower rate both for the buildup and the drawdown test. During a buildup test, the enthalpy of the exiting fluid decreases because of the increased time that the fluid is in the well. As the enthalpy decreases, the fluid can condense or compress more for the same pressure so more fluid flows into the well with a smaller pressure rise. Also the time required until a semilog straight line is measured increases and the slope of this line changes from that predicted in the petroleum industry (see Milller 1979b).

PLANNED ACTIVITIES

In the future, it would be of interest to investigate the drawdown response for a multilayer reservoir when the time response of the reservoir is relatively fast. It is also of interest to investigate the pressure response when flashing occurs in the reservoir itself instead of just in the well and to consider the effects of slip between the phases of the well test results.

REFERENCES CITED

Miller, C. W., 1979a. Numerical model of transient two-phase flow in a well bore. Berkeley, Lawrence Berkeley Laboratory, LBL-9056.

____, 1979b. Wellbore storage effects in geothermal wells. Dallas, Society of Petroleum Engineers, SPE-8203.

Narasimhan, T. M., and Witherspoon, P. A., 1977. Reservoir evaluation tests on RRGE 1 and RRGE 2, Raft River Geothermal Project, Idaho. Berkeley, Lawrence Berkeley Laboratory, LBL-5958.

HYDRAULICS OF A WELL INTERCEPTING A SINGLE HORIZONTAL FRACTURE

G. S. Bodvarsson, T. N. Narasimhan, and C. F. Tsang

INTRODUCTION

Since the 1960s, considerable work has focused on the problem of isothermal flow to a well intercepting a single fracture. The primary emphasis has been placed upon understanding the flow characteristics of a system with a vertical fracture; the horizontal fracture case has received relatively less attention. The interest in vertical fracture stems from the common belief that vertical fractures generally result from hydraulic fracturing experiments.

The orientation of fractures created by hydraulic fracturing techniques is controlled by the in-situ stress condition at each specific site. Because the fracture propagates perpendicular to the least principal stress, horizontal fractures are generally created at shallow depths, and vertical ones at greater depths. Recent studies by Zoback et al. (1977) have indicated that horizontal fractures can be created at considerable depths in certain tectonically active regions.

Fractures are also commonly found naturally. For example, in volcanic regions, the primary fluid conduits may be the contact zone between adjacent lava beds (Thorsteinsson and Eliasson, 1970; Benson et al., 1979). The contacts will in general behave as horizontal fractures of large areal extent in well tests. An understanding of the flow characteristics to a well intercepting a horizontal fracture is very important in the analysis of well tests in groundwater and geothermal reservoirs.

This brief report focuses on the pressure response in a well intercepting a finite-capacity horizontal fracture. The model used is calibrated against an analytical solution for the uniform-flux horizontal fracture case. Some examples of the effects of fracture permeability and radial extent on the pressure response are given.

PREVIOUS WORK

A number of studies have focused on fracture network problems using a grid of equally spaced horizontal fractures (Kazemi, 1979; Boulton and Streltsova, 1977; Najurieta, 1979). Hartsock and Warren (1961) studied numerically the psuedo-steady-state behavior of horizontally fractured wells. They calculated skin factors for different geometric and material parameters, assuming radial flow four fracture radii away from the well. Warren (1962) later extended the study, developing an expression for the skin factor.

Gringarten (1971) studied the unsteady-state pressure response in a well intersecting a horizontal fracture. In the study he considered a confined aquifer with a single horizontal fracture (Figure 1). All of the flow into the well was assumed to be via the fracture and the fluid entering the fracture was assumed to enter uniformly over the fracture area (uniform flux). The results of the study were presented in a set of type curves (Figure 2). Gringarten found that the system under the assumed conditions could be characterized by two dimensionless parameters (dimensionless time and pressure) in addition to the parameter

$$h_D = \frac{h}{r_f}\sqrt{\frac{kr}{k_z}} \quad .$$

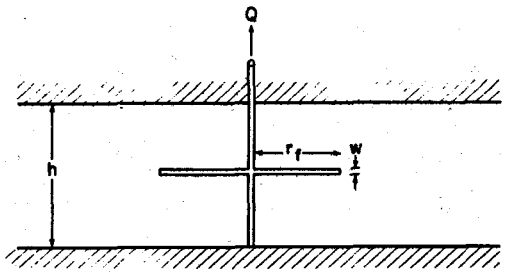

Figure 1. Cross section of a horizontal fracture model. (XBL 804-7003)

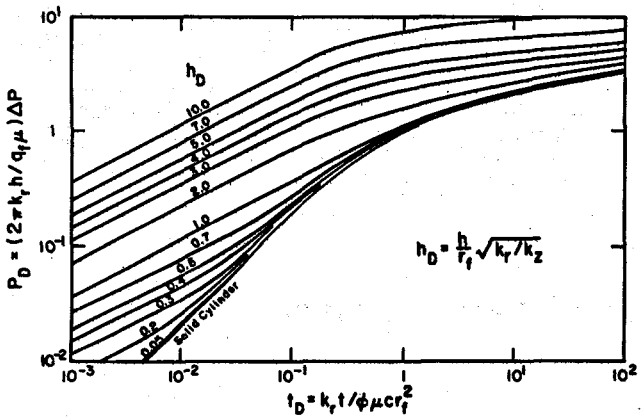

Figure 2. Type curves for a uniform flux horizontal fracture system (Gringarten, 1971). (XBL 804-7009)

NUMERICAL STUDIES

For this study the numerical code TERZAGI was used. The program solves the mass balance equation for isothermal fluid flow. It employs the integrated finite-difference method (IFDM) to characterize the flow regime (Narasimhan and Witherspoon, 1978) and solves the sets of nonlinear equations using an efficient sparse solver (Duff, 1977).

An axisymmetric mesh was used in the study (Figure 3). Gravity effects and tip flow were neglected. Due to symmetry, only half of the flow field needed to be considered. The block size was increased logarithmically in the radial direction. Ten to twenty fracture elements were used, depending upon the permeability and radial extent of the fracture.

Comparison with Gringarten's Solution

The first problem solved using the numerical simulator was identical to the one solved analytically by Gringarten (1971).

In the problem as defined by Gringarten there is actually no well; rather the fracture behaves as a source (sink). Thus for the purpose of comparison with Gringarten's solutions, in the numerical simulation the well element had to be removed and sources (sinks) of variable strength placed in the fracture elements. In this way, one of the most

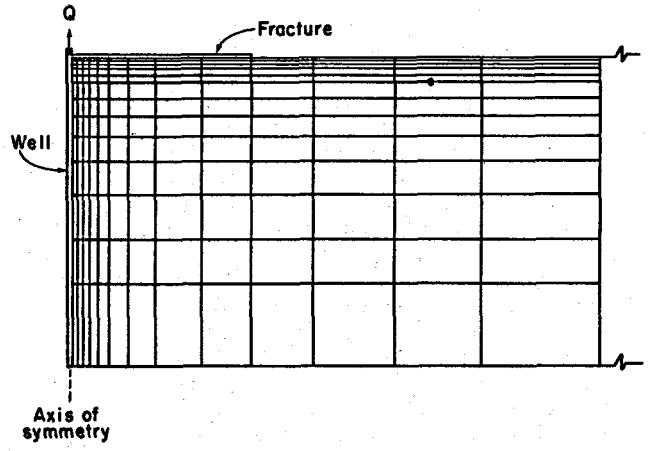

Figure 3. The mesh used in the numerical simulation studies. (XBL 804-7003)

critical assumptions made by Gringarten, the uniform flux assumption, was satisfied. Two cases were simulated, i.e., $h_D = 1$ and $h_D = 4$. Figure 4 shows the comparison between the numerical and the analytical solutions for one of these cases.

Finite Conductivity Horizontal Fracture

The horizontal fracture problem solved analytically by Gringarten was based upon several important assumptions. The most critical assumption is that the same mass of fluid enters the fracture everywhere (uniform flux conditions). This assumption should not be critical at early times when linear vertical flow from the reservoir to the fracture occurs. At later times, however, radial flow to the fracture region starts to dominate and the bulk of the fluid enters the fracture close to the tip of the fracture. The uniform flux assumption therefore creates an unrealistically large pressure drop in the fracture elements close to the well.

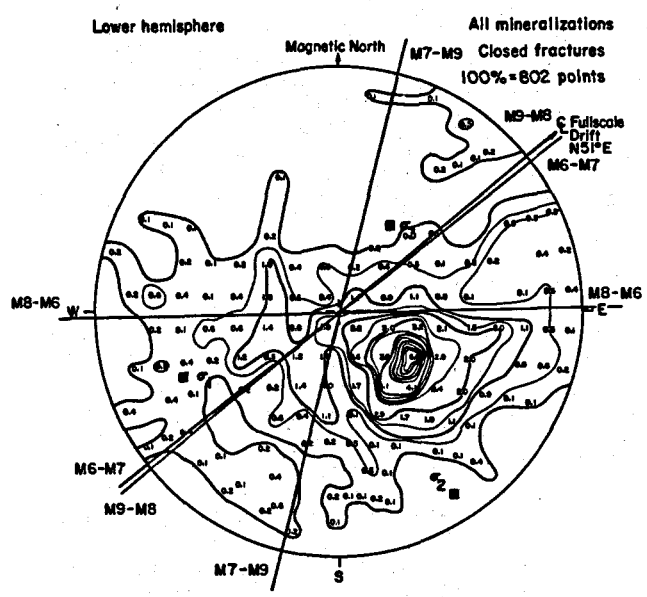

Figure 4. Schmidt equal-area pole plot for vertical E and M holes, H9% occurrence. (XBL 801-6786A)

In our numerical study we allow unrestricted flow to the fracture and the well. Fluid is allowed to flow from both the fracture and the rock matrix to the well depending upon the pressure gradients (Darcy's law). The fracture has a finite but constant permeability and contains only slightly compressible fluid (water).

Typical curves of dimensionless pressure versus dimensionless time at the well are shown in Figure 5. For all of the three curves the same k_f/k_r ratio is used, but with different fracture radii (r_f). All other parameters remain the same. At early times the curves coincide, as wellbore effect and fracture storage effects dominate the pressure response. Later on, as the pressure pulse hits the fracture radial boundary and fluid from the formation starts to enter the fracture, the curves start to diverge from the mother curve. The less the radial extent of the fracture (r_f), the sooner the curves start to divert. Theoretically, the early part of the curves can be used to determine the transmissivity (kw) and the storativity ($\phi_f \mu c_f$) at the fracture. The time of departure from the mother curve can be used to determine the fracture radius r_f. The later time data can be analyzed to obtain the parameters of the in-situ rock.

The permeability ratio between the fracture and the residual rock, $k_D = k_f/k_r$, is an important parameter that can be used to characterize a finite conductivity horizontal fracture system. Our studies have shown that this parameter is unique at practical dimensionless times. That is, if the k_D is kept constant, the pressure response at the well will remain the same, regardless of individual values of the rock and the matrix permeabilities. Figure 6 shows P_D vs t_D curves at the well for different values of the parameter k_D. In these runs a rather large wellbore (8 in.) was used, as reflected distinctly in the long duration of the unit slope (wellbore effects). The bottom curves correspond to an infinite fracture permeability, whereas the top curve represents the Theis curve with wellbore storage ($C_D = 0.466$). The dotted line represents Gringarten's analytical solution for $h_D = 1$, which is the value used in the simulation. As the figure shows, the analytical curve compares fairly well with the curves representing very high fracture conductivity.

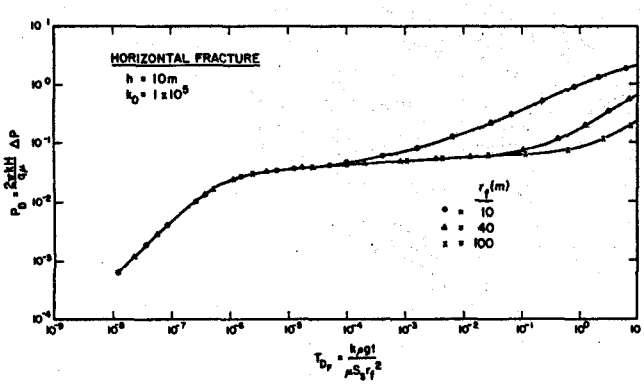

Figure 5. Typical pressure response at a well intercepting a finite conductivity horizontal fracture. (XBL 804-7002)

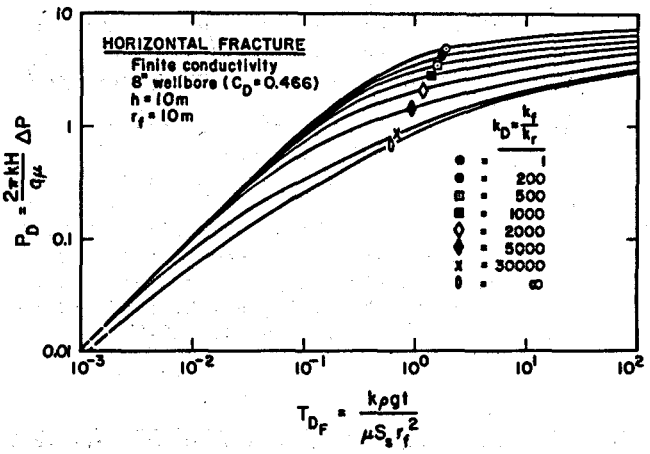

Figure 6. The effects of kp on the pressure response at the well. (XBL 804-6897)

The effects of wellbore storage, chocked fracture, fracture skin and skin around the wellbore have also been studied. The limited space in this report does not allow elaboration upon the results obtained.

The numerical studies have shown that the dimensionless parameter h_D, as defined by Gringarten (1971) is not a unique parameter for the horizontal fracture model we used. The reason for this is probably that we do not employ the apparently unrealistic "uniform flux" assumption in our model. The use of the presently available type curves for horizontal fracture systems may, therefore, lead to serious errors in the determination of the fracture and formation parameters.

FISCAL YEAR 1980 ACTIVITIES

During the next fiscal year our studies will be continued. Emphasis will be placed upon identifying the important dimensionless parameters that can be used to characterize finite conductivity horizontal fracture systems.

REFERENCES CITED

Benson, S., Goranson, C., and Schroeder, R., 1979. Evaluation of City Well 1, Klamath Falls, in Annual Report Earth Sciences Division, 1979 (this volume).

Boulton, N. S., and Streltsova, T. D., 1977. Unsteady flow to a pumped well in a fissured water-bearing formation. Journal of Hydrology, v. 35, p. 257-269.

Duff, I. S., 1977. MA28: A set of FORTRAN subroutines for sparse unsymmetric linear equations. Harwell/Oxfordshire, Great Britain. Report AERE-R8730.

Gringarten, A. C., 1971. Unsteady state pressure distribution created by a well with a single horizontal fracture, partial penetration, or restricted entry (Ph.D. dissertation). Stanford University, 110 p.

Hartsock, J. H., and Warren, J. E. The effect of horizontal hydraulic fracturing on well performance. Journal Petroleum Technology, v. 1, p. 1050-1056.

Kazemi, H., 1969. Pressure transient analysis of naturally fractured reservoirs with uniform fracture distribution. Soc. Petr. Eng., v. 9, p. 451-462.

Najurieta, H. L., 1979. Interference and pulse testing in uniformly fractured reservoirs. Dallas Society of Petroleum Engineers. SPE-8283.

Narasimhan, T. N., and Witherspoon, P. A., 1978. An integrated finite difference method for analyzing fluid flow in porous media. Water Resources Research, v. 14, no. 2, p. 255-261.

Thorsteinsson, T., and Eliasson, J., 1970. Geohydrology of the Laugarnes hydrothermal system in Iceland, in Proceedings, U.N. Symposium on the Development and Utilization of Geothermal Resources. Geothermics, Special Issue 2, v. 2, part 2, p. 1191-1204.

Warren, J. E., 1962. Discussion on a mathematical model for water movement about bottom-water drive reservoirs. Society Petroleum Engineers Journal, v. 14, p. 367-368.

Zoback, M. D., Healy, J. H., and Roller, J. C., 1977. Preliminary stress measurements in central California using the hydraulic fracturing technique. Pageoph. v. 115, p. 135-152.

PRELIMINARY STUDY OF SUBSIDENCE AT WAIRAKEI, NEW ZEALAND, USING A NUMERICAL MODEL

T. N. Narasimhan and K. P. Goyal

INTRODUCTION

Significant ground subsidence (4.5 m maximum) has been observed at Wairakei, New Zealand, following geothermal fluid extraction since the late 1950s (Stilwell et al., 1975). The observed subsidence presents two peculiar features. The first is that the subsidence bowl is offset from the main production area (Figure 1). Secondly, a plot of reservoir pressure drop versus subsidence at benchmark A97 (Figure 2) shows that the rate of subsidence with reference to pressure increases drastically after the pressure drop exceeds approximately 15 bars. While this combination of observed behavior should be explainable in more than one way, it appears that a combination of heterogeneity and preconsolidation of the formation material could provide a logical framework for characterizing Wairakei subsidence.

The purpose of the present study is to investigate in a phenomenological fashion whether the observed features at Wairakei can be reasonably explained in terms of heterogeneity and preconsolidation. This work is not intended as a detailed model of the Wairakei system; rather, it is merely a preliminary investigation as to whether heterogeneity and preconsolidation can provide a practical basis for understanding in the Wairakei phenomenon.

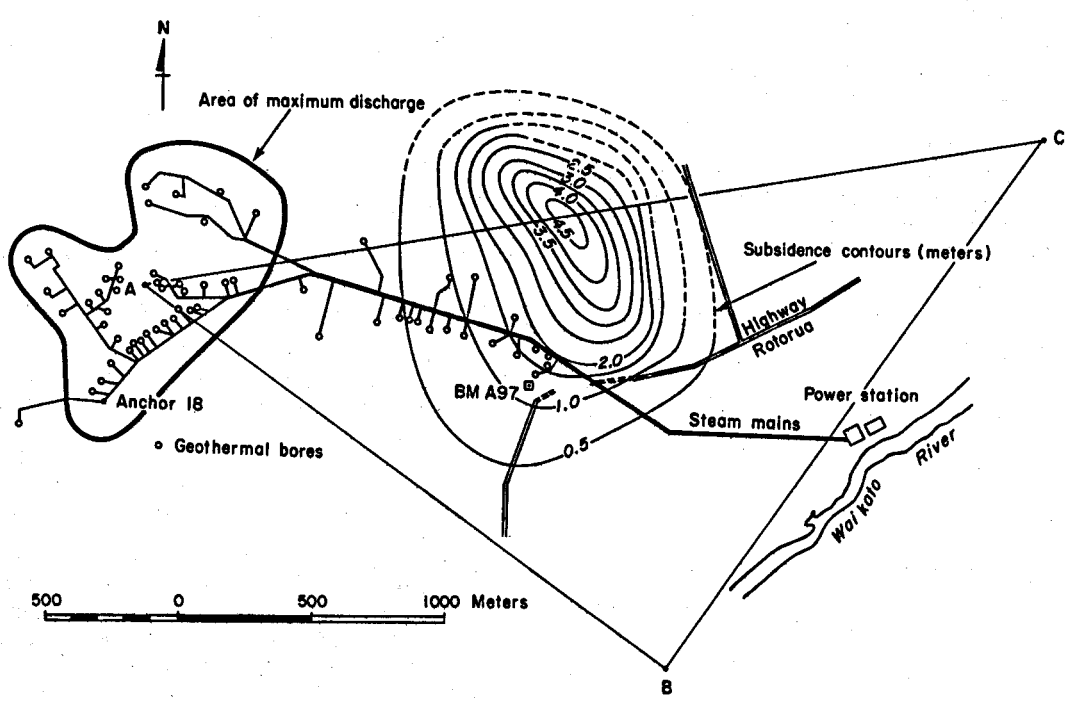

Figure 1. Total subsidence contours at Wairakei, New Zealand, and the area of investigation ABC (from Stilwell et al., 1975). (XBL 7911-13203)

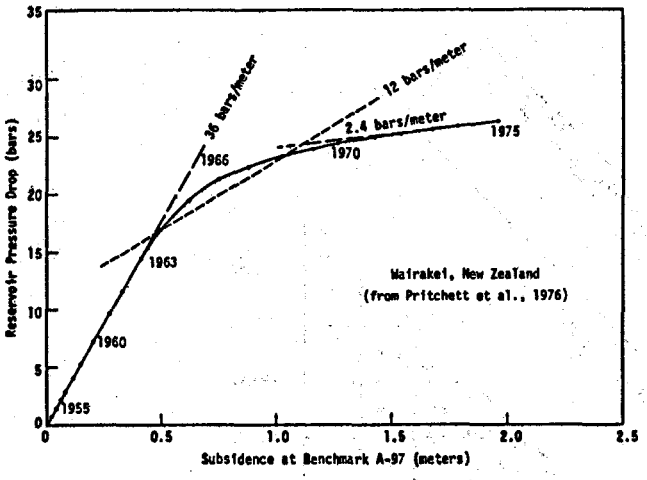

Figure 2. Reservoir pressure drop versus subsidence observed at the Wairakei geothermal field, New Zealand. (XBL 773-8173)

RESULTS

The geology of the Wairakei field has been discussed by Grindley (1965), Healy (1965), and Grange (1937); reservoir engineering data have been compiled by Pritchett et al. (1978). It can be noted from Figure 1 that the subsidence bowl is offset from the main production area. This subsidence pattern is possible if the Huka Falls formation (assumed to be relatively more compressible than the Wairakei formation layer) is thicker in that region. Or, alternatively, the compressibility of the formation in the highly subsidized zone is greater than in other areas. In our idealized model, we use the first approach with a reasonable compressibility value of the Huka Falls formation. It can be noted from Figure 2 that the drop in the reservoir pressure is linearly proportional to subsidence during early production times. However, in later periods, reservoir pressure seems to stabilize while subsidence continues. Such behavior could be explained if one assumes that the deforming material passes from a state of preconsolidation to one of normal consolidation. Our preliminary model, then, studies the effect of heterogeneity and plasticity on the subsidence phenomenon.

For purposes of simulation, we can idealize the system as consisting of Waiora aquifer, the Huka Falls formation, and the overburden which extends to the ground surface. This idealized model is shown in Figure 3. The thickness of the overburden (Holocene Pumice and Wairakei Breccia) is assumed to be 200 m (Pritchett et al., 1978, Table 5.1, p. 30). The depth of the reservoir, including Huka Falls formation, is assumed to be 400 m. The maximum thickness of the Huka Falls formation is assumed to be 200 m near the zone of maximum subsidence (Pritchett et al., 1978, Figure 5.21, p. 52).

To model subsidence, we have used an idealized graded thickness of the Huka Falls formation of 40, 80, 120, 160, and 200 m (Figure 4). The maximum thickness of 200 m over the nodes 138, 145, and 146 corresponds to the area of maximum subsidence (Figure 1). Node 107 is modeled as a production zone, indicative of the area of maximum discharge in Figure 1. To offset the subsidence bowl from the main production area, the thickness of the overburden is increased to 360 m over the nodes 207 to 216. The rest of the volume elements represent the Waiora formation. Impermeable boundary conditions are imposed on the sides AB and AC. An initial potential of 600 m of water is specified everywhere in the system. Material properties used in the model are as follows:

<u>Huka Falls Formation</u>

Permeability = $10^{-14}m^2$ (Mercer et al., 1975).
Coefficient of compressibility for virgin curve (a_v) = $5 \times 10^{-8}m^2/N$
Coefficient of compressibility for swelling curve (a_{vs}) = $5 \times 10^{-9}m^2/N$

<u>Waiora Formation</u>

Permeability = $8.5 \times 10^{-14}m^2$
Coefficient of compressibility for virgin as well as swelling curve ($a_v = a_{vs}$) = $10^{-10}m^2/N$
Relative density of the saturated soil = 2.

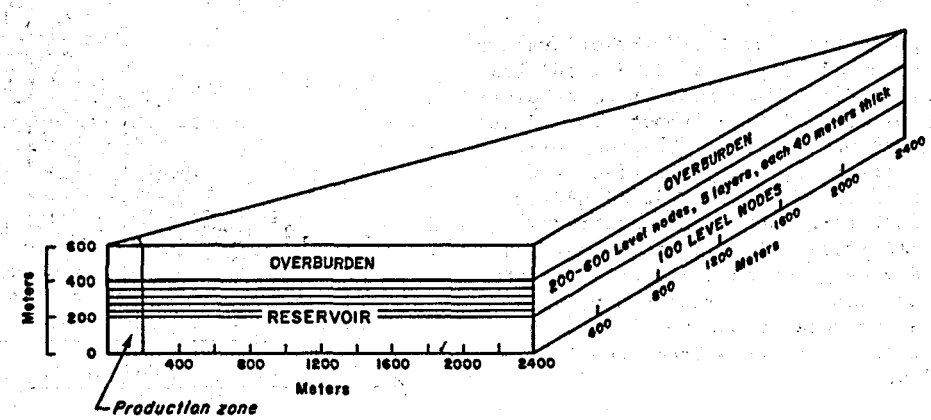

Figure 3. An idealized three-dimensional subsidence model of the Wairakei geothermal system. (XBL 7911-13085)

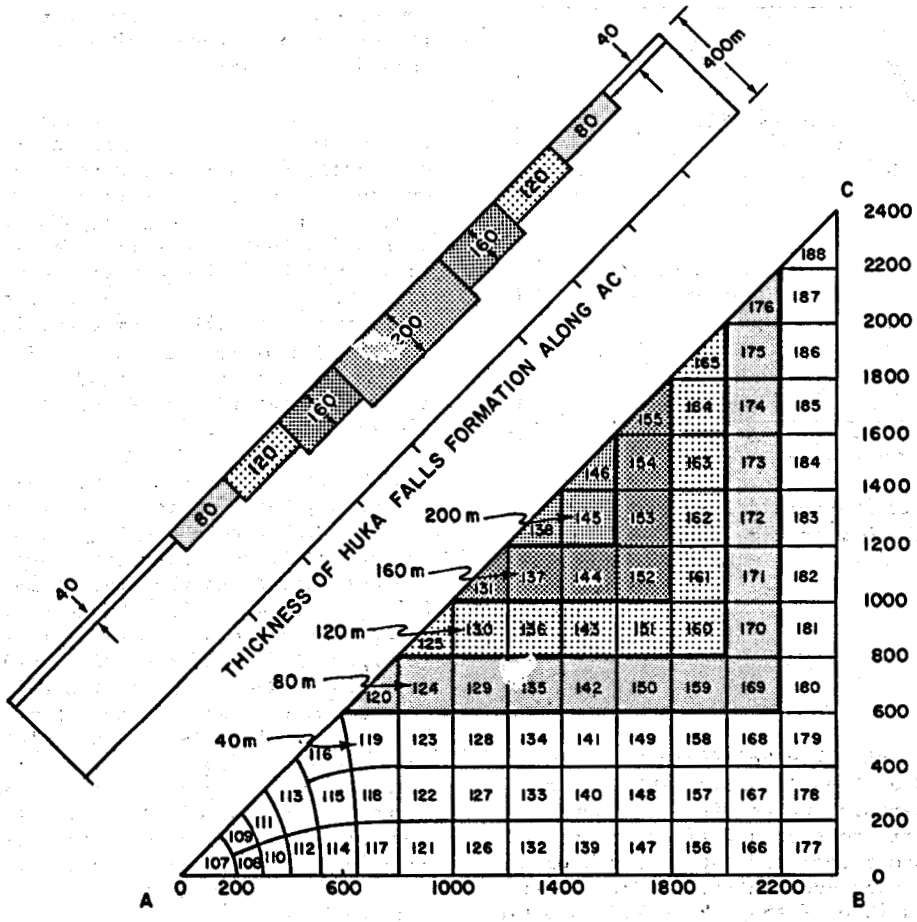

Figure 4. The thickness of the Huka Falls formation and the node numbers used in the model. (XBL 7911-13083)

This model also assumes that the soil is preconsolidated. The preconsolidation pressure over and above hydrostatic pressure is about 225 m of water. The properties used for the liquid are:

Viscosity = 0.2 centipoise
Density = 940 kg/m^3
Compressibility = 4.9 x 10^{-10}m^2/N

Total mass production for the Wairakei/Tuahara system as of December 31, 1976, was 2329 x 10^9 lbs (Pritchett et al., 1978). This amounts to an average volumetric production rate of about 1.48 m^3/sec. Since our triangular model (Figure 4) considers only 1/8 of the total area, the production rate is correspondingly reduced to about 0.185 m^3/sec. It can be noted that this rate applies to both Wairakei and Tuahara fields. To consider only the area of maximum discharge (Figure 1), this amount should be somewhat reduced. In this study, we have considered an average production rate of 0.1 m^3/sec. This amount is produced from node 107 at the depth of 500 m.

Subsidence produced under aforementioned conditions is shown in Figure 5. A comparison with Figure 1 shows that the results are qualitatively

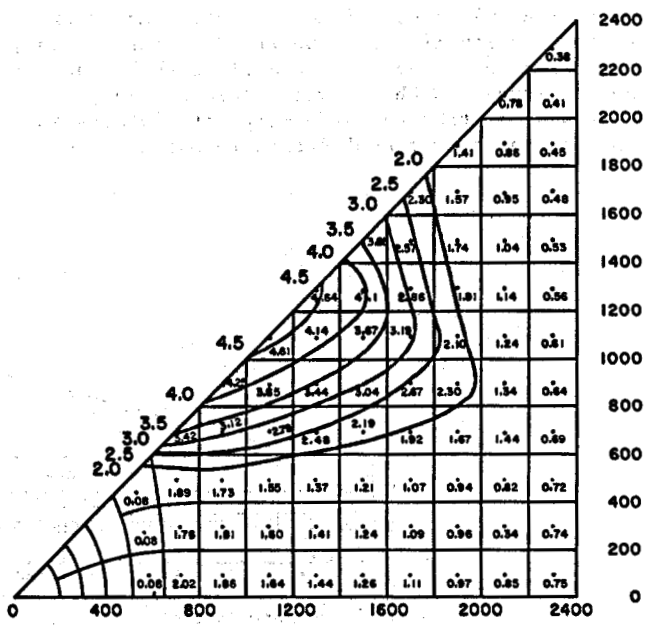

Figure 5. Subsidence contours in meters after 21 years of production. (XBL 7911-13091)

similar. Measured and calculated reservoir pressure drop vs subsidence at the benchmark A97 and node 142 are shown in Figure 6. A qualitatively similar pattern is seen for the preconsolidated soil. This figure also shows the behavior of the normally consolidated soil, which is quite different from that of the preconsolidated soil.

In summary, we developed and tested a preliminary model to explain subsidence at the Wairakei field and obtained results which are qualitatively similar to those measured at the site. The effect of preconsolidation stresses seems to be important in explaining the changing slope of the reservoir pressure-subsidence relationship shown in Figure 2.

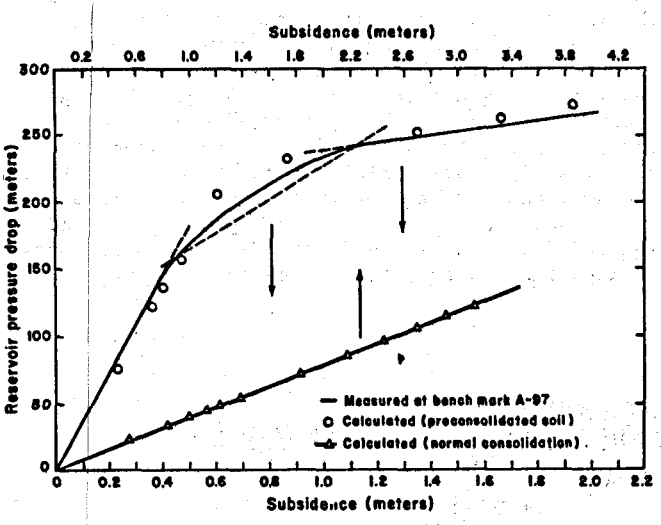

Figure 6. Comparison of the measured subsidence with that calculated at node 142.
(XBL 7911-13408)

REFERENCES CITED

Grange, L. I., 1937. The geology of the Rotorua-Taupo Subdivision, Rotorua and Kaimanawa Divisions. DSIR Bulletin 37.

Grindley, G. W., 1965. The geology, structure, exploitation of the Wairakei field, Taupo, New Zealand. N.Z. Geol. Surv. Bull. 75, 131.

Healy, J., 1965. Geology of the Wairakei geothermal field. Proceedings, Eighth Commonwealth Mining and Metallurgical Congress, Australia and New Zealand, New Zealand Section.

Mercer, J. W., Pinder, G.F., and Donaldson, I. G., 1975. A Galerkin-Finite element analysis of the hydrothermal system at Wairakei, New Zealand. Journal of Geophysical Research, v. 80, no. 17, p. 2608-2621.

Pritchett, J. W., Garg, S. K., and Brownell, D. H., 1976. Numerical simulation of production and subsidence at Wairakei, New Zealand. Stanford Geothermal Program, Report SGP-TR-20. Stanford, California, p. 310-323.

Pritchett, J. W., Rice, L.F., and Garg, S. K., 1978. Reservoir engineering data: Wairakei geothermal field, New Zealand. La Jolla, California, Systems, Science and Software, SSS-R-78-3597-1, v. 1.

Stilwell, W. B., Hall, W. K., and Tawhai, J., 1975. Ground movements in New Zealand geothermal fields. Proceedings of the Second United Nations Symposium on the Development and Use of Geothermal Resources, v. 2, p. 1427-1434.

USE OF PRESSURE TRANSIENT ANALYSIS IN MODELING THE HYDRAULIC FRACTURING PROCESS

W. A. Palen and T. N. Narasimhan

The flow of fluids in reservoirs containing large fractures is vitally important in many geoenergy resource systems. The use of massive hydraulic fracturing (MHF) for the creation of large hydraulic fractures of up to 500 m in length is used extensively in the petroleum industry to stimulate tight gas formations whose very low permeability (0.5 to 5 x 10^{-16} m^2) severely curtails production. The use of hydraulic fracturing is also visualized in the geothermal area for the creation of circular vertical fractures used in the hot-dry-rock (HDR) concept. In HDR, the fracture is created at depth in a region exhibiting high geothermal temperatures. Water is swept over the fracture faces, and the heated fluid is pumped to the surface utilization facilities. Horizontal fractures are used in some coal gasification processes to create coal bed channels for mixing of steam, oxygen, and air necessary for gas production.

To evaluate the success and to predict the future performance of such systems, it is important to know the physical properties of the created fracture system. Such properties include the average width, w, and the characteristic half-length, x_f, or radius r_f, of the fracture. Several methods published in the petroleum literature have resulted in type curves for the analysis of pressure build-up data in systems involving a well intercepting a single, vertical, rectangular fracture. These methods include analytical treatments assuming no pressure gradients (infinite fracture conductivity) in the fracture (Gringarten et al., 1975); semi-analytical treatments correcting for a finite fracture conductivity (Cinco-Ley et al., 1978); and numerical methods employing a finite difference scheme (Agarwal et al., 1979).

Previous work has included another approach to analyzing the pressure behavior of a well intercepting a finite vertical fracture. Program TERZAGI was employed in calculating pressure build-up type curve data similar to that generated by the above-mentioned authors.

THE YEAR'S ACTIVITIES

TERZAGI is a fully numerical program developed by LBL to handle three-dimensional, single-phase, isothermal transient flow. The computational algorithm is based on the integrated finite-difference method (Narasimhan and Witherspoon, 1976) and handles arbitrarily nonlinear variations in permeability in addition to one-dimensional consolidation. The program was modified to handle Darcy flow in fractures and to handle permeability variation in the fracture in the case where a constant fracture width, w, cannot be reasonably assumed. The fracture permeability K_f was made a function of the pressure distribution in the fracture; i.e., the fracture was allowed to "breathe."

The work was summarized by Narasimhan and Palen (1979). The publication includes the effects of: wellbore storage, skin factor around the fracture (due to poor fluid cleanup), effects of fracture storage; uneven wing length (asymmetrical fracture), choked flow (uneven proppant dispersal), and pressure dependent permeability on the type curves. Results indicated that in a sufficiently large fracture, fracture storage will dominate wellbore storage during early time data for a significant period and must be corrected for. The effect of choking the fracture was also found to be dramatic. A permeability reduction of 10 in the choked region increases the drawdown of the system throughout the duration of the test for wells with an r_r = 7.62 cm. The effect of reducing the choked area permeability by 100 was observed to produce a test result that could invalidate the conventional calculation of the physical properties of the system.

An important conclusion of the work was that a variety of conditions may occur in a realistic fracture situation that would make type curve analysis extremely difficult, if not impossible. A similar study was carried out by LBL researchers for the case of a horizontal fracture (Bodvarsson and Narasimhan, 1980).

Consideration of this problem has led to the development of program HYDFR. Program HYDFR was designed to handle the problem of analyzing the pressure transient data recorded during the actual hydraulic fracturing process. It was hoped that a parameter analysis could provide insight not only into the dimensions of the fracture system but also into the in-situ rock stresses and formation strength.

CURRENT WORK

HYDFR is a program designed specifically to handle the highly nonlinear problem of a growing hydraulic fracture. As such, it borrows heavily from its parent program, TERZAGI, and shares the common IFDM formulation. The extra computational effort involved in solving the growing fracture was expedited by replacing the iterative solver in the original program with a direct solver that is many times faster (Bodvarsson et al., 1980). The increased speed of the solution algorithm allowed the preliminary modeling to be done that otherwise would have been cost prohibitive.

The program is based on a surface energy concept of fracture extension. The fracture system before extension is modeled in Figure 1. Initially, nodal elements exist representing the surface pumps and tubing, the pressurized tubing in the well, the packer cavity, and an initial fracture surface. Once the pumping is initiated, the program monitors the cavity pressure until the rupture pressure P_b is reached. Once this pressure is reached, flow is allowed into the first fracture element. The total available energy of the system is defined as the PV work done to inject fluid into the fracture less the work done overcoming the earth stresses in the formation and the energy lost in creating the fracture surface. If sufficient energy is available in the system and the pressure in the initial fracture element exceeds the earth stress, the fracture grows outward as a plane. The program generates its own mesh, creating the additional fracture elements and simple reservoir elements to allow for fracturing fluid penetration (leak off). The two requirements for extension are available excess surface energy to extend the fracture and the sufficient pressure in the downstream elements to open the fracture against earth stresses.

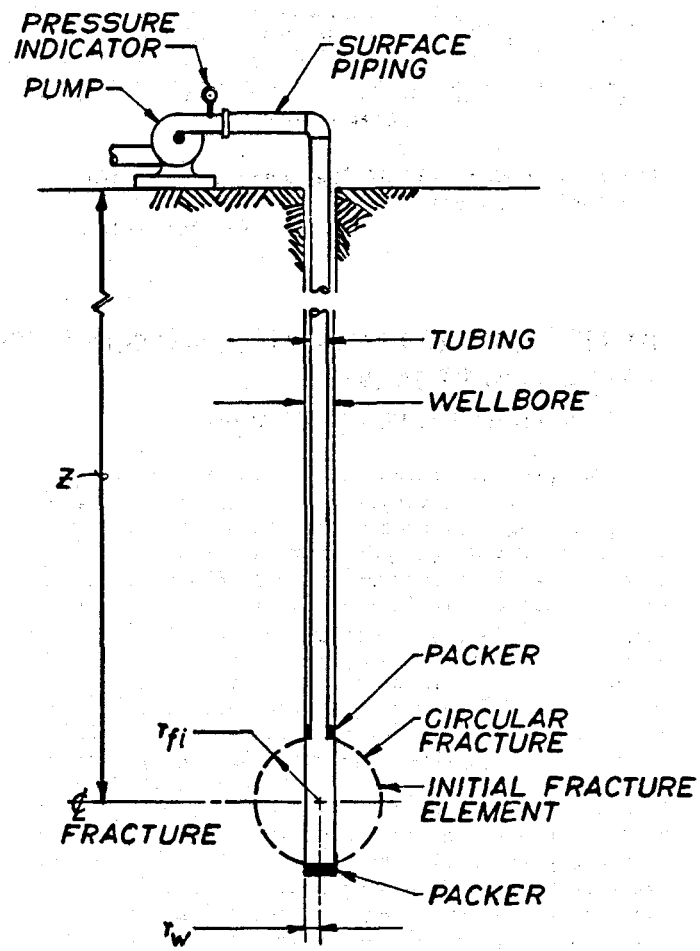

Figure 1. Initial representation of growing fracture mesh. (XBL 806-9919)

Two basic geometries have been modeled with HYDFR. A rectangular geometry is used to study vertical fracture development in layered anisotropic formations such as oil fields. A circular geometry is used to model vertical fractures in an isotropic medium such as used in geophysics and HDR experiments (where gravity effects are neglected) or for a horizontal fracture.

The pressure profile generated by the model is depicted in Figure 2. Shown here is the simulator's transient pressure profile vs actual field data gathered by Mark Zobak of the U.S. Geological Survey. Agreement is generally good over the first two pressure cycles. Adjusting the parameters of the model indicate that the fracture radius at the end of the second fracture cycle was 9.5 m and that the maximum stable width was approximately 10^{-4} m. Other parameters may be inferred from the study of these particular data, but while the range of variation of these parameters of the earth stresses, formation strength, and surface energy requirements is small, it cannot be stated that the best fit data is unique due to the interrelationship of the parameters in the model.

PLANNED ACTIVITIES

The simulation will be used to examine the possibility of using the fluid viscosity and pumping rate to control the growth of the fracture system. This is hoped to aid in not only optimizing the fracture penetration when desired, but also to control the growth when working in sensitive formations.

REFERENCES CITED

Agarwal, R. G., Carter, R. D., and Pollock, C. B., 1979. Evaluation and performance prediction of low permeability gas wells simulated by massive hydraulic fracturing. Journal of Petroleum Technology, p. 362-372.

Bodvarsson, G. S., Lippmann, M. J., and Narasimhan, T. N., 1980. Recent modifications of the numerical code CCC, in Earth Science Division Annual Report 1979 (this volume).

Bodvarsson, G. S., and Narasimhan, T. N., 1980. Hydraulics of a well intercepting a single horizontal fracture, in Earth Sciences Division Annual Report 1979 (this volume).

Cinco-Ley, H., Samaniego, F., and Domínguez, A., 1978. Transient pressure behavior for a well with a fracture-conductivity vertical fracture. Society of Petroleum Engineers Journal, v. 18, no. 4.

Gringarten, A. C., Ramey, H. J., and Raghavan, R., 1975. Applied pressure analysis for fractured wells. Journal of Petroleum Technology, v. 15, p. 887-892.

Narasimhan, T. N., and Palen, W. A., 1979. A purely numerical approach for analyzing flow to a well intercepting a vertical fracture. Dallas, Society of Petroleum Engineers, SPE-7983.

Narasimhan, T. N., and Witherspoon, P. A., 1976. An integrated finite difference method for analyzing fluid flow in porous media. Water Resources Research, v. 12, no. 1, p. 57-66.

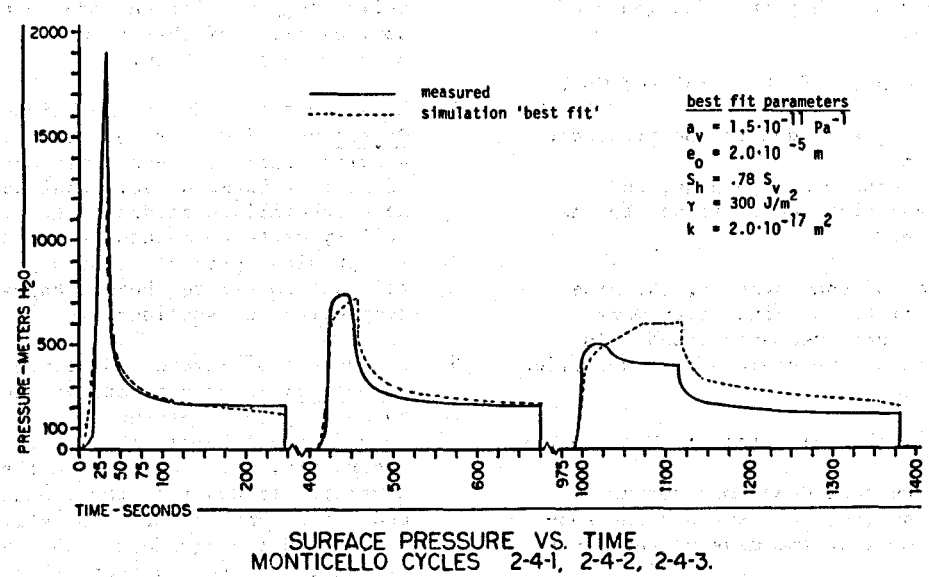

Figure 2. Calculated vs observed pressure transient of the Monticello data. (XBL 806-9931)

Geothermal Environmental Research

GEOTHERMAL SUBSIDENCE RESEARCH PROGRAM

J. E. Noble

INTRODUCTION

As with the development of any energy source, problems encountered may limit development. For geothermal energy, one such problem may be land deformation associated with the removal or injection of geofluids in the reservoir.

The objective of geothermal subsidence research is to control or mitigate, within predictable limits, potential subsidence associated with geothermal development. This objective will be accomplished by understanding the compaction subsidence phenomena associated with geothermal energy development. The Geothermal Subsidence Research Program (GSRP) is designed to develop a comprehensive understanding of the compaction-subsidence phenomena and provide:

1. The means for developers to build and operate geothermal facilities within prescribed limits of land subsidence and deformation.

2. The basis for policy-makers to regulate geothermal facilities with respect to potential subsidence.

A workshop was held in October 1978 for the purpose of making a mid-course correction to the original subsidence research plan. The goals of the workshop were to:

- Review the results of the completed GSRP research
- Advise on changes needed to the program's research plan
- Assess the adequacy of the plan, and
- Make recommendations on revisions to the original plan.

As a consequence of the workshop, the nine research categories of the original plan were grouped into three general research areas. In turn, these major areas were divided into specific research topics:

1. Subsidence Research Monitoring and Measurement

   - Direct surface subsidence monitoring
   - Indirect technique, both surface and subsurface, to monitor and measure reservoir compaction
   - Wellbore measurements to directly monitor and measure reservoir compaction

2. Reservoir Compaction and Subsidence Prediction

   - Understanding the physical processes that cause compaction and subsidence
   - Laboratory studies of the compaction and subsidence phenomena
   - Assessment and development of compaction-subsidence models

3. Compaction and subsidence impact assessment

   - Compaction and subsidence case studies
   - Assessment of the economic costs and environmental effects of compaction and subsidence.

PROGRAM PROGRESS IN FISCAL YEAR 1979

At the start of fiscal year 1979, several general contract objectives were stated for the Geothermal Subsidence Research Program:

1. Supplemental Case History--Chocolate Bayou
   Objective: Expand the Chocolate Bayou case study in order to make the study more comprehensive. An expanded study could also be useful as a model to researchers at the Brazoria Geopressure field located south of the Chocolate Bayou field.

2. Hostile Environment Tool Development
   Objective: The four suggestions made by Woodward-Clyde Consultants for improved wellbore extensometers will be component tested.

3. Assessment of Radioactive Bullets
   Objective: Additional review of radioactive bullet logging will be made to assess the applicability of this technique to monitoring subsurface compaction.

4. Assessment of Indirect Techniques
   Objective: Indirect measurement methods, i.e. gravity, resistivity and microseismicity, have promise as inexpensive, areal survey techniques. Research will be conducted to evaluate the ability of these methods to detect changes in the physical properties of a geothermal reservoir and to relate these changes to reservoir compaction and subsidence.

5. Assessment of Physical Subsidence Theories
   Objective: A step toward greater predictive capability is assessing existing subsidence theory and its applicability to geothermal reservoirs. Most subsidence theories were developed to describe the compaction of oil and gas reservoirs or of relatively shallow unconsolidated aquifers. The applicability of these theories to deep, thermodynamically complex geothermal systems will be examined.

6. Creep Phenomena and Inelasticity
   Objective: Related to the assessment of existing subsidence theory is an assessment of rock creep and inelasticity at high temperature and high pressure. The effects of these phenomena are little understood and limit accuracy in predicting subsidence. Research will be conducted to study their contribution to compaction and subsidence.

During fiscal year 1979, contracts were issued to accomplish each of these objectives. Some of these contracts will be continued in fiscal year 1980. The following is a review of the fiscal year 1979 accomplishments of the contracts issued:

1. Supplemental Case History--Chocolate Bayou

Principal Investigator: Barbara Turner (ESA Associates)

Objective. Expand the Chocolate Bayou Case Study to make it more comprehensive. An expanded study will be useful as a model to researchers at the Brazoria Geopressure Field located south of the Chocolate Bayou Field.

Progress. The ESA data assessment availability and evaluation study is completed. The general, conclusions and recommendations are:

1. Sufficient data appear to be available for modeling the Chocolate Bayou field, although some data on material properties may have to be extrapolated from well testing and core analysis of the Pleasant Bayou wells.

2. The 1978 to 1979 releveling data show that subsidence of Chocolate Bayou is continuing but at a lower rate than previously. Maximum subsidence between 1943 and 1979 was 2 ft (0.61 m).

3. The relationships among observed subsidence, groundwater production, and hydrocarbon extraction were investigated in more detail for this report. The results of this analysis indicate that hydrocarbon production has contributed to the observed subsidence. In particular, a comparison of the 1959 to 1973 elevation changes at shallow benchmarks with changes at deep benchmarks set on abandoned oil and gas well casings shows a very close correspondence between the amounts and rates of subsidence. It is expected that collection and analysis of more site-specific fluid extraction data would make it possible to determine how much subsidence has been due to groundwater production and how much from producion of deep fluids.

2. Subsidence Instrumentation Development

Principal Investigator: A. Veneruso (Sandia Laboratories)

Objective. Provide LBL technical guidance and support in the development of hostile environment instrumentation for subsurface subsidence research.

Progress. With the successful testing of seven switches (all to 300°C), the reed switch testing was completed. The switches were all built by the Hamlin Company of Lake Mills, Wisconsin, and are all commercially available from component suppliers. The switches tested were:

Type	Description
MRHDT	Dry Reed (SPDT)
MTHG2	Mercury Wetted (all position)
MARH2	Miniature Dry Reed
MINI-2S-115	Miniature Dry Reed
MMRR-2-185	Microminiature Dry Reed
MSDR4	Miniature Dry Reed
DRR-129-425	High Current (3.0 amps)

Because there are many different current, voltage, size and performance variations, selection of a particular switch is dependent on the specific application.

The development of high-temperature magnetic materials, refractory thin-film resistors, capacitators, conductor interconnections, and the high-temperature line driver has been accelerated. Some of the line driver circuits have been fabricated in tandem, rather than in sequence.

3. Assessment of Radioactive Formation Markers to Monitor Reservoir Compaction

Principal Investigator: Dr. M. Dorfman (U. of Texas)

Objective. To assess the usefulness of radioactive bullet logging in measuring and monitoring differential compaction on a geothermal reservoir.

Progress. A comprehensive literature review has been carried out, followed by personal discussions with engineers of Atlantic-Richfield, Schlumberger, Dresser Atlas, and Welex. The first three companies have been involved in significant compaction measurement studies using radioactive bullets at Prudhoe Bay, Alaska; Gronigen, Holland; and Long Beach, California, respectively. The last three companies are major well-logging businesses. Using the best tools and procedures, the distance between radioactive bullets spaced about 40 ft apart can be determined with a standard deviation of 0.01 ft.

The temperature limit is about 500°F for all components except the bullets, for which the limitation is approximately 350°F. Radioactive jet markers are available which have a limit of 500°F. The pressure limit is approximately 20,000 psi.

The uniaxial compaction coefficients measured on Frio cores from the Pleasant Bayou #2 well (Brazoria County, Texas) range from about 5×10^{-7} to 10^{-6} psi, taking into account both short-term and long-term (creep) effects. For this well, the above precision of bullet location should permit meaningful compaction measurements when flowing pressure drawdown from the initial reservoir pressure is more than about 360 psi to 180 psi, respectively.

There is some evidence that laboratory measurements of compaction coefficients on cores are not always reliable in predicting compaction in the field. For example, at Groningen, Holland, predicted compaction based on laboratory data was three times greater than observed compaction using radioactive bullets. In other words, the above estimate of required pressure drawdown for meaning-

ful compaction measurements with radioactive bullets should be used with caution.

Also, the above estimate does not take into account any possible "strengthening" of the system near the wellbore due to the steel casing and cement. The radioactive bullet will probably not penetrate more than 6 in. to 1 ft from the wellbore. This is the region with the greatest pressure drawdown when the well is flowing and hence has the greatest potential for compaction. For wells with several thousand pounds drawdown, and with good bonds between casing and cement and between cement and formation, the compaction in the region occupied by the bullets would almost certainly not be as great as that measured in the absence of the relatively strong casing and cement. It is possible that this effect contributed to the discrepancy between observed and predicted compaction at Groningen.

For reservoirs in basement or metamorphic rocks, with relatively low porosity such as found at The Geysers, California, the observed compaction coefficients are expected to be considerably smaller than calculated, and the required pressure drawdowns correspondingly larger for meaningful compaction measurements. Since these wells are usually completed without running casing through the producing interval, the "strengthening" effect discussed above would not occur here. Also, in hard rocks, use of radioactive jets as markers might be preferable to radioactive bullets, since bullet penetration might be extremely variable.

4. Indirect Methods: Seismic Assessment

Principal Investigator: Dr. T. V. McEvilly (U.C. Berkeley)

Objective. To map lateral and vertical variations in velocity and attenuation (both P and S waves) throughout the production zone. Also studied are the source dynamics of the microearthquakes so that we might infer stress orientation, stress drops, and source dimensions relative to production activities (withdrawal, reinjection) and the reservoir boundaries. If subsidence occurs on a significant scale these data may be able to delineate regions of discrete movement or stress release.

Progress. During fiscal year 1979 the major effort was directed toward fabrication of the Automatic Seismic Processor (ASP) and an in-field vehicle to house the ASP.

Gravity Assessment

Principal Investigator: Dr. R. B. Grannell (Long Beach State University)

Objective. To assess the applicability of surface gravity measurements to monitoring the response of a geothermal reservoir to exploitation. If gravity surveys can be shown to be applicable, it could provide a cost-effective indirect method to indicate net mass changes in the subsurface due to extraction and/or injection of geothermal fluids. Some causes of net mass changes could be alteration of the subsurface chemical/thermodynamic environment, changes in the volume of subsurface formations, or changes in formation void ratios. How these changes are subsidence-related is of paramount interest to the Geothermal Subsidence Research Program.

In fiscal year 1979 the following tasks were accomplished:

Task 1: An assessment was made of the applications of surface gravity measurements to monitoring the various subsidence-related net-mass formation changes that could be caused by exploitation of a geothermal reservoir. Each application required a well-documented theoretical basis, a technical feasibility statement indicating the accuracy by which the changes could be repeatably measured, and a review of the instruments and techniques currently available for such studies.

Task 2: A comprehensive plan was recommended for implementation of a gravity study to investigate and monitor subsidence-related formation changes. Of particular interest were methods of repeatable data acquisition and analysis, and the use of corroborating surface geophysical techniques such as seismic velocity studies.

Task 3: A suitable site was identified where the recommended plan could be implemented, including sufficient corroborating geological, geophysical, and geothermal resource data to support the selected sites. Discussions with the field operators have begun to gain permission to conduct a field gravity survey in fiscal year 1980.

5. Assessment of Physical Theory

Principal Investigators: Dr. M. Carroll (U.C. Berkeley) and Dr. John Rudnicki (U. of Illinois)

Objective. To assess the adequacy of constitutive theory to define deformation.

Progress. Dr. Carroll (UCB): A report has been submitted on the study of analytical and numerical solutions for elastic deformation of weakened half-space under gravity. In the report, constitutive relations are developed for mechanical response of dry or fluid-saturated porous material beyond the linear range. The main emphasis is on hydrostatic loading and unloading response, although deviatoric effects are also treated. The technique focuses on the manner in which localized shear stresses in the solid material are treated. A theoretical derivation of an initial yield surface for porous material is also described.

Dr. Rudnicki (University of Illinois): As part of the work on time-dependent behavior of brittle rock, Dr. Rudnicki has reviewed experimental work on the growth of cracks in brittle rock. This experimental work provides an indication of the kinetic relations that link the rate of microscale deformation mechanisms to applied stress. Rudnicki has started to evaluate the role of coupling between deformation and pore-fluid diffusion in elastic fluid-infiltrated porous bodies. This coupling is often neglected in modeling studies, but has proven to be of importance in a variety of geophysical and geotechnical problems. The problem chosen for study is the simplest problem for a finite

body exhibiting full coupling, that of a hollow sphere subjected to radial stress and pore fluid pressure at its boundary.

6. Physical Properties of Rocks Associated with Subsidence

Principal Investigators: A. Abou-Sayed, John Schatz, and Ken Wolgemuth (Terra Tek, Inc.)

Objective. To study high temperature and pressure compressibility of cores from geothermal reservoirs at East Mesa, California, and Cerro Prieto, Mexico.

Progress. All basic mechanical testing has been completed on both Cerro Prieto and East Mesa cores. Essentially completed are the elastic or short-term compaction studies of East Mesa cores, and these same studies are nearly completed on cores from Cerro Prieto. In addition to the elastic tests, Cerro Prieto core permeablities have been measured and presented in a paper at the Second Symposium on the Cerro Prieto Geothermal Field, held in Mexicali, Mexico.

Long-term compaction (creep) studies of the Cerro Prieto cores have continued. Future work, after completion of all short-term tests, will emphasize a relatively small number of high-quality creep tests on both East Mesa and Cerro Prieto cores. Both fine-grain and coarse-grain material are being studied to evaluate the effect of grain size or rock compaction.

Of notable interest were the apparent chemical changes occurring in the cores during compaction tests, especially long-term tests. Long-term testing had a strong tendency to increase the silica content of the fluid. The final silica content of the fluid from several of these tests exceeded the total solubility of silica at test conditions. It is hypothesized that pressure point dissolution of silica causes the formation fluid to be supersaturated.

Basic conclusions at this time are as follows:

1. For short-term tests, the reservoir is stiffer for pore pressure reduction than it is for confining pressure increase.

2. Short-term compaction moduli are consistent with the behavior of sandstone at this porosity.

3. Creep compaction occurs and is a significant effect, leading to long-term compaction moduli that are several times smaller than short-term.

4. Rebound moduli are significantly larger than compaction moduli indicating the irreversibility of the behavior.

5. Silica concentration in fluids goes up with time during testing, hinting that pressure solution may be associated with the compaction.

6. Permeability decreases both with temperature increase and time. The precise magnitude of reductions or its importance is uncertain.

In addition to the above contracts, several contracts issued in the last quarter of fiscal year 1978 were substantially concluded in fiscal year 1979. The following is a review of the accomplishments of those contracts:

1. Modeling of the Physical Processes of Subsidence

Principal Investigator: Ian Miller (Golder Associates, Inc.)

Objective. To assess the individual attributes of particular mathematical models in their own right and to determine, through studies of both real and hypothetical subsidence case histories, the significance of different mathematical model attributes. The result of this research will be synthesized to give detailed assessments of the available models, recommendations for the capabilities of desirable new models, and a general perspective on the limits of mathematical models.

Progress. Proficiency assessment has been completed on the following models:

- Hand calculation of one-dimensional compaction
- One-dimensional calculation stress-seepage model
- Nucleus of strain
- Boundary integral equation method
- Displacement discontinuity method
- Finite element model
- CCC

Conclusions of their assessment are as follows:

Overall Approach: It appears that the development of highly sophisticated, coupled models for reservoir flow and deformation is not desirable at this time. Not only is the use of overly sophisticated models not justified by available data, but, as was shown in the Austin Bayou case study, coupling of flow deformations increases cost more than it does accuracy. Conceptual models should be developed to as great a level of sophistication as is permitted by available data. Mathematical models should be selected that are appropriate to the sophistication of the conceptual model. In some cases, where production can be assumed known, reservoir flow modeling may not be necessary. This was the case at Austin Bayou.

Reservoir Flow Models: Further theoretical development of reservoir flow models appears to be appropriate. At present, lack of adequate reservoir flow theory represents a significant limitation to predicting the subsidence of geothermal reservoirs. Current theories have not, in general, been adequately tested. In addition, further theoretical work might be appropriate in the fields of multiphase and fracture/porous media flow. We anticipate a rapid evolution in the state-of-the-art of heat/fluid flow over the next few years. Mathematical models should be developed not only using state-of-the-art theoretical developments, but also using simplifying assumptions such that the model could be implemented by the lay engineer. Possible simplifying assumptions include lower dimensionality, restricted physical processes, and

limitation of calculation to static equilibrium conditions.

Deformation Models: Current theory appears to be adequate for all practical deformation modeling problems. Although assumptions of homogeneity, isotropy, and linear elasticity are frequently gross, they often appear to be adequate considering the level of inaccuracy introduced by lack of data. There is no single model that is superior to all others. Golder tested six different models and found that each one was valuable in some situations and that none of them was good in all situations. The range of mathematical models now available is sufficient for most reservoir deformation problems. What is needed is not newer, more sophisticated mathematical models, but more useable versions of current models. Some criteria for models are:

- Available in the public domain
- Well-documented with regard to both theory and usage
- Simplified input and automatic element generation
- Clear, comprehensive output, and where appropriate, plotting capabilities
- Improved efficiency
- Increased flexibility by development of models that incorporate a variety of current techniques in a single model.

Availability in the public domain might be facilitated by development of a public library of well-documented mathematical models.

In addition to the contracts, Lawrence Berkeley Laboratory conducted its own investigation into subsidence phenomena during fiscal year 1979. A study was made of the Wairakei subsidence problem using the LBL computer subsidence simulator TERZAGI. The objective of this study was to develop a subsidence model of a geothermal field qualitatively similar to the Wairakei field.

Results of the study pertain solely to reservoir deformation according to the one-dimensional consolidation theory. It was assumed that the vertical displacements obtained at the interface of the reservoir and overburden are completely transmitted to the ground surface. The purpose of the present study was to make a preliminary study of the ground subsidence observed over the geothermal field at Wairakei, New Zealand, and to find whether the field observations can be reasonably explained in terms of the well-known geotechnical principles of consolidation. As the study is preliminary in nature, the geothermal system has been treated as an isothermal, liquid system.

Subsidence predicted by the TERZAGI code qualitatively matches the observed Wairakei subsidence feature. The study successfully demonstrated the development and testing of a preliminary model to explain subsidence in the Wairakei field and to obtain results which are qualitatively similar to those measured at the site.

PLANS FOR FISCAL YEAR 1980

The following projects have been planned for fiscal year 1980.

1. The LBL computer code TERZAGI will be modified to model lateral reservoir deformation and be further validated. CCC, a nonisothermal compaction model, will be modified to compute coupled reservoir-overburden deformation.

2. The creep study of geothermal reservoir cores will continue and be expanded to investigate the role of pressure solution and microcrack progagation as a mechanism for creep compaction.

3. Sandia and LBL will make an assessment of service company borehole tools that show promise for being upgraded to use under geothermal conditions. They will be field tested, and recommendations for enhancement will be made.

4. The Geysers and Cerro Prieto geothermal fields will be evaluated using the Automatic Seismic Processor system. Data from these monitoring surveys will be used to analyze and model compaction-related reservoir stress changes.

5. A high-precision surface gravity study will be conducted at the Cerro Prieto and Heber geothermal fields. The objective will be to establish a base line for detection of net-mass changes related to withdrawal or injection of geofluids.

REFERENCES CITED

Earth Sciences Division, Lawrence Berkeley Laboratory, 1979. News from subsidence. Berkeley, Lawrence Berkeley Laboratory, PUB-286.

Grimmud, P., Turner, B. L., and Framer, P. A. (Systems Control, Inc.), 1978. Areas of ground subsidence due to geofluid withdrawal. Berkeley, Lawrence Berkeley Laboratory, LBL-8618, GSRMP-4.

O'Rourke, J. E., and Ranson, B. B. (Woodward-Clyde Consultants), 1979. Instruments for subsurface monitoring of geothermal subsidence. Berkeley, Lawrence Berkeley Laboratory, LBL-8669, GSRMP-2.

Pinder, G. F., 1979. State-of-the-art review of geothermal reservoir modeling. Berkeley, Lawrence Berkeley Laboratory, LBL-9093, GSRMP-5.

Van Til, C. J. (Woodward-Clyde Consultants), 1979. Guideline manual for surface monitoring of geothermal areas. Berkeley, Lawrence Berkeley Laboratory, LBL-8617, GSRMP-3.

Vaughan, C. K., and Harding, R. C., 1979. Environmental economic effects of subsidence. Berkeley, Lawrence Berkeley Laboratory, LBL-8615, GSRMP-1.

INDUCED SEISMICITY STUDIES AT THE CERRO PRIETO, MEXICO, AND EAST MESA, CALIFORNIA, GEOTHERMAL FIELDS

E. L. Majer and T. V. McEvilly

INTRODUCTION

The utility of microearthquake studies in geothermal regions is not restricted to exploration applications. Information from these studies may be important in delineating reservoir boundaries and in monitoring environmental effects such as subsidence and induced seismicity in producing geothermal fields. By utilizing the variation in propagation characteristics of P and S waves as well as the source characteristics of microearthquakes, information relating to the stress field, temperature, and fluid state can, in principle, be obtained. Continuous monitoring of these properties in producing geothermal fields may provide a means to detect dynamic reservoir boundaries, areas of recharge, and changing fluid state.

As a reservoir is produced there will undoubtedly be relatively large stress and/or thermal gradients produced by the withdrawal and reinjection of fluids. Stress gradients may affect the nature of seismicity, especially in a region as tectonically active as the Salton Trough. Although the Cerro Prieto field and other geothermal regions in the Imperial Valley (such as East Mesa, Brawley, and Herber) are fluid dominated, continued production may induce areas of steam domination. Recent laboratory wave-propagation studies (Nur and Winkler, 1979) indicate that relative P and S wave attenuation studies may be particularly useful for delineating regions of partial saturation. Therefore, it is hoped that continuous microearthquake monitoring with occasional detailed wave propagation studies will be able to detect subtle changes in the static and dynamic properties of the reservoir.

CERRO PRIETO

In Februrary 1978 a velocity, attenuation, and preliminary microearthquake study was carried out at Cerro Prieto (Majer et al., 1979). Based on the results of that study, a permanent five-station array was designed to monitor continuously the temporal and spacial variation in seismicity throughout the production zone. The five closely spaced stations were located to supplement the data from the CICESE stations surrounding the production region, as shown in Figure 1. Also shown in Figure 1 are the regions of high seismicity detected during the 1978 study. As can be seen, none of the seismically active regions (shaded) lie within the production zone. Only several events with magnitude greater than 1 were detected in the reservoir region, these all occurring on one day. The permanent stations were located such that minimum ambiguity would occur in fault plane solutions for events within the reservoir. The 1978 study indicated that the events within the field were on northwest-southeast trending faullts with right lateral strike-slip motion. However, if the Cerro Prieto field is in a region of transverse faulting, (i.e. a spreading center) normal faulting would be expected.

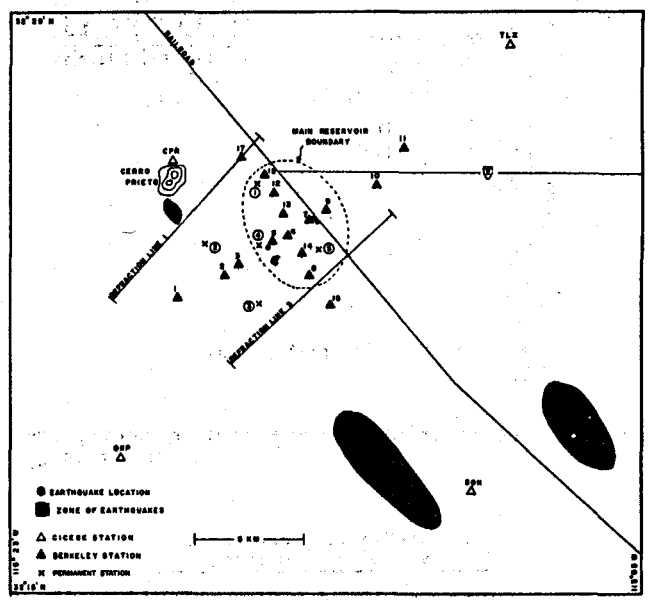

Figure 1. Station locations of permanent array relative to 1978 Cerro Prieto study. Seismic activity is indicated by the shaded regions. (XBL 789-10723)

Data are collected at each station with a three-component 4.5-Hz geophone package in a 100-m borehole. The holes were drilled and cased by the Comision Federal de Electricidad de Mexico. At the top of each hole an instrument box houses a Sprengnether DR-100 event recorder and five 2.5-V McGraw-Edison air-cell batteries (Figure 2). Air-cell batteries were chosen for long life because of their high amp-hour rating (1200 A-hr), although their peak output is only between 1/2 and 1 A. The batteries should last one year with the DR-100. The DR-100 is a triggered digital cassette recorder. The recorders are set at 200 samples/sec with triggering levels (short-term and long-term average) appropriate for microearthquake detection (Figure 3). Although the signal-to-noise ratio is improved by 20 dB by placing the geophones at depth, other problems were encountered. In addition to the disadvantage of the permanence of the borehole sites, the near 100°C temperature of the water produced O-ring deterioration in the sondes, thus causing the geophone packages to leak. Standard O-rings had to be replaced with Viton or silicon rings. It was also necessary that the standard rubber cable be replaced with a PVC-shielded cable. For continuous monitoring above 100°C, Teflon-coated wire is recommended.

Each station is connected by a single-twisted pair of wires, forming a loop around the array (Figure 4). Also in the loop is a central site housing a visual monitor and time-code clock. The triggering of the recorders is controlled by the recorder at a selected site. Except for this site

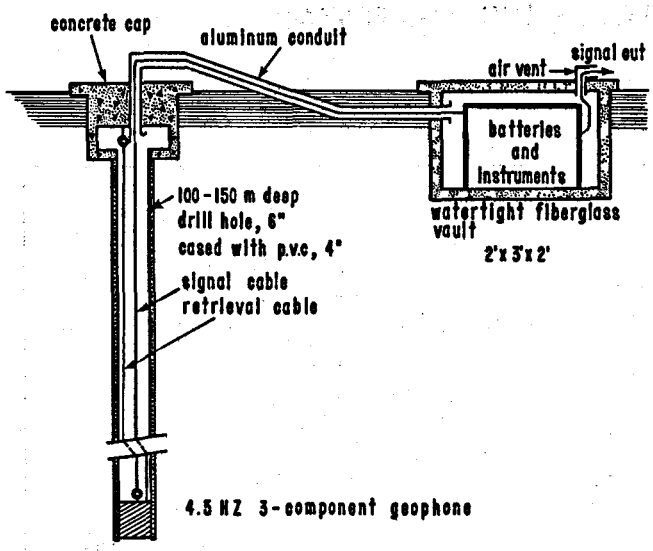

Figure 2. Cerro Prieto network station configuration. (XBL 787-1966)

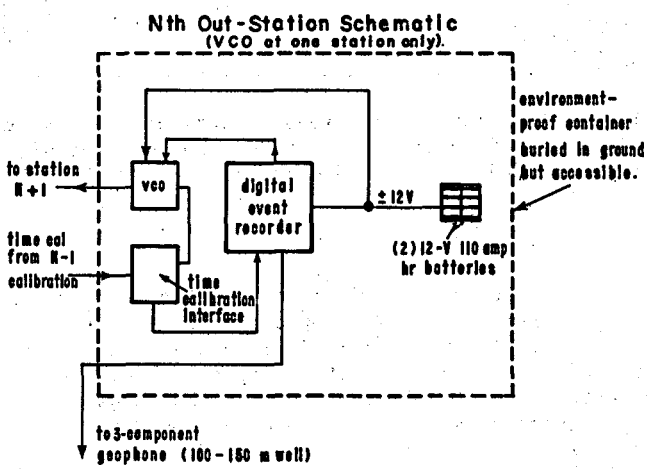

Figure 3. Cerro Prieto station electronics showing a trigger control and vco for visual monitor at central sie. (XBL 787-1968)

(the quietest) all other recorders have their internal triggering disabled. When the selected site detects an event it sends a trigger pulse to the other recorders via the wire loop. A separate twisted pair from the quiet site (the station nearest the volcano) carries an FM signal to a discriminator at the central site for visual monitoring on a drum recorder. The original plan was to send a time code fiducial to each station via one wire of the twisted pair loop and to carry the FM signal from any selected site on the remaining wire of the twisted pair loop. Each station was to trigger separately; however, due to constant construction many false triggers would often run the tapes out before any earthquakes could be recorded. Also, if the twisted part was broken it had to be reconnected with the proper polarity for the time fiducial and visual monitor to function.

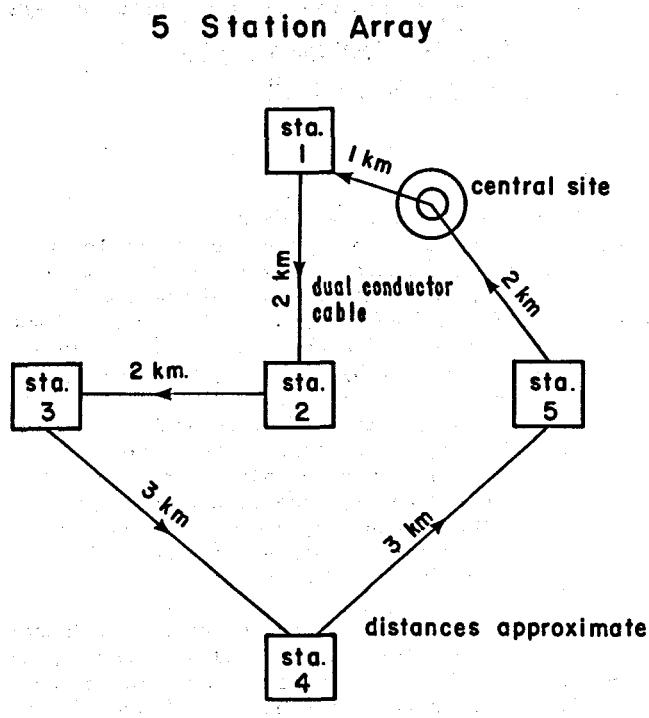

Figure 4. Cerro Prieto array plan, showing connection to central site with twisted pair. (XBL 787-1967)

As configured now, the twisted pair carrying the trigger pulse can be connected without regard to polarity, thus significantly reducing repair time. However, there is no longer a time pulse fiducial carried to each station. Due to simultaneous triggering there is no longer a need for one.

The array became operational in September 1979. However, since the magnitude 6.5 Imperial Valley earthquake of October 15, 1979, the array has been saturated with aftershocks of this sequence. Other problems are being addressed such as high noise levels in the field (particularly when downhole packages failed and we resorted to surface geophones), effects of high ambient temperatures in the summer, and wire breakage due to construction activity. These problems have been overcome and the downhole sensors are again operational, yielding a five-station, 15-component array providing high-quality digital data which will allow detailed studies of the microearthquake activity associated with the production of the Cerro Prieto geothermal reservoir. Seismic source parameters such as fault orientation and slip direction, in addition to moment and corner frequency, will provide details of source dynamics relative to the withdrawal and reinjection of fluids. Complementing the data will be extensive geophysical, hydrological, and geochemical studies currently being carried out.

EAST MESA

In April 1979 a three-component 4.5-Hz geophone in a 100-m well and a triggered digital cassette recorder were placed at the East Mesa

geothermal test facility in the Imperial Valley, California. The hole is centered among the geothermal leases of Republic Geothermal, Magma Power, and the East Mesa test facilities. The purpose of the project is to collect background seismicity data ($M_L > 1.0$) before and during commercial production. Magma Power intended to place 13 MW of power on line in the summer of 1979, with Republic adding 11 MW soon after. However, as of February 1980, routine power generation had not begun.

Before this study, there had been several other seismicity studies at the East Mesa geothermal area. One study (Combs and Hadly, 1977), claims a seismicity rate in the region of 1 to 2 events a day, $1.5 < M < 2.98$. (December 1974 to December 1975). However, subsequent monitoring by the U.S. Bureau of Reclamation (1976 to 1978) detected no locatable events in the same area, $M_L > 1.5$ (Howard et al., 1978).

As of February 1980, the present instrument had not detected any events with S-P times of less than 2.5 sec, i.e., within 15 to 20 km. However, since October 1979, the cassette recorder has been saturated with the aftershocks of the October 15 Imperial Valley earthquake (epicenter 20 km to the west). Within several months the number of aftershocks will have fallen off sufficiently to have continuous monitoring with a bi-monthly rate of tape change. It is interesting to note that the earthquake sequence associated with the main shock on October 15 had no detectable effect on seismicity or well performance in the production zone at East Mesa and Cerro Prieto.

REFERENCES CITED

Combs, J., and Hadley, D., 1977. Microearthquake investigations of the East Mesa geothermal anomaly, Imperial Valley, California. Geophysics, v. 42, p. 17.

Howard, J. H., Apps, J. A., Benson, S. M., Goldstein, N. E., Graf, A. N., Haney, J. P., Jackson, D. D., Juprasert, S., Majer, E. L., McEdwards, D. G., McEvilly, T. V., Narasimhan, T. N., Schechter, B., Schroeder, R. C., Taylor, R. W., van de Kamp, P. C., and Wolery, T. J., 1979. Geothermal resource and reservoir investigations of U. S. Bureau of Reclamation leaseholds at East Mesa, Imperial Valley, California. Berkeley, Lawrence Berkeley Laboratory, LBL-7094.

Majer, E. L., McEvilly, T. V., Albores, A. L., Diaz, S. C., 1979. Seismological studies at Cerro Prieto, in Proceedings, First Symposium on the Cerro Prieto Geothermal Field, Baja California, Mexico, September 1978. Berkeley, Lawrence Berkeley Laboratory, LBL-7098, p. 239-249.

Nur, A., and Winkler, K., 1979. The relative effects of pore fluids on seismic attenuation and velocities. Presented at the 29th Meeting Society of Exploration Geophysicists, New Orleans, La.

REMOVAL OF SILICA FROM CERRO PRIETO BRINES

O. Weres and L. Tsao

INTRODUCTION

The work reported here was conducted in support of the ongoing studies of brine reinjection at Cerro Prieto being conducted by the personnel of the Comisión Federal de Electricidad (CFE) and the Instituto Investigaciones Eléctricas (IIE). It was part of the research project at the Lawrence Berkeley Laboratory (LBL) which is part of the CFE/DOE Cooperative Program at Cerro Prieto.

The geothermal brine at the Cerro Prieto field in Baja California, Mexico, is among the hottest in the world, and contains a large amount of dissolved silica. When the brine is flashed down to atmospheric pressure, the dissolved silica rapidly polymerizes, and begins to precipitate out. In the past, this has not caused serious problems because the separated brine was disposed of by dumping it into a large evaporation pond. However, the capacity of the field has now been doubled, and brine reinjection is now considered essential to maintain productivity. Reinjection of untreated brine is not possible because the colloidal silica in it would rapidly plug the reinjection well. We were given the assignment of researching the chemistry of silica in the flashed brine at Cerro Prieto, and proposing a practical brine treatment process for field testing.

EXPERIMENTAL METHODS

We worked in the laboratory with synthetic brines formulated to closely resemble the freshly flashed brine at Cerro Prieto. Two such synthetic brine formulations were used. They differed from real Cerro Prieto brines only in that they contained a buffering compound to control the pH during the experiment, and did not contain any bicarbonate. (We did not seek to experimentally study the precipitation of calcium carbonate.)

The experiments were run at near 100°C. Two solutions, one acid and one alkaline, were prepared and preheated. They were then mixed to actually constitute the synthetic brine and initiate the silica polymerization reaction. During the experiments, both dissolved and total silica (i.e., including the colloidal silica) were periodically determined. The dissolved silica concentration was directly determined by the molybdate yellow method. To determine total silica, the sample was first reacted with sodium hydroxide solution to dissolve the colloidal silica, and then analyzed by the molybdate yellow method. The difference between the two values is the amount of colloidal silica present in the brine. The experimental methods and results of this work are discussed in detail by Weres and Tsao (1980) and Weres and Iglesias (1980).

RESULTS

The pH of the freshly flashed brine at Cerro Prieto is typically about 7.35. At this pH and 100°C, the dissolved silica in the brine polymerizes rapidly, but the colloidal silica thus formed does not settle out well. However, it may be caused to settle out ("flocculate") better by increasing the pH. This is illustrated in Figure 1. This figure presents the results of two experiments. In one of them the brine pH was not changed after the experiment was started, while in the other, the pH was increased by adding base after dissolved silica concentration had dropped to a steady value. Increasing the pH quickly caused most of the colloidal silica to flocculate and settle out.

In our laboratory work sodium hydroxide was used as a matter of convenience. In practice, lime (CaO) would be used because it is much cheaper. Theoretical calculations of the buffering capacity of the brine indicate that only about 30 g of lime would be needed per metric ton of brine to effect the treatment (see Weres et al., 1980, and Iglesias and Weres, this volume). The cost of this little lime would be negligible, even if the total brine flow at Cerro Prieto were treated. Because the needed pH increase is so small (about one-half unit) undesirable side effects, such as the precipitation of calcium carbonate should not arise. (See Weres et al., 1980, and Iglesias and Weres, this volume.)

We also tested a variety of commercially available organic flocculating agents. Of these, only compounds of the quaternary ammine type were found to be effective, and even these were effective with only one of the synthetic brine formulations but not with the other. Adding base to increase the pH, on the other hand, was invariably effective with either synthetic brine.

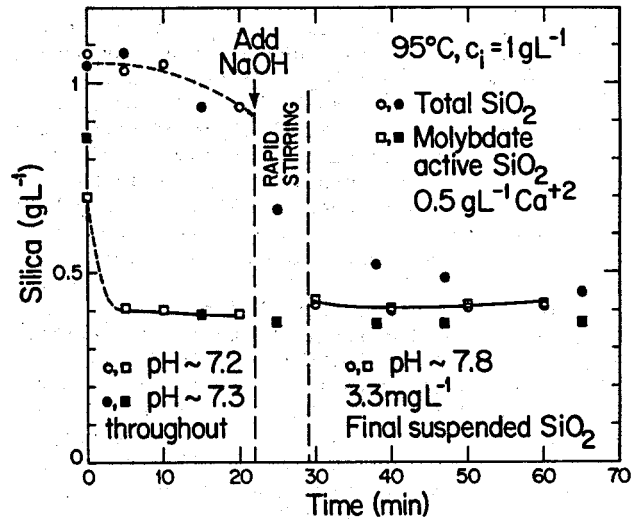

Figure 1. Results of two experiments on Cerro Prieto brines. (XBL 799-2976)

These results were confirmed in the field at Cerro Prieto using freshly flashed brine from the two wells M-14 and M-30. In both cases, increasing the pH caused the silica to flocculate out. The quaternary amines were effective with brine from M-14, but not with that from M-30. All in all, increasing brine pH appears to be the cheap and reliable treatment of choice.

These results led us to recommend the following brine treatment to our Mexican colleagues: age the fresh brine for a few minutes to allow the dissolved silica to polymerize, add lime slurry, stir the brine rapidly for a few minutes, and then separate the flocculated silica from the brine in a clarifier. A schematic of a pilot plant to test this process as well as closely related similar processes is shown in Figure 2.

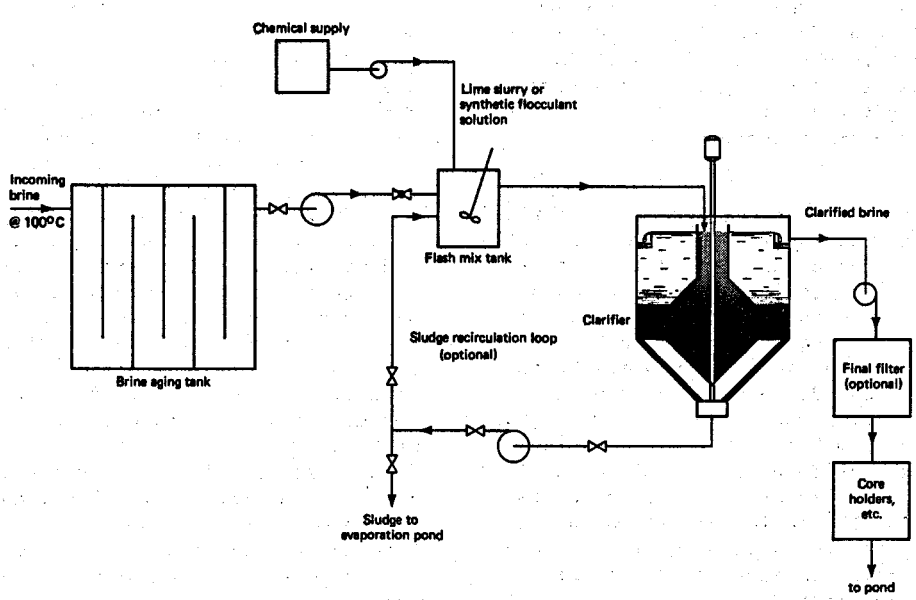

Figure 2. Schematic pilot plant to test the recommended brine treatment process. (XBL 799-2849)

This pilot plant has actually been built and operated by the IIE chemists at Cerro Prieto, and the results confirm those of our laboratory work (R. Hurtado J., report in preparation).

REFERENCES CITED

Weres, O., and Tsao, L., 1980. The chemistry of silica in Cerro Prieto brine, in Proceedings, Second Symposium on the Cerro Prieto Geothermal Field, Baja California, Mexico, October 1979. Mexicali, Comisión Federal de Electricidad (in press).

Weres, O., Tsao, L., and Iglesias, E., 1980. The chemistry of silica in Cerro Prieto brine. Berkeley, Lawrence Berkeley Laboratory, LBL-10166.

THEORETICAL STUDIES OF CERRO PRIETO BRINES CHEMICAL EQUILIBRIA

E. R. Iglesias and O. Weres

INTRODUCTION

Surface equipment scaling and formation damage due to mineral deposition are risks normally associated with the reinjection of geothermal brines (Howard et al., 1978; Cuellar, 1976). Prereinjection treatment of the brines can provide a solution to these problems (Quong et al., 1978; Weres et al., 1980), which are essentially site-specific due to the wide variation in chemical composition found in geothermal reservoirs (Ellis and Mahon, 1977; Wahl, 1977). Because of our involvement in the Mexican-American Cooperative Project we are interested in prereinjection treatment of Cerro Prieto brines. A scheme for silica removal from separated brines, based on an increase of the natural pH, has been developed by Weres and Tsao (1979). In a related effort, which is the subject of this report, we studied the potential for scaling induced by the silica removal treatment and found it significant. We then proposed and discussed a way to avoid this potential problem which we found both technically and economically feasible.

The chemical equilibrium model used in these studies is described in the next section. The important mineral saturation ratios and the proposed treatment are discussed in the last section.

THE CHEMICAL MODEL

The adopted model is described in detail elsewhere (Iglesias and Weres, 1980). This model has been implemented in a compact, fast FORTRAN package called HITEQ. The data base covers the range 0 to 300°C. Input parameters are confining pressure, total enthalpy, composition and (optional) pH. The output provides temperature, enthalpies of water, steam and noncondensible gases, partial pressure of the gas phase components, steam and water masses, pH, ionic strength, the liquid concentrations of the dissolved species, and the saturation ratios of calcite ($CaCO_3$), aragonite ($CaCO_3$), witherite ($BaCO_3$), strontianite ($SrCO_3$), anhydrite ($CaSO_4$), gypsum ($CaSO_4 \cdot 2H_2O$), barite ($BaSO_4$), and celestite ($SrSO_4$).

PREREINJECTION TREATMENT

Elsewhere (Quong et al., 1978; Weres and Tsao, 1979), a scheme for silica removal from separated brines, based on increasing their pH, is discussed. This change of pH may induce unwanted supersaturation of the brines with respect to other minerals such as calcite or witherite.

In order to assess the possible side effects of this silica removal scheme in Cerro Prieto brines, we used HITEQ to compute the chemical equilibrium of a representative brine (Table 1) and then varied the pH by addition of H_2SO_4 and $Ca(OH)_2$. The corresponding saturation ratios are presented in Figure 1. These results have been checked against computations kindly undertaken by D. L. Lessor at Battelle Northwest Laboratories, in an attempt to detect possible discrepancies. It was reassuring to find good agreement with the updated (September 1979 data base) version of Battelle's code.

Increasing the brine pH brings about potential scaling problems as indicated by the high saturation ratios calculated for the carbonates. These problems can be circumvented by reducing the bicarbonate content of the brine before the silica removal treatment is applied. This can be accomplished by first decreasing the brine pH at intermediate pressures ($P_{wellhead} \gtrsim P > 1$ atm) thus inducing conversion of sizable amounts of solution bicarbonate into carbon dioxide, which then can be stripped from the solution by allowing the pressure to decrease and thereby causing further flashing. A possible implementation of this scheme is shown in Figure 2. The first separator pressure has been adopted according to current practices (Alonso et al., 1979).

Table 1. Average brine composition of Cerro Prieto geothermal fluids.

Chemical	ppm	molal
Na	6,610	0.288
K	1,436	0.037
Mg	1.2	0.00005
Ca	328	0.008
Sr	15.8	0.00018
Ba	11.3	0.000082
B	11	0.001
Cl	11,970	0.340
CO_2	44	0.001
$SO_4^=$	9.6	0.0001
$SiO_2 \simeq 500$ (1000)*		0.008 (0.016)
pH (100°C) $\simeq$ 7.35		

*In solution after (before) amorphous silica precipitation.

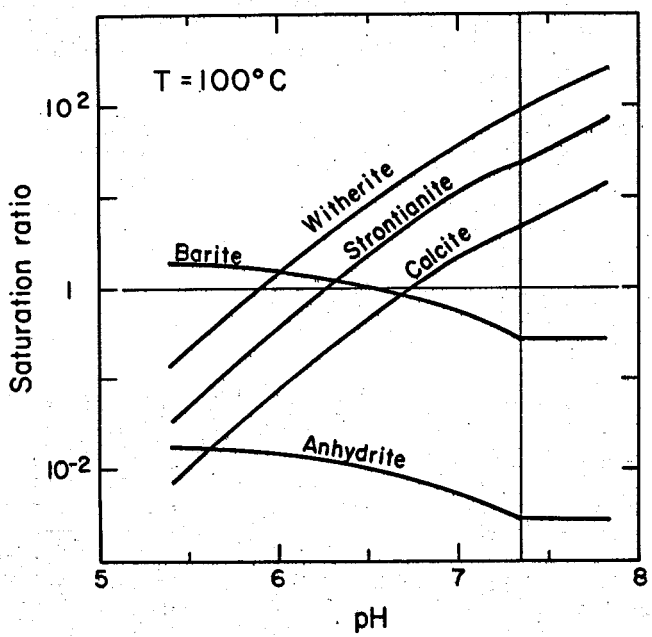

Figure 1. Effects of adjusting pH on saturation ratios of carbonate and sulfate minerals for a typical separated Cerro Prieto brine. (XBL 7912-13481)

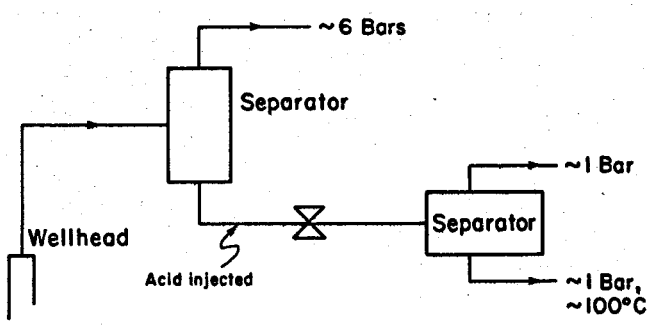

Figure 2. Schematic of the proposed scheme of acid injection for inhibition of carbonate minerals deposition. (XBL 7912-13484)

Using HITEQ we find that the reconstructed brine at 6 bars and 159°C ($SiO_2 \simeq 1000$ ppm before silica precipitation) has a pH = 7.02 and equilibrium ratios CO_2:HCO_3^-:$CO_3^=$::0.22:0.773:0.007. Figure 3 shows the computed equilibrium shift when H_2SO_4 is added. At pH = 5 we find CO_2:HCO_3::0.961:0.039; 0.6 mmoles/kg of added H_2SO_4 were required to lower the pH to this value. We envision no or minor corrosion problems at this moderate pH value. The computed saturation ratios in this condition, depicted in Figure 4, indicate that barite may be a limiting factor for use of inexpensive H_2SO_4.

Flashing the acidified brine to P $\simeq$ 1 bar we compute pH = 6.34 and the total amount of carbon dioxide and bicarbonate remaining in the liquid phase is reduced.

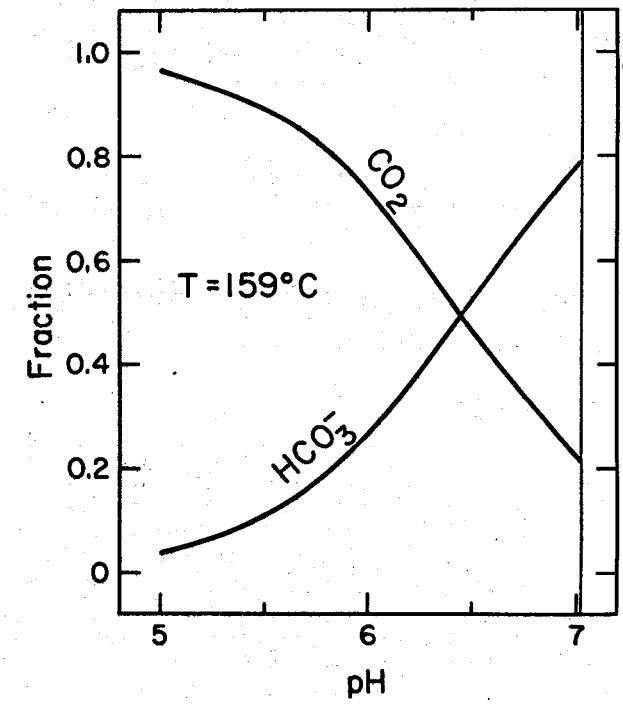

Figure 3. Carbon dioxide partition in the first separator (P $\simeq$ 6 bars) as a function of pH. (XBL 7912-13483)

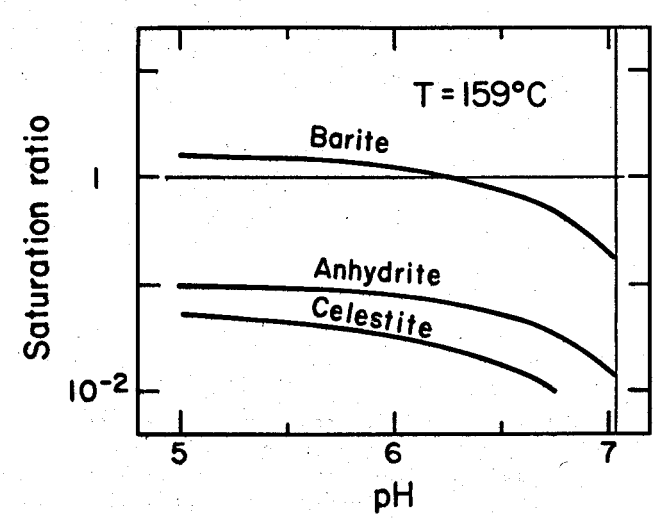

Figure 4. Effects of adding sulfuric acid on the saturation ratios of sulfate minerals (carbonate minerals out of scale) in the first separator. (XBL 7912-13480)

Increasing the pH of the separated brine by addition of $Ca(OH)_2$ we find the saturation ratios of Figure 5, which indicate that the proposed scheme can indeed control carbonate precipitation in treated Cerro Prieto brines. The amount of $Ca(OH)_2$ necessary to increase the pH of the separated brine to $\simeq$7.8, as required by the silica removal treatment, was found to be about 0.5 mmole/kg. The

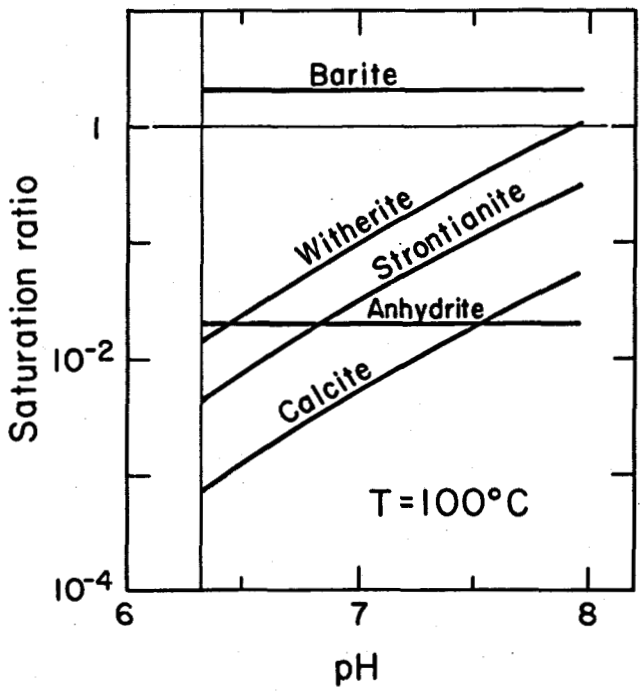

Figure 5. Effects of then adding calcium hydroxide on the saturation ratios of relevant minerals in the second separator (P ≃ 1 bar). (XBL 7912-13482)

brine is found to be supersaturated with respect to barite. This problem may be solved by replacing H_2SO_4 by HCl, though at higher cost.

Adopting 20 kg of separated brine per kWhr we estimate that the treatment with H_2SO_4 cost 2.0 x 10^{-5} \$/kWh; using HCl instead, we find a cost of 2.17 x 10^{-4} \$/kWh. The cost of the lime treatment is, in both cases, 2.00 x 10^{-5} \$/kWh. The prices of chemicals were taken from the Chemical Marketing Reporter (January 21, 1980) as \$15.00/ton for tanks of smelter grade 100% H_2SO_4; \$62.50/ton for HCl 18° Baume (29% by weight HCl); and \$32.50/ton for CaO pebble. Prices of the acids are for the West Coast; the lime price is f.o.b.

We concluded that the proposed scheme for the prereinjection brine treatment in Cerro Prieto is both technically and economically feasible. This tentative conclusion should be confirmed by experimental work due to uncertainties (e.g., validity of the Debye-Hückel approximation, values of the equilibrium constants) associated with the chemical model.

REFERENCES CITED

Alonso, H., Dominguez, B., Lippmann, M. J., Molinar, R., Schroeder, R. C., and Witherspoon, P. A., 1980. Update of reservoir engineering activities at Cerro Prieto, in Proceedings of the Fifth Annual Stanford Geothermal Reservoir Engineering Workshop.

Cuellar, G., 1976. Behavior of silica in geothermal waste waters, in Proceedings, Second United Nations Symposium on the Development and Use of Geothermal Resources. San Francisco, May 1975. U.S. Government Printing Office, v. 2, p. 1243.

Ellis, A. J., and Mahon, W. A. J., 1977. Chemistry and geothermal systems. New York, Academic Press.

Howard, J., Apps, J. A., Benson, S., Goldstein, N. E., Graf, A. N., Haney, J., Jackson, D., Juprasert, S., Majer, E., McEdwards, D., McEvilly, T. V., Narasimhan, T. N., Schechter, B., Schroeder, R., Taylor, R., van de Kamp, P., and Wolery, T., 1979. Geothermal resources and reservoir investigations of U.S. Bureau of Reclamation leaseholds at East Mesa, Imperial Valley, California.

Quong, R., Schoepflin, F., Stout, N. D., Tardiff, G. E., and McLain, F. R., 1978. Processing of geothermal brine effluents for injection. Geothermal Resources Council, Transactions, v. 2, p. 551.

Wahl, E. F., 1977. Geothermal Energy Utilization. New York, John Wiley and Sons.

Weres, O., and Tsao, L., 1980. The chemistry of silica in Cerro Prieto brines, in Proceedings, Second Symposium on the Cerro Prieto Geothermal Field, Baja California, Mexico, October 1979. Mexicali, Comisión Federal de Electricidad.

Weres, O., Tsao, L., and Iglesias, E., 1980. The chemistry of silica in Cerro Prieto brines. Berkeley, Lawrence Berkeley Laboratory, LBL-10166 (in press).

GEOSCIENCES

The summary papers which follow describe fundamental studies addressing a variety of earth science problems in support of the U. S. Department of Energy's missions. They have applications in such diverse areas as energy conservation, geothermal energy, oil and gas recovery, and radioactive waste isolation.

Funding for studies described by the papers comes from the U. S. Department of Energy, Division of Energy Storage Systems (STOR), Office of Basic Energy Sciences (OBES), Division of Fossil Energy (DFE), and Lawrence Berkeley Laboratory's Director's Development Fund. Most of the studies are conducted under ongoing projects. For descriptions of earlier work, the reader is referred to the 1977 and 1978 annual reports of the Earth Sciences Division (LBL-7028 and 8648) and the 1975 and 1976 annual reports of the Energy and Environment Division of Lawrence Berkeley Laboratory (LBL-5299 and LBL-5982).

In the following paragraphs, a brief discussion of the papers is given so the reader may appreciate the diversity of the work being accomplished and may easily locate the subjects of most interest to him.

The first five papers by C. F. Tsang and his coworkers cover problems relating to the storage of heated or chilled water in underground porous rock reservoirs. Three papers report the results of research supported by STOR; the remainder report results of work sponsored by OBES. Aquifer thermal energy storage possesses great potential as a means of storing heated or chilled water for periods up to six months, at which time the energy can be recovered for space heating or cooling. Substantial energy savings could thereby be realized. However, problems relating to the storage process must be resolved for this method to be economical.

There follows, under OBES support, a series of eight papers by T. N. Narasimhan, C. F. Tsang, and others concerning problems of dynamic subsurface groundwater movement in porous or fractured rocks. These papers deal with fundamental physical and chemical properties of reservoirs, and numerical methods of simulating transient and steady-state processes that occur in these reservoirs under natural or artificial conditions.

Also under OBES support are a series of papers addressing chemical and physical properties of natural systems. Three papers, one by K. S. Pitzer and coworkers, and two by S. L. Phillips and coworkers, are concerned with the thermodynamic and transport properties of aqueous inorganic electrolytes at elevated temperatures. In the first paper the authors discuss progress being made in the measurement of heat capacities and densities of solutions of geothermal interest, with particular attention being paid to NaCl and Na_2SO_4 solutions. The second and third papers summarize available literature data on properties of NaCl solutions.

Two papers are concerned with the results of heterogenous processes occurring in water-saturated rocks. J. A. Apps and J. M. Neil discuss the solubility of the rock-forming mineral, albite, in sodium chloride solutions at elevated temperatures, as part of a wider ranging study of mineral-water interactions, whereas C. L. Carnahan reports on his investigations concerning the transport in water-saturated porous rocks of ions that sorb on mineral surfaces. In addition, he has investigated the temperature dependence of the adsorption of cesium ions on smectites.

I. S. E. Carmichael and others give their latest findings in a paper on the thermodynamic properties of silicate liquids, particularly as they relate to magmas and the minerals that crystallize from them. In addition, they are investigating the heats of fusion of major rock-forming minerals and are presently attempting to determine this parameter for the mineral anorthite.

Continuing investigation under OBES funding involves study of the physical properties of rock-fluid systems at elevated pressures and temperatures. In this work, W. H. Somerton describes the measurement of a wide range of physical properties—as many as possible made simultaneously, on sedimentary rocks under conditions encountered in deep high-temperature oil and gas reservoirs, and other subsurface reservoirs where elevated temperatures and pressures are found.

In another paper relating to the oil industry, C. J. Radke and W. H. Somerton present the results of research supported by the DFE and designed to establish conditions required for tertiary mode displacement of acidic oils in oil reservoirs and to elucidate the dominant mechanisms of displacement so that improved recovery methods using caustic solutions may be developed.

To complete this section, four short reports are given by S. M. Klainer, J. A. Apps, and M. C. Michel on projects supported by the Director's Development Fund. The projects, concerned primarily with instrumental development for geoscience applications, cover a range of innovative concepts. These include the continued development of high-precision mass spectrometry for isotopic dating techniques; the development of techniques for measuring organic fluorocarbon tracers in groundwaters; a novel technique for measuring crystallographic properties of minerals using nuclear quadrupole resonance spectroscopy; and finally, an ultrasensitive method for measuring trace quantities of actinides in groundwaters.

Basic Sciences Studies

BUOYANCY FLOW AND THERMAL STRATIFICATION IN AQUIFER HOT-WATER STORAGE

G. Hellstrom, C. F. Tsang, and J. Claesson

INTRODUCTION

In the research area of hot-water storage in aquifers, a number of key problems remain to be studied. Their solution would define best-operation conditions and parameters and optimize the storage-recovery ratio. Solution of these problems would not only yield a basic understanding of thermohydraulics in porous media, but may be crucial in the eventual success of this process.

One critical problem is thermal buoyancy flow in which, because of the difference in density and viscosity of waters with different temperatures, hot water tends to flow to the top of cold water. This induces a mixing of hot and cold water, resulting in heat dissipation that decreases the energy recovery ratio. When hot water is injected into an aquifer, the interface between hot and cold water is primarily vertical. This vertical interface is unstable and will tend to tilt outward from the injection well. The rate at which the system tends to equilibrium, i.e., with the hot water on top of the cold water, is a decisive factor in determining the feasibility of a system with vertical injection and production wells. A strong disturbance of the temperature field will lead to higher heat loss (larger surface area of the hot region and increased heat dispersion). It will also require a more complicated extraction system in order to avoid excessive mixing of hot and cold water in the well.

CURRENT STUDY

Our study aims to find an explicit order-of-magnitude expression for the influence of the buoyancy flow. It is then possible to estimate the rate at which the thermal front "tilts," without resorting to numerical models. The analysis is based on a number of analytical solutions for a vertical thermal front in cylindrical and two-dimensional Cartesian coordinates. The diffusiveness of the thermal front is also taken into account. Several assumptions about the thermal front's behavior must be made in order to modify the analytical solutions for nonvertical situations. Finally, the tilting rate for a given system is quantified by a characteristic tilting time-constant, which equals the time required for an initially vertical front to tilt 45°. Major conclusions include:

1. Buoyancy flow is proportional to the density difference between stored and native waters, and to the square root of the product of vertical and horizontal permeabilities of the aquifers, and inversely proportional to aquifer thickness and average viscosity of the injected and native waters. The dependence on aquifer thickness and permeabilities will suggest a criterion for selecting potential storage aquifers. The density and viscosity dependence will introduce a guideline for optimal storage temperatures.

2. With forced convection, the injected hot water (for the case of hot-water storage) tends to flow more easily into regions of higher temperatures because of the lower viscosity. Formulas are derived to quantitatively calculate this flow. In some cases, this flow counteracts the buoyancy flow process.

3. Two key lumped parameters are derived which would make it possible to relate results of different cases by means of a similarity transformation.

The most important parameter is the product of the vertical and horizontal permeabilities. The tilting time-constant is inversely proportional to the square root of this product. In order to verify the assumptions made when deriving the analytical solution, a number of simulations have been made using the numerical model CCC (Conduction, Convection, and Compaction). These simulations confirm that the assumptions are reasonable.

As an illustration of the results, we give the following example. Consider a 20-m-thick alluvial aquifer with a vertical permeability that is 1/10 of the horizontal one. The heat capacity of the aquifer is 2.7 MJ/m^3K. The temperature of the injected water is 85°C, and the ambient water is 15°C. Figure 1 shows the tilting angle (assuming a straight front) as a function of permeability (m^2) and storage time (days). Let us require that the thermal front should not tilt more than 60° during a storage period of 90 days. The corresponding maximum allowable permeability is then about 3×10^{-11} m^2. This example does not include the effects of a superposed forced convection, which will cause a further increase in the tilting angle.

*Permanent address: Department of Mathematical Physics, Lund University, P. O. Box 725, S-22007 Lund 7, SWEDEN.

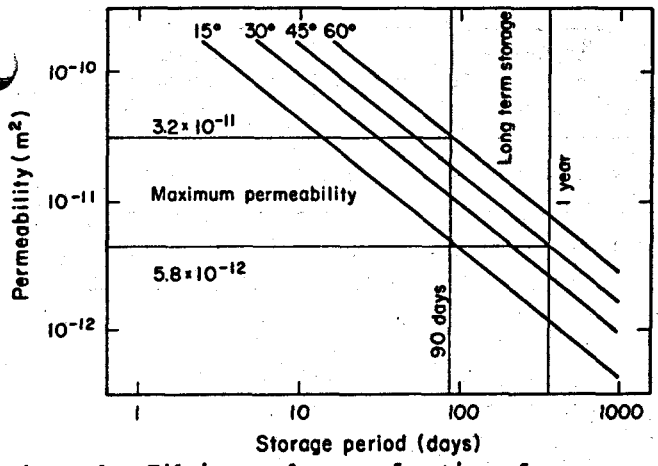

Figure 1. Tilting angle as a function of permeability and storage time. (XBL 7910-13050)

In the field tests conducted so far, water at rather low temperatures (~55°C) has been injected into aquifers of relatively high permeability. The length of the storage cycle is about three months. To avoid excessive influence of buoyancy flow during an annual storage cycle with higher temperatures (~85°C), it is necessary to use less permeable aquifers.

PLANS FOR NEXT FISCAL YEAR

Work will continue on the same basic subjects. Main emphasis will be on the derivation of key lumped parameters and calculation of the storage-recovery ratio as a function of these variables. The results will be of use in the selection of aquifers and procedures for thermal energy storage.

DAILY SENSIBLE HEAT STORAGE IN AQUIFERS FOR SOLAR ENERGY SYSTEMS

C. F. Tsang, P. Fong, C. W. Miller, and M. J. Lippmann

INTRODUCTION

Recently much interest has been generated by the concept of long-term seasonal storage of hot water in aquifers. However, the possibility of daily storage-retrieval cycles has not been explored in much detail. This note will describe the results of numerical simulation studies of hot-water storage in aquifers.

ACCOMPLISHMENTS DURING FISCAL YEAR 1979

At Lawrence Berkeley Laboraory, a powerful numerical model for three-dimensional liquid-saturated porous systems has been developed, initially for geothermal applications. This model, called CCC (Conduction, Convection, and Compaction) computes heat and mass flow while simulating the vertical deformation of the aquifer system, by using the one-dimensional consolidation theory of Terzaghi. CCC has been validated against many analytical solutions and has been applied to the study of geothermal reservoir dynamics as well as the modeling of aquifer seasonal storage systems (Tsang et al., 1976, 1978a,b).

For the present work, this model is coupled with a wellbore conduction computer program. This wellbore program computes the heat loss away from the wellbore into the formation as hot water flows up or down the well. The coupled model is applied to the case of a "typical" aquifer 20 m thick and 200 m deep. A moderate flow rate of 2.0×10^5 kg/day of 220°C water, is assumed for two different hot water storage-retrieval schemes:

1. Twelve hours of injection into the aquifer followed by 12 hours of production;
2. Eight hr of injection in the daytime followed by 4 hr of production in the evening, then shut-in for 8 hr at night, and finally, a second 4-hr production period in the early morning.

The parameters used for these calculations are summarized in Table 1. As an illustration of the wellbore heat-loss effects, Figure 1 shows the temperature at the well bottom during the first 8-hr injection period (case B) when 220°C water is injected at the top of the well.

Three cycles were calculated for each case and the results are shown in Figures 2 and 3 for case A and Figures 4 and 5 for case B. These figures display the temperatures at the bottom of the well (Figures 2 and 4) and temperatures at the top of the well (Figures 3 and 5) during the production and shut-in periods. A difference in temperature of a few degrees is noticed between the top and bottom due to heat losses or gains as water flows along the well. The large heat loss near the top of the well during the shut-in period is apparent in Figure 5.

If we define the energy of the stored water as represented by its temperature above the ambient 20°C, the energy recovery, as a percentage of stored energy, is shown in Table 2. On the whole, a recovery ratio of over 70% is computed.

Table 1. Material and fluid parameters used.

Material	Dimensions m	Porosity	Density kg m^{-3}	Heat capacity j kg^{-1}•c	Thermal conductivity j $s^{-1}m^{-1}$•c^{-1}	Permeability m^2	Specific storage $kn^{-1}m^2$
Aquifer	200 deep 20 thick	0.20	2.6×10^3	9.7×10^2	2.894	1.0×10^{-13}	2.0×10^{-4}
Aquitard	200 deep 20 thick	0.15	2.5×10^2	9.3×10^2	2.20	1.0×10^{-17}	2.0×10^{-4}

Fluid Parameters

Viscosity (cp)	Temperature (°C)	Heat capacity c(j kg^{-1}•c^{-1}	Temperature (°C)
1.005×10^{-3}	20	4.182×10^3	20
5.450×10^{-4}	50	3.894×10^3	75
2.800×10^{-4}	100	3.652×10^3	125
1.820×10^{-4}	150	3.341×10^3	200
1.350×10^{-4}	200		

Expansivity (°c^{-1})	3.17×10^{-4}
Flow rate (kg day^{-1})	200448
Injection temperature at surface (°C)	220

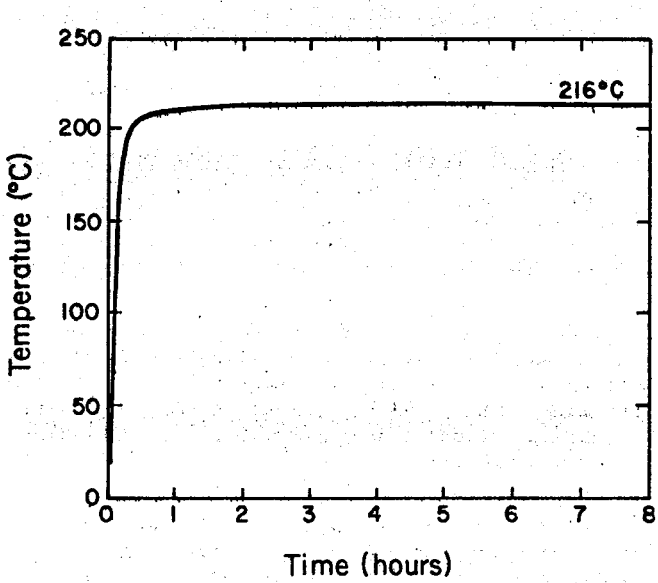

Figure 1. Temperature at the well bottom with injection of 220°C water at top (case B). (XBL 795-854)

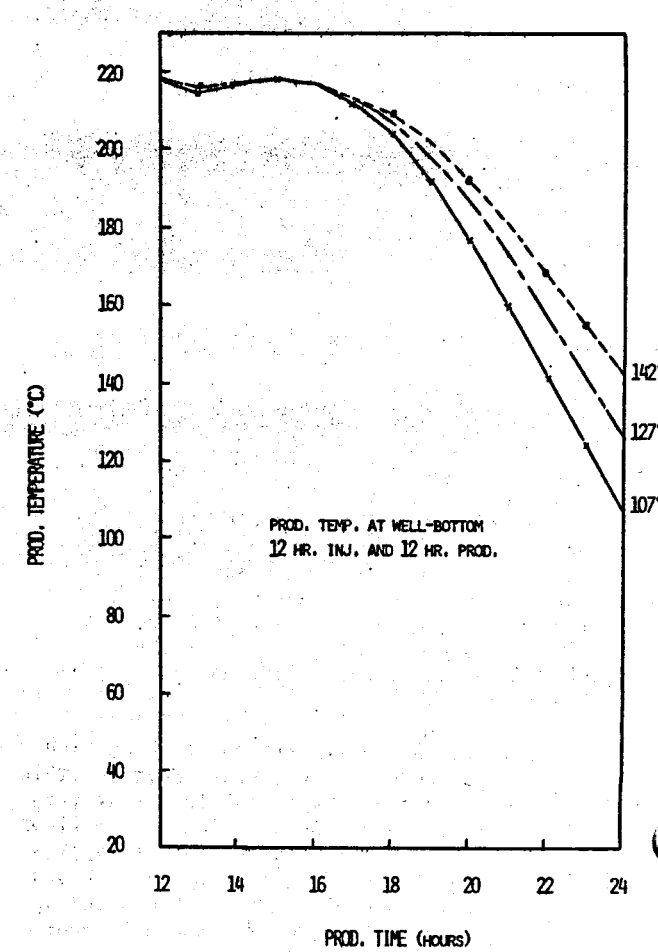

Figure 2. Temperature at the bottom of the well during production periods, case A, 12-hr injection and 12-hr production. (XBL 7811-12942)

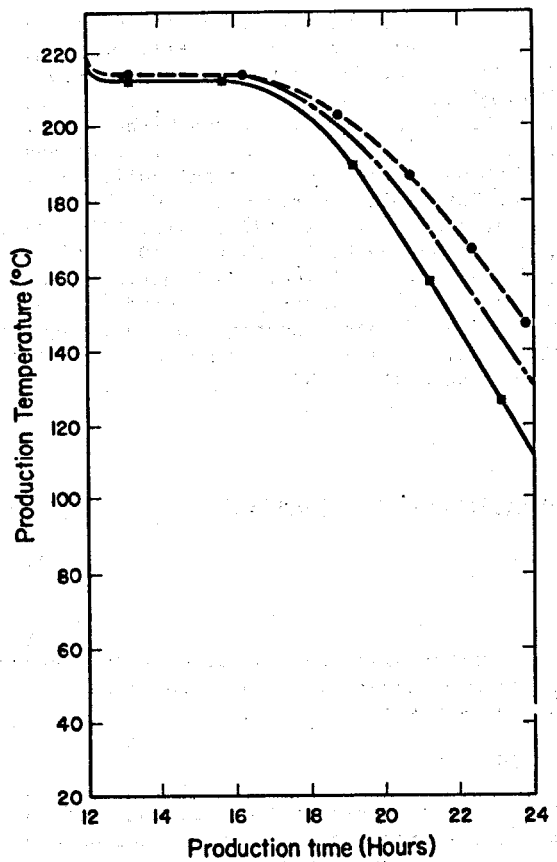

Figure 3. Temperature at the top of the well during production periods, case B. (XBL 807-10694)

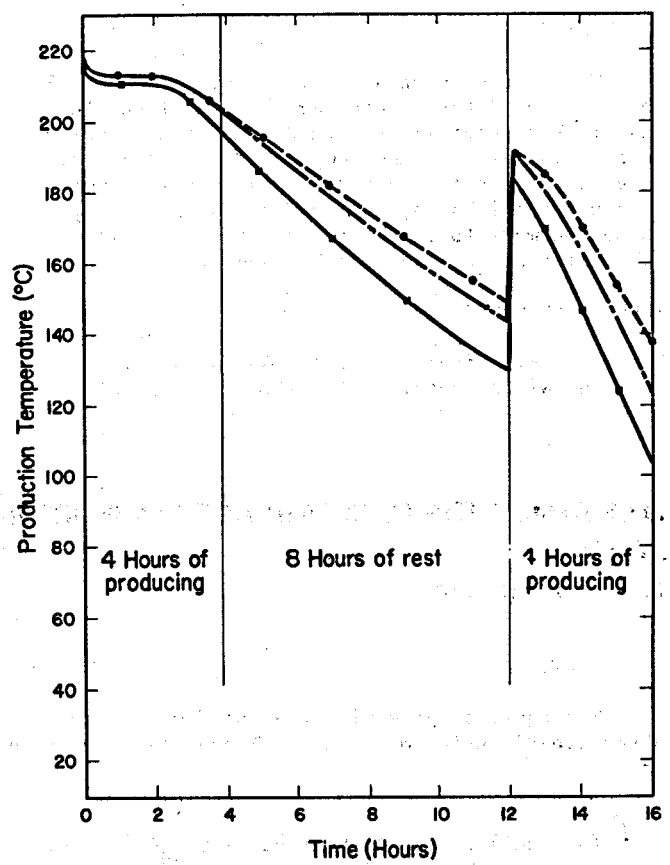

Figure 5. Temperature at the top of the well during production and shut-in periods, case B. (XBL 807-10695)

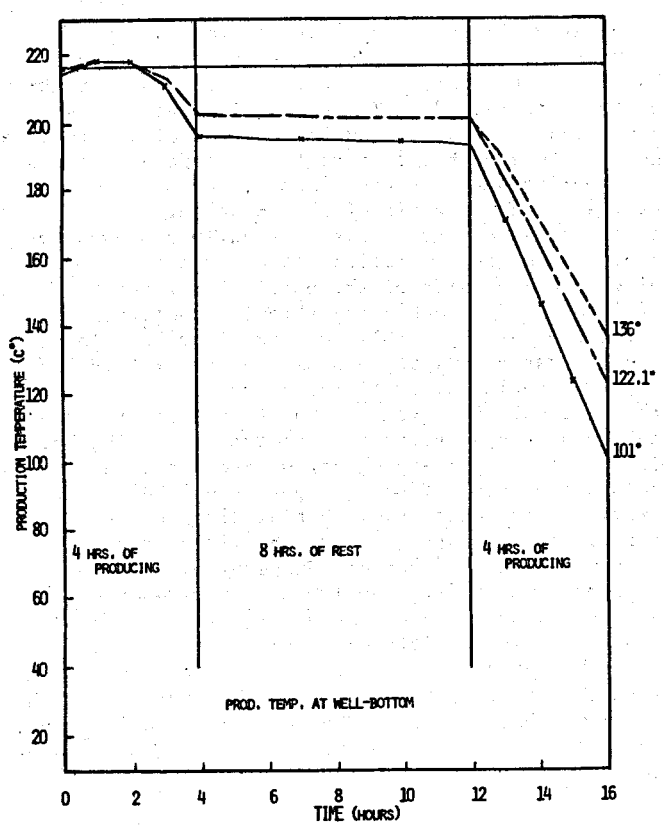

Table 2. Percentage of energy recovery.

	Cycle 1	Cycle 2	Cycle 3
Case A:			
12-hour production	82%	86%	88%
Case B:			
First 4-hour production	95%	96%	97%
Second 4-hour production	63%	71%	75%
Total	79%	83%	86%

Figure 4. Temperature at the bottom of the well during production and shut-in periods, case B. (XBL 7811-12944)

CONCLUSIONS

The results suggest that it may be reasonable to store hot water in aquifers on a daily-cycle basis; this possibility should be further studied. Once a storage rate and temperature are decided, based on a practical scenario, parametric studies of aquifer thickness, permeability, and porosity should be made to select an aquifer which will make daily storage an economic venture.

REFERENCES CITED

Tsang, C. F., Lippmann, M. J., Goranson, C. B., and Witherspoon, P. A., 1976. Numerical modeling of cyclic storage of hot water in aquifers. Presentation, AGU Fall Meeting, San Francisco, California, December 6-10, 1976, (also LBL-5929).

Tsang, C. F., Lippmann, M. J., and Witherspoon, P. A., 1978a. Underground aquifer storage of hot water from solar energy collectors. Proc. Int. Solar Energy Cong., New Delhi, India, January 16-21, 1978, (also LBL-7034).

Tsang, C. F., Buscheck, T., Mangold, D., and Lippmann, M. J., 1978b. Mathematical modeling of thermal energy storage in aquifers, in Proceedings, Therm. Energy Storage in Aquifers Workshop. Berkeley, Lawrence Berkeley Laboratory, LBL-8431, p. 37-45.

ONE-DIMENSIONAL CHEMICAL TRANSPORT IN AN ADVECTION-DOMINATED SYSTEM

T. N. Narasimhan

INTRODUCTION

The equation governing the one-dimensional advective-diffusion of a chemical species is written as

$$-\int_\Gamma (\vec{q}\cdot \mathrm{n}d\Gamma)c_\Gamma + \int_\Gamma D_L \vec{\nabla}c\cdot\vec{n}d\Gamma = V_v\frac{\partial c}{\partial t} \qquad (1)$$

where $\vec{q}\cdot\vec{n}$ is Darcy velocity along the outer normal $\vec{n}$ to the surface segment $d\Gamma$, c_Γ is the mean concentration at $d\Gamma$, D_L is the longitudinal diffusion coefficient, assumed to be constant; V_v is the pore volume within the elemental volume bounded by the surface Γ; and $\partial c/\partial t$ is the mean time derivative over the elemental volume. In (1), we assume that the fluid flow field is steady and that q is independent of time. The more familiar differential form of (1) is

$$q\,\nabla c + D_L\nabla^2 c = \frac{\partial c}{\partial t} \quad . \qquad (2)$$

Both (1) and (2) are subject to initial and boundary condition.

The numerical solution of the above equations is reasonably straightforward providing that the magnitude of diffusion is strong relative to advection, as quantified by the Peclet Number,

$$P_e = \frac{q\Delta x}{D_L} \quad . \qquad (3)$$

It is widely known that when P_e is larger than about 2, the numerical solution of the above equation is masked by a dispersion or a smearing out of the concentration front caused by the solution process itself. This is known as numerical dispersion.

This report discusses one attempt to overcome the problems of numerical dispersion in one-dimensional systems.

DISCUSSION

To understand numerical dispersion, let us consider the extreme case of pure advection where $D_L = 0$. In this case, equation (1) reduces to:

$$-\int_\Gamma (\vec{q}\cdot\vec{n}d\Gamma)c_\Gamma = V_v\frac{\partial c}{\partial t} \quad . \qquad (4)$$

If we view (4) in an explicit fashion, all the geometric quantities and the Darcy velocity are known, and the only unknown is c_Γ, the concentration at the interface $d\Gamma$. In numerical models, c is specified (initially) and $\partial c/\partial t$ computed at discrete node centers rather than at the interfaces between neighboring node centers. Hence, c_Γ is to be evaluated on the basis of the known values of c at the node centers. This is usually achieved by a process of interpolation between known values of c on either side of the particular interface of interest. In achieving this interpolation, there are three possible sources of error. These are (1) variations of c_Γ over the time interval Δt; (2) the spatial discretization errors inherent in the interpolation process; and (3) errors inherent in the discrete values used in the interpolation. Of the three, time-integration errors can be handled relatively easily from a computational point of view. Of the other two, spatial discretization errors have perhaps received the widest attention as the source of numerical dispersion. Attempts have been made, for example, to minimize numerical dispersion by using upstream weighting in conjunction with finite difference approximations or by using higher order approximations in conjunction with the finite element method. However, not much attention has apparently been paid in the literature to exploring the third error source as a major source of error. We now consider this in detail.

Consider a volume element of width Δx, within which the concentration front is residing. Since we are considering pure advection, the concentration at the node center of the volume element has to be either 1 or 0, depending on whether or not the front has crossed the location of the node center. However, since concentrations are treated as averages over the volume element, the concentration at the node center will gradually vary from 0 to 1 as the front migrates from the upstream to the downstream end of the volume element. As a result, a fundamental error is introduced into the interpolation process as long as one uses an average concentration for the volume element in which the sharp front is residing. This basic error cannot generally be eliminated by improved interpolation schemes.

One possible way to eliminate the aforesaid error is to avoid using, in the interpolation process, the erroneous average concentration of the volume element in whch the front is residing. Instead, one simply uses a procedure of extrapolation, rather than interpolation. In order that this could be implemented, one should know, a priori, the node in which the front is residing. This information, nevertheless, is known as long as the problem involves steady fluid flow field.

This method of minimizing numerical dispersion was explored by implementing the extrapolation technique for evaluating the concentrations at the surfaces bounding the volume element in which the front resides and using the conventional interpolation scheme everywhere else. The method indeed gave excellent results for pure advection as well as advection-dominated problems with or without exponential decay of the solute. In addition, due to the extremely small diffusion, the volume elements have relatively large time-constants and hence enabling explicit evaluation of time-derivatives as long as C_Γ's are evaluated accurately. As long as the method is implemented correctly, the solution process is not limited by $\Delta\Gamma$.

The main limitation of the method is the need to store, in memory, the fluid flux field in an appropriate fashion. Although this is not a serious problem for one-dimensional situations, extensions to two and three dimensions is cumbersome in practice although simple in principle. Yet, in its present state, the method offers attractive possibilities for studying a variety of advection-dominated problems such as transport in a fissured, two-dimensional porous medium in which all the flow occurs in the fissures while diffusion governs chemical transport in the porous rock.

RESPONSE OF AQUIFERS TO EARTH TIDES

T. N. Narasimhan and B. Y. Kanehiro

INTRODUCTION

Since Grablovitz's early observation in 1880, many field workers have reported the response of confined aquifers to earth tide fluctuations as evidenced by water level or fluid pressure fluctuations in wells. This response is basically governed by the relative compressibilities of water and the porous matrix of the aquifer. Attempts have therefore been made in the past (Bredehoeft, 1967; Bodvarsson, 1970; Arditty and Ramey, 1978) to estimate reservoir compressibility based on the aquifer pressure response relative to the changes in gravitational potentials induced by changes in earth tides. Whereas Bredehoeft considered a horizontal aquifer of finite thickness, Bodvarsson and Arditty idealized the system to use a spherical geometry. Bredehoeft's idealization, similar to what follows in the present work, leads to a direct estimation of specific storage as a ratio between observed dilation and the associated pressure response in the aquifer.

The present work deals with the analysis of aquifer response data from three field cases: Raft River Valley, Idaho; East Mesa, California; and Marysville, Montana. All the wells were deeper than 1 km. An example of a well record is shown in Figure 1. The work consisted of two parts. First, the data were processed using finite Fourier analysis to identify the primary tidal components from the pressure transient data. An example of the spectra resulting from finite Fourier analysis is shown in Figure 2. The second part of the task was to evaluate the aquifer storativity using the relationship between the observed fluid pressure change and the corresponding stress changes induced by the earth tides. In this respect, the present work differs somewhat from Bredehoeft's analysis in that we did not directly compute storativity as he did. Instead, we first calculated the bulk modulus of the porous medium before evaluating specific storage.

We also carried out a numerical investigation of the effect of wellbore storage on governing the phase-lag between the aquifer response and the associated response in the well.

THEORY

Consider a horizontal, homogeneous, areally infinite aquifer, pierced by a fully penetrating well. The well is non-pumping and is merely an observational device. In the first case, assume that the well is small and reacts instantaneously to any changes in the fluid potential in the aquifer. We will consider the noninstantaneous well response later.

Because the motions of the earth, moon, and sun are well understood, it is possible to estimate the changing gravitational potential at all points in the earth as a function of time. On cursory examination, it might seem reasonable to assume that the changing acceleration due to gravity, implied by the changing gravitational potential, results in the fluctuation of the weight of the overburden of the reservoir and, hence, the fluctuating pore-fluid pressure as seen at the well.

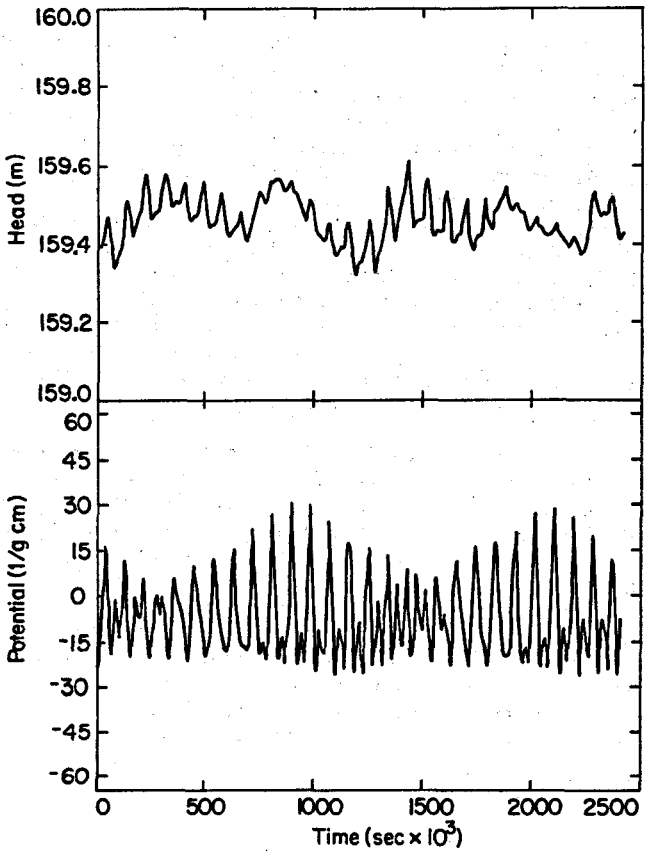

Figure 1. Well record (TOP) and calculated earth tides record (BOTTOM) for the same site. Response of the aquifer may be determined by comparing the two. (XBL 799-2889)

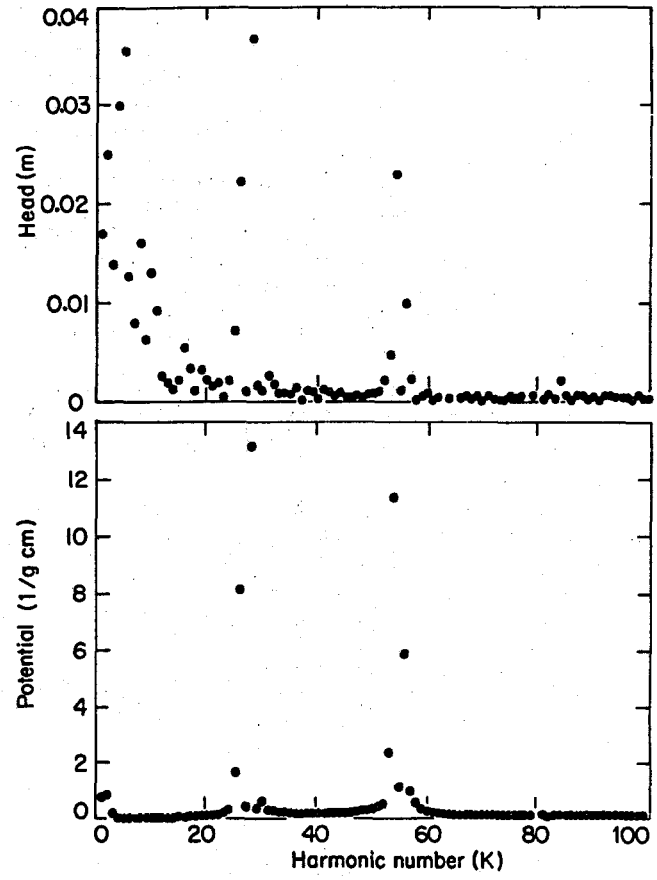

Figure 2. Spectrum of the well record (TOP) and the earth tide record (BOTTOM) for the same site. (XBL 799-2888)

Rough calculations, however, show that this mechanism is not large enough to account for the magnitude of the observed pore-fluid pressure fluctuation seen in moderately deep reservoirs. The bulk of the change in pore-fluid pressure in the aquifer apparently results from some other mechanism.

This mechanism is related to the nonrigidity of the earth. The driving force may be viewed as a bulging of the earth resulting from the gravitational attraction of the moon or sun on the one side and centrifugal force on the other. Because of the motions of the sun, moon, and earth relative to one another, the deformation appears to be periodic.

In a gross sense, the aquifer may be considered to be a sealed deformable packet of saturated sand imbedded in the earth's crust. This packet deforms periodically in response to the deformation of the earth as a whole. The deformation implies that there is a change in the pressure of the pore fluid within the aquifer that can be measured at the well. If the section of the well exposed to the aquifer is sealed off (packed) with rubber packers, then the pressure measured in that section of the well should reflect the pressure of the pore fluid within the aquifer. If, on the other hand, the well is open to the atmosphere and the water level in the well fluctuates in response to the changing pore-fluid pressure, there will be both an attenuation and a lag between the pressure fluctuation of the pore fluid and the fluctuation as measured in the well. The attenuation and phase lag reflect wellbore storage and result from filling and emptying the well with each pressure fluctuation. The problem is then one of relating the known changing gravitational potential to the pressure fluctuation as seen at the well in terms of meaningful aquifer characteristics.

Although the nature of the changing gravational potential is reasonably well understood, the inhomogeneous anisotropic nature of the earth complicates the stress-strain picture of the deforming aquifer. In general, however, reasonable assumptions and empirically determined coefficients can be invoked to estimate the stress imposed on the aquifier by the earth tides. In the case of the packed-off well, the relationship between this stress and the pressure fluctuation as seen at the well is a function of two aquifer characteristics--specific storage and porosity. In the case of an open well, the relationship also depends on the permeability of the aquifer.

It is well known that for the undrained problem (see Skempton, 1954; Domenico, 1972), the ratio of fluid pressure change to the total stress change induced by earth tides is governed by the porosity of the aquifer as well as the compressibilities of water and the aquifer matrix. Thus,

$$\frac{\Delta p_f}{\Delta \sigma_m} = \frac{1}{1 + (nc_w/m_v)} \quad (1)$$

where Δp_f is pore pressure change, $\Delta\sigma_m$ is change in B mean principal (total) stress, n is porosity, c_w is water compressibility, and m_v is coefficient of volume change. Hence, by rearrangement of terms we may write,

$$m_v = \frac{nc_w \Delta p_f}{\Delta \sigma_m} \quad (2)$$

and S_s, specific storage, is given by:

$$S_s = \gamma_w nc_w \left[1 + \frac{\Delta p_f}{\Delta \sigma_m}\right] \quad (3)$$

where γ_w is unit weight of water. As seen from (3), S_s can be estimated if n and $\Delta\sigma_m$ are known, with Δp_f denoting the measured earth tide response and $\Delta\sigma_m$ representing the total mean stress change induced by the earth tide. Thus, an important task is to estimate $\Delta\sigma_m$. It can be shown that Δ, the dilatation due to earth tides, can be approximated as

$$\Delta = \frac{W_2}{ag} \quad (4)$$

where W_2 is tidal potential, a is mean radius of the earth and g is acceleration due to gravity. In view of (4), if we can use a reasonable estimate for the bulk modulus for the region of the earth in which the aquifer is situated, then we can estimate $\Delta\sigma_m$ by the relation,

$$\Delta\sigma_m = K\Delta$$

where K is the estimated bulk modulus.

Under these conditions,

$$S_s = n\gamma_w c_w \left[1 + \frac{\Delta p_f ag}{KW_2}\right]. \quad (5)$$

Using (5), field data collected from Marysville, Montana; East Mesa, California; and Raft River, Idaho, were analyzed. The results obtained, using $K = 5 \times 10^{10}$ Pa, are given in Tables 1, 2, and 3.

In arriving at the results in Tables 1, 2, and 3, it was assumed that the well responded instantaneously to changes in the aquifer potential. This is true in the case of a small-diameter well or a well that is packed off at the top and bottom of the formation.

The second problem considered was that of pulse lag between the pressure transient as seen at the well and the stress imposed by the earth tides. This corresponds to the case of a relatively large open well, which is more difficult to deal with than the packed-off well. The easiest approach was to use numerical modeling. Because there were no data complete enough to verify any modeled real-world situation, we only considered hypothetical cases. The problem involved an axisymmetric well-aquifer system with a sinusoidally varying driving force. This sinusoidal term corresponds to a single component of the real-world tide that may be separated by Fourier analysis. A pressure-versus-time record of a simulation run is shown in Figure 3. Here the upper curve represents the tide and the lower curve represents the

Table 1. Results of the analysis of the record from the well at East Mesa, California (bulk modulus of 5×10^{10} Pa assumed for the region around the aquifer).

Tidal Component	ΔW_2 (x 1/gm)	Δp_f (Pa)	S_s/n (1/m)
O1	7.060×10^{-2}	2.924×10	5.052×10^{-6}
P1, K1	7.362×10^{-2}	4.745×10	5.416×10^{-6}
N2	3.754×10^{-2}	1.102×10	4.881×10^{-6}
M2	1.704×10^{-1}	5.526×10	4.923×10^{-6}
S2	9.235×10^{-2}	3.717×10	5.035×10^{-6}

Ss/n (mean) = 5.06×10^{-6} 1/m

Standard Deviation = 2.11×10^{-7} 1/m

Table 2. Results of the analysis of the record from the well at Raft River, Idaho (bulk modulus of 5×10^{10} Pa assumed for the region around the aquifer).

Peak Identification	ΔW_2 (x 1/gm)	ΔP_f (Pa)	S_s/n (1/m)
1	3.900×10^{-1}	9.655×10^{2}	1.265×10^{-5}
2	5.300×10^{-1}	1.172×10^{3}	1.061×10^{-5}
3	6.000×10^{-1}	1.172×10^{3}	9.165×10^{-6}
4	6.100×10^{-1}	1.517×10^{3}	1.276×10^{-5}
5	5.600×10^{-1}	1.310×10^{3}	1.151×10^{-5}

S_s/n (mean) = 1.13×10^{-5} 1/m

Standard Deviation = 1.50×10^{-6} 1/m

Table 3. Results of the analysis of the record from the well at Marysville, Montana (bulk modulus of 5×10^{10} Pa assumed for the region around the aquifer).

Tidal Component	ΔW_2 (x 1/gm)	ΔP_f (Pa)	S_s/n (1/m)
O1	8.126×10^{-2}	2.176×10^{2}	1.485×10^{-5}
P1, K1	1.318×10^{-2}	3.581×10^{2}	1.535×10^{-5}
N2	2.315×10^{-2}	4.600×10	9.351×10^{-6}
M2	1.133×10^{-1}	2.260×10^{2}	9.366×10^{-6}
S2	5.863×10^{-2}	9.782×10	7.962×10^{-6}

S_s/n (mean) = 1.14×10^{-5} 1/m

Standard Deviation = 3.45×10^{-6} 1/m

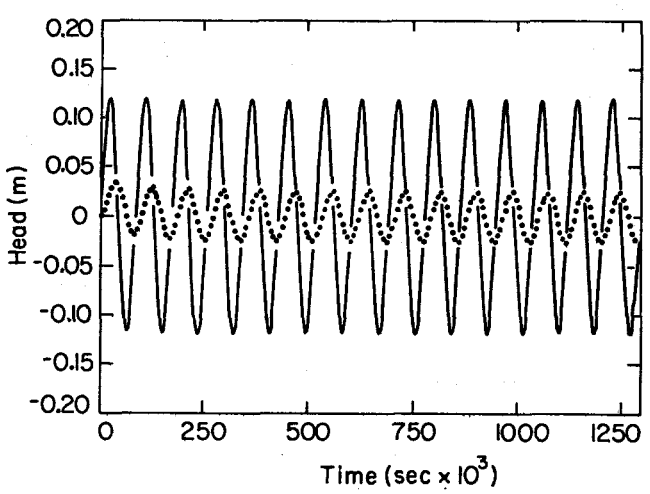

response of the aquifer. Note that in the case of the open well, there is a phase lag as well as an attenuation of the signal. Application of this model to the real world becomes an inverse problem that, although straightforward in principle, may be relatively tedious. The possibility of systematizing the solution of the inverse problem, perhaps through the use of type-curve generation, was investigated. Although some potential was

Figure 3. Pressure fluctuation in the well element (points) and an element distant from the well element (line) in the case of a well open to the atmosphere. The period of the sinusoidal generation term is 86,400 sec (24 hr). (XBL 799-2886)

shown, verification of such methodology requires more and better data than that what is presently available.

Using the response of aquifers to earth tides as a means of estimating aquifer characteristics has good potential, particularly in areas where pump tests cannot be run. Ideally, however, since the method does involve a number of assumptions (as do pump test analyses), and since it provides information that is often complementary as well as overlapping with that obtained from the pump test, both types of tests should be run. Similar values from the two methods could give us considerably more confidence in the results than either method alone, since the methods are independent of one another.

REFERENCES CITED

Arditty, P. C., and Ramey, H. J., Jr., 1978. Response of a closed well-reservoir system to stress induced by earth tides. 53rd Ann. Fall Tech. Conf. and Exhib., SPE of AIME, Houston, TX, October 1-3, paper 7484.

Bodvarsson, G., 1970. Confined fluids as strain meters. 1970. J. Geophys. Res., v. 75, no. 4, p. 2711-2718.

Bredehoeft, J. D., 1967. Response of well-aquifer systems to earth tides. J. Geophys. Res. v. 72, no. 12, p. 3075-3087.

Domenico, P. A., 1972. Concepts and models in groundwater hydrology, New York, McGraw-Hill.

Skempton, A. W., 1954. The pore pressure coefficients, A and B. Geotechnique, v. 4, p. 143-147.

PROBABILISTIC SIMULATION OF TRANSIENT SUBSURFACE FLOW USING A NUMERICAL SCHEME

T. N. Narasimhan and T. Buscheck

INTRODUCTION

Long-term decision-making tasks in regard to the hydrogeologic environment have to rely heavily on outputs from mathematical models. However accurate the computational scheme may be, the model output has only limited reliability due to uncertainties inherent in the input data and parameters. It is now being increasingly well recognized that a quantitative appreciation of the output uncertainty is of great practical value in arriving at optimal decisions. As a result, several workers are turning their attention to incorporating parameter uncertainty into the computational model in such a manner as to obtain confidence limits on the model output.

OUTLINE OF STUDY

The purpose of this study is to develop a probabilistic model to simulate the flow of fluids through porous media. It is important to clarify the distinction between stochastic (or probabilistic) and deterministic models. Clark (1973) made this distinction in terms of hydrologic modeling.

A system can be defined as a set of physical processes which convert an input variable (or variables) to an output variable (or variables). A variable is a characteristic of the system which can be measured and which assumes different numerical values at different times. A variable is differentiated from a parameter, which is a quality characterizing the system that does not change with time. In hydrologic modeling one must be able to mathematically model the relationships between hydrologic variables that describe the system's behavior.

A model is defined as stochastic or deterministic depending on whether or not it contains random variables. In the case where any of the input or output variables have a probability distribution, the model is stochastic. One possible source of a probabilistic structure for an output variable could be a probabilistic distribution of one or more of the parameters.

The stochastic model developed in this study makes use of a well-defined probabilistic structure. The probabilistic distribution is modeled by discrete values. Each of these values (or magnitudes) has associated with it some probability of occurrence. For any given frequency distribution, the sum of the probabilities corresponding to each discrete value must equal 1.0. Given a probabilistic distribution, one can generate any number of discrete values and their associated probabilities using a graphical technique. The accuracy of modeling a well-defined probabilistic structure will improve with the number of discrete values chosen. Each probabilistic distribution is therefore modeled by a determined number of pairs of values, a discrete value for the magnitude and its associated probability. These probabilistic structures represent the inherent uncertainty of the variable or parameter in question.

As pointed out by Freeze (1977), the applied sciences of groundwater hydrology, soil physics, and soil mechanics make use of mathematical solutions to deterministic models of flow through porous media. These models make the assumption that individual soil layers and geologic formations are uniformly homogeneous. Even when numerical mathematical models are used for complex heterogeneous systems, the heterogeneities describe the differences in parameter values among various layers, not within an individual layer. At some scale, it is tacitly assumed a single number can be assigned to each hydrogeologic parameter within some spatial geologic unit.

It is generally accepted, however, that there is physically no such entity as a truly uniform and homogeneous geologic unit. Single-number representations or deterministic predictions involve uncertainties because of inherent nonuniformity of porous media as well as the uncertainty of measure-

ment. This study considers the effect of modeling such uncertainties with stochastic parameters. Stochastic modeling allows one to study the properties of statistical distributions of the output variables that result when input parameters are modeled with probabilistic distributions.

Three parameters are usually associated with hydrologic modeling: hydraulic conductivity, porosity, and compressibility. For the analysis of one-dimensional, steady-state, saturated flow between two specified boundary heads, the equations of flow contains only one hydrogeologic parameter, hydraulic conductivity. It is this parameter that is stochastically modeled in this work.

Strong field evidence indicates that the probability density function for hydraulic conductivity is usually log normal. Using this evidence, and given a mean value and standard deviation for a typical rock or soil, the lognormal distribution for hydraulic conductivity is modeled as outlined above.

ACCOMPLISHMENTS

During fiscal year 1979, a theoretical basis was developed, based on axiomatic foundations of probability theory, to define the meaning of algebraic operations involving two-probability distributions. A computer algorithm was then successfully developed to implement the algebra of distributions. Briefly stated, the algorithm works as follows. Suppose we have two random variables, A and B, with distributions specified as histograms with N discrete values and associated probabilities. That is, we are given A_i, $P(A_i)$, B_i and $P(B_i)$, $i = 1,2,3,\ldots N$ where A_i and B_i denote the magnitudes of the ith component of each variable while $P(A_i)$ and $P(B_i)$ denote the associated probabilities. Obviously we have

$$\sum_{i=1} P(A_i) = \sum_{i=1} P(B_i) = 1 \quad . \tag{1}$$

Suppose we now wish to add the two distributions to obtain their sum in the form of a third variable C_i with associated probabilities $P(C_i)$. To find C, we will proceed as follows:

$$C'_{ij} = A_i + B_j, \quad i = 1,2,3,\ldots N \qquad j = 1,2,3,\ldots N \tag{2}$$

where C'_{ij} is the outcome if events A_i and B_j were to be realized simultaneously. According to the axiomatic foundations of probability theory, the probability of events A_i and B_j occurring simultaneously is:

$$P(C'_{ij}) = P(A_i)\, P(B_i) \tag{3}$$

and

$$\sum_{i=1}^{N} \sum_{j=1}^{N} P(C'_{ij}) = 1 \tag{4}$$

Thus, the outcomes C'_{ij} constitute N^2 discrete values and associated magnitudes. In order that the computational efforts are reasonable, we would now like to have the variable C'_{ij} expressed as an equivalent variable C_i with N discrete values rather than the N^2 discrete values of the former. This we now achieve by dividing the range min C'_{ij} to max C'_{ij} into N equal intervals. The mean magnitude C_i of the ith interval ($i = 1,2,3,\ldots N$) denotes an appropriate average for that interval. For example, it can either simply be the midpoint of that interval, or, as we have done, it could be a weighted average of all the C'_{ij} values falling within that interval. The probability associated with that interval C_i is the sum of the probabilities of all the C'_{ij}'s falling within that interval. These procedures have been incorporated into a subroutine called PRODIST for implementing equations (1) and (2) and a subroutine called COLAPS to go from N^2 values of C'_{ij} to N values of C_i.

WORK PROPOSED FOR FISCAL YEAR 1980

The aforesaid routines will be incorporated into computer program TERZAGI, which solves groundwater flow problems in ratinated, multidimensional systems. Using TERZAGI in the explicit mode so that independence between potential changes between adjoining subdomains during a given time step is assured, we propose to apply this model to some simple one- and two-dimensional problems. We will also verify our results against the Monte Carlo simulations by Freeze (1975).

REFERENCES CITED

Clarke, R. T., 1973. A review of some mathematical models used in hydrology, with observations on their calibration and use. J. of Hydrol., v. 19, pp. 1-20.

Freeze, R. A., 1975. A stochastic conceptual analysis of one-dimensional groundwater flow in nonuniform homogeneous media. Water Res. Res., v. 11, no. 5, pp. 225.

Freeze, R. A., Probabilistic one-dimensional consolidation. Journal of Geotechnical Engineering Division, v. 103, no. GT7.

A NOTE ON VOLUME AVERAGING

T. N. Narasimhan

INTRODUCTION

In characterizing fluid flow in subsurface systems through such devices as fluid potential, Darcy's Law and storativity, one implicitly assumes statistical uniformity on a macroscopic scale. In this context, the notion of "point" value, such as porosity, density, pressure and so on, actually implies an average evaluated over an appropriately small region to which the point of interest is interior. A fundamental appreciation of the power, as well as the limitations, of the equations governing subsurface fluid flow therefore requires a proper appreciation of the manner in which various physical quantities are related to volume-averaging.

EXTENSIVE AND INTENSIVE PROPERTIES

Fundamental to volume-averaging is the distinction between extensive and intensive properties. Extensive properties (e.g., mass, energy, and volume) are such that their magnitudes are dependent on the size of the regions they occupy. Intensive quantities, on the other hand are independent of the size of the region they occupy. They denote the concentration or the intensity of an extensive property and frequently constitute potentials. Intensive properties may either by volume-normalized (e.g., porosity, density, concentration) or mass-normalized (e.g., temperature). A fundamental difference between the two is that the former possess the "additive" property while the latter does not. That is, the total mass or energy contained in two distinct regions is equal to the sum of the mass or energy contained in the two regions. A corollary statement is that mass or energy can exist if and only if space is available for them to occupy.

The physical reality of the mathematics of integration stems from the additivity property of the extensive property. In the theory of integration, the mathematical equivalent of the extensive property is the "measure" which is a set function possessing the additive property. The magnitude of a measure is zero over a null set. Both mass and energy are defined over a set of spatial points and are measures.

VOLUME AVERAGING

Given the spatial distribution of an intensive quality over a subset of space, the aim of volume-averaging is to evaluate a macroscopic average value of the property over the given subset. This is to be achieved by integrating the property over the subset of interest in some meaningful fashion and normalizing the sum by the volume of the subset. That is,

$$\langle\psi\rangle = \frac{1}{V}\int_V \psi dV \qquad (1)$$

where ψ is an intensive quantity.

If the above procedure is to be physically realistic, then, the integrand dV must be an extensive property or a measure. While many intensive properties such as porosity and density satisfy the requirement that ψdV be additive, there exist several other intensive quantities which do not satisfy that requirement. In order to accomodate all intensive quantities within the folds of a single definition, we introduce the notion of a "capacity" function and rewrite (1) as,

$$\langle\psi\rangle = \frac{1}{V\langle c\rangle}\int_V c\psi dV \qquad (2)$$

where c is the capacity function.

If equation (2) were to be used for defining average temperature, then c is volumetric specific heat. If ψ denotes fluid pressure in the porous medium, then c denotes the compressibility of the solid-fluid porous complex. For a given combination of extensive and intensive quantities (e.g., heat and temperature; fluid mass and fluid pressure) the corresponding capacity function denotes the rate of change of the former with reference to the latter.

As shown in other papers (Narasimhan, 1978, 1980), equation (1) is strictly valid only in steady-state systems or in homogeneous materials with constant capacity. From a generalized perspective, indiscriminate extension of (1) to transient problems can lead to erroneous results or conclusions.

VOLUME-AVERAGING AND MATHEMATICAL MODELING

The basic task of mathematical modeling in dealing with subsurface fluid flow is to simulate the observations made in the real world through a computational mode. The success of simulation depends very much on the manner in which physical observations and volume averages are placed in mutual correspondence with each other.

Within the computational model, the computed volume averages are associated with a discrete point interior to the subset of integration. The potential gradients that exist between these discrete points provide the driving force for subsurface fluid movement. A very important question that requires resolution concerns the conditions under which the volume-average assigned to the spatial point will match the physical obseration made at the real location corresponding to the spatial point of interest. Analysis (Narasimhan, 1980) seems to indicate that for homogeneous materials with constant properties, the above match will be obtained when the intensive property of

interest varies linearly over the subdomain of interrest. This linearity requirement, coupled with the importance of the capacity function strongly suggest that there is a need to reassess some of our current notions in regard to numerically solving transient fluid flow in heterogeneous porous media.

REFERENCES CITED

Narasimhan, T. N., 1978. Perspective on numerical analysis of the diffusion equation. Advances in Water Resources, v. 1, no. 3., pp. 147-155.

____, 1980. A note on volume averaging. Advances in Water Resources (in press).

GROUNDWATER MODELING IN SUBSURFACE NUCLEAR WASTE DISPOSAL—AN OVERVIEW

T. N. Narasimhan

INTRODUCTION

The role of groundwater modeling in subsurface nuclear waste disposal technology consists of (1) analyzing regional groundwater flow in order to select a site with maximum path-length and travel-time to the biosphere; (2) evaluating the perturbation caused to the regional flow by the repository; and (3) studying the transport of radioactive contaminants to the biosphere over tens or even hundreds of thousands of years. This paper attempts to assess the ability of existing models to simulate realistic problems of groundwater flow and contaminant transport. Toward this end, the governing equations will first be given, followed by a brief description of the computational methods used to implement the governing equations. Finally, the various difficulties that challenge the credibility and effectiveness of the models will be examined.

GOVERNING EQUATIONS

For studying long-term effects, thermal phenomena can be ignored and two types of conservation equations, one for flow of water and one for each of the chemical species transported must be considered. For an appropriately small, arbitrarily shaped macroscopic volume element, the conservation equations are:

Fluid Flow

$$G_W(\Psi,t) + \int_\Gamma \rho_W(\Psi)\,\frac{k_{ij}(\Psi)\rho_W(\Psi)\,g}{\mu}\,\frac{\partial}{\partial x_j}\,(z+\Psi)\;d\Gamma = M_c(\Psi)\,\frac{D\Psi}{Dt}\,, \qquad (1)$$

where G_W is the mass of water generated, Γ is the closed surface bounding the element, ρ_w is the water density, k_{ij} is the permeability tensor, g is gravity, μ is viscosity, z is elevation, Ψ is pressure head, and M_c is fluid mass capacity (Narasimhan and Witherspoon, 1977).

Solute Transport

$$\underbrace{G_s(c,t)}_{source} + \underbrace{\int_\Gamma (-\bar{q}\cdot n d\Gamma)\bar{c}_\Gamma}_{advection} + \underbrace{\left\{\begin{array}{l}\int_\Gamma (-\tilde{q}\cdot n d\Gamma)\tilde{c}_\Gamma \\ \int_\Gamma D_{ij}\frac{\partial c}{\partial x_j}\,d\Gamma\end{array}\right\}}_{hydrodynamic\ dispersion} + \underbrace{\int D^*_{ij}\,\frac{\partial c}{\partial x_j}\,d\Gamma}_{molecular\ diffusion} = V_w\,\frac{Dc}{Dt}\,, \qquad (2)$$

where G_s is mass of solute generated due to chemical changes; $\bar{q}$ is the average (Darcy) velocity; $\bar{c}_\Gamma$ is mean concentration over $d\Gamma$; $\tilde{q}$ and $\tilde{c}$ are measures of the deviations from $\bar{q}$ and $\bar{c}$ over $d\Gamma$; D_{ij} is hydrodynamic dispersion tensor; D^*_{ij} is the molecular diffusion tensor; and V_w and c are volume of water contained in, and the average concentration over, the volume element. In (2) advection is handled in terms of the average quantity, $\bar{q}$. Due to the variability of fluxes within pores along $d\Gamma$, convective mixing occurs at a microscopic level causing conentration profiles to spread. Numerous workers have treated such spreading effects as an equivalent macroscopic diffusion process through the hydrodynamic dispersion coefficient D_{ij} which is a function of $\bar{q}$. Equations (1) and (2) are subject to boundary and initial conditions. With suitable assumptions, the two equations can also be extended to fractured media.

MATHEMATICAL MODELS

For applying (1) and (2) in a most general fashion, numerical methods are preferable to analytical methods. The theme of numerical methods is to partition the flow domain into an appropriate number of subdomains and apply the conservation equations to each subdomain, subject

to compatibility of fluxes and potentials between neighbors. The subdomains could be explicitly defined [integrated finite difference method (Narasimhan and Witherspoon, 1976)] or implicitly defined [method of weighted residuals (Finlayson, 1972; Narasimhan, 1978)]. Critical to the evaluation of the integrals in (1) and (2) are the mean concentrations c_Γ and the gradients $\partial\Psi/\partial x$ and $\partial c/\partial x$ at the interface $d\Gamma$. These could be evaluated using simple finite differences or using the more general finite element techniques (Gray and Pinder, 1976). Because pure advection does not involve mixing, the concept of averages used in (1) and (2) can lead to spurious "numerical dispersion" in advection-dominated systems. While some workers (e.g., Chaudhary, 1971; Gray and Pinder, 1976) have overcome this problem through correction factors, improved gradient approximations, and other artifices, others have used alternate approaches such as the method of characteristics (Pinder and Cooper, 1970) or random-walk techniques (Ahlstrom et al., 1977) to handle advective transport.

CHALLENGES TO MODELING

Despite active research, the credibility of groundwater models for long-duration predictions of natural systems is yet to be firmly established. The challenges in this regard stem from (1) the gaps between the physical system and the conceptual model, (2) the gaps between the conceptual model and the computational model, and (3) the difficulties associated with the computational procedure itself. In regard to (1), some workers have questioned the validity of the dispersion coefficients to quantify the mixing phenomena observed on porous media. As for (2), flow and transport in geologic systems are approximately ordered phenomena in an essentially disordered geometry (Philip, 1973). All model parameters are therefore subject to uncertainties due to the size of the portion of flow region sampled by the measuring device and the number of samples taken. As a result, one has not only to specify beforehand the scale of monitoring but also to obtain sufficient population of field data to assure confidence in the model output. Computationally, problems exist with respect to minimizing integration errors, handling discontinuities and so on. In addition, considerable difficulties exist in handling the interaction of statistical quantities that are mutually dependent or correlated.

It appears that many of the computational difficulties can be overcome by improved solution strategies. However, the basic problems related to parameter uncertainties may continue well into the future.

REFERENCES CITED

Ahlstrom, S.W., Foote, H.P., Arnett, R.C., Cole, C.R., Serne, R.J., 1977. Multi-component mass transport model: theory and numerical implementation (discrete-parcel-random walk version). Richland, Washington, Battelle Pacific Northwest Laboratory.

Chaudhary, N.M., 1971. An improved numerical technique for solving multidimensional displacement equations. Society of Petroleum Engineers Journal, v. 11, p. 277-284.

Finlayson, B.A., 1972. The method of weighted residuals and variational principles. New York, Academic Press.

Gray, W.G., and Pinder, G.F., 1976. An analysis of the numerical solutions of the transport equation. Water Resources Research, v. 12(3), p. 547-555.

Narasimhan, T.N., 1978. A perspective on numerical analysis of the diffusion equation. Advances in Water Resources, v. 1(3), p. 147-155.

Narasimhan, T.N., and Witherspoon, P.A., 1976. An integrated finite difference method for analyzing fluid flow in porous media. Water Resources Research, v. 12(1), p. 57-64.

——, 1977. Numerical model for saturated-unsaturated flow in deformable porous media: Part I, Theory. Water Resources Research, v. 13(3), p. 657-664.

Philip, J.R., 1972. Flow in porous media, in Proceedings, 13th Intl. Cong. Theor. and Appl. Mech., Moscow. Amsterdam, Springer-Verlag.

Pinder, G.F., and Cooper, H.H.,Jr., 1970. A numerical technique for calculating the transient position of the salt water front. Water Resources Research, v. 6(3), p. 875-888.

ROLE OF PORE PRESSURE ON DEFORMATION IN GEOLOGIC PROCESSES

T. N. Narasimhan

SUMMARY

Water is known to occur even at great depths in the earth's crust. Due to its slight compressibility as well as to capillary action, water exerts fluid pressure on the pores containing it, thereby modifying the existing state of stresses on the rock matrix. The contrast that exists between the deformation properties of the rock and the fluid, the modification of the stress field by the fluid pressure, and the continuous changes in fluid pressure induced by the dynamics of flowing groundwater contribute profoundly to the deformation behavior of the geologic systems.

The importance of understanding the deformation behavior of fluid-permeated geologic systems is readily apparent in more than one context: the development of oil, gas, water, and geothermal resources; the cause and the modification of earthquakes; the utilization of soil or rock masses to support engineering structures; the response of the earth's crust to electrical and mechanical waves; the formation of hydrothermal ore deposits, and others.

Scientists and engineers in many disciplines are actively striving toward a better understanding of the physical mechanisms that govern the

deformation behavior of geological systems subjected to the ubiquitous influence of water. With a view to bringing together the current ideas and observations on this important natural phenomenon, a Penrose Conference, sponsored by The Geological Society of America, was convened by the author with W. N. Houston of the University of California, Berkeley, and Amos Nur of Stanford University as co-conveners, during November 9-13, 1979, at San Diego, California.

The conference was strongly interdisciplinary and drew participants from the following fields: structural geology and geophysics, hydrogeology, geotechnical engineering, geochemistry, rock mechanics, applied mechanics, and ocean engineering. In keeping with the Penrose ideals, the conference provided an excellent forum for a free exchange of ideas among the participants, and generated new research contacts.

This report is a brief summary of the conference highlights. During the conference, a collection of important reprints, textbooks, and reports on the conference subject matter was assembled for the participants' benefit. In response to participants' suggestions, a list of these references has been prepared for distribution. Those interested in obtaining a free copy may contact the first author. Although the conference was essentially self-supporting, partial financial support was provided by the Earth Sciences Division of the Lawrence Berkeley Laboratory.

The discussions of the conference concentrated on the following general areas: effective stress laws; stress-strain relations; seismicity and pore pressure; hydraulic fracturing and geopressured systems. Most of the main points covered in the various sessions are discussed below.

Perhaps the most significant feature that sets apart a fluid-filled porous medium from a dry one, insofar as deformation is concerned, is that fluid pressures acting outward from within counter the external stresses acting inward. Inasmuch as matrix deformation is governed strictly by the stresses borne by the matrix, and since the hydrodynamics of fluid flow is governed by fluid pressure, a constitutive relation is a priori imperative if one is to couple fluid flow and skeletal deformation in a general conceptual framework. The notion of an effective stress, originally proposed by Terzaghi more than 50 years ago, provides the basis for such a constitutive relation. Although there is little dispute about the general concept of effective stress, there still appears to exist many a question about the specific, quantitative meaning of this quantity, as was evident from the deliberations of the first two conference sessions.

It was pointed out that there is no unique effective stress law or relation satisfying all mechanical properties, and that an effective stress law may not be needed if a given property is known for any combination of total stress and pore pressures. Some of the questions raised relevant to the effective-stress concept included: What are the limits of the simple effective-stress relation proposed by Terzaghi, $\sigma' = \sigma - P$? How important are physical-chemical forces of interaction? Can the state of a soil be uniquely defined by void ratio, effective stress, and overconsolidation ratio? What happens to effective stress when temperature changes or phase transformations occur? What is the correct relation when more than one fluid phase is present?

Following the discussions on effective-stress relations, theoretical developments were presented for the elastic as well as nonelastic response of fluid-saturated porous media. The possibility of applying the theory to such problems as flow in abnormally pressured systems, suddenly pressurized cavities, growing tensile cracks, and suddenly introduced dislocations were discussed. The derivations carried out for isotropic linearly elastic materials included undrained as well as drained responses and showed that the single Terzaghi relation is strictly valid only for plastic deformation.

From a practical standpoint, one of the most intriguing questions of fundamental interest is the maximum depth to which interconnected pore spaces exist, facilitating deep circulation of groundwater. Indirect evidence, based on electrical resistivity measurements, seems to suggest that circulation may persist down to a depth of 20 km. Permeabilities of the order of a nanoDarcy or higher have been inferred to exist down to a depth of 10 km through earthquake, isotope, and heat flow studies.

A variety of experimental results were presented and discussed in relation to the stress-strain behavior of fluid-saturated rocks. Some of these experimental results suggested that in some rocks (e.g., Cosco Granite) the bulk modulus is sensitive to saturation while in some others (e.g., Solenhofen limestone) it may not be; in clayey sandstones, permeability may be more sensitive to pore fluid pressure than effective stress; in certain fault-gouge materials, permeability is related to strain rate, and this material may exhibit strain-hardening properties with increasing sand fraction. Pressure solution effects may be important in certain joints subjected to nonhydrostatic stresses.

The phenomenon of earthquake instability is basically related to frictional sliding along a fault plane. A large number of laboratory experiments have indicated that the shear strength of fractures is related to the normal stress by the approximate relation, $\tau \approx 0.85\sigma'$, $\sigma' > 2$ kb, and $\tau \approx 0.5 + 0.6\sigma'$, $\sigma' \geqslant 2$ kb. If, because of pore pressure rise, σ' is so diminished that falls below the shear stress in situ, the resulting sliding should lead to seismicity. This appears to be an adequate model for seismicity, provided that we can reasonably predict the time-dependent variation of pore pressures leading to a progressive decline in normal effective stresses. A principal concern is therefore the permeability of the in situ material and the factors that influence its change. Experimental evidence indicates that the presence of compressible clayey materials in fractures considerably influences the permeability versus effective stress relation. Thus, permeability is related generally to $(\tau - \alpha p)$ with $\alpha < 1$ for clean fractures and $\alpha < 1$ for fractures with clay. A knowledge of these

properties at hypocentral depths is essential to predict induced seismicity.

That fault movement occurs as the pore pressure exceeds a critical value causing frictional sliding was demonstrated in the case of the Rangely earthquakes through the use of mathematical simulation of the hydrogeologic system. In this case there was a definite correlation between the frequency and location of the earthquakes and the local fluid pressures.

Considerable research activity is currently in progress in studying reservoir induced seismicity. Among the carefully collected data at these sites are included: the measurement of in situ stress, permeability and fracture characteristics, and the monitoring of earthquake loci and magitudes. Depending on the permeability of the in situ rocks, the time-lag between lake filling and seismicity may vary from a few months to as many as several years. It is quite probable that the migration of pore pressure transients is critical to induced seismicity. Is there a reasonable chance of modeling the phenomenon accurately enough to achieve reliable prediction? An outstanding problem still defying solution is that of predicting earthquake magnitudes.

While the factors that cause seismicity are important for earthquake prediction, it is equally essential to study those factors which help mitigate earthquake hazards. Over the past decade, geotechnical engineers have established that abnormal pore pressure generation in shallow, cohesionless soils leads to soil liquefaction. Indeed, the study of many earthen dams and foundations subjected to strong earth motions shows that abnormal pore-pressure generation commonly accompanies cyclic loading in alluvial soils and earth structures. Experimental study of pore pressure generation using shaking tables simulating cyclic loading is therefore a very active area of research. Theoretical studies as well as experimental results from shaking table experiments were presented and discussed.

It was noted that in situ stress measurements are of great importance in delineating areas of potential seismicity. The technique of measuring stress in situ using hydraulic fracturing is extensively employed. In addition, hydraulic fracturing is also beneficially employed to stimulate low-permeability reservoir rocks to augment production of oil, water and geothermal fluids.

The nature and disposition of hydraulic fractures depend on the orientation of the local principal stresses, the toughness of the rock, and the fluid pressure gradient within the fracture. Assuming elastic properties for the crack, theoretical relations have been developed to distinguish conditions of stable and unstable fracture growth. Theoretical analysis has also been performed to study the growth of long, elliptical cracks, and the controlling parameters. Field and laboratory studies indicate that the rate of fluid pressurization is important in controlling fracture disposition. Rapid pressurization favors vertical fractures while slow pressurization leads to horizontal fractures.

The technique of hydraulic fracturing is undergoing development in terms of both hardware and interpretive techniques. The interpretation of pressure transient data from hydraulic fracturing tests is particularly involved due to the presence of well compliance effects, as well as the time-dependent variations in fracture geometry, aperture, and stiffness. The successful application of a numerical model towards interpreting an actual field test and the estimation of the minimum principal test was presented. Whether powerful mathematical models can help improve the design of hydraulic fracturing tests appears to be a fruitful area of inquiry. Perhaps the most important field problem in hydraulic fracturing at the present time is that of determining the maximum principal stress, since it is the difference between the maximum and minimum stresses that governs frictional sliding.

In the foregoing discussions, the main emphasis was placed on the mechanical aspects of pore-pressure generation and the interaction between pore pressure and skeletal stresses. However, in certain geological environments, chemical effects can act in conjunction with mechanical effects and contribute greatly to the creation of anomalously high pore pressures. The following mechanisms are believed to contribute to abnormally high pressures: aquifer head due to natural recharge, "fossil" head due to exhumation and erosion, tectonic compression, rapid loading and compaction, influx of juvenile water, gas infiltration, mineral dissolution or precipitation, phase changes (gypsum ↔ anhydrite, smectite ↔ illite, heavy hydrocarbon to light hydrocarbon), expansivity to temperature changes, and osmotic (clay-membrane) phenomena. There were considerable discussions as to which of the aforesaid mechanisms was the most dominant in geopressured systems. The phenomenon of nonequilibrium compaction, that is rapid deposition without adequate time for drainage, is perhaps the most dominant of all the mechanisms. In this mechanism, the role of permeability is very important. If rapid burial is accompanied by reduction in permeability due to precipitation and related effects, abnormal pore pressures are augmented. Among the other mechanisms, mineral-phase transformations, aquathermal effects, and osmotic effects are probably the most significant, in general.

CONCLUSIONS

It became obvious from the lively discussions and the diversity of presentations, that the role of pore pressure in geological deformation processes is not only an important area of investigation, but is emerging as a broad, all-encompassing one. Many of the vital or critical problems society faces today--resource exploration, evaluation recovery, earthquake hazards, and ground stability, to name the more important ones--are linked to the role of pore pressure. Although our understanding of the intricate behavior of geological material and the interaction between physical and chemical processes in the presence of pore fluids is far from adequate, the conference did show that we are rapidly gaining understanding of what the

important problems are--a first step to solving them. We all agreed that a great deal of new active research in the area of pore pressure is to be expected and encouraged in the coming decade.

AN ANALYTIC STUDY OF GEOTHERMAL RESERVOIR PRESSURE RESPONSE TO COLD-WATER INJECTION

Y. W. Tsang and C. F. Tsang

Introduction

Many authors have studied various aspects of the reinjection of cooled geothermal water into a geothermal reservoir. One consideration of practical relevance is the calculation of the pressures required for reinjection. These pressures determine the pumping requirements that are important inputs to the technical and economical feasibilities of the project. The pressures may also be used as baseline data. If, for example, the measured pressure becomes much greater with time than the calculated values, some kind of plugging may be occurring, and remedial action would have to be taken.

For isothermal cases where the injected water is at the same temperature as the reservoir water, the pressure change is simply given by the Theis solution in terms of an exponential integral. The solution shows that this pressure change is directly proportional to the viscosity, with viscosity a strong function of temperature. From 100°C to 250°C, the viscosity changes by a factor of 3 (whereas the density of water changes by about 20%).

The injection of cold water into a hot reservoir is a moving boundary problem. On the inside of a boundary enclosing the injection well, the parameters correspond to that of the injected cold water; on the outside, the parameters correspond to those of the reservoir hot water. Due to heat conduction between the hot and cold water, the boundary is, of course, not sharp. The width of the boundary depends on the aquifer heat conductivity and capacity, and it increases with time as the boundary (or cold temperature front) moves outward from the injection well.

There exist numerical models to solve such a problem. In earlier work, we made a simple study using the numerical model CCC developed at Lawrence Berkeley Laboratory. A sample of calculated results is shown in Figure 1. The present work is an analytical calculation of such a problem when several approximations are applied. Solutions are obtained in terms of well-known functions or in terms of one integral. These calculations are checked against numerical model results.

Mathematical Approach

Three equations — the equation of continuity, Darcy's equation, and the equation of state — are combined into one governing equation in radial symmetric coordinates, in which viscosity (μ) and density (ρ) are assumed to be dependent variables. Applying the Boltzman transformation and the boundary condition of constant line-source flow rate Q at the injection well, one obtains, after

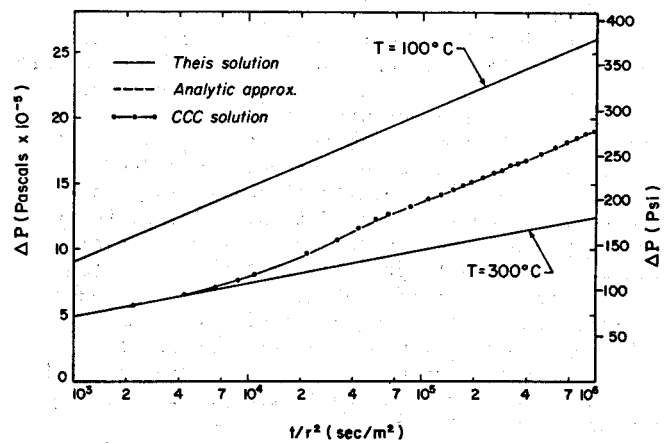

Figure 1. Pressure change at well versus t/r^2 when water at 100°C is injected into a reservoir of 300°C water. Results obtained by numerical model CCC are compared with isothermal Theis solutions. (XBL 789-2077)

some manipulation, the transient pressure P(z) as a function of $z = r^2/t$:

$$P(z) = P_o - \frac{Q}{4\pi h}\int_z^\infty \frac{1}{K(z)z}\exp\left(-\frac{c}{4}\int_0^z \frac{1}{K(z')}\,dz'\right)dz\,, \qquad (1)$$

where the parameters are h (reservoir thickness), $c = \beta\phi$ (compressibility times porosity), P_o (the initial pressure), and $K = k/\mu$ (permeability divided by viscosity value). Here K is density-dependent and, since we assume that the Boltzman transformation is possible, it is a function only of $z = r^2/t$. For our current calculations, the reservoir temperature distribution during injection is represented by a Fermi-Dirac function

$$K(z = r^2/t) = \frac{K_R - K_I}{1 + e^{-(z-d)/a}} + K_I\,. \qquad (2)$$

The function takes on the values of K_I, K_R, and $(K_I + K_R)/2$ respectively at $z = 0$, $z = \infty$, and $z = d$ (see Figure 2a). The function varies appreciably only in the neighborhood of $z = d$; the parameter a characterizes the range of z over which K(z) is appreciably different from K_I and K_R. The derivative dK/dz is a symmetrical function about $z = d$. The full-width half-maximum of dK/dz about this point may be shown to be 3.52 a (see Figure 2b). This behavior of K(z) may be understood as follows: near the wellbore, the function takes on the value of $K = k/\mu = K_I$, equal to that of injected water;

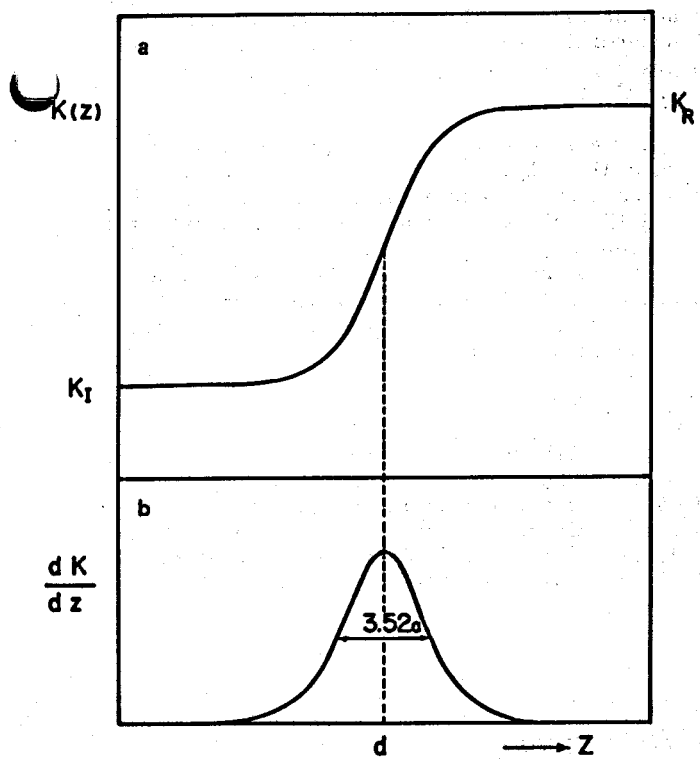

Figure 2. The function K(z) assumed in the calculations. (XBL 791-7306)

at large radial distances from the well, it takes on the value K_R, equal to that of the reservoir. With this K(z), we have

$$\int_0^z \frac{c}{4K(z')}\,dz' = \frac{c}{4}\,\frac{z}{K_R} + \frac{ca}{4}\left(\frac{1}{K_R} - \frac{1}{K_I}\right) \times \ln \frac{K_I \exp(-(z-d)/a + K_R)}{K_I \exp(d/a) + K_R} \qquad (3)$$

and

$$P(z) = P_o - \frac{Q}{4\pi h}\exp\left(\frac{-cd}{4K_I}\right)\int_z^\infty \frac{1 + \exp(-(z'-d)/a)}{K_R + K_I \exp(-(z'-d)/a)} \times \frac{1}{z'}\,\frac{[K_R + K_I \exp(-(z'-d)/a)]^{(1/K_I - 1/K_R)\,ca/4}}{\exp\left(\frac{c}{4K_R}\,z'\right)}\,dz' \qquad (4)$$

This equation is integrated numerically. Figures 3 and 4 show the variation of $P(z) - P_o$ with z for various values of d and a. Table 1 summarizes the parameters used.

Discussion

The most interesting feature of these plots is that the curve follows, for small values of t/r^2,

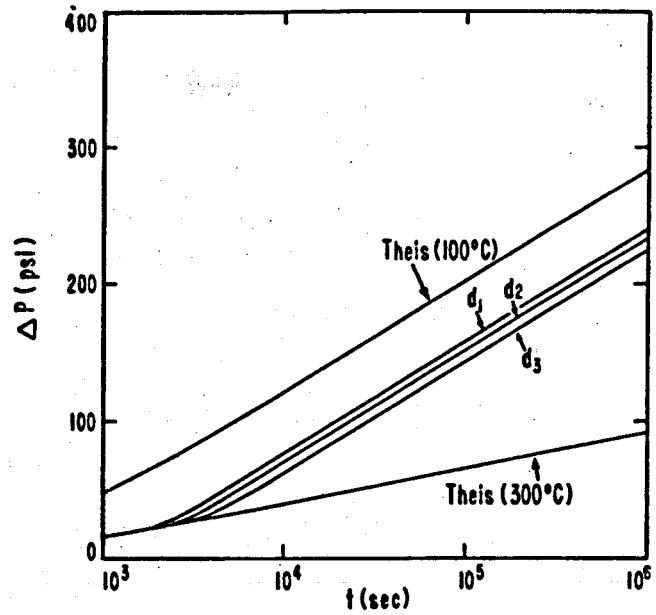

Figure 3. Analytic results of pressure change ΔP versus time t for different values of $d \propto Q/h$. (XBL 804-9357)

a Theis line with parameters corresponding to those of the native hot water, and for large t/r^2, it approaches a line parallel to a Theis line with parameters corresponding to those of the injected water. The transition occurs at $z = d$, or $t/r^2 = 1/d$, where d may be expressed in terms of the flow rate, heat capacities, and reservoir thickness. Thus injection well test data can yield the transition point d.

This additional parameter, when coupled with the two which are normally obtained (transmissivity

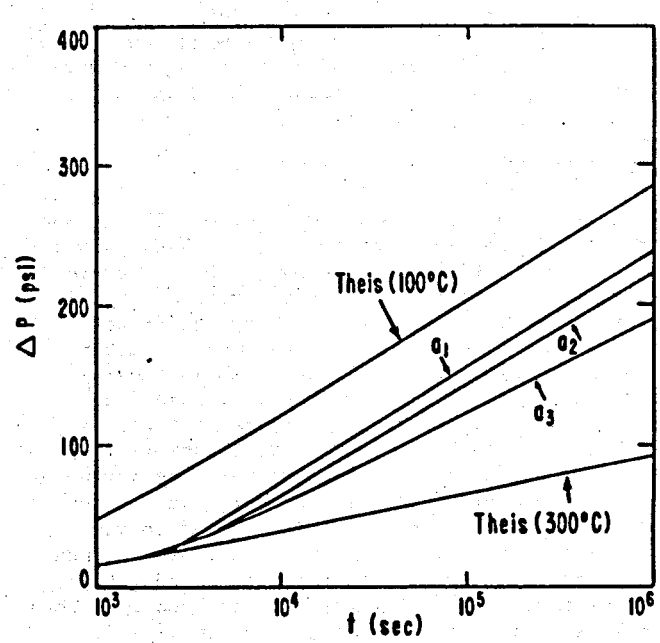

Figure 4. Analytic results for ΔP versus t for different values of $a \propto \kappa_a/C_a\rho_a$. (XBL 804-9358)

TABLE 1. Parameters used in calculations.

$$Q = 80 \text{ kg/sec}$$

$$h = 150 \text{ m}$$

$$c = \phi\beta = 1.2168 \times 10^{-8} \text{ ms}^2/\text{kg}$$

$$K(300°C) = (k/\mu)300°C = 5.4705 \times 10^{-10} \text{ m}^3\text{s/kg}$$

$$K(100°C) = (k/\mu)100°C = 1.7857 \times 10^{-10} \text{ m}^3\text{s/kg}$$

$$d = \begin{cases} 3.2568 \\ 4.2568 \times 10^{-4} \text{ m}^2/\text{s} \\ 5.2566 \end{cases}$$

$$a = \begin{cases} 0.1 \\ 1.0 \times 10^{-4} \text{ m}^2/\text{s} \\ 2.0 \end{cases}$$

kh and storativity $\phi\beta h$) affords the possibility of determining the parameters h, ϕ, and k separately, provided the heat capacities are known.

In well-test analysis, Figures 3 and 4 may be used directly. The early data first may be compared with the curve for $t/r^2 = 1/d$, yielding kh and $\phi\beta h$ values. Matching later data will give parameter d from which h may be estimated. Thus, k, $\phi\beta$, and h are evaluated. Of course, in actual field-data analysis, other possible effects (e.g., boundaries) may enter, and great care has to be exercised.

Plans for Next Year

This work will be extended to include cases of a step function and a trapezoidal function to simulate the transition in temperature between the injected cold and native hot water zones. The applications of derived formulae to practical field cases will be studied.

THERMAL EFFECTS IN WELL TEST ANALYSIS

D. C. Mangold, C. F. Tsang, M. J. Lippmann, and P. A. Witherspoon

INTRODUCTION

The effect on the pressure response due to fluid and rock temperature-dependent properties is a challenge to our ability to interpret well test results from nonisothermal reservoirs. Zones of different temperatures in the reservoir may resemble permeability boundaries, so that care in interpreting results is required (Tsang et al., 1978). In this study we examine these temperature effects on well test data in which the producing well is completed in the center of a hot zone surrounded by a concentric cooler water region. The investigation was done with a view toward comparing the results of such tests with the classical Theis solution, and discovering the ways in which temperature differences can be accounted for in well test data analysis.

ACCOMPLISHMENTS DURING FISCAL YEAR 1979

This study employed a numerical model (Lippman et al., 1977) developed at Lawrence Berkeley Laboratory called CCC (Conduction Convection, Compaction) to simulate a geothermal reservoir with a central hot cylindrical region surrounded by colder water. The program has coupled energy and mass transport equations to simulate single-phase nonisothermal saturated porous systems. Viscosity, specific heat, and density of water are properly taken as temperature-dependent properties. The program also can consider pressure and temperature-dependent rock and fluid properties in general, but for this study only water properties were allowed to vary with temperature. In particular, intrinsic permeability was held constant throughout in order to study variability due to viscosity and density alone (see Table 1 for the rock properties employed). Pure liquid water was assumed; the effects of salt solution of a 3 wt% brine in our present problem are negligible (see below). This model has been validated against a variety of analytical and semi-analytical solutions, as well as field data (Mangold et al., 1978; Tsang et al., 1977, 1980).

STUDY OF THERMAL EFFECTS IN WELL TEST ANALYSIS: 100 m ANOMALY

In this case, the temperature within the cylindrical geothermal anomaly is 250°C; the remainder of the simulated region is at 100°C. When the usual semilog plot of ΔP versus log time is made, the slope, m, of the straight line will reflect the influence of the temperature on the water viscosity, μ, and the mass flow rate, q, due to changes in water density, ρ:

$$m = 0.183234 \frac{qB\mu}{\rho kh}$$

Table 1. Properties of the aquifer used in the simulations.

Thickness, h (m)	50
Porosity, ϕ	0.1
Intrinsic Permeability, k ($10^{-3}\,\mu\,m^2$)	29
Specific Storage Coefficient, S_s (m^{-1})	3.9×10^{-5}
Density, ρ_a (kg/m^3)	2650
Heat Capacity, C_a (J/kg·K)	970
Thermal Conductivity, K_M (W/m·K)	2.8935

For early times, the slope should reflect the values of μ and ρ for 250°C. However, after the influence of 100°C region is felt, the slope will change. Since the viscosity ratio of the water at these two temperatures is 1:2.6, and the fluid density ratio is 1:0.83, the combined effect from the different temperatures on the semilog slope is approximately 1:2. This is the change in slope m that would be expected in the presence of a linear permeability barrier, if the common assumption of an isothermal reservoir is made. Figure 1 shows the results from 39 days of production from the 100-m radius hot spot, and for the later times the semilog slope is evidently about twice that of the initial slope. Such a thermal effect could therefore cause a mistaken interpretation in the well test analysis.

The underlying pressure distribution for this case is seen in Figure 2, where the effect of the different temperature waters is evident. Even after a month of production, the boundary of the colder water still provides a significant change in the pressure decline curves. Furthermore, the thermal front has barely moved during these 39 days. In practice, the "moving boundary" of the thermal front would probably appear to be stationary during a well test, because the radius of an actual hot spot would likely be greater than 100 m, and the mass of fluid withdrawn would only slightly affect the position of the front. Thus, the thermal boundary would not be detectable as a moving boundary, making interpretation of this change in semilog slope even more difficult to distinguish from a permeability barrier.

THE 50 m ANOMALY: PRODUCTION FOR 120 DAYS

For the remainder of this study, a 50-m-radius hot spot was assumed, in order to investigate effects when the production period is long enough to manifest the moving boundary of the thermal front. In this case, production was continued for 120 days, that is, until all the 250°C water was extracted from the reservoir, which then was

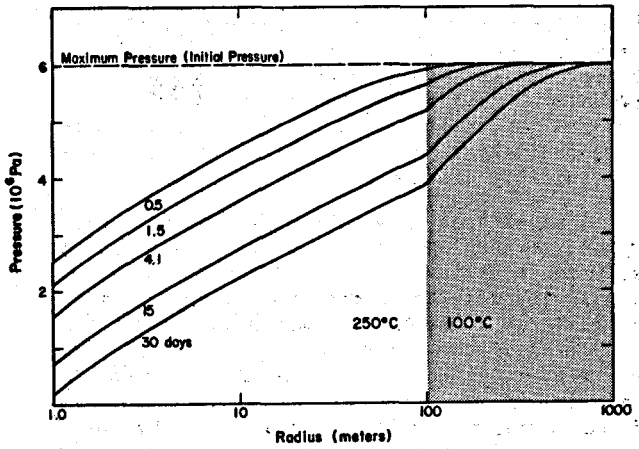

Figure 2. Radial pressure distribution for a 100-m hot spot (shaded region is 100°C). (XBL 797-7574A)

at 100°C throughout. The progression in pressure change from the initial hot spot condition to the end is shown in the semilog plot of Figure 3, where there are several discernible periods of different response. During the earliest times (up to nearly 0.5 day) the pressure follows the 250°C Theis behavior, as expected. There follows a transition time (from 0.5 to 2 days) where the curve shifts to run parallel to the 100°C Theis curve, but still below it in magnitude (from 2 to 20 days). Then the curve again shifts upward (20 to 60 days) until the temperature front begins to reach the observation well. At this point the pressure changes drastically, with the curve sloping steeply upward to join the 100°C Theis curve (for times greater than 60 days) as it should, since by the end of the 120 days the entire reservoir is at 100°C.

The practical application of this "second shift" is made by locating an observation well at some distance away from the production well.

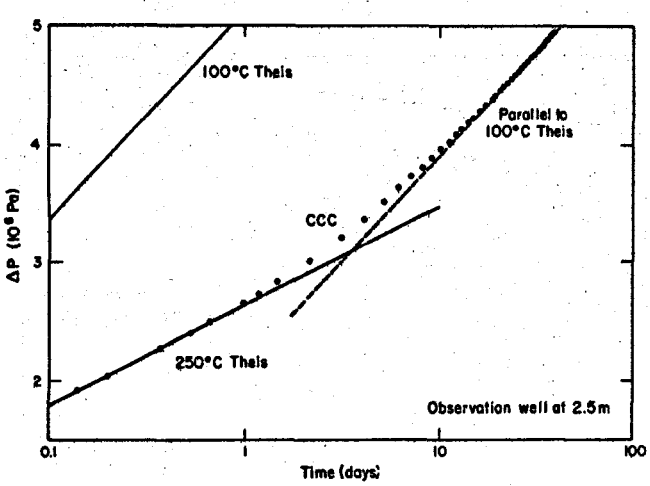

Figure 1. Drawdown curve for 100-m hot spot (r = 2.5 m). (XBL 797-7570)

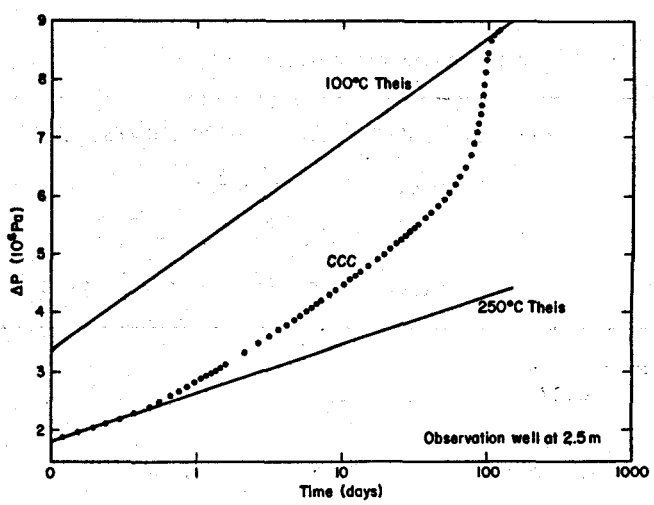

Figure 3. Drawdown history of 120 days production from 50-m hot spot (r = 2.5 m). (XBL 798-11480)

At such an observation well, the effect of the moving thermal front occurs much earlier, e.g., at approximately 15 days when observed at a distance of 19.5 m from the production well. Thus the length of time for the moving boundary to be manifested can be minimized by data taken at a suitably distant observation well.

A usual type curve matching procedure was applied to the log-log plot of r = 2.5 m data to estimate transmissivity (kh/μ) and storativity (ϕch). The results of the type curve analysis are given in Table 2. The match with the very early part of the curve yields a good estimate for kh/μ, as expected. But under such a direct analysis, if the analyst matched the later portion of the curve, he would be seriously mistaken. The estimated values for ϕch reflect the sensitivity of type curve matching, even for the early time data. Again, matching with the latest portion of the curve would lead to serious errors by direct analysis.

The progress of the temperature front is interesting to follow. In Figure 4, a sequence of curves shows how the front moves slowly at first, and quite rapidly at the end, reflecting differences in radial volume under a constant pumping rate. The diffusion of the front is very apparent. This diffusion of the temperature front may also account for some of the shifting of the pressure change data curves over the period of production.

THE 50 m ANOMALY: BUILD-UP TESTS

The build-up tests performed in this series of simulations confirm the same general behavior observed in the production tests, but the effects occur at earlier times. Figure 5 shows a Horner plot of a build-up test after 30 days of production from the 50-m hot spot of the previous section. At the earliest times the points are parallel to the 250°C analytical curve, but after less than one day the points shift toward the 100°C curve. By 5 days the pressure is already following characteristic 100°C build-up behavior.

Table 2. Theis curve matching.

50-m-radius, 250°C inside, 100°C outside $q/p = 6.0602 \times 10^{-2}$ m³/s	kh/μ (10^{-8} m³/Pa·s)	ϕch (10^{-7} m/Pa)
Early times (to 0.37 d)	1.21	4.33
Later times (from 1.50 d)	0.66	48.40
Actual value	1.36	2.50

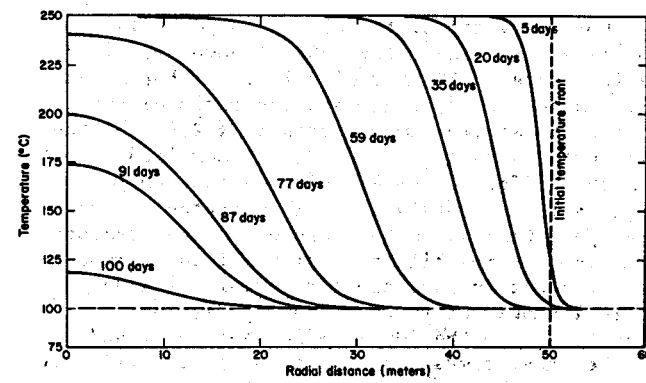

Figure 4. Radial distribution of temperature for 120 days production from 50-m hot spot. (XBL 798-11488)

REINJECTION AND PRODUCTION OF COLD WATER

In their study of cold water reinjection, Tsang et al. (1978) employed numerical model CCC to inject 100°C water into a 300°C reservoir, obtaining results such as those displayed in Figure 6. The characteristic pressure behavior noted in the previous sections for drawdown and build-up tests is also apparent here. This pattern of behavior is confirmed by the analytical solution of Tsang and Tsang (1978).

PARTIAL PENETRATION CASE

The previous sections have assumed a single layer model where there is necessarily full penetration, and gravity is not an influence. To study thermal effects in the common situation of partial penetration, a multilayered cylindrical mesh was used. The results are displayed in Figure 7.

The same general pattern of the previous sections is apparent for partial penetration. The analytical solutions are taken from Witherspoon et al. (1967), and are semilog straight lines for

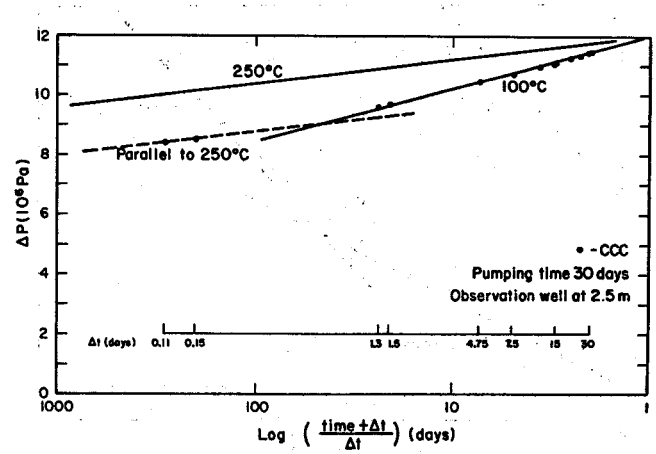

Figure 5. Buildup curves for 50-m hot spot, 250°C and 100°C (after 30 days pumping, r = 2.5 m). (XBL 798-11486)

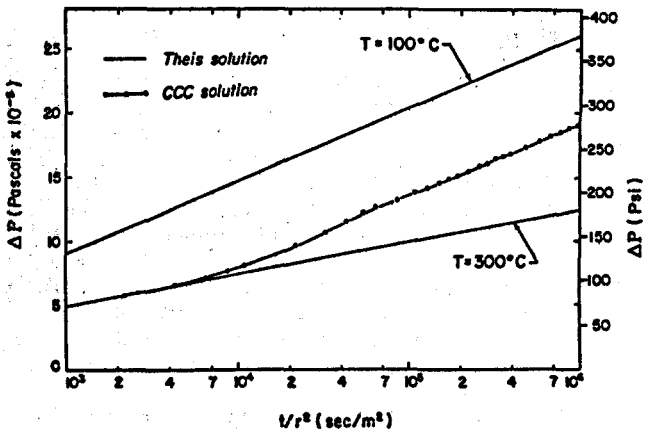

Figure 6. Drawdown curve for t/r^2 for cold water injection into a hot reservoir (log-log plot). (XBL 789-2077)

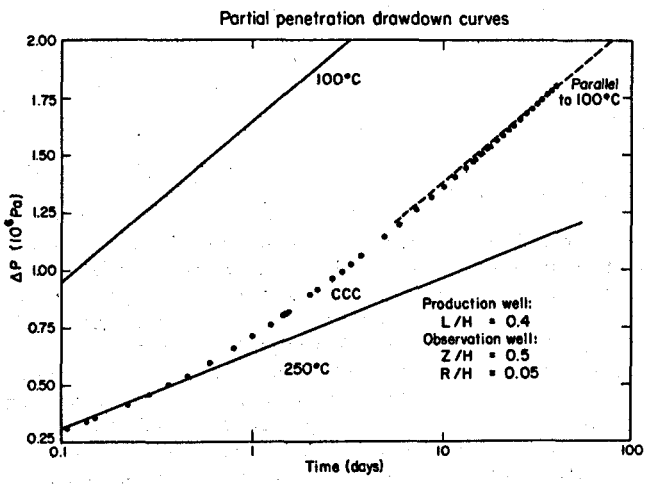

Figure 7. Drawdown curve for 40% partial penetration in 48-m hot spot. (XBL 798-11481)

the times plotted for the reservoir parameters used. This result confirms the effect of viscosity differences on the pressure response during a drawdown test, even when the well is partially penetrating.

THREE ADDITIONAL FACTORS

Three factors have a possible influence on the above results: the effects of natural convection, brine solution and a diffuse front.

To study the effect of natural convection, a simulation was performed using the partial penetration mesh of five layers under the initial temperature and pressure conditions, but with no production at the well. After 27.5 days the mass flow cycle in simulation achieved a quasi-steady-state, and no further mass flow was computed. The results were compared with analytical formulas recently derived by Hellstrom et al. (1979) for buoyancy tilting of a thermal front in an aquifer, including the effect of a diffuse front. The numerically computed flow velocity at the front was within 0.8% of the analytical solution at 27.5 days. The maximum flow velocity due to natural convection from both the analytic and numerical calculations was found to be 1.455×10^{-7} m/sec, compared with the flow velocity from pumping, which was 4.285×10^{-6} m/sec at 30 days, a factor of nearly 30:1. These results confirm that the use of a single-layer mesh for the major part of this investigation was acceptable, since natural convection should have negligible effect on reservoir pressure for the time periods considered (up to approximately 40 days).

The effect of a brine solution instead of pure water was examined using estimation formulas from Wahl (1977) for physical properties of geothermal brines. The difference in properties between a 3 wt% brine and water is negligible for ρC, and approximately 6% for μ or (k/μ). However, the error of 6% applies equally to the 250° and 100°C waters, so that the viscosity ratio remains the same. Thus, encountering a brine solution in place of pure water in a field test should not affect the results reported here.

Finally, the diffuseness of the thermal front will have an effect on the slope of the semilog plot, as shown in Tsang and Tsang (1978). According to their numerical results, the values used in this investigation should be similar to their analytical calculations (see Figure 6). Because the pressure behavior presented here does follow their reported pattern, the present set of simulations does confirm their analytical formulas for the effect of such a diffuse zone.

CONCLUSION

This paper has shown that the effects of viscosity from regions of different temperature water can appear in well test data in a way that may be mistaken as permeability barriers in some cases. This effect can be recognized by a pumping test of sufficient duration with observation wells located at a suitable distance from the production well. The questions of identifying the moving thermal boundary, applications of the method to build-up tests, and partially penetrating wells have been discussed. The possible influences of gravity and buoyancy (i.e., natural convection), water salinity, and the size of the diffuse zone have also been considered.

PLANS FOR FISCAL YEAR 1980

The present investigation can be extended to cover other cases, such as a Cerro Prieto reinjection model (Tsang et al., 1980). Further work may be done to explore other possibilities for detecting thermal effects in well test analysis.

REFERENCES CITED

Hellstrom, G., Tsang, C. F., and Claesson, J., 1979. Heat storage in aquifers: Buoyancy flow and thermal stratification problems. Lund, Sweden, Lund Institute of Technology, Department of Mathematical Physics.

Lippmann, M. J., Tsang, C. F., and Witherspoon, P. A., 1977. Analysis of the response of

geothermal reservoirs under injection and production procedures. 47th Ann. Calif. Reg. Meeting, SPE-AIME, Bakersfield, CA., April 13-15. Dallas Society of Petroleum Engineers, paper SPE-6537.

Mangold, D., Wollenberg, H., and Tsang, C. F., 1978. Thermal effects on overlying sedimentary rock from in-situ combustion of a coal seam. Berkeley, Lawrence Berkeley Laboratory, LBL-8172.

Tsang, C. F., Lippmann, M. J., Goranson, C. B., and Witherspoon, P. A., 1977. Numerical modeling of cyclic storage of hot water in aquifers. Berkeley, Lawrence Berkeley Laboratory, LBL-5929.

____, 1978. Numerical modeling studies in well test analysis, in Proceedings, 2nd Invitational Well Testing Symposium. Berkeley, Lawrence Berkeley Laboratory, LBL-8883, p. 47-57.

Tsang, C. F., Buscheck, T., and Doughty, C., 1979. Aquifer thermal energy storage--a numerical simulation of Auburn University field experiments. Berkeley, Lawrence Berkeley Laboratory, LBL-10210.

Tsang, C. F., Mangold, D. C., and Lippmann, M. J., 1980. Simulation of reinjection at Cerro Prieto using an idealized two-reservoir model, in Proceedings, Second Symposium on the Cerro Prieto geothermal field, Baja California, Mexico, October 1979: Mexicali, Comision Federal de Electricidad (in press).

Tsang, Y. W., and Tsang, C. F., 1978. An analytic study of geothermal reservoir pressure response to cold water reinjection, in Proceedings, 4th Stanford Workshop on Geothermal Reservoir Engineering. Stanford, Stanford University, p. 322-331.

Wahl, E. F., 1977. Geothermal energy utilization. New York, Wiley-Interscience, 302 p.

Witherspoon, P. A., Javandel, I., Neuman, S. P., and Freeze, R. A., 1967. Interpretation of aquifer gas storage conditions from water pumping tests. New York, American Gas Association, 273 p.

THERMODYNAMICS OF HIGH-TEMPERATURE BRINES

K. S. Pitzer, D. J. Bradley, P. Z. Rogers, and J. C. Peiper

INTRODUCTION

An understanding of brines is essential for the technical utilization of many geothermal resources. Consequently, in 1975 we began a study of the solution thermodynamics of brine systems, both simple and complex, weak and strong, covering a wide temperature and pressure range, and combining both modeling and experimental work.

The initial work involved analysis of existing thermodynamic data on simple electrolyte systems using equations developed by Pitzer and co-workers (Pitzer, 1973; Pitzer and Mayorga, 1973, 1974; Pitzer and Kim, 1977). The goal of the modeling was to provide a compact set of equations capable of reproducing, at various temperatures and pressures, the existing data within experimental error up to practical concentrations (6M) in terms of parameters having physical significance.

The program to measure heat capacities and densities arose because of inadequate experimental data on electrolyte systems. The primary goal of the experimental program is to supply data on simple and complex electrolyte systems at high temperatures and pressures both along and away from the liquid-vapor saturation curve. In addition, these data will provide a base for checking and refining various models.

Although the modeling and experimental work relate directly to electrolyte systems common to geothermal brines, the results are applicable to such areas as biological fluids, battery electro lytes in aqueous and non-aqueous solvents, plating baths, waste effluents, materials corrosion from electrolyte systems, and marine chemistry.

PROGRAM IN 1979

Experimental projects conducted during the past year have emphasized the high-temperature/high-pressure properties of solutions of geothermal interest. Both a calorimeter and a densimeter, designed to operate at elevated temperatures and pressures, have been used to obtain data on aqueous electrolyte solutions common in geothermal and geochemical systems. Data acquisition has been coupled to a computational program designed to compile and evaluate existing thermodynamic data on geothermal solutions.

The densimeter has been designed to operate in the temperature range 25 to 400°C and at pressures to 800 bar. It is essentially a dilatometer, which directly measures the volume expansion of a solution due to a temperature increase. The volume change is then converted to a density determination. The densimeter has been used to obtain the volumetric properties of NaCl solutions at 20 bar and 25 to 200°C with a precision of 15 ppm. Experiments are now under way to obtain similar data at 100 bar and 25 to 300°C. These data are necessary to complete a computer fit of the volumetric properties of NaCl solutions to 300°C and 1 kbar. The volumetric data to 100 bar are also needed to correct existing saturation heat capacity data to constant pressure values.

The flow microcalorimeter has been designed for operation to 300°C and 600 bar. It is a differential calorimeter, in which the heat capacity difference between water and an aqueous solution is determined directly. The calorimeter has been used to obtain heat capacity data for Na_2SO_4 solutions from 0.05 to 2.5 molal. The data extend

from 30 to 200°C at saturation pressure and at 200 bar. Work in progress will extend the temperature range of the data to 300°C. Precision of the data obtained is 3 x 10^{-4} cal/deg g, and the agreement between the present data and that of other workers in a small region of overlap is excellent. The heat capacity data will be used to complete an evaluation and computer fit of all the thermodynamic data for Na_2SO_4. A similar study of $MgSO_4$ solutions is also planned, along with an extension of the pressure range of the measurements to 500 bar. The calorimeter will also be rebuilt using a special corrosion resistant alloy, so that heat capacity data can be obtained for other geothermally important salts.

Modeling calculations during 1979 included a revision of the earlier work of Silvester and Pitzer (1977) on aqueous NaCl at saturation pressure to 300°C. The new Debye-Hückel parameters (Bradley and Pitzer, 1979) were introduced as well as some experimental enthalpy data which had been published recently. Figures 1 and 2 show the osmotic coefficient and the heat capacity, respectively, and compare our calculated curves with experimental data shown as points. The agreement is excellent except for the heat capacity at 300°C, Certain correction terms related to pressure derivatives of thermodynamic quantities were unavailable and were omitted; these are negligible at lower temperatures but not for the heat capacity at 300°C. These results were released as an LBL report (Pitzer et al., 1979). Before general publication, however, the volumetric data for aqueous NaCl, including our own measurements, will be modeled within the same general system of equations. With pertinent thermodynamic relationships, this will generalize

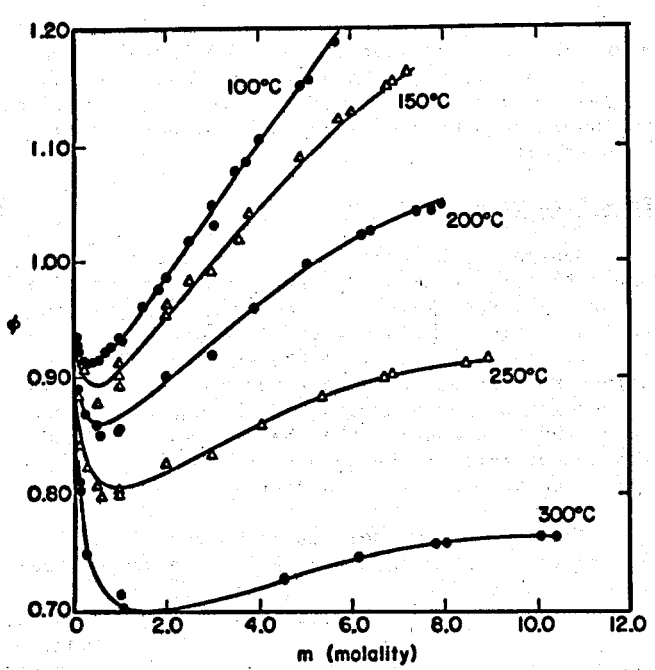

Figure 1. The osmotic coefficient of aqueous NaCl; curves are calculated, points are experimental from sources cited by Pitzer et al., 1979.
(XBL 803-8837)

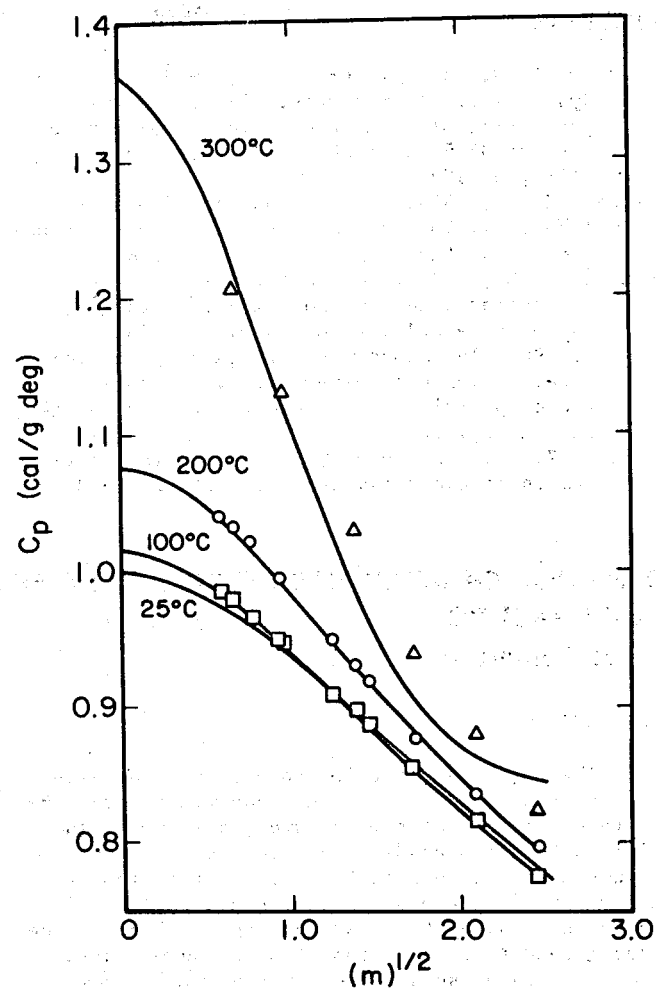

Figure 2. The total specific heat capacity of aqueous NaCl; details are the same as for Figure 1.
(XBL 803-8836)

the treatment of various properties to the above-saturation pressure domain. Also it will evaluate the correction terms mentioned above and allow a fully self-consistent treatment.

Reviews of the full system of modeling equations, including various applications, were prepared and presented (Pitzer, 1979a,b) to conferences on aqueous geochemistry and on the thermodynamics of aqueous systems with industrial application.

FUTURE WORK

Calorimetric and density measurements will continue for solutes of geochemical interest as indicated above. Also, the modeling program is being extended to deal with above-saturation pressures. Since carbonic acid and bicarbonates are weak electrolytes, their dissociation equilibria must be considered in addition to the usual strong electrolyte effects. Our modeling program will be extended in 1980 to include carbonates.

REFERENCES CITED

Bradley, D. J., and Pitzer, K. S., 1979. Thermodynamics of electrolytes: 12, Dielectric properties of water and Debye-Huckel parameters to 350° and 1 kbar. J. Phys. Chem., v. 83, p. 1599.

Pitzer, K. S., 1973. Thermodynamics of electrolytes: I, Theoretical basis and general equations. J. Phys. Chem., v. 77, p. 268.

Pitzer, K. S., 1979a. Characteristics of very concentrated aqueous solutions. Berkeley, Lawrence Berkeley Laboratory, LBL-9660.

____, 1979b. Thermodynamics of aqueous electrolytes at various temperatures, pressures, and compositions. Berkeley, Lawrence Berkeley Laboratory, LBL-9788.

Pitzer, K. S., and Mayorga, G., 1973. Thermodynamics of electrolytes: II, Activity and osmotic coefficients for strong electrolytes with one or both ions univalent. J. Phys. Chem., v. 77, p. 2300.

____, 1974. Thermodynamics of Electrolytes: III, Activity and osmotic coefficients for 2-2 electrolytes. J. Sol. Chem., v. 3, p. 539.

Pitzer, K. S., and Kim, J. J., 1974. Thermodynamics of electrolytes: IV, Activity and osmotic coefficients for mixed electrolytes. J. Am. Chem. Soc., v. 96, p. 5701.

Pitzer, K. S., Bradley, D. J., Rogers, P. S. Z., and Peiper, J. C., 1979. Thermodynamics of high-temperature brines. Berkeley, Lawrence Berkeley Laboratory, LBL-8973.

Silvester, L. F., and Pitzer, K. S., 1977. Thermodynamics of Electrolytes: VIII, High temperature properties including enthalpy and heat capacity with application to sodium chloride. J. Phys. Chem., v. 81, p. 1822.

BEHAVIOR OF ROCK-FLUID SYSTEMS AT ELEVATED PRESSURES AND TEMPERATURES

W. H. Somerton

INTRODUCTION

The objective of this project is to develop methods and apparatus for the measurement of rock-fluid properties at temperatures, pressures, and fluid-saturation conditions encountered in deep, high-temperature oil and gas reservoirs, geothermal reservoirs, and other subsurface reservoirs in which elevated temperatures are involved in the underground process. Properties being measured under simulated subsurface environmental conditions include porosity, permeability, and electrical resistivity factor; thermal properties, including thermal expansion, pore and bulk compressibilities; compressional and shear wave velocities, and the dynamic elastic constants derived from these properties.

Methods of measuring most of the above properties have been developed as reported in an earlier work (Somerton, 1977). However, the presently available apparatuses permit measurement of, at the most, only two properties at a time and are limited to measuring temperatures of 200°C and stress of one kbar. It is difficult to correlate results of measurements of properties in different apparatuses, using different test specimens, and with the possibility of different temperature-stress histories. Therefore, a second objective of this work is to develop an apparatus in which all or most of the desired properties may be measured at the same time on the same test specimen under identical test conditions. Basic design of this apparatus has been presented elsewhere (Somerton, 1979).

Measurements of physical properties and behavior of rock-fluid systems at elevated temperatures and pressures are difficult and time consuming. Therefore, a third objective of the present work is to develop models and correlations that will make possible the prediction of properties and behavior from more easily measured characteristics of the rock-fluid system. An example is the progress made in modeling thermal properties. Having estimates of such characteristics as mineral composition, porosity, and grain size, models have been developed for predicting thermal conductivity under any fluid saturation condition at a base pressure and temperature. Correlations have also been developed to permit prediction of thermal behavior at other pressure and temperature conditions. Well log data may also be used to predict thermal properties.

RESEARCH ACTIVITIES FISCAL YEAR 1979

Much of the research accomplished during fiscal year 1979 has been reported by Chou (1979), Cruz (1979), Kuo (1979), Sahnine (1979), and Somerton (1979). Other work in progress by Ashqar, Ghaffari, Greenwald, and Wong will be reviewed briefly in this report.

Rock Properties Apparatus

Design of the computer control for new multi-properties measurement apparatus was completed and reported by Kuo (1979). This design is based on the assumption that a new LSI-11 microcomputer system will be employed since the existing PDP 11/34 computer would be inadequate for the purpose. The sequencing of measurements and the control of pressures and temperatures have been formulated, and the computer-interface components required for these operations have been designed.

The pressure vessel has been ordered and delivery is expected in early 1980. The vessel consists of a monolithic forging with closures at both ends. Working space within the interior of the vessel is 7 in. in diameter and 20 in. long. The vessel has a maximum allowable working pressure of 25,000 psi (1.7 kbars) and meets LLL safety rules for "manned area operation."

The confining pressure system will use a diaphram compressor with argon as the pressuring fluid.

The pressure control system is designed for an accuracy of 2.5% but can be easily modified for an accuracy of 0.25% if required. This system is ready to be installed as soon as the test facility's final location has been determined.

Detailed drawings of the inner test assembly are nearing completion. Nearly all of the design aspects are complete and further development awaits construction and testing of the assembly.

Rock Properties Measurement

Significant developments were made on the compressibility thermal-expansion apparatus. After extended testing of the linear displacement transducers, they were found to be unreliable for the pressure and temperature conditions under which the tests were to be conducted. The transducers were replaced by high-temperature strain gauges mounted directly on the rock test specimen. Successful measurements of bulk compressibility and bulk thermal expansion have been obtained by this technique. In conjunction with these tests, measurements were also made of pore volume compressibility and pore volume thermal expansion. Preliminary results (unpublished) obtained by Greenwald and Ashqar in this latter work are shown in Figures 1-3.

Study of the effects of temperature and stress on the permeability of porous rocks continues and will be reported soon by Wong. His work has shown that the effect of temperature on permeability is coupled with the stress levels to which the rock is subjected. At low stress the effect of temperature is negligible, but at higher stress levels

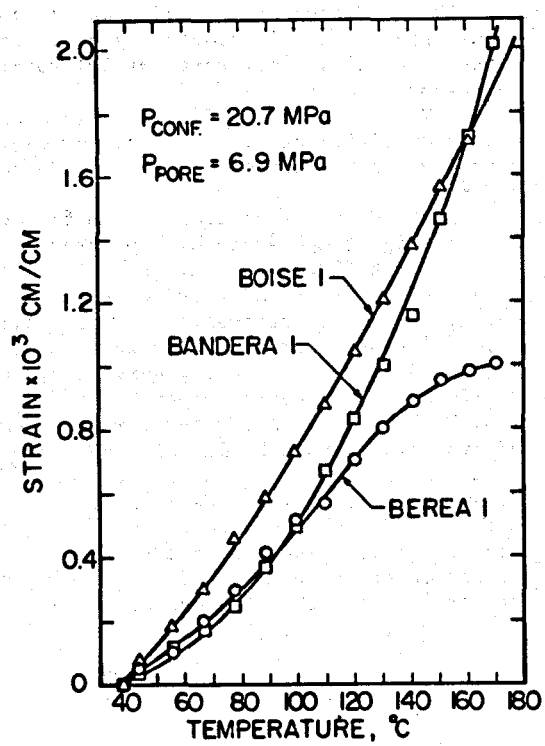

Figure 1. Axial strain versus temperature. (XBL 803-8752)

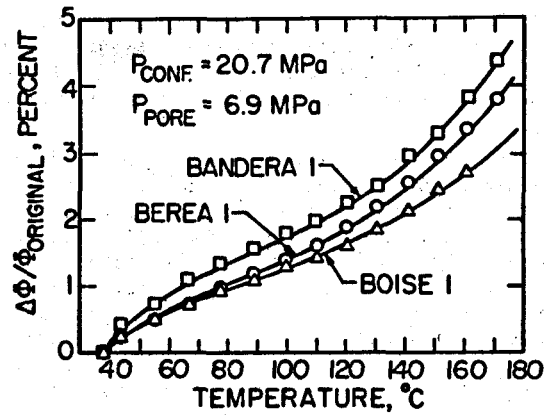

Figure 2. Fractional pore volume change versus temperature. (XBL 803-8753)

the effect of temperature is to reduce permeability to only a fraction of the room-temperature value. Because permeability reduction is likely related to release of, and plugging by, "fines" in the core, the rate of fluid flow effects and rate of heating effects are being investigated.

Theoretical Modeling

The theoretical model for predicting pore volume compressibility is being modified to account for the presence of clays in the pore spaces. To provide input data for the model, compressibility characteristics of clays must be measured as a

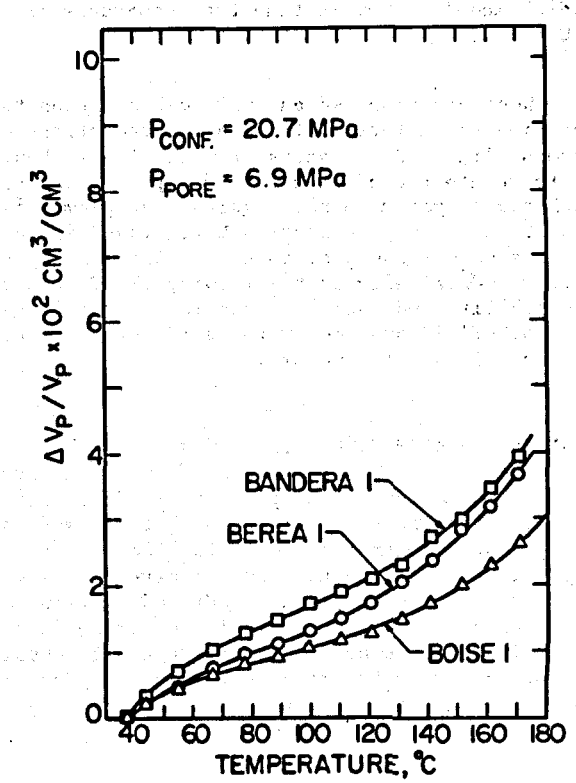

Figure 3. Fractional porosity change versus temperature. (XBL 803-8754)

function of hydrostatistic stress and temperature. These measurements are in progress, and the data will be used by Greenwald in comparing model results with measured pore volume compressibilities.

Two of the completed reports provided information needed by Ghaffari for completion of the model for thermal conductivity of multi-fluid saturated porous media. The work of Cruz (1979) showed rather conclusively that a grain size parameter needed to be included in the theoretical model. The work of Sahnine (1979) on the other hand, demonstrated that there was only a slight correlation between thermal conductivity and sonic velocity in porous media. This is contrary to reports by other investigators and casts doubt on the use of sonic log data to predict in-situ thermal conductivities.

In other thermal work, Chou (1979) developed a one-dimensional finite-difference model to test the importance of the VCC (vaporization-condensation-capillary) effect in causing heat transfer in porous media. His model results showed that the VCC effect is probably negligible in steam injection or production in subsurface formations. However, the effect may not be negligible in wellbore heat loss where heat-thief sands penetrated by the wellbore could extract large amounts of heat from injected or produced steam. One problem in using the model was the lack of data on capillary and relative permeability for liquid-vapor systems. A possible application of this work is the extraction of these data by comparing model results with experimental data from an existing laboratory model. Su is conducting his own investigation of this subject and is developing a two-dimensional radial model for evaluating the importance of the VCC effect.

Wong has proposed an empirical equation to describe the effect of temperature and stress on permeability. He suggests the next steps should be to relate the effects of other properties of the rock-fluid system to the magnitude of permeability reduction. These properties being investigated include quartz and clay contents of the rock, velocity and salinity of the flowing fluid, and compressibility and thermal expansion coefficients of the rock-fluid system. Details of this work will be given in a later report.

PLANNED RESEARCH FISCAL YEAR 1980

Upon receipt of the pressure vessel, it will be installed and tested along with the compressor and pressure control system. The inner test assembly will be constructed, and the several design elements will be tested and modified as required. Computer control equipment will be purchased and assembly and testing will be started. It should be possible to make initial tests on standard rock samples by the end of the year.

Rock properties tests will continue, using the presently available apparatus, primarily to provide data for testing models and for testing new procedures to be used in the multiproperties apparatus. Measurements of bulk and pore compressibility and thermal expansions will be made over a wider range of test conditions and on several different rock types. Permeability tests will also be continued to provide data for testing correlations and a theoretical model of the effects of temperature and stress on permeability.

Experimental techniques yet to be finalized include measurements of thermal conductivity by the probe method and electrical resistivity using a radial electrode system. The thermal conductivity probes have been designed and will be sent out for bids early this fiscal year. Testing of the probes and the method can be done in one of the present pressure vessels. Electrical resistivity will be measured using the outer sheathing of the thermal conductivity probes as the inner electrode. This method can also be tested in existing apparatus.

Two models are scheduled for completion during this fiscal year. The thermal conductivity model for multifluid saturated porous media will be completed by Ghaffari and the model for predicting the effect of stress on pore compressibility will be completed by Greenwald. Progress will be made on two other model. The permeability model developed by Wong will continue to be studied by Okah. Ashqar's work on bulk and pore thermal expansions will be continued by Janah, and he will begin development of a model of these properties.

REFERENCES CITED

Chou, C., 1979. Vaporization-condensation-capillary (VCC) effects in oil recovery by steam injections. Berkeley, University of California, MS research report.

Cruz, J., 1979. The effect of grain size on thermal conductivity of fluid saturated media. Berkeley, University of California, MS research report.

Kuo, W., 1979. Computer control system for measurement of high temperature high pressure properties of rock-fluid systems. Berkeley, University of California, MS research report.

Sahnine, B., 1979. Relationship between sonic velocities and thermal conductivities of fluid saturated rocks. Berkeley, University of California, MS research report.

Somerton, W. H., 1977. Apparatus for measurement of properties and behavior of rock-fluid systems at high temperatures and pressures. Berkeley, University of California, Petroleum Engineering Laboratories report.

____, 1979. Status report on the design and construction of an apparatus for measuring the properties of rocks at elevated temperatures and pressures. Berkeley, University of California, Petroleum Engineering Laboratories.

SOLUBILITY OF LOW ALBITE IN NaCl SOLUTIONS AT 250°C

J. M. Neil and J. A. Apps

INTRODUCTION

Understanding the solubility of the major rock-forming minerals in low temperature, hydrothermal environments is important for successful modeling of diagenetic or metasomatic processes; or for predicting the effects of injecting cooled, geothermal fluids into a geothermal reservoir; or for using an aquifer for hot-water storage. Albite, one of the end-members of the feldspar mineral series, is an ideal candidate for the initial study because it is found in a wide variety of geological environments.

This is the third progress report on studies of the solubility of rock-forming minerals in the aqueous phase. The initial report (Apps and Neil, 1978) dealt with the selection of low-albite starting material and its chemical and physical characterization. The second report (Neil and Apps, 1979) dealt with the initial experiments of albite solubility at 250°C in 0.1 N NaCl solutions. This report is a summary of the albite solubility measurements in varying NaCl concentrations at 250°C and in the presence of a water vapor phase.

EQUIPMENT

The equipment used for albite solubility measurements has been described previously (Neil and Apps, 1979). Several additions and modifications have been made to improve the measurement of temperature and pressure within the autoclave and to increase the system's safety.

Initially the temperature was measured with a chromel-alumel thermocouple and read from the Speedomax H, model S, strip chart recorder of the Leeds & Northrup Series 60 D.A.T. Control Unit. A second chromel-alumel thermocouple has been placed in the thermocouple well of the 1-liter autoclave and is connected to an Omega Model 2170 A-K digital thermometer which is accurate to ±1°C.

The pressure was initially measured on a 4-in.-diameter, 0 to 10,000 psi, Bourdon tube guage manufactured by Ashcroft and supplied by the autoclave manufacturer. The gauge was filled with water and isolated from the autoclave proper by a gauge isolator to prevent chemical attack of the Bourdon tube. A BLH model GP-HR, 0 to 10,000 psi, High-Temperature Pressure Transducer with a BLH Model 450 Transducer Indicator has been added to the gauge side of the isolator to give greater precision pressure measurements. The transducer's sensitivity is rated at 3mV/V ±0.25%, equivalent to a precision of ±10 psi.

The safety improvements made to the autoclave system include the addition of two more rupture disk assemblies to the high pressure line. One assembly is in the oil line between the pump and the oil-water separator; the other is in the water line between the oil-water separator and the valve that isolates the solution recharging reservoir from the rest of the system. This prevents any portion of the system from being isolated from a fail-safe pressure relief device, and these modifications put the entire system in compliance with the LBL safety requirements.

The thermocouple located in the furnace windings has been connected to an Omega Model 20 Limit Temperature Controller. This will shut off the furnace if it becomes hotter than the temperature set point of the controller or if the thermocouple fails.

EXPERIMENTAL PROCEDURES

The experimental procedure followed in measuring the dissolution of albite has been described previously (Neil and Apps, 1979). However, several modifications have been made as a result of additional work and more refined data evaluation.

Each albite charge is sonicated in acetone to remove the very small (<1 μm) albite grains that adhere to the larger grains. This procedure is repeated until the acetone remains clear after 5 minutes of sonication. SEM images of the albite treated in this manner show very few fines adhering to the larger grains (Figure 1). Also, the residual solution in the autoclave at the end of an experiment is free of suspended fines.

By collecting and handling the aqueous samples as well as measuring the pH under a CO_2-free nitrogen atmosphere, it has been possible to get stable measurements for the pH. The solution samples appear to be very efficient scavengers of atmospheric CO_2. The nitrogen is passed through a CO_2 trapping agent (Ascorite) to remove any CO_2 contamination which might be present.

Two different techniques were investigated for sodium determinations in the aqueous phase. Neither specific ion potentiometry (Orion Research, 1977a) nor atomic absorption spectrophotometry (AA) (Perkin-Elmer, 1976) have proven to be entirely acceptable. The electrode instability limits the accuracy to approximately 3%, while very large (on the order of 10^4) dilutions cause an uncertainty of a similar magnitude for the higher NaCl (1.0 N to 0.01 N) concentrations with the AA technique. Because it is faster, the AA technique is preferred although the Na electrode is still used for solutions with very high Na concentrations.

Two different techniques were also evaluated for chloride determinations. Both methods use a chloride-specific ion electrode. In one method the potentials of the samples are compared with the potentials of standards with known chloride concentration, while in the other the electrode is used to detect the end-point of a silver nitrate tritration for chloride (Orion Research, 1977b). The methods gave similar results although there was a small systematic error. The potentiometric method was selected becasue it is more rapid.

Samples were analyzed for calcium in the first albite solubility run and for potassium in subsequent runs by atomic absorption spectroscopy. Both

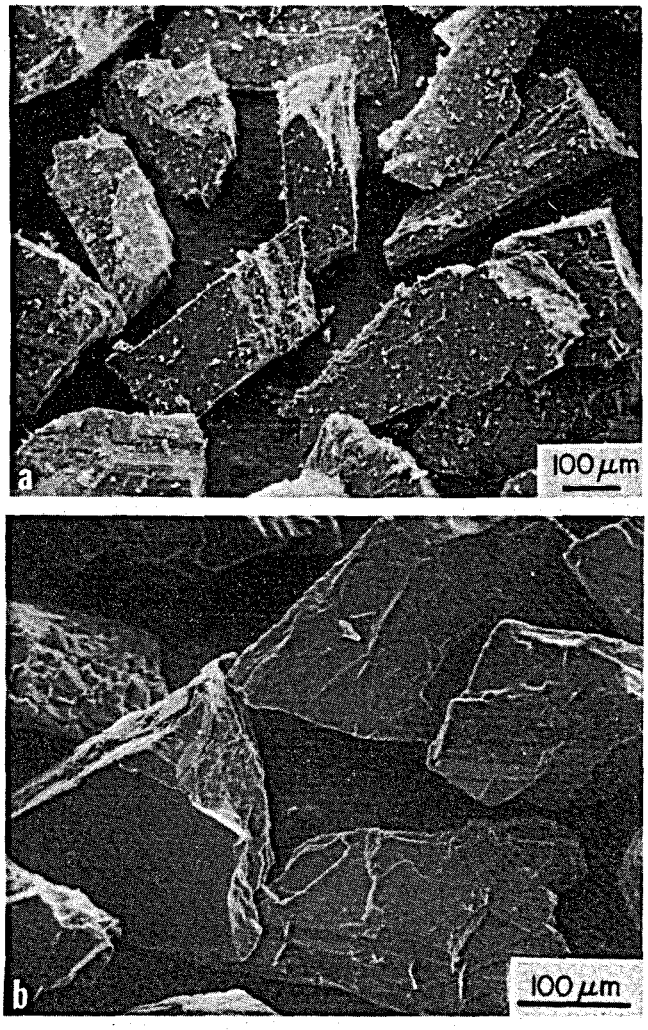

Figure 1. (a) Starting material before sonication to remove adhering fines. (b) Starting material after sonication showing the degree to which adhering fines were removed.
(XBB 804-5029, XBB 799-11265)

elements are normally present in insignificant concentrations. There were, however, several experiments where there was some potassium contamination that was due to the use of 1 M KOH between experiments to remove scale adhering to the autoclave. More stringent cleaning procedures have eliminated this problem.

The surface area of the 65^- to 100^+ mesh sized albite has not been determined. It is difficult to make accurate measurements on this size fraction using conventional techniques becasue of the small specific surface area.

Summary of Experiments

Table 1 lists all the albite solubility experiments which have beem completed to date, and it notes operating conditions and the observations made during each run.

Evaluation of Data

After the chemical analyses of each experimental trial are completed, the results are evaluated using a proprietary computer code, FASTPATH, developed by Kennecott Corporation. This code, which models aqueous solution-mineral interactions and reactions progress, is similar in its function and was derived from an earlier code by Helgeson (1969a). The code calculates the concentration of the aqueous species present, their activities, and the activity quotients, log Q, of solid phases that can appear in the system. This information allows the evaluation of the approach to equilibrium between the albite and the aqueous phase and indicates the consistency of the data between runs.

The general procedure is to calculate the initial speciation in solution at 25°C by specifying the pH and balancing the charge by adjusting the sodium concentration until electro-neutrality is achieved. Comparison can then be made between the measured and calculated concentrations of sodium as a measure of the quality of the analytical data. The new sodium value is then specified to calculate the distribution of species at 250°C, and the minor corrections to electro-neutrality taken up by adjusting the concentration of H^+. Figure 2 illustrates the distribution of species as a function of time for albite equilibrated in 0.1 N NaCl starting solution. The saturation concentration of H_4SiO_4 in equilibrium with quartz is also plotted on the figure for comparison.

Log $Q_{(albite)}$ can be calculated from the solubility reaction defined as:

$$NaAlSi_3O_8 + 4H^+ + 4H_2O = Na^+ + Al^{+++} + 3H_4SiO_4$$

$$Q_{(albite)} = \frac{[Na^+][Al^{+++}][H_4SiO_4]^3}{[H^+]^4[H_2O]^4[NaAlSi_3O_8]} .$$

Log Q, where the square-bracketed species denote activities of those species calculated from the FASTPATH species distribution, is plotted in Figure 3 for the run illustrated in Figure 2, to show the approach to apparent equilibrium. Because of the observed occurrence of analcime as a product in several of the runs, the analogous log $Q_{(analcime)}$, where

$$Q_{(analcime)} = \frac{[Na^+][Al^{+++}][H_4SiO_4]^2}{[H^+]^4[H_2O][NaAlSi_2O_6 \cdot H_2O]}$$

is also included. Log $K_{(albite)}$ and log $K_{(analcime)}$, calculated from calorimetric data, are also plotted in Figure 3 and are enclosed by an uncertainty envelope expressing the estimated error in the calorimetric data of ±1.0 kcal. Agreement between the independently calculated log Qs and log Ks are quite good after steady-state conditions have been attained. This also reflects indirectly the overall precision of the analytical data.

Comparison of log $Q_{(albite)}$ from several runs with different initial concentrations of sodium chloride starting solutions and with plain water

Table 1. Albite dissolution experiments.

Run	Temperature Run (°C)	Solution Composition (N Nacl)	Solution Volume (ml)	Weight albite (g)	Duration of run (hr)	Number of samples taken during run	Comments
B	250	0.1	700	17.77	72	13	Al-Si ppt. formed before samples were analyzed.
C	205	0.1	700	25.00	102	12	20 ml sample added to 5 ml 0.01 M KOH to prevent Al-Si ppt.
D	250	0.1	700	25.01	137	13	Hydrazine buffered the pH (in sample bottles).
E	125	0.1	860	25.00	264	17	Samples centrifuged to remove any suspended material prior to adding 0.01 M KOH.
F	250	0.1	750	25.00	55	15	
G	250	0.1	770	25.62	105	15	Starting material sonicated; pH measured under N_2.
H	250	1.0	770	25.69	104	14	Al-Si ppt. while samples were centrifuged.
I	250	0.01	770	25.65	100	13	
J	250	0.1	770	25.71	25	15	Sampled every hour from 10-20hr.
J†	250	0.1	750	~20 g material recovered from Run J	480	11	Analcime scale recovered from side; cemented albite in bottom of autoclave.
K	250	1.0	770	25.69	58	13	Sampled directly into bottle with KOH to avoid problem of Run H.
L	250	0.001	780	25.73	101	15	Analcime scale on the side; cemented mass of albite on the bottom of autoclave.
M	250	0.1 w 75 ppm SiO_2 spike	750	None	200	15	Effect of different sampling procedures tested.
N	250	0.0	780	25.00	156	15	Mass of cemented albite on the bottom.

†Starting material was the albite recovered from Run J. By allowing the system to operated for an extended period of time it was hoped that large crystals of the secondary phases could be recovered.

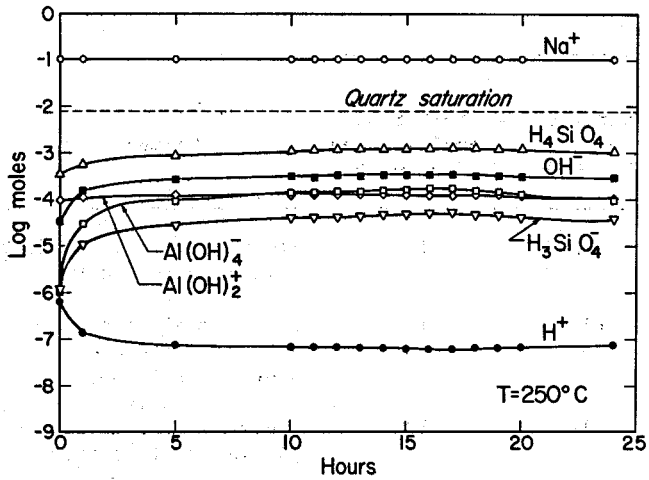

Figure 2. Aqueous species distribution as a function of time as calculated by FASTPATH. (XBL 799-2749)

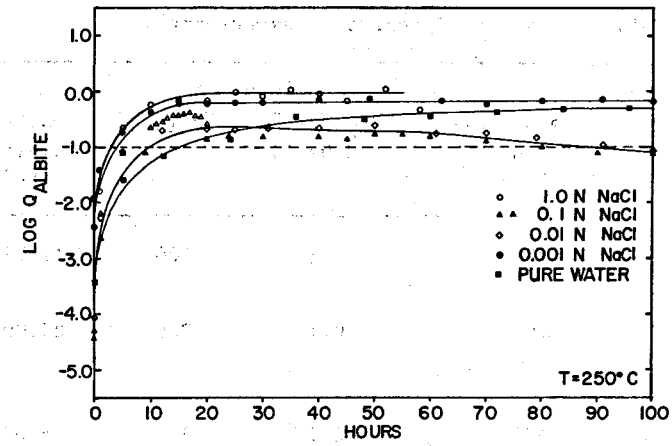

Figure 4. Log Q_{albite} as a function of time and NaCl concentration. (XBL 799-11397)

are given in Figure 4. All results indicate that apparent equilibrium is reached, and that the final values of log $Q_{(albite)}$ differ by no more than one log unit.

SECONDARY PHASE FORMED

Evidence for the formation of secondary phases were observed both on macroscopic and microscopic scales. Although examination of the material collected from 13 runs is incomplete, the observations to date are consistent with the interpretation of the solution analyses.

From the long duration run (J*) and from the lowest concentration NaCl (0.001 N) run (L), sufficient crystals and scale were recovered from the side of the autoclave and the baffle assembly (an internal fitting within the autoclave to create turbulence during agitation) to prepare samples for x-ray powder diffraction photographs. The J* run

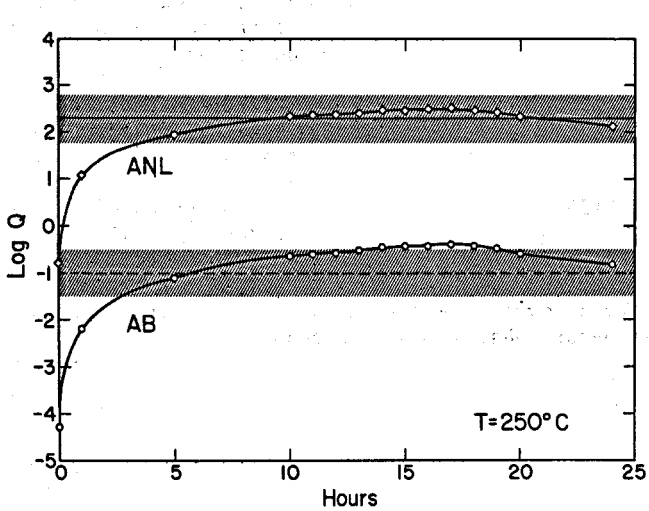

Figure 3. Log Q_{albite} and log $Q_{analcime}$ as a function of time. (XBL 799-2750)

material indexed as analcime plus albite, while the L material indexed as analcime plus four unidentified lines. In most of the other runs, similar material was produced but was too small to characterize.

A scanning electron microscope (SEM) examination of the Run L scale has shown that the major phase present is analcime as shown in Figure 5 (a,b). The pitting on the faces is not yet understood. Several other crystal forms have been observed but remain unidentified (Figure 5c,d).

Samples of the albite charge recovered from Runs B through L have been examined by the SEM. The grains themselves show slight rounding of sharp edges; and in the case of the 0.001 N NaCl solution run, there is etching of dislocations as well. The material recovered from the long duration (J*) run shows much greater etching, which often appears to be preferential to specific cleavage faces. In all these samples, an occasional cleavage fragment is also observed encrusted with small crystallites, concentrated along the edges and ridges. Six crystal morphologies have been observed: cubes with truncated corners, regular polyhedrons, irregular polyhedrons, interpenetrating blades of two different types, and small spherules. The latter were often massed together (see Figure 5c,d,e).

Chemical analyses of the crystallites with the Energy Dispersion Analyses of x-ray (EDAX) attachment of the SEM have been attempted. However, the surfaces are irregular, which gives poor geometry and makes elemental ratios very inaccurate. The electron beam may also be activating the material under the grain as well as the grain itself. All the EDAX analyses, so far, show the composition to be primarily Na, Al, and Si. Several analyses also reveal a small (<2 wt%) amount of chlorine.

In runs J* and L as well as the pure water run (N), a mass of cemented albite was found in the bottom of the autoclave. A diffraction pattern of the Run L material indexed as albite. None of this material has yet been examined with the SEM.

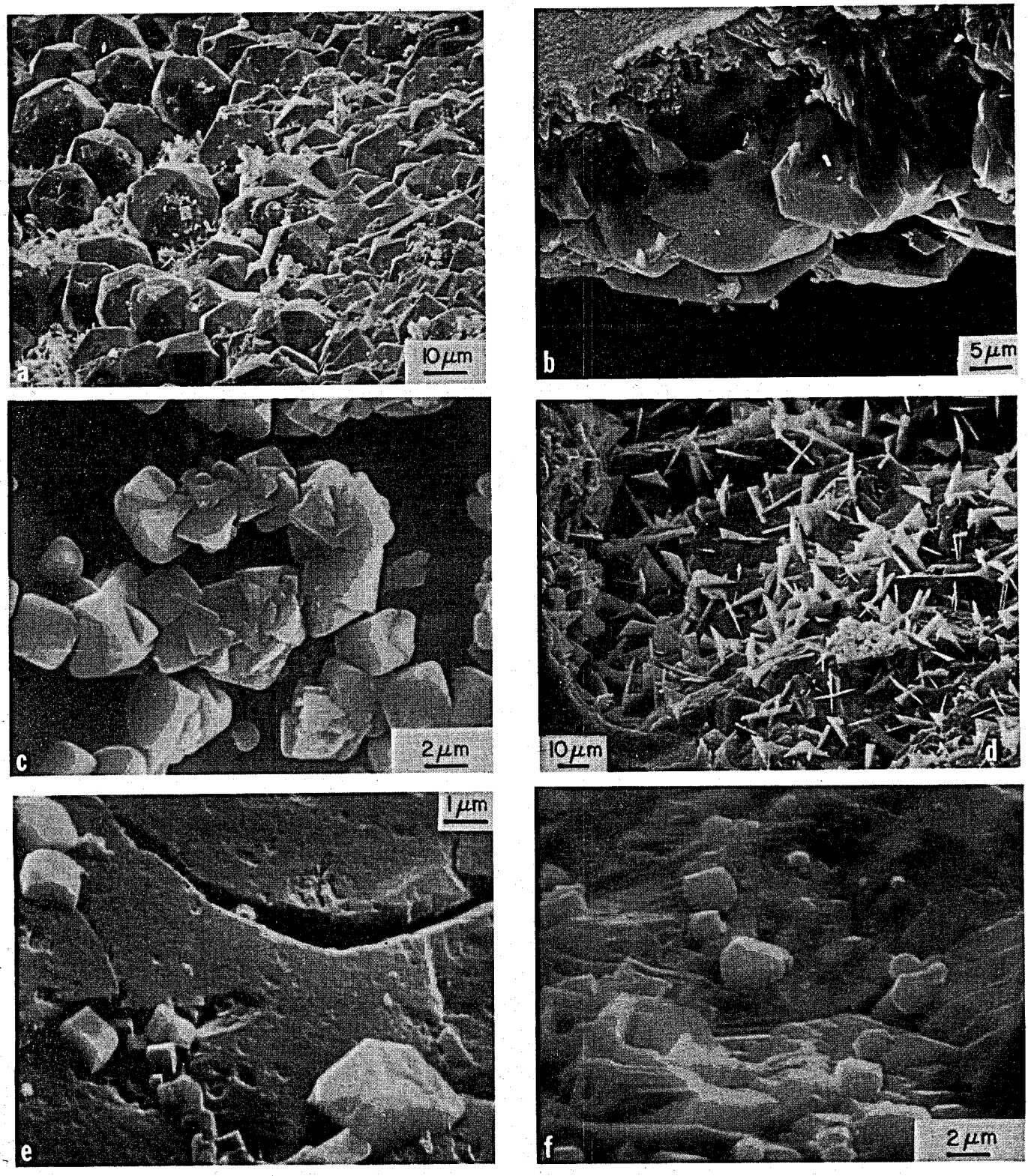

Fig. 5. SEM images of secondary phases formed during the dissolution of albite at 250°C: (a) analcime polyhedron, (b) massive analcime, (c) blades, type 1, (d) blades, type 2 on massive analcime, (e) cubes with truncated corners, (f) irregular (hexagonal?) polyhedron.
[(a) XBB 804-5031, (b) 804-5030, (c) 799-11277, (d) 804-5032, (e) 804-5033, (f) 799-11270]

Discussion

Figure 6 illustrates the phase relations as a function of pressure and temperature in the degenerate ternary system H_2O-$NaAlSiO_4$-SiO_2, containing the phases nepheline ($NaAlSiO_4$), jadeite ($NaAlSi_2O_6$), analcime ($NaAlSi_2O_6 \cdot H_2O$), albite ($NaAlSi_3O_8$), quartz (SiO_2), and water. These relations were calculated from experimentally determined univariant relations between the phases (Apps, 1970). The results of the albite solubility measurements reported here are consistent with these relations, and show that albite, when in the presence of water alone, will dissolve to produce a three-phase assemblage consisting of albite, analcime, and the aqueous phase.

There remains an undesirable scatter in the calculated log $Q_{(albite)}$ and log $Q_{(analcime)}$ between different albite dissolution runs at different ionic strengths (NaCl starting concentrations). This may be due to inadequacies in the simple formulation of activity coefficients of the aqueous species in solution (Helgeson, 1969b) using the extended form of the Debye-Huckel expression.

$$-\log \gamma_i = \frac{A(z_i)^2 \sqrt{I}}{1 + a_i B \sqrt{I}} + B^{\cdot} .$$

It may also be due to the presence of unaccounted aqueous species, such as $Al(OH)_3^o$, to errors in the dissociation constants used to calculate the distribution of species at 250°C, or to failure to correct for the activity of water. Finally, not all dissolution runs appear to have attained thermodynamic equilibrium. In some runs, particularly the 0.1 N NaCl and 0.01 N NaCl, the Al and SiO_2 concentrations attain a maximum before declining progressively to the end of the run. This is also reflected in a maximum in log $Q_{(albite)}$ and log $Q_{(analcime)}$, as illustrated in Figure 2. The growth of secondary phases may contribute to the phenomenon, and caution should therefore be used in interpreting these preliminary results.

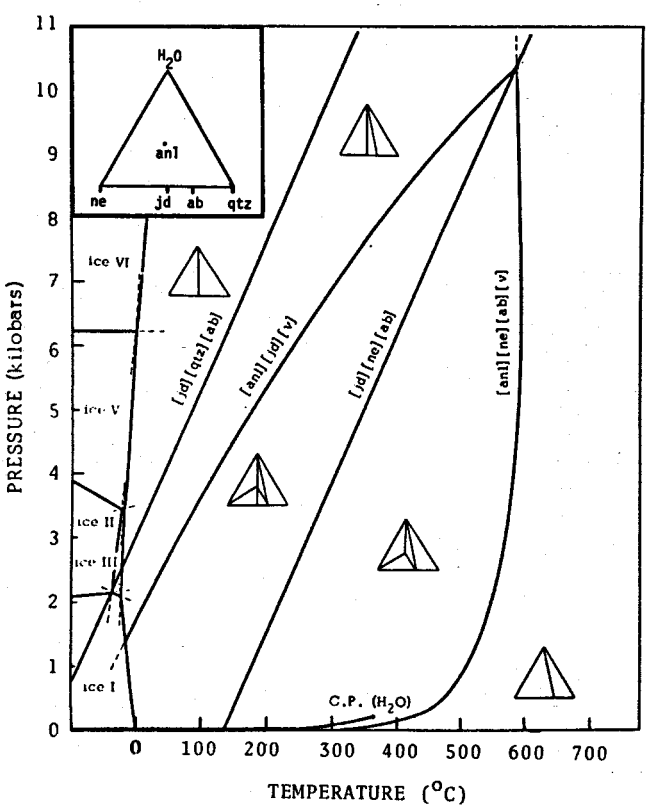

Figure 6. Phase relations in the degenerate tenancy system H_2O-$NaAlSiO_4$-SiO_2. (XBL 804-9367)

FUTURE PLANS

The next experimental step in this project will require additional checks to establish that thermodynamic equilibrium between albite and the aqueous phase is achieved. Solution samples will be taken at 25°C intervals up and down the water saturation curve between 125°C and 350°C with a between sample equilibration interval of 24 hours. If the system achieves equilibrium at each temperature, log Q for a given temperature should be independent of the direction from which equilibration was approached. Once it is established that equilibrium is achieved and the time interval needed is determined, a systematic determination of log $Q_{(albite)}$ in P-T space will begin. The temperature interval to be investigated will be 125°C to 400°C, and the pressure interval will be 1 to 500 bars.

Technicon autoanalyzer will be set up to speed up analyses in solution of Al and SiO_2. Also, further effort will be made to improve the sodium analyses. Finally, the characterization of the secondary phases will be attempted.

The long-term portions of this project include an updating and refinement of the data base and an expansion of the data base so that 25°C temperature intervals can be used in FASTPATH. If this does not prove feasible, the other water-mineral equilibrium programs (SOLMNEQ, WATEQZ, and others) will be evaluated for their suitability. In addition, data from earlier albite dissolution experiments in the literature will be evaluated.

REFERENCES CITED

Apps, J. A., 1970. The stability field of analcime (Ph.D. dissertation). Cambridge, Massachusetts, Harvard University, 347 p.

Apps, J. A., and Neil, J. M., 1978. Selected albites as candidates for hydrothermal solubility measurements. Berkeley, Lawrence Berkeley Laboratory, LBL-7058, p. 16-19.

Helgeson, H. C., 1969a. Program No. 1000-Path I. American Society for Information Science, NAPS Document No. 00774.

____, 1969b. Thermodynamics of hydrothermal systems at elevated temperatures and pressures. Amer. J. Sci., v. 267, p. 729-804.

Neil, J. M., and Apps, J. A., 1979. Solubility of albite in the aqueous phase at elevated temperatures. Berkeley, Lawrence Berkeley Laboratory, LBL-10349, p. 16-21.

Orion Research, 1977a. Instruction manual, sodium electrodes: model 94-11 and model 96-11. Cambridge, Massachusetts, Orion Research, Inc., 28 p.

____, 1977b. Instruction manual, halide electrodes: model 94-17 and model 94-35, model 94-53,

and model 96-17. Cambridge, Massachusetts, Orion Rsearch, Inc., 31 p.
Perkin-Elmer, 1976. Na standard conditions, in Analytical methods for atomic absorption spectra photometry. Norwalk, Connecticut, Perkin-Elmer Corp.

THERMODYNAMIC PROPERTIES OF SILICATE MATERIALS

I. S. E. Carmichael, M. S. Ghiorso, L. Moret, S. A. Nelson, M. Rivers, and J. Stebbins

INTRODUCTION

The main emphasis of this research program is to measure various properties of silicate liquids, especially as functions of composition and temperature. Thus one objective is to be able to describe the density of any natural silicate liquid as a function of pressure and temperature, which at the moment cannot be done. This program will also contribute significantly to the data on the molar heats of fusion of silicate materials, for few are known at the moment, and until they are, no crystallization paths of multicomponent silicate liquids can be calculated.

ACTIVITIES IN 1979

One of the goals of igneous petrology is to understand, on a quantitative level, the relationships among temperature, pressure and the compositions of coexisting solids crystallizing from magnetic (natural silicate) liquids. Enough thermodynamic data on silicate liquids are available over a sufficiently broad temperature and compositional range to allow certain generalizations to be made regarding the solution behavior of oxide components in these liquids. The observations of the absence of excess volume (Nelson and Carmichael, 1979) and of excess heat capacity (Carmichael et al., 1977) have been considered along with published experimental results on the compositions of solids and liquids coexisting at elevated temperatures and pressures, and combined with thermodynamic data obtained from P-T fusion curves for the pure components, to yield a regular solution expression for the free energy of mixing of silicate liquids.

This model can be inverted and used to predict temperatures from the compositions of coexisting quenched mineral-glass pairs (volcanic rocks). It has proved reliable in predicting liquid phase immiscibility in lunar basalts and rocks of andesitic and rhyolitic composition and accurately yields silica activities which are independently corroborated by solid-liquid buffer assemblages.

Attempts are currently being made to expand the compositional range of the experimental data base used to evaluate the thermodynamic excess properties (ΔH^{ex}) necessary for construction of the free energy surface. Computer software is also under development to calculate, using the derived solution model, the cooling products of natural silicate liquids of variable composition.

Few systematic and careful measurements of the compressibility of silicate liquids have been made, and preliminary investigations of ultrasonic velocities in liquids using solid buffer rods demonstrated that multiple modes and echoes within the rods masked the arrival of weak signals that had passed through the liquid. We have pursued, therefore, a design involving a liquid buffer medium. The silicate liquid sample floats on a column of liquid metal (65% Ga, 15% Sn, 20% In). The sample is within a furnace at T < 1500°C, while the base of the liquid metal column, which is supported by an ultrasonic transducer, is water cooled outside the bottom of the furnace. The base of the tungsten reflector rod is immersed in the silicate liquid, and is precisely moved by a micrometer assembly mounted on top of the furnace. The time delay between the echo from the Ga-silicate liquid interface and the silicate-tungsten interface is measured as a function of reflector position, using a modification of the pulse-echo overlap method. To date we have measured the velocity of standard materials at room temperatures to determine the sensitivity and accuracy of the technique. We obtain a value for the velocity of sound in deionized water at 23.4°C of 1492.14 m/sec, which is within 0.01% of the value published by the Naval Research Laboratory, 1972. Accuracy is limited by our capability to control and measure the temperature of the water. We have tested a column filled with liquid metal (Hg) at 23.5°C, and obtained 1448.9 m/sec within 0.1% of the accepted value. The apparatus to conduct high temperature measurements has recently been completed, and such experiments are about to begin.

During 1979, a venerable high-temperature drop calorimeter was brought back into operation with several modifications to improve precision and accuracy. The instrument can measure the enthalpy difference between furnace temperatures as high as 1880 K and the calorimeter temperature of 300 K, for a wide variety of materials. After a period of testing and calibration, a program was begun to determine enthalpies and heat capacities of glasses and liquids in the system $NaAlSi_3O_8$-$CaAl_2Si_2O_8$-$CaMgSi_2O_6$. This system is a relatively simple model of many naturally occurring igneous rock compositions, and is therefore useful in understanding geologically important crystallization and melting phenomena. Determinations of mixing heats will also help constrain models of solution chemistry, which may in turn be generalized to more complex silicate systems.

Measurements on five compositions along the $NaAlSi_3O_8$-$CaAl_2Si_2O_8$ join have been completed. Of immediate interest is a new determination of the heat of fusion of anorthite, whose melting point of 1830 K makes experiment on the pure composition difficult and has led to widely varying estimates of this fundamental property. The combination of our data with published solution calorimetric results gives a heat of fusion at the melting point

of 32.0 ± 0.3 kcal/mol, with a heat capacity of 102 ± 1 cal/mol/k.

Our study of the density of silicate liquids began in 1978, was completed in 1979, and values for the partial molar volumes of eight oxide components as a function of temperature were derived. It was found that within the experimental limits of 1 to 2%, silicate liquids mix ideally with respect to volume over the composition-temperature range of the experiments; these results have been reported by Nelson and Carmichael (1979).

A Perkin-Elmer differential scanning calorimeter has been used in two studies to determine the heat capacity at constant pressure (C_p). Sixteen compositions in the system $NaAlSi_3O_8$-$CaAl_2Si_2O_8$-$CaMgSi_2O_6$ have been measured in the range 300 to 500 K with a view to establishing the mixing properties in the metastable glassy state. The second study is designed to measure the effect of coordination changes in silicate liquids as a function of pressure. Under high pressure, the coordination change of aluminum with oxygen changes from fourfold to sixfold, clearly demonstrated in the stability of minerals at high pressure with respect to those at low pressure. Coordination changes in liquids at high pressures will markedly affect the physical properties of these liquids, such that the liquids may in fact be more dense than the solids from which they were derived. Simply put, the bouyancy drive for liquids to reach the surface of the earth may disappear at high pressures. Presently missing is decisive evidence for the existence of this coordination change in silicate liquids and, of the techniques available to identify this change in coordination, the change in heat capacity should be one of the most effective.

Turning now to experiments at comparatively low temperatures, the utility of mineral solubility experiments lies in the potential for extracting thermodynamic data from measured hydrolysis constants over a wide temperature range. Furthermore, whether dissolution be congruent or incongruent, useful kinetic data can always be obtained as the reactions tend towards equilibrium. We have initiated a program to measure solubility products of two common hydrothermal minerals, kaolinite [$Al_2Si_2O_5(OH)_4$] and alunite [$KAl_3(SO_4)_2(OH)_6$], in dilute solutions of hydrochloric and sulfuric acids, respectively, over the temperature range 30 to 90°C and 1 bar. These two minerals were chosen because of their common occurrence as hydrothermal alteration products and the high uncertainties in existing thermodynamic data (ΔH_f) for these phases at 25°C. Purified natural mineral samples are being used. The experiments are carried out in a thermally equilibrated shaker/water bath, and solutions (200 mls) are contained in Teflon bottles. Solubility is determined from chemical analyses of the fluids, by computation of the activity product of the appropriate mineral hydrolysis reaction. Preliminary data from unreversed alunite runs at 90°C indicate a $\Delta H_{f,25°C}$ more positive by 16.7 kJ (about 4 kcals) than that reported by Kelley et al. (1946).

REFERENCES CITED

Carmichael, I. S. E., Nicholls, J., Spera, F. J., Wood, B. J., and Nelson, S. A., 1977. High temperature properties of silicate liquids: applications to the equilibration and ascent of basic magma. Phil. Trans. R. Soc. Lond., A 286, p. 373-431.

Kelley, K. K., Schomate, C. H., Young, F. E., Naylor, B. F., Salo, A. E., and Juffman, E. H., 1946. Thermodynamic properties of ammonium and potassium alums and related substances with reference to extraction of alumina from clay and alunite. U.S. Bur. Mines Tech. Paper #688, 104 p.

Nelson, S. A., and Carmichael, I. S. E., 1979. Partial molar volumes of oxide components in silicate liquids. Contrib. Mineral. Petrol., v. 71, p. 117-124.

CHEMICAL TRANSPORT IN NATURAL SYSTEMS

C. L. Carnahan

Problems involving the transport of chemical species in porous or fractured flow systems, accompanied by chemical reactions, arise frequently in geochemical investigations. Such investigations range from studies of ore deposition in past geological time to predictions about the fate of nuclear waste depositories thousands of years from now. On a more immediate time scale, consideration of chemical transport processes is an important part of evaluating environmental effects and possible biological hazards of, for example, subsurface disposal of toxic wastes, acid mine drainage, insitu retorting of oil shale, and other disturbances of nature caused by human activities.

Chemical transport processes in natural systems are, in general, very complex and very difficult, if not impossible, to simulate in extreme detail by mathematical and numerical models. A large body of work has treated various isolated aspects of chemical transport, yet much work remains to be done. This project is an investigation of fundamental thermodynamic aspects of solute transport with chemical reactions, including explicit consideration of irreversible processes in derived models. Thus, the approach is strongly based on the thermodynamics of irreversible processes, and leads to mathematical descriptions of transport processes which are different from classical descriptions in some important respects.

To establish a basis against which future results could be compared, analytical solutions were derived for the classical transport equation (in which gradients of mass concentration are the driving forces for diffusive transport) with chemical sorption obeying linear rate expressions. These solutions are inherently useful in the context of the classical theory. They are derived for point releases of solute into uniform, three-dimensional fields of groundwater flow velocities,

resulting in a distribution of solute in groundwater which is symmetrical about an axis parallel to the direction of flow. The solutions for point releases can be used to develop solutions for releases from extended sources (lines, planes, volumes) by integration with regard to the appropriate spatial dimension(s). Other characteristics of the derived solutions are different coefficients of longitudinal and transverse hydrodynamic dispersion and radioactive decay of the transported solute. Solutions were obtained for time-dependent (nonequilibrium) sorption following three solute injection characteristics: instantaneous injection of a finite mass of solute, continuous injection of solute varying in time, and injection for a specified time followed by transport with no further injections. Solutions were obtained for solute concentrations in the fluid phase and on the solid phase as functions of location and time. The solutions obtained are not expressible directly in terms of known mathematical functions. Instead, solutions have the form of single or double integrals, with regard to time, of products of known functions, e.g., products of exponential functions and Bessel functions. Numerical results must be computed using numerical quadrature methods; computer codes to perform these calculations have been written.

When account was taken of changing populations of sorption sites on the solid phase, a nonlinear rate expression for nonequilibrium sorption and desorption was obtained; when this expression was coupled to the classical solute transport equation, the resulting nonlinear system was not solvable analytically. An algorithm for numerical simulation of this system was constructed.

Introduction of the formalism of the thermodynamics of irreversible processes produced a transport equation in which the driving force for diffusional transport is the transported solute's chemical potential gradient. The time-dependent form of the transport equation is then nonlinear because of the nonlinear relationship between mass concentration and chemical potential of a solute. However, the transport equation for the steady state is linear because temporal derivatives of mass concentrations do not appear. Also, chemical reaction rates are now expressed in terms of their thermodynamic affinity, a linear combination of chemical potentials of reactants and products. Because of these simplifying features, simple steady-state systems with chemical reactions were studied before proceeding to time-dependent systems. The initial studies of steady-state systems pointed out the possibility of using a minimum property of such systems as a tool for analysis of complex reacting and diffusing systems. This property is a nonzero, minimum value of the rate of entropy production by irreversible processes in the steady state of an open system. It is analogous to the minimum value of Gibbs free energy reached by a closed system at equilibrium. Use of this property for analysis of steady-state systems is currently being investigated.

THERMAL CONDUCTIVITY OF AQUEOUS NaCl SOLUTIONS FROM 20°C TO 330°C

H. Ozbek and S. L. Phillips

INTRODUCTION

An important aspect of the development and use of geothermal energy is our use of thermodynamic and transport data for hot brines, which transport heat, and for vapors, which drive turbines to produce electricity. although geothermal brines contain a large number of dissolved electrolytes and gases, the main constituent is NaCl. Consequently, modeling and other studies that require basic data on geothermal brines are generally based on those of aqueous NaCl solutions (Lyon and Kolstad, 1974; Silvester and Pitzer, 1977). Although data on many basic properties are needed, this report covers a survey of the available data on the thermal conductivity of aqueous NaCl solutions for regions of geothermal interest: temperatures to 350°C, pressures to 500 bars (50 MPa), and concentrations up to saturation.

The published literature on the thermal conductivity of NaCl solutions to high temperatures is not extensive; this is especially true for studies of NaCl at temperatures exceeding 80°C. Only one series of measurements are available to 150°C: these are the data published by Korosi and Fabuss for application to seawater desalination (Fabuss and Korosi, 1968; Korosi and Fabuss, 1968). By far, the most extensive data are contained in graphical form in the publication by Yusufova et al. (1975) with over 50 data points between 100°C and 330°C. However, accurate values cannot be read from the graphs.

Unless otherwise noted, the data were compiled from the original publications. Numerical values were converted where necessary to units of °C, molal concentration, and W/m·°C. The density data needed to convert molar to molal concentrations were obtained from the paper by Rowe and Chou (1970). Data on the thermal conductivity of water and the corresponding correlation equation are contained in publications of the International Conference on the Properties of Steam (Haywood, 1966; Kestin and Whitelaw, 1966).

Additional information on the theory and instrumentation is obtained from Thermal Conductivity (Touloukian et al., 1970); theory and correlations from the publications by Kestin and Whitelaw (1966), Riedel (1951), Korosi and Fabuss (1968), Fabuss and Korosi (1968), and Yusufova et al. (1975). Tabulated data for sodium chloride solutions are given in Table 1. Of special interest are the survey by Jamieson et al. (1975), and the correlation developed for sea water by Jamieson and Tudhope (1970).

Scope of Compilation

The time span covered is mainly from 1929 to 1979; earlier data are found in the International Critical Tables (Washburn, 1929). Besides data on

the thermal conductivity of aqueous NaCl solutions, selected portions of the available literature are included on theory, instrumentation, data estimation methods, other salts (e.g., potassium chloride), and sea water.

Analytical Expressions and Correlations

Yusufova et al. (1975) measured the thermal conductivity of aqueous sodium chloride solutions for temperatures ranging from 20°C to 330°C and concentrations of 5, 10, 15, 20, and 25 wt% NaCl. They developed the following correlation equation, which reproduces their experimental data for over 50 values with a reported deviation of 2%:

$$\frac{\lambda}{\lambda_w} = 1.0 - (2.3434 \times 10^{-3} - 7.924 \times 10^{-6}\, T + 3.924 \times 10^{-8}\, T^2)\, S + (1.06 \times 10^{-5} - 2 \times 10^{-8}\, T + 1.2 \times 10^{-10}\, T^2)\, S^2 , \qquad (1)$$

where

$$S = \frac{5844.3 \times m}{1000 + 58.443 \times m} .$$

The correlation given by Yusufova et al. is the only one available that represents a large number of data points in the temperature and pressure range of geothermal interest. As seen, equation (1) is the ratio of the thermal conductivity of NaCl solutions to that of pure water. Yusufova et al. used the following liquid water equation which appeared in the publications of the Sixth International Conference on the Properties of Steam (Haywood, 1966; Kestin and Whitelaw, 1966).

$$\lambda_w = -0.92247 + 2.8395 \left(\frac{T + 273.15}{273.15}\right) - 1.8007 \left(\frac{T + 273.15}{273.15}\right)^2 + 0.52577 \left(\frac{T + 273.15}{273.15}\right)^3 - 0.07344 \left(\frac{T + 273.15}{273.15}\right)^4 \qquad (2)$$

Equation (2) is valid for temperatures ranging from 0°C to 330°C at saturation pressures.

Equations (1) and (2) were selected in this work to reproduce and interpolate data on the thermal conductivity of NaCl solutions. Figure 1 shows the variation in thermal conductivity for concentrations from 0 to 5 m NaCl and temperatures between 50°C and 300°C. As shown, the thermal conductivity decreases almost linearly at each temperature as the concentration increases. Figure 2 is a plot of thermal conductivity versus temperature with concentration as a parameter. The thermal conductivity increases with increasing temperatures up to a broad maximum near 140°C, then decreases with concentration, by a maximum of 7% for 5 m NaCl as compared with pure water. Table 1 consists of smoothed values for the thermal conductivity of

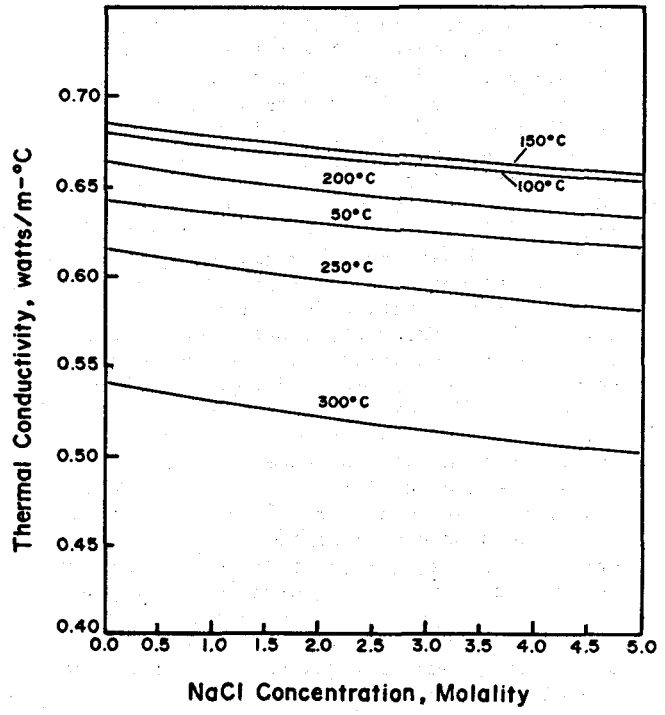

Figure 1. Thermal conductivity of aqueous NaCl solutions as a function of NaCl concentration at temperatures indicated. (XBL 802-8167)

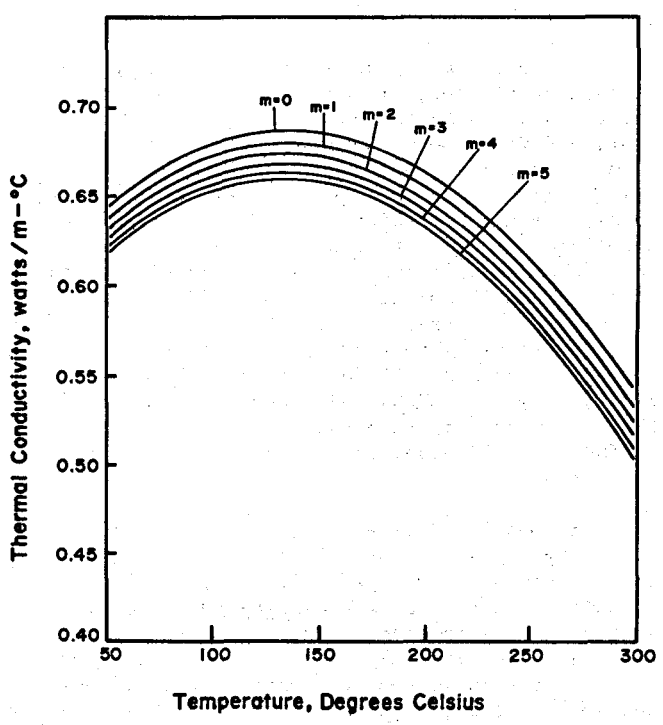

Figure 2. Thermal conductivity of aqueous NaCl solutions as a function of temperature at molalities shown. (XBL 802-8168)

Table 1. Recommended values for the thermal conductivity of aqueous NaCl solutions, calculated from Equations (1) and (2), W/m-°C (λ).

Temperature (°C)	Concentration (m)					
	0	1	2	3	4	5
20	0.603	0.596	0.590	0.585	0.580	0.577
30	0.618	0.611	0.605	0.600	0.595	0.592
40	0.632	0.624	0.618	0.613	0.609	0.605
50	0.643	0.636	0.630	0.625	0.621	0.617
60	0.653	0.646	0.640	0.635	0.631	0.627
70	0.662	0.655	0.649	0.644	0.640	0.636
80	0.670	0.663	0.657	0.652	0.647	0.643
90	0.676	0.669	0.663	0.658	0.653	0.649
100	0.681	0.674	0.668	0.662	0.658	0.654
110	0.684	0.677	0.671	0.666	0.661	0.658
120	0.687	0.679	0.673	0.668	0.664	0.660
130	0.688	0.680	0.674	0.669	0.664	0.661
140	0.688	0.680	0.674	0.669	0.664	0.660
150	0.687	0.679	0.673	0.667	0.663	0.659
160	0.684	0.677	0.670	0.665	0.660	0.656
170	0.681	0.673	0.667	0.661	0.656	0.652
180	0.677	0.669	0.662	0.656	0.651	0.647
190	0.671	0.663	0.656	0.650	0.645	0.641
200	0.665	0.656	0.649	0.643	0.638	0.633
210	0.657	0.648	0.641	0.635	0.630	0.625
220	0.648	0.640	0.632	0.626	0.620	0.616
230	0.639	0.630	0.622	0.616	0.610	0.605
240	0.628	0.619	0.611	0.604	0.599	0.594
250	0.616	0.607	0.599	0.592	0.586	0.581
260	0.603	0.594	0.586	0.579	0.573	0.567
270	0.589	0.580	0.571	0.564	0.558	0.553
280	0.574	0.565	0.556	0.549	0.543	0.537
290	0.558	0.548	0.540	0.532	0.526	0.520
300	0.541	0.531	0.522	0.515	0.508	0.503
310	0.523	0.512	0.504	0.496	0.489	0.484
320	0.503	0.493	0.484	0.476	0.470	0.464
330	0.482	0.472	0.463	0.455	0.449	0.443

aqueous NaCl solutions from 20°C to 330°C over the concentration range 0 to 5 m.

Summary and Conclusions

The correlation in Equation (1) generally reproduces the experimental data to better than ±2% between 20°C and 80°C; an exception are the data of Korosi and Fabuss where the deviation ranges from +5.3 to +13.8%. Between 100°C and 150°C, the deviation between the calculated values and the data of Korosi and Fabuss increases to +31.6% at 150°C. However, we assume their values to be incorrect partly because they are consistently higher than the other values at temperatures below 80°C, and partly because Korosi and Fabuss felt their measurements should be considered tentative (Korosi and Fabuss, 1968; Fabuss and Korosi, 1968; Jamieson and Tudhope, 1970). In addition, the values obtained for sea water concentrations to 150°C are consistently lower than those of Jamieson and Tudhope.

PLANNED ACTIVITIES IN FISCAL YEAR 1980

Fiscal year 1980 is expected to see a revision of our previous work on the viscosity of NaCl solutions to include recent data to 350°C. We also expect to expand our evaluation by surveying the basic properties of selected elements with relevance to nuclear waste isolation.

REFERENCES CITED

Fabuss, B. M., and Korosi, A., 1968. Properties of sea water and solutions containing sodium chloride, potassium chloride, sodium sulfate and magnesium sulfate. Washington, D.C., U.S. Department of the Interior, Office of Saline Water Resource Development Program, report 384.

Haywood, R. W., 1966. 6th Intl. Conf. on Properties of Steam. Trans, ASME, Journal of Engineering and Power, v. 88, p. 63.

Jamieson, D. T., and Tudhope, J. S., 1970. Physical Properties of Sea Water Solutions. Desalination, v. 8, p. 393.

Jamieson, D. T., Irving, J. B., and Tudhope, J. S., 1975. Liquid thermal condictivity: A data survey to 1973. Edinburgh, Her Majesty's Stationery Office.

Kestin, J., and Whitelaw, J. H., 1966. 6th Intl. Conf. on Properties of Steam. Trans. ASME,

Journal of Engineering and Power, v. 88, p. 82.
Korosi, A., and Fabuss, B. M., 1968. Thermophysical properties of saline water. Office of Saline Water Resource Development Program, report no. 363.
Lyon, R. N., and Kolstad, G. A., eds., 1974. A recommended research program in geothermal chemistry. U.S. Department of Energy, WASH-1344.
Riedel, L., 1951. Thermal Conductivity of Aqueous Solutions of Strong Electrolyutes. Chem. Ing. Technik., v. 23, p. 59.
Rowe, A. M., and Chou, J. C. S., 1970. PVTC Relation of Aqueous NaCl Solutions. Journal of Chemical Engineering Data, v. 15, p. 61.
Silvester, L. F., and Pitzer, K. S., 1977. Thermodynamics of Electrolytes. 8. Journal of Physical Chemistry, v. 81, p. 1822.
Touloukian, Y. S., Liley, P. E., and Saxena, S. C., 1970. Thermal conductivity. New York, IFI/Plenum Data Corporation, v. 3.
Yusufova, V. D., Pepinov, R. I., Nikolaev, V. A., and Guseinov, G. M., 1975. Thermal Conductivity of Aqueous NaCl Solutions. Inzh. Fiz. Zh., v. 29, p. 600.
Washburn, E. W., ed., 1929. International critical tables. New York, McGraw-Hill, v. 5.

AQUEOUS SOLUTIONS DATA BASE TO HIGH TEMPERATURES AND PRESSURES, SODIUM CHLORIDE SOLUTIONS

S. L. Phillips, R. J. Otto, H. Ozbek, and M. Tavana

INTRODUCTION

Lawrence Berkeley Laboratory is funded by the U.S. Department of Energy to provide a comprehensive data base on the basic properties of aqueous solutions involved in geothermal energy (Lyon and Kolstad, 1974). The compilation, which includes critical evaluation and correlation, constitutes a source of recommended values to be used in research and development of both electric power generation and direct use. In addition, the results of this work include identification of those areas where data are either lacking or are inadequate, and recommendations for research designed to provide the needed data. Because data on the basic properties of individual geothermal brines vary from site to site and are virtually nonexistent, it is common practice to rely on those of aqueous sodium chloride solutions as a substitute. In this paper it is not possible to cover all data for each solution of interest. (More complete information is obtained from Haas, 1976; Potter et al., 1977; Phillips et al., 1979; Pitzer et al., 1979; Ozbek et al., 1977; Ozbek and Phillips, 1979; Marshall and Jones, 1974; Holmes et al., 1978; Smith-Magowan and Goldberg, 1978; Silvester and Pitzer, 1977.)

This report is limited to a survey of the experimental data and correlations for NaCl solutions up to 350°C temperatures and 50 MPa pressures. The objectives of the work are mainly to: (1) obtain correlation equations that reproduce the available experimental data on the basic properties of aqueous NaCl solutions over a range of temperatures up to 350°C and pressure to 50 MPa; (2) to develop tables of smoothed data based on the correlation expressions and to provide reasonable estimates of these properties through extrapolation, where necessary, into the region of geothermal interest; and (3) to prepare a handbook containing evaluation procedures, equations, tables of smoothed data, and recommendations for future research in areas where the current data are either lacking or inadequate (Phillps et al., 1979).

ACCOMPLISHMENTS IN FISCAL YEAR 1979

The basic properties of NaCl solutions can be organized in several ways; it is convenient here to separate them as indicated in Table 1. The table lists these classes of basic enegy data for NaCl solutions and the measurement means commonly used to obtain the data.

A review of the current status of data on selected properties of NaCl solutions in the temperature range 0° to 350°C and pressures up to 50 MPa shows that only limited data are available for providing tables of smoothed values. (See Table 2 for references to selected correlations for the data.) Experimental data are needed mainly for pressures different from vapor saturation, and at temperatures above about 150 to 200°C for viscosity, thermal conductivity, enthalpy, and heat capacity. All properties need to be correlated as new data are made available; this will result in both improved fits of the equations and in better extrapolation procedures.

After reviewing current data in terms of the geothermal energy program's needs, we found that the "ideal" data obtainable from published literature should include the following:

1. Experimental values in tabular form showing concentration, temperature, pressure, and the measured value of the basic property. The data can then be used to develop correlation expressions and for calculations of mean values and deviations from the mean.

2. Measurements on the basic properties of site-specific geothermal brines under operating conditions, or from samples that are preserved to the greatest extent possible. These measurements would permit a comparison between NaCl solutions and the various brines.

3. Use of a consistent set of units for the various data. Experimental values are currently published using a variety of units for temperatures, pressure, concentration, and property; these must then be converted to a standard form before evaluation. The International System of units should be used.

4. A description of any special instrumentation or materials used in obtaining the experimental

Table 1. Selected basic energy properties of sodium chloride solutions and commonly used methods of measurement to high temperatures.

Basic property	Temperature (°C)	Method
Heat of solution	0-100	Calorimeter (glass)
	100-200	Calorimeter (Ti)
	300	Calorimeter (Ti-Pd)
Heat of dilution	10-100	Calorimeter
		Flow calorimeter
	184-712 (51; 100 MPa)	Calorimeter (Hastelloy)
Heat of solution at infinite dilution	0-300	Calorimeter; vapor pressure
Heat capacity	1-85	Calorimeter (stainless steel)
		Flow calorimeter
		Bomb calorimeter (gold-plated beryllium copper)
Vapor pressure	25-100	Manometer
	75-700	Differential manometer (Pt cups)
		Isotensicope
		Bomb (stellite)
Viscosity	25-150	Cannon glass capillary
		Ostwald and Ubbelohde
		Oscillating disk
Thermal conductivity	25-50	Coaxial cylinders
	25-150	Continuous line source
	25-330	Flat plate
Electrical conductivity	0-800	Conductance cell (Pt-Ir)
		Four-electrode cell (ceramic, Pt)
Density	0-200	Sinker
	20-75	Pycnometer
	25-350	Hydrostatic weighing
	150-500	Autoclave, filling temperature
Solubility	0-300	Sample analysis
	148-425	Pressure-temperature (Pt vessel)

values. Sodium chloride solutions are highly corrosive at high temperatures and pressures. This can cause undesirable side reactions and interfere with measurement of the property.

5. Data on the effects of other substances (e.g., KCl, $CaCl_2$, CO_2) on the properties of NaCl solution. Geothermal brines are complicated solutions that consist of a large number of substances besides NaCl; these are present in amounts which may significantly change the properties of the NaCl solution as the temperature and pressure are changed.

6. Foreign language publications with an English language abstract, and English language headings for both tables of data and for graphs. There is much delay in evaluating data when there is a need for translations.

Table 2. Selected correlations for the basic energy properties of NaCl solutions and pure water to high temperatures.

NaCl Solutions					
Property	Temperature (°C)	Concentration (m)	Pressure (MPa)	Accuracy	References
Thermal conductivity	20-300	0-5	saturation	± 2%	Ozbek and Phillips, 1979
Viscosity	0-150	0.5-5	to 30	± 1.5%	Ozbek et al., 1977
	0-300	0-6	saturation	± 1%	Potter, 1978
Electrical conductivity	0-800	0.001-0.1	to 400		Quist and Marshall, 1968
Electrical resistivity	22-375	0.2-4 molar	30	± 2%	Ucok et al., 1979
Solubility	0-600		saturation		Potter et al., 1977
Specific volume	40-280	0.001-1.5	10		Gorbachev et al., 1979
	0-175	0-25%w	to 350 kg-cm^{-2}	1.5 ppt	Rowe and Chou, 1970
Density	20-150	0-6	to 35		Kestin et al., 1978
	80-325	0-30	saturation	± 0.002 g/cm^3	Haas, 1976
					Ozbek and Phillips, 1979
Vapor pressure	75-325	0-saturation		0.32%	Haas, 1976
Heat of solution	0.01-300	0.25-25%w	saturation	<5 KJ/mole	Pitzer et al., 1979
Heat of solution at infinite dilution	0-300		saturation		Pitzer et al., 1979
Heat of dilution					Pitzer et al., 1979
Heat capacity	0-300	0.25-25%w	saturation	0.004-0.17 J/mole-°C	Pitzer et al., 1979
Total enthalpy	0-300		saturation		Pitzer et al., 1979
Specific heat capacity	0-300		saturation		Pitzer et al., 1979

Water			
Energy property	Temperature (°C)	Pressure (MPa)	References
Thermal conductivity	0<T<800	0.1<P<100	Haywood, 1966
Viscosity	0<T<800	0<P<100	IAPS, 1976
Specific enthalpy	0.01<T<374	0.0006113<P<22.09	Keenan et al., 1978
Specific volume	0.01<T<374	0.0006113<T<22.09	Keenan et al., 1978
Vapor pressure			Keenan et al., 1978
Heat capacity			Keenan et al., 1978

EXPECTED RESULTS IN FISCAL YEAR 1980

In fiscal year 1980, we expect to complete a survey of data on other electrolytes (e.g., KCl, $CaCl_2$) and gases (e.g., H_2S, CO_2). A revision to an earlier report on viscosity is also expected.

REFERENCES CITED

Gorbachev, S. V., Kondratev, V. P., Androsov, V. I., and Kolupaev, V. G., 1974. Specific volumes of aqueous solutions of alkali-metal chlorides. Russian Journal of Physical Chemistry, v. 48, p. 2789-2791.

Haas, J. L., Jr., 1976. Physical properties of the coexisting phases and thermochemical properties of the H_2O component in boiling NaCl solutions. U.S. Geological Survey Bulletin 1421-A.

Haywood, R. W., 1966. Sixth international conference on the properties of steam--supplement on transport properties. Journal of Engineering and Power, v. 88, p. 63-66.

Holmes, H. F., Baes, C. F., Jr., and Mesmer, R. E., 1978. Isopiestic studies of aqueous solutions at elevated temperatures. I. Journal of Chemical Thermodynamics, v. 10, p. 983.

International Association for the Properties of Steam, 1976. Release on dynamic viscosity of water substances. Mechanical Engineering, v. 98, p. 79.

Keenan, J. H., Keyes, F. G., Hill, P. G., and Moore, J. G., 1978. Steam tables. New York, John Wiley and Sons.

Kestin, J., Abe, Y., Grimes, C. F., Khalifa, H. E., Sookiazian, H., and Wakeham, W. A., 1978. The effect of pressure on the viscosity of aqueous

NaCl solutions in the temperature range 20-150°C. Journal of Chemical Engineering Data, v. 23, p. 328.

Lyon, R. N., and Kolstad, G. A., eds., 1974. A recommended research program in geothermal chemistry. Springfield, Virginia, National Technical Information Service, report WASH-1344.

Marshall, W. L., and Jones, E. V., 1974. Liquid-vapor critical temperatures of aqueous electrolyte solutions. Journal of Inorganic Nuclear Chemistry, v. 36, p. 2312-2318.

Ozbek, H., Fair, J. A., and Phillips, S. L., 1977. Viscosity of aqueous sodium chloride solutions from 0-150°C. Berkeley, Lawrence Berkeley Laboratory, LBL-5931.

Ozbek, H., and Phillips, S. L., 1979. Thermal conductivity of aqueous NaCl solutions from 20°C to 330°C. Berkeley, Lawrence Berkeley Laboratory, LBL-9086.

Phillips, S. L., Otto, R. J., Ozbek, H., and Tavana, M., 1979. Aqueous solutions data base to high temperatures and pressures NaCl solutions. Berkeley, Lawrence Berkeley, Laboratory, LBL-9621.

Pitzer, K. S., Bradley, D. J., Rogers, P. S. Z., and Peiper, J. C., 1979. Thermodynamics of high temperature brines. Berkeley, Lawrence Berkeley Laboratory, LBL-8973.

Potter, R. W., II., 1978. Viscosity of geothermal brines. Trans., Geothermal Resources Council, v. 2, p. 543-544.

Potter, R. W., II., Babcock, R. S., and Brown, D. L., 1977. A new method for determining the solubility of salts in aqueous solutions at elevated temperatures. Journal of Research of U.S. Geological Survey, v. 5, no. 3, p. 389-395.

Quist, A., and Marshall, W. L., 1968. Electrical conductances of aqueous sodium chloride solutions from 0 to 800° and at pressures to 4000 bars. Journal of Physical Chemistry, v. 72, p. 684-703.

Rowe, A. M., Jr., and Chou, J. C. S., 1970. Pressure-volume-temperature-concentration relation of aqueous NaCl solution. Journal of Chemical Engineering Data, v. 15, no. 1, p. 61-66.

Silvester, L. F., and Pitzer, K. S., 1977. Thermodynamics of electrolytes. 8. High temperature properties, including enthalpy and heat capacity, with application to sodium chloride. Journal of Physical Chemistry, v. 81, no. 19, p. 1822-1828.

Smith-Magowan, D., and Goldberg, R. N., 1978. A bibliography of sources of experimental data leading to thermal properties of binary aqueous electrolyte solutions. Washington, D. C., National Bureau of Standards.

Ucok, H., Ershaghi, I., and Olhoeft, G. R., 1979. Electrical resistivity of geothermal brines. Dallas, Society of Petroleum Engineers, paper SPE-7878.

Applied Research Studies

ENHANCED RECOVERY WITH MOBILITY AND REACTIVE TENSION AGENTS

C. J. Radke and W. H. Somerton

INTRODUCTION

The objectives of the present study are (1) to establish the conditions requisite for tertiary-mode displacement of acidic oils with pH agents, and (2) to elucidate the dominant recovery mechanisms and hence permit development of an improved caustic flooding package. The overall project includes studies on restored-state core displacements of Ranger Zone Wilmington oil sands, chemical transport, emulsion flow and displacement, and interfacial tensions. Progress during 1979 is summarized.

CORE DISPLACEMENTS

During 1979, eight additional core tests were performed, aimed at recovering tertiary oil from resaturated Ranger Zone sand packs at reservoir temperature (125°F) and rate (1.5 ft/day). The flooding procedure is identical to that described previously (Radke and Somerton, 1978), except that the cores are no longer packed in the completely frozen state. The focus is on tertiary oil recovery, and the brine flood is continued until water-to-oil ratios in excess of 10^3 are attained. The brine contains no hardness ions (i.e., calcium or magnesium), so flooding results are not complicated by any ion-exchange phenomena. During flooding, the effluent production history and pH are monitored, and the core pressure drop is recorded so that dynamic relative permeabilities may be determined (Johnson et al., 1959).

Typical flooding results are shown in Figure 1. Waterflood performance shows very early breakthrough followed by oil production at high water-to-oil ratios. This is the result of the high viscosity of the well B108 crude oil used in all our testing. Figure 2 shows that this oil's viscosity at reservoir temperature (~50°C) exceeds 100 cp giving an oil-to-water viscosity ratio of more than 200. Also shown in Figure 2 is the viscosity of well C331 crude oil, suggesting large variability in properties of the Wilmington Ranger zone crude.

Initial pH of the water flood was varied between 11 and 13 in three tests. The pH 11 tertiary flood was used to test the importance of interfacial tension, which is low under these conditions (Radke and Somerton, 1978.) A pH near 12 is anticipated for the Wilmington field test (City of Long Beach, 1978), and the higher pH 13 tertiary flood is used to examine possible oil production with earlier caustic breakthrough. All tertiary recoveries are almost independent of the caustic and salt concentration. Caustic breakthrough time, however, decreases dramatically with increasing pH.

To gain a basic understanding of the tertiary recovery performances, the simplified chemical

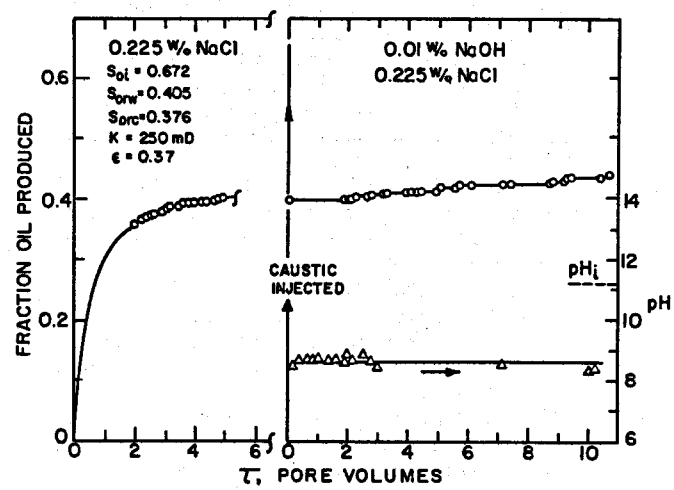

Figure 1. Production performance and pH history of B108 oil by pH 11 caustic. (XBL 797-6603)

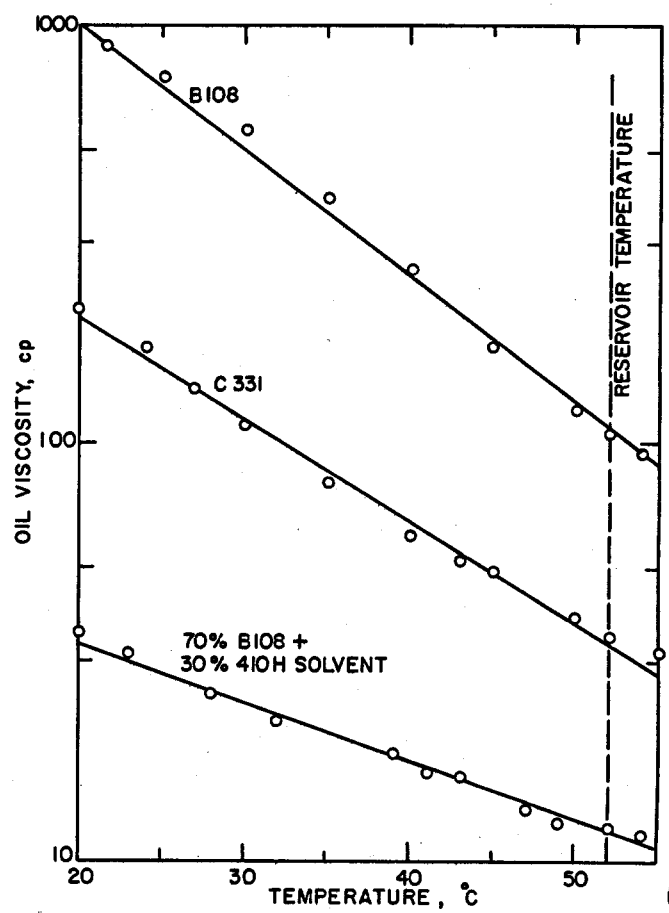

Figure 2. The viscosity of Wilmington-Ranger zone crude oils as a function of temperature. (XBL 797-6605)

flooding model of Fayers and Perrine (1959), Claridge and Bondor (1974), and Castor (1979) was applied. In the model, the saponified surfactants are assumed to alter the relative permeability to the oil phase. Further, since the in-situ hydrolyzable acids exist as surfactants only in the alkali, they are presumed to chromatograph with the caustic. Caustic elution in turn is controlled by a reversible adsorption isotherm with a nominal breakthrough delay at pH 12 of 5 pore volumes. The fractional flow curves to water and chemical are taken to be those of Craig (1971).

To ascertain the possible benefits of mobility control, the B108 well crude oil was diluted by a thinner. The viscosity of this mixture is shown in Figure 2, and the flooding results are portrayed in Figure 3. Tertiary production is still poor, but does occur earlier, as predicted. Of course, this experiment is not definitive because dilution of the crude oil also dilutes the concentration of natural acids.

The conclusion at present is that in low-permeability cores of high sorptive capacity, caustic flooding of viscous crude oils recovers minimal additional oil when commenced at high water-to-oil ratios. The caustic process must be augmented; mobility control is a prime candidate.

CHEMICAL TRANSPORT

The chromatographic movement of chemical species in Wilmington oil sands is important to the caustic process because these unconsolidated sands have high sorptive capacities. The transport of hydroxyl ions and the ion exchange between sodium and calcium are being studied. The procedure used is frontal analysis chromatography in which the column effluent concentration is monitored after a step change in concentration is imposed at the column inlet (Radke and Somerton, 1978). Material balance then determines the sorptive consumption (Radke and Somerton, 1978; Wang et al., 1978). Analysis of the shapes of such breakthrough curves also permits identification of the kinetics of the sorption process (Radke and Somerton, 1978; Trogus et al., 1976; Ramirez et al., 1979), and hence, extrapolation to field conditions.

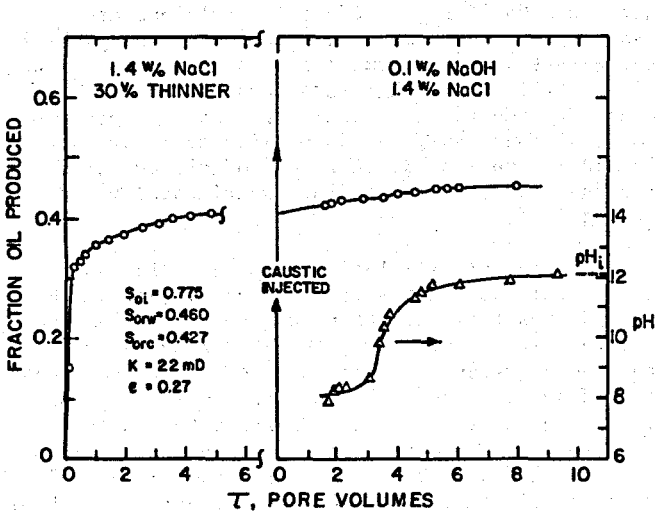

Figure 3. Production performance and pH history of thinned B108 oil by pH 12 caustic. (XBL 797-6602)

Caustic Loss

Caustic loss in a reservoir can be due to several causes including surface adsorption, solid dissolution, solid reaction, insoluble salt formation (by hardness ions), and neutralizatin of acids in the crude oil. The first four factors are studied in this work. Caustic consumption by saponification of the crude oil is minimal for all but extremely high acid number oils.

Figure 4 shows the caustic consumption by Wilmington oil sand is a function of pH at various temperatures and salt concentration. Reservoir temperature is approximately 50°C, and 1 wt% salt corresponds to anticipated flooding conditions (City of Long Beach, 1978). Caustic consumption is approximately Langmuirian, and increases with increasing temperature, but decreases with increasing salt. Sodium orthosilicate (SiO_2/Na_2O = 0.5) consumption at pH ~12 is equivalent to caustic, indicating no buffering action. Further, orthosilicate requires a higher weight concentration to achieve the same pH as caustic soda.

Figure 4 may be used in conjuction with equilibrium chromatographic theory (DeVault, 1943) to predict the elution behavior of caustic in the oil displacement tests. At pH 11, no elution is expected until after 10 pore volumes, which explains why caustic has not arrived at the core exit in Figure 1.

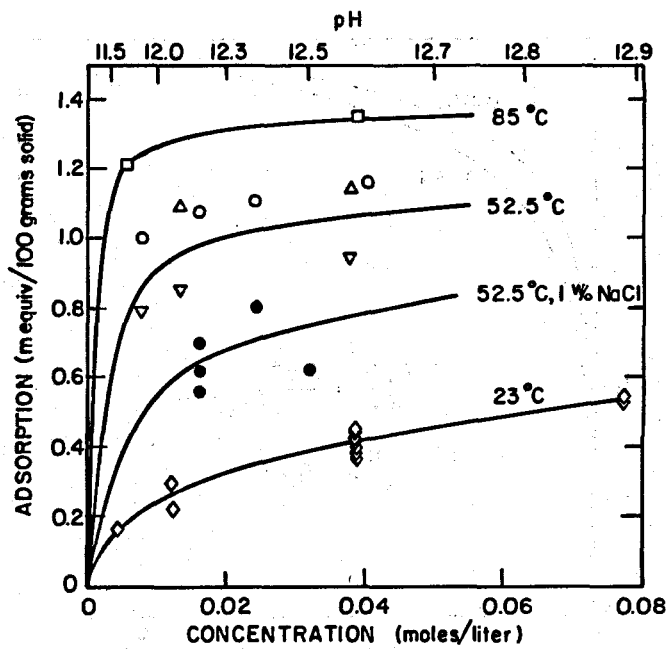

Figure 4. Caustic adsorption on Ranger-Zone reservoir sand as a function of hydroxyl concentration. (XBL 788-5600)

Several investigations of alkali flooding have suggested that caustic is consumed by dissolution of reservoir rock especially at higher temperatures (Ehrlich and Wygal, 1976; Cooke et al., 1974; Robinson et al., 1977). No evidence of mineral dissolution in column testing has been seen. One explanation is that the effluent response for caustic is a combination of linear reversible sorption kinetics and irreversible first-order rock dissolution. For laboratory studies with short cores and amenable superficial velocities, the caustic dissolution rate constant is apparently too small to have a noticeable influence on the caustic effluent response curves. Nevertheless, one can establish an upper bound of 10^{-7} sec^{-1} for k_D (first-order dissolution rate constant) of Wilmington oil sand at 50°C in 1 wt% sodium chloride. It is critical to ascertain how important this value will be under reservoir conditions.

Ion Exchange

Because hardness (i.e., calcium and magnesium) is present in the Wilmington waterflooded zones, it may impair caustic flooding performance by precipitation of divalent soaps which are generated by saponification of the acid oils. Hence, soft water preflushing is desirable. The cation exchange capacity (CEC) of Wilmington oil sands at 50°C has been determined to be approximately 2.5 milliequivalents per 100 g of reservoir sands. Frontal analysis chromatography at several sodium-to-calcium inlet concentration ratios and levels shows that the exchange isotherm is well represented as a mass action relationship. Figure 5 shows the ion-exchange isotherm for two salinities of 0.18 and 0.36 equivalents per liter, which corresponds to 1 and 2 wt% sodium chloride solutions, respectively. Figure 5 permits design of soft water preflush slugs by equilibrium chromatography theory.

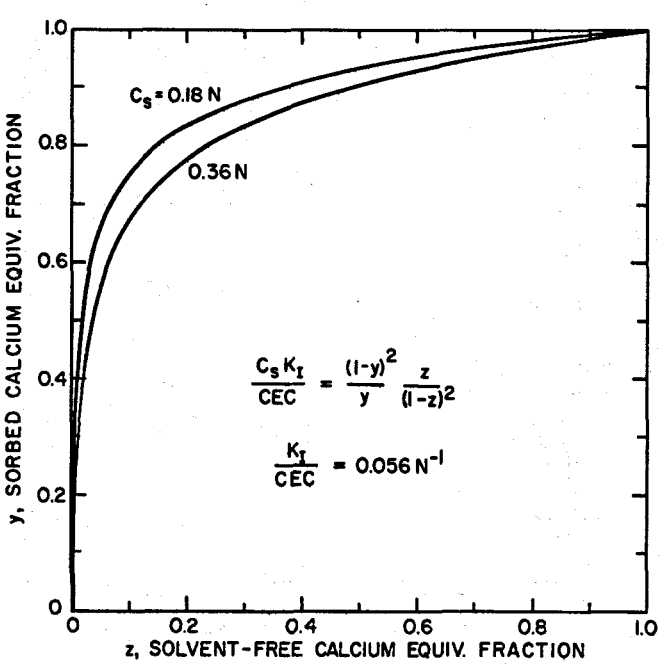

Figure 5. Sodium/calcium ion exchange isotherm at 52.5°c and at two salinities.

(XBL 797-6592)

EMULSION FLOW

Filtration Model

As a prelude to investigating emulsions as mobility control agents, the flow of dilute stable emulsions in unconsolidated porous media is being studied. The contention is that emulsified oil drops transport according to filtration principles. The details of the filtration model are available elsewhere (Radke and Somerton, 1977, 1978; Soo and Radke, 1979). Here, the only salient features are reviewed.

Equations have been developed that characterize emulsion flow behavior by three parameters: (1) a filter coefficient, (2) an interpore diversion factor, and (3) a local flow restriction factor. These expressions show that the filter coefficient controls the sharpness of the emulsion front, the diversion parameter dictates the steady-state retention, and the flow restriction parameter describes the effectiveness of retained drops in reducing permeability.

New transient permeability and effluent suspension concentration data are obtained for dilute oil in water emulsions of mean drop size ranging from 2 to 10 μm flowing in cores of 0.06 and 1.2 Darcy permeabilities at superficial velocities of 0.42 and 1.9 cm/min. The low-viscosity oil drops cause permeability reductions up to 90% with 4 to 5 μm sized drops and lower flow rates being most effective.

Emulsion Flooding

A major problem with the caustic flooding process is the lack of mobility control. Polymers may be used but they must be effective in and withstand the alkaline, high clay-content environment at elevated temperatures. The cost of the process also rises dramatically with use of polymer additives. An alternative is to use dilute emulsions. Because the mechanism of mobility control is solely by permeability reduction, emulsion effectiveness is quite impervious to temperature and alkalinity. With acid California crude oil, emulsions are easily prepared in alkaline water with no synthetic surfactants. Hence, emulsions would be less expensive mobility-control agents than polymers. However, fundamental questions arise as to whether or not emulsions can actually provide mobility control. Secondary emulsion displacement of viscous oils is, therefore, being studied experimentally and theoretically.

A standard oil-flooding apparatus is under construction. A commercial HPLC pump (Altex Model 101) drives the oil, water, and emulsion via mercury displacement. Presently, the HPLC pump is unable to handle mercury because of check balls whose densities are less than that of mercury. Also, in injecting emulsion, it is important to supply a uniform drop concentration over long time periods. This is difficult because of creaming. The emulsion is stirred in a displacement reservoir without using high-pressure seals. An external magnet reciprocates vertically in a concentric tube moving an internal magnet, which provides the stirring action. The magnets' poles are opposed so that

the internal magnet is pushed upward. It then settles by gravity. Emulsion displacement both in homogeneous cores, and in heterogeneous systems will be studied to ascertain possible improvements in sweep efficiency.

In 1980, many of the research areas discussed herein will be investigated to improve the basic understanding of the factors that affect enhanced recovery with mobility and reactive tension agents and thus further establish the viability of this approach.

REFERENCES CITED

Castor, T. 1979. Enhanced recovery of acid oils by alkaline agents. (Ph.D. dissertation). Berkeley, University of California, Mechanical Eng. Department.

City of Long Beach, Department of Oil Properties and THUMS Long Beach Company, 1978. Caustic Waterflooding Demonstration Project, Ranger Zone, Long Beach unit, Wilmington field, California. City of Long Beach, 2nd Ann. Report.

Claridge, E. L., and Bondor, P. L., 1974. A graphical method for calculating linear displacement with mass transfer and continuously changing mobilities. Society Petroleum Engineering Journal, Dec., pp. 609-618.

Cooke, C. E., Williams, R. E. and Kolodzie, P. A., 1974. Oil recovery by alkaline waterflooding. Journal of Petroleum Technology, v. 26 no. 12.

Craig, F. F., Jr., 1971. The reservoir engineering aspects of waterflooding. Dallas, Soc. of Pet. Eng. of AIME, monograph, v. 1, chap. 8.

DeVault, D. The theory of chromatography, 1943. Journal Americal Chemical Society, v. 65, p. 532.

Ehrich, R. and Wygal, R. J., 1976. Interrelation of crude oil and rock properties with the recovery of oil by caustic waterflooding. Presented at the Improved Oil Recovery Symp. of the SPE, Tulsa, March 22-24.

Fayers, F. J., and Perrine, R. L., 1959. Mathematical description of detergent flooding in oil reservoirs. Trans. AIME, v. 216, pp. 277-283.

Johnson, E. F., Bossler, D. P., and Naumann, V. O., 1959. Calculation of relative permeability for displacement experiments. Trans. AIME v. 216, p. 370-372.

Radke, C. J., and Somerton, W. H., 1977. Enhanced recovery with mobility and reactive tension agents," in Proceedings, Third ERDA Symp. on Enhanced Oil and Gas Recovery and Improved Drilling Methods. U.S. Department of Energy, v. 1, p. B-5.

____, 1978. Enhanced recovery with mobility and reactive tension agents, in Proceedings, Fourth DOE Symposium on Enhanced Oil and Gas Recovery and Improved Drilling Methods. U. S. Department of Energy. v. 1A, p. B-2.

Ramirez, W. F., Shuler, P. J., and Friedman, F., 1979. Mass transport of surfactants in porous media. Presented at the 1979 California Regional Meeting of the Society of Petroleum Engineers of AIME. SPE-7951.

Robinson, R. J., Bursell, C. G., and Restine, J. L., 1977. A caustic steamflood pilot-Kern River field, preprint for 47th Ann. CA Reg. Meet. of SPE of AIME, Bakersfield, SPE-6523.

Soo, H., and Radke, C. J., 1979. Stable emulsion flow in porous media. 86th Nat. Meet. of AICHE, Houston.

Trogus, F., Sophany, T., Shechter, R. S., and Wade, W. H., 1976. Static and dynamic adsorption of anionic and nonionic surfactants. Presented at the 51st Ann. Fall Tech. Conf. and Exhib. of SPE AIME, New Orleans.

Wang, H. L., Duda, J. L., and Radke, C. J., 1978. Solution adsorption from liquid chromatography. J. Colloid. Int. Sci., v. 66, no. 1, p. 153. SPE-6004.

HIGH-PRECISION MASS SPECTROMETRY

M. C. Michel and W. R. Keyes

Previous research (Michel et al., 1978) has shown that the basic idea of simultaneous collection of ion beams can be applied to high-precision isotope ratio measurements of relatively heavy elements (e.g., strontium and neodymium). This year's work was directed at determining the factors limiting the precision of this system.

It had been found that the ion source used, which is necessitated by ion optical properties of the large mass spectrometer, caused considerably greater fractionation of isotopes during the useful life of the sample than more conventional ion sources. Because the isotope ratio of interest must be corrected for this fractionation by use of an internal standard, it is clearly desirable to minimize this correction to reduce the added errors involved in this calculation. Preliminary data indicate that spreading the sample over a large surface area substrate (such as silica gel) reduced the total fractionation range. More work needs to be done with controlled substrates to see if further reduction is possible.

With the development of sample handling techniques, measurements of isotope ratios on a NBS standard strontium sample were reproducible to about four parts in 100,000 even with the still large fractionation effects. This is comparable with the best work done by conventional sequential measurement techniques. Analyses of four basalt samples for the strontium isotope ratio ($^{87}Sr/^{86}Sr$) are summarized in the Table 1. These results demonstrate that, for such chemically processed samples, residual rubidium contamination limits the precision to the same degree as conventional techniques. It must be again noted that because of the special properties of the ion source, the interference may be somewhat worse. This is so because chemical separation by volatility difference may be slower for the cavity source over an open configuration. In addition, the closed ion source may encourage

Table 1. Analyses of four basalt samples for $^{87}Sr/^{86}Sr$.

Sample	1	2	3	4
$^{87}/^{86}Sr$	0.70753 ±0.00004	0.70759 ±0.00002	0.70531 ±0.00002	0.70509 ±0.00003

early diffusion of rubidium into the source metal surface to be re-emitted later during the sample measurement. This reduces the time during which the strontium ionization is free from rubidium.

It has been concluded that the advantages of simultaneous collection outweigh the disadvantages. Many possible avenues exist for improvement that have not been investigated. This work has been terminated for the present, but a relatively modest effort could yield precision levels that may not be available by conventional techniques. This would not necessarily be of general interest but the growing importance of Sm-Nd geochronology, where precision is even more important, indicates there may soon be a need for upgraded technology, as discussed herein.

REFERENCE CITED

Michel, M. C., Mosier, D. F., and Keyes, W. R., 1978. Four-channel simultaneous collection system for high precision mass spectrometry, in Earth Sciences Division Annual Report. Lawrence Berkeley Laboratory, LBL-8648, p. 189-191.

STATE-OF-THE-ART TRACER TECHNIQUES

S. M. Klainer and J. A. Apps

INTRODUCTION

During fiscal year, 1979 a research program was undertaken to evaluate whether improved tracers could be selected (or, if necessary, developed) to help define the characteristics of underground systems. In addition, techniques for detecting the chosen tracers have been considered. The tracer program was undertaken because much additional information was needed in at least four in-situ systems:

1. Evaluation of hydrological properties. The addition of tracer(s) in groundwaters will provide information on permeability, flow rate, etc.

2. Integrity of groundwater chemistry. The addition of tracer(s) to drilling fluids will provide the necessary marker(s) to assure that groundwater samples collected for analyses are representative and have not been contaminated during drilling.

3. Suitability of storage sites for nuclear waste. The addition of tracer(s) to a potential underground nuclear waste repository will aid in demonstrating the repository's integrity.

4. Measurement of chemical transport in natural systems. The addition of nonabsorbing tracers to dissolved radionuclides during injection provides a convenient means of measuring the retardation of radionuclide migration in groundwaters relative to the nonadsorbing tracer.

Presently employed tracer materials include the use of radioisotopes; S-F compounds; fluorescent dyes; and, most recently, C-F materials or fluorocarbons (Davis et al., 1980). Of these, only the C-F compounds have the potential of meeting both immediate and future tracer needs. We have, therefore, chosen to pursue the fluorocarbons as tracers because of their intrinsic chemical and physical properties and because of our ability to alter these with simple chemical procedures to meet specific needs. In addition, the presence of C-F compounds as natural backgrounds is nonexistent, except in contemporary waters where contamination has occurred due to the use of aerosol spray cans and refrigerants.

SELECTION OF TRACERS

The fluorocarbons that have tentatively been chosen for tracers are of three basic classes:

1. The low molecular weight compounds, such as $^{12}CF_4$ and $^{13}CF_4$,

2. The heavier molecular weight materials in the C_4 and C_5 range, with initial emphasis on these compounds:

```
      F   F
      |   |
  F - C - C - F

  F - C - C - F
      |   |
      F   F
```

3. Substituted C_4 and C_5 fluorocarbons.

The higher molecular weight compounds are of particular interest because they are much more specifically identifiable, and because their vapor pressure is much higher than one would expect for compounds in the 200 to 400 molecular weight range.

To determine the suitability of C-F compounds as tracers, these tracers must be tested in the laboratory for their adsorptive properties using columns packed with crushed rock or minerals to represent approximately in-situ conditions. Known concentrations of the tracer candidates, dissolved in water, will be passed through these columns.

The rate of elution, mass balance, and amount of fluorocarbon remaining on the column will be determined using gas chromatography and mass spectroscopy.

RECOVERY OF TRACER COMPOUNDS FROM NATURAL SYSTEMS

The physical state of the tracer at the point of detection and quantification will dictate, to a major extent, which analytical techniques are appropriate. In all cases the prerequisite for continuous measurements (as opposed to batch processes) on location will be adhered to as a primary requirement.

One concept is to filter the solids from the solution containing the tracer and then measure the dissolved fluorocarbons directly using optical spectrometry. Initial calculations indicated that sensitivities below the parts-per-million-range (sufficient for this program) should be theoretically obtainable. In natural systems, such as groundwaters, however, the indeterminate number of commonly present soluble constituents and their variable concentrations may present a background signal which will degrade system performance. This possibility was investigated by Dr. Peter Griffiths of Ohio University, using FT/IR (Fourier transform infrared) spectroscopy, and a preliminary report on his results indicates potential success. Even if the optical detection of fluorocarbons in solutions proves to be sufficiently sensitive, however, it will not be possible to discern the isotopic species, because of the width of the spectral bands, using mixtures of, for example $^{12}CF_4$ and $^{13}CF_4$ would not be possible.

A second approach now being seriously considered is to quantitatively remove the fluorocarbons from the solution, as a vapor, before analysis. This represents a realistic possibility as fluorocarbons, even in the C_4 and C_5 molecular weight range, are usually gases. The use of heating techniques to effect this separation do not appear feasible because of the amount of water which will be vaporized and because this method, of necessity, will reduce analyses response times so it may be no faster than batch techniques. The method being considered, therefore, is forced selective diffusion, which is akin to membrane separation. Albert Copeland, Jr., NASA, Johnson Spacecraft Center, Houston, Texas, has provided evidence that such separation techniques have been found feasible in mass spectrometry.

In this situation, tracer diffusion through the walls of fluorinated silicone tubing is the objective. The presence of the fluorine groups in the silicone matrix should make it possible to preferentially pass the fluorocarbon species. The inside of the silicone tubing will be at atmospheric pressure while its outside walls will be in a vacuum ($\sim 10^{-3}$ torr). The solution containing the tracer is filtered, to remove the particulates and other materials which may coat the walls of the tubing. It is then passed through the silicone tubing, and the tracer material is permitted to diffuse through the walls into the low pressure side of the system. Once it has been demonstrated that this method of tracer separation is either complete, or accurately predictable, then subsequent detection and quantification becomes relatively easy.

DETECTION INSTRUMENTATION

At the present time, instrumentation for measurements on tracer materials, both in the vapor and dissolved states, is being pursued. Experts in the field of instrumental analyses have been visited, and arrangements are being made whereby some basic information, needed to evaluate the various methods, can be obtained cost-effectively. As previously mentioned, Dr. Griffiths has done some FT/IR measurements. Raman or dipole laser infrared measurements have not yet been made. It is expected that the data supplied by Dr. Griffiths combined with information available in the literature will permit an "order-of-magnitude" estimation of sensitivity to be calculated for these latter two approaches.

Finally, now that there is a potential, as a result of membrane separation or reduced-pressure vapor sampling of the fluorocarbon, the use of a mass spectrometer becomes an attractive choice as a detector. Miniature mass spectrometers, suitable for in-field use, have been built by Lawrence Livermore Laboratory (LLL) and NASA. Discussions have been held with both organizations, and it appears that LLL will permit us to test our postulations on their unit.

SUMMARY

During fiscal year 1979, potential fluorocarbon tracer materials have been selected and undergone preliminary evaluation. These tracers offer great versatility because it should be possible to selectively change their chemical and physical behavior (especially absorptive properties) by proper substitution of other chemical groups at one or more of the fluorine sites.

At least two detection methods have been tentatively evaluated (infrared and mass spectrometry), and both systems appear to have the required sensitivity and specificity when presented with gas (vapor) samples. In addition, either instrument can be engineered for in-field use. The extraction of the tracer as a vapor from a liquid background matrix has been considered. In principle, selective membrane separation appears feasible. The practicality of this is yet to be achieved.

Continuation of this work will be done under funding from the Office of Nuclear Waste Isolation.

The authors wish to thank Dr. Maynard Michel of Lawrence Berkeley Laboratory for his inputs on mass spectrometry.

REFERENCE CITED

Davis, S. M., Thompson, G. M., Bently, H. W., and Stiles, G., 1980. Ground-water tracers: A short review. Groundwater, v. 18, p. 14-23.

CRYSTALLOGRAPHIC PROPERTIES USING THE NQR TECHNIQUE

S. M. Klainer and J. A. Apps

INTRODUCTION

The research performed in fiscal year 1979 was to identify and evaluate the potential use of Nuclear Quadrupole Resonance (NQR) Spectroscopy in the geosciences and particularly for energy-related problems. At this early stage of the evaluation, the possible uses of this method appear to be numerous and very important.

Many DOE mission areas such as nuclear waste isolation, contintental drilling, fossil fuel recovery, and geothermal energy require an in-depth understanding of earth sciences. Of particular interest is the development of new analytical techniques to develop a better understanding of mineralogy.

Presently, available instrumental techniques for studying mineralogical problems such as x-ray, electron and neutron diffraction, nuclear magnetic resonance (NMR), electron microscopy, and transmission electron microscopy have inherent limitations. These techniques are unable to characterize mineral samples fully, especially if the samples are polycrystalline.

Nuclear Quadrupole Resonance (NQR) spectroscopy offers the potential for obtaining accurate high-resolution spectra. These can then be interpreted to give structural information which can be related to local electronic structure, atomic arrangement, order/disorder phenomena, and crystal phase transformation. In addition, molecular dynamics in the solid state can be studied. Furthermore, since NQR data are sensitive to changes in temperature and pressure, stress/ strain information may be obtained.

A selection of potential applications to various energy technologies is listed in Table 1. It should be emphasized that implementation of the applications described in this table may take many years of effort in the theoretical, experimental, and instrumental development fields. An initial research goal is to establish what this potential is and how much development is required before NQR spectroscopy becomes a fully viable technique for geoscience and related disciplines.

Each of the potential applications listed in Table 1 can be placed into one of three broad categories: (1) crystallographic information, (2) stress determination, and (3) the identification of a specific chemical compound or atomic arrangement. These are all congruous with the NQR method, which is known to give specific information on chemical, physical, and crystallographic properties of solids which contain any degree of crystal order.

NQR THEORY

The basic mathematics of NQR have been described by Lucken (1969) and Das and Hahn (1958). The content of their discussions may be summarized as follows. Compounds may be studied which contain nuclei with a nuclear spin ≥ 1. This includes molecules which contain such probe nuclei as N^{14}, O^{17}, Na^{23}, Al^{27}, Cl^{35}, Cl^{37}, Cu^{63}, and Cu^{65}, as well as many of the rare earths and actinides. The NQR method is used to study the electron density distribution.

The charged particles in the atomic nucleus precess around the direction of the nuclear spin while the charged particles outside the nucleus remain virtually stationary over the averaging time. Thus, the charge distribution in the nucleus may be regarded as axially symmetric. In a coordinate system with the z-axis directed along the symmetry axis of the nucleus, the off-diagonal terms of the quadropole moment tensor Q_{jk} are zero while the diagonal terms are related by the equality $eQ_{xx} = eQ_{yy} = -1/2\ eQ_{zz}$. As a result, the quadrupole moment tensor is determined by one component, which is designated as the nuclear quadrupole moment:

$$eQ_{zz} = \int \rho(3z^2 - r^2)d\tau \quad , \tag{1}$$

where ρ is the charge density in the nucleus, and $d\tau$ is the volume element in the nucleus system, x, y, z. In the case of spherical symmetry, the righthand side of equation (1) vanishes, and the quadrupole moment is thus a measure of the deviation of the nuclear charge distribution from spherical symmetry.

The electric field gradient (EFG) around the nucleus is produced by charges situated outside the nucleus. The EFG tensor is diagonal in the principal axes. The Hamiltonian of the nuclear quadrupole interaction contains the three components of this tensor, which are related by

$$\nu_{zz} = \frac{\partial E_z}{\partial z} > \nu_{yy} = \frac{\partial E_y}{\partial y} > \nu_{xx} = \frac{\partial E_x}{\partial x} \quad , \qquad \nu_{zz} + \nu_{yy} + \nu_{zz} = 0 \quad . \tag{2}$$

Two of these components, ν_{zz} and ν_{yy}, are in general unequal. We can thus define the EFG asymmetry parameter

$$\eta = \frac{\nu_{xx} - \nu_{yy}}{\nu_{zz}} \quad , \tag{3}$$

which varies within the range $0 \leq \eta \leq 1$. For the particular case of an axially symmetric EFG tensor ($\nu_{xx} = \nu_y = -1/2\ \nu_{zz}$) $\eta = 0$. The Hamiltonian of the nuclear quadrupole interaction is

Table 1. Potential applications of NQR to energy related problems.

Mission	Potential application
Nuclear waste	Identification of lattice sites of radionuclides in glasses, synthetic, and natural minerals. In situ measurement of stress in salt. In situ measurement of stress in rock formations.
Continental drilling program	Downhole sensing of elemental compositions and the crystal structures that contain them. In situ measurement of stress at depth.
Fossil fuels	Continuous measurement of the distribution of sulfur between organic and inorganic phases in coal. Measurement of organic complexes of V, Cu, Ni, and S in crude oil. Stability of mining excavations, i.e., by wall, room, and pillar mining methods in coal mines, block caving, and in situ retorting of oil shales.
Geothermal energy	Use of compounds containing stable isotopes as tracer materials.
Uranium resources	Downhole measurement of uranium ore grade and type, both in and adjacent to the bore-hole wall. Continuous monitoring of uranium in cores and mill feed, and identification of the mineral phases containing uranium. Monitoring of uranium by-product elements such as Cu, V.
Fundamental research in support of energy development	Characterizing phase transitions in common rock-forming minerals, i.e., feldspars, pyroxenes, amphiboles, support of phyllosilicates, and zeolites. Interpreting ordering in minerals with respect to thermodynamic properties. Evaluating localized stress in nonisotropic materials.

$$H_Q = \frac{e^2qQ}{4I(2I-1)} \left[3I_z^2 - I(I+1) + 1/2\eta(I_+^2 + I_-^2)\right] , \quad (4)$$

where I is the nuclear spin operator with the components I_z, I_x, and I_y, and $I_\pm = I_x + iI_y$. For the particular case $\eta = 0$, the energy eigenvalues of the quadrupole interaction are given by

$$E_m = \frac{e^2qQ}{4I(2I-1)} [3m^2 - I(I+1)] . \quad (5)$$

If $\eta \neq 0$, the energy eigenvalues are found by solving the secular equation for (4).

The quadropole interaction energy is small, and the NQR frequencies, therefore, fall within the radio-frequency range between 0 and 1000 MHz. The nuclear quadropole moment is approximately constant and does not depend on the nature of the chemical bonds of the given atom. The electric field gradient, conversely, characterizes the electron density distribution and is thus highly sensitive to the nature of the bonds in the given atom and in all other atoms in the molecule, whether or not they are directly bonded to the resonant nucleus. As a result, the position and the number of lines in a NQR spectrum will depend on the molecular and crystal structure of the compound being studied. Accordingly, NQR spectroscopy provides an indication of the state of the electron surrounding the resonant nucleus, and thus gives information on the electron density distribution in the molecule.

SELECTION OF PROBE NUCLEUS

The first requirement is selection of a probe nucleus. Given the areas of interest, aluminum-27 is a rational choice as the probe nucleus for initial studies because of its natural abundance. Among the elements of the lithosphere it ranks third, with 8 wt%. Oxygen (47 wt%) and silicon (28 wt%) are the only two elements with greater abundance. Both of these more abundant elements are ruled out because they have no abundant isotopes which have spin $I \geq 1$, and, therefore, are not subject to the NQR interaction. Aluminum-27, however, has a sufficient high nuclear spin ($I = 5/2$), and

natural isotopic abundance (~100 wt%) to satisfy the basic experimental requirements. In addition, its relative abundance in the lithosphere leads to the expectation that it may be a generally useful probe nucleus, but still dilute enough so that signals from more than one crystal site can be unraveled. Unfortunately aluminum-27 represents a nucleus whose NQR spectral characteristics have not been measured and, therefore, obtaining this information is the first avenue of experimental research which must be pursued.

The oxygen-17 nucleus offers many advantages to the current problem (ubiquitous occurrence in rock forming minerals, favorable frequency region for the NQR frequencies) but suffers from a low natural abundance. This results in instrumentation which requires several orders of magnitude more sensitivity. If sensitivity is improved, oxygen-17 may become very attractive as a probe nucleus.

Less severe experimental problems would be expected in the detection of elements such as copper or chlorine covalently bonded in minerals. Here, NQR frequencies in the tens of MHz are expected on the basis of extensive investigations carried out by NQR spectroscopists for many years. However, the usefulness of these nuclei is rather limited given their relatively low abundance in geologic materials.

The possibility of using NaCl as the test material is also presented because of the great interest in storing radioactive waste in salt domes. This, however, represents a special NQR case. Normally, the cubic symmetry forces the quadropole interaction e^2qQ to vanish. Two situations, however, can overcome this difficulty acting separately or concurrently. First, the presence of substitutional impurities in NaCl, e.g., Br^- for Cl^-, results in a distortion of the cubic symmetry of the chloride site which allows a measurable quadrupole interaction. Second, the presence of axial stress on the salt also changes the symmetry and yields a spectrum. In either or both events, it should be possible to obtain a measure of the kind and magnitude of strains present. The extent interest in salt seems sufficiently high to justify its use.

RESEARCH AREAS DEFINED

The proposed program has a very broad technical scope and will have to be limited to mission-oriented research. The typical program as defined during fiscal year 1979 may be broken into two areas: (1) mineralogical problems and (2) strain measurement. A brief overview of these areas is included herein.

Mineralogical Considerations

There are several mineralogical problems that are of interest when considering energy related problems and these can be researched once the response of the NQR spectrometer to aluminum-containing compounds is fully understood.

Over 70% of the continental crust consists of alumino-silicates. The feldspars, predominant aluminosilicates, occur as solid discontinous solutions of the three end-member components, microcline ($KAlSi_3O_8$), albite ($NaAlSi_3O_8$), and anorthite ($CaAl_2Si_2O_8$). Thus, any model of chemical, structural, and deformation processes occurring in the earth must almost always include the properties of feldspars. They are present in many rocks, including those which may be suitable hosts for radioactive waste repositories; those forming reservoirs associated with the production of geothermal energy; and in many sedimentary rocks containing or associated with fossil fuels.

Aluminum in feldspars is tetrahedrally coordinated. AlO_4 and SiO_4 tetrahedra form a continous three-dimensional framework. In feldspars formed at low temperature, Al and Si are usually fully ordered. The plagioclase feldspars form a solid solution series at elevated temperatures, from albite ($NaAlSi_3O_8$) to anorthite ($CaAlSi_2O_8$). This has been found to contain different ordering schemes at lower temperatures, such as shown in Figure 1. In albite, there are 4 nonequivalent tetrahedral positions, (Figure 1a), while in anorthite there are 8 (Figure 1c). In intermediate compositions, such as labradorite, partial disorder occurs (Figure 1b). At high temperatures (close to the melting point), Al and Si are disordered. Ordered and disordered phases have significantly different free energies. Such differences are important in calculations of stability relations in multicomponent geochemical systems, and it is essential to determine their Al-Si distribution in order to correlate disorder with this and other important thermodynamic parameters.

Unfortunately, Al and Si have very similar atomic numbers and direct determination of site occupancies by x-ray diffraction measurements is, therefore, not possible. Neutron diffraction studies have been met with more success since scattering amplitudes for Al and Si show a greater difference, but this technique is very costly to implement and suitable equipment is available only in a few places with high-flux neutron reactors, such as the Oak Ridge National Laboratory.

It is common to assume a linear bond length occupancy relationship, and one might expect a linear change in bond length with the chemical

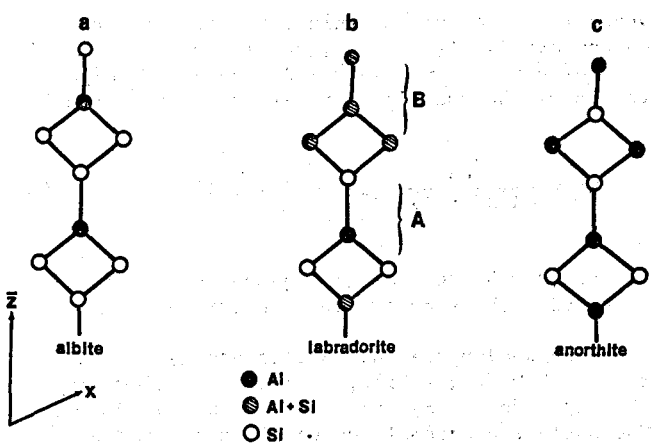

Figure 1. Si/Al arrangements in plagiolases. (XBL 793-8875)

composition of plagioclase. Recent structure refinements of several plagioclases have shown that this is not the case. Particularly, small substitutions of Si on the Al-site have a very strong effect on bond lengths, while substitutions of Al on Si sites follow closely a linear relationship. This could be due to the existence of superstructures with more complex ordering patterns, but it is suspected that it may be caused by a nonlinear bond length occupancy relationship. A linear relation corresponds to an ideal solution model with ideal mixing and no interaction between substituting atoms. The authors suspect that mixing may follow regular solution behavior, particularly for the Al site, with Al being close to the transition from tetrahedral to octahedral coordination. There is no way to confirm this hypothesis with x-ray techniques. It is fortunate that NQR is very sensitive to the local Al environment and may permit the determination of the site occupancies directly and, thereby help evaluate the possibility of nonlinear forces during atom substitutions.

Another area where information is needed is the phase transformation from an ordered to a disordered Al-Si distribution. The state of ordering at specific temperatures can be determined both with indirect x-ray and direct NQR measurements. This will allow quantitative investigation of the thermodynamics of these phase transformations. Whether this process is first or second order is still unclear. The results of such an investigation are important in establishing and understanding the behavior of igneous rocks (particularly volcanic rocks) during cooling.

Because NQR is most sensitive to the immediate environment of a nucleus, it should be applicable to study differences between truly disordered structures and those with short-range order. A distinction between these two is very difficult on the basis of x-ray data. It can be suggested that there is considerable order over a few unit cells based on diffuse background scattering, but this is unconfirmed. This problem is presently being investigated with transmission electron microscopy (TEM), which also supports a model with short-range order. Confirming this postulation using NQR could have great impact on understanding ordering kinetics.

Feldspars are an ideal system to test the applicability of NQR techniques on Al-Si order for two reasons. First, it is possible to define specific research as previously discussed, and second, samples of albite from the California Coast Ranges (Franciscan), labradorite from Plush, OR, and anorthite from Grass Valley, CA, have already been analyzed in some detail by the existing techniques, thus providing an initial data base.

At a later stage, as the NQR technique matures, it would be desirable to apply it to other minerals such as the phyllosilicates to determine the emphasis on the degree of order in the tetrahedral sites. In this way it should be possible to learn whether some micas posses higher ordering and lower symmetry than has previously been believed. Furthermore, since NQR does not require large single crystals, it seems ideally suited to study clays and finely crystalline zeolite minerals which are of great importance in the weathering or diagenesis of rocks, and potentially important ion-exchangers when in contact with groundwater.

The Possibility of Measuring In-Situ Strain

In the area of rock mechanics, the most pressing problem is a good method of determining stress/strain in situ. As part of this initial research effort, NQR was considered as a potential measuring technique. It was fully appreciated at the start that this represented a situation to which NQR had never been applied before.

Inasmuch as strain is related to the characteristics of the chemical bond and changes in electron density distribution as nuclei change their geometric position relative to each other, the potential of the NQR approach becomes obvious. These effects are reflected in the resonance frequencies, line shape, and number of NQR lines. Further information is also available due to the fact that, in solids, resonance frequency is also dependent on temperature and hydrostatic pressure. The first requirement, therefore, is to derive a set of equations (model) which relates measurable NQR parameters to those needed to define strain.

For the purpose of confirming the model, samples must be chosen with a representative probe nucleus. Several possibilities exist but aluminum-27 is by far the most promising nucleus.

INSTRUMENTATION

One of the authors (Klainer, 1979) has been involved in the development of NQR instrumentation for several years. It was, therefore, not necessary to focus on this aspect of the program in fiscal year 1979.

At present, two state-of-the-art NQR spectrometries exist, which can be adapted for use on this research. Both instruments were originally designed and constructed for studying nitrogen-14 as the probe nucleus. Plans are underway to modify one of these spectrometers from a nitrogen-14 (spin, $I = 1$) to an aluminum-27 (spin, $I = 5/2$) system. The initial instrument modification necessary, to prove the suitability of NQR to the research problems previously discussed, will be done, for the most part, with commercial components so that the preliminary measurements can be done within the shortest time possible. Performance information from the modified instrument will also be used as a guide for the construction of an optimized system at a later date.

SUMMARY

During fiscal year 1979, the Director's Development Plan assessed the suitability of NQR spectrometric techniques to energy-related geoscientific applications. Preliminary results were most encouraging. The NQR technique appears to have the potential to complement existing analytical systems in the broad areas of mineralogy. Specific areas where its use appears beneficial are in the areas of phase transitions, atomic arrangement, crystal order, and bond characterization. Furthermore, indications are that NQR can be applied to the very important rock mechanics problem of in-

situ stress measurement. Finally, an extended, detailed NQR research program has been formulated which will permit the confirmation of conclusions drawn during this initial study.

ACKNOWLEDGMENTS

The authors wish to acknowledge the contributions to this program by Dr. T. Hirschfeld, Lawrence Livermore Laboratory; Professor R. Marino, Hunter College of the City University of New York; and Professor R. Wenk of the University of California, Berkeley.

REFERENCES CITED

Das, T. P., and Hahn, E. L., 1958. Nuclear quadrupole resonance spectroscopy. New York, Academic Press.

Harding, J. C., Wade, D. A., Marino, R. A., Sauer, E. G., and Klainer, S. M., 1979. A pulsed NQR-EFT spectrometer for nitrogen-14. Journal Mag. Res., v. 36, p. 21.

Lucken, E. A. C., 1969. Nuclear quadrupole coupling constants. New York, Academic Press.

TRACE ANALYSIS OF GROUNDWATERS

S. M. Klainer and J. A. Apps

A sensitive monitor to measure the presence of trace quantities of actinides in groundwaters is essential for detecting minute leaks from nuclear waste repositories and for monitoring the periphery of a waste repository. When this program was initiated it was felt that present nuclear monitors are capable of detecting major losses from a waste storage area, but that no suitable instrumentation existed for detecting and quantifying mishaps which are not readily obvious. In particular, monitoring had to be developed to detect the escape of very small quantities of actinides through "pin holes," i.e., hairline cracks in waste packages, or by diffusion through engineered barriers.

When discussing the monitoring problem with DOE and ONWI staff, it quickly became apparent that no definite answer could be obtained to the two essential questions: (a) what species must be measured, and (b) what concentration ranges must be covered? The best advice we received was strive for both maximum sample coverage and sensitivity. A program was thus devised which postulated that the best place to monitor for actinide leaks is in the groundwater surrounding the repository, and that this effort should be directed at the detection of those radionuclides which have very long half lives ($>10^4$ years).

For the purpose of program definition, plutonium (Pu) was chosen as the element of interest and detectability as low as 10^{-15} molar was hypothesized. The suggestion that the concentration may be so low is based on two inputs: (a) By definition the proposed monitor is for detecting the smallest conceivable leakage, and (b) most actinides have a very low solubility in water (in this case, the groundwater). In addition, groundwater samples no larger than 100 ml and analysis times not exceeding 2 hours were established as criteria for making measurements.

To calibrate the program goals, nuclear detection techniques were first evaluated, and it was established that nuclear counting techniques (presently considered the most sensitive methods of analysis) would not meet the postulated requirements. Calculations indicate that, as a minimum, nuclear detection methods may reach 10^{-12} molar for Pu. A concentration of 10^{-10} molar appears more reasonable for routine measurements. It should also be noted that Pu represents a "best case" situation, because there is no natural background of the material. By contrast, uranium detection, where uranium will normally be present in groundwaters in abundances greater than the proposed detection limit, will be less sensitive due to its normal background contribution.

The analytical approach that was evaluated for this investigation employs two special cases of resonance fluorescence. The actinides are unique in that their fluorescent spectra have very narrow bands and are easily resolved. Thus the components of an actinide mixture can be identified and quantified. Without any sample preparation, or instrumentation advances, resonance fluoresence (the most sensitive of the light interaction techniques) already has a sensitivity to Pu of 10^{-11} molar.

The use of resonance fluorescence was considered from two points of view: (a) the development of the most sensitive and specific system possible to help define the ultimate requirements of a respository monitor, and (b) the fluorescence approach which may be most amenable to a long term in-situ measurement system.

For establishing the monitoring requirements, much more fluorescence sensitivity is to be gained by employing special coprecipitation techniques. The formation of the coprecipitate serves several functions: (a) It concentrates the sample by removing the water, (b) it performs an initial separation of the actinides which greatly reduces the complexity of the fluorescence spectra, (c) it removes many of the contaminating compounds which represent background interferences, and (d) it provides a better matrix in which the actinide can resonate. Furthermore, if the coprecipitated sample is calcined before analysis, the volatile compounds, which represent the principal background, will be removed. Thus, using a combination of coprecipitation and resonance fluoresence, sensitivities to 10^{-15} molar should be readily attainable while several orders of magnitude improvement still appear practical. This is based on our calculations and the work of Gustafson and Wright (1979) and Johnston and Wright (1979) for lathanides. It predicts a 10^{-15} molar calcined sample of Pu will give a signal-to-noise ratio of

greater than 5:1 for a 1-sec. analysis time using a 1 W argon laser as the irradiating source.

To prove the potential of the technique, a 10^{-8} molar sample of UO_2^{2+} was measured. The choice of 10^{-8} molar concentration was based on the purity of available spectrographically pure reagents. Figure 1 is the spectrum obtained with the operating conditions listed in Table 1. From the data given, that is a spectrum with a S/N ≈ 4×10^4:1, an instrument sensitivity which has been deliberately reduced by a factor of 10^4, and the inordinately short analysis time of 0.3 sec, it can easily be seen that a sensitivity of better than 10^{-15} molar UO_2^{2+} appears feasible for situations where there is no uranium background. This value may be considerably less when groundwaters are analyzed.

When it actually becomes desirable to instrument a repository, the collection and treatment of samples may become impractical. In this case, fiber optics could be strategically placed around the canister, in the backfill material, in the groundwater, and elsewhere. Fiber optics, 100 μ in diameter, can be used so that their mass will be small compared with the media into which they are imbedded, and little or no perturbation of the diffusion process will occur. Bundles of fiber optics of varying lengths can be used to correct for signal loss due to distance. To perform an analysis, pulsed laser radiation is transmitted through the fiber where it excites the fluoresence of the actinide. The actinide then emits light at a particular wavelength, and this travels back through the fiber optic (at the interval between laser pulses) to a spectral sorter, detector, and the necessary signal-processing electronics. The intensity of the signal will be a measure of how much actinide is in the fiber's vicinity. By using

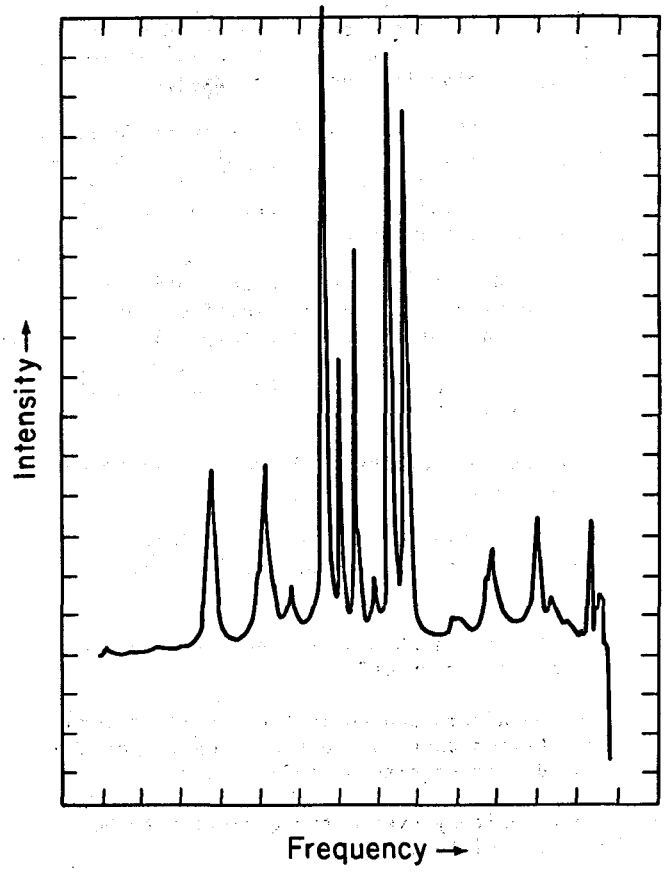

Figure 1. Fluorescence spectrum of 10^{-8} M UO_2^{2+} coprecipitated with CaF_2. LEGEND: laser frequency, 5146 Å; laser power, 8 mW; time constant, 0.3 sec; resolution, 3 cm^{-1}; slit width, 100 μ; collector, f/1.2; peak count rate, >10^6 cps. (XBL 806-7206)

Table 1. Potential sensitivity of fluorescence coprecipitation technique to actinides.

Technique	Operating conditions	Available	Available enhancement
Laser frequency	5145 Å	?	?
Laser power	8 mW	8W	10^2
Time constant	0.3 sec	5 min	30
Background	1	?	?
Slit width	100 μ	400 μ	4
Collector	f/1.2	?	?
S/N	>1000:1	5:1	4×10^4
Minimum total enhancement available			5×10^8
Projected sensitivity to UO_2^{2+} (no background conditions			10^{-16}M

several strategically placed fiber bundles, it should be possible to obtain a three-dimensional concentration plot for the actinide.

As a result of the initial study performed in fiscal year 1979, it has been possible to define several questions that need to be investigated before a final system can be designed. For the test system these include:

1. What complexity of actinide separation is required for unambiguous identification of the contents of groundwater samples?

2. How many suitable coprecipitation materials are available?

3. Does the coprecipitant add to the fluorescent background?

4. Is it possible to confirm the projected sensitivity to all of the actinides of interest?

5. What technique should be used for obtaining groundwater samples?

6. Can containers and collection media or both be obtained that assure the integrity of the groundwater samples at 10^{-15} molar?

For the repository system the questions to be answered are different:

1. What effect does the use and selection of fiber optics have on ultimate sensitivity?

2. Can the fiber optics be coated to increase sensitivity?

3. What is the optimum design for the end of a fiber optic to assure maximum sensitivity, self-cleaning, etc.?

4. What are the requirements of the spectral sorter when no preparation of the sample is possible?

5. What is the ultimate sensitivity of the resonance fluorescence technique using fiber optics?

These and other questions that may arise will be answered during a three-year program beginning in mid fiscal year 1980, funded by the Office of Nuclear Waste Isolation.

The authors wish to thank Dr. T. Hirschfeld of Lawrence Livermore Laboratory for obtaining the spectrum (Figure 1) on his laser fluorimeter Dr. D. Perry of Lawrence Berkeley Laboratory prepared the UO_2^{2+} samples.

REFERENCES CITED

Gustafson, F. J., and Wright, J. C., 1979. Trace analysis of lanthanides by laser excitation of precipitates. Anal. Chem., v. 51, p. 1762.

Johnston, M. V., and Wright, J. C., 1979. Trace analysis of non-fluorescent ions by associative clustering with a fluorescent probe. Anal. Chem., v. 51, p. 1774.

SURVEY OF AQUIFER THERMAL ENERGY STORAGE PROJECTS

C. F. Tsang, D. L. Hopkins, and G. Hellstrom

INTRODUCTION

The disparity between energy production and demand has led to increased research into using aquifers for long-term, large-scale storage of thermal energy. Aquifers are well suited to thermal energy storage because of their low heat conductivities, large volumetric capacities, and ability to contain water under high pressures. At present, there are several field experiments and feasibility and modeling studies in which the technical, economic, and environmental aspects of aquifer storage are being studied. A survey of aquifer projects throughout the world (Tsang et al., 1980) was prepared for a conference, Recent Trends in Hydrogeology, held at Lawrence Berkeley Laboratory in Februrary 1979. The following summary describes some of the projects surveyed.

SUMMARY OF CURRENT PROJECTS

Field experiments have been conducted in Switzerland, France, the United States, Japan, and the People's Republic of China. In 1974, at the University of Neuchatel, Switzerland, 494 m^3 of hot (51°C) water was injected into a shallow, phreatic aquifer. After a storage period of 122 days, 16,370 m^3 of water (more than 30 times the injection volume) was withdrawn. The small injection volume, together with the high permeability of the aquifer which caused the lighter hot water to rise, resulted in a large heat loss through the upper unconfined layer and a heat recovery ratio of only 40%.

Field work in France began in 1976 with the Bonnaud experiments. The first series of experiments consisted of three successive injection and production cycles and was followed by a second series consisting of four cycles. The Campuget experiment (1977 to 1978) was a full-scale storage project intended to store enough heat to meet the needs of 100 housing units. During a three-month injection period, 20,000 m^3 of warm (33.5°C) water, heated by simple solar collectors and heat pumps, was injected into a shallow unconfined aquifer. The experiment consisted of two waiting and withdrawal periods during which 17,000 m^3 of water was withdrawn. As in the case of the Swiss experiment, the water was stored in a shallow, phreatic

*Visiting scientist from University of Lund, Sweden

aquifer, resulting in a large heat loss through the unsaturated zone and a low energy recovery ratio (20%). Contributing to the loss of efficiency was a decrease in air temperature and a decrease in the thickness of the unsaturated zone from 3 m to 1 m during the experiment.

At Auburn University in the United States, a series of hot water storage experiments are in progress. For a preliminary experiment initiated in 1975, 7,688 m^3 of warm (36.4°C) water was obtained from the effluent discharge canal of a powerplant and injected into a confined aquifer. After a storage period of 44 days, 14,260 m^3 of water was withdrawn, yielding an enegy recovery ratio of 68%. For a second set of experiments, 54,784 m^3 of water was obtained from a shallow semiconfined aquifer; the water was then heated and injected into the deeper confined aquifer. After 51 days of storage, 55,345 m^3 of water was withdrawn, yielding an energy recovery rate of 65%. For a second cycle, just completed, an energy recovery rate of 74% was obtained. The improvement can largely be attributed to the aquifer still being warm from the previous cycle in which production stopped at a temperature 13°C above ambient.

At Texas A&M University, the economic and technical feasibility of cold water storage in aquifers is being studied. In the winter of 1978 to 1979, water was pumped from a shallow aquifer into a 5000 ft^2 cooling pond. When wet-bulb temperatures dropped below 50°F, water was pumped through a spray system and cooled to the air temperature. A total of 31,800 m^3 of chilled (8.9°C) water was reinjected into the aquifer and stored until summer when it was withdrawn and used in a heat-exchange process for air conditioning.

A second cold water storage experiment is under way at Yamagata University in Japan. During summer, cold water is withdrawn and used to air-condition a commercial building while warm waste water is passed through a spray system on the roof of the building for heat collection. After passing through a filtration tower, the water is further heated by a heat exchanger and recharged through a second well. The process is reversed during winter when warm water is withdrawn and used to melt snow. For the first experiment, a total of 8,843 m^3 of warm (23.7°C) water was injected into a confined, 19 m thick, sand-and-gravel aquifer. After a storage period of three months, 9,930 m^3 of water was withdrawn yielding an energy recovery ratio of approximately 40%. Between January and March 1978, some 9,430 m^3 of cold (5.3°C) water from melted snow was injected into the aquifer. Water withdrawn 4 months later had an average temperature of 14°C. Failure to get cooler water may be attributed to the small volume of injected water and the short distance between injection and production wells, which resulted in the mixing of warm and cold water.

In China, use of aquifers for thermal energy storage largely developed out of reinjection experiments in Shanghai designed to reduce subsidence and raise groundwater levels that had dropped because of widespread use of groundwater by factories. Based on large-scale experiments conducted during the 1960s, hydrogeologists in Shanghai concluded that by using reinjection they were able to effectively control subsidence and groundwater levels, and that it was possible to store cold water in winter for summer use in air conditioning. These conclusions led to a city-wide reinjection program in which 70 factories used 134 deep wells for simultaneous recharge. Groundwater produced during summer had a very low temperature, and thus became a new source of chilled water for industrial use. The program grew in subsequent years so that there are now several hundred wells in use; and it has been expanded to include summer injection of hot water for winter use. Because of the success at Shanghai, many cities have adopted similar reinjection and thermal energy storage programs.

Generally, field projects to date have been of relatively small scale and have used water of moderate temperatures (not greater than 55°C or less than 5°C). Most of these experiments focused on obtaining pressure and temperature data with the objectives of understanding heat and fluid flow in the aquifer and validating numerical models. A need exists to both extend the temperature range of the investigations and to examine the concept of energy storage on a larger scale.

Several numerical models to study energy storage in aquifers are under development although details for most are yet to be reported. Among these are studies being conducted by Lund University, Sweden; Bureau de Recherches Géologiques et Minières, France; Institute de Production d'Energie de l'Ecole Polytechnique Fédérale de Lausanne, Switzerland; and Lawrence Berkeley Laboratory.

At Lund University, Sweden, a two-dimensional, finite-difference model has been developed to study hot-water storage in eskers (long and narrow glacial deposits of high permeability). Analytical studies have also been conducted to examine topics related to thermal storage, including buoyancy tilting of a vertical thermal front, entropy analysis of numerical dispersion, and effect of temperature-dependent viscosity in a two-well extraction-injection system.

Several models have been developed by the Bureau de Recherches Géologiques et Minières (BRGM), France, to study fluid and heat flow, dispersion, and the effect of varying physical parameters and operating conditions on the temperature of water produced from a single well system. Programs developed at BRGM have been used to model the Bonnaud experiments, described previously.

A three-dimensional finite-element model for diffusion and convection has been developed by the Institut de Production d'Energie de l'Ecole Polytechnique Fédérale de Lausanne, Switzerland. The model has been used to simulate an aquifer heat-storage system with vertical flow between two horizontal networks of drain pipes.

At Lawrence Berkeley Laboratory, we are using program CCC (conduction, convection, and compaction) to model the Auburn University field experiments (see Tsang, et al., this report) and to perform parameter sensitivity studies. CCC employs the integrated finite-difference method and is a fully three-dimensional model incorporating the effects of complex geometry, temperature-dependent fluid

properties, gravity, and land subsidence or uplift. The code has been validated against a number of semianalytic solutions and has been used for several generic studies of aquifer thermal energy storage.

We have obtained some initial results from our parameter sensitivity study. In simulating the Auburn University field experiment, the vertical/horizontal permeability ratio (K_v/K_h) in the aquifer, and the permeability and storativity in the aquitards, could not be determined directly and had to be estimated. Our parameter study indicates that the estimated recovery factor is very sensitive to permeability and the K_v/K_h ratio. In the Auburn simulation, using a value of K_v/K_h equal to 0.1 is critical to obtaining good agreement with the field data. Increasing aquitard permeability by a factor of 10 had only a slight effect on energy recovery. The effect on energy recovery was also slight when thermal conductivity was increased by a factor of 2, but significant changes were observed when thermal conductivity was increased by a factor of 20.

To study the effect of partial well penetration on the results of the Auburn experiments, a simulation was run assuming full penetration of the well. Energy recovery was estimated to be 0.69, which differed only slightly from the value 0.68 obtained for the partial-penetration case.

In addition to field experiments and modeling studies, a number of feasibility studies of energy storage in aquifers are also under way. Projects range from general economic and systems analyses to evaluation and design of pilot plants. The technical work being done entails field and laboratory investigations of the hydrogeological, chemical, and biological aspects of aquifer storage. Several programs call for regional geological surveys to locate possible storage sites and many studies are aimed at specific applications.

Experiments to date illustrate the need for further research and development to ensure successful implementation of an aquifer storage system. Areas identified for further research include shape and location of the hydrodynamic and thermal fronts, optimal flow rate and formation permeability, thermal dispersion, natural regional flow, land subsidence or uplift, thermal pollution, water chemistry, wellbore plugging and heat exchange efficiency, and corrosion control.

REFERENCE CITED

Tsang, C. F., and Hopkins, D. L., 1980. Aquifer thermal energy storage, a survey, in Narasimhan, T. N., ed., Recent trends in hydrogeology. Berkeley, Lawrence Berkeley Laboratory, LBL-8977 (in prep.).

MULTIPLE-WELL VARIABLE-RATE WELL TEST ANALYSIS OF THE AUBURN UNIVERSITY AQUIFER THERMAL ENERGY STORAGE FIELD DATA

C. A. Doughty, D. G. McEdwards, and C. F. Tsang

INTRODUCTION

Reservoir engineers often consider well test analysis as an initial, short-term field test carried out before other reservoir activities can begin. When conventional type-curve analysis is employed, this is generally true because flow rates must be held constant or carefully controlled during the well test. However, LBL has developed a computer-assisted well test analysis method, program ANALYZE (McEdwards, 1979), that allows arbitrarily varying flow rates of several production or injection wells. The method can also treat simultaneous measurements from several observation wells. Hence, well tests can be conducted concurrently with other reservoir activities, as long as flow rates and pressures are measured.

As an example of long-term well test analysis, ANALYZE has been used with data obtained from an aquifer thermal energy storage field experiment conducted by Auburn University in Mobile County, Alabama (Molz et al., 1977, 1979). Parts of two hot water injection/storage/recovery cycles, as well as a conventional 36-hr pumping test were analyzed. Results of the three tests are consistent and agree well with the results of the USGS (Papadopulos and Larson, 1978) obtained using conventional type-curve analysis of the 36-hr pumping test.

PROGRAM ANALYZE

The program ANALYZE treats well test data for the reservoir characteristics transmissivity, kh/μ, storativity, ϕch, the location, and type (barrier or leaky) of a linear hydrologic boundary. The program rigorously handles variable production rates from as many as 20 production wells, and can simultaneously analyze pressure data from as many as 20 observation wells. The program models production wells as fully penetrating line sources or sinks and the reservoir as a constant thickness, laterally infinite, isotropic, porous medium.

The computation basis of ANALYZE is a least-squares minimization routine that uses parameters kh/μ, ϕch, and the angle and distance to a hydrologic boundary to calculate the pressure change at locations and times corresponding to observed pressure data. The routine then adjusts the values of the parameters (collectively called x_j) so that the sum of the normalized squared difference between calculated pressure changes and observed pressure changes is a minimum. The set of parameters associated with the minimum is then accepted as representative of the reservoir and well system. Written mathematically, we minimize

$$\chi^2 = \frac{1}{I} \sum_{i=1}^{I} \left[\frac{\Delta P^{(i)}_{calc}(X_j) - \Delta P^{(i)}_{obs}}{\Delta P^{(i)}_{obs}} \right]^2 , \quad (1)$$

in which the summation is taken over all the times and locations at which I observed pressure changes are specified. To enable the user to judge the reasonableness of a minimum and its associated parameters, the observed and calculated pressure changes, the differences and ratios between them, and times of observation are listed for each observation well. Following this a log-log plot of pressure vs time, comparing the observed and calculated pressure changes is printed.

WELL TEST ANALYSIS

ANALYZE was applied to each of the three data sets from Auburn: two variable flow rate injection periods and one constant flow rate pumping test. Results from the first injection test will be discussed below.

The aquifer used by the Auburn experiment is about 21 m thick and lies between 40 and 61 m below the surface. It is primarily sand confined above and below by clay layers. Two production/injection wells and 14 observation wells penetrate the aquifer. Figure 1 shows the well field layout. Because the injection/production well I_1 is screened only in the middle portion of the aquifer, an emphasis is placed on results from the more distant observation wells.

Warm water (35°C) was injected into well I_1, at a variable rate for 74 hr, followed by a quiescent period of 93 hr after which injection was restarted. The injection data were reported as cumulative flow only, so flow rate was represented by step changes calculated from these data.

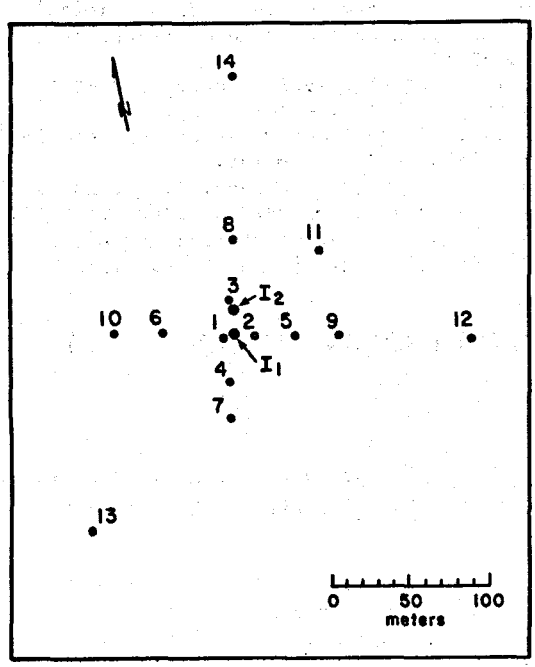

Figure 1. Top view of the Auburn well field. (XBL 795-7445)

Two-Parameter Analysis

Individual well analyses. Sequential two-parameter individual well analyses were done for data with latest pressure data considered ranging from 10 to 167 hours ($10 \le \tau max \le 167$). Figure 2 shows the variation of kh/μ and ϕch with τmax for wells 7, 9, and 10. The similarity of the results from different wells exhibits the overall homogeneity of the reservoir.

Multiwell analysis. Because the individual well analyses give similar values for reservoir parameters, it is reasonable to do sequential two-parameter multiwell analyses to yield spatially averaged values of kh/μ and ϕch. The results of multiwell analyses using data from wells 7, 9, and 10 are shown in Figure 3. The decrease in kh/μ corresponding to an increase in χ^2 for $\tau max \le 20$ indicates the presence of a barrier boundary.

Boundary Analysis

Multiwell analysis. At least three observation wells are required to locate a boundary unambiguously. A four-parameter multiwell analysis using data from wells 7, 9 and 10 was used to locate the barrier indicated by the two-parameter analysis sequence. Because more distant boundaries may also exist, a sequence of four parameter analyses was done with τmax ranging from 4.6 to 167 hr (see Figure 4; distance is measured from the origin in Figure 1; angle is measured clockwise from the +y axis). Trends in χ^2 and kh/μ values indicate the presence and type of the next-encounterd boundary.

To interpret these results, note that the χ^2 values for all times are much less than the corresponding χ^2 values for the two-parameter no-barrier analysis (Figure 3). Thus, for all times, the assumption of one barrier fits the data better than no barrier. The increase in χ^2 for $12 \le \tau max \le 20$ indicates that the influence of one barrier fits the data less well for these times. This increase in χ^2 for $12 \le \tau max \le 20$, coupled with the decrease

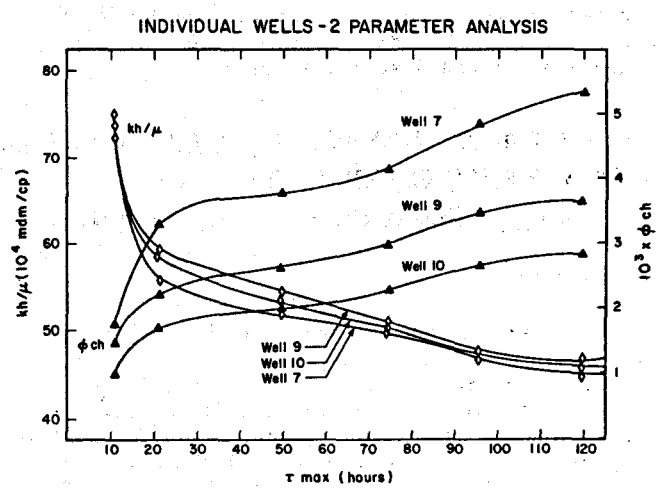

Figure 2. Variation of kh/μ and ϕch with τmax for wells 7, 9, and 10. (XBL 795-7497)

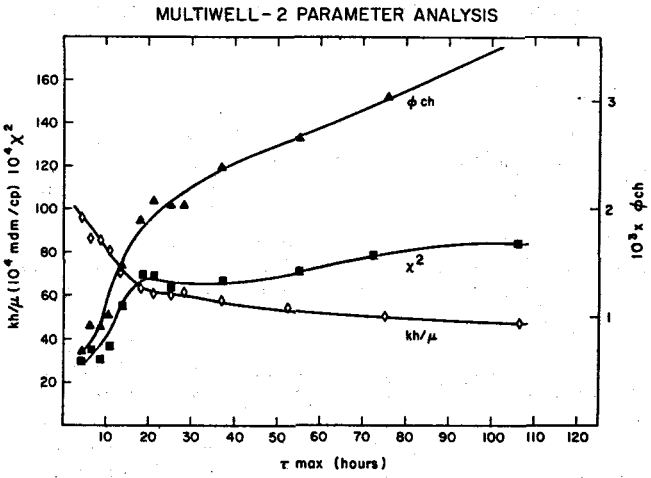

Figure 3. Multiwell analyses using data from wells 7, 9, and 10. (XBL 795-7471)

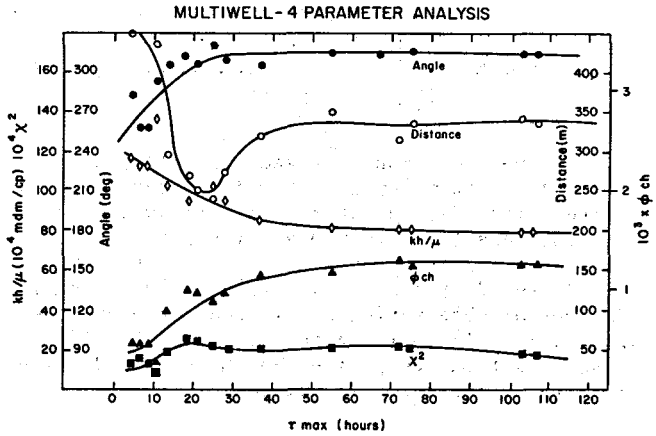

Figure 4. Four parameter analyses: distance is measured from the origin in Figure 1, angle is measured clockwise from the +y axis. (XBL 795-7476)

in kh/μ for the same time period, suggests that a second barrier influences pressure data for t > 12 hours. Thus, the shortest time data, 4.6 ≤ τmax ≤ 12, determines the reservoir parameters and the location of the first barrier, while subsequent variation in kh/μ and χ^2 indicates the presence, but not the location, of a more distant barrier. The scatter of data and unaccounted-for variations may be due in part to the variable flow rate and manner in which it was modeled. Also, very few data points are available for small values of τmax, so the results of small τmax analyses may not be as meaningful as results of large τmax analyses. Although the influence of a second barrier is indicated after 12 hr, analysis of data for large values of τmax may still be used to determine the location of the first barrier, if its effect is dominant. Angle and distance values are less scattered for this range of τmax than for smaller values of τmax, so the barrier location given by the analyses for which τmax < 12 is thought to be the most realistic result.

In view of the above discussion, the set of parameters chosen to represent the aquifer are: kh/μ = 0.115 x 10^7 mdm/cp; φch = 0.464 x 10^{-3}; angle = 315°; and distance = 330 m.

CONCLUSION

The values of kh/μ, φch and distance agree well with the USGS results, which made use of the 36-hr constant flow rate pumping test. In addition, the use of ANALYZE allows determination of the angle to the barrier, which is not possible using type curve analysis. These results are substantiated by analysis of the pumping test and a later injection period using ANALYZE.

REFERENCES CITED

McEdwards, Donald, 1979. Multiwell variable rate well test analysis (Ph.D. dissertation). Berkeley, Lawrence Berkeley Laboratory, LBL-9459.

Molz, F. J., et al., 1977. Subsurface waste heat storage. Experimental study.

____, 1979. Thermal energy storage in confined aquifers. WRRI preprint.

Papadopulos, S. S., and Larson, S. P., 1978. Aquifer storage of heated water; Part II, numerical simulation of field results. Ground Water, v. 16, no. 4, p. 242-248.

NUMERICAL SIMULATION OF AUBURN UNIVERSITY AQUIFER THERMAL ENERGY STORAGE FIELD EXPERIMENTS

C. F. Tsang, T. Buscheck, and C. A. Doughty

INTRODUCTION

Earlier LBL work on seasonal thermal energy storage in aquifers has included comprehensive generic calculations based on a numerical model to calculate the coupled heat and fluid flows in a three-dimensional, complex-geometry aquifer system. Many of the results have been published in a series of papers (Tsang, Lippmann, and Witherspoon, 1976, 1978; Tsang et al., 1978). During fiscal year 1979, LBL work has included a numerical simulation of the hot water storage field experiments recently completed by Auburn University in Mobile County, Alabama.

The purpose of such a study is twofold. First, in the Auburn field experiment will be obtained. This will not only give us knowledge of the relevant heat and flow behavior, but will focus on the effects of unexpected factors that may exist in a field experiment, such as injection well clogging. Secondly, a good simulation of the field data will

validate our numerical model and give us confidence in its use as a design and prediction tool.

SIMULATION OF THE AUBURN FIELD EXPERIMENTS

The experiments by Auburn University involved two injection-storage-recovery cycles. (Details may be found in Molz et al., 1980). The first six-month injection-storage-production cycle involved the storage of 55,000 m^3 of water at about 55°C. The injection took 79.2 days, the hot water was then stored for 52.5 days, after which it was produced at an average rate of 245.6 gpm until the recovered water temperature fell to 32.8°C. At that point 66% of the injected energy had been recovered. The second injection-storage-production cycle was carried out in essentially the same manner, using 58,000 m^3 of water at an average temperature of 55.4°C. When the production temperature had dropped to 33°C, a recovery of 76% of the injected energy had been realized.

The first stage of the simulation involved the determination of the hydraulic parameters of the aquifer (the transmissivity and storativity), and the location of a linear hydrologic barrier through well test analysis. Conventional well test type curve analysis techniques require a constant or carefully controlled flow rate. To get around this limitation, LBL has developed a computer-assisted analysis method, program ANALYZE (Tsang et al., 1977; McEdwards and Tsang, 1977) that can handle a system of several production and injection wells, each flowing at an arbitrarily varying flow rate. This program was applied to the Auburn case, treating the injection period also as part of the well test data (Doughty et al., 1979).

With parameters thus obtained, the LBL three-dimensional, complex geometry, single-phase model, CCC, was used to make detailed modeling studies. A radially symmetric mesh was assumed. There is one major hydrologic parameter that was not determined by well test analysis. This parameter, the ratio of vertical to horizontal permeability, has to be inferred from field experience and parameter studies. After making a preliminary parameter study, we decided to use the value of 0.10 for this ratio. The same ratio was suggeted by the USGS (Papadopulos and Larson, 1978).

Because neither the injection flow rate nor temperature was held constant, it was necessary to break up both the injection (and production) periods into segments having average flow rate and temperature values, conserving injected mass and energy (Figure 1). Results of the simulation include the recovery factor, plots of production temperatures versus time, and temperature contour plots and temperature profiles at various times during the injection, storage, and production periods. Both the first and second cycles have been successfully simulated.

For the first cycle, the simulated recovery factor of 0.68 agrees well with the observed value of 0.66. For the second cycle the simulated value is 0.78, and the observed value is 0.76. The details of the comparison between simulated and observed energy recovery can be studied in production

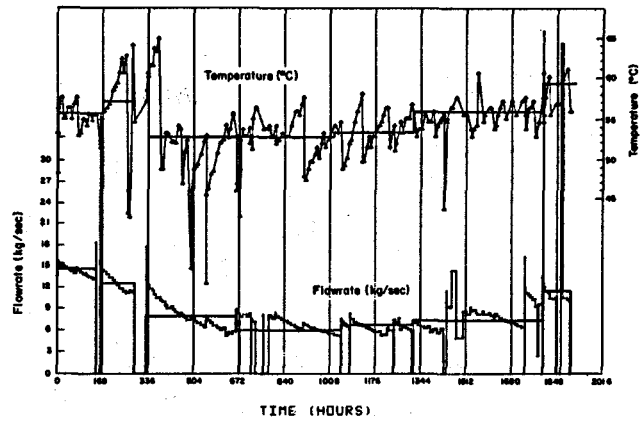

Figure 1. Injection flow rate and temperature versus time, and the average segments used in the simulation. (XBL 795-7460)

temperature versus time plots (Figures 2 and 3). For both cycles, the initial simulated and observed temperatures agree (55°C). During the early part of the production period, the observed temperature decreases slightly faster than the simulated temperature. During the latter part, the simulated temperature decreases faster than the observed temperature so that by the end of the production period the simulated and observed temperatures again agree (33°C). The discrepancy over the whole range is, at most, 1 to 2 degrees.

Temperature contour maps of vertical cross-sections of the aquifer at given times (Figure 4) show the details of buoyancy flow, heat loss through the upper and lower confining layers, and the radial extent of the hot water in the aquifer. Buoyancy flow is important in this rather permeable system. Comparison with temperatures recorded in observation wells throughout the aquifer show that the simulated temperature distribution agrees generally with observed temperatures. However, the

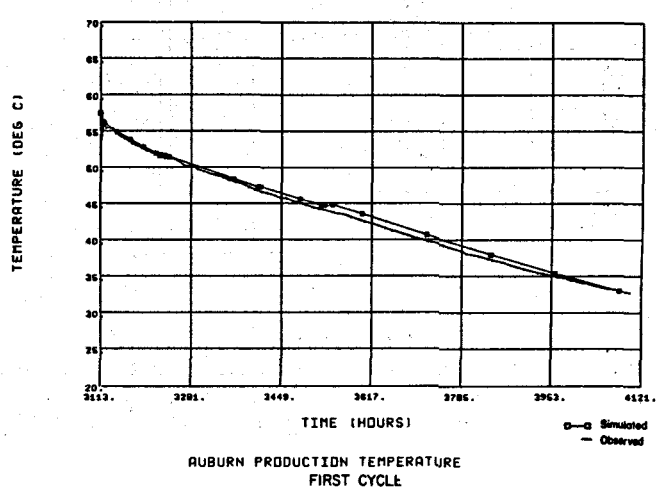

Figure 2. Observed and simulated production temperature as a function of time for the first cycle. (XBL 798-11428)

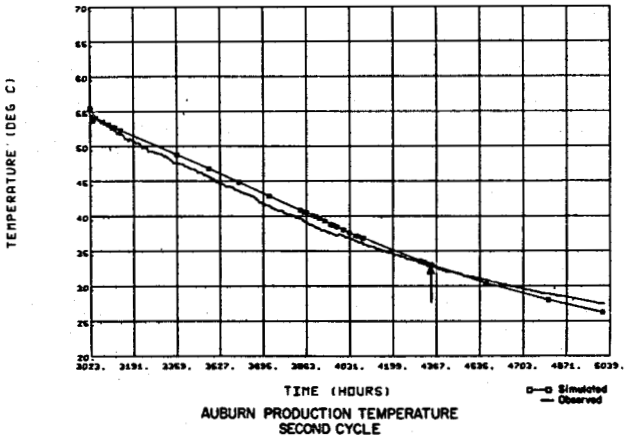

Figure 3. Observed and simulated production temperature as a function of time for the second cycle. (XBL 798-11426)

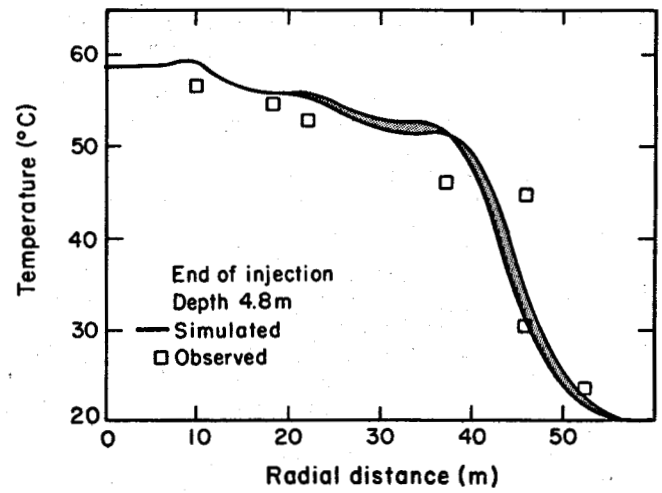

Figure 5. Temperature versus radial distance at the end of injection period for the first cycle. Shaded curve indicates simulated values, boxes show observed values. (XBL 795-7463)

discrepancies are much larger than the differences between calculated and observed production temperatures. Apparently there are local variations in the aquifer which tend to average out. Temperature versus radial distance at given depths and times are also plotted (Figures 5 and 6) and, from these profiles, the effects of thermal conductivity and dispersion on the shape of the thermal front can be studied.

In order to prove the mesh-independence of these results, the first cycle has been modeled again, using first a coarser mesh (double the radial step) and then a finer mesh (half the radial step). The coarse mesh recovery factor is 0.67, to be compared with a value of 0.68 using our first mesh. Interestingly, the coarse mesh simulation yields a recovery factor slightly closer to the observed value than does the original simulation, so the increased numerical dispersion may be more closely simulating thermal dispersion due to local heterogeneities in the aquifer. Temperature as a function of radial distance (Figure 7) and the production temperature as a function of time (Figure 8) show the insensitivity of the results to the mesh chosen.

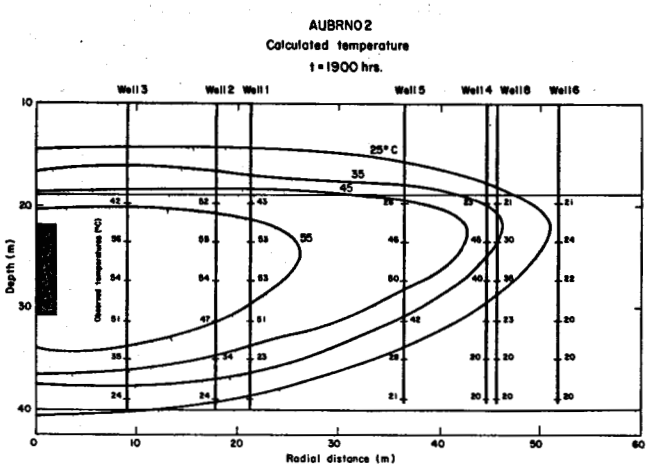

Figure 4. Simulated temperature contours in a vertical cross section of the aquifer at the end of the injection period of the first cycle, observed temperatures are also indicated. (XBL 795-7452)

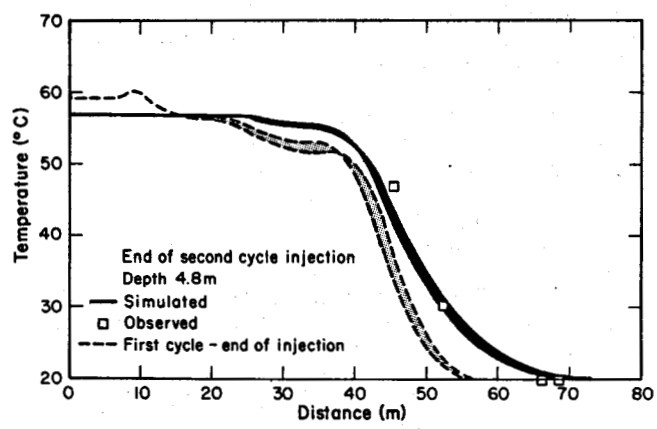

Figure 6. Temperature versus radial distance at the end of injection period for the second cycle. The broken curves shows the simulated values for the first cycle, for comparison. (XBL 798-11429B)

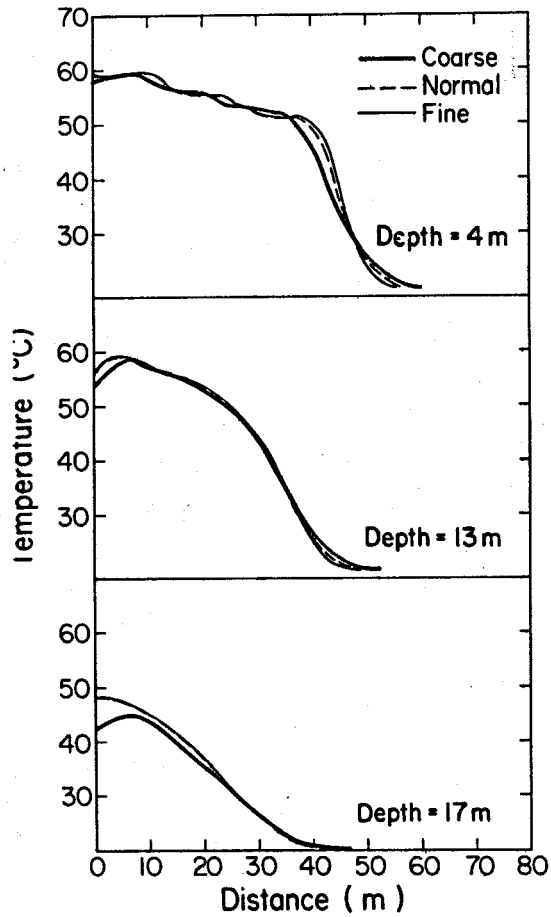

Figure 7. Simulated temperature versus radial distance at the end of the injection period for the coarse, normal, and fine meshes. (XBL 7911-13295A)

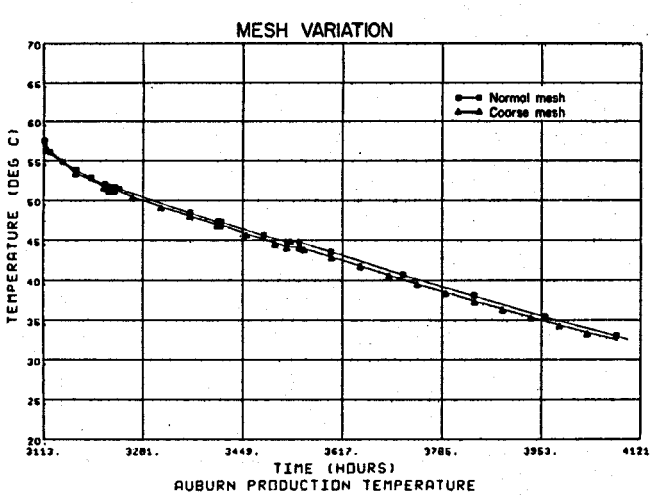

Figure 8. Production temperature versus time for the coarse and normal meshes. (XBL 7912-13756)

PLANS FOR NEXT YEAR

In the coming year, further generic and parameter studies will be made, including calculations of effects of varying the ratio of vertical and horizontal permeabilities, the storativity parameter, the injection temperature and effects of the well partially or fully penetrating the aquifer.

REFERENCES CITED

Doughty, C., McEdwards, D., and Tsang, C. F., 1979. Multiple well variable rate well test analysis of data from the Auburn University thermal energy storage experiment. Berkeley, Lawrence Berkeley Laboratory, LBL-10194.

McEdwards, D., and Tsang, C. F., 1977. Variable rate multiple well testing analysis, in Proceedings, Invitational Well Testing Symposium. Berkeley, Lawrence Berkeley Laboratory, LBL-7027, p. 92-99.

Molz, F. J., Parr, A. D., and Andersen, F. P., 1980. Experimental study of the storage of thermal energy in confined aquifers. Water Resources Research Institute, Auburn, Alabama, 37 p.

Papadopulos, S. S., and Larson, S. P., 1978. Aquifer storage of heated water; part II, numerical simulation of field results. Ground Water, v. 16, no. 4., p. 242-248.

Tsang, C. F., Lippmann, M. J., and Witherspoon, P. A., 1976. Numerical modeling of cyclic storage of hot water in aquifers. (Presented at Symposium on Use of Aquifer Systems for Cyclic Storage of Water). Tulsa, American Geophysical Union.

____, 1978. Underground aquifer storage of hot water from solar energy collectors, in Proceedings, International Solar Energy Congress. Pergamon Press.

Tsang, C. F., McEdwards, D., and Narasimhan, T. N., and Witherspoon, P. A., 1977. Variable flow well test analysis by a computer assisted matching procedure. Dallas Society of Petroleum Engineers, SPE-6547.

Tsang, C. F., Buscheck, T., Mangold, D., and Lippmann, M. J., 1978. Mathematical modeling of thermal energy storage in aquifers, in Proceedings, Aquifer Thermal Energy Storage Workshop. Berkeley, Lawrence Berkeley Laboratory, LBL-8431.

A number of different rock types are now being evaluated, both in the United States and elsewhere, as potential repository host rocks for nuclear waste. Properties such as mechanical response to thermal loading, fluid flow through fractures, and chemical sorptivity have not been systematically investigated for fractured rocks, yet they and their interactions must be understood or their magnitude ascertained before confidence can be had in predictions about disposing of wastes in repositories in fractured media. Thus fundamental investigations on geological aspects of fractured media continue to be expanded as well as experimental and field research projects of more applied natures.

The Swedish-American cooperative program, begun in July 1977, is a first-of-its-kind experiment for fractured rocks. The fundamental questions about how to characterize materials and properties and how to measure them are being approached both experimentally and theoretically. Preliminary results from experiments in the mine at Stripa, Sweden, have already been obtained. The correspondence of these results with predictions promises to lead to better predictions and to shape the next generation of experiments, which will improve our understanding of the physical and chemical phenomena that control waste migration.

LBL is also investigating a variety of other topics central to radioactive waste isolation; these range from theoretical to laboratory studies, surveys of the literature, and computational studies.

Transport through backfill--the engineered barrier between waste canister and rock--along with transport through the rock itself is being considered. Groundwater dating, via the $^{234}U/^{238}U$ technique, to enable determination of the flow of water in aquifers, is under development for small sample sizes. Theoretical studies of temperature-driven circulation in fractures around a repository are being calculated, and a study was made to catalog existing or recently abandoned mines in crystalline rocks that could possibly be used for in-situ test facilities for rock mechanics, hydrology, and geochemistry. Additional work is in progress on understanding rock-water-waste interactions in basalt and on theoretical and experimental evaluation of waste transport in basalt, shale, and quartz monzonite.

The projects are conducted under the University of California Contract W-7405-ENG-48 with the U.S. Department of Energy. Funding for the Nuclear Waste Isolation Program is administered by the Office of Nuclear Waste Isolation at Battelle Memorial Institute.

By its many interrelated activities, the Earth Sciences Division is actively involved in developing the science and technology that will be necessary to isolate wastes. Details of these activities are given in the following section.

Swedish-American Cooperative Program

THERMOMECHANICAL EXPERIMENTS AT STRIPA

M. Hood, T. Chan, and P. Nelson

INTRODUCTION

One of the main areas of concern regarding the disposal of radioactive waste materials in subsurface geologic repositories is the response of the in-situ rock mass, comprising the respository and the surroundings, to the thermomechanical loading that will be induced by the heat generating waste canisters. In order to assess quantitatively the response of a granitic rock mass to loading of this type, a series of experiments is being conducted at the Stripa mine in Sweden. The layout and design of these experiments are described in previous annual reports (1977 and 1978) of the Earth Science Division and by Hood (1979) and Cook and Witherspoon (1978). These experiments were begun in June 1978, and are continuing. During 1979 the heaters were turned off and the response of the rock during the cool-down period was observed. In a radioactive waste repository the rock mass will undergo both a heating and a cooling cycle. Therefore it is important that the behavior of the rock during both phases of the cycle be determined.

THIS YEAR'S ACTIVITIES—DATA ANALYSIS AND MODEL DEVELOPMENT

A consistent, and puzzling, feature of the results from these heater tests is that although the temperatures measured through the rock mass accord well with predictions, the displacements and stresses are less than those predicted by a factor of more than 2. This result is difficult to explain since if the rock is being heated then expansion should be taking place. Checks were made of the performance of the instruments and the calculation routine, but errors sufficient to explain this large discrepancy were not discovered. The analysis investigating this discrepancy has concentrated on the displacement measurements since these are easier to make and much easier to interpret than stress measurements. Displacement readings by the extensometers demonstrate two distinct modes of behavior. First an initial phase is observed immediately after turn-on of the heaters when displacements are completely unpredictable and are very much less than the calculated values. The second phase occurs when the measured displacements are less than the predicted values by a constant amount. For many of these instruments the ratio of the measured to the predicted displacements during this second phase is about 0.4 (Hood, 1979).

The initial nonlinear phase is difficult to explain and possibly may be caused by absorption of the early expansions of the rock into pre-existing discontinuities within the mass. This hypothesis is supported by evidence from an independent experiment where an increase in the velocity of ultrasonic waves through the rock in the vicinity of the heater was observed (Hood et al., 1979). The subsequent phase indicates that the rock is responding to the loading in a predictable manner but with a magnitude less than the calculations forecast. Behavior of this kind is consistent with a difference in values for the rock properties for an in-situ rock mass and for those used in the calculations.

The original calculations for the temperature, displacement, and stress fields, which were made before the start of the heater experiments, idealized the rock as a homogeneous, isotropic, perfectly elastic continuum with constant material properties. The main reason for using these assumptions was that the thermal and thermomechanical properties for Stripa granite had been determined by laboratory testing using a very limited number of small intact rock specimens at the time the calculations were carried out. Only thermal conductivity had been measured as a function of temperature and this had been found to decrease linearly with temperature at the rate of about 0.1 percent per degree Centigrade.

The thermal field was obtained using a closed-form solution of the linear heat conduction equation for a finite-length line source (Chan et al., 1978). This temperature distribution then was applied as thermal loads to calculate thermoelastic displacements and stresses using a modified version of the finite element code SAP IV (Bathe et al., 1974). The SAP IV code has been modified to achieve higher computational efficiency and to improve the accuracy of thermal strain and stress calculations. This Lawrence Berkeley Laboratory/Lawrence Livermore Laboratory version has been documented by Sackett (1979). The constant material properties used in these calculations are given in Table 1.

The model used for prediction of displacements and stresses in the experiments described in this paper was axisymmetric and used boundary conditions that took account of the mine excavations. Details of these thermoelastic calculations are given in a report by Chan and Cook (1978).

The effect of changing these constant material properties on predictions for temperature, displacement, and stress was investigated. It was found that the thermal conductivity has only a small effect on the parameters. From the classical theory of linear thermoelasticity it can be shown (Chan and Cook, 1978; Timoshenko and Goodier, 1951; Boley and Weiner, 1960) that, for an axially symmetric system, displacements and stresses are proportional, respectively, to the following combinations of thermomechanical properties

$$\alpha \frac{1+\nu}{1-\nu}$$

and

$$\frac{\alpha E}{1-\nu}$$

Table 1. Constant material properties used in the calculations.

Material property	Symbol	Value	Units
Thermal conductivity	k	3.2	W/m°C
Thermal diffusivity	$= k/\rho c_p$	1.47×10^{-6}	m^2/s
Coefficient of linear thermal expansion	α	11.1×10^{-6}	/°C
Young's modulus	E	51.3	GPa
Poisson's ratio	ν	0.23	

Illustrative calculations, both analytical and using the finite-element method, have been performed to show the effect of changing one or more of these parameters on predictions for rock displacement and stress. An example of these calculations is given in Table 2. This example shows radial displacements and stresses at a point in the rock mass a radial distance 1 m from the axis of the 5-kW heater at the heater midplane. Three sample calculations are given in this table where one property at a time is varied and the corresponding effects of this on displacement and stress can be seen. From this it is evident that, as expected, u and σ scale proportionally with α; a large change in ν results in a relatively small change in either u or σ; and E causes no change in u and a proportional change in σ.

A limited number of laboratory tests of intact small samples of Stripa granite were conducted in parallel with the in-situ heater experiments. These tests were carried out to determine the properties of this rock as functions of temperature, and in some cases, confining stress. The results of these tests for the rock properties of interest from the viewpoint of calculation of displacement and stress are illustrated in Figure 1.

Because the thermomechanical properties all exhibit significant variations with temperature, as shown in Figure 1, numerical calculations were carried out to investigate the influence of these temperature-dependent properties on predicted displacements and stresses. To include temperature-dependent thermal conductivity a nonlinear finite-element code, DOT (Polivka and Wilson, 1976) was used for the thermal modeling. (Specific heat and density were found by Pratt et al. (1977) to vary insignificantly with temperature over the temperature range concerned. The DOT code has been modified at LBL to take advantage of large core memory of the CDC-7600 computer.) These thermal calculations also account for the nonuniform initial temperature distribution in the rock and convective boundary conditions at the surfaces of the heater borehole and the drifts. The results of these thermal calculations have been summarized by Javandel and Chan (1979).

Thermally induced displacements and stresses were calculated using the finite-element code SAP IV. To delineate the effect of the temperature dependence of each individual rock property shown in Figure 1, several computer runs have been made in which one, two, three, or four temperature-dependent properties are included. Figure 2 illustrates the influence of each parameter in turn on calculated displacement, and compares these results with the observed relative displacement. These displacements are for a vertical extensometer located

Table 2. Sample calculations showing the effect of a variation of nontemperature-dependent material properties on displacements and stress predictions.

	α (10^{-6}/°C)	ν	E GPa	u (mm)	σ (MPa)	δ property (%)	δu (%)	δ/σ (%)
Base Case	11.1	0.23	51.3	0.71	51.5			
Case 1	<u>8.0</u>	0.23	51.3	0.51	37.1	-28	-28	-28
Case 2	11.1	<u>0.12</u>	51.3	0.57	44.9	-48	-20	-13
Case 3	11.1	0.23	<u>37.0</u>	0.71	37.1	-28	0	-28

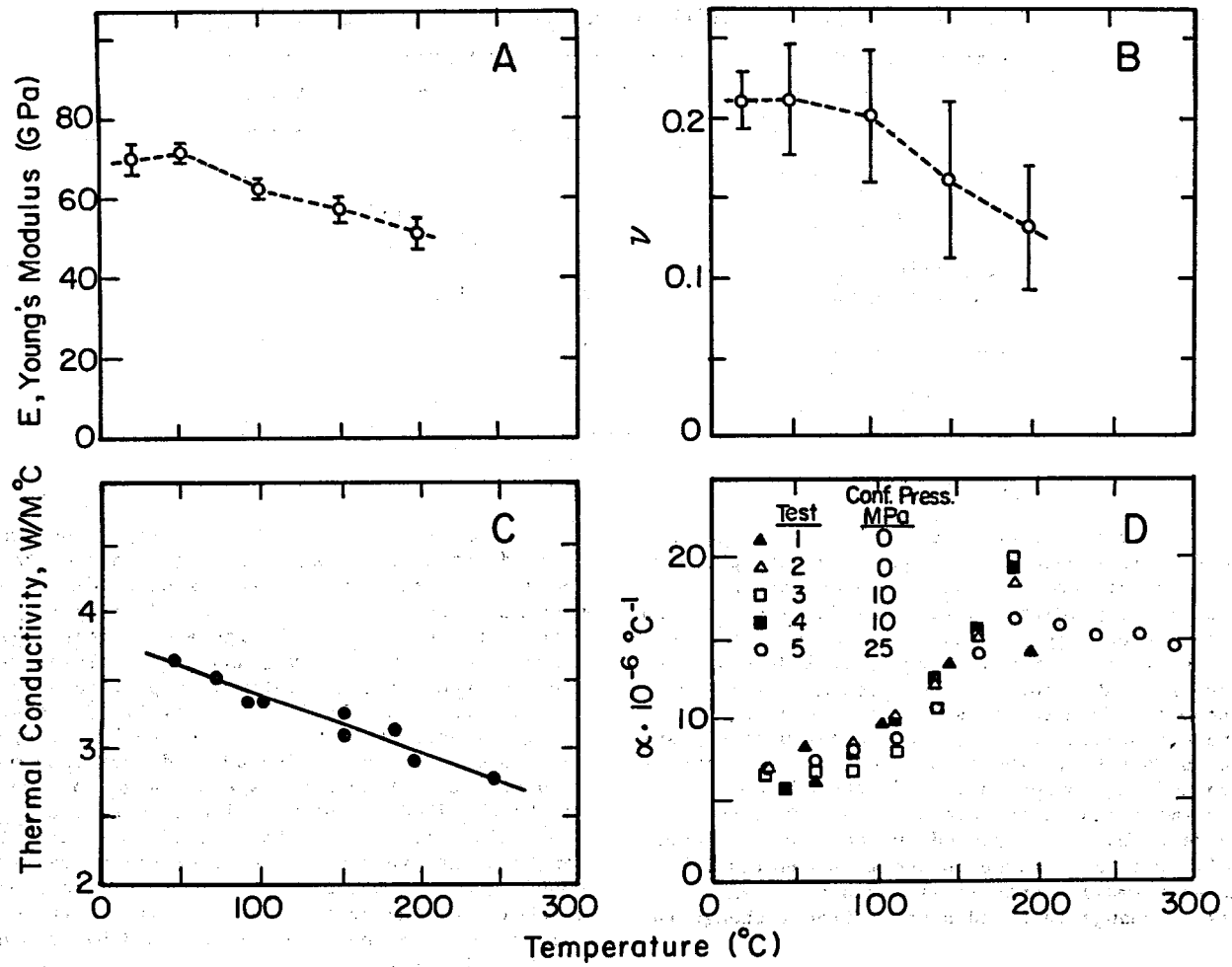

Figure 1. Results from the limited amount of laboratory testing showing the temperature dependence of material properties of Stripa granite. Results given in Plots A and B are after Swan (1978) and results given in Plot C are after Pratt et al. (1977). (XBL 801-4613)

at 2 m radial distance from the heater between anchor points 2.24 m above and below the midplane of the 5-kW heater.

From Figure 2A it can be seen that the weak temperature dependence of thermal conductivity of Stripa granite (Figure 1C) has only minor effects on the vertical displacements.

Figure 2B and 2C show that the temperature dependence of Young's modulus, E, affects the displacements more than the temperature dependence of Poisson's ratio, ν, although the latter property varies more rapidly with temperature. This is in contrast with the situation for constant rock properties where the magnitude of E does not affect the thermal displacements at all.

Finally, the very strong temperature dependence of the thermal expansion coefficient, α, of Stripa granite is reflected in its dramatic effect on the displacements, as depicted in Figure 2D. Note that the absolute values of the vertical displacements predicted using all temperature dependent properties are now somewhat smaller than the measured values.

At present only a small portion of the displacement data has been examined. For this limited amount of vertical displacement data the same general trend seems to hold.

In the thermal expansion coefficient measurements some hysteresis was observed during the heating-cooling cycle. It is of interest to determine whether hysteresis of this type is observed in the measurements of displacement for the in-situ rock mass during the cool-down phase of the heater experiments. This result is of importance in terms of the overall design of a repository because, as a result of the decay of thermal power from the waste canisters the rock surrounding the repository will undergo a thermal pulse (St. John, 1978). The rock temperatures will reach a maximum within one or two centuries and after this cooling will occur. The behavior of the rock during both the heating and the cooling phases will govern the stress field

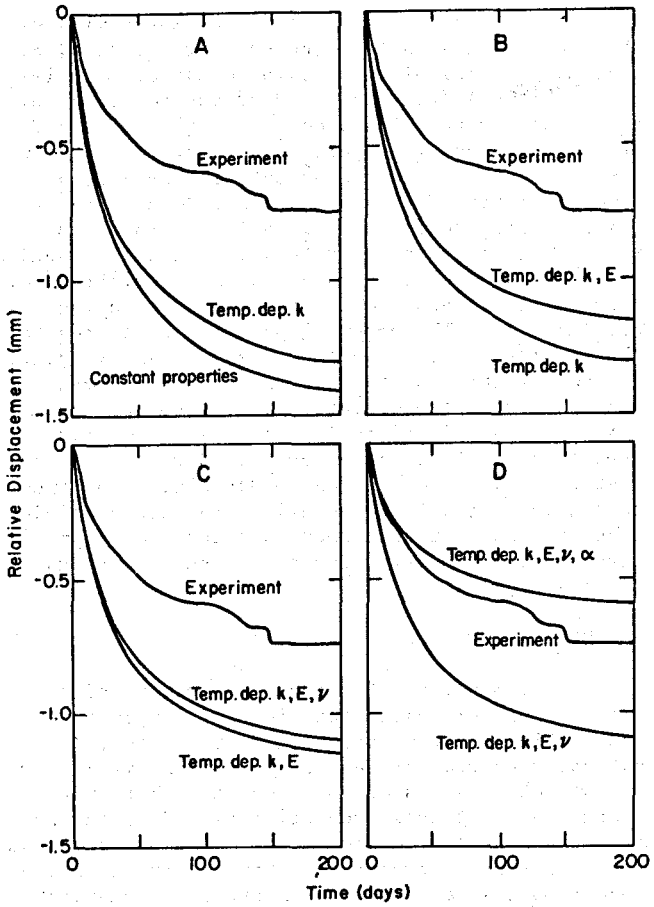

Figure 2. A series of graphs comparing measured rock displacements in the vertical plane between anchor points 2.24 m above and below the heater midplane for an extensometer at a radial distance 2 m from the 5-kW heater with calculated values for these displacements. The plots illustrate the sensitivity of these predicted displacements to the temperature dependence of the material properties. The plots A-D illustrate the effect of incorporating into the model an additional material property as a function of temperature. (XBL 801-4612)

induced, and the rates of groundwater flow through the rock mass. Demonstration of an ability to predict the rock behavior during both of these phases will be a prerequisite for repository design.

Some preliminary work has been done in this direction. An example is given in Figure 3, in which the measured and calculated relative displacements between a pair of anchor points across the heater midplane on a vertical extensometer at radial distance of 1 m from the 3.6-kW heater has been plotted as function of time, including the cooling period, i.e., beyond 398 days. No apparent difference can be discerned at this moment between the heating and cooling portions of the curves. The measured curve still follows the predicted curve for temperature dependent properties quite closely, but the absolute values of the measured displacements are again slightly higher.

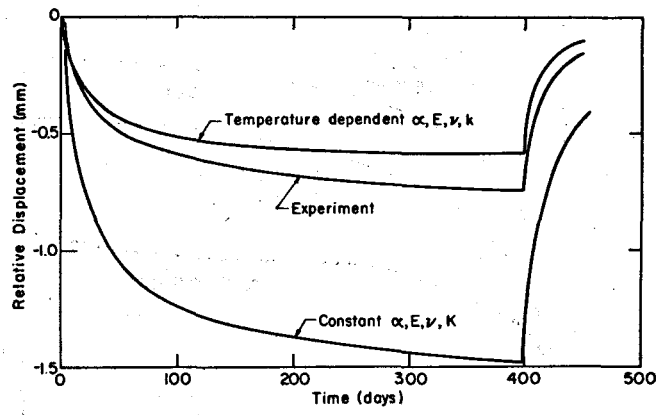

Figure 3. A plot comparing measured rock displacements in the vertical plane between anchor points 2.24 m above and below the heater midplane for an extensometer at a radial distance of 1 m from the 3.6-kW heater. This graph shows the predicted displacements for both temperature dependent and temperature independent material properties. Also illustrated in this Figure are the displacements, both measured and predicted during the cool down after the heater was turned off. (XBL 801-4611)

Interpretation of the measurements for changes in rock stress is still in progress. In the field better experience has been achieved with the vibrating-wire Creare gauges than with the U.S. Bureau of Mines borehole deformation gauges. For this reason analysis of results from the former is more advanced. Figure 4 illustrates the influence of temperature dependent properties on the calculations for radial stress at a point in the rock at radial distance 1.5 m from the 5-kW heater and 0.85 m above the midplane. From Figure 4 it is seen that, although using temperature-dependent rock properties reduces the discrepancy between measured and calculated stresses, the improvement is not as impressive as that for displacements.

As a sensitivity analysis, the calculations using temperature dependent rock properties were repeated with a scaled down Young's modulus

$$E(T) = \frac{37}{69} \times E_{lab}(T)$$

The rationale for this choice of scaling factor is that a suite of measurements were made of the in-situ rock modulus, at the Stripa heater test site using the Colorado School of Mines cell (Hustrulid, 1979). Results of these measurements, which showed considerable scatter, showed a mean value for the modulus of 37 GPa compared with the laboratory value of 69 GPa at 10°C (Swan, 1978). As expected the calculated radial stress was found to be scaled down by the same ratio, Figure 4B.

Incidentally, scaling down Young's modulus does not affect the displacements. This should be contrasted to the effect of temperature dependent

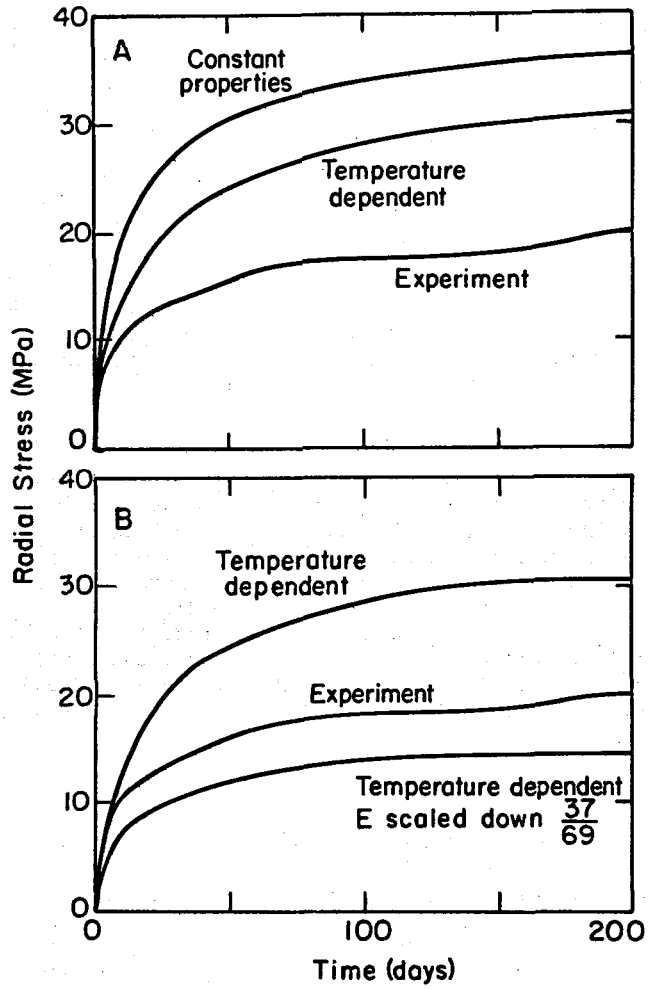

Figure 4. Two sets of curves both of which give the stress measured in a direction radial to the 3.6-kW heater with a vibrating-wire Creare gauge. Also given in these curves are calculations for the stress at this point demonstrating the effect of temperature-independent and temperature-dependent material properties together with the effect of incorporating a scaled down value for the Young's modulus to approximate more closely the rock modulus in-situ. (XBL 801-4614)

Young's modulus on displacements shown in Figure 2B. Apparently, the functional dependence on temperature affects the displacements, whereas a constant of proportionality does not.

CONCLUSIONS

The work described in this paper must be regarded as preliminary since data from laboratory tests for the properties of Stripa granite at elevated temperatures and pressures are limited and only a small portion of the field data have been compared with the modified finite-element calculations. Nevertheless the calculations for the displacements and stresses that are induced in the in-situ rock mass during the heater experiments demonstrate the dependence and the sensitivity of these quantities on the rock properties, k, ν, E, and, α. The calculations using constant material properties validate the standard thermomechanical equations for the dependence of displacement and stress on material properties. Also, calculations using temperature-dependent material properties demonstrate the fairly significant dependence of the rock displacements on Young's modulus. This is in contrast with the situation where the modulus is independent of temperature when calculations of rock displacements remain independent of changes in rock modulus. The material property that affects the predicted rock displacements most significantly is the variation of the coefficient of thermal expansion with temperature. Variations of thermal conductivity and Poisson's ratio with temperature have little effect on the predicted rock displacements. Changes in the rock properties with temperature have less effect overall on the stress field that is induced in the rock mass than incorporating into the model a value for the measured in-situ Young's modulus.

RECOMMENDATIONS FOR FUTURE WORK

The importance of accurate knowledge of material properties as functions of temperature and confining stress has been demonstrated. An extensive program of laboratory testing is required to collect these data. We recommend that these measurements of rock properties be made both for intact and fractured specimens. We also recommend that tests be conducted to determine the effect of rock sample size on these properties. Some work of this kind is planned at the Lawrence Berkeley Laboratory. Concurrently, further finite-element analysis should be performed to minimize the inaccuracy introduced by the geometrical approximation of the models, to study the influence of stress-dependent properties, and to determine more precisely the appropriate ranges of temperatures and confining stresses as well as the required accuracy of laboratory rock property measurements.

REFERENCES CITED

Bathe, K. J., Wilson, E. L., and Peterson, F. E., 1973. SAP IV, a structural analysis program for static and dynamic response of linear systems. Berkeley, University of California, College of Engineering, report EERC 73-11.

Boley, B. A., and Weiner, J. H., 1960. Theory of thermal stresses. New York, John Wiley and Sons.

Chan, T., and Cook, N. G. W., 1978. Calculated thermally induced displacements and stresses for Stripa heater experiments. Berkeley, Lawrence Berkeley Laboratory, LBL-7061.

Chan, T., Cook, N. G. W., and Tsang, C. F., 1978. Theoretical temperature fields for heater project at Stripa. Berkeley, Lawrence Berkeley Laboratory, LBL-7082.

Cook, N. G. W., and Witherspoon, P. A., 1978. In-situ heating experiments in hard rock: Their objective and design, in Proceedings, Seminar on In-Situ Heating Experiments in Geological Formations. Ludvika, Sweden, Organisation for Economic Cooperation and Development.

Hood, M., 1979. Some results from a field investigation of thermomechanical loading of a rock mass when heater canisters are emplaced in the rock, in Proceedings, 20th U.S. Symposium on Rock Mechanics. Austin, University of Texas.

Hood, M., Carlsson, H., and Nelson, P. H., 1979. The application of field data from heater experiments conducted at Stripa, Sweden, to parameters for repository design, in Proceedings, Internat. Symp. on the Underground Disposal of Radioactive Wastes. Helsinki, Organisation for Economic Cooperation and Development, Nuclear Energy Agency.

Hustrulid, W. A., and Schrauf, T., 1979. Borehole modulus measurements with the CSM cell in Swedish granite, in Proceedings, 20th U.S. Symp. on Rock Mechanics. Austin, University of Texas.

Javandel, I., and Chan, T., 1979. Detailed analysis of temperatures from underground heating experiments in granite. EOS, Transactions, American Geophysical Union, v. 60, no. 46, Abstract T96.

Polivka, R. M., and Wilson, E. L., 1976. Finite-element analysis of nonlinear heat transfer problems. Berkeley, University of California, Department of Civil Engineering, Report UC SESM 76-2.

Pratt, H. R., et al., 1977. Thermal and mechanical properties of granite, Stripa, Sweden. Salt Lake City, Terra Tek, Report TR 77-92.

Sackett, S. J., 1979. Users' manual for SAP 4 on modified and extended version of the University of California Berkeley SAP IV code. Livermore, Lawrence Livermore Laboratory, UCID-18226.

St. John, C. N., 1978. Computer models and the design of underground radioactive waste repositories, prepared for Current Developments in Rock Engineering. Cambridge, Massachusetts Institute of Technology.

Swan, G., 1978. The mechanical properties of Stripa granite. Berkeley, Lawrence Berkeley Laboratory, LBL-7074.

Timoshenko, S. P., and Goodier, J. N., 1951. Theory of elasticity, 3rd ed. New York, McGraw Hill, Engineering Society Monographs.

FRACTURE HYDROLOGY STUDIES AT STRIPA

J. E. Gale, C. P. Wilson, and P. A. Witherspoon

INTRODUCTION

The overall hydrology program at Stripa (Gale and Witherspoon, 1979) is summarized in Figure 1. The five major areas of research are: (1) assessment of directional permeabilities; (2) geochemical and isotope studies; (3) tracer studies; (4) an underground macropermeability experiment to measure rock-mass seepage; and (5) pump tests. The geochemical and isotope studies and the macropermeability experiment are discussed elsewhere in this report. The tracer studies have not been initiated at this time. Thus, this paper deals primarily with the first part of the program, assessing directional permeabilities of the Stripa granite, which is the major activity of the fracture hydrology program.

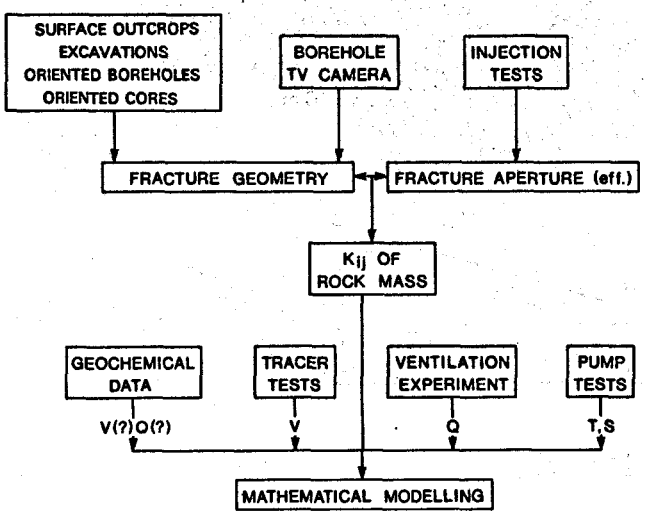

Figure 1. Block diagram of fracture hydrology program at Stripa. (XBL 7811-2144)

Fracture hydrology tests have been performed in both surface and subsurface boreholes. The surface boreholes consist of six water-table wells, WT-1 through WT-6, a pump test well WT-7, and three long inclined boreholes, SBH-1, SBH-2, and SBH-3 (Figure 2). SHB-1 is an open, 76-mm-diameter, diamond-core hole, 385 m long, that angles downward at 45 degrees, passes over the top of the test excavations, and terminates at approximately the 290-m level. SBH-2, also diamond-cored, was drilled from the west toward the test excavations. This borehole is 365 m long, angles downward at 52 degrees, and terminates in the position shown in Figure 2 at approximately the 290-m level. SHB-3, 315 m long, also diamond-cored, is drilled from the north at an angle of approximately 50 degrees south toward the test excavations, terminating in the position shown. All three inclined surface boreholes were oriented to optimize their intersection with the major fracture sets.

The subsurface hydrology boreholes (Figure 3) are located at the north end of the test excavations. This group of boreholes are all diamond-core holes, 30 m long and 76 mm in diameter, except R-1 and R-6, which are 40 m long.

ACTIVITIES IN FISCAL YEAR 1979

The geological log of the drill core, distribution of major fracture zones, RQD values, and the bottom-hole porewater pressures for SBH-1 are pre-

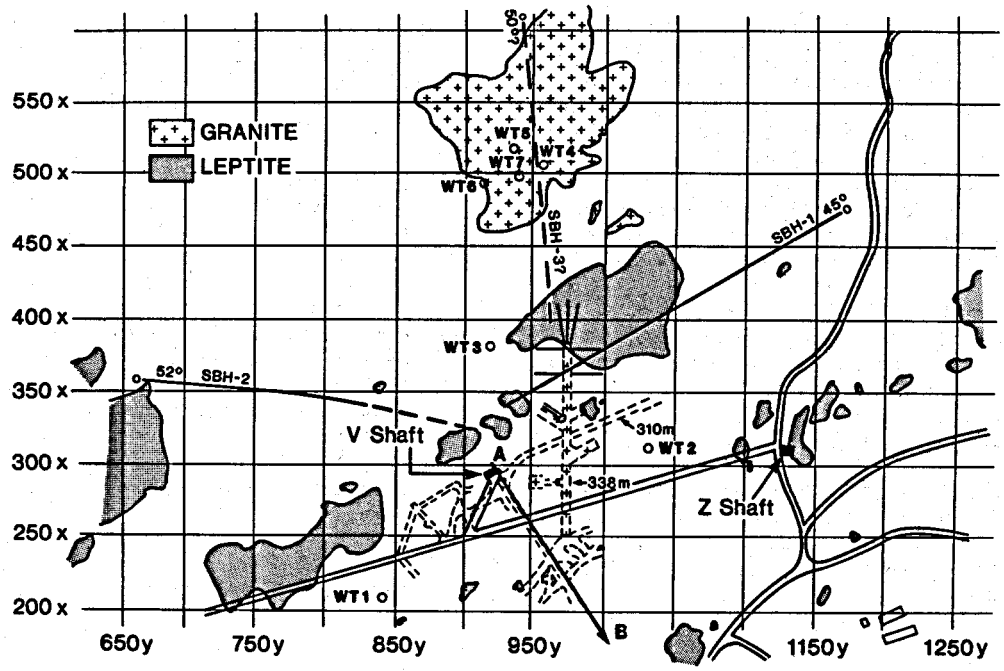

Figure 2. General geology and hydrology borehole locations. Squares are 50 m on a side.
(XBL 7811-13105)

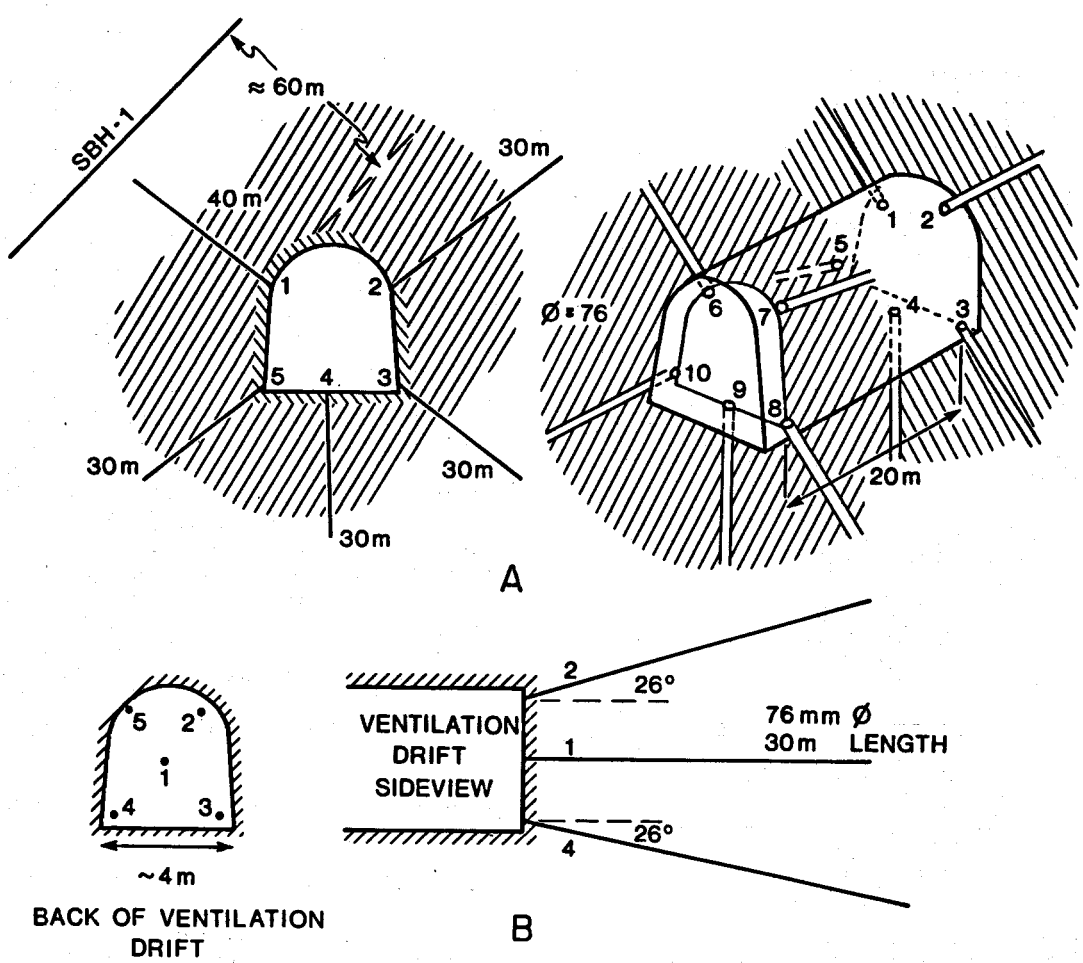

Figure 3. Location and orientation of subsurface hydrology boreholes. (XBL 7811-13108)

sented in Figure 4. The porewater pressures, measured in a bottom hole, 3 to 4 m long, cavity sealed off with an inflatable packer as the drilling advanced, show that at 100 m or so below the surface, the mine has reduced the water pressures in the rock mass.

The borehole injection test program was designed to provide information on the distribution of effective fracture apertures. The basic test equipment consists of a two-packer assembly with downhole pressure and temperature probes. During each test the fluid pressures were measured both in the injection zone and above and below the injection zone. In all of the boreholes, packer tests were carried out using (1) a fixed packer spacing of 2 m along the entire length of the boreholes; (2) packer spacings sufficient to isolate and test single fractures; and (3) packer spacing of approximately 6 to 10 m to test the main fracture-geophysical zones. This testing program enables one to develop fracture aperture distribution data for different parts of the rock mass from a statistical analysis of the fluid pressure, flow rate and fracture frequency data.

The results of injection tests in 2-m intervals in two sections of SBH-1 are shown in Figures 5 and 6. Flow rates for these 2-m packer spacings ranged from less than 0.01 ml/min to approximately

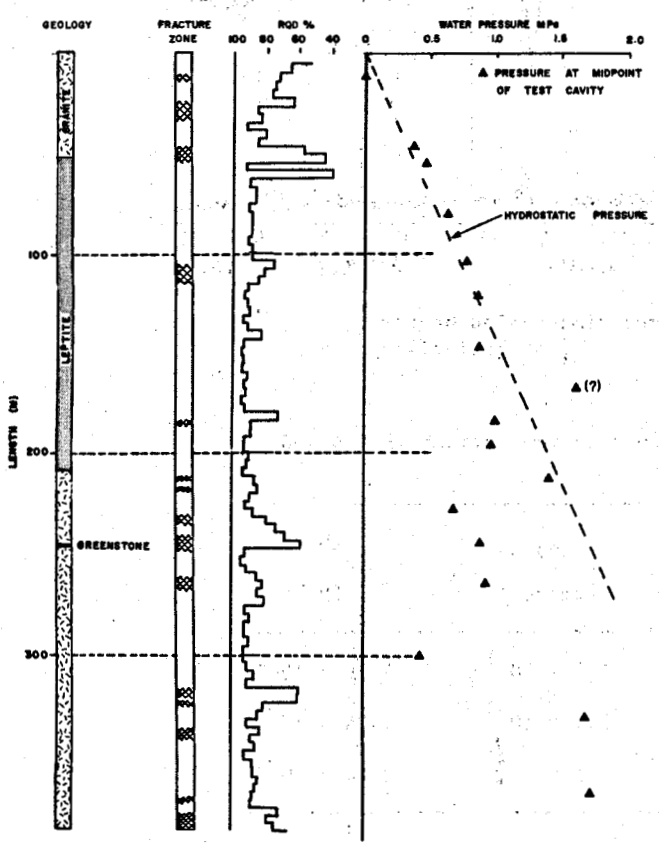

Figure 4. General geology, fracture zones, RQD values, and bottom-hole fluid pressures, measured during drilling, for SBH-1. (XBL 7811-13104)

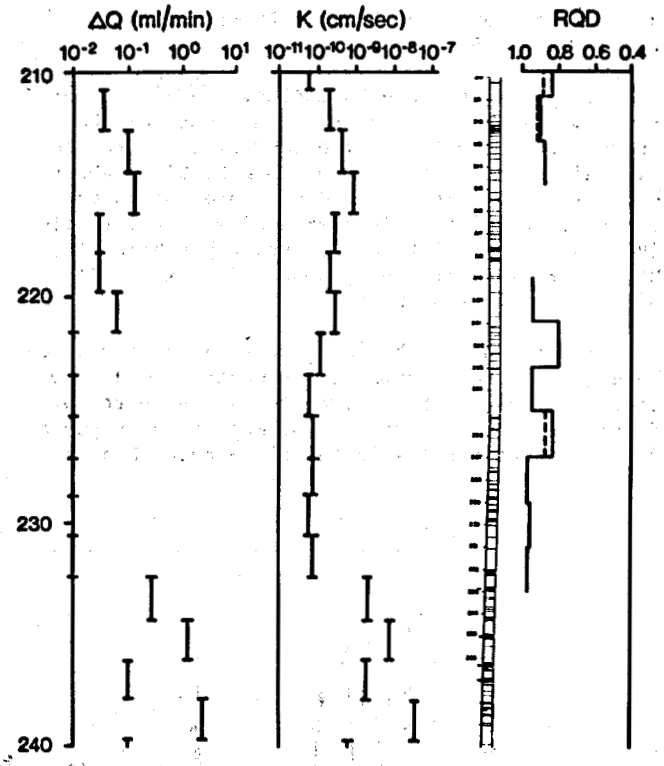

Figure 5. Injection test and fracture data from SBH-1, 210- to 240-m section. (XBL 804-9416)

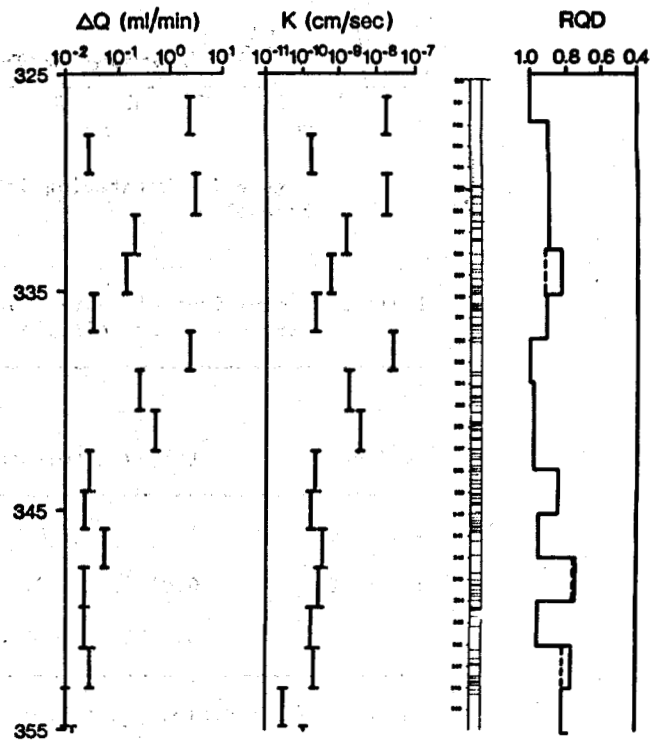

Figure 6. Injection test and fracture data from SBH-1, 325 to 355 m section. (XBL 802-8225)

3 ml/min for both the 210- to 240-m section and the 325- to 355-m section.

In the subsurface boreholes, the excess pore pressures in the rock mass at the depth of the excavations resulted in flow out of the boreholes. Typical outflow rates ranged from 0.001 to about 6 ml/min, and in-situ fluid pressures measured in 2-m packer intervals over a 30-m long borehole (R4) ranged from 0.4 to 0.8 MPa. This borehole, R4, is drilled vertically downward from the floor of the ventilation drift.

Dewatering of the instrument and heater boreholes during the thermal experiments showed flow rates similar to those given for R4 and parts of SBH-1. Figure 7 shows the volumes of water pumped from two heater holes in the time-scaled heater experiment room. These boreholes are about 11 m long and the average rate of inflow, over several months, of 1 to 2 ml/min represents the flow out of a fairly large volume of rock. Although injection rates up to 500 ml/min have been measured in some test zones, the flow rates given above are generally representative of most of the granite rock mass at Stripa.

PLANNED ACTIVITIES

A detailed interpretation of the data presented herein in terms of the fracture hydrology of the Stripa granite will be initiated in fiscal year 1980. As a form of preliminary interpretation, it is instructive to consider the measured flow rates in the context of the data presented in Table 1.

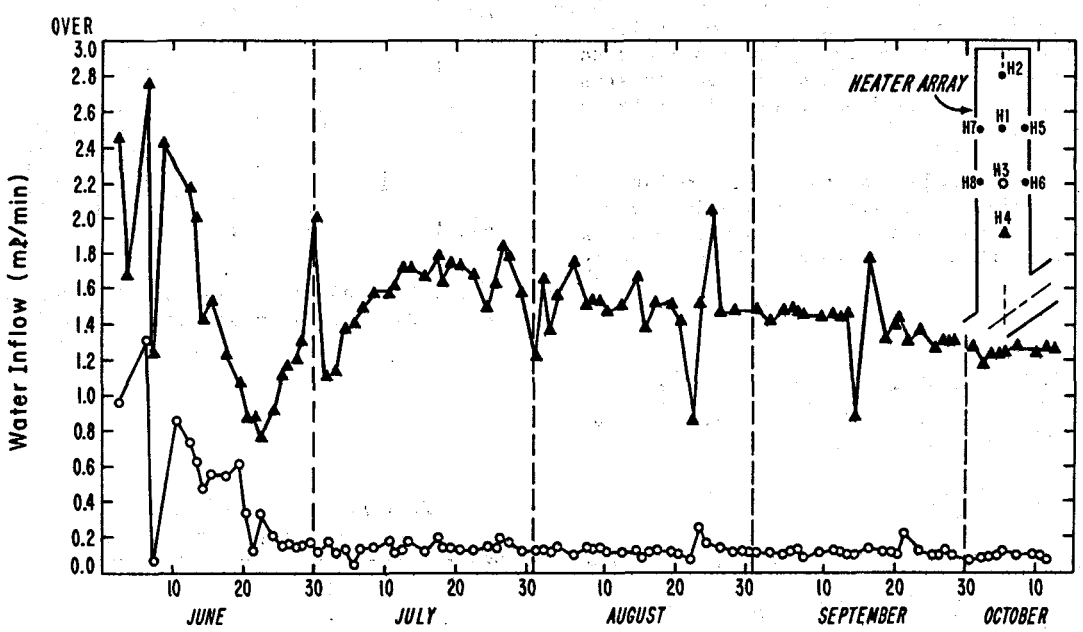

Figure 7. Dewatering data from time-scaled heater boreholes. (XBL 7811-2143)

Table 1. Comparison of equivalent porous medium permeabilities and fracture permeabilities.

K_p (cm/sec)	Q (ml/s)	Q (ml/min)	K_f (cm/sec)	2b (M)
4.5×10^{-6}	1	60	1.9×10^{-1}	4.82×10^{-5}
4.5×10^{-8}	0.01	0.6	8.8×10^{-3}	1.04×10^{-5}
4.5×10^{-10}	0.0001	0.006	4.1×10^{-4}	2.24×10^{-6}

Radial Flow Conditions, r = 0.038 m,

r_p = 10 m, H_b = 0, H_w = 10 m

Fracture Spacing = 2 m

There, we have calculated porous media hydraulic conductivities for a range of flow rates, subject to a given set of boundary conditions. If instead of a porous medium we have, as may very well be the situation, a single fracture intersecting the 2 m test interval, we can calculate the hydraulic conductivity of this single fracture. As shown in Table 1, there is a considerable difference in the impression created depending on whether we choose to express the results in terms of fracture or equivalent porous medium hydraulic conductivities. One important point to remember is that the volume of fluid moving through rock mass is generally independent of the model chosen to interpret the field data, but the rate of movement and the nature of the pathway followed is not.

REFERENCE CITED

Gale, J. E., and P. A. Witherspoon, 1979. An approach to the fracture hydrology at Stripa --preliminary results. Berkeley, Lawrence Berkeley Laboratory, LBL-7079.

MACROPERMEABILITY STUDIES AT STRIPA

C. R. Wilson, J. C. S. Long, R. M. Galbraith, A. O. DuBois, M. J. McPherson, and P. A. Witherspoon

INTRODUCTION

The macropermeability experiment is an attempt to improve permeability characterization techniques to analyze regional groundwater flow through low-permeability rock in the vicinity of a nuclear waste repository. This experiment consists of monitoring flow into, and pressure surrounding a 5 x 5 x 33 m long drift called the ventilation drift at the 335-m level of the Stripa mine (Figure 1). This paper examines the theoretical problems associated with making such a measurement and describes the actual experiment now in progress.

A major problem in regional hydrologic analysis is to determine the permeability of large volumes of low-permeability rock from in-situ tests. In high-permeability soils or rocks, standard well tests can be run such that large volumes of the flow system are perturbed by the test in reasonable periods of time. However, in low-permeability rock, standard well tests may only affect the flow system within a few meters of the well. Determination of large-scale permeability values can therefore be attempted in two ways. The first way is to synthesize large-scale values from a series of small-scale tests done in boreholes. The second way is to create a large-scale sink (or source), which will perturb a large volume of the flow system, i.e., a macroscopic permeability test.

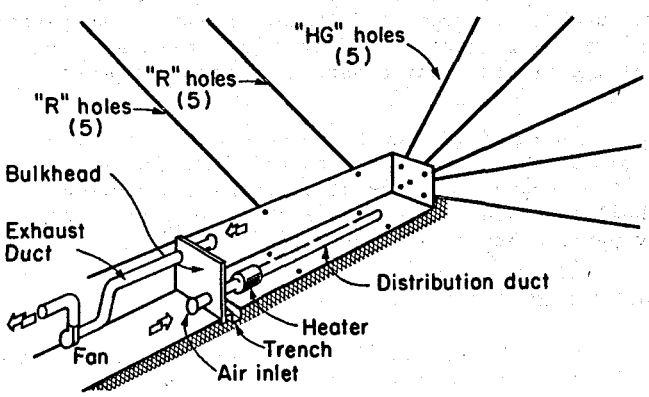

Figure 1. Perspective section through the ventilation drift showing air flow pattern and hydrology instrumentation boreholes. (XBL 7910-13004)

Small-scale borehole tests will probably remain the mainstay of hydrologic investigations since boreholes are the only practical means of extensively exploring deeply buried rocks. Therefore, reliable methods for predicting macroscopic permeability from borehole data are needed. In order to perfect such methods they will have to be checked by performing large scale in-situ tests at the same place where the borehole data have been collected. The macroscopic permeability test at Stripa represents a large-scale measurement that will be used to check the analysis of an extensive series of small-scale borehole tests (Gale and Witherspoon, 1979).

ACTIVITIES IN FISCAL YEAR 1979

Pressure Measurement

At Stripa, 15 boreholes 30 to 40 m long have been drilled from the ventilation drift into the surrounding rock (Figure 1). These boreholes are divided into three groups of five each. Two groups (the R-holes) are radial holes and one group (the HG holes) extend from the face of the drift. Each of these holes has been instrumented to monitor pressure. A total of 94 packers have been installed at approximately 5-m intervals. This prevents the boreholes from acting as drains into the drift and creates a three-dimensional array of 94 zones, 90 of which are individually connected by tubing to pressure gages.

During the experiment air in the drift will be kept at constant temperature. Pressures in the boreholes and water flow into the drift will be monitored until they are steady. Then the air temperature in the drift will be raised and the experiment repeated.

Between constant temperature experiments two

further experiments will be conducted. The first will be small-scale permeability tests in which each zone in one or two boreholes will be drained. The flow rate from each zone will be monitored separately until approximately steady conditions are reached. By repeating this test after each constant-temperature experiment, it may be possible to detect local changes in permeability due to changes in temperature. These changes can then be correlated to changes in permeability detected for the whole macroscopic test.

At Stripa we will not be able to examine average pressure parallel to the theoretical average isopotentials. However, since the average gradient is not expected to be very large at the outer ends of the boreholes, we will be able to approximately examine the effect of zone length on pressure by hydraulically interconnecting adjacent zones through the pressure tubing and allowing the system to come to equilibrium. Head losses in the tubing will be known and the pressure in each of the interconnected zones can be calculated. Because flow rates between zones are in most cases expected to be quite low, the pressures in the zones should be nearly equal. The average of the pressures will be taken as an estimate of the pressure the zones would have if the packer between them were removed.

Flow Measurement

In most permeability tests, the water can be collected in a tube or pipe and the flow rate measured in a straightforward manner. However, in the low-permeability rock of this experiment, the flow rate into the drift is so low and the surface area is so great that a significant proportion of the inflow would be lost to evaporation and the remainder would collect on the floor of the drift too slowly to measure in a reasonable amount of time.

One of the purposes of this experiment is to examine the utility of measuring low flow rates by evaporating all the water into the ventilation air while measuring the change in water vapor content between the incoming and exhaust air streams. To operate successfully, the ventilation system should provide an air flow rate and temperature capable of vaporizing and carrying away all of the influx water (McPherson, 1979). In addition, all parameters must be steady enough to allow identification of the equilibrium conditions. Also, the differential relative humidity between the air entering and leaving the experiment area must be great enough to provide acceptable water vapor measurement accuracy. As a point of reference, 1.0 m^3/sec (2,100 cfm) of air flowing at normal atmospheric pressure, 20°C, and 100% relative humidity will transport about 1 liter of water vapor per minute.

A sketch of the experimental setup was shown in Figure 1. An air- and vapor-tight bulkhead seals off a 33-m length of the ventilation drift. This wall consists of a structural wooden frame covered with a 0.15-mm-thick sheet of PVC, as a vapor barrier, and fiberglass insulation to prevent condensation. The vapor barrier and the structure are keyed into a 20-mm-deep notch on all four sides, with foamed plastic sealing in the notch to prevent the loss of water through the blast damaged surface rock. A frozen-food-locker type door provides access through the bulkhead.

The general mine ventilation system delivers about 1.4 m^3/sec of fresh air to a point just outside the bulkhead. The experimental ventilation system admits a portion of this fresh air into the sealed room to pick up the water (as vapor), which flows into the sealed room through the surrounding rock. This secondary ventilation system is driven by a fan located in the exhaust duct so that a slightly negative pressure will exist within the sealed room. Any air leaking through the bulkhead will be into the room and it will be the same air as that entering through the inlet duct. In this way, the inlet wet and dry bulb measurements will be representative of both the intentionally admitted air and the leakage air. The flow measuring station as well as the exhaust wet- and dry-bulb sensors are in the exhaust duct. These sensors sense the total air flow including leakage.

The air entering the sealed room passes through an electric duct heater. It is then distributed through an insulated duct with multiple openings along the length of the room. The air issuing from these openings will be directed preferentially onto any damp spots on the rock surface (most of the water arrives by seeping along discrete fractures). We expect to maintain the walls of the drift in an almost dry condition, with fans used where necessary to provide a high air velocity over particularly damp spots.

The climatic conditions within the room will be controlled by manually selecting a suitable air flow rate (by adjusting a damper on the fan exhaust) and then adjusting the heater power as required to maintain the desired air temperature in the room. The energy input from the heater is used in three ways: (1) the sensible heat of the exhaust air will be increased; (2) the heat of vaporization for the water will be provided; and (3) the rock will be heated. As equilibrium conditions are approached the third contribution would become negligible. The 45-kW heater is divided into six sections, which are separately controlled. Five sections are under manual control and one is under automatic on-off control with feedback from a room-temperature sensor. The heater voltage is regulated to isolate it from the large voltage fluctuations observed in the mine power system.

A 75-mm-deep trench has been cut across the floor of the drift just inboard of the bulkhead. If the trench and floor of drift remain dry, we shall conclude that all available water is being evaporated at its arrival rate.

PLANNED ACTIVITIES

The bulk permeability measurements are expected to be completed during fiscal year 1980. Data reduction will be initiated in fiscal year 1980 and completed in fiscal year 1981 when the results of the borehole hydrology tests will become available for comparison. In addition to the bulk permeability measurements, a series of borehole

permeability and tracer tests using fluid withdrawal methods are planned using installed equipment from macropermeability test.

REFERENCES CITED

Gale, J. E., and P. A. Witherspoon, 1979. An approach to the fracture hydrology at Stripa: Preliminary results. Berkeley, Lawrence Berkeley Laboratory, LBL-7069, SAC-15.

McPherson, M. J., 1979. Psychrometry: The measurement and study of moisture in air. Nottingham University Mining Magazine, University of Nottingham, United Kingdom.

A PROGRAM OF GEOLOGIC STUDIES AT STRIPA

H. A. Wollenberg, L. Andersson, and S. Flexser

INTRODUCTION

A number of geomechanical, hydrologic, and geochemical tests have been conducted since late fall 1977 in granitic rock at the Stripa, Sweden, mine. Results have been the subjects of over 20 reports describing the hydrologic setting and the response of the rock to heating. The results of these tests will be used (1) to establish techniques to measure the hydrologic, geomechanical, and geochemical settings of proposed nuclear waste repositories, and (2) to determine the properties of a granitic rock mass which would be critical to the long-term isolation of radioactive waste.

To validate the transferability of these techniques and properties from Stripa to the evaluation of potential repository rock masses, it is necessary to know the geologic setting and petrology of the Stripa pluton. The experiments at Stripa are being conducted in a granitic rock mass within ~200 m of its contact with older metamorphic rock called leptite (Olkiewicz and others, 1978). Yet, little is known of the size and configuration of the Stripa pluton. On the recently published geologic map of the Lindesberg SV quadrangle (Geological Survey of Sweden, 1979), the pluton is shown exposed over a relatively small area (~0.3 km radius). However, the extensive cover of glacial debris obscures the true size and shape of the pluton at the surface. The configuration with depth of the contact between the pluton and the metamorphic rock is well defined only to the south, afforded by the extensive workings of the old iron mine. Contacts to the north, west, and east are concealed at the surface and unexplored at depth. Thus, the questions of whether the granitic rock mass at Stripa is among other things a dike-like body, a stock, or the exposed portion of a much larger pluton, are unanswered and as such the position of the experiments within the pluton also remain in question.

ACTIVITIES IN FISCAL 1979

To help answer these questions a program of geologic studies was started in the summer of 1979 to determine the size, configuration, and composition of the Stripa pluton. Efforts concentrated on collection of samples of granitic and metamorphic rocks from the surface and underground at Stripa and at other plutons within the Lindesberg region. Samples of cores were also selected from the holes SBH 1 and 2, drilled diagonally from the surface toward the experimental area, and from the vertical hole drilled to a depth of 465 m from the mine's 410 m level. This set of samples then covers a vertical extent from the surface to a depth of nearly 900 m and encompasses samples of pegmatite, various granitic compositions, diabase, and leptite. The sample set also contains representatives of the classes of fractures encountered in the Stripa pluton: those predominately filled by chlorite, epidote and sericite, quartz, and carbonate minerals. At many locations on the surface and underground, hand specimens were oriented at the time of collection for strike and dip, to permit subsequent petrofabric determinations.

Along with collection of surface and subsurface samples, field radiometric measurements were made with a portable gamma-ray spectrometer to determine the uranium, thorium, and potassium concentrations within the various rock units. These measurements give preliminary indications of the geochemical homogeneity of the pluton and permit calculation of the radiogenic heat production, a useful parameter that, when combined with the conductive heat flow, may be used to estimate the size of the pluton.

The conductive heat flow through the Stripa pluton was calculated, based on the product of the temperature gradient (17.5 $^{o}C/km$) observed by the Swedish Geological Survey in the vertical hole drilled from the 410 level, and a mean conductivity of 3.4 $W/m^2/^{o}C$ (Pratt et al., 1979). The resulting value of 59.5 mW/m^2 compares closely with the regional conductive heat flow for the south-central portion of Sweden, as indicated by Cermak (private communication, 1979). Preliminary results of field gamma spectral measurements indicate that the radiogenic heat production of the Stripa granite is nearly four times that of the neighboring leptite, and 1.6 times the average heat production of the other plutons within the region. Therefore, the high radiogenic heat production of the Stripa granite, coupled with regionally "normal" heat flow measured within the pluton, suggest that the relatively radioactive granitic body is small; it appears to have little if any effect on the regional heat flow.

PLANNED ACTIVITIES

Continuing activities in fiscal year 1980 will include petrographic descriptions of the classes of fractures, as well as descriptions of

relatively unfractured Stripa granite and granitic rocks from other plutons in the region. Age dates will be obtained to determine the relative ages of the plutons and the fracture filling material. The location and abundance of uranium within the fractures and the relatively unfractured rock will be mapped by the fission-track method, permitting estimates of the source term for the high ^{222}Rn contents observed in water from boreholes in the experimental area (Nelson et al., in prep.).

A program of geophysical measurements and surface boreholes has been proposed to penetrate the glacial debris covering the Stripa area to delimit the concealed contacts between the pluton and the surrounding leptite. Together with petrologic studies of cores from underground horizontal holes expected to be drilled in 1980, and comparisons of the age and petrology of the Stripa granite and granitic bodies in the surrounding region, these measurements should furnish a definition of the size and configuration of the Stripa pluton and the position of the experiments within the pluton.

REFERENCES CITED

Geological Survey of Sweden, 1979. Bedrock map 11F, Lindesburg SV, SGU Ser. Af-nr. 126.

Olkiewicz, A., Hansson, K., Alnién, K-E, and Gidlund, G., 1978. Geologisk och hydrogeologisk grunddokumentation ar Stripaforsoksstation, K.B.S. Teknisk Rapport no. b3.

Pratt, H. R., Schrauf, T. W., Bills, L. A., and Hustrulid, W. A., 1977. Thermal and mechanical properties of granite: Stripa, Sweden. Salt Lake City, TerraTek Summary report TR-77-92.

Research and Development Investigations

REVIEW OF THE STATE-OF-THE-ART OF NUMERICAL MODELING OF THERMO-HYDROLOGIC FLOW IN FRACTURED ROCK MASSES

J. S. Y. Wang, R. A. Sterbentz, and C. F. Tsang

INTRODUCTION

This review is a result of the attention currently being given to the isolation of nuclear wastes by underground storage in geological formations. The wastes generate heat, which raises the temperature of the surrounding fractured rock masses, inducing buoyancy flow and pressure changes in the groundwater. These effects introduce the potential hazard of radionuclides being carried to the biosphere. A number of numerical models are now available to investigate these physical processes.

The objectives of this project are to develop a list of models and to study the governing equations, numerical methods, computer code, validation and applications of a selection of models relevant to the simulation of thermohydrologic flow around a repository in fractured rock masses. The work plan consists of the following steps: (1) initial literature survey, (2) selection of models, (3) detailed evaluation, (4) workshop, and (5) final report.

ACTIVITIES IN FISCAL YEAR 1979

Literature Survey

An initial literature survey was conducted of journals and data bases. An information request letter has been sent to over 50 modelers in the United States and abroad. Additional preprints, reports, and information on model developments were received. Over 500 papers and reports were catalogued and filed.

Selection of Models

A number of models were selected for detailed survey. We preferred discrete fracture and double porosity models over porous medium models, and nonisothermal models over isothermal models. The relevant applications are in radioactive waste storage as well as in groundwater movement, geothermal reservoirs, aquifer thermal storage, and thermal recovery of petroleum.

The final sets of models can be divided into three groups. The first group contains models used in handling the characterizing fractured rock masses. The model ROCMAS (PORFRC) of U.C. Berkeley solves the coupled flow and stress equations in discrete fractures and in porous medium blocks. The applied stress can also be thermally induced. The models of Duguid of ONWI and O'Neill of Princeton are double porosity models for fluid flow and for heat transfer, respectively. In a double porosity model, each point in space is represented by two values of pressure and two values of temperature, one set representing the macroscopically averaged values over the fractures, and the other set for the porous rock medium blocks. The model TERZAGI of LBL has been used for the study of fluid flow in a deformable fracture network and demonstrates the flexibility of the integrated finite difference method for modeling complex geometry. The nonisothermal model CCC and the two-phase model SHAFT79 of LBL use the same methodology. CCC has been recently used for discrete fracture simulations.

The second group of models are nonisothermal saturated flow models currently being used in several repository studies. The model GWTHERM of Dames and Moore has been used in generic studies of crystalline rocks. The model FINI of Acres has been used in the Swedish KBS studies in granite. The model SWIFT of Intera has been used in the WIPP and Nuclear Regulatory Commission studies in salt. The model CFEST of Battelle Pacific Northwest Laboratory is developed for the Waste Isolation Safety Assessment Program studies. The modeling experience from these studies is valuable for the prediction of thermal effects of a repository. More realistic representation of the fractured rock mass will be modeled in the future.

The third group of models are nonisothermal, two-phase (steam and water) models developed recently for geothermal reservoir engineering. The possibility of liquid water turning into steam near a waste canister indicates the need for simulating two-phase phenomena for waste storage studies. The model of Coats of Intercomp has simulated the steam flashing within fractures. The model of Faust and Mercer of Geotrans has been applied to an areal simulation of the Wairakei geothermal field in New Zealand. The model MUSHRM of Systems, Science, and Software has been used in a vertical simulation of Wairakei, and in Gulf Coast geopressure simulation. The model SHAFT79 of LBL is a newly developed, efficient code currently used in geothermal simulations in Italy, Iceland, and Baca, New Mexico, and also in repository simulations in NTS studies.

Detailed Evaluation

For each model, the following features have been studied.

1. Governing equations
2. Numerical methods
3. Computer code
4. Validation

5. Applications

An outline of the subjects covered under each of the five features follows:

Governing equations. This section will cover the equations to be solved by the numerical method for both fluid flow and heat transfer. Fluid movement depends on the porosity and permeability of a formation, the density and viscosity of the fluid, and the fluid sources. The formation-related properties are the main concern here. A rock mass can be modeled in three ways: (1) as a system with discrete fractures within a porous rock medium; (2) as a porous medium with two porosities, one representing the fractures and another the rock medium; or (3) as a porous medium with a simple porosity. Additional terms or additional equations to handle the responses of porosity and permeability to changes in pressure, temperature, or stress will be discussed. The porosity and permeability, together with pressure and buoyancy driving forces, determine the fluid particle velocity. The velocity field is used in the simulation of the migration of radioactive nuclides through fractured rock masses.

Heat transfer depends on the conduction and dispersion through the rock, convection by the fluid, and characteristics of the heat sources. Heat generated by the waste affects the fluid flow directly through changes of fluid properties and indirectly through changes of rock stresses which may alter the permeability and porosity of a formation. At high temperature, liquid water may turn into steam indicating that two-phase phenomena must be treated. The temperature field determined by a thermohydrologic model can be used to interface with a rock stress study and a geochemical reaction rate study.

Numerical methods. Different methods can be used to discretize the space and to evaluate the gradients. The governing equations are usually solved by either finite-difference or finite-element methods. For the fluid-flow equations, treatment of the fluid capacity and fluid flux terms are discussed. For the heat-transfer equation, treatment of the convective and dispersive terms are discussed. For nonisothermal models, the solution sequence and time step control for the two equations are discussed. Also the direct or iterative procedure used to solve the nodal values of the variable on the grid mesh is described.

Computer code. The user's manual, code development, and other computers specific features are described. Versatility in grid mesh design for modeling is considered, especially discretization of the spatial domain which is applicable to fracture simulation. The required input of material properties for the model is described, including the capability to treat heterogeneity and anisotropy. Input data and calculations for fluid properties are also described.

The availability of source and sink terms for running problems are noted and the input data at initial and program restart times are described as well as the treatment, by the program, of various boundary conditions. The procedures used in the model for checking accuracy of solutions are discussed and, in addition, the printer and graphic output of the results are mentioned.

Validation. One area of importance in the review of a numerical model is the validation of the code. One can have little confidence in a model that is not validated. In our review we will identify and list the analytic solutions and field experiments against which the code has been validated. Comparisons with results from other numerical models will also be documented.

Applications. Major areas of application are listed to illustrate the variety of problems solved by the code, including references to published studies. This will give an indication of their versatility and range of applicability. Procedures in using the code with other codes are also described.

ACTIVITIES PLANNED FOR FISCAL YEAR 1980

Workshop

A workshop was held February 19-20, 1980, on the subject of modeling fractured rock masses. The developers of the selected models presented informal talks on the model or made other relevant comments on fracture flow modeling or repository simulation. The workshop included selected technical experts in model development, and representatives from ONWI.

Final Report

Following the workshop, the report on the evaluation and on the workshop will be finalized and distributed.

ACKNOWLEDGMENT

This study is sponsored by the Office of Nuclear Waste Isolation, U.S. Department of Energy.

REFERENCES CITED

Ayatollahi, M. S., 1978. Stress and flow in fractured porous media, Ph.D. dissertation. Department of Material Science and Mineral Engineering, University of California, Berkeley, California, 154 p.

Coats, K. H., 1977. Geothermal reservoir modeling. SPE-6892. Presented at the 52nd Annual Fall Technical Conference and Exhibition of the Society of Petroleum Engineers of AIME, Denver, Colorado, 33 p.

Dillon, R. T., Lantz, R. B., and Pahwa, S. B., 1978. Risk methodology for geologic disposal of radioactive waste: the Sandia waste isolation flow and transport (SWIFT) model. SAND78-1267, NUREG/CR-0424. Sandia Laboratories, Alburquerque, New Mexico.

Duguid, J. O., Jr., 1973. Flow in fractured porous media, Ph.D. dissertation. Department of Civil and Geological Engineering, Princeton University, Princeton, New Jersey.

Faust, C. R., and Mercer, J. W., 1979. Geothermal reservoir simulation: 2. Numerical solution techniques for liquid- and vapor-dominated hydrothermal systems. Water Resources

Research, v. 15, no. 1, p. 31-46.
Garg, S. K., Pritchett, J. W., Brownell, D. H., Jr., and Riney, T. D., 1979. Geopressured geothermal reservoir and wellbore simulation. System, Science and Software, report SSS-R-78-3639. La Jolla, California.
Gupta, S. K., Cole, C. R., Kincaid, C. P., and Kaszeta, F., 1980. Three-dimensional finite element model for coupled solution of flow, energy and solute transport in porous medium. Presented at the Fracture Hydrology Workshop, Lawrence Berkeley Laboratory, Berkeley, California.
KBS, 1977. Groundwater movements around a repository. KBS teknisk rapport 54:01-06, Hagconsult AB, Karnbranslesakerhet, Stochholm, Sweden.
Lippman, M. J., Tsang, C. F., and Witherspoon, P. A., 1977. Analysis of the response of geothermal reservoirs under injection and production procedures. SPE 6537. Presented at the 47th Annual California Regional Meeting SPE-AIME, Bakersfield, California.
Narasimhan, T. N., Witherspoon, P. A., and Edwards, A. L., 1978. Numerical model for saturated-unsaturated flow in deformable porous media. 2. The algorithm. Water Resources Research, v. 14, no. 2, p. 255-261.
O'Neill, K., 1978. The transient three-dimensional transport of liquid and heat in fractured porous media, Ph.D. dissertation. Dept. of Civil Engineering, Princeton University, Princeton, New Jersey.
Pruess, K., and Schroeder, R. C., 1979. Geothermal reservoir simulation with SHAFT79. LBL-10066. Presented at the 5th Geothermal Reservoir Engineering Workshop, Stanford, California.
Runchal, A., Treger, J., and Segal, G., 1979. Program EP21 (GWTHERM): Two-dimensional fluid flow, heat and mass transport in porous media. Technical note TN-LA-34. Advanced Technology Group, Dames and Moore, Los Angeles, California. September.

MIGRATION OF RADIONUCLIDES IN GEOLOGIC MEDIA

T. H. Pigford

During 1978-79 the research group in Nuclear Engineering has developed a sound mathematical foundation for predictive modeling of the migration of radionuclides in geologic media. We have provided a clear derivation of the differential equations of hydrogeological transport of radionuclides undergoing both radioactive decay and chemical/physical interaction with the porous solid. The differential equations are formulated to be applied both to one-dimensional flow, which is the subject of the studies for 1979-80, and to multidimensional flow in nonisotropic media. The source term characterizing the rate of dissolution of radionuclides, in the event that water enters the waste repository, can be arbitrarily specified for each of the elemental species. The differential equations allow arbitrary specification of the character of the rate of sorption and desorption of dissolved radionuclides as they permeate through the porous solid.

During 1978-79 emphasis has been placed upon developing analytical solutions for the migration of radionuclide chains in one-dimensional flow through isotropic porous media, with the assumption of local sorption equilibria. Solutions have been developed for band-release sources, resulting from dissolution of the waste matrix and its contained radionuclides at a constant rate, and also for preferential dissolution characterized by constant fractional rates of dissolution for individual radionuclides.

A superposition theorem has been developed that allows the solution for a band release to be synthesized from relatively simple time-displaced solutions for a hypothetical step release occurring over an infinite time.

Explicit solutions have also been developed for the space-time-dependent concentrations for a plane source in a medium of finite thickness surrounded by another medium of infinite extent in the direction of flow.

These analytical solutions are exact within the assumptions of the differential equations and boundary conditions, are easily programmed on a simple computer, and are useful for predictive modeling of long-term radionuclide releases from a geologic repository and as benchmark solutions to validate the mathematical accuracy of numerical solutions used in other national efforts on radioactive waste management.

Work in progress for fiscal year 1980 emphasizes the further generalization of these analytical solutions, demonstration of the important effects of different parameters such as dissolution rates and hydrogeological and geochemical properties, extension to nonequilibrium sorption, and extension to two-dimensional flow and propagation.

The research team consists of Professor Paul Chambré, Makoto Harada, and Thomas Pigford; Research Associates Fumio Iwamoto, Susumu Muraoka, and Sumio Masuda; and graduate students Marc Albert, Mauro Foglia, David Leung and Daniel Ting.

ULTRA-LARGE ROCK CORE EXPERIMENTS

D. J. Watkins, R. Thorpe, W. E. Ralph, R. Hsu, and S. Flexser

INTRODUCTION

The safe underground storage of radioactive waste requires accurate determination of the hydraulic properties of rock. Fracture systems in the rock play a dominant role in its hydraulic behavior. Because fractures are deformable, changes in fluid pressure or applied stress will change the fracture apertures within a rock mass and will have significant influence on fracture conductivity and fluid pressure distribution (Witherspoon et al., 1977). Models of the movement of fluids in a fracture are generally based on the analogy of flow between parallel plates. For steady, laminar, isothermal flow, the flux per unit head can be expressed as:

$$Q/\Delta h = C/f\ (2b)^3 \qquad (1)$$

where Q is flow rate, Δh is difference in hydraulic head, C is constant depending upon flow geometry and fluid properties, f is a factor accounting for roughness and nonparallelism, and 2b is the fracture aperture. The equation expresses the "cubic law" for fracture flow. Its validity has been established for laminar flow through open fractures (Witherspoon et al., 1979b) but further work is required to investigate its applicability to the wide range of fracture types and flow conditions that are encountered in nature. Laboratory research has traditionally been performed using rock specimens with dimensions of several centimeters. However, there is evidence that the measured hydrological properties of rock are influenced by the size of the sample (Witherspoon et al., 1979a). Thus it is important to obtain measurements on rock samples of dimensions closer to that of practical concern, namely meters rather than centimeters. To meet these needs, a facility development and research program for laboratory investigations using samples on the order of 1 m diameter by 2 m high is in progress at the University of California, Richmond Field Station. This work is part of the Nuclear Waste Isolation Group's overall research program on the hydraulic and thermomechanical properties of fractured crystalline rock (Witherspoon et al., 1979c).

ACTIVITIES IN FISCAL YEAR 1979

Test Facility

The ultra-large triaxial testing machine at the Richmond Field Station was originally constructed in 1968 for testing rock-fill materials. The machine (Figure 1) has 5.2 MPa confining pressure and 17.8 MN axial loading capacities. During the fiscal year the machine and facility have been rehabilitated and modernized. A servo-control system, including a new hydraulic power supply, has been installed that provides automated control of axial load and displacement. This equipment together with new apparatus for supply and regulation of confining pressure, pore pressure and fluid injection pressure will enable the test machine to be used for research on the hydraulic properties of ultra-large, fractured and intact specimens of crystalline rocks and other materials of importance to the design of underground nuclear waste isolation repositories.

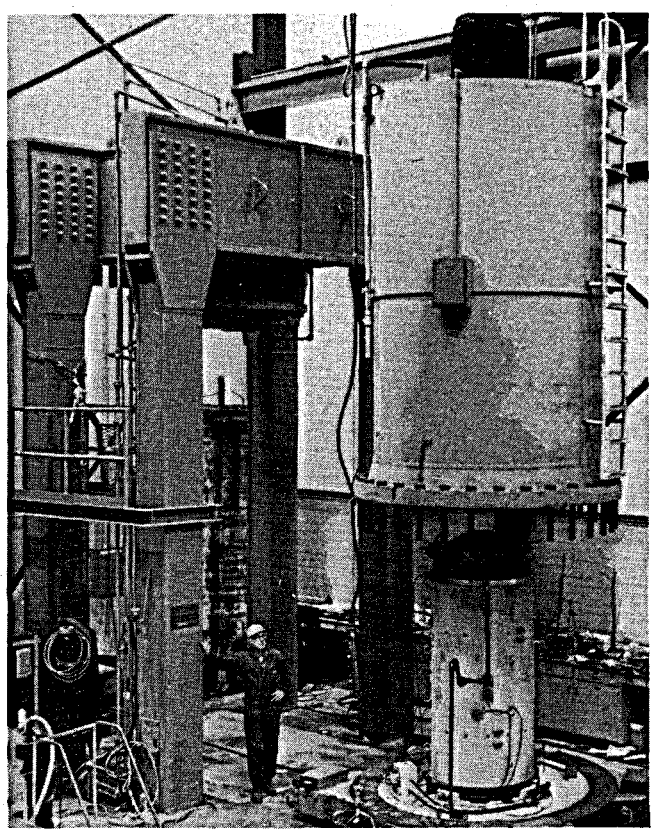

Figure 1. Large triaxial machine. (XBB 753-1977)

Depending upon the complexity of the specimen under test, permeability experimentation on ultra-large cores of fractured rock can involve large instrument arrays that typically include LVDT's, strain gauges, load cells, pressure transducers and thermocouples. The hydraulic and mechanical rock properties are highly stress-history dependent and efficient test control requires rapid reduction of data into engineering format and the capability to simulate complex stress-paths. To meet this need an advanced data acquisition/control system (DAS) has been designed by LBL's Real Time Systems Group. This installation will be based on a Hewlett-Packard System 45 modular DAS. It will be installed at the test facility in 1980 with an initial 80-channel capability and provision for future expansion.

Ultra-Large Stripa Core

In support of the Swedish-American Cooperative Program on Radioactive Waste Storage in Mined Caverns in Crystalline Rock (Witherspoon and Degerman, 1978) a 0.95-m-diameter, 1.9-m-high core, weighing 3628.7 kg, has been obtained from the mine at Stripa, Sweden (Halén and Andersson, 1978).

Tests using the large triaxial machine will be performed on this core to investigate fracture conductivity, matrix permeability, and the mechanical properties of the fractured rock under varying states of stress and stress history. The results will assist in understanding the hydrology of the Stripa mine, allow comparison of simple parallel plate models of fracture flow with data from a complex system of natural fractures, and provide deformation moduli that will contribute to the analysis of the thermomechanical behavior of the rock in the simulated waste repository.

During fiscal year 1979 the large core was prepared for testing by construction of reinforced concrete end caps (Figure 2) and drilling a 7.62-cm-diameter hole through the long axis, which serves for injection of water. The fractures contained within the core have been mapped and characterized. The rock is pervasively fractured down to the microscopic scale but fluid flow is dominated by two principal sets of fractures; one oriented approximately normal to the core axis and one at about 30 degrees to the axis. The major fractures are shown in Figure 3. A petrographic study of the core has been made using thin section, x-ray diffraction, and microprobe and soft x-ray fluorescence techniques. The rock matrix is a quartz monzonite and the fracture filing is intimately related to matrix alteration, with chlorite, sericite, and calcite minerals predominating. In preparation for tests in the large triaxial machine, simple, falling-head permeability tests have been made to obtain preliminary estimates

Figure 2. Ultra-large Stripa core. (BBC 796-8237)

of the conductivity and interconnection of flow paths through the fractures and matrix of the core. The results show that, depending upon the injection interval, there are a multiplicity of primary and complex secondary flow paths through the core that can accommodate flows as high as 5 l/min under injection pressure as low as 0.01 Pa. When the injection interval is not intersected by a major discontinuity the tests indicate a matrix permeability on the order of 10^{-6} cm/sec.

For the purpose of qualitative comparison of conductivity of different intervals within the core test, results have been presented in the form of Figure 4. The term kG is a combined "permeability-geometry coefficient" taken from the modified form of the Darcy equation:

$$Q = kGh \quad . \qquad (2)$$

where Q is flow rate, h is the injection head, k is the coefficient of permeability, and G is a geometry factory that depends upon the cross-sectional area and length of the flowpath.

The ultra-large core is scheduled to be installed in the triaxial vessel in January 1980 and will be instrumented to obtain measurements of changes in fracture aperture and radial deformation during injection and withdrawal permeability testing under controlled cycles of increasing and decreasing axial load. To estimate the maximum load that can be safely applied to the core, a series of point-load tension tests, direct tension tests, uniaxial compression tests, and triaxial compression tests were performed on naturally fissured and intact, 5.2-cm-diameter cores obtained from core-holes in the Stripa mine. Lower-bound Mohr failure envelopes for the fractured and intact rock have cohesion intercepts of 7.3 and 24.0 MPa and angles of friction of 55° and 65° respectively. From these results we estimate that the ultra large core has a load- bearing capacity approximately twice the 17.8 MN maximum axial loading capability of the triaxial machine.

Size-Effect Studies

To extend understanding of the fundamental laws governing flow through fractures in crystalline rock, particularly with respect to flow through natural fractures and the influence of sample size on measured hydraulic properties, a research program using the ultra-large core test facility is planned to begin in 1980. This work will complement research on smaller cores currently under way at the University of Waterloo. During fiscal year 1979 a search for sources of suitable samples of naturally fractured rock was made jointly by LBL and the University of Waterloo. We identified several quarries containing suitable rock and equipped with the large-scale rock dressing and handling equipment necessary for recovery of ultra-large cores, in the Sierra Nevada foothills near Fresno, California, in the vicinity of St. Cloud, Minnesota, and at Lake Placid, New York (Gale, 1979). A massive block of granite at the Charcoal Black Quarry, Cold Spring, Minnesota, that contained a single well-defined natural fracture (see Figure 5) was selected to demonstrate the feasibility of sample recovery and preparation techniques. By the end

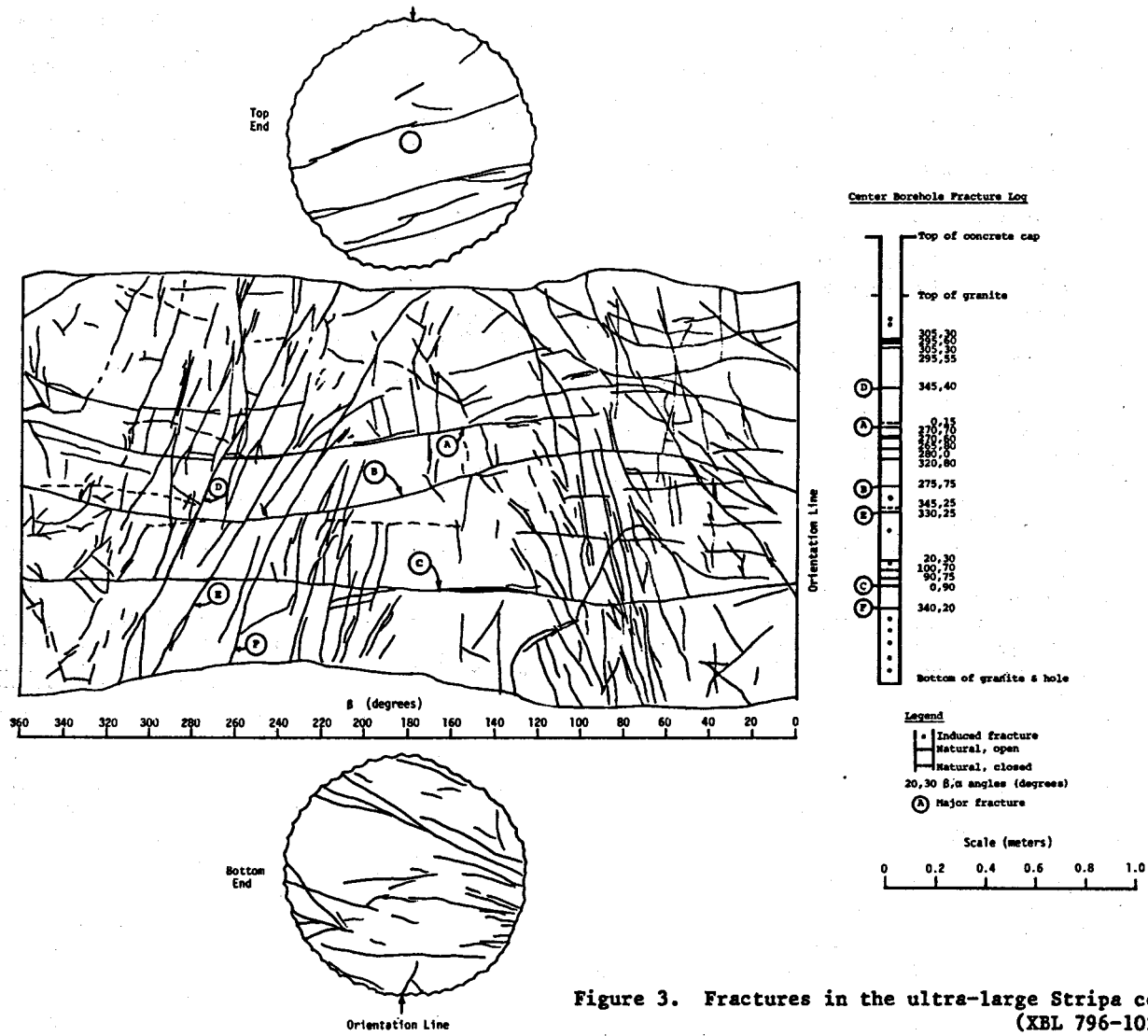

Figure 3. Fractures in the ultra-large Stripa core. (XBL 796-10210)

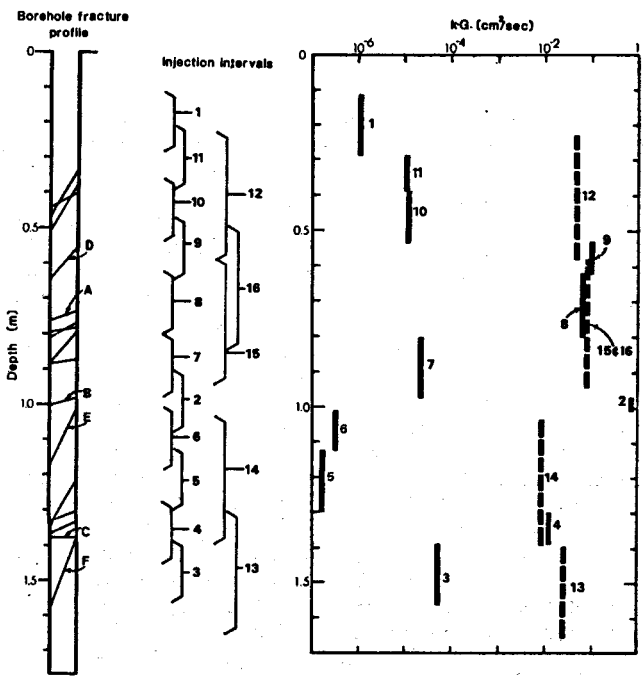

of fiscal year the granite block had been successfully moved from the quarry to the rock dressing plant where it will be formed into 0.91-m-diameter, 1.83-m-high cylindrical sample that is scheduled for delivery to the ultra-large core test facility at Richmond, California, in January 1980.

Figure 4. Relative conductivities--ultra large Stripa core. (XBL 801-7785)

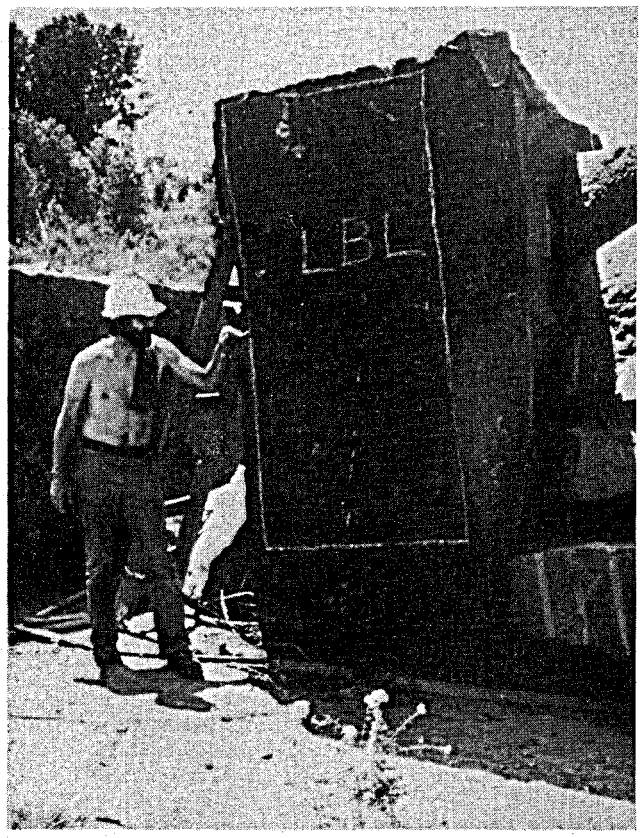

Figure 5. Fractured block of Charcoal Black granite. (CCB 798-10084)

REFERENCES CITED

Gale, J. E., 1979. Testing facilities for ultra-large rock cores: Task 1: identification of sites for sample gathering. University of Waterloo WRI 904-02.

Halén, P. A. and Andersson, B., 1978. Mining methods used in the underground tunnels and test rooms at Stripa. Berkeley, Lawrence Berkeley Laboratory, LBL-7081, SAC-08.

Witherspoon, P. A., Amick, C. H., Gale, J. E., 1977. Stress-flow behavior of a fault zone with fluid injection and withdrawal. Berkeley, University of California, Department of Materials Science and Mineral Engineering, Report No. 77-1, 159 p.

Witherspoon, P. A., and Degerman, O., 1978. Swedish-American Cooperative Program on Radioactive Waste Storage in Mined Caverns in Crystalline Rock. Berkeley, Lawrence Berkeley Laboratory, LBL-7049, SAC-01.

Witherspoon, P. A., Amick, C. H., Gale, J. E., and Iwai, K., 1979a. Observations of a potential size-effect in experimental determination of the hydraulic properties of fractures. Berkeley, Lawrence Berkeley Laboratory, LBL-8571, SAC-17.

Witherspoon, P. A., Wang, J. S. Y., Iwai, K., and Gale, J. E., 1979b. Validity of cubic law for fluid flow in a deformable rock fracture. Berkeley, Lawrence Berkeley Laboratory, LBL-9557.

Witherspoon, P. A., Watkins, D. J., Cook, N. G. W., Hood, M., and Gale, J. E., 1979c. Laboratory investigations on the hydraulic and thermo-mechanical properties of fractured crystalline rocks. Berkeley, Lawrence Berkeley Laboratory, LBL-9582.

$^{234}U/^{238}U$ DISEQUILIBRIUM STUDIES

M. C. Michel and W. R. Keyes

The disequilibrium between ^{234}U and ^{238}U observed in most ground waters can, in principle, serve as a clock to enable dating of the ground water reservoir (time since recharge) or, more appropriately, to indicate the rate of flow of the aquifer (Cherdynatev et al., 1955; Isabaev et al., 1960; Thorber, 1962; Cowart and Osmond, 1974.) This type of information is of interest in assessing the suitability of a particular site as a nuclear waste repository based on the assumption that a slowly moving (old) aquifer represents a lower probability that mobilized wastes will return to the environment. All this presupposes failure of all the other means to avoid such mobilization. Because the time for ^{234}U to reach secular equilibrium is the same order of magnitude (~250,000 years) as the criteria for waste isolation, the determination of $^{234}U/^{238}U$ disequilibrium gives a measurement of the proper interval.

The secular equilibrium between ^{234}U/ and ^{238}U established in most rocks and uranium deposits yields a mass ratio of 18,300. The ratio of alpha radioactivities is by definition equal to 1. Direct alpha particle counting is applicable to the study of the disequilibrium in uranium and almost all the work to date has been done in this way. Because deep groundwaters often have only a few parts per trillion of uranium, measurements by this method often require several tens of liters of sample, an amount difficult to recover from deep wells or drill holes, especially without serious contamination by other waters. It was, therefore, proposed that direct mass spectrometric measurement of this ratio be made. This is a technique that should allow measurements on samples of only a few tens of mililiters. This size sample can easily be obtained by the use of remote samplers presently in use or currently being designed.

The work in 1979 was related to the ability to recover meaningful data from such small samples of uranium without introducing either natural or other uranium contamination during the necessary chemical separation procedures. Sensitivity of the mass spectrometer itself is much greater than can be used with present levels of uranium background. Isotopic dilution analysis (using pure ^{233}U) has been used to determine the "blank" levels

of the chemical separations and the uranium content of various reagents and materials. Since, except for the ^{234}U isotope, the samples are indistinguishable from natural uranium, it is necessary to reduce blank levels well below the sample sizes to assure the integrity of the results. Fortunately, natural uranium contamination affects the ^{234}U abundance less as the observed enrichment increases, and since a precision of 1 or 2% is sufficient for this work, amounts of natural uranium below 1% of the sample size represents an acceptable level.

In dealing with very small amounts of materials in chemical separations, where there is the possibility of introduction of the same material from the environment, it is always desirable to minimize the number of chemical operations and reagents used. A very simple scheme has been developed for separation of uranium from groundwater. This involves treating the groundwater with HCl gas to produce about 4 M HCl followed by near saturation with sulfur dioxide gas (to reduce Fe^{3+} to Fe^{2+}). This solution is then passed through an ion exchange column packed with the chloride form of a quaternary amine, a strong base anion exchange resin. Under these conditions almost all of the major cations and non-ionic impurities pass through the column without holdup. Only uranium and a few other elements present in low abundance are sufficiently complexed in 4 M HCl to adsorb strongly. Washing with 4 M HCl followed by elution of the uranium (and a few other noninterfering trace elements) in 0.1 M HCl completes the separation. The sample is obtained in a small volume, which is further reduced by closed-system evaporation with flowing dry nitrogen. This sample is then transferred to the ion source and dried. At this point it is ready for mass analysis.

Mass analysis is performed in the 5-ft-radius mass spectrometer as the UO_2^+ ion, and using single ion counting techniques. Because of the high vacuum, the high ion energy (40 keV) and the large radius of this instrument, gas scattering from ^{238}U at the ^{234}U position can be reduced to the order of 1 ppm and only ionization of organic impurities of the appropriate mass can create a significant ion background. Proper sample conditioning can reduce this background to levels below 0.01 c/sec. Since it is possible to allow total ion count rates of several thousand per second at mass 238, signal-to-background ratios of 100:1 can be attained at mass 234 with total sample sizes of the order of 1 ng or less. In such samples the amounts of ^{234}U are equal to or less than 0.05 pg (10^8 atoms). During isotopic dilution analyses, quantities of individual isotopes have been identified at levels of 10^{-15} grams (3×10^6 atoms) with a precision of at least 10%.

Early in development of the $^{234}U/^{238}U$ technique, it was discovered that small amounts of natural uranium are found in almost all reagents and this could easily be reduced to acceptable levels. The ion exchange resin, however, in addition to small amounts of natural uranium, was found to contain uranium in a different chemical form enriched in ^{235}U (and containing an almost constant fraction of ^{234}U). This enrichment was not in constant proportion to the natural uranium but depends on the source of the resin. In addition, with the same resin, the relative amounts of the two types of uranium contamination introduced into blank runs depends on details of the operation of the column that are not readily understood. From the level of ^{234}U and the observation of occasional samples with unusually high levels of ^{235}U, it seems possible to conjecture that the uranium containing the ^{235}U is approximately of the composition of weapons grade uranium, which is produced in gaseous diffusion plants. This contamination may be introduced into the resin manufacturing process through recovery of slightly contaminated reagents or (less likely) through generalized contamination of a plant or process. The amounts are small enough that they represent no conceivable health or safety problem and, therefore, could easily have escaped detection.

Further work demonstrated that the ^{235}U enriched uranium is released from the resin only when a concentration gradient is passed down the column as is necessary when going from the concentration phase of the chemical separation to the elution phase. Washing the column with a constant concentration of the complexing anion (Cl^-) removes a much smaller (and not significant) amount of ^{235}U. It is possible to deplete the uranium reservoir to some extent (with some batches of resin this may be a slow process) and eventually reach small enough background contamination to permit the $^{234}U/^{238}U$ analyses to be performed. Because of the extremely simple chemical separation allowed by the ion exchange technique, alternative separation schemes have not been tested. This is because other approaches involve more steps, more sources of accidental contamination and, therefore, a more laborious program of blank monitoring.

It should be pointed out that the enriched $^{235}U/^{234}U$ mixture is particularly damaging because it not only increases the ^{234}U blank but also destroys the known $^{235}U/^{238}U$ ratio in the samples. This removes a very valuable internal standard with which to assure proper operation of the entire mass spectrometer and data collection system. Of course, since the $^{235}U/^{234}U$ ratio is easily determined for a particular column, corrections to the data can be made, but only with a loss in precision and this should be avoided.

We expect that further work will allow elimination of the source of non-natural background. If this can be accomplished, no other barrier to successful measurements of the uranium disequilibrium appears to remain. Because of the small sample size, $^{238}U/^{234}U$ ratios at very low total uranium concentrations can be measured, which is a necessary requirement for deep drill holes. In addition, because of the ability to examine small samples, we anticipate that the disequilibrium in uranium deposited in secondary minerals, especially in fracture-type aquifers in basically solid rock, can be investigated. These secondary minerals may contain information on the history of the disequilibrium in the groundwater. A laboratory simulation of the alpha-particle recoil enrichment of ^{234}U will also be attempted to determine the effect, on enrichment yield, of the chemical environment. This is a serious consideration since the decay proceeds by way of ^{234}Th with a half life of almost

a month and with entirely different chemistry than uranium.

REFERENCES CITED

Cowart, J. B., and Osmond, J. K., 1974. ^{234}U and ^{238}U in the Carrizo Sandstone Aquifer of South Texas. IAEA-SM-182/35.

Cherdyntsev, V. V., Chalov, P. I., and Khaidarov, G. Z., 1955. Transactions of the 3rd Session of the Committee for Determination of Absolute Ages of Geological Formations. Izv. Akad. Nauk., USSR, Moscow, 175.

Isabaev, E. A., Usatov, E. P., and Cherdynbtsev, V. V., 1960. Isotopic composition of uranium in natural samples. Soviet Radiochemistry, v. 2, p. 97.

Thurber, D. L., 1962. Anomalous $^{234}U/^{238}U$ in nature. Journal of Geophysical Research, v. 67, p. 4518.

SEARCH FOR UNDERGROUND OPENINGS FOR IN-SITU TEST FACILITIES IN CRYSTALLINE ROCK

H. A. Wollenberg, B. Strisower, D. J. Corrigan, A. N. Graf, and M. T. O'Brien

The literature on underground mines and civil works in the United States was surveyed in the first phase of a search for sites for in-situ test facilities in crystalline rock. Such sites would be utilized for geomechanical, geochemical, and hydrogeologic tests pertinent to the isolation of radioactive wastes in crystalline rock. For the purposes of this study, crystalline rocks were limited to plutonic rocks and medium- to high-grade metamorphic rocks.

Literature searches were done, primarily using the Minerals Availability System data base of the U.S. Bureau of Mines; to a lesser extent, the Computerized Resources Information Bank compiled by the U.S. Geological Survey; and GEOREF. From these sources and from consultants, a list of approximately 6100 mines and civil works in known rock types was compiled.

Criteria used to judge each site included workings:

- in crystalline rock
- at depths below 600 ft
- of adequate size to provide for a Stripa-sized facility
- open within the past 10 years and not flooded or caved
- below the water table, and
- with good rock support.

The selection process, diagrammed in the flow chart in Figure 1, resulted in the identification of 26 mines and 4 civil works (designated Class 1 sites), which met all the criteria. Thirty mines that probably meet the criteria (but could not be verified based on information in the open literature) were listed as Class 2 sites.

Potential underground workings range in size from a few thousand lineal feet, with the capacity to employ a few tens of miners, to several hundred miles, employing hundreds of miners. Depths range from near the threshold limit of 600 ft to over 8000 ft.

Names of all 60 of the Class 1 and Class 2 sites are listed in Table 1 and locations are shown on the accompanying map of the United States (Figure 2).

Class 1 mines or civil works in tectonically stable mid-continent or eastern regions of the United States include one in Maine, two in Minnesota, two in New Jersey, two in New York, and one in South Carolina. The remaining Class 1 sites are in the Rocky Mountain region and westward. Of the civil works, pumped storage facilities incorporating underground and appurtenant galleries may offer the best prospects for in-situ test facilities, because, even though they may be operating, access may still be available to test and support galleries.

Many of the workings in Class 1 mines are in hydrothermal vein deposits, at or near contacts between plutonic and older sedimentary, volcanic or metamorphic rocks. Test facilities at these sites would therefore be located relatively near the margins of crystalline rock masses. Notable exceptions are the Climax, Urad, and Henderson mines in Colorado, mines in the Butte district, Montana, the San Manuel-Kalamazoo in Arizona, and mines in the Duluth Gabbro, Minnesota. All of these ore bodies are located well within plutons.

Mines within medium- to high-grade metamorphic rock masses include the Homestake, South Dakota, the Schwartzwalder and Colorado School of Mines' experimental mine in the Colorado Front Range, the Mt. Hope/Scrub Oaks, New Jersey, and mines of the Lyon Mountain district, New York.

Structural settings of mining districts are dominated by the aforementioned contact zones, by strong folding and faulting in the case of mines in metamorphic rocks, and by zones of intersecting faults in mines in plutonic rocks. Because of their stability requirements, underground hydroelectric facilities in crystalline rocks are located in relatively stable tectonic settings, usually away from the contacts with other rock types. Accessible openings associated with hydroelectric facilities may offer rock property conditions most similar to rock properties of potential waste isolation sites.

A program was recommended which would definitively evaluate the available and accessible underground workings. This program would result in the identification of one or more sites where a concordance exists between rock type and struc-

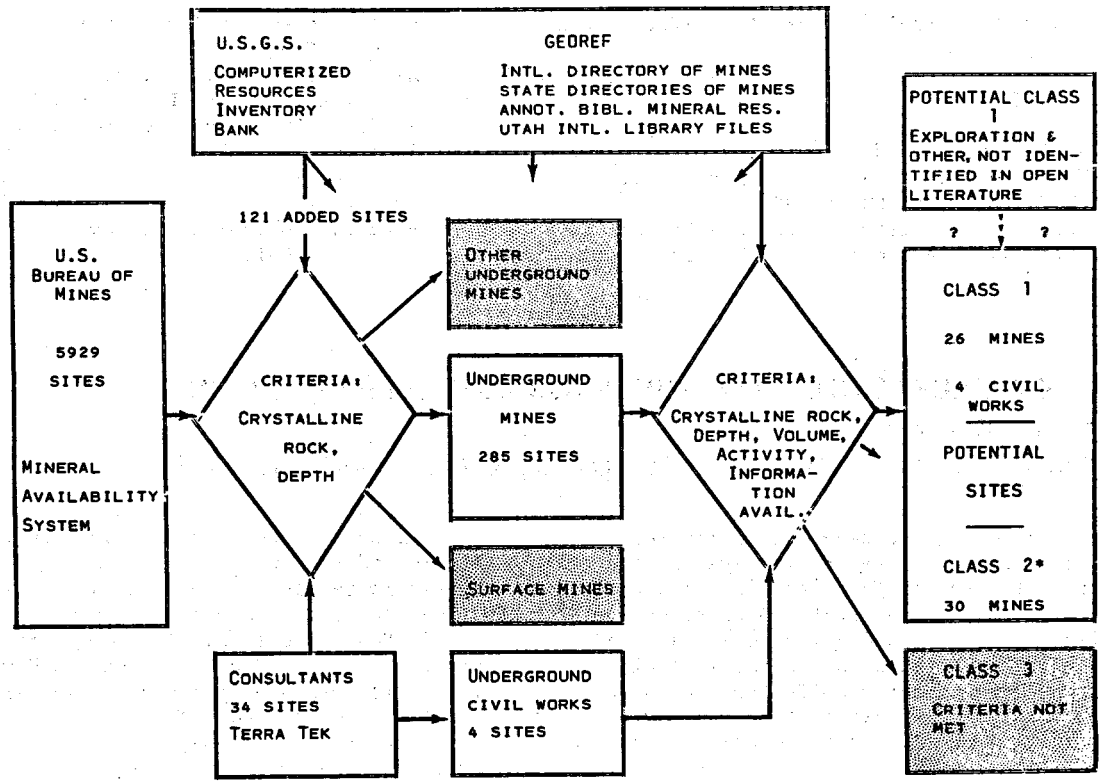

Figure 1. Identification and selection process for potential underground sites. * = all criteria met, some information not validated in the open literature. (XBL 806-10533)

Table 1. Locations of underground workings on map of the United States (Figure 2).

Class "1" Mines
Arizona
1. Lakeshore Mine
2. Miami East Mine
3. San Manuel/Kalamazoo Mine
California
4. Pine Creek Mine
Colorado
5. Climax Mine
6. Schwartzwalder Mine
7. Urad/Henderson Mine
8. Colorado School of Mines, Experimental Mine
Idaho
9. Lost Packer Mine
Coeur D'Alene District
10. Dayrock Mine
11. Star-Morning Mine
12. Coeur Mine
Maine
13. Black Hawk (Second Pond)-Blue Hill Mine
Minnesota
14. Minnamax Project, Ely Prospect
Montana
15. Black Pine Mine
Butte Mining District and Butte Underground Mines
16. Leonard Mine
17. Steward Mine
18. Granite-Bimetallic Mine
Nevada
19. Tem Piute District
New Jersey
20. Mount Hope and Scrub Oaks Mines
New Mexico
21. Questa Molybdenum Mine
New York
22. Balmat-Edwards District Mines
23. Lyon Mountain District
South Dakota
24. Homestake Mine
Washington
25. Holden Mine
Wyoming
26. Sunrise Mine

Class "2" Mines
Arizona
27. Bagdad Mine
28. Oracle Ridge
California
29. Atolia District
Colorado
30. Black Cloud Mine
Idaho
31. Kentuck Mine
32. Silver City Region
Michigan
33. Indiana Mine
34. Iroquois Mine
Minnesota
35. Ely Prospect
Montana
36. Butte Highlands Mine
37. Dacotah Mine
Nevada
38. Gooseberry Mine
39. Mill City Mine
40. Ruby Hill Mine
41. Searchlight District
42. Summit King Mine
43. Sutton No. 2 Mine
44. Taylor Mine
New Jersey
45. Sterling Mine
New Mexico
46. Continental Underground
47. Groundhog Mine
North Carolina
48. Cranberry Magnetite
49. Tungsten Queen Mine
Tennessee
50. Ducktown District
Utah
51. Ontario Mine
52. Mayflower Mine
53. Park City Mine
Washington
54. Midnite Mine
55. Sherwood Mine
56. Sunrise Breccia Deposit

Civil Works
California
57. Helms Underground Powerhouse Pumped Storage Project
Idaho
58. Dworshak Dam Site
Nevada
59. Nevada Test Site-Climax Stock
South Carolina
60. Bad Creek Pumped Storage Project

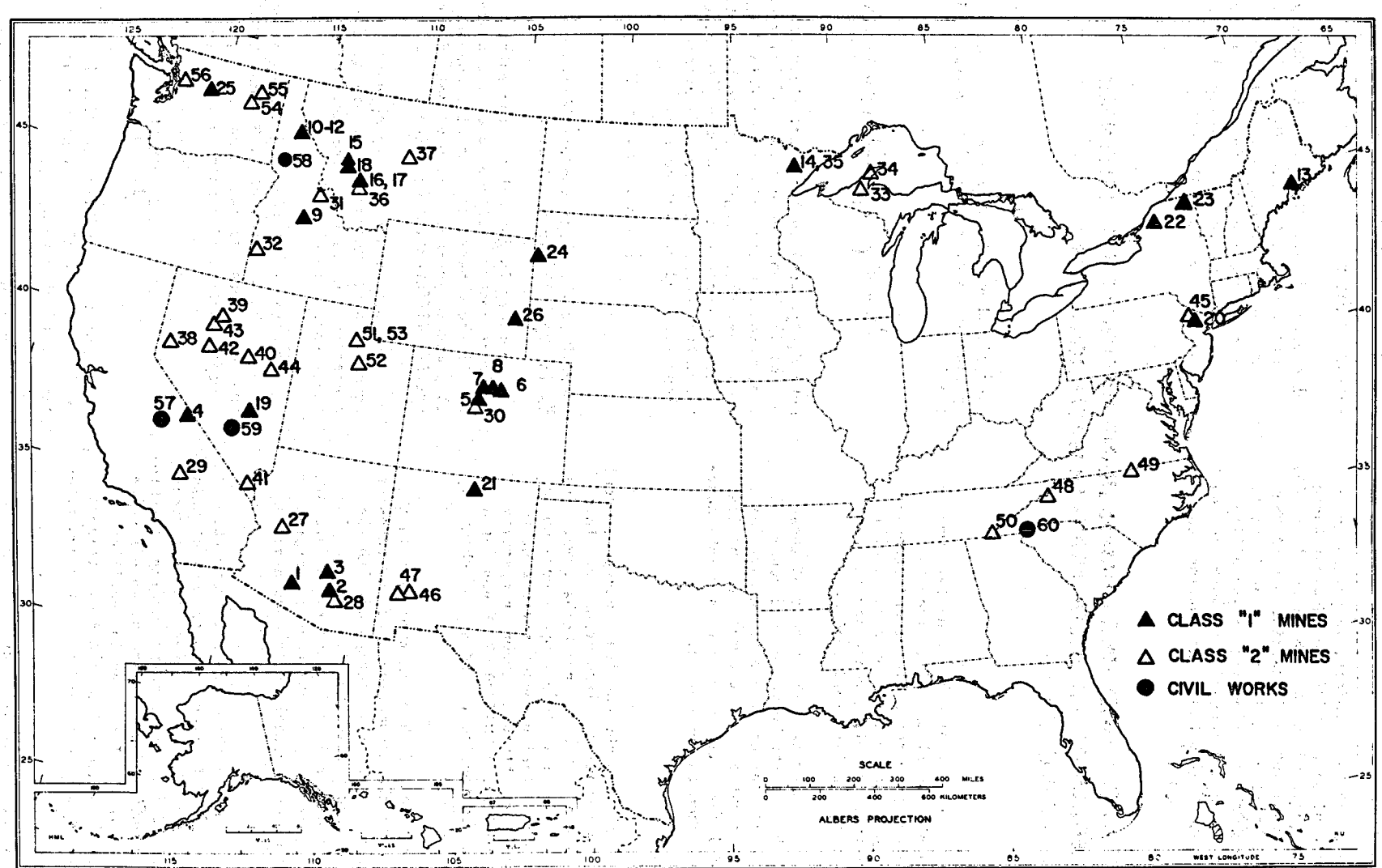

Figure 2. Map showing the locations of Class 1 mines, Class 2 mines, and civil works identified in this study. (XBL 802-7992)

tural setting and depth, company amenability, accessibility, facilities, and hydrogeologic setting.

The results of this project, supported by the U.S. Department of Energy Office of Nuclear Waste Isolation, are reported by Wollenberg et al. (1980). The report includes detailed descriptions of the 26 mines and 4 civil works designated as Class 1. Information includes location and accessibility, geologic setting, and description of workings and facilities. Tables give known information and indicate the missing data for Class 2 mines. A bibliography lists the 945 references consulted during the course of the study.

REFERENCE CITED

Wollenberg, H. A., Strisower, B., Corrigan, D. J., Graf, A. M., O'Brien, M. T., Pratt, H., Board, M., and Hustrulid, W., 1980. Search for underground openings for in-situ test facilties in crystalline rock. Berkeley, Lawrence Berkeley Laboratory, LBID-077, 469 p.

THERMOCHEMICAL MODELING OF MASS TRANSPORT PROCESSES IN THE NEAR-CANISTER REGION OF A BASALTIC NUCLEAR WASTE REPOSITORY

L. V. Benson and P. C. Lichtner

INTRODUCTION

The emplacement of high-level nuclear wastes (HLW) in a basalt repository will alter the chemical physical properties of the underground environment. Changes in these properties will induce a variety of chemical reactions in both the near-canister and far-field regions.

In order to understand the effect of these reactions on the redistribution of radiochemical species in the natural environment, we have initiated the development of a multicomponent chemical transport model that will be used to simulate near-canister thermochemical processes.

MODEL DEVELOPMENT

In its final form the chemical transport model will include complexation, dissolution, precipitation, and sorption (ion exchange) mechanisms. Its range of validity will include temperatures up to 100°C and aqueous solution concentrations up to a few molal. Heat and fluid transport properties will be simulated using SHAFT79 (K. Pruess et al., LBL) which will be coupled to the set of chemical reaction calculations.

The description of chemical processes in the model is based on the assumption that the rates of chemical reactions are "fast" compared with the advective or diffusive flow rates. This enables the use of chemical equilibrium theory to determine the local concentrations of the various chemical species in terms of a conveniently chosen set of basis species.

According to this theory reaction product concentrations are determined from the law of mass action as products of basis species concentrations raised to the power of their corresponding stoichiometric coefficients and multiplied by an effective equilibrium constant. The effective equilibrium constants depend in general on the local temperature, pressure, and concentrations of the constituent elements.

The transport equations describing the time evolution of the basis component concentrations, $c_j(\vec{r},t)$, then follow from mass balance relations applied to an elemental fluid volume and are of the form

$$\left\{\hat{L} - \frac{\partial}{\partial t}\right\} F_j = \frac{\partial S_j}{\partial t} \quad (j = 1,\ldots N) \tag{1}$$

Here $F_j(c_1\ldots c_N)$ is the total fluid concentration of the jth component composed of its free ion concentration $c_j(r,t)$ and that contained in fluid complexes; $S_j(c_1\ldots c_N)$ is the total sorbed and precipitated concentration of the jth component, and the differential operator $\hat{L}$ describes diffusive/dispersive and convective flow

$$\hat{L} = \nabla \cdot D\nabla - \nabla \cdot \vec{v}_o \quad , \tag{2}$$

where D is the diffusion/dispersion coefficient and $\vec{v}_o$ is the bulk fluid velocity.

Because in general the concentration of one basis component will depend on the concentrations of all the others, the set of transport equations (1), are in general a coupled set of nonlinear partial differential equations.

To solve equations (1) appropriate boundary conditions are necessary specifying the initial concentrations of each component in the fluid and their source terms.

The total adsorbed and precipitated concentration of the jth component, S_j, may be eliminated from equations (1) by noting that S_j is proportional to the total fluid concentration, F_j

$$S_j = K_j F_j \quad . \tag{3}$$

The quantity K_j, called the distribution coefficient, is in general a nonlinear function of the fluid concentrations, c_j.

Use of definition (3) for the distribution coefficient allows the transport equations (1),

to be written in the form

$$\left\{\hat{L} - (1 + K_j)\frac{\partial}{\partial t}\right\} F_j = \frac{\partial K_j}{\partial t} F_j \quad . \tag{4}$$

From this result it follows that whenever the distribution coefficient may be approximated by a constant, there is no coupling between different components and each component moves independently from the others governed by the retarded flow operator, $\hat{L}_{jret}$, given by

$$\hat{L}_{jret} = \nabla \cdot D_{jret} \nabla - \nabla \cdot \vec{v}_{jret} \tag{5a}$$

where

$$D_{jret} = \frac{D}{1 + K_j} \tag{5b}$$

and

$$\vec{v}_{jret} = \frac{\vec{v}_o}{1 + K_j} \tag{5c}$$

This approximation is called the retarded flow approximation.

In general, however, neither will the distribution coefficient be constant nor will its time derivative appearing in equation (4) be necessarily small. In this case, the retarded flow approximation will no longer be valid and the time evolution of the basis components may be significantly altered.

The major objectives of the initial part of the project were to derive the chemical transport equations including a sorption algorithm.

In addition a simplified two-component sorption model (TCSM) was studied to investigate the effects of competition for sorption sites. Finally the limiting form of the transport equations for trace concentrations was investigated and was shown to reduce to the retarded flow approximation with distribution coefficients whose forms are a function of the valence of the particular ion under consideration. Future work will concentrate on developing a computer code to solve the transport equations under conditions appropriate to HLW storage in underground repositories. It is expected that a considerable effort will be devoted to verification of the chemical transport model by comparing results with various laboratory experiments. Of special interest will be the modeling and design of engineered barrier systems that can be used to retard the migration of radionuclides species.

THEORETICAL AND EXPERIMENTAL EVALUATION OF WASTE TRANSPORT IN SELECTED ROCKS

R. J. Silva, L. V. Benson, A. W. Yee, and G. A. Parks

INTRODUCTION

The licensing procedure for the storage of nuclear waste in underground geologic media will involve a safety assessment of the proposed site. Since the time scale being considered is 100,000 to 1,000,000, predictions based on realistic modeling studies provide the main avenue of assessment. Modeling studies are only as reliable as the data on which they are based. For the prediction of radionuclide migration in geologic media, it is essential that the systems involved be well understood.

The objective of the program is to develop quantitative data and methods to describe the interactions that control the transport of radionuclides in geologic environments anticipated for terminal radioactive waste storage facilities. The program covers a theoretical and experimental evaluation of the physical and chemical processes governing sorption phenomena, with the goal of establishing a basis on which distribution coefficients might be reliably predicted for any given radionuclide with a variety of geologic materials and groundwater types.

The first year of this program, fiscal 1977, was devoted to a review of the literature on the thermodynamic data for aqueous complexes and solid phases of Pu, Np, Am, and Cm likely to form in the natural environment and on the transport mechanisms of radionuclides in water-saturated rocks. An assessment of factors influencing the radionuclide-rock interactions for conditions expected in a terminal storage facility was made (Apps et al., 1978).

During fiscal year 1978, a theoretical and experimental program was developed with the purpose of identifying the most important parameters governing the transport of five actinides (U, Np, Pu, Am, and Cm) in the three rock types: Umtanum basalt (Hanford), Eleana shale (NTS), and Climax quartz monzonite (NTS). The work demonstrated that the behavior of the actinides in groundwater and their sorption on rocks was dependent on the oxidation state of the actinide and on the solubility of stable precipitates such as oxides, hydroxides, and carbonates. Furthermore, it was determined that secondary alteration phases such as clays and zeolites appeared to sorb actinides preferentially over other rock-forming minerals such as silica and feldspars (Silva et al., 1978).

THIS YEAR'S ACTIVITIES

In fiscal year 1979, experimental and theoretical efforts were concentrated on a study of the sorption of cesium on the substrates quartz (Min-u-sil) and montmorillonite (Belle Fourche clay)--two representative geologic materials that

*Stanford University

are widely distributed and frequently coat weathered surfaces. This study was undertaken in order to begin to delineate the principle parameters in sorption processes. Cesium was chosen for these beginning studies because it exhibits rather simple chemical behavior under most solution conditions.

The experimental effort was aimed at:

1. A characterization of the solid phases which included determinations of chemical compositions, particle size distributions, surface areas and cation-exchange capacities.

2. A determination of the surface acid dissociation and electrolyte binding constants of the solid phases from the results of acid/base titrations of their aqueous sols.

3. The measurement of Cs sorption isotherms on the two substrates at 26°C over a wide range of Cs concentrations, pH, and concentration of supporting electrolyte from batch-type experiments using finely crushed materials. Sodium chloride was selected as the supporting electrolyte because of the current interest in salt domes as a waste repository. In addition, one mixed electrolyte of a composition similar to the groundwaters from Columbia River basalts was selected to simulate a natural system. It had an ionic strength of about 0.003 m.

   Cesium sorption isotherms using the sodium form of the Belle Fourche clay and Min-u-sil were obtained for initial Cs concentrations of 10^{-3}, 10^{-5}, 10^{-7}, and 10^{-9} m for the clay and 10^{-4}, 10^{-5}, 10^{-6}, 10^{-7}, 10^{-8}, and 10^{-9} m for the quartz; pH values were 5, 6, 7, 8, 9, and 10; electrolyte solutions were 0.002, 0.01, 0.1, and 1 m NaCl, and in the simulated basalt groundwater the starting Cs solutions were "spiked" with ^{137}Cs tracer and Cs concentrations in solution before and after sorption determined by γ-ray counting the solutions.

Because the concentration (and radioactivity) of the influent Cs solutions had previously been measured, the determinations of the ^{137}Cs radioactivities (and thus total Cs concentrations) in the effluent solutions allowed the calculation of K_d's.

$$K_d = \frac{1-f}{f} \cdot \frac{v}{w}$$

$$= \frac{\text{Concentration of Cs per gram of Solid}}{\text{Concentration of Cs per milliliter of Solution}}$$

where

f = fraction of influent Cs remaining in solution
v = volume of solution (ml)
w = weight of clay or quartz (g).

As examples, results for the Belle Fourche clay and Min-u-sil are presented in Figures 1 and 2. They show the variation of K_d with Cs loading of

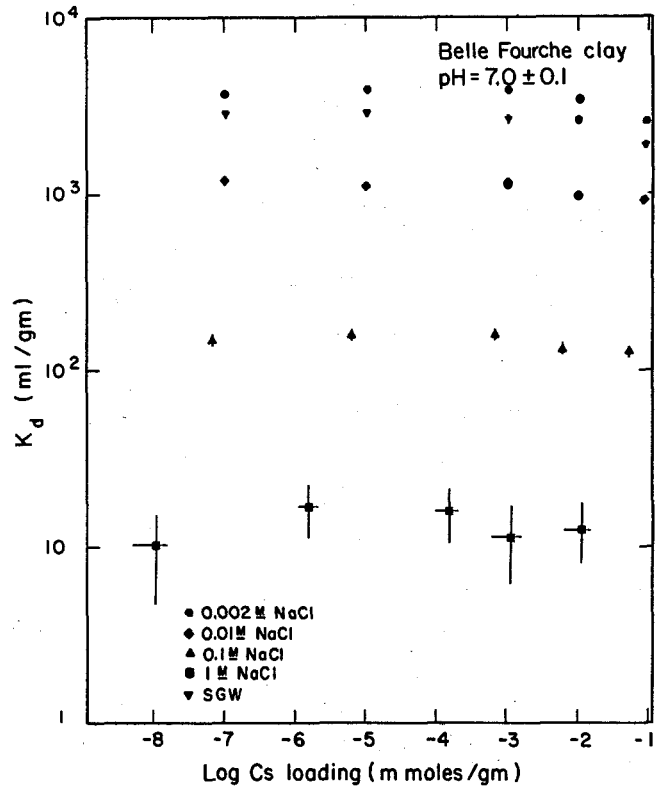

Figure 1. Distribution coefficients, K_d, for Cs measured at 26°C on the Na form for the Belle Fourche clay as a function of Cs loading at pH 7 for several electrolyte compositions. SGW = simulated basalt groundwater. (XBL 799-11576)

the solid substrate and electrolyte concentration at pH = 7.

The equation for the exchange of the monovalent cations Cs^+ and Na^+ between the solid surface, s, and the aqueous solution, a, may be written as (Helfferich, 1962)

$$SO^-Na^+_s + Cs^+_a \rightleftarrows SO^-Cs^+_s + Na^+_a$$

where SO^- represents the surface sorption sites. The mass action expression for the thermodynamic equilibrium constant is

$$K_{Cs/Na} = \frac{[SO^-CS^+]_s[Na^+]_a}{[SO^-Na^+]_s[Cs^+]_a} \cdot \frac{\gamma_{Na^+}\gamma_{SO^-}\gamma_{Cs^+}}{\gamma_{Cs^+}\gamma_{SO^-Na^+}}$$

where the first term is expressed in concentrations of ions on the surface and in the solution phases and the second term contains the corresponding activity coefficients. The latter equation can be written as

$$K_{Cs/Na} = K_d \cdot \frac{[Na^+]_a}{[SO^-Na^+]_s} \cdot \Gamma$$

where Γ is the quotient of the activity coefficients. If Cs is present on the absorber at trace

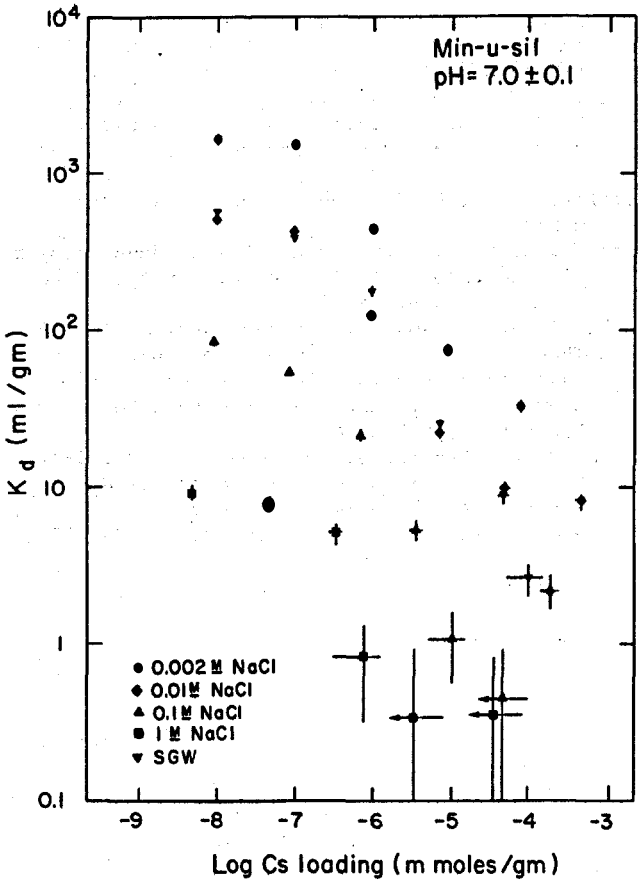

Figure 2. Distribution coefficients, K_d, for Cs measured at 26°C on Min-u-sil as a function of Cs loading at pH 7 for several electrolyte compositions. SGW = simulated basalt groundwater. (XBL 799-11584)

loadings, i.e., at only a few percent of the capacity, then $[SO^-Na^+]_s$ remains nearly constant and is equal to the cation exchange capacity. Assuming $K_{Cs/Na}/\Gamma$ to be a constant, K_d should vary only with $[Na^+]_a$ and not with pH or Cs loading.

For the Belle Fourche clay, the measured K_d values showed only a small dependence on pH and Cs loading but a large, inverse dependence on electrolyte concentration as expected from the simple mass action expression of the exchange of Cs for Na. However, for the Min-u-sil, the K_d values showed a large dependence on all three parameters that could not be explained by the simples expression. For both substrates, the variation of K_d with pH indicated that the competition of H^+ for surface site occupancy should also be included. The K_d values for the synthetic groundwater were similar to those of the NaCl solutions of nearly the same ionic strength, i.e., 0.002 m NaCl, for the clay but were more nearly like the values of the 0.01 m NaCl solutions for the Min-u-sil.

The theoretical efforts were aimed at developing and testing an advanced sorption model (Yates, 1974; Silva, 1978) to predict k_d values. This model is reasonably complete in that physical and chemical interactions are considered simultaneously in the calculation of surface sorption and solution chemical equilibria for major electrolyte ions and dilute solutes. The model can also include the effects of the development of surface charge on the surface sorption reactions, i.e., the effects due to the development of an electrical double layer (Grahame, 1947). The model requires a knowledge of the thermodynamic constants of the surface reactions as well as those governing the solubilities and complexation of the solution species. A computerized version of the model, called MINEQL, was brought to operational status at LBL. MINEQL is designed to accept a list of components of a solution and solid phase and their total analytical concentrations, solve the appropriate set of mass balance and equilibrium expressions, and produce a list of the identities and concentrations of all species formed by the interaction among the components and between them and/or water, e.g., precipitates, complexes and sorbed species.

Input parameters required by MINEQL were determined and sorption isotherms for Cs on the Belle Fourche clay were calculated over the same range of parameters as the experimental measurements. As an example, the results of the calculations are shown in Figure 3 (curves) along with the experimental values (points) for an initial Cs solution

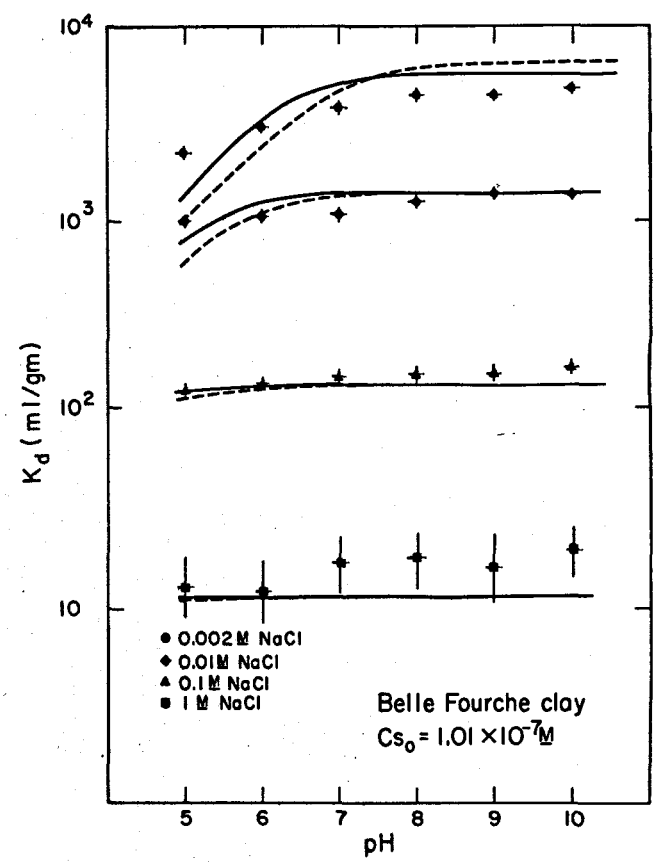

Figure 3. Variation of distribution coefficients for Cs with pH for an initial Cs solution concentration of 1.01 x 10^{-7} m for several NaCl electrolyte concentrations. Solid points represent the experimental data. Solid and dashed curves result from calculations using MINEQL without and with the inclusion of electrical double layer effects, respectively. (XBL 7911-113448A)

concentration of 1.01×10^{-7} m. Figure 3 shows the variation of K_d with pH for the different NaCl electrolyte concentrations. The solid curves were calculated without the inclusion of the electrical double layer effects; the dashed curves results when they are included. Where the solid and dashed curves coincide, only the solid curve is shown. Further comparisons of the calculations with the Belle Fourche clay experimental data demonstrated that MINEQL was able to simulate the Cs sorption isotherms for the clay reasonably well over the range of parameters studied. The results were quite encouraging and further testing of the model with other substrates and radionuclides is in progress.

REFERENCES CITED

Apps, J. A., Lucas, J., Mathur, A. K., and Tsao, L., 1978. Theoretical and experimental evaluation of waste transport in selected rocks: 1977 Annual Report. Berkeley, Lawrence Berkeley Laboratory, LBL-7022.

Davis, J. A., James, R. O., and Leckie, J. O., 1978. Surface ionization and complexation of the oxide water interface. J. Colloidal Interface Sci., v. 3, p. 480-499.

Helfferich, F., 1962. Ion exchange. New York, McGraw-Hill.

Grahame, D. C., 1947. The electrical double layer and the theory of electrocapillarity. Chem. Rev., v. 41, p. 441-501.

Silva, R. J., Benson, L. V., and Apps, J. A., 1978. Theoretical and experimental evaluation of waste transport in selected rocks: 1978 Annual Report. Berkeley, Lawrence Berkeley Laboratory, LBL-8094.

Yates, D. E., Levine, S., and Healy, T. W., 1974. Site binding model of the electrical double layer at the oxide/water interface. J. Chem. Soc. Faraday Trans. I., v. 170, p. 1897-1818.

MARINE SCIENCES

The Marine Science Group is a multi-disciplinary unit in the Earth Sciences Division responsible for research and development of programs whose basic sphere of reference is the oceans. Four marine-oriented disciplines are represented in the training and experience of the staff:

Applied Oceanography (Ocean Engineering)
Biological Oceanography
Chemical Oceanography
Geological Oceanography

The knowledge of the staff is reinforced by a science advisory council of internationally recognized experts in the various oceanographic disciplines. Funding is provided by the Ocean Systems Branch, Division of Central Solar Technology, U.S. Department of Energy.

The Marine Science Group was formally incorporated into the Earth Science Division in 1979 as an outgrowth of LBL's Ocean Thermal Energy Conversion (OTEC) Program. The major research activity of the group is still related to the environmental assessment and measurement program for OTEC. Other activities include compiling marine geologic and other oceanographic data for the west coast of the United States. The series consists of six map sheets each covering 3° of latitude with references; the northern five sheets have been printed. The Marine Science Group also is working on the potential for petroleum accumulation in the deep sea off central California as a cooperative effort with the U.S. Geological Survey.

Ocean Thermal Energy Conversion

ENVIRONMENTAL AND RESOURCE ASSESSMENT PROGRAM FOR OCEAN THERMAL ENERGY CONVERSION

P. Wilde

INTRODUCTION

Ecologically sound operations of projected Ocean Thermal Energy Conversion (OTEC) plants can be insured by careful attention to the marine environment during the design phase. This requires quality information from regions of potential OTEC interest, coordinated with required assessment studies to insure legal compliance. Currently, preliminary or actual surveys and laboratory studies are being conducted in the waters of Puerto Rico, the Gulf of Mexico, Hawaii, and Guam for potential moored or seacoast OTEC plants and in the equatorial South Atlantic for proposed plant-ship operations to provide such benchmark and baseline data. These data plus existing archival information can be used to model effects of OTEC operations based on projected design schemes. Four major areas of concern are: (1) redistribution of oceanic properties, (2) chemical pollution, (3) structural effects, and (4) legal and socioeconomic effects. Eleven key issues associated with OTEC deployment have been identified. In general, mitigating strategies can be used to alleviate many deleterious environmental effects of operational problems as biostimulation and outgassing. Various assessment research studies on toxicity, biocide releases, and other hazards are under way or planned to investigate areas where no clear mitigating strategy is available. Data from the monitoring and assessment programs are being integrated into a series of environmental compliance documents including a comprehensive programmatic environmental impact assessment.

ENVIRONMENTAL CONCERNS

The four major classes of environmental concerns and the key issues in these classes associated with OTEC deployment and operations are:

1. Redistribution of oceanic properties (ocean water mixing, impingement/entrainment, climatic/thermal)

2. Chemical pollution (biocides, working fluid leaks, corrosion)

3. Structural effects (artifical reef, nesting/migration)

4. Legal and socioeconomic effects (worker safety, enviro-maritime law, secondary economic impacts)

PRESENT PROGRAM

Monitoring

The monitoring strategies are designed for shipboard operations, manned platforms, and instrumented buoys. This program is to be integrated with those proposed by OTEC groups for bio-fouling and corrosion, and by NOAA for synoptic oceanographic parameters. An additional goal is to develop a packaged monitoring program which can be mobilized rapidly to aid in site selection for larger OTEC platforms (Figure 1). Data collection and monitoring strategies will be done in view of compliance with NEPA and EPA, Corps of Engineers, and Coast Guard regulations.

Specifically, the program initiated preoperational studies in four areas (Figure 2):

1. Hawaii--one site off the Kona coast (OTEC-1 site)
2. Puerto Rico--one site near Punta Tuna
3. Gulf of Mexico--regional survey using two station locations: west of Tampa; and south of Biloxi
4. South Atlantic--regional survey, 5 to 10°S, 20 to 30°W, and affected zone

In the areas considered for the sea coast or moored OTEC option--Hawaii, Gulf of Mexico, and Puerto Rico--a program has been initiated to take background data before placement of any operating OTEC system in these areas. This is required to insure that baseline information is available to evaluate the effects of OTEC on the ambient environment and to provide environmental data useful in the design of the operating system. At this time, only attractive thermal regions are known with any certainty. It is premature, therefore, to pick exact sites for potential OTEC plants until knowledge of other important environmental siting factors is obtained. Accordingly, for the initial studies each thermal region is divided into subregions in which it is expected that the basic environmental conditions relating to OTEC are spatially homogeneous, although likely to vary seasonally.

To characterize each subregion, a reconnaissance benchmark is located. A benchmark is defined as a specific location, typical of a subregion, where serial data are taken and to which historical data may be referred. Because of the lack of serial, long-term records of any kind in attractive thermal regions, we believe that the benchmark approach is more valuable in the long term than initiating broad regional surveys where variations in measurements may be attributed to site as well as time variability. Where substantial subregional variability is found, the benchmarks will be used as starting points for potential regional surveys.

The intent of taking measurements at benchmarks is to provide data at a specific location, which will form the basis, in conjunction with previously obtained data from the area, for defining longer

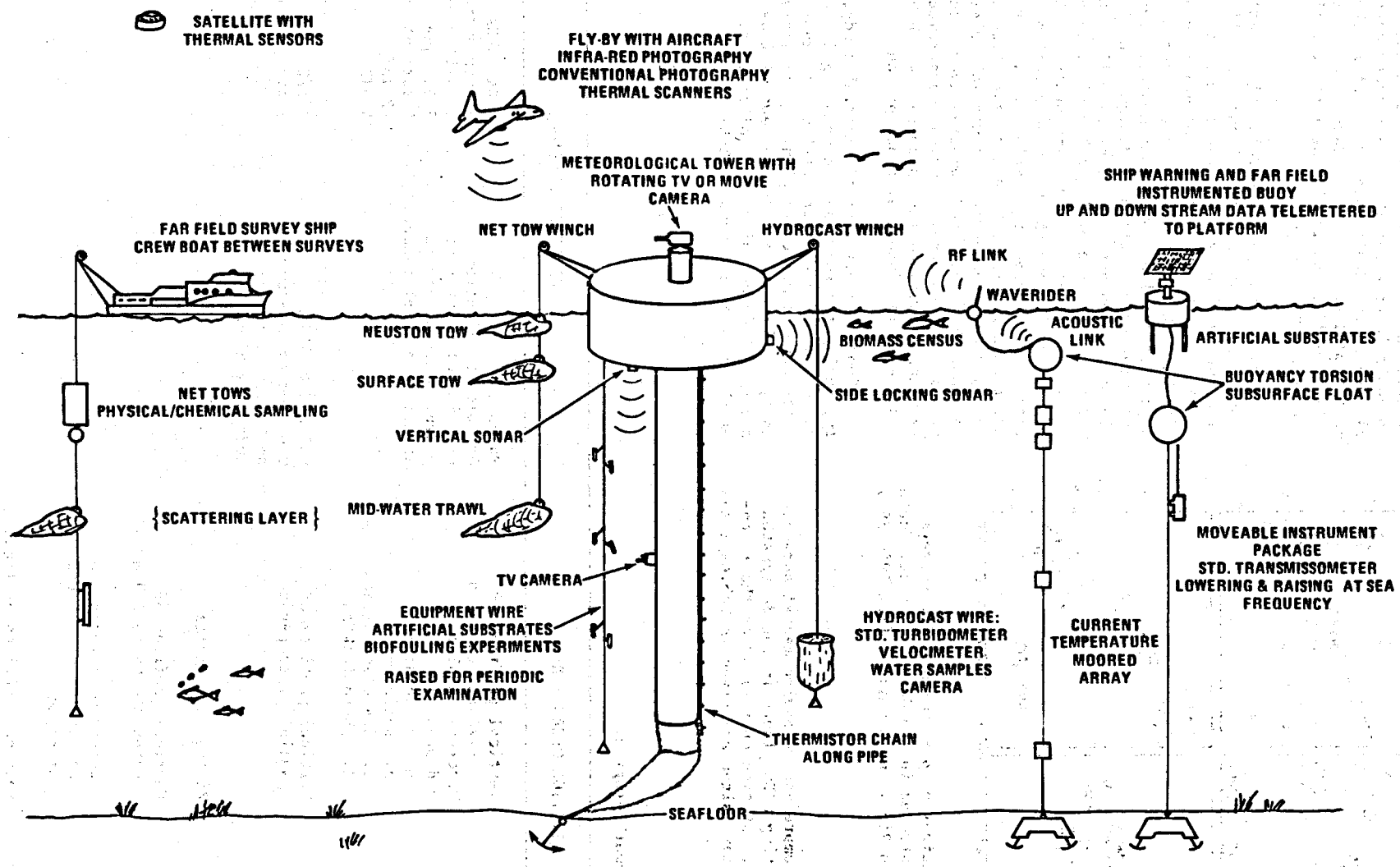

Figure 1. Schematic of OTEC environmental monitoring station. (XBL 804-9189)

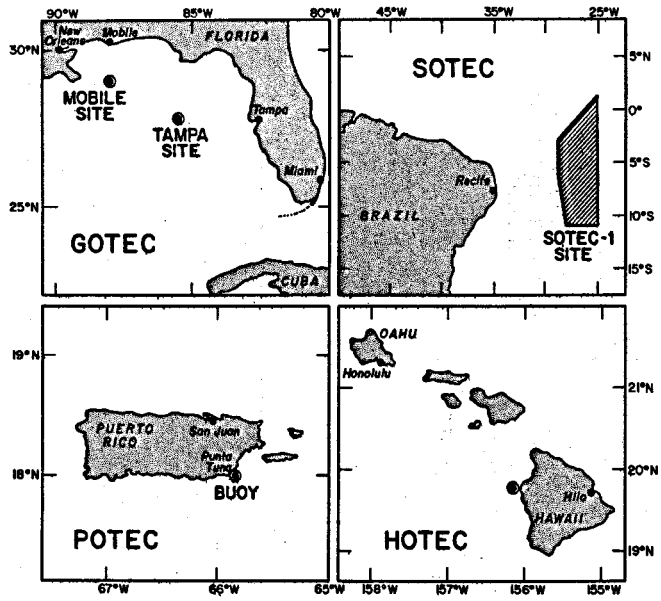

Figure 2. Locations of preliminary OTEC surveys and laboratory studies in the Gulf of Mexico, South Atlantic, Puerto Rico, and Hawaii. (XBL 795-1393)

term and more comprehensive environmental surveys required for siting OTEC plants in the designated thermal regions. Station operations at the reconnaissance benchmark sites are given in Tables 1 and 2. In addition to this station operation at each benchmark, a current profiler runs during station operations, except in Hawaii due to the loss of the Holoholo in December 1978. A current meter array is planned at the Hawaii benchmark before the deployment of OTEC-1. Satellite data, when available, will be used to assist in the interpretation of data from the arrays.

Because of costs and reliability factors, measurements for the initial surveys will be mainly from survey ships rather than from instrumented buoys. The survey ship will occupy each benchmark site bi-monthly for a minimum of three days with augmented sampling every four months. Sampling at each station occupation is designed to give, at a minimum, day-night variations as well as bi-monthly variations for the biologically significant parameters. Parameters sampled bi-monthly are thought to have variations which may be detected at that frequency. Parameters sampled every four months are thought: (1) to have less variation annually, or (2) to have potential but unresolved significance to OTEC. The augmented sampling every four months also is done to develop optimal measurement and sampling techniques for parameters which become routine during future site occupations.

Upon completion of the initial study, (actually, during the surveys) the sampling frequencies and choice of parameters will be re-examined. Results from augmented samplings, from serial samplings, and historical data reviews will be used to design subsequent site data collections. Status of these sites is shown in Table 3.

Table 1. Benchmark program.

STATION OPERATION		CLASS OF STATIONS	
Profiler	Vertical profiles of horizontal currents	PRIMARY Occupied in locations of prime OTEC interest -sampling frequency to ascertain diurnal changes	3-DAY DURATION 2 deep hydrocasts 2 shallow hydrocasts 2 oblique net tows 4 current profilers 12 XBT 4 STD
Hydrocast	Discrete samples at depth of: a. temperature b. salinity c. dissolved oxygen d. phytoplankton		
STD	Vertical profiles of salinity, temperature	CURRENT PROFILER Occupied to determine spatial variability of current regime	2/1/2 HOUR DURATION 1 current profile
Net tows	Biological samples		
XBT	Vertical profiles of temperatures to 750 m		
Current meter arrays	Discrete measurements of horizontal water currents at depth		
Transmissometer	Vertical profiles of light transmittance		

Table 2. Ecological/chemical parameters.

Parameter	Station operation	Station frequency	Sampling frequency
Temperature	Hydrocast	Bi-monthly	All hydrocasts
Temperature	STD, XBT	Bi-monthly	4 STD, 12 XBT
Salinity	Hydrocast	Bi-monthly	all hydrocasts
Salinity	STD	Bi-monthly	2 STD
Water Currents	Current meter	Continuous	One/30 min
	Profiler	Bi-monthly	4 casts
Light transmittance	Transmissometer	Bi-monthly	2 traces/cruise
Dissolved oxygen	Hydrocast	Bi-monthly	2 casts
Orthophosphate	Hydrocast	Bi-monthly	2 casts
Total phosphate	Hydrocast	Every 4 months	2 casts
Silicate	Hydrocast	Bi-monthly	2 casts
Nitrate	Hydrocast	Bi-monthly	2 casts
Ammonia	Hydrocast	Every 4 months	2 casts
Urea	Hydrocast	Every 4 months	2 casts
Total nitrogen	Hydrocast	Every 4 months	2 casts
Alkalinity	Hydrocast	Yearly	2 casts
Trace metals	Hydrocast	Yearly	1 cast
Chlorophyll/phaeophytin	Hydrocast	Bi-monthly	2 shallow casts
ATP	Hydrocast	Every 4 months	2 shallow casts
Phytoplankton census	Hydrocast	Bi-monthly	1 shallow cast
^{14}C uptake	Hydrocast	Every 4 months	1 cast
POC	Hydrocast	Yearly	1 cast
DOC	Hydrocast	Yearly	1 cast
Zooplankton census	Net tow	Bi-monthly	6 tows

Table 3. OTEC number of visits/site (July 1977 - January 1980).

	Measurements		
Site/region	Physical	Chemical	Biological
Mobile	8	8	6
Tampa	5	5	5
South Atlantic	3	3	3
Puerto Rico	6	6	6
Hawaii	6	6	6

Assessment

Complementary to the monitoring program are a series of studies to ascertain those effects of potential OTEC operations that are not site-dependent but are generic to OTEC. Also included in such studies are the legal compliance activities (Sands et al., 1979) and model studies. Initial studies on toxicity to organisms of various OTEC operations are under way at the Gulf Coast Research Laboratory. The toxicities of aluminum (heat exchanger material), ammonia (working fluid), and chlorine (biocide) are being investigated by bioassays of mullet (fish) and copepods (zooplankton). Biostimulation studies using ^{14}C uptake techniques investigating the potential for artificial upwelling effects due to redistribution of nutrients have been started in conjunction with nitrogen fixation studies. Studies of entrainment/impingement, artificial upwelling effects due to redistribution of nutrients have been started in conjunction with nitrogen fixation studies. Entrainment/impingement, artificial reef, and chlorine studies are being done through DOE's Office of Health and Environmental Research (OHER).

REFERENCE CITED

Sands, M. D., et al., 1979. Environmental assessment, Ocean Thermal Energy Conversion (OTEC) program preoperational test platform. Washington, D. C., U. S. Department of Energy, Division of Solar Technology, DOE/EA 0062.

COMPILATION OF MARINE GEOLOGIC AND OCEANOGRAPHIC DATA OFF THE WEST COAST OF THE UNITED STATES

P. Wilde

A series of oceanographic compilation sheets for the area off the west coast of the United States are being produced in cooperation with the U.S. Geological Survey. The aim of this study is to provide a sheet of convenient size that:

1. Summarizes the oceanographic data to date for a particular area.

2. Can be used as a base map for marine geologic investigations.

3. Can be a working chart during shipboard operations.

4. Can be easily revised as new information becomes available.

To date, five of the six sheets, covering the area from the Canadian border (49°N) to the Mexican border (32°N) have been issued (Table 1). The format of the sheets consist of a base bathymetric map at oceanographic plotting scale (approximately 1:750,000 at 45° latitude) with depth contours at 100-m intervals (Figure 1). The base map is supplemented with a series of small maps where items of special interest are plotted. The content of the small maps varies somewhat with each sheet but topics have included geologic and geographic features, earthquake epicenters, bottom sampling stations, heat flow stations, magnetic contours, monthly surface current, monthly sea surface temperatures, gravity-values, seismic stations including track lines with reflection profiling information, seasonal wave heights, and water mass data. Several typical reflection profiles are shown for each sheet. Where applicable, summary logs from deep-sea drilling sites are given.

For actual navigation, a table of available NOAA-NOS sailing and general charts is shown. Finally, pertinent oceanographic and particularly marine geologic references are listed. The maps, tables, and diagrams are useful as indices to available data in a more detailed form. Each data source is listed so the reader/user can contact the groups responsible for the data for additional information.

REFERENCES

Chase, T. E., Normark, W. R., and Wilde, P., 1975. Oceanographic data of the Monterey Deep Sea Fan. University of California, San Diego, IMR Tech. Rept. Series TR-58.

Wilde, P., Normark, W. A., and Chase, T. E., 1976. Oceanographic data off Central California 37° to 40° north including the Delgada deep sea fan. Berkeley, Lawrence Berkeley Laboratory, Pub. 92.

Wilde, P., Chase, T. E., Holmes, M. L., Normark, W. R., and Thomas, J. A., 1977. Oceanographic data off Washington 46° to 49° north including the Nitinat deep sea fan. Berkeley, Lawrence Berkeley Laboratory, Pub. 223.

Wilde, P., Chase, T. E., Holmes, M. L., Normark, W. R., McCulloch, D. S., and Kulm, L. D., 1978. Oceanographic data off northern California-southern Oregon 40° to 43° north including the Gorda deep sea fan. Berkeley, Lawrence Berkeley Laboratory, Pub. 251.

Wilde, P., Chase, T. E., Holmes, M. L., Normark, W. R., and others, 1979. Oceanographic data off Oregon 43° to 46° north including the Astoria deep sea fan. Berkeley, Lawrence Berkeley Laboratory, Pub. 253.

Table 1. Charts in the series.

Principal feature	Location	Publication	Date of Issue
Nitinat Fan	40°-49°N	Pub. 223	1977
Astoria Fan	43°-46°N	Pub. 253	1979
Gorda Fan	40°-4343°N	Pub. 251	1978
Delgada Fan	37°-40°N	Pub. 92	1976
Monterey Fan	24°-37°N	IMR Tech. Rept. 56	1975
Southern California Borderland	32°-35°N	in preparation	--

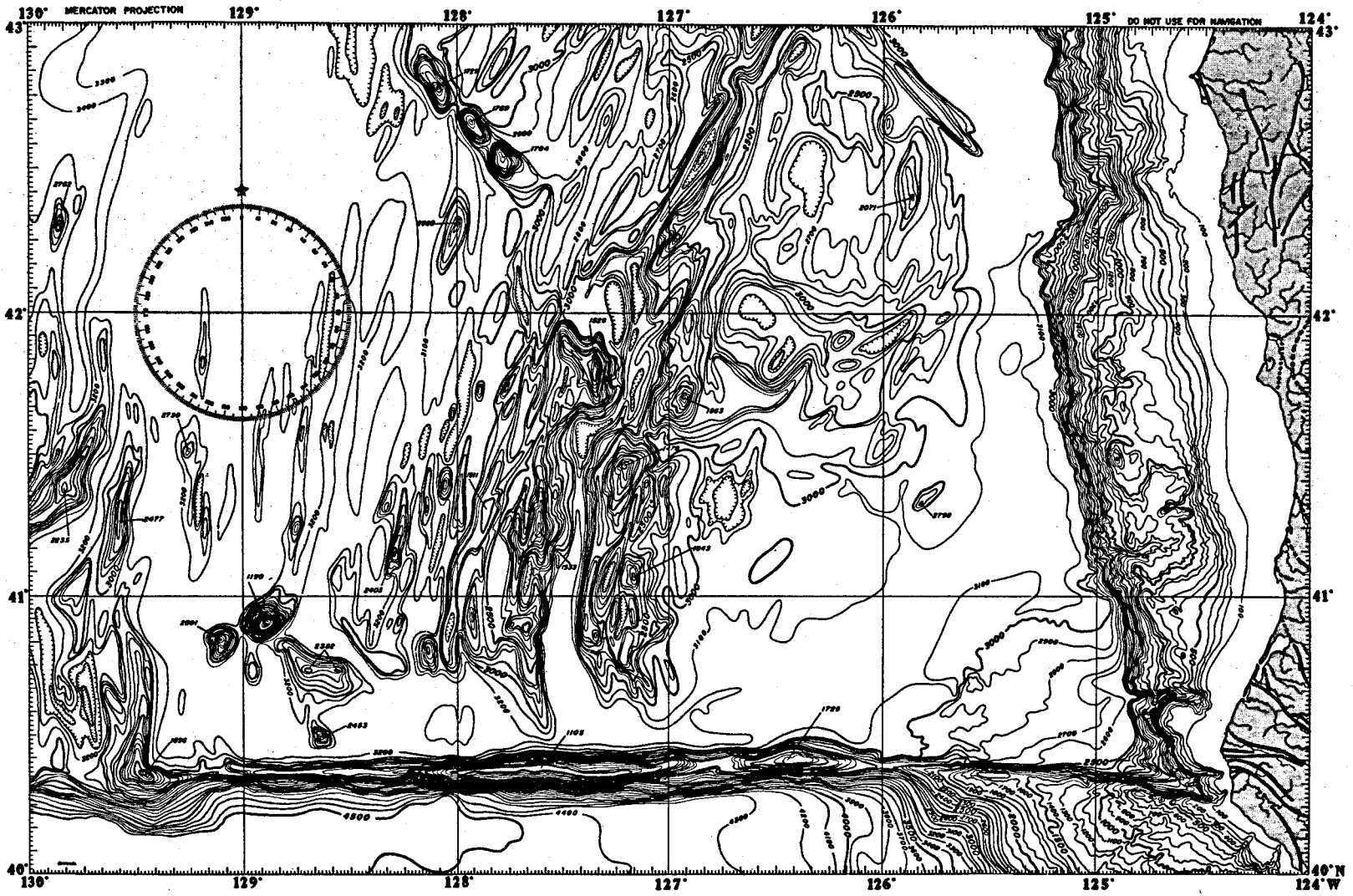

Figure 1. Oceanographic data off northern California/southern Oregon, 40° to 43° North, including the Gorda deep sea fan. (XBL 804-9359)

APPENDIXES

APPENDIX A: PUBLICATIONS

Alonso, H. E., Domínguez, B. A., Lippmann, M. J., Mañon, A. M., Schroeder, R. C., and Witherspoon, P. A., 1978. Recent activities at the Cerro Prieto field (Mexican-American Cooperative Program at the Cerro Prieto Geothermal Field), LBL-8538, CP-02, December 1978.

Apps, J. A., 1978. The simulation of reactions between basalt and groundwater. UCID-8066, October 1978.

Apps, J. A., Doe, T., Doty, B., Doty, S., Galbraith, R., Kearns, A., Kohrt, B., Long, J. C., S., Monroe, A. P., Narasimhan, T. N., Nelson, P. H., Wilson, C. R., and Witherspoon, P. A., 1979. Geohydrological studies for nuclear waste isolation at the Hanford Reservation. Volume I, Executive Summary; Volume II, Final Report. LBL-8764, August 1979.

Benson, S. M., Goranson, C. B., Haney, J. P., and Schroeder, R. C., 1979. The status of the resource evaluation at Susanville, California (presented at the 1979 annual meeting, Geothermal Resources Council, Reno, Nevada, September 24-27, 1979). LBL-9469, July 1979.

Berlin, B., 1979. Statistical analysis of the correlation of earthquakes with radon concentration in water from shallow wells near Oroville, California. LBL-10139, April 1979.

Burleigh, R. H., Binnall, E. P., DuBois, A. O., Norgren, D. U., and Ortiz, A. R., 1979. Electrical heaters for thermo-mechanical tests at the Stripa Mine (Swedish-American Cooperative Program on Radioactive Waste Storage in Mined Caverns in Crystalline Rock). LBL-7063, SAC-13, January 1979.

Chan, T., 1978. Modeling of heater experiments related to radioactive waste storage (presented at the Geological Society of America Penrose Conference, Vail, Colorado, November 13-17, 1978). LBL-8447 (ABS), November 1978.

Chan, T., and Cook, N. G. W., 1979. Calculated thermally induced displacements and stresses for heater experiments at Stripa, Sweden, linear thermoelastic models using constant material properties (Swedish-American Cooperative Program on Radioactive Waste Storage in Mined Caverns in Crystalline Rock). LBL-7061, SAC-22, December 1979.

Chan, T., and Remer, J. S., 1978a. Preliminary thermal and thermomechanical modeling for the near surface test facility heater experiments at Hanford. LBL-7069, December 1978.

_____,1978b. Semi-analytic thermal calculations for arrays of nuclear waste canisters buried in rock (presented at the Americal Geophysical Union 1978 fall meeting, San Francisco, December 4-8, 1978). LBL-8433 (ABS), November 1978.

Clarke, J., Gamble, T. D., Goldstein, N. E., Goubau, W. M., Koch, R., and Miracky, R. F., 1979. Field analysis of magnetotelluric data (presented at the 49th International Meeting, Society of Exploration Geophysicists, New Orleans, Louisiana, November 4-8, 1979). LBL-9268 (ABS), May 1979.

Cliff, W. C., Apley, W. J., and Greer, J. M., 1979. Evaluation of potential geothermal well-head flow sampling and calorimeter methods [Battelle Pacific Northwest Lab, subcontractor]. LBL-9248, GREMP-7, June 1979.

Commins, M. L., and Horne, A. J., 1979. Zooplankton from OTEC sites in the Gulf of Mexico and the Caribbean (presented at the 6th Annual Ocean Thermal Energy Conversion Conference, Washington, D. C., June 19-22, 1979). LBL-9053, June 1979.

Cook, N. G. W., 1979. Field measurement techniques —status and needs (presented at the Workshop on the Thermochemical Modeling for a Hardrock Waste Repository, sponsored by ONWI and Lawrence Livermore Laboratory, Berkeley, California, June 25-27, 1979). LBL-9425, June 1979.

Cook, N. G. W., Gale, J. E., and Witherspoon, P. A., 1979. Waste disposal in granite--preliminary results from Stripa, Sweden (presented at the 19th Annual ASME Symposium, Geological Disposal of Nuclear Waste, Albuquerque, New Mexico, March 15-16, 1979). LBL-9424, March 1979.

Cook, N.G.W., and Hood, M., 1978. Full-scale and time-scale heating experiments at Stripa, preliminary results (Swedish-American Cooperative Program on Radioactive Waste Storage in Mined Caverns in Crystalline Rock). LBL-7072. SAC-11, December 1978.

Cook, N. G. W., and Witherspoon, P. A., 1978. Mechanical and thermal design considerations for radioactive waste repositories in hard rock: Part I - An appraisal of hard rock for potential underground repositories of radioactive wastes; Part II - In-situ heating experiments in hard rock, their objectives and design (Swedish-American Cooperative Program on Radioactive Waste Storage in Mined Caverns in Crystalline Rock). LBL-7073, SAC-10. October 1978.

DuBois, A. O., Binnall, E. P., Chan, T., McEvoy, M. B., Nelson, P. H., and Remer, J. S., 1979. Heater test planning for the near surface test facility at the Hanford Reservation. LBL-8730, March 1979.

Earth Sciences Division, 1978a. Proceedings of the First Symposium on the Cerro Prieto Geothermal Field, Baja California, Mexico, San Diego, California, September 20-22, 1978. LBL-7098, September 1978.

_____, 1978b. Earth Sciences Division annual report 1978. LBL-8648.

_____, 1978c. Geothermal exploration technology, annual report 1978. LBL-8603.

_____,1978d. Proceedings of the Second Invitational Well-Testing Symposium, Berkeley, California, October 25-27, 1978. LBL-8883.

_____, 1978e. Geosciences Program annual report, 1978. LBL-10349.

_____, 1978f. Aquifer Thermal Energy Storage Newsletter (ATES). PUB-272, v. 1, no. 1 , October 1978.

_____, 1979a. Earth Sciences Division Newsletter. PUB-283, v. 2, no. 1 (January 1979), v. 2, no. 2 (September 1979).

_____, 1979b. News from Geothermal Reservoir Engineering Management Program (GREMP). PUB-285, v. II, no. 1 (February 1, 1979), v. II, no. 2 (May 1, 1979), v. II, no. 3 (August 31, 1979).

_____, 1979c. News from Geothermal Subsidence Research Management Program (GSRMP). PUB-286, v. I, no. 1 (February 1, 1979), v. I, no. 2, (June 1, 1979).

_____, 1979d. Aquifer Thermal Energy Storage Newsletter (ATES). PUB-294, v. I, no. 2 (January 1979), v. I, no. 3 (May 1979), v. I, no. 4 (September 1979).

_____, 1979e. News of Geothermal Energy Conversion Technology (GECT). PUB-308, v. I, no. 1 (July 1979), v. I, no. 2 (December 1979).

Fritz, P., Barker, J. F., and Gale, J. E., 1979. Geochemistry and isotope hydrology of groundwaters in the Stripa granite, results and preliminary interpretation (Swedish-American Cooperative Program on Radioactive Waste Storage in Mined Caverns in Crystalline Rock). LBL-8285, SAC 12, April 1979.

Fulton, R. L., 1979. Geothermal energy for industrial application (presented at the Association of Energy Engineers Conference, San Francisco, March 21-23, 1979). LBL-8918, March 1979.

Gale, J. E., and Witherspoon, P. A., 1979. An approach to the fracture hydrology at Stripa, preliminary results (Swedish-American Cooperative Program on Radioactive Waste Storage in Mined Caverns in Crystalline Rock). LBL-7079, SAC-15, May 1979.

Goldstein, N. E., 1979. Geothermal energy development from the Salton Trough to the High Cascades (presented at the Third National Conference and Exhibition on Technology for Energy Conservation, Tucson, Arizona, January 23-25, 1979). LBL-8703, January 1979.

Goranson, C. B., and Schroeder, R. C., Site specific geothermal reservoir engineering activities at Lawrence Berkeley Laboratory (presented at the 1979 annual meeting, Geothermal Resources Council, Reno, Nevada, September 24-27, 1979). LBL-9463, July 1979.

Goranson, C. B., Schroeder, R. C., and Haney, J. P., 1979. Evaluation of Coso geothermal exploratory hole No. 1 (CGEH-1), Coso Hot Springs, known geothermal resource area, China Lake, California (presented at the Fourth Annual Workshop on Geothermal Reservoir Engineering, Stanford University, Palo Alto, California, December 13-15, 1978). LBL-8675, January 1979.

Goyal, K. P., and Kassoy, D. R., 1978. Heat and mass transfer studies of the East Mesa anomaly (presented at the Fourth Workshop on Geothermal Reservoir Engineering, Stanford University, December 1978). LBL-9330, December 1978.

_____, 1979a. Fault zone controlled charging of a liquid dominated geothermal reservoir (submitted to the Journal of Geophysical Research). LBL-9327, July 1979.

_____, 1979b. Heat and mass transfer in a saturated porous wedge with impermeable boundaries (submitted to the International Journal of Heat and Mass Transfer). LBL-9328, June 1979.

_____, 1979c. Fault zone controlled charging of an aquifer (presented at the 18th ASME-AICHE National Heat Transfer Conference, San Diego, August 5-8, 1979). LBL-09329 (ABS), December 1979.

Grannell, R. B., Tarman, D. W., Aronstam, P., Clover, R. C., Leggewie, R. M., Eppink, J., and Kroll, R., 1979. Precision gravity measurements in the Cerro Prieto geothermal area (presented at the Second Symposium on the Cerro Prieto Geothermal Field, Mexicali, Mexico, October 17-19, 1979). LBL-9551 (ABS), July 1979.

Haney, J. P., Goranson, C. B., Solbau, R., and Schroeder, R. C., 1979. A review of LBL geothermal well testing equipment (presented at the 1979 annual meeting, Geothermal Resources Council, Reno, Nevada, September 24-27, 1979). LBL-9462, July 1979.

Hood, M., 1979. Experimental results from Stripa (presented at the Workshop on Thermomechanical Modeling for a Hard Rock Waste Repository, Berkeley, June 25-27, 1979). LBL-9426, June 1979.

Howard, J. H., Apps, J. A., Benson, S. M., Goldstein, N. E., Graf, A. N., Haney, J. P., Jackson, D. D., Juprasert, S., Majer, E. L., McEdwards, D. G., McEvilly, T. V., Narasimhan, T. N., Schechter, B., Schroeder, R. C., Taylor, R. W., Van de Kamp, P. C., and Wolery, T. J., 1978. Geothermal resources and reservoir investigations of U. S. Bureau of Reclamation leaseholds at East Mesa, Imperial Valley, California. LBL-7094, October 1978.

Howard, J. H., and Davey, J. V., 1979. Geothermal resources and the U. S. pulp and paper industry (submitted to Paper Trade Journal). LBL-8735.

Howard, J. H., and Schwarz, W. J., 1979. Status of geothermal reservoir engineering research projects supported by U. S. Department of Energy Division of Geothermal Energy (presented at the 1979 annual meeting, Geothermal Resource Council, Reno, Nevada, September 24-27, 1979). LBL-9326, July 1979.

Javandel, I., and Witherspoon, P. A., 1979a. A study of partial penetration in a two-layered aquifer: I, Analytical solution. LBL-9479, May 1979.

_____, 1979b. A semi-analytical solution for partial penetration in two-layer aquifers (submitted to Water Resources Research). LBL-9427, June 1979.

Jeffry, J. A., Chan, T., Cook, N. G. W., and Witherspoon, P. A., 1978. A least squares method for determining in situ thermal properties from temperatures caused by a finite length heater (presented at the American Geophysical Union 1978 Fall Meeting, San Francisco, December 4-8, 1978). LBL-8423 (ABS), November 1978.

_____, 1979. Determination of in situ thermal properties of Stripa granite from temperature measurements in the full-scale heater experiments, method and preliminary results (Swedish-American Cooperative Program on

Radioactive Waste Storage in Mined Caverns in Crystalline Rock). LBL-8423, SAC-24, May 1979.

Johnson, P. W., and Horne, A. J., 1979. Phytoplankton and biomass distribution at potential OTEC sites, (presented at the 6th Annual Ocean Thermal Energy Conversion Conference, Washington, D. C., June 19-22, 1979). LBL-9054, June 1979.

Kassoy, D. R., and Goyal, K. P., 1979. Modeling heat and mass transfer at the Mesa geothermal anomaly, Imperial Valley, California [University of Colorado, subcontractor]. LBL-8784, GREMP-3, February 1979.

Lamers, M. D., 1979. Measurement requirements and methods for geothermal reservoir system parameters, an appraisal [Measurement Analysis Corp., subcontractor]. LBL-9090, GREMP-6, August 1979.

Lippmann, M. J., and Tsang, C. F., 1979. Three-dimensional numerical simulation of single-phase, non-isothermal, fluid flow in porous reservoirs (submitted for the meeting of the Society of Petroleum Engineers of AIME, Denver, Colorado)., LBL-7056 (ABS), January/February 1979.

Mangold, D. C., Tsang, C. F., Lippmann, M. J., and Witherspoon, P. A., 1979. A study of thermal effects in well test analysis (presented at the 54th Annual Fall Technical Conference and Exhibition of the Society of Petroleum Engineers of AIME, Las Vegas, Nevada, September 23-26, 1979). LBL-9769, September 1979.

Marconcini, R., Neri, G., Pruess, K., Ruffilli, C., Schroeder, R. C., and Witherspoon, P. A., 1979. Simulation of the depletion of two-phase geothermal reservoirs (presented at the 54th Annual Technical Conference and Exhibition, Society of Petroleum Engineers of AIME, Las Vegas, Nevada, September 23-26, 1979). LBL-9310 (ABS), June 1979.

McEdwards, D. G., 1979. Multiwell variable rate well test analysis (presented at the 54th Annual Fall Technical Conference and Exhibition of the Society of Petroleum Engineers of AIME, Las Vegas, Nevada, September 23-26, 1979). LBL-9460, SPE-8392, September 1979.

McEdwards, D. G., and Benson, S. M., 1978. Injection test results from wells 5 1 and 18 28 East Mesa known geothermal resource area (presented at the Second Invitational Well Testing Symposium, Berkeley, October 24-27, 1978). LBL-8362 (ABS), October 1978.

McEvoy, M. B., 1979. Data acquisition, handling, and display for the heater experiments at Stripa (Swedish-American Cooperative Program on Radioactive Waste Storage in Mined Caverns in Crystalline Rock). LBL-7062, SAC-14, February 1979.

Miller, C. W., 1979. Wellbore storage effects in geothermal wells (presented at the 54th annual Fall Technical Conference, Society of Petroleum Engineers of AIME, Las Vegas, Nevada, September 23-26, 1979). LBL-8844, July 1979.

Miller, C. W., and Haney, J. P., 1978. Pressure transient response of a fluid in a capillary tube (presented at the Second Invitational Well Testing Symposium, Berkeley, October 24-27, 1978). LBL-8361 (ABS), October 1978.

Miller, C. W., and Zernan, J. M., 1979. Downhole pressure changes measured with a fluid filled capillary tube (presented at the annual meeting of the Society of Petroleum Engineers, Las Vegas, Nevada, September 23-27, 1979). LBL-9303, October 1978.

Morrison, H. F., Goldstein, N. E., Hoversten, M., Oppliger, G., and Riveros, C. A., 1978. Description, field test and data analysis of a controlled-source EM system (EM-60). LBL-7088, October 1978.

Morrison, H. F., Lee, K. H., Oppliger, G., and Dey, A., 1979. Magnetotelluric studies in Grass Valley, Nevada. LBL-8646, January 1979.

Narasimhan, T. N., 1979. Groundwater modeling in subsurface nuclear waste disposal--an overview (submitted to Transactions of the American Nuclear Society). LBL-8742, January 1979.

Narasimhan, T. N., 1979. A note on volume averaging (submitted to Advances in Water Resources). LBL-8792, February 1979.

Narasimhan, T. N., and Palen, W. A., 1979. A purely numerical approach for analyzing flow to a well intercepting a vertical fracture (presented at the Society of Petroleum Engineers California Regional Meeting, Ventura, California, April 18-20, 1979). LBL-8816, March 1979.

Narasimhan, T. N., and Witherspoon, P. A., 1978. Numerical model for saturated unsaturated flow in deformable porous media. Water Resources Research, v. 14, no. 8, p. 1017-1034, and LBL-7037, December 1978.

Narasimhan, T. N., and Kanehiro, B. Y., 1979. A note on the meaning of storage coefficient (submitted to Water Resources Research). LBL-8295, January 1979.

Narasimhan, T. N., and Witherspoon, P. A., 1979. Geothermal well testing (published in the Burke Maxey Volume of the Journal of Hydrology, 1979). LBL-8290, January 1979.

Nelson, P. H., Paulsson, B. N. P., Rachiele, R., Andersson, L., Schrauf, T., Hustrulid, W., Duran, O., and Magnusson, K. A., 1979. Preliminary report on geophysical and mechanical borehole measurements at Stripa (Swedish-American Cooperative Program on Radioactive Waste Storage in Mined Caverns in Crystalline rock). LBL-8280, SAC-16, May 1979.

Nelson, S. A., and Carmichael, I. S. E., 1979. Partial molar volumes of oxide components in silicate liquids (submitted to Contributions to Mineralogy and Petrology). LBL-9210, July 1979.

Neretnieks, I., 1979. Age dating of groundwater in fissured rock--the influence of water volume in micropores (submitted to Science). LBL-9473, July 1979.

O'Brien, M. T., Cohen, L. H., Narasimhan, T. N., Simkin, T. L., Wollenberg, H. A., Brace, W. F., Green, S., and Pratt, H. P., 1979. The very deep hole concept--evaluation of an alternative for nuclear waste disposal. LBL-7089, July 1979.

Olkiewicz, A., Gale, J. E., Thorpe, R. K., and Paulsson, B. N. P., 1979. Geology and fracture system at Stripa (Swedish-American

Cooperative Program on Radioactive Waste Storage in Mined Caverns in Crystalline Rock). LBL-8907, SAC-21, February 1979.

O'Rourke, J. E., and Ranson, B. B., 1979. Instruments for subsurface monitoring of geothermal subsidence [Woodward-Clyde Consultants, subcontractor]. LBL-8616, GSRMP-2, July 1979.

Payne, S. F., 1979. The marine mammal fauna of potential OTEC sites in the Gulf of Mexico and Hawaii (presented at the 6th annual Thermal Energy Conversion Conference, Washington, D. C., June 19-22, 1979). LBL-9055, May 1979.

Pinder, G. F., 1979. State-of-the-art review of geothermal reservoir modeling [Golder Associates, subcontractors]. LBL-9093, GSRMP-5, March 1979.

Pitzer, K. S., 1979. Characteristics of very concentrated aqueous solutions (presented to the Nobel Symposium on Chemistry and Geochemistry of Solutions at High Temperature and Pressure, Bofors, Karlskoga, Sweden, September 16-21, 1979, and published by the Royal Swedish Academy of Sciences). LBL-9660, August 1979.

Pope, W. L., Pines, H. S., Fulton, R. L., and Doyle, P. A., 1978. Heat exchanger design: Why guess a design fouling factor when it can be optimized? (presented at the Energy Technology Conference and Exhibition, Houston, Texas, November 5-9, 1978, and to appear in Bradley, W. B., ed., Emerging Energy Technologies American Society of Mechanical Engineers). LBL-7067, June 1978.

Pritchett, J. W., Rice, L. F., and Garg, S. K., 1979. Summary of reservoir engineering data--Wairakei geothermal field, New Zealand [Systems, Science, and Software, subcontractor]. LBL-8669, GREMP-2, January 1979.

Pruess, K., Bodvarsson, G., Schroeder, R. C., and Witherspoon, P. A., 1979. Simulation of the depletion of two-phase geothermal reservoirs (presented at the Society of Petroleum Engineers 54th Annual Technical Conference, Las Vegas, Nevada, September 23-26, 1979). LBL-9606, August 1979.

Pruess, K., Schroeder, R. C., and Zerzan, J. M., 1978. Studies of flow problems with the simulator SHAFT78 (presented at the Fourth Geothermal Reservoir Engineering Workshop, Stanford University, December 13-15, 1978). LBL-8515, November 1978.

Pruess, K., and Schroeder, R. C., 1979. Basic theory and equations used in the two-phase multidimensional geothermal reservoir simulator, SHAFT79 (presented at the 1979 annual meeting, Geothermal Resource Council, Reno, Nevada, September 24-27, 1979). LBL-9464, July 1979.

Pruess, K., Zerzan, J. M., Schroeder, R. C., and Witherspoon, P. A., 1979. Description of the three-dimensional two-phase simulator SHAFT78 for use in geothermal reservoir studies (presented at the 1979 meeting, Society of Petroleum Engineers of AIME, 5th Symposium on Reservoir Simulation, Denver, Colorado, February 1-2, 1979). LBL-8802, January 1979.

Quinby-Hunt, M. S., 1979. Comparison of nutrient data from four potential OTEC sites (presented at the 6th annual Ocean Thermal Energy Conversion Conference, Washington, D. C., June 19-22, 1979). LBL-9052. June 1979.

Riveros, C. A., and Goldstein, N. E., 1979. Design and application of a mega-moment electromagnetic dipole source (presented at the 49th International Meeting, Society of Exploration Geophysicists, New Orleans, Louisiana, November 4-8, 1979). LBL-9273 (ABS), May 1979.

Sands, M. D., 1979. Programmatic environmental impact assessment for operational OTEC platforms--A progress report (presented at the MTS Oceans 1979 Conference, San Diego, September 1979). LBL-9183, May 1979.

Silva, R. J., Benson, L. V., Yee, A. W., and Parks, G. A., 1979. Waste isolation safety assessment program, task 4--collection and generation of transport data, theoretical and experimental evaluation of waste transport in selected rocks (annual progress report, October 1, 1978 - September 30, 1979). LBL- 9945.

Sudol, G. A., Harrison, R. F., and Ramey, H. J., Jr., 1979. Annotated research bibliography for geothermal reservoir engineering [Terra Tek, Inc., subcontractor]. LBL-8664, GREMP-1, August 1979.

Stark, M., Goldstein, N. E., Wollenberg, H. A., Strisower, B., Hege, M. L., and Wilt, M. J., 1979. Geothermal exploration assessment and interpretation, Klamath Basin, Oregon, Swan Lake and Klamath Hills area. LBL-8186, May 1979.

Thorpe, R. K., 1979. Characterization of discontinuities in the Stripa granite time-scale heater experiment (Swedish-American Cooperative Program on Radioactive Waste Storage in Mined Caverns in Crystalline Rock). LBL-7083, SAC-20, July 1979.

Tleimat, B. W., Laird, A. D. K., Hsu, I. C. W., and Rie, H., 1979. Baseline data on film coefficient for heating isobutane inside a tube at 4.14 MPA (600 PSIA). (Presented at the joint ASME/AIME 18th National Heat Transfer Conference, San Diego, August 6-8, 1979). LBL-9720, April 1979.

Tleimat, B. W., Laird, A. D. K., Rie, H., Hsu, I. C. W., and Seban, R. A., 1979. Hydrocarbon heat transfer coefficients--preliminary isobutane results. LBL- 8645, February 1979.

Tsang, C. F., 1979. A review of current aquifer thermal energy storage projects (presented at the International Assembly on Energy Storage, Dubrovnik, Yugoslavia, May 27-June 1, 1979). LBL-9834, May 1979.

Tsang, C. F., Lippmann, M. J., Schroeder, R. C., Narasimhan, T. N., Zerzan, J. M., Pruess, K., Bodvarsson, G., and Mangold, D. C., 1978. Numerical modeling studies in well test analysis (presented at the Second Invitational Well Testing Symposium, Berkeley, October 24-27, 1978). LBL-8363 (ABS), October 1978.

Tsang, Y. W., and Tsang, C. F., 1978. An analytic study of geothermal reservoir pressure response to cold water reinjection (presented at the Fourth Annual Workshop

on Geothermal Reservoir Engineering, Stanford University, December 13-15, 1978). LBL-9001, November 1978.

Van Til, C. J., 1979. Guidelines manual for surface monitoring of geothermal areas [Woodward-Clyde Consultants, subcontractor]. LBL-8617, GSRMP-3, May 1979.

Vetter, O. J., and Campbell, D. A., 1979. Scale inhibition in geothermal operations experiments with Dequest 2060 phosponate in Republic's East Mesa field [Vetter research and Republic Geothermal, Inc., subcontractor]. LBL-9089, GREMP-5, June 1979.

Viets, V. F., Vaughan, C. K., and Harding, R. C., 1979. Environmental and economic effects of subsidence [EDAW and ESA, subcontractor]. LBL-8615, GSRMP-1, May 1979.

Vonder Haar, S., and Gorsline, D., 1979. Flooding frequency and sedimentation unit correlation of tidal flat and coastal salina facies along the upper Gulf of California, Mexico, (presented at the Geological Society of America Annual Conference, San Diego, November 7-9, 1979). LBL-9285 (ABS), June 1979.

Vonder Haar, S., and Howard, J. H., 1978. Geology and geothermal resources of the Salton Trough, California, in relation to rift zone tectonics (presented at the 1978 International Symposium on the Rio Grande Rift, Santa Fe, New Mexico, October 8-17, 1978). LBL-9556, October 1978.

Vonder Haar, S., and Puente Cruz I., 1979. Transform faulting related to geothermal energy in Baja California, Mexico, (presented at the Geological Society of America Annual Conference, San Diego, November 5-8, 1979). LBL-9272 (ABS), June 1979.

Vonder Haar, S., and Puente Cruz, I., 1979. Fault intersections and hybrid transform faults in the southern Salton Trough geothermal area, Baja California, Mexico. (Presented at the annual meeting, Geothermal Resources Council, Reno, Nevada, September 24-27, 1979). LBL-9458, July 1979.

Vonder Haar, S., Noble, J. E., and Puente Cruz, I., 1979. Vertical movement along the Cerro Prieto transform fault, Baja California, Mexico--A mechanism for geothermal energy renewal. LBL-8905, March 1979.

Weres, O., Yee, A. W., and Tsao, L., 1979. The mechanisms of amorphous silica precipitation from geothermal brines (presented at the Geothermal Scaling and Corrosion Symposium at the American Chemical Society National Meeting, Honolulu, Hawaii, April 1-6, 1979). LBL-8326 (ABS), October 1978.

Wilde, P., 1979. Environmental monitoring and assessment program at potential OTEC sites (presented at the 6th annual Ocean Thermal Energy Conversion Conference, Washington, D. C., June 19-22, 1979). LBL-9051, June 1979.

Wilde, P., Chase, T. E., Holmes, M. L., Normark, W. R., Thomas, J. A., McCulloch, D. S., and Kulm, L. D., 1978. Oceanographic data off northern California/southern Oregon, 40 degrees to 43 degrees north including the Gorda Deep Sea Fan. PUB-251, Map, 1st ed., November 1978.

Wilde, P., Chase, T. E., Holmes, M. L., Normark, W. R., Thomas, J. A., McCulloch, D. S., Carlson, P. R., Kulm, L. D., and Young, J. D., 1979. Oceanographic data off Oregon 43 degrees to 46 degrees north including the Astoria Deep Sea Fan. PUB-253, Map, 1st ed., July 1979.

Wilde, P., Sandusky, J., and Jassby, A., 1978. Assessment and control of OTEC ecological impacts (presented at the U. S. DOE Environmental Control Symposium, Washington D. C., November 28-30, 1978). LBL-8967, December 1978.

Wilt, M. J., and Goldstein, N. E., 1979. Resistivity monitoring at Cerro Prieto (presented at the Second Symposium on the Cerro Prieto Geothermal Field, Mexicali, Mexico, October 17-19, 1979). LBL-9549 (ABS), July 1979.

Wilt, M. J., Goldstein, N. E., Hoversten, M., and Morrison, H. F., 1979. Controlled-source EM experiment at Mt Hood, Oregon (presented at the Geothermal Resources Council annual meeting, Reno, Nevada, September 24-27, 1979). LBL-9399, July 1979.

Witherspoon, P. A., Amick, C. H., Gale, J. E., and Iwai, K., 1979. Observations of a potential size-effect in experimental determination of the hydraulic properties of fractures (Swedish-American Cooperative Program on Radioactive Waste Storage in Mined Caverns in Crystalline Rock). LBL-8571 SAC-17, May 1979.

Witherspoon, P. A., Gale, J. E., and Cook, N. G. W., 1979. Investigations in granite at Stripa, Sweden, for nuclear waste storage (presented at the 25th annual meeting, American Nuclear Society Special Session on Geological Repositories for Nuclear Wastes, Atlanta, Georgia, June 3-8, 1979). LBL-9400, June 1979.

Witherspoon, P. A., Gale, J. E., and Cook, N. G. W., 1979. Investigations in granite at Stripa, Sweden, for nuclear waste storage (presented at the 1979 annual meeting of the American Nuclear Society, Atlanta, Georgia, June 3-8, 1979). LBL-8801. January 1979.

Witherspoon, P. A., Nelson, P. H., Doe, T., Thorpe, R. K., Paulsson, B. N. P., Gale, J. E., and Forster, C., 1979. Rock mass characterization for storage of nuclear waste in granite (Swedish-American Cooperative Program on Radioactive Waste Storage in Mined Caverns in Crystalline Rock). LBL-8570, SAC-18, February 1979.

Wollenberg, H. A., Bowen, R. E., Bowman, H. R., and Strisower, B., 1979. Geochemical studies of rocks, water, and gases at Mt Hood, Oregon. LBL-7092, February 1979.

APPENDIX B: EARTH SCIENCES DIVISION STAFF

PAUL A. WITHERSPOON*

Associate Director, Lawrence Berkeley Laboratory
Division Head, Earth Sciences Division

DIVISION ADMINISTRATION

Kenneth F. Mirk, Deputy Division Head
Karl Olson, Assistant Division Head
Monique Adam, Division Office Administration

STAFF OF FISCAL YEAR 1979

Jack Angevine
John Appa
Lois Armetta
Mohammed Ayatollahi

Lawrence Beaulaurier
Larry Benson
Sally Benson
Eugene Binnall
Gudmundur Bodvarsson
Mary Bodvarsson
Milford Bookman
Harry Bowman
Daniel Bradley
Wendy Brubaker
Annette Bunge
Thomas Buscheck
Timothy Buscheck
Patricia Butler

Hans Carlsson
Ian Carmichael*
Coen Carmiggelt
Chalon Carnahan
Joseph Chan
Tin Chan
Mitchell Che
Eric Cheney
Jerry Chin
Clement Chou
Jeri Chu
John Clarke*
Marcie Commins
Lewis Cohen*
Neville Cook*
Donald Corrigan
Alain Curneir

James Davey
Robert Davis
E. F. De Zabala
Thomas Doe
Cathy Donnelly
Christine Doughty
Padraic Doyle
Allan Dubin
Andrew DuBois
Peter Duncan

Houshana Ebrahimi
Laurel Egenberger

Paul Elias
Janice Elliot
Eugene Eno
Daniel Estrella
James Evans

James Ferguson
Steve Flexser
Conny Frisch
Mauro Foglia
Philip Fong
Ted Fujita
Robert Fulton

Robert Galbraith
Thomas Gamble
Anoushiravan Ghaffari
Susan Gillett
Beverly Gimeno
Orah Goldman
Norman Goldstein
Colin Goranson
Wolfgang Goubau
Keshav Goyal
Alexander Graf
Joyce Graves
Thomas Green
Roy Greenwald

Joseph Haney
Leif Hansen
Makoto Harada
Rosemary Hart
Niamh Harty
Ramsey Haught
Kunio Higashi
Deborah Hopkins
Alex Horne*
John Howard
Michael Hood*
Richard Hsu

Eduardo Iglesias
Jeffrey Irvine

Dennis Jamison
Alan Jassby
Abdul Rahim Jaouni
Julie Jeffrey
Anthony Jones
Keith Jones

Randall Jones
Sirisak Juprasert

Brian Kanehiro
Allen Kearns
William Keyes
Tjiep Kho
Stanley Klainer
Steven Kramer
Brent Kohrt
Pavel Kurfurst

Cheng-Hsien Lai
Raymond Lee
Wayne Lee
David Leung
Donald Lippert
Marcelo Lippmann
Nicholas Littlestone
Jane Long
Steve Lundgren

Ernest Majer
Donald Mangold
Donald McCarthy
Susan McCormick
Donald McEdwards
Thomas McEvilly*
Maurice McEvoy
Ellen McKeon
Janet McQuillan
Maynard Michel
Constance Miller
Susan Miller
James Mitchell
Sofia Mitina
Milton Moebus
Alison Monroe
Leuren Moret
H. Frank Morrison*
Susumu Muraoka

T. N. Narasimhan
John Neil
Philip Nelson
Helen Nicholas
John Noble
Duane Norgren
Yvonne Norpchen

Maura O'Brien

---

*Faculty member, University of California.

John Oldson
Irmgard Orzech

Walter Palen
George Parks
Bjorn Paulsson
Susan Payne
Christopher Peiper
Scott Peterson
Ronald Philips
Thomas Pigford*
Howard Pines
Kenneth Pitzer*
William Pope
Karsten Pruess

Richard Rachiele
Clayton Radke*
William Ralph
Pascal Rapier
Ruthie Redic
Janet Remer
Carlos Riveros
Marc Rivers
Morris Roach
Gene Rochlin
Pamela Rogers
Donald Rondeau
James Roth

Eliezer Rubin
Theresa Ruiz
Jacqueline Runnells

James Sandusky
Marie Schauer
Bruce Schechter
Peter Schein
David Schmidt
Dee Schmidt
Ronald Schroeder
Werner Schwarz
Robert Silva
Lenard Silvester
Terrance Simkin
Ray Solbau
Wilbur Somerton*
Hwaili Soo
Barbara Srulovitz
Mitchell Stark
Andrew Stromdahl
Rebecca Sterbentz
Robert Stolzman
Beverly Strisower
Ho-Jeen Su

Lisa Teague
Jerome Thomas
Richard Thorpe

Marc Trujillo
Chin Fu Tsang
Leon Tsao
Badawi Tleimat
Richard Vallentine
William Villet
Jen Edgar-Vogt
Stephen Vonder Haar

David Watkins
Cheri Walker
Oliver Wan
Joseph Wang
Christopher Weaver
Virginia Weaver
Oleh Weres
Jerry West
Richard Whiteman
Pat Wilde
Charles Wilson
Michael Wilt
Harold Wollenberg, Jr.
Lester Wong
William Wong

Andrew Yee

John Zerzan

---

*Faculty member, University of California.